BioMed Research International

How Microgravity Affects the Biology of Living Systems

Guest Editors: Mariano Bizzarri, Monica Monici, and Jack J. W. A. van Loon

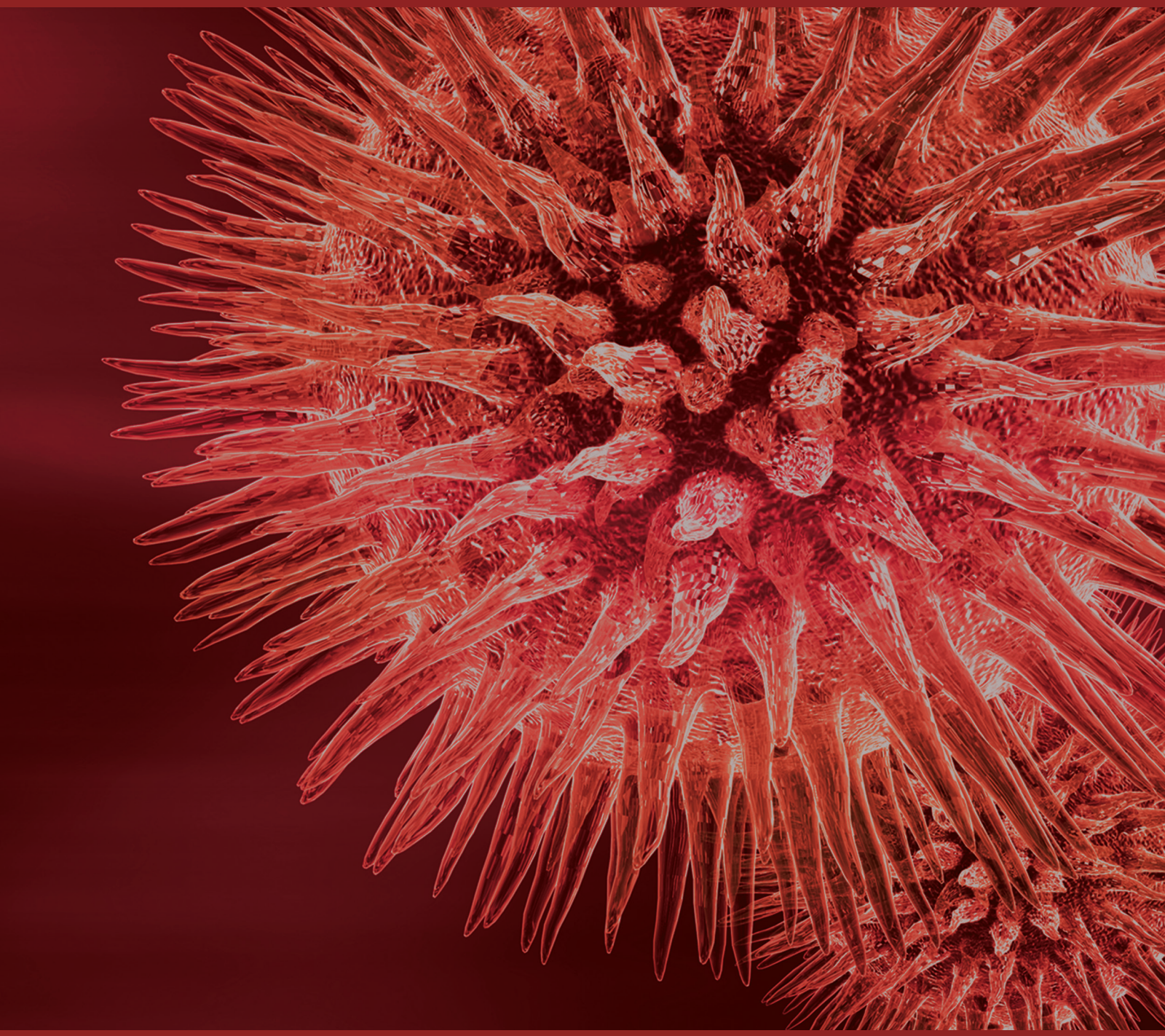

How Microgravity Affects the Biology of Living Systems

BioMed Research International

How Microgravity Affects the Biology of Living Systems

Guest Editors: Mariano Bizzarri, Monica Monici, and Jack J. W. A. van Loon

Contents

Hindawi Publishing Corporation
BioMed Research International
Volume 2015, Article ID 863075, 4 pages
http://dx.doi.org/10.1155/2015/863075

Editorial

How Microgravity Affects the Biology of Living Systems

Mariano Bizzarri,[1] Monica Monici,[2] and Jack J. W. A. van Loon[3]

[1]*Department of Experimental Medicine, Systems Biology Group, University La Sapienza, 00161 Rome, Italy*
[2]*ASAcampus Joint Laboratory, ASA Research Division, Department of Experimental and Clinical Biomedical Sciences, University of Florence, 50121 Florence, Italy*
[3]*Department of Oral and Maxillofacial Surgery/Oral Pathology, VU-University Medical Center, 1081 HZ Amsterdam, Netherlands*

Correspondence should be addressed to Mariano Bizzarri; mariano.bizzarri@uniroma1.it

Received 20 November 2014; Accepted 20 November 2014

Gravity has constantly influenced both physical and biological phenomena throughout Earth's history. The gravitational field has played a major role in shaping evolution when life moved from water to land, even if, for a while, it has been generally deemed to influence natural selection only by limiting the range of acceptable body sizes, according to Galilei's principle. Indeed, to counteract gravity, living organisms would need to develop systems to provide cell membrane rigidity, fluid flow regulation, and appropriate structural support for locomotion. However, gravity may influence in a more deep and subtle fashion the way the cells behave and build themselves.

The first empirical experiments, mostly done by Russian scientists in the 60s, were unable to unravel major changes after exposure to microgravity, thus nurturing the false notion for which near weightlessness does not get any appreciable effects on living organisms [1, 2]. However, as fundamental investigations began in the space environment, it became evident that biological properties change as gravitational force is diminished, underscoring the relationship between physical force and biological function. Cells exposed to microgravity can indeed be profoundly affected by the physical changes that occur in this unique environment, which include the loss of gravity-dependent convection, negligible hydrodynamic shear, and lack of sedimentation [3–5]. Cell-substrate adhesions, as well as cell-to-cell junctions, are consequently profoundly affected at Earth's gravity, impairing multicellular aggregates and tissue formation, while such structures can be more easily sustained for days or months in microgravity [6]. These modifications eventually lead to a significant change in the way the cell mechanosensor apparatus responds to a wide array of environmental and internal biophysical stresses [7]. As a consequence, enzymatic, genetic, and epigenetic pathways change in concert, leading to several modifications in cells and tissues shape, function, and behavior [8, 9]. Fruitful insights about the involvement of several molecular pathways during microgravity exposure are reported in this issue by the studies of V. Gasperi et al. (unravelling new pathways involved in immune function impairment during spaceflight) and E. Albi et al. (overexpression of Galectin-3 in thyroid follicles due to microgravity-induced membrane remodelling). Namely, a sophisticated analysis of mRNA expression in human blood lymphocytes, carried out by C. Girardi et al., confirmed that microgravity induces a generalized inhibition of proliferation and a contemporary increase in apoptosis rate.

Indeed—and unfortunately—near weightlessness dramatically impairs biological functions and thereby, contrary to what was previously thought [2], cells cannot be considered "blind" with respect to gravity.

The microgravity space environment may result in a challenging threat for living beings, as aptly documented by the paper from C. Nislow et al., showing that spaceflight has subtle but significant effects on core cellular processes including growth control via RNA and ribosomal biogenesis, metabolism, modification, and decay pathways. It is noteworthy that, despite the fact that some reference-genes remain stable during microgravity exposure, several others, investigated in the study of C. S. Thiel et al., change quite dramatically, thus reinforcing the concept that exposure to

near weightlessness may have a profound impact on living processes. Namely, it seems that genes involved in ROS detoxification are especially impaired in such condition, as reported by the paper from S. Fengler et al., therefore suggesting how relevant could be the role sustained by the redox status in counteracting at least some downstream consequences of microgravity. Yet, as reported in the article of S. Mugnai et al., both nitric oxide and ROS are likely to play a previously unrecognized role as messengers during the gravitropic response in many root tips. Relevance of oxidative processes during microgravity exposure was also reported by the study of A. M. Rizzo et al., in which a significant increase in oxidative stress has been observed in tardigrades exposed to spaceflight.

Cells may "sense" changes in the microgravitational field through (a) an indirect mechanism (mainly based on the modification of physical properties of their microenvironment); (b) the development of specialized structures for the mechanical perception and transduction of gravitational forces (like the cytoskeleton); and (c) changes in the dynamics of enzymes kinetics or protein network self-assembly. It is worth noting that the latter two processes are dramatically affected by nonequilibrium dynamics. Nonlinear dynamical processes far from equilibrium involve an appropriate combination of reaction and diffusion, and the pattern arising from those interactions is tightly influenced by even minimal changes in reactant concentrations or modification in the strength of the morphogenetic field [10]. Processes of this kind are called Turing or dissipative structures, given that a consumption of energy is required to drive and maintain the system far from equilibrium. That prerequisite is needed in order to allow the system to promptly change its configuration, according to the system's needs. In turn, the dissipative energy provides the thermodynamic driving force for the self-organization processes. Some experimental evidence has already been provided that change of the gravitational field may significantly affect some nonlinear reactions occurring within cells and tissues [11, 12]. Herein, a further confirmation is provided by the article of M. G. Masiello et al., in which the near weightlessness condition is shown to drive the systems towards different attractor states, thus enabling cells to acquire new and unexpected phenotypes in the course of a true phase transition [13]. According to such results, gravity seems to be an "inescapable" constraint that obliges living beings to adopt only a few configurations among many others. By "removing" the gravitational field, living structures will be free to recover more degrees of freedom, thus acquiring new phenotypes and new functions/properties. That statement raises several crucial questions. Some of these entail fundamentals of theoretical biology, as they question the gene-centered paradigm, according to which biological behavior can be explained by solely genetic mechanisms [14].

What are the mechanism(s) through which microgravity may so profoundly modify cell function and structure? Several studies included in this issue deal with that topic, calling into the question the pivotal role sustained by the cytoskeleton in mediating several microgravity-based effects.

A common outcome in nearly all cell types exposed to microgravity is indeed the alteration of cytoskeletal elements: actin, microfilaments, and microtubules [15, 16]. Disorganization of basic cellular architecture can affect activities ranging from cell signalling and migration to cell cycling and apoptosis. In this issue, K. Paulsen and colleagues investigated how surface expression of ICAM-1 protein and expression of ICAM-1 mRNA in cells of the monocyte/macrophage system change in microgravity. Given that ICAM proteins are essential for cell-to-cell adhesion as well as for cytoskeleton proper functioning, such results outline the involvement of the cytoskeleton system in mediating at least some effects due to microgravity. That statement is further reinforced by the paper from F. Louis et al. in which dramatic decrease in RhoGTPases activity has been documented. RhoGTPases represent a unique hub for integration of biochemical and mechanical signals. As such, they are probably very rapidly involved in a cell's adaptation to microgravity-related conditions. Additionally, RhoGTPases activity is tightly and mechanistically bound to alterations of the cytoskeleton, adhesion, and fibrillogenesis as well as to an enhancement of ROS delivery. As a result, RhoGTPases may be considered true mechanosensitive switches responsible for cytoskeletal dynamics and cells commitment. Relevant modification of the cytoskeleton architecture and microtubule organization in testicular cells has been also reported in the study by F. Ferranti et al., where a significant correlation between cytoskeleton abnormalities induced by simulated microgravity and enhanced autophagy was recorded. Yet, cytoskeleton changes affect different cell types, including endothelial cells. In the paper of J. Maier et al., it is shown that endothelial cells are highly sensitive to gravitational stress, as microgravity leads to changes in the production and expression of vasoactive and inflammatory mediators and adhesion molecules, which mainly results from changes in the remodelling of the cytoskeleton and the distribution of *caveolae*. In addition, by keeping in mind that the cytoskeleton dynamics is a fundamental player in cell proliferation and migration, it is not surprising that microgravity significantly affects the flytrap closure, a process involving not only the actin dynamics but also the ion channels and aquaporin activities, as evidenced in the article from C. Pandolfi et al.

Cytoskeleton changes have also profound consequences on both cell shape and tissue modelling. Simulated near weightlessness in human volunteers is associated with a significant change in arterial geometry, flow, stiffness, and shear rate as documented by C. Palombo et al. Microgravity is acting on endothelial cells also through modulation of P2-receptor and the release of several cytokines, as reported by the study from Y. Zhang et al. Given that P2-receptor artificial ligands are applied as drugs, it is reasonable to assume that they might be promising candidates against the cardiovascular deconditioning the astronauts experience during spaceflight.

Overall the alterations occurring in microgravity have undoubtedly significant backwashes on the physiological homeostasis of the whole organism. Such aspect is highlighted by two papers from the group of F. Lacquaniti et al. dealing with the effects of near weightlessness on nervous system function. Gravity is indeed crucial for spatial perception, postural equilibrium, and movement generation. The brain

may deal with the gravitational field by integrating a wide array of different signals, thus enabling the system to trigger the most appropriate response. F. Lacquaniti et al. provide compelling evidence that this ability depends on the fact that gravity effects are stored in brain regions which integrate visual, vestibular, and neck proprioceptive signals, where the nervous system combines this information with an internal model of gravity effects. The second study evidenced in turn the beneficial effect of the neurophysiologic adaptation to near weightlessness and how knowledge acquired on this field may even enhance the development of innovative technologies for gait rehabilitation.

Research on microgravity and hypergravity effectively advances our knowledge on physiology and biochemistry, thus providing valuable data and models for the understanding for some important human diseases. Moreover, space-based research has played and presumably will continuously play an important role in reformulating the theoretical framework in biology and physiology and may serve as a novel paradigm for innovation. Namely, microgravity-related research fostered the development of new tools-like for culturing cells in three dimensions. It is now well understood that 3D growth environments that facilitate unrestricted cell-cell interactions are mandatory for defining the biology of cancer cells and tissues, including tumour formation, tumour microenvironment, and tumour progression [17, 18]. Indeed, three-dimensional culture in real and simulated microgravity allows a more precise appreciation of the role the biophysical constraints play in shaping cell phenotypes and functions. In turn, such devices may help in improving tissue-engineering techniques. Experimental models of cells/tissues cultures in both simulated and real microgravity need, however, to be further improved in order to obtain more reliable and reproducible data and to minimize the impact of confounding factors. Such studies may indeed provide valuable information about modulations in signal transduction, cell adhesion, or extracellular matrix induced by altered gravity conditions. These systems also facilitate the analysis of the impact of growth factors, hormones, or drugs on these tissue-like constructs in order to better address issues like pharmacokinetics and pharmacodynamics. Paradigmatic examples of such studies are reported in this issue by the articles of several groups (C. Ulbrich et al.; C. Morabito et al.; V. Gupta et al.), some of which (S. L. Wuest et al.) critically reviewed the reliability of available technical tools (like the Random Positioning Machine). These facilities may also allow investigating developmental and organogenesis processes.

The motivation for this focussed issue of the Biomed Research International Journal is to take stock of the state of research and identify possible areas for future development. There is an urgent need for this, as the last comprehensive collection of studies devoted to space biomedicine research dates back to the 90s [19].

As editors we have collected an eclectic mix of articles, provided by research groups fully involved in space biomedicine research and actively participating in studies carried out both on the International Space Station and on the ground, by means of different techniques enabling performing conditions of simulated near weightlessness and increased gravity. This is not a "one view fits all" approach. It is rather one to "let a hundred flowers bloom." Yet, they provide a fruitful overview on what is going to come from space biomedicine research. Overall, studies reported in the issue demonstrated how relevant physical cues may be in shaping biological phenotypes and function, influencing so in depth molecular and genetic pathways. It is regrettable to notice that such influences have been for so long overlooked by the scientific mainstream [20, 21]. Furthermore, microgravity studies forced us to develop new technological solutions and more appropriate experimental models. Thereby, knowledge gathered in space research has offered an invaluable support in understanding both human physiology and pathology, fostering technological innovation and the development of priceless medical and experimental devices.

This is why it has been argued that the ultimate reason for human space exploration is precisely to enable us to discover ourselves. Undoubtedly, the microgravity and space related research present an unlimited horizon for investigation and discovery. Controlled studies conducted in microgravity can advance our knowledge, providing amazing and unforeseen insights into the biological mechanism underlying physiology as well as many relevant diseases like cancer [22].

Mariano Bizzarri
Monica Monici
Jack J. W. A. van Loon

References

[1] P. O. Montgomery Jr., J. E. Cook, R. C. Reynolds et al., "The response of single human cells to zero gravity," *In Vitro*, vol. 14, no. 2, pp. 165–173, 1978.

[2] M. G. Tairbekov, G. P. Parfyonov, E. Y. Shepelev, and F. V. Sushkov, "Experimental and theoretical analysis of the influence of gravity at the cellular level: a review," *Advances in Space Research*, vol. 3, no. 9, pp. 153–158, 1983.

[3] J. J. W. van Loon, "The gravity environment in Space experiments," in *Biology in Space and Life on Earth. Effects of Spaceflight on Biological Systems*, E. Brinckmann, Ed., pp. 17–32, Wiley-VCH, 2007.

[4] T. G. Hammond and J. M. Hammond, "Optimized suspension culture: the rotating-wall vessel," *American Journal of Physiology—Renal Physiology*, vol. 281, no. 1, pp. F12–F25, 2001.

[5] P. Todd, "Gravity-dependent phenomena at the scale of the single cell," *ASGSB Bulletin*, vol. 2, pp. 95–113, 1989.

[6] L. E. Freed, R. Langer, I. Martin, N. R. Pellis, and G. Vunjak-Novakovic, "Tissue engineering of cartilage in space," *Proceedings of the National Academy of Sciences of the United States of America*, vol. 94, no. 25, pp. 13885–13890, 1997.

[7] J. Klein-Nulend, R. G. Bacabac, J. P. Veldhuijzen, and J. J. W. A. Van Loon, "Microgravity and bone cell mechanosensitivity," *Advances in Space Research*, vol. 32, no. 8, pp. 1551–1559, 2003.

[8] S. J. Pardo, M. J. Patel, M. C. Sykes et al., "Simulated microgravity using the Random Positioning Machine inhibits differentiation and alters gene expression profiles of 2T3 preosteoblasts," *American Journal of Physiology—Cell Physiology*, vol. 288, no. 6, pp. C1211–C1221, 2005.

[9] M. Monici, F. Fusi, M. Paglierani et al., "Modeled gravitational unloading triggers differentiation and apoptosis in preosteoclastic cells," *Journal of Cellular Biochemistry*, vol. 98, no. 1, pp. 65–80, 2006.

[10] G. Nicolis and I. Prigogine, "Introduction," in *Self-Organization in Nonequilibrium Systems: From Dissipative Structures to Order Through Fluctuations*, John Wiley & Sons, New York, NY, USA, 1977.

[11] P. J. Stiles and D. F. Fletcher, "The effect of gravity on the rate of a simple liquid-state reaction in a small, unstirred cylindrical vessel," *Physical Chemistry Chemical Physics*, vol. 3, no. 9, pp. 1617–1621, 2001.

[12] C. Papaseit, N. Pochon, and J. Tabony, "Microtubule self-organization is gravity-dependent," *Proceedings of the National Academy of Sciences of the United States of America*, vol. 97, no. 15, pp. 8364–8368, 2000.

[13] M. Bizzarri and A. Giuliani, "Represeenting cancer cell trajectories in a phase-space diagram: switching cellular states by biological phase transitions," in *Applied Statistics for Network Biology: Methods in Systems Biology*, M. Dehmer, F. Emmert-Streib, A. Graber, and A. Salvador, Eds., pp. 377–403, Wiley, New York, NY, USA, 2011.

[14] M. Bizzarri, A. Cucina, A. Palombo, and M. Grazia Masiello, "Gravity sensing by cells: Mechanisms and theoretical grounds," *Rendiconti Lincei*, vol. 25, no. 1, pp. 29–38, 2014.

[15] M. L. Lewis, "The cytoskeleton in spaceflown cells: an overview," *Gravitational and Space Biology Bulletin*, vol. 17, pp. 1–11, 2004.

[16] D. Vorselen, W. H. Roos, F. C. MacKintosh, G. J. L. Wuite, and J. J. W. A. van Loon, "The role of the cytoskeleton in sensing changes in gravity by nonspecialized cells," *FASEB Journal*, vol. 28, no. 2, pp. 536–547, 2014.

[17] D. Grimm, M. Wehland, J. Pietsch et al., "Growing tissues in real and simulated microgravity: new methods for tissue engineering," *Tissue Engineering Part B: Reviews*, vol. 20, no. 6, pp. 555–566, 2014.

[18] G. R. Souza, J. R. Molina, R. M. Raphael et al., "Three-dimensional tissue culture based on magnetic cell levitation," *Nature Nanotechnology*, vol. 5, no. 4, pp. 291–296, 2010.

[19] D. Schmitt, "Workshop purpose and structure," *The FASEB Journal*, vol. 13, supplement S1, no. 9001, 1999.

[20] M. Bizzarri, A. Pasqualato, A. Cucina, and V. Pasta, "Physical forces and non linear dynamics mould fractal cell shape. Quantitative morphological parameters and cell phenotype," *Histology and Histopathology*, vol. 28, no. 2, pp. 155–174, 2013.

[21] M. Monici and J. van Loon, *Cell Mechanochemistry. Biological Systems and Factors Inducing Mechanical Stress, Such as Light, Pressure and Gravity*, Trivandrum Research Signpost/Transword Research Network, 2010.

[22] J. L. Becker and G. R. Souza, "Using space-based investigations to inform cancer research on Earth," *Nature Reviews Cancer*, vol. 13, no. 5, pp. 315–327, 2013.

Hindawi Publishing Corporation
BioMed Research International
Volume 2015, Article ID 971474, 8 pages
http://dx.doi.org/10.1155/2015/971474

Review Article

Simulated Microgravity: Critical Review on the Use of Random Positioning Machines for Mammalian Cell Culture

Simon L. Wuest,[1] Stéphane Richard,[1] Sascha Kopp,[2] Daniela Grimm,[2] and Marcel Egli[1]

[1] *Lucerne University of Applied Sciences and Arts, School of Engineering and Architecture, CC Aerospace Biomedical Science and Technology, Space Biology Group, Lucerne University of Applied Sciences and Arts, Seestraße 41, 6052 Hergiswil, Switzerland*
[2] *Institute of Biomedicine, Pharmacology, Aarhus University, Wilhelm Meyers Allé 4, 8000 Aarhus C, Denmark*

Correspondence should be addressed to Marcel Egli; marcel.egli@hslu.ch

Received 15 May 2014; Revised 12 September 2014; Accepted 6 October 2014

Academic Editor: Jack J. W. A. Van Loon

Random Positioning Machines (RPMs) have been used since many years as a ground-based model to simulate microgravity. In this review we discuss several aspects of the RPM. Recent technological development has expanded the operative range of the RPM substantially. New possibilities of live cell imaging and partial gravity simulations, for example, are of particular interest. For obtaining valuable and reliable results from RPM experiments, the appropriate use of the RPM is of utmost importance. The simulation of microgravity requires that the RPM's rotation is faster than the biological process under study, but not so fast that undesired side effects appear. It remains a legitimate question, however, whether the RPM can accurately and reliably simulate microgravity conditions comparable to real microgravity in space. We attempt to answer this question by mathematically analyzing the forces working on the samples while they are mounted on the operating RPM and by comparing data obtained under real microgravity in space and simulated microgravity on the RPM. In conclusion and after taking the mentioned constraints into consideration, we are convinced that simulated microgravity experiments on the RPM are a valid alternative for conducting examinations on the influence of the force of gravity in a fast and straightforward approach.

1. Introduction

Gravity is an omnipresent force on Earth, and all living organisms have evolved under the influence of constant gravity. Some organisms have learned to take advantage of the force of gravity by using it as a reference for orientation. The condition of microgravity (or near weightlessness) and its effects on living organisms, on the other hand, have always presented a fascinating scenario in biology and medicine. With the first manned space flights, it became clear that the human organism reacts with a series of adaptations to microgravity. Interestingly, some of the symptoms observed in space, such as wasting muscle mass and decreasing bone density, are typically diagnosed in the elderly as well [1–3]. This is one important factor that fostered scientists' interest in doing space research.

Numerous studies on mammalian organisms, for example, have demonstrated that the absence of gravity has severe effects not only on a systemic level but also on a cellular level. Short-term effects of microgravity (on the order of seconds) can be studied on research platforms such as drop towers or airplanes that fly in parabolic maneuvers. In contrast, long-term effects can only be studied on board sounding rockets (on the order of minutes) and space vehicles in flight. Due to the extensive preparation effort, safety constraints and rare flight opportunities, however, access to space experiments is limited. For many years, the random positioning machine (RPM), besides other tools, has been successfully used to simulate microgravity for screening studies, pre- and postflight experiments, and hardware testing. The principle of the RPM (a specialized, two-axis form of the clinostat) is based on gravity vector averaging to zero [4]. The typical RPM system comprises two gimbal-mounted frames, which are each driven by independent motors. Through dedicated algorithms, the samples placed on the inner frame are constantly reoriented, such that the gravity vector is distributed

in all directions over time. Thus, from the sample's point of view the constantly reorienting gravity vector's trajectory averaged over time shall converge toward zero. However, 1 g is always acting on the sample at any given instant. It is assumed that the gravity vector needs to point in a specific direction for a minimal period of time in order to allow biological systems, like cells, to adapt to the gravity vector. But if the gravity vector constantly changes its orientation, the cells will lose the sense of direction and thus experience a state similar to microgravity (removed gravity vector). Therefore, the rotation of the frames shall be faster than the biological process studied [5]. However, the rotation cannot be too fast, as centrifugal forces will become effective [6]. Therefore, the RPM is typically used to examine slow processes, which are observed at least on the timescale of hours. It remains a legitimate question whether the RPM can reliably simulate microgravity. In this review we attempt to provide an answer to that question by comparing data of mammalian cells obtained at real microgravity in space and at simulated microgravity generated by using the RPM. In the first part, however, a summary is provided on the latest technical development as well as new applications of the RPM.

2. RPM Development and Technology

2.1. RPM Systems. Today's RPMs were introduced by Japanese plant researchers for conducting their particular studies [7, 8]. Later on, a similar machine was developed in The Netherlands (Dutch Space) [5]. Although both systems were commercialized [6], their range of use for doing space-related experiments was limited. For instance, scientific studies with mammalian cells that are very sensitive to temperature fluctuations were difficult to carry out because of a missing temperature control unit. Thus, these kinds of experiments had to be operated in a temperature-controlled room (e.g., a growth chamber). One approach to overcome this limitation was to miniaturize the RPM to fit into an ordinary cell culture incubator (max. size 50 × 50 × 50 cm) that offers precisely controlled temperatures (also referred to as desktop RPM) [4]. Through this RPM modification, the installation of large climate chambers around RPMs became unnecessary. We have recently reported another approach to upgrading the RPM by installing a commercial CO_2 incubator onto the rotating frames. This RPM, called "random positioning incubator" (RPI) [9, 10], has the advantage of being independent of large laboratory incubators (Figure 1). Furthermore, the closed chamber of the incubator isolates the environment of the culture flasks and thus prevents exposure of biological samples to vapor and wear from the machinery, for example, [10]. Besides differences in the design of the three RPM types (regular RPM, small desktop RPM, and RPI), there appear to be slightly different concepts of how to average the gravity vector. The algorithm implemented on the Japanese RPM (referred to as a regular RPM) lets the RPM run with random rotational speeds and changes the velocity after two possible predefined periods (e.g., 30 or 60 s) [8]. The Dutch systems (referred to as regular and desktop RPMs) rotate with random speeds that are varied at random time points [6]. In contrast, our RPI rotates with constant velocity,

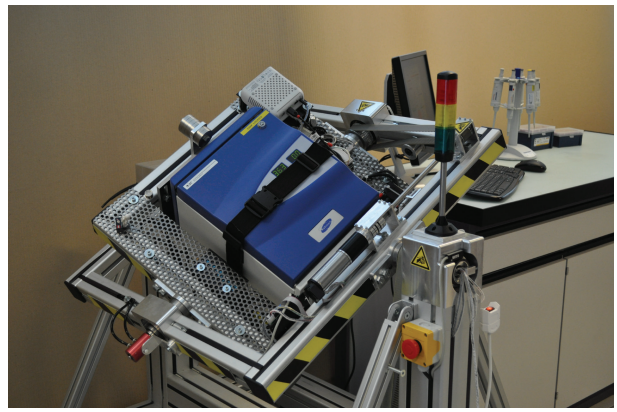

Figure 1: Random positioning incubator (RPI) featuring a fully integrated CO_2 incubator (developed by the Institute for Automation, University of Applied Science Northwestern Switzerland).

but the rotation direction is inverted at random time points. The transition from forward to backward takes place at a predefined rotational acceleration [10]. All three algorithms employed by the different RPM types are reported to be reliable in averaging gravity. To our current knowledge, these algorithms are equivalent from a biological point of view.

2.2. Live Cell Imaging on the RPM. Microscopy is a common analytical tool used in cell biology. Even though microscopes are used on clinostats (rotation around one horizontal axis) [11, 12], until recently live cell imaging was not successful on an operating RPM. To date, most of the optical microscopy techniques applied under simulated microgravity conditions have been realized in the field of physical sciences. For such experiments, microscopes with a low numerical aperture and poor imaging performances were used because of their intrinsic robustness to environmental disturbances such as vibrations. In life science, however, high magnification is needed to detect modifications at the cellular or subcellular level. Because most of the ground-based microgravity research platforms are not vibration-free, high-performance microscopy has not been applicable. Thus, studies involving cell imaging have been conducted in ground laboratories after chemical fixation of the cell in microgravity. This approach implies a series of static shots, which cannot truly reveal the dynamic processes and labile cellular events occurring in cells in response to microgravity exposure.

Until recently, there was no system available that allowed high-quality real-time images taken at cellular or subcellular level under (real or simulated) microgravity. The breakthrough came with the use of a digital holographic microscope (DHM) that we have combined with an epifluorescent microscope. In this dual-mode microscope, the two imaging modes (DHM and fluorescent) operate sequentially. The DHM is an innovative interferometric microscope that is less sensitive to vibrations. The technological advantages of the DHM, which comprise continuous and fast digital autofocusing with a short exposure time, allow high-resolution imaging [13–16]. We tested the DHM on the RPM as well as during parabolic flights, and in both cases we obtained good data

[13–16]. For instance, we followed reorganization of the actin cytoskeleton and fluctuations of the intracellular calcium concentration under simulated microgravity (unpublished data).

3. Partial Earth Gravity Load

During past years, RPM development was focused on the improvement of the hardware. We have also been working on an upgrade of the software responsible for controlling the motion of the RPM. Three different algorithms were introduced recently that simulated partial Earth gravity (0 to 0.6 g), allowing simulation of moon- or Mars-like gravity conditions [9]. All algorithms are adaptations of the random walk algorithm originally designed to simulate microgravity [10]. As described above, simulated microgravity is achieved by rotating both frames with constant velocity and inverting the rotation direction at random times. Partial gravity is achieved by altering the random walk in a way that the Earth's gravity vector is not completely randomized anymore and points (from the sample's point of view) for a prolonged time in a specific direction. In one algorithm version, this is accomplished by slowing down the rotational velocity while the gravity vector (considered in the sample frame) is pointing downwards. Otherwise, the frames rotate with the predefined velocity. The ratio of the two velocities finally determines the mean gravity (gravity vector averaged over time). In the other two algorithm versions, the random walk is interleaved with static intervals in which the frames stand still in a predefined orientation. However, the timing of these static intervals (start point and duration) is handled differently. In one case the timing is flexible and adjusted online as the experiment runs. In the other case the timing is strictly periodic and predefined before the experiment starts [9].

All three algorithms were tested on suspended human T cells and adherent mice myoblasts. Chemically activated T cells showed a decreased activation rate that correlates strongly to the decreasing simulated mean gravity values [9]. The results were similar for all algorithms. The adhered myoblast (C2C12 cell line) showed a decreased proliferation rate with decreasing mean gravity [9]. Interestingly, this effect is algorithm dependent. The correlation between mean gravity and proliferation was reduced or disappeared in the two algorithms involving static intervals [9]. Ideally, these types of partial gravity experiments are carried out in space by using a centrifuge. To our knowledge, no comparable space experiments have been conducted so far, except during particular parabolic flight campaigns of the European Space Agency (ESA). Therefore, a direct comparison to space is not possible at this time. However, these experiments demonstrate that simulation of partial gravity opens a new field of scientific questions that attracts other research groups. Dutch Space was attracted by the new topic as well and thus recently introduced a modified desktop RPM (presented at the ELGRA meeting 2013) allowing partial gravity simulations. Partial Earth gravity enabling RPMs increase the application range substantially, allowing investigation of the influence of gravity—like on the moon or Mars, for example,—on cells and small organisms at affordable cost.

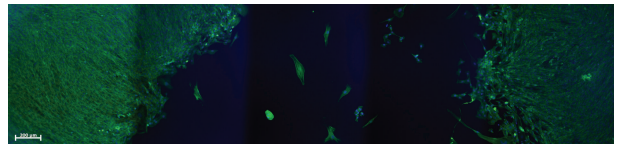

Figure 2: Mouse myoblasts (C2C12 cell line) were cultured until near confluence and subsequently exposed to a frequently passing air bubble. The culture chamber filled with medium was swinging upside down, such that the intentional air bubble frequently passed the same trajectory. The sample was fixed and stained for actin (green) and DNA (blue) thereafter. The cells in the trajectory of the air bubble got detached from the substrate (dark central area), while cells in the unaffected area kept proliferating (lateral green areas). Interestingly, detached cells could reattach to the opposite side of the culture chamber. Measuring bar 200 μm. (Due to the limited field of view, this image has been stitched together from five images.)

These results may help to estimate the biological response of cells or even whole organisms when exposed to the gravity loads of other planets or moons.

4. RPM Use and Experiment Quality

4.1. Cultivation Method of Mammalian Cells. In order to obtain comparable data, it is important to standardize cell culture methods. One of the most important aspects of doing so is a stable cultivating environment. When cultivating cells on the moving RPM, additional aspects have to be considered, such as avoiding air bubbles in the culture chambers [4]. Experiments have shown that an air bubble passing by adherent cells at the same trajectory repetitively (as the culture chamber moves in a "swinging motion"), the cells can detach from the substrate (Figure 2, unpublished observation). Interestingly, these cells often reattach at the opposite side of the culture chamber wall. Using air- and gas-tight culture chambers on the RPM has the advantage of being more independent of the culture environment. However, a gas-tight culture chamber requires a culture medium that does not require CO_2 for pH buffering, which reduces the overall cultivation period in which the culture flasks do not have to be manipulated. Gas-tight chambers in turn can cause problems when cultivating gas-producing cells, such as yeast cells.

4.2. Artifacts through Kinematic Rotation. In addition to a standardized cultivation method, artifacts caused by the kinematic rotation need to be considered. While the Earth's gravity vector is distributed in a way that the mean gravity converges to zero over time, the accelerations caused by the RPM's kinematics are not well controlled. In order to avoid artifacts, the rotational velocity, the sample's distance to the center of rotation, and the rotational acceleration (during velocity transitions) have to be chosen appropriately. Since there has been no systematic study on acceptable limits, scientists have to rely on their common sense. The following considerations can be used as guidelines. For explanatory reasons, we also refer here to the somewhat simpler case of clinorotation around one axis. Clinorotation and the related rotating wall vessel (RWV) bioreactor are alternative methods commonly used in many laboratories to simulate

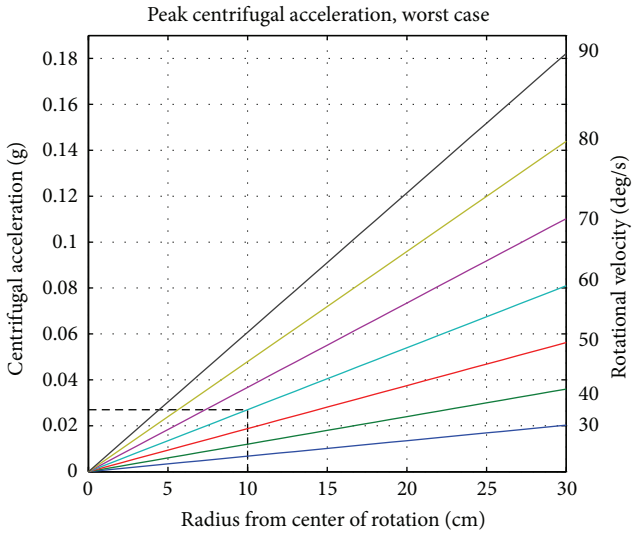

Figure 3: The worst-case peak centrifugal acceleration on an RPM depending on the distance to the center of rotation ($a_{pc} \approx 2.41 \cdot \omega^2 \cdot r$). For example, a moderate rotational velocity of 60 deg/s (cyan line) and a distance of 10 cm from the center of rotation (vertical dashed line) results in a peak centrifugal acceleration of approximately 0.03 g (horizontal dashed line).

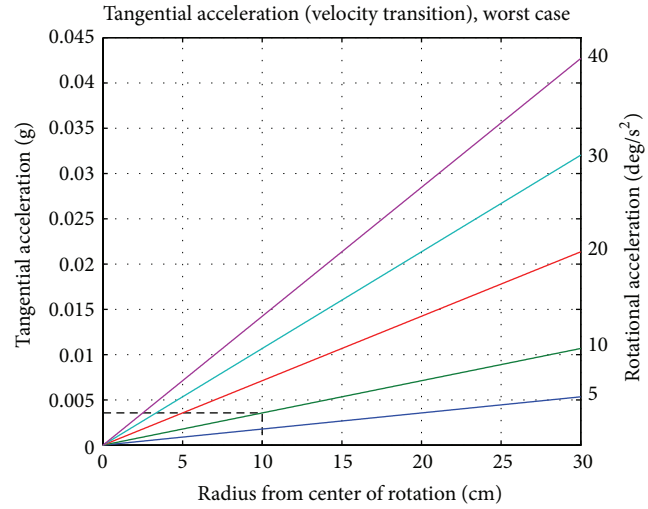

Figure 4: The worst-case tangential acceleration depending on the distance from the center of rotation ($a_t = 2 \cdot \alpha \cdot r$). For a smooth velocity transition of, for example, 10 deg/s^2 (green line) and 10 cm distance from the center of rotation (vertical dashed line), a tangential acceleration of approximately 0.004 g is expected (horizontal dashed line).

microgravity on the ground. These methods simulate microgravity by rotating samples around a horizontal axis. (Selecting the appropriate rotation velocity for suspended cells in clinostat experiments has been discussed elsewhere [17].)

To minimize centrifugal acceleration, the rotational velocity and the sample's distance to the center of rotation should be set as low as the experiment allows. As mentioned earlier, the rotation shall be clearly faster than the biological processes investigated [5]. For mammalian cell experiments, many scientists have used a rotational velocity of 60 deg/s [4]. In the case of chemically activated T cells (as discussed further below), we could also create a microgravity-like environment with a rotational velocity of 40 deg/s [10]. For rotation around one axis, as in a clinostat or centrifuge, the centrifugal acceleration (in m/s^2) is time independent and is computed by $a_c = \omega^2 \cdot r$, where ω is the rotation velocity (in rad/s) and r is the distance from the center of rotation (in meters). For rotations around two perpendicular axes, as is the case for RPMs, the centrifugal acceleration becomes time dependent. Thus the centrifugal acceleration depends now on the two rotation velocities, the sample's position in space and time. It is no longer trivial to make a statement on the effective centrifugal acceleration at the samples within the cultivation chamber. For the simplified case where both velocities are equal and constant, the centrifugal acceleration becomes periodically oscillating. By focusing on a worst-case scenario in terms of centrifugal acceleration, the analysis provides easy equations: in such a scenario, the peak centrifugal acceleration (in m/s^2) can be approximated to $a_{pc} \approx 2.41 \cdot \omega^2 \cdot r$ (Figure 3), where ω is the rotation velocity of both frames (in rad/s) and r is the distance from the center of rotation (in meters). As the equation indicates, all cells are ideally placed at the center of rotation. Therefore, the scientist is responsible for compactly placing the samples around the center of rotation. By using the distance to the center of rotation from the sample farthest away from this point (worst case), the largest expected centrifugal acceleration can be estimated. For a moderate velocity of typically 60 deg/s [4] and a moderate distance from the center of rotation (e.g., 10 cm), the centrifugal acceleration is in the order of 10^{-2} g. Such small forces are detectable by some specialized cells [18]. Since at any instance in time the Earth's gravity vector (which is averaged to zero over time) is present as well, the centrifugal acceleration is two orders of magnitude smaller, and we therefore consider it to be negligible. In addition, the transitions of the frames' rotational velocities introduce additional accelerations and thus should be smooth, by selecting a small rotational acceleration. For the clinostat, this tangential acceleration (in m/s^2) is $a_t = \alpha \cdot r$, where α is the rotational acceleration (in rad/s^2). For the RPM, the tangential acceleration becomes $a_t = 2 \cdot \alpha \cdot r$ in the worst case, when both frames accelerate simultaneously (Figure 4). For a smooth velocity transition of 10 deg/s^2 and a moderate distance from the center of rotation (e.g., 10 cm), the tangential acceleration is well below 10^{-2} g.

Besides these parasitic accelerations, rotation introduces fluid motion in the culture flask, leading to shear forces and enhanced convection (Figure 5). This condition is unlike space conditions, where no convection is present. Therefore, the nutrition supply on the RPM is enhanced as compared to static or space experiments. In order to avoid additional mechanical stimulation such as shear stress, a moderate rotational velocity needs to be chosen, and the velocity transitions have to be smooth [19]. Because the behavior of fluid motion has not been fully elucidated yet, the acceptable limits for rotation velocity and acceleration are not clarified.

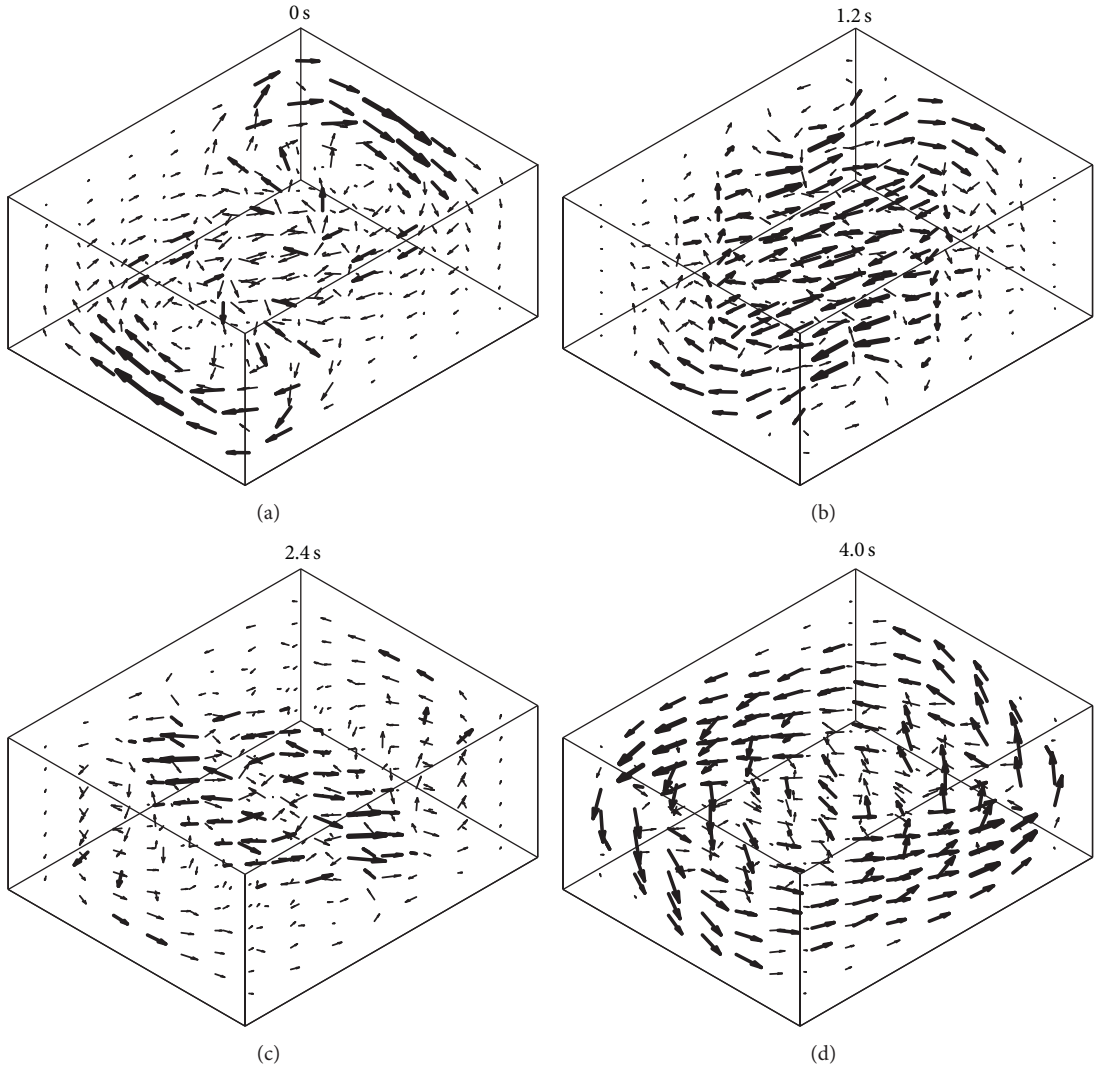

Figure 5: The RPM rotation introduces fluid motion in the culture flask, leading to shear forces and enhanced convection. Therefore, a moderate rotational velocity needs to be chosen, and the velocity transitions have to be smooth in order to minimize the introduction of additional mechanical stimulation of the samples. In this numerical illustration, the fluid motion is shown if both frames rotate at 60 deg/s. This results in a periodic motion of 6 seconds. The four images indicate snapshots of the velocity at 0 s (a), 1.2 s (b), 2.2 s (c), and 4 s (d).

However, the values provided above are a good starting point and have been successfully used in previous experiments [9, 10].

5. Experiment Reporting

As new and innovative technologies expand the range of possible experiments, it is becoming important to document the used hardware precisely. In accordance with good laboratory practice (GLP), any researcher who is using RPMs or clinostats should follow the "Bonn Criteria." In this document it is stated that "Experimental reporting should include the properties of the culture vessel, culture media and carrier beads. These should also include dimensions and rotation speed of vessels, chemical consistency including density and viscosity of media, size, density, and porosity of beads, size, density, and porosity of cells, whether cells are motile or non-motile, density of beads with cells attached, as well as time of rotation, nature of controls, operating temperature, and gas content [20]." As described above, improper use of the RPM can introduce additional forces leading to unwanted mechanical stimulation of the sample cells. Interpreting results from such experiments could lead to wrong conclusions and could thus jeopardize a whole study.

6. RPM Application in Mammalian Cell Culture

6.1. Can the RPM Reproduce Microgravity Conditions? Despite the long history of RPM usage, the difference between simulated and real microgravity in space shall be critically examined when interpreting experimental results. Particularly, for adhered cells, the rotation generated by the RPM could provide an unwanted source of mechanical stimuli

[6]. Unfortunately, only a few researches have systematically compared experiments performed in a real microgravity environment and on an RPM. Most of these comparative studies have been done on leukocytes, for which the RPM showed good agreement with space experiments: it is well known that T lymphocytes fail to activate in microgravity after being exposed to the activator Con A [21]. This effect was reproduced numerous times on an RPM [9, 10, 22, 23]. Similarly, Villa and colleagues have shown slower proliferation of the human leukemic myelomonocytic cell line U937 exposed to simulated microgravity on the RPM [24]. The same phenomenon was previously observed on a space shuttle experiment [25]. In a study on cell mobility under microgravity with the human leukemic monocyte/macrophage cell line, the RPM predicted real microgravity results. Monocyte locomotion ability was clearly reduced in real as well as in simulated microgravity. The authors suggest that this is linked to changes in the cytoskeletal structures, since they observed reduced density of actin filaments and disruption of the β-tubulin architecture [26, 27]. Furthermore, peripheral blood mononuclear cells cultured for 48 hours onboard the International Space Station (ISS) showed remarkably increased apoptotic hallmarks, which could also be reproduced under simulated microgravity [28].

In recent years, two investigators directly compared the results from RPM experiments to results obtained in space conditions, performed simultaneously: in the first experiment, primary porcine chondrocytes from articular cartilage were flown for 16 days aboard the ISS. Cells exposed to microgravity showed higher collagen II/I ratio and reduced aggrecan/versican ratio at the mRNA level. In addition, cell density was significantly reduced, and the extracellular matrix straining was weaker on the ISS samples. The samples that were simultaneously exposed to simulated microgravity on an RPM generally showed results that were similar to those of the space samples but not as prominent [29]. In the second experiment, cells from the human thyroid carcinoma cell line FTC-133 were flown aboard the Shenzhou-8 spacecraft and fixed after 10 days in space. Cells exposed to spaceflight appeared to form three-dimensional tumor spheroids, while the inflight 1 g controls remained in two-dimensional monolayers. The FTC-133 cells exposed to simulated microgravity on the RPM also formed three-dimensional spheroids, even though the spheroids appeared to be smaller than those formed in space [30]. In addition, EGF and CTGF gene expression was upregulated in both real and simulated microgravity. Interestingly, EGF expression was lower and CTGF expression was higher in the RPM samples than the space samples [30]. The reason the RPM sample showed intermediate effects between the 1 g control and the space samples is not clear at this point. Since the RPM can only be used for slow processes, one possible speculation is that some of the underlying molecular processes might be too fast for RPM-simulated microgravity.

In conclusion, the RPM has been shown to mimic microgravity responses reliably for several, but not all, experimental conditions. Particularly, for leukocytes, several effects seen in space were reproduced on the RPM. Particular studies designed to investigate differences in cellular responses between space samples and samples exposed to simulated microgravity elucidated an underestimation or overestimation of simulated versus real microgravity. Overall, the RPM generally seems to underestimate the spaceflight effects. Therefore, results from RPM experiments need to be interpreted with caution and, if possible, more directly compared to experiments under real microgravity in order to fully assess their capability to support gravitational biology studies.

6.2. Novel Applications of the RPM. The exact mechanisms by which mechanical stimuli initiate cellular modifications have still not been fully elucidated [31]. This is the motivation of mechanobiologists to expose cells to various mechanical stimuli such as distinct patterns of shear flow, tensile stretch, or mechanical compression at various parametric combinations of magnitude, duration, or frequency [31]. The RPM can be regarded as an additional mechanical device for reducing the long-term effects of the mechanical force of gravity. Due to the constant reorientation of samples on the RPM, gravity-dependent intracellular responses will not be triggered anymore. Thus one can say that the RPM generates a state of a mechanically unloaded environment in which the longer-lasting impact of gravity can be studied.

Monolayer (two-dimensional) cell cultures have been successfully used for many decades, allowing a better understanding of many cellular and molecular processes. They actually represent an important source of information prior to animal experimentation. Despite numerous advantages, the monolayer model cannot simulate organs or tissues realistically. Therefore, three-dimensional cell culturing has emerged over the last decades as an alternative to mimic better tissue-like organization with the idea of closing the gap of uncertainty between tissue-like and monolayer cell culture. The RPM in that context appears as an alternative approach to generating a three-dimensional culture [32]. The random repositioning of the cells around the gravity vector over time allows constant redistribution of gravity forces, which thus leads to the formation of cell aggregates that can form microspheroids (Figure 6) [32–34]. Spheroids organized as multilayers are closer to *in vivo* tissue situation than monolayer cells [32]. Such samples are therefore more accurate as a model integrating the three-dimensional real surroundings of a cell in an *in vivo* tissue. Thus, spheroid structures open a new field of applications, such as test systems for drug therapies or diagnosis [35]. The spheroid structure is actually a good model to screen for penetration characteristics of drugs or antibodies through tissue.

7. Conclusion

Several RPMs have evolved during the past years that feature different designs, functions, and motion patterns. They all have reliably proven to simulate microgravity conditions. Developments to RPM hardware and software have expanded the experimental possibilities substantially. The successful operation of digital holographic microscopy (DHM) on the RPM and the implementation of partial gravity algorithms have opened new fields in gravitational research, particularly in mechanobiology.

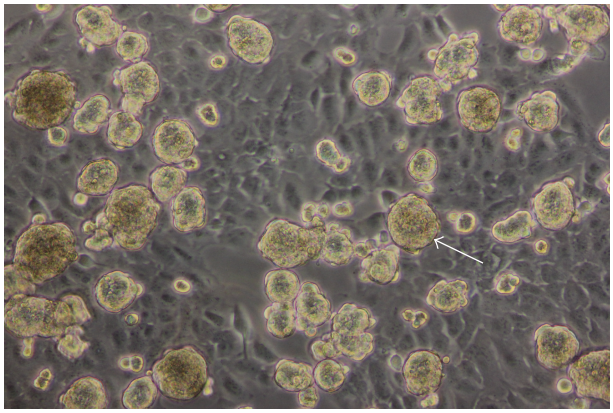

Figure 6: Thyrocytes cultured for seven days on the RPM organized to spheroid structures (arrow).

In order to obtain reliable and comparable data, the appropriate use of the RPM and application of standardized cultivation methods are of central importance. The RPM has been established as a reliable tool supporting ground-based microgravity studies. Effects seen in real microgravity were reproduced with good agreement on RPMs. Some RPM studies, however, also showed cellular effects that were between those of the real microgravity and 1 g ground control results. The RPM is furthermore an ideal tool for preliminary microgravity tests, screening studies in which simulated microgravity effects are checked on various organisms and hardware testing. Particularly, for suggesting live science experiments for the conduction under real microgravity in space, the presentation of preliminary data showing modifications under simulated microgravity is becoming very important. Advances in RPM engineering and live science qualify the RPM as an interesting tool for novel applications, such as three-dimensional cell culturing as well as tissue engineering.

Conflict of Interests

The authors have no conflict of interests regarding the publication of this paper.

Acknowledgments

The authors thank their coworkers at the CC Aerospace Biomedical Science and Technology and especially Nicole Wittkopf for the support and critical discussions. Furthermore, they would like to thank Adrian Koller and Mariana Reyes Perez from the CC of Mechanical Systems, Lucerne School of Engineering and Architecture, for interesting discussions and close collaboration. Special thanks also go to Jörg Sekler and his coworkers at the Institute for Automation, University of Applied Science Northwestern Switzerland, for the fruitful collaboration.

References

[1] R. H. Fitts, S. W. Trappe, D. L. Costill et al., "Prolonged space flight-induced alterations in the structure and function of human skeletal muscle fibres," *Journal of Physiology*, vol. 588, no. 18, pp. 3567–3592, 2010.

[2] D. A. Riley, J. L. W. Bain, J. L. Thompson et al., "Decreased thin filament density and length in human atrophic soleus muscle fibers after spaceflight," *Journal of Applied Physiology*, vol. 88, no. 2, pp. 567–572, 2000.

[3] S. W. Trappe, T. A. Trappe, G. A. Lee, J. J. Widrick, D. L. Costill, and R. H. Fitts, "Comparison of a space shuttle flight (STS-78) and bed rest on human muscle function," *Journal of Applied Physiology*, vol. 91, no. 1, pp. 57–64, 2001.

[4] A. G. Borst and J. J. W. A. van Loon, "Technology and developments for the random positioning machine, RPM," *Microgravity Science and Technology*, vol. 21, no. 4, pp. 287–292, 2009.

[5] D. Mesland, "Novel ground-based facilities for research in the effects of weight," *ESA Microgravity News*, vol. 9, pp. 5–10, 1996.

[6] J. J. W. A. van Loon, "Some history and use of the random positioning machine, RPM, in gravity related research," *Advances in Space Research*, vol. 39, no. 7, pp. 1161–1165, 2007.

[7] T. Hoson, S. Kamisaka, Y. Masuda, and M. Yamashita, "Changes in plant growth processes under microgravity conditions simulated by a three-dimensional clinostat," *The Botanical Magazine Tokyo*, vol. 105, no. 1, pp. 53–70, 1992.

[8] T. Hoson, S. Kamisaka, Y. Masuda, M. Yamashita, and B. Buchen, "Evaluation of the three-dimensional clinostat as a simulator of weightlessness," *Planta*, vol. 203, no. 1, pp. S187–S197, 1997.

[9] T. Benavides Damm, I. Walther, S. L. Wüest, J. Sekler, and M. Egli, "Cell cultivation under different gravitational loads using a novel random positioning incubator," *Biotechnology and Bioengineering*, vol. 111, no. 6, pp. 1180–1190, 2014.

[10] S. L. Wuest, S. Richard, I. Walther et al., "A novel microgravity simulator applicable for three-dimensional cell culturing," *Microgravity Science and Technology*, vol. 26, no. 2, pp. 77–88, 2014.

[11] M. Cogoli, "The fast rotating clinostat: a history of its use in gravitational biology and a comparison of ground-based and flight experiment results," *ASGSB Bulletin*, vol. 5, no. 2, pp. 59–67, 1992.

[12] R. Hemmersbach, M. von der Wiesche, and D. Seibt, "Ground-based experimental platforms in gravitational biology and human physiology," *Signal Transduction*, vol. 6, no. 6, pp. 381–387, 2006.

[13] M. F. Toy, J. Kühn, S. Richard, J. Parent, M. Egli, and C. Depeursinge, "Accelerated autofocusing of off-axis holograms using critical sampling," *Optics Letters*, vol. 37, no. 24, pp. 5094–5096, 2012.

[14] C. Pache, J. Kühn, K. Westphal et al., "Digital holographic microscopy real-time monitoring of cytoarchitectural alterations during simulated microgravity," *Journal of Biomedical Optics*, vol. 15, no. 2, Article ID 026021, 2010.

[15] M. F. Toy, S. Richard, J. Kühn, A. Franco-Obregón, M. Egli, and C. Depeursinge, "Enhanced robustness digital holographic microscopy for demanding environment of space biology," *Biomedical Optics Express*, vol. 3, no. 2, pp. 313–326, 2012.

[16] M. F. Toy, C. Pache, J. Parent, J. Kühn, M. Egli, and C. Depeursinge, "Dual-mode digital holographic and fluorescence microscopy for the study of morphological changes in cells under simulated microgravity," in *Three-Dimensional and Multidimensional Microscopy: Image Acquisition and Processing XVII*, pp. 7570–7573, 2010.

[17] D. M. Klaus, P. Todd, and A. Schatz, "Functional weightlessness during clinorotation of cell suspensions," *Advances in Space Research*, vol. 21, no. 8-9, pp. 1315–1318, 1998.

[18] D. Driss-Ecole, V. Legué, E. Carnero-Diaz, and G. Perbal, "Gravisensitivity and automorphogenesis of lentil seedling roots grown on board the International Space Station," *Physiologia Plantarum*, vol. 134, no. 1, pp. 191–201, 2008.

[19] C. A. Leguy, R. Delfos, M. J. B. M. Pourquie et al., "Fluid motion for microgravity simulations in a random positioning machine," *Gravitational and Space Biology Bulletin*, vol. 25, no. 1, 2011.

[20] T. Hammond and P. Allen, "The Bonn criteria: minimal experimental parameter reporting for clinostat and random positioning machine experiments with cells and tissues," *Microgravity Science and Technology*, vol. 23, no. 2, pp. 271–275, 2011.

[21] M. Cogoli-Greuter, "The lymphocyte story—an overview of selected highlights on the *in vitro* activation of human lymphocytes in space," *Microgravity Science and Technology*, vol. 25, no. 6, pp. 343–352, 2014.

[22] M. Schwarzenberg, P. Pippia, M. A. Meloni, G. Cossu, M. Cogoli-Greuter, and A. Cogoli, "Signal transduction in T lymphocytes—a comparison of the data from space, the free fall machine and the random positioning machine," *Advances in Space Research*, vol. 24, no. 6, pp. 793–800, 1999.

[23] I. Walther, P. Pippia, M. A. Meloni, F. Turrini, F. Mannu, and A. Cogoli, "Simulated microgravity inhibits the genetic expression of interleukin-2 and its receptor in mitogen-activated T lymphocytes," *FEBS Letters*, vol. 436, no. 1, pp. 115–118, 1998.

[24] A. Villa, S. Versari, J. A. Maier, and S. Bradamante, "Cell behavior in simulated microgravity: a comparison of results obtained with RWV and RPM," *Gravitational and Space Biology Bulletin*, vol. 18, no. 2, pp. 89–90, 2005.

[25] J. P. Hatton, F. Gaubert, M. L. Lewis et al., "The kinetics of translocation and cellular quantity of protein kinase C in human leukocytes are modified during spaceflight," *The FASEB Journal*, vol. 13, supplement, pp. S23–S33, 1999.

[26] M. A. Meloni, G. Galleri, G. Pani, A. Saba, P. Pippia, and M. Cogoli-Greuter, "Space flight affects motility and cytoskeletal structures in human monocyte cell line J-111," *Cytoskeleton*, vol. 68, no. 2, pp. 125–137, 2011.

[27] M. A. Meloni, G. Galleri, P. Pippia, and M. Cogoli-Greuter, "Cytoskeleton changes and impaired motility of monocytes at modelled low gravity," *Protoplasma*, vol. 229, no. 2-4, pp. 243–249, 2006.

[28] N. Battista, M. A. Meloni, M. Bari et al., "5-Lipoxygenase-dependent apoptosis of human lymphocytes in the international space station: data from the ROALD experiment," *The FASEB Journal*, vol. 26, no. 5, pp. 1791–1798, 2012.

[29] V. Stamenković, G. Keller, D. Nesic, A. Cogoli, and S. P. Grogan, "Neocartilage formation in 1 g, simulated, and microgravity environments: implications for tissue engineering," *Tissue Engineering—Part A*, vol. 16, no. 5, pp. 1729–1736, 2010.

[30] J. Pietsch, X. Ma, M. Wehland et al., "Spheroid formation of human thyroid cancer cells in an automated culturing system during the Shenzhou-8 Space mission," *Biomaterials*, vol. 34, no. 31, pp. 7694–7705, 2013.

[31] J. Wang, D. Lü, D. Mao, and M. Long, "Mechanomics: an emerging field between biology and biomechanics," *Protein & Cell*, vol. 5, no. 7, pp. 518–531, 2014.

[32] J. Pietsch, A. Sickmann, G. Weber et al., "A proteomic approach to analysing spheroid formation of two human thyroid cell lines cultured on a random positioning machine," *PROTEOMICS*, vol. 11, no. 10, pp. 2095–2104, 2011.

[33] D. Grimm, J. Bauer, C. Ulbrich et al., "Different responsiveness of endothelial cells to vascular endothelial growth factor and basic fibroblast growth factor added to culture media under gravity and simulated microgravity," *Tissue Engineering Part A*, vol. 16, no. 5, pp. 1559–1573, 2010.

[34] C. Ulbrich, "Characterization of human chondrocytes exposed to simulated microgravity," *Cellular Physiology and Biochemistry*, vol. 25, no. 4-5, pp. 551–560, 2010.

[35] A. Ivascu and M. Kubbies, "Rapid generation of single-tumor spheroids for high-throughput cell function and toxicity analysis," *Journal of Biomolecular Screening*, vol. 11, no. 8, pp. 922–932, 2006.

Hindawi Publishing Corporation
BioMed Research International
Volume 2015, Article ID 538786, 18 pages
http://dx.doi.org/10.1155/2015/538786

Research Article

Regulation of ICAM-1 in Cells of the Monocyte/Macrophage System in Microgravity

Katrin Paulsen,[1] Svantje Tauber,[1,2] Claudia Dumrese,[1,3] Gesine Bradacs,[1] Dana M. Simmet,[1,2] Nadine Gölz,[1] Swantje Hauschild,[1,2] Christiane Raig,[1] Stephanie Engeli,[1] Annett Gutewort,[1,2] Eva Hürlimann,[1] Josefine Biskup,[1] Felix Unverdorben,[2] Gabriela Rieder,[1] Daniel Hofmänner,[1] Lisa Mutschler,[1] Sonja Krammer,[1] Isabell Buttron,[1] Claudia Philpot,[4] Andreas Huge,[5] Hartwin Lier,[6] Ines Barz,[7] Frank Engelmann,[6,7] Liliana E. Layer,[1] Cora S. Thiel,[1,2] and Oliver Ullrich[1,2,8,9]

[1]*Institute of Anatomy, Faculty of Medicine, University of Zurich, Winterthurerstraß 190, 8057 Zurich, Switzerland*
[2]*Department of Machine Design, Engineering Design and Product Development, Institute of Mechanical Engineering, Otto-von-Guericke-University Magdeburg, Universitätsplatz 2, 39106 Magdeburg, Germany*
[3]*Flow Cytometry Facility, University of Zurich, Winterthurerstraß 190, 8057 Zurich, Switzerland*
[4]*German Aerospace Center, Space Agency, Königswinterer Straße 522-524, 53227 Bonn, Germany*
[5]*Integrated Functional Genomics (IFG), University of Muenster, Roentgenstraß 21, 48149 Muenster, Germany*
[6]*KEK GmbH, Kemberger Straße 5, 06905 Bad Schmiedeberg, Germany*
[7]*University of Applied Science Jena, Carl-Zeiss-Promenade 2, 07745 Jena, Germany*
[8]*Zurich Center for Integrative Human Physiology (ZIHP), University of Zurich, Winterthurerstraß 190, 8057 Zurich, Switzerland*
[9]*Study Group "Magdeburger Arbeitsgemeinschaft für Forschung unter Raumfahrt- und Schwerelosigkeitsbedingungen" (MARS), Otto-von-Guericke-University Magdeburg, Universitätsplatz 2, 39106 Magdeburg, Germany*

Correspondence should be addressed to Oliver Ullrich; oliver.ullrich@uzh.ch

Received 14 May 2014; Revised 22 September 2014; Accepted 9 October 2014

Academic Editor: Jack J. W. A. Van Loon

Cells of the immune system are highly sensitive to altered gravity, and the monocyte as well as the macrophage function is proven to be impaired under microgravity conditions. In our study, we investigated the surface expression of ICAM-1 protein and expression of ICAM-1 mRNA in cells of the monocyte/macrophage system in microgravity during clinostat, parabolic flight, sounding rocket, and orbital experiments. In murine BV-2 microglial cells, we detected a downregulation of ICAM-1 expression in clinorotation experiments and a rapid and reversible downregulation in the microgravity phase of parabolic flight experiments. In contrast, ICAM-1 expression increased in macrophage-like differentiated human U937 cells during the microgravity phase of parabolic flights and in long-term microgravity provided by a 2D clinostat or during the orbital SIMBOX/Shenzhou-8 mission. In nondifferentiated U937 cells, no effect of microgravity on ICAM-1 expression could be observed during parabolic flight experiments. We conclude that disturbed immune function in microgravity could be a consequence of ICAM-1 modulation in the monocyte/macrophage system, which in turn could have a strong impact on the interaction with T lymphocytes and cell migration. Thus, ICAM-1 can be considered as a rapid-reacting and sustained gravity-regulated molecule in mammalian cells.

1. Introduction

Several limiting factors for human health and performance in microgravity have been clearly identified arising from the immune system, and substantial research activities are required in order to provide the basic information for appropriate integrated risk management. The gravity-sensitive nature of cells of the immune system renders them an ideal biological model in search for general gravity-sensitive mechanisms to understand how the architecture and function

of human cells are related to the gravitational force and therefore adapted to life on Earth. Cells of the immune system are highly sensitive to altered gravity (for review see [1–4]). T lymphocytes as well as monocytes and macrophages are impaired severely in their functions under microgravity conditions [2–4]. T cell activation is severely disturbed under microgravity conditions as shown in the blood of astronauts during and after space flight [5] and in numerous *in vitro* experiments (reviewed by [6]). In monocytes the secretion of the cytokines IL-1, IL-6, TNF-alpha, and IL-10 is altered under microgravity conditions [7, 8]. Substantial changes in gene expression of monocytes and in gene induction associated with the differentiation of monocytes into macrophages have been observed [8].

Migration and adhesion of immune competent cells at areas of infection, inflammation, or structural disorders are indispensable for the immune response [9]. For these processes the communication and connection between cells are essential. The integrins of the LeuCAM family (LFA-1 and MAC-1) and their ligands, the intercellular adhesion molecules (ICAMs), are receptors that mediate the attachment between cells (cell-cell contact) and of cells and the extracellular matrix (cell-matrix contact) [10]. ICAMs are transmembrane proteins that are expressed on epithelial cells, endothelial cells, and cells of the immune system including T cells and macrophages. Binding of ICAM-1 (CD54) to receptors on endothelia of blood vessels enables leucocytes to attach and migrate through the endothelia to sites of inflammation [11]. Later on in the immune reaction close and strong interaction between ICAM-1 and LFA-1 is indispensable for the immunological synapse formation between T cells and antigen-presenting cells such as monocytes [12].

ICAM-1 expression is known to be upregulated during mechanical stress [13], in a long-term microgravity environment [14], in the NASA-developed Rotary Cell Culture Systems (RCCS) as well as during short-term microgravity in parabolic flights [15] in endothelial cells. While these studies show gravity sensitivity of ICAM-1 in endothelial cells, less is known about the effects of microgravity on cells of the 2 monocyte/macrophage system (MMS). Therefore in this study we investigate whether the ICAM-1 surface expression is regulated by altered gravity in these cell types. The MMS belongs to the innate immune system and represents the body's first line of defense. The innate immune system is characterized by a fast, but unspecific immune reaction, and it activates the adaptive immune response. This activation occurs through interaction of antigen-presenting cells (APCs)—dendritic cells and macrophages [16]—with T lymphocytes. Macrophages are relatively long-lived, carry a variety of surface receptors, and reside in many tissues including the gastrointestinal tract, the respiratory tract, the liver, the spleen, bones, and connective tissues [17]. Microglial cells are the brain-resident macrophage population which crucially controls and regulates immune reactions inside the central nervous system (CNS).

In our study, we investigated the surface expression of ICAM-1 protein and expression of ICAM-1 mRNA in cells of the monocyte/macrophage system in microgravity. As cell models we used primary cells (macrophages, T cells) as well as cell lines (U937 myelomonocytic cells, macrophage-like differentiated U937 cells, and BV-2 microglial cells). We conducted experiments with different durations of microgravity in clinorotation, parabolic flight, sounding rocket, and orbital flight experiments.

2. Methods

2.1. U937 Cell Culture and Macrophage-Like Differentiation. U937 cells (ATCC CRL-1593.2) are a human monocytic cell line that preserves the main monoblastic characteristics of monocytes including the ability to differentiate into a macrophage-like phenotype. U937 cells were cultured in RPMI 1640 medium with or without 20 mM HEPES (Biochrom, Berlin, Germany), supplemented with 10% fetal calf serum (FCS, Biochrom) or 10% human serum (HS, Biowest), 2 mM glutamine (PromoCell), 100 U/mL penicillin, and 100 μg/mL streptomycin (Gibco). Subcultivation was done at a cell density of 1×10^6 cells/mL. Stimulation and differentiation were performed by adding 25 nM phorbolmyristylacetate (PMA) (Sigma-Aldrich) in dimethylsulfoxid (DMSO, 0.1%) (Sigma-Aldrich) at a cell density of 0.5×10^6 cells/mL. Differentiation medium was supplemented with 10% HS, 2 mM glutamine, 100 U/mL penicillin, and 100 μg/mL streptomycin. Cells were differentiated on polycarbonate (Makrolon) slides (SIMBOX/Shenzhou-8) or in cell culture flasks (parabolic flights and clinorotation experiments) for 72 h at 37°C with 5% CO_2 into a macrophage-like phenotype. U937 macrophage-like cells were detached by Macrophage Detachment Solution DXF (PromoCell) following manufacturer's protocol. After detaching, cells were filled immediately into Nutrimix bags (B. Braun Melsungen) ($1\text{-}2 \times 10^7$ cells in 10 mL medium each bag) for parabolic flight or in serological pipettes (1 mL cell suspension with $0.25\text{–}0.5 \times 10^6$/mL) for clinorotation experiments [18, 19].

2.2. Primary Human Macrophages. Human primary M2 macrophages (PromoCell) were cultivated with M2-Macrophage Generation Medium DXF (PromoCell). Cells were detached by Macrophage Detachment Solution DXF (PromoCell) following the manufacturer's protocol. After detaching, cells were filled immediately into Nutrimix bags (B. Braun Melsungen) (2×10^6 cells in 10 mL medium each bag) for parabolic flight, or in serological pipettes (1 mL cell suspension with $0.25\text{–}0.5 \times 10^6$/mL) for clinorotation experiment [18, 19].

2.3. BV-2 Microglia Cell Culture. Since primary microglia are not available in quantities required for parabolic flight experiments, we used the murine cell line BV-2, whose function resembles that of tissue macrophages and which share many properties with both peripheral macrophages and monocytes [20]. BV-2 microglial cells were cultured in DMEM medium (Biochrom, Berlin, Germany) supplemented with 10% FCS and without antibiotics. 72 hours before parabolic flight experiment, the cells were set on only 2% FCS (serum starved) for the transport and were supplemented again

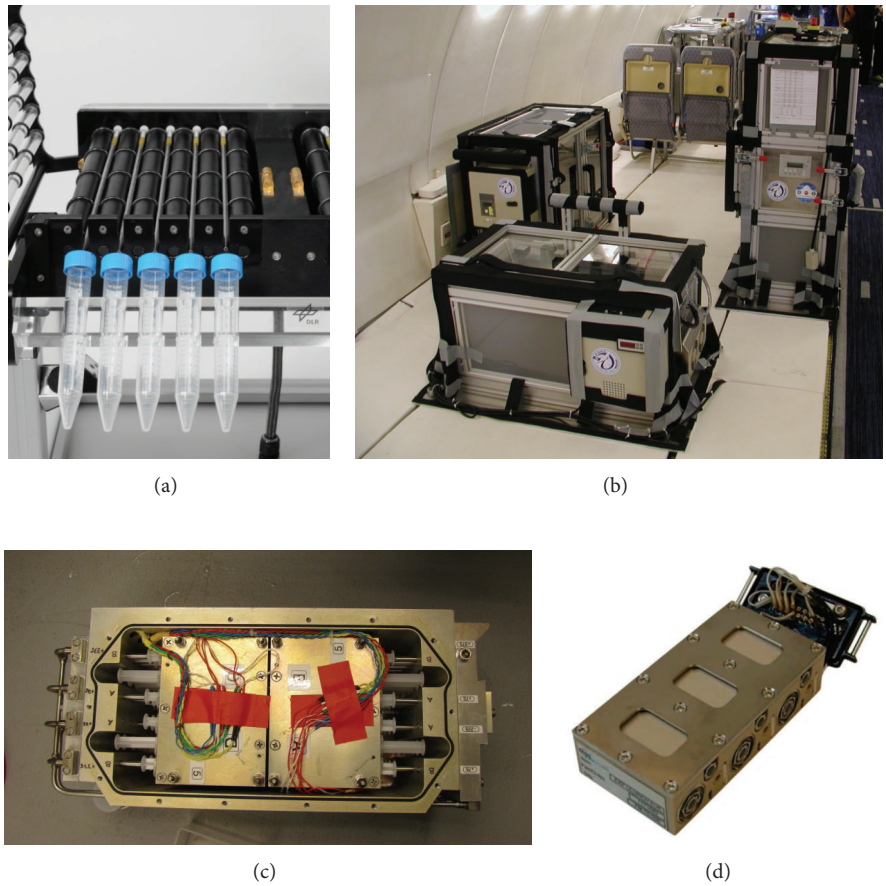

(a) (b)

(c) (d)

Figure 1: Technology for cell culture experiments in different microgravity research platforms. (a) Fast-rotating two-dimensional (2D) clinostat manufactured by the German Aerospace Center (DLR, Cologne, Germany) was used to provide simulated microgravity. Under the chosen experimental conditions (60 rpm, 4 mm pipette diameter) a maximal residual acceleration of 4×10^{-3} g is achieved at the outer radius of the pipette and decreases towards the center. (b) Experimental hardware structure which consists of an incubator rack to store the cell containers temporarily before the experiment at 37°C (left), an experimental rack in which all active aggregates are accommodated and where the living cells are handled during altered gravity (right) and a cooling rack to temporarily store all cell containers after the injection of the stop/fixation liquid at 4°C until landing (front). (c) Payload of TEXUS-49 sounding rocket tempered and vacuum-resistant container with experiment syringe systems. (d) Plunger unit EUE for SIMBOX (Science in Microgravity Box) incubator system, support structure (housing made of PEEK), which includes three culture chambers and six supply units, two for each culture compartment. Each culture chamber represents an independent loop. The culture chambers filled with medium are closed on the top of the housing by means of polycarbonate specimen window slides, where the adherent cells are attached beforehand. The housing is tightened by silicon sealing and covered by an aluminum plate (cover) fixed with screws.

with 10% FCS after arrival. Before transport to Bordeaux-Mérignac airport, BV-2 cells were transferred into 200 mL Nutrimix bags (B. Braun Melsungen, Melsungen, Germany) at a density of 3×10^6 cells in 15 mL medium.

2.4. Experiments in Simulated Microgravity (2D Clinorotation). A fast-rotating two-dimensional (2D) clinostat manufactured by the German Aerospace Center (DLR, Cologne, Germany) was used to provide simulated microgravity (Figure 1(a)). The principle of clinorotation-induced microgravity is the rotation of a cell suspension in a serological pipette perpendicular to the Earth's gravity. The microgravity produced is an averaging of the gravity vector, if the clinostat rotates with 40–100 rpm. Under the chosen experimental conditions (60 rpm, 4 mm pipette diameter) a maximal residual acceleration of 4×10^{-3} g is achieved at the outer radius of the serological pipette and decreases towards the center. The clinostat device was placed in an incubator providing constant 37°C. Fifteen serological pipettes rotated at the same time with 60 rpm. 1 g controls were placed at the ground plate of the clinostat without rotation but the same environmental conditions are as the μg samples. The density of the cell suspension was 0.5×10^6/mL (U937 macrophage-like cells), $0.25–0.5 \times 10^6$/mL (human primary macrophages), or 0.75×10^6/mL (BV-2 microglial cells) in 1 mL volume each. The duration of the filling procedure was not longer than 10 min for all 30 serological pipettes. Cells were cultured in the serological pipettes for 24 h–96 h. After clinorotation, cells

were fixed by the addition of 500 μL of 3% PFA (Sigma-Aldrich)/2% sucrose (Sigma-Aldrich) solution for 30 min, washed with PBS and analyzed after immunocytochemical staining by flow cytometry.

2.5. Parabolic Flights as Microgravity Research Platform. During a parabolic maneuver, an aircraft is weightless by flying on a Keplerian trajectory, described as an unpropelled body in ideally frictionless space subjected to a centrally symmetric gravitational field [21]. During this free-fall trajectory, the resultant of all forces acting on the aircraft other than gravity is zeroed. During a flight campaign, which normally consists of three individual flights, 31 parabolas are flown on each flight, with 93 parabolas in total. On each parabola, there is a period of increased gravity (1.8 g) which lasts for 20 seconds immediately prior to and following the 20-second period of reduced gravity (acceleration in x-, y-, and z-axis was below 2×10^{-3} g at all times during the μg parabola, Figure 1(a)). During the parabolic flight maneuver, the aircraft gradually pulls up its nose and starts climbing at an angle of approximately 45 degrees. This phase lasts for about 20 seconds, during which the aircraft experiences an acceleration of around 1.8 g. The engine thrust is then reduced to the minimum required to compensate for air-drag, and the aircraft is then in a free-fall condition, lasting approximately for 20 seconds, during which weightlessness is achieved. At the end of this phase, the aircraft must pull out the parabolic arc, a maneuver which gives rise to another 20 second period to 1.8 g on the aircraft, after which it returns to normal level flight attitude. Special designated flight areas were above the Atlantic Ocean and the Mediterranean Sea. Experiments were conducted during the 10th and 19th DLR parabolic flight campaigns of the German Aerospace Center ("Deutsches Zentrum für Luft- und Raumfahrt", DLR) in Bordeaux, France. The campaign used the only large aircraft that is licensed in Europe to perform parabolic flights for research purposes, the Airbus A300 ZERO-G. This aircraft is a specially configured test aircraft operated by NOVESPACE (Bordeaux, France) according to the standing orders of NOVESPACE (A300 ZERO-G Rules and Guidelines RG-2001-1, RG-2008-1, RG-2008-2, RG-2009-1, and RG-2009-02) and the CEV (Centre d'essai en vol).

2.6. In-Flight Hardware for Parabolic Flight Experiments. A custom-made hardware meeting the requirements for experiments with human cell culture on board the Airbus A300 ZERO-G was developed in collaboration with KEK GmbH, Germany (Figure 1(b)). The system has already been used successfully for cell culture experiments during 9 parabolic flight campaigns [18, 19]. The system consists of double-sealed cell containers holding the cells of the monocyte-macrophage system and three experimental modules that supply storage of samples before the experiment, half-automated performance of the experiment, and storage of the processed samples. The first module holds the cell containers at 36.5°C in a hanging position. From there, containers are transferred into the second module manually. In this module, cells were fixed by the addition of fixation reagent upon triggering. Triggering was done manually at defined time intervals (20 sec) after the onset of the gravitational condition of interest. The third experimental module served as in-flight storage for the fixated samples at 4°C. Three samples could be processed in parallel. Sample exchange required approximately one minute of a defined procedure by three trained persons.

2.7. Procedures during Parabolic Flight Experiments. Transport of in-flight cell culture bags in in-flight-configuration and of fixed samples after the parabolic flight was provided by the Swiss Air Force from Zurich to Bordeaux during each flight day of the 13th DLR Parabolic Flight Campaign or by train during each flight day of the 19th DLR Parabolic Flight Campaign. After arrival at the flight location on the evening before the flight, cells were incubated overnight at 37°C and handled very carefully in order to avoid any mechanical or temperature cell stress. All steps of the entire cell preparation and transport procedure had been tested extensively with respect to cell viability and function beforehand. All procedures during the parabolic flight campaign had been tested several times and highly standardized following an extensive and detailed standard protocol. During the campaign, all procedures were documented and double-checked. In-flight μg and 1 g control experiments were performed in 200 mL Nutrimix bags [18, 19] used as in-flight cell culture bags containing 3×10^7 cells in 15 mL. During the onset of μg or during 1 g (in-flight control experiments), 10 ng PMA/mL (with 0.01 residual DMSO) or 10 ng TNF-α/mL or plain cell culture medium were added to the cells. After 20 sec of μg or 1 g, cells were fixed by addition of 1% formaldehyde (Sigma-Aldrich) (for cytometry analysis) or lysed by RLT buffer (Qiagen) (for RNA analysis) and cooled immediately (4°C) during the remaining flight. Experiments were performed at least three times during independent flights and separate flight days. After the flight, fixed cells were transported to the laboratories on the same day, harvested, and subjected to analysis.

2.8. TEXUS-49 Sounding Rocket Experiment. For the TEXUS-49 campaign at ESRANGE (Kiruna, Sweden), U937 cells were cultivated in the fully installed laboratories on site. Cells were seeded with a density of 0.2×10^6 cells/mL and the medium was exchanged every 48 hours as described above. On the launch day, cells were visually inspected, harvested, counted, and pooled to a concentration of 5×10^7 cells/mL. 0.5 mL of this cell suspension was filled into a sterile 3 mL plastic syringe shortly before the launch. Additionally, one syringe was filled with 0.3 mL of cell culture medium and another one with 1 mL Trizol LS (Life Technologies, Germany). The three syringes were mounted on a plastic block with a tubing system connecting them. This unit was finally integrated into the automatically operated experiment system (Figure 1(c)). In total 35 of these experiment units were prepared and kept at 37°C until the integration into the payload of the rocket. During the experimental run, first the 0.3 mL of medium, as a potential placeholder for an activation solution, and then the 1 mL of Trizol LS were injected to the cell suspension at defined time points to lyse the cells and preserve the current status of differential gene

expression. Injections were performed at 75 sec after launch to monitor a so-called baseline (BL) directly before the μg phase, and at 375 sec after launch at the end of the μg phase. A group of 1 g ground controls was treated immediately after the μg sample group. TEXUS-49 consisted of a VSB-30 engine (S-30 solid rocket stage with an S-31 second stage) and of the payload. The rocket was launched on March 29, 2011, at 06:01 am from the ESRANGE Space Center near Kiruna, Sweden. During the ballistic suborbital flight, an altitude of 268 km and 378 sec of microgravity with a quality of 10^{-5} g were achieved.

2.9. SIMBOX Incubator System with Plunger Experiment Insert. SIMBOX (Astrium GmbH Friedrichshafen, Germany; Kayser Italia, Livorno, Italy) is a programmable, space-qualified incubator for biological research in space equipped with a 1 g in-flight centrifuge for 1 g control experiments. The incubator allows for fully automatic execution of biological experiments with limited use of commands during orbital flight in a controlled thermal environment. The SIMBOX incubator (internal volume 34 liters, dimensions 461 × 551 × 273 mm, empty mass 16 kg, fully integrated mass 34.5 kg, max. power 130 W) accommodates 40 experiment unique equipment (EUEs) with 24 EUEs on the μg-platform and 16 EUEs on the 1 g-centrifuge. The plunger experiment insert (Figure 1(d)) was developed by Astrium GmbH and is described in the *Astrium Space Biology Product Catalog* [22]. It allows medium exchange and chemical fixation of adherent cell cultures. There are two plungers which can be filled with any liquid and automatically activated to inject it into the experimental volume. The EUEs consisted of a support structure (housing made of PEEK) which includes three culture chambers (CCs) and six supply units (SU, plungers), two per culture compartment. Each CC has two SUs and represents an independent loop. The CCs are closed on the top of the housing by Specimen Slides (SS) made of polycarbonate, on which the adherent cells were attached. The chamber (covered by the window slide) contained the medium. The housing is tightened by silicon sealing and covered with an aluminum plate (cover), which is fixed with screws. The container lid of the Biorack standard type I container is mounted onto the housing. The Biorack standard is based on the accommodation of various EUEs into experiment containers which provide the interface to facilities and support infrastructure [22]. The plunger unit is qualified for an unmanned capsule mission and for use on the International Space Station (ISS).

The unmanned Shenzhou-8 spacecraft was launched on October 31, 2011, at 21:58 UTC (November 1, 2011, 05:58 LT) on board of a Long March 2F (CZ-2F) rocket from the Jiuquan Satellite Launch Center (JSLC) in Inner Mongolia. On November 17, the capsule was autonomously deorbited and landed at 12:38 UTC (20:38 LT) around 500 km north of Beijing. The SIMBOX was recovered immediately and transported by helicopter and jet aircraft to the PITC, Beijing. Total early retrieval time was 6 hours. On arrival at the PITC, the SIMBOX was opened, and the EUEs were removed and inspected. The samples were recovered and stored in cold (4°C) PBS until arrival in Zurich for analysis.

2.10. SIMBOX Experiment Execution. Medium was changed before integration of the slides into the EUEs. Inside the EUEs, the slides were bedded in 0.5 mL fully CO_2 saturated RPMI 1640 medium with 10% HS, 2 mM glutamine, 100 U/mL penicillin, 100 μg/mL streptomycin, and 250 ng/mL amphotericin B (PromoCell). Bellow 1, 3, and 5 of the EUEs [23] were filled with RPMI 1640 medium, 10% HS, 100 U/mL penicillin, 100 μg/mL streptomycin, 250 ng/mL amphotericin B, 2 mM glutamine, 1% PFA, and 0.6% sucrose. Bellow 2, 4, and 6 of the EUEs [23] were filled with PBS, 100 U/mL penicillin, 100 μg/mL streptomycin, and 250 ng/mL amphotericin B. Two EUEs (6 chambers) were prepared for the μg-position, and one EUE (3 chambers) was prepared for the 1 g position. The gravity vector of the 1 g position was perpendicular to the surface of sample slides (z-axis). During the unpowered transport from the laboratory to the spacecraft and installation in the spacecraft (total time 3 h 06 min), the temperature was always above 21°C. Shenzhou-8 launch was on October 31, 2011, 21:58 UTC and the spacecraft attained orbit at 22:08 UTC. The SIMBOX timeline started at 22:34 UTC. Active temperature control was set to 23°C. The centrifuge speed for the 1 g reference centrifuge was 74.40 rpm. Plungers 1, 3, and 5 of all three EUEs were activated between 120:50:00 and 120:55:20 (hours:min:sec) of the timeline sequences of 40 seconds. Plungers 2, 4, and 6 of all three EUSs were activated between 122:50:00 and 122:55:22 (hours:min:sec) of the timeline sequences of 40 seconds. Human macrophage-like U937 cells were cultivated for 5 days inside the SIMBOX hardware on board of the Shenzhou-8 spacecraft in μg and 1 g conditions, fixed with 1% PFA/sucrose solution for 2 h, and stored in PBS on board at 23°C until landing. After landing, the polycarbonate slides were removed, washed, and then stored in PBS at 4°C for 2 weeks until analysis. The ground control experiment was executed analogously to the flight scenario. Details about the experiment were published previously [23].

2.11. Quantification of ICAM-1 by Flow Cytometry. Surface expression of ICAM-1 on BV-2 microglial cells and U937 monocytic and macrophage-like cells as well as primary human macrophages was analyzed by flow cytometry. Cells were collected from the Nutrimix bags (parabolic flight) or standardized serological pipettes (clinorotation) fixated in PFA/sucrose solution. After the washing procedure (PBS without Ca/Mg, Biochrom) cells were stained with ICAM-1 monoclonal antibody (BV2: Invitrogen, FITC labeled; U937 and primary macrophages: cell signaling, PE labeled). Analysis was performed using a flow cytometer (FACSCanto II, BD Biosciences, Heidelberg, Germany), collecting at least 20000 cells per sample. Mean fluorescence intensity Ratio (MFI) was calculated as MFI of sample/MFI of isotype control.

2.12. ICAM-1 Analysis in BV-2 Cells from Parabolic Flight Experiments. Cells were quadruple stained for ICAM-1, apoptosis (TUNEL), cell delineation (HCS cell mask), and

DNA (DAPI). In brief, cells were cytospinned onto glass slides washed 3x with PBS, permeabilized for 1 min with 0.1% Triton-X 100 (Sigma-Aldrich, Buchs, Switzerland), and washed again 3x with PBS and incubated with the TUNEL labeling mix (Boehringer, Mannheim, Germany) according to the manufacturer's instructions. For TUNEL staining, rhodamine coupled dUTP was used. Subsequently to overnight incubation, cells were washed again 3x with PBS, blocked with 0.5% BSA, and stained with FITC labeled ICAM-1 antibody (BD Pharmingen, San Jose, USA) at a concentration of 0.05 mg/mL for 2 h. After additional washing, cells were stained entirely with HCS cell mask deep red cytoplasmic and nuclear stain (Invitrogen, Basel, Switzerland) using a dilution of 1 : 20000 and nuclei were labeled with DAPI (Invitrogen) at 1 μg/mL for 10 min. Labeled cells were imaged using a Leica microscope DMI 6000 and LAS AF software (Leica Microsystems, Wetzlar, Germany). For automated imaging, the unified random sampling module was utilized, 63 randomized images of each sample were recorded, and at least 500 single cells from 3 independent experiments from 3 different parabolas were analyzed. From each image cells were identified according to the following criteria: nucleus of a predefined size and brightness, being TUNEL negative, and containing HCS staining over a certain threshold. Surface calculation of these cells was performed with Imaris and automated for all images using batch coordinator (Bitplane AG, Zurich, Switzerland). Therefore, the mean intensity of the ICAM-1 signal was analyzed in living cells exclusively and binned into ICAM-1 intensity categories of 50 gray levels. Statistical analysis was carried out using GraphPad Prism software (GraphPad Software, Inc., La Jolla, USA) and Student's t-test was applied for all analyzed data.

2.13. ICAM-1 Analysis in Differentiated U937 Cells from the SIMBOX Experiment. Polycarbonate slides were cut by a water jet method into 16 T-shaped pieces. Each piece was stained individually. In order to differentiate between dead (necrotic/apoptotic) and living cells before fixation, slides were stained with CellMask-deep red plasma membrane stain (Invitrogen) and TUNEL reagent (Fluorescein-12-dUTP, Roche). In addition, cells were labeled with different mono- and polyclonal primary antibodies directed against the cytoskeleton components and immunological relevant surface molecules (reported in [17]) and ICAM-1 in concentrations according to the manufacturers' protocols. After blocking with 1% BSA in PBS for 1 h, primary antibodies were detected by species specific secondary antibodies used in a dilution of 1 : 1000 in 0.5% BSA in PBS. Secondary antibodies were labeled with Alexa-Fluor405 or Alexa-Fluor568 (Invitrogen). Slide pieces were analyzed by confocal laser scanning microscopy (Leica, SP5). Only cells positive for CellMask and negative for TUNEL were subjected to further analysis, since these represent the living cell population in the experiment. Digital image analysis was performed using Imaris software (Bitplane).

2.14. RNA Isolation from the Parabolic Flight Experiments. After the return of the aircraft and transport of the samples to the on-site laboratory facilities, the containers were disassembled, the Nutrimix bags were gently agitated, and the lysed cell solution from each bag was filled into a T75 straight neck cell culture flask. The cell solution was vortexed for 10 sec and passed four times through a Ø 0.8 × 120 mm needle (B. Braun Melsungen, Germany) fitted to a 50 mL syringe. 50 mL of absolute ethanol was added and precipitates were resuspended by vigorous shaking. A valve and a sterile connective piece were placed on a Qiavac 24 plus vacuum system (Qiagen, Germany) and an RNA maxi column (Qiagen, Germany) was attached to the connective piece. A vacuum of −200 mbar was adjusted and the column was loaded with the lysed cell suspension. Then, the valve was closed and the column was centrifuged at 4000 g for 3 min. 15 mL of buffer RW1 (Qiagen, Germany) was applied for washing membrane bound RNA. After centrifugation at 4000 g for 7 min, the flow was discarded, and two washing steps with 10 mL RPE buffer (Qiagen, Germany) followed each with centrifugation at 4000 g for 3 min and 10 min, respectively. The column bound RNA was eluted by application of 600 μL of RNase-free water (Qiagen, Germany), incubation for 1 min at room temperature, and centrifugation for 4 min at 4000 g. The elution step was repeated with the first eluate. The RNA was transported at approximately −150°C in a Cryo Express dry shipper (CX-100; Taylor-Wharton, USA) prepared with liquid nitrogen and stored at −80°C until the processing of the RNA for the microarray analysis.

2.15. RNA Isolation during the TEXUS-49 Sounding Rocket Campaign. Directly after landing, localization, and recovery of the payload, the experiment modules were dismantled and handed over to the scientists. The cell suspension was sheared three times with a 20 G needle (B. Braun Melsungen, Germany) and distributed in two 2.0 mL tubes. 0.1 mL of chloroform (Sigma-Aldrich, Germany) was added, and the solution was vortexed for 15 sec and incubated for 5 min at room temperature before a 15 min centrifugation step at 11000 g and 4°C. The upper phase of both 2.0 mL tubes was transferred into a 15 mL tube and 4 mL of RLT buffer and 3 mL of absolute ethanol were added and mixed. 4 mL of this solution was pipetted on an RNA Midi column (Qiagen, Germany) and centrifuged for 30 sec at 3000 g at room temperature. The flow was discarded, and the residual 4 mL of RNA solution was loaded on the column and centrifuged for 5 min at 3000 g at room temperature. Then, the columns were washed twice with 2.5 mL of RPE buffer and centrifuged for 2 min and 5 min, respectively, at 3000 g and room temperature. The RNA was eluted by the addition of 250 μL RNase free water (Qiagen, Germany) to the column, incubation for 1 min at room temperature, and centrifugation for 3 min at 3000 g and room temperature. The eluate was loaded again onto the column, followed by a 1 min incubation and centrifugation for 5 min at 3000 g, and room temperature. The isolated RNA was transferred into sterile Cryo-tubes and stored until the return transport at approximately −150°C in a Cryo Express dry shipper (CX-100; Taylor-Wharton, USA) prepared with liquid nitrogen. After arrival in the home

laboratory, samples were stored at −80°C until processing the RNA for the microarray analysis.

2.16. RNA Processing and Microarray Analysis for Parabolic Flight and TEXUS-49 Sounding Rocket Campaign Samples. RNA quantity and purity were analyzed spectrophotometrically using a Nanodrop 1000 (Thermo Scientific). Isolated RNA samples were all of high quality with 260/280 nm ratios between 1.9 and 2.1. The RNA integrity was measured using an Agilent 2100 Bioanalyzer (Agilent Technologies, USA). Only RNA with an RNA Integrity Number (RIN) > 8.7 was used for the following microarray analysis. 400 ng total RNA was applied to Cy3-labeling with the "Low RNA Input Linear Amplification Kit, PLUS, One-Color" (Agilent Tech-nologies) and hybridized for 17.5 h to a NimbleGen expression microarray (12 × 135000 features) employing the "Gene Expression Hybridization Kit" (Agilent Technologies, USA). Afterwards, arrays were washed and scanned by the Micro Array Scanner G2505B (Agilent Technologies, USA).

The image files of the scanner were analyzed with the NimbleScan Software 2.6 using the Robust Multi-Array Analysis (RMA) with the default parameters. RMA, a probe-level summarization method, identifies probes that are outliers in the overall behavior of the expression measured for a given gene. The contribution of outlier probes is reduced in the reported gene expression level, which has been demonstrated to improve the sensitivity and reproducibility of microarray results. In addition to screening outlier probes, NimbleScan software's implementation of RMA used quantile normalization and background correction. The normalized microarray data were analyzed using Partek Genomics Suite 6.6. Statistical analysis was performed using the one-way ANOVA and the false discovery rate (FDR) for multiple testing corrections. Further, the coefficient of variation (CV) expressed in percent was calculated, also known as "relative variability," which equals the standard deviation divided by the mean. Genes of interest were identified and the log2 values of the measured fluorescent intensities returned by the Partek software were back calculated to linear values. Then, means of all values of the same gene generated by different probes were calculated, if at least three values existed excluding outliers. Subsequently, standard deviations were calculated for the means and an unpaired t-test with Welch correction was performed to test statistical significance.

2.17. Pathway Enrichment Analysis. The pathway enrichment analysis was performed using Partek Genomics Suite 6.6 and the KEGG human pathway library [24, 25]. The P values were calculated by the Fisher exact test. Enrichment analysis was applied on the genes showing differential expression with P values of <0.05 and fold change >+1.5 or < −1.5.

2.18. Statistical Analysis. Data are expressed as median or as median ± SE. Groups contain the analysis of 200–1000 cells (SIMBOX, shown in box-plots) or data of three independent experiments with 1–5 samples (n = 3–15, shown in columns). Data were analyzed by one-way ANOVA followed by Wilcoxon or unpaired t-test using GraphPad Prism 5. $^{*}P < 0.1$ was considered to be significant, $^{**}P < 0.05$ as significant, and $^{***}P < 0.01$ as very significant.

3. Results

3.1. Clinorotation of Downregulated ICAM-1 Expression in BV-2 Microglial Cells. First, we analyzed ICAM-1 expression in BV-2 microglial cells after 24 h clinorotation (60 rpm, 4 mm pipette diameter, maximal residual acceleration of 4×10^{-3} g at the outer radius of the pipette). The clinostat device was placed in an incubator, which provides constant 37°C. Fifteen serological pipettes rotated at the same time with 60 rpm. 1 g controls were placed at the ground plate of the clinostat without rotation but with the same environment condition like μg samples. A 1 g control group of BV-2 cells was filled into 1 mL serological pipettes in the same way as the clinorotation cell group but was not clinorotated. Another control group was kept at regular cell culture conditions in the incubator (37°C, 5% CO_2). Cells were subsequently stained for cell surface ICAM-1, apoptosis (TUNEL), cell delineation (HCS CellMask), and DNA (DAPI) (Figure 2). ICAM-1 expression analysis by flow cytometry revealed two distinct subtypes of cells in the clinorotated group (μg group) compared to the 1 g control group and the incubator control group consisting of only one subtype, respectively (Figure 2(a)). The first of the two subtypes was small and stronger granulated (subtype 1) than the second subtype, which appears taller but less granulated (subtype 2). Apoptotic cells were excluded from the analysis by TUNEL staining. Subtype 1 could possibly represent an activated state. Subtype 1 was found in the μg group as well as in the 1 g control group, whereas the incubator control did virtually not contain this subtype. Subtype 2 was represented in all three cell groups, μg, 1 g control, and incubator control cell group. However, it was primarily present in the μg and in the incubator control group and less present in the 1 g control group. The population distribution within cell groups is illustrated in Figure 2(b), showing the relative cell numbers of each population in each cell group. Since the incubator control group consisted almost exclusively of cells in subtype 2, this number was nearly 100%, whereas subtype 1 was close to 0%. The μg group had almost as many cells in subtype 2 as in subtype 1 with a slight predominance in subtype 2. In Figure 2(c), the mean fluorescence intensity of the cell subtypes in the different cell groups was depicted. While the ICAM-1 expression in the incubator control group was stable in both subtypes (2158 ± 234.4 RFU versus 2082 ± 171 RFU), and the μg cell group displayed significantly less expression of ICAM-1 in subtype 1 compared to subtype 2. ICAM-1 expression was significantly reduced in the μg group compared to the 1 g control and the incubator control group. Cells in the 1 g control group exhibited a similar ICAM-1 expression distribution as cells from the μg group. The mean fluorescence intensities between subtype 2 of different groups did not change dramatically, except a significant difference between the 1 g control group and the incubator control group. In summary, we suppose that ICAM-1 expression was downregulated in microglia cells in simulated microgravity.

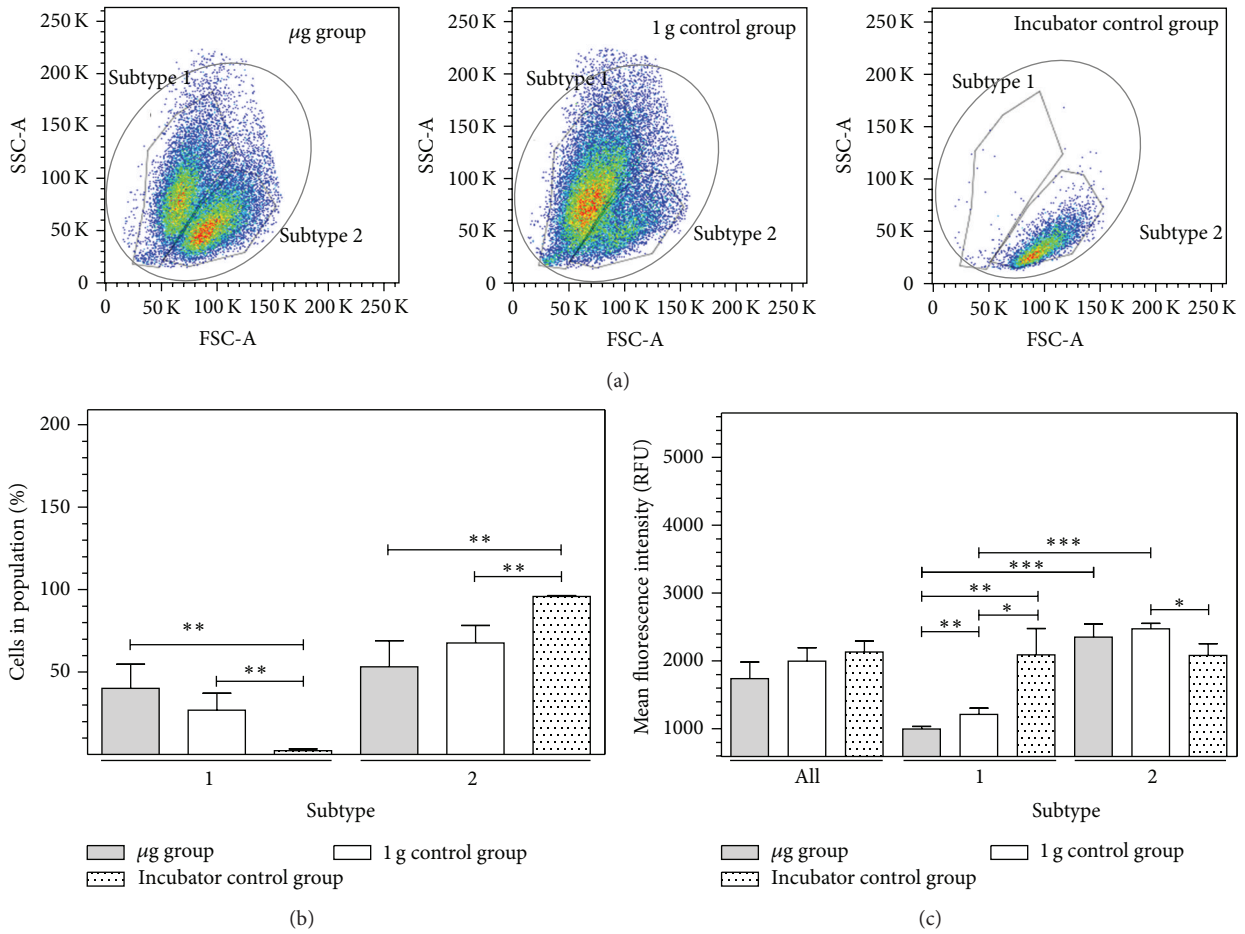

Figure 2: Cytometry analysis of ICAM-1 expression in BV-2 microglial cells in simulated microgravity (2D clinorotation). BV-2 microglial cells were exposed to either clinorotation (μg), placed in the clinostat but not rotated (1 g control group), or cultured under standard cell culture conditions (incubator control) for 24 h. Cells were stained for ICAM-1 surface expression and analyzed by flow cytometry. The level of ICAM-1 surface expression is represented by the mean fluorescent intensity assessed by flow cytometry. (a) In forward/sideward scatter detection mode of flow cytometry, two gates were set to separate two subtypes of BV-2 microglial cells that appeared different in size and granulation (subtypes 1 and 2 in dot plots). (b) Distribution of BV-2 microglial cells in subtypes 1 and 2 after exposure to different gravity conditions. (c) Quantification of ICAM-1 expression after exposure to different gravity conditions within subtypes 1 and 2. Data are given as median ± SE ($^{*}P < 0.1$, $^{**}P < 0.05$, $^{***}P < 0.01$, $n = 3$, according to one-way ANOVA followed by Wilcoxon or unpaired t-test).

3.2. Rapid and Reversible Downregulation of ICAM-1 Surface Expression in BV-2 Microglial Cells in Real Microgravity. In the next step, we investigated the cell surface expression of ICAM-1 in real microgravity provided by parabolic flights in murine BV-2 microglial cells. During parabolic flight experiments, cells were activated at the onset of μg (or during 1 g for in-flight control experiments) by the addition of PMA or TNF-α or not activated by the addition of medium only. After a 20 sec period of altered gravity, cells were fixed by the addition of formaldehyde.

During the 13th DLR parabolic flight campaign, we also addressed the issue that, during parabolic flight experiments, cells are generally subjected to irregular stress by cell preparation and handling and by the in-flight situation itself. This combination of interference factors always leads to a significant degree of damaged or dead cells, which could affect the experiment results and mask a possible microgravity-related effect, even under presence of internal controls. For this reason, we developed an automated analysis method, which allows for the specific analysis of alive and morphologically intact cells at the moment of fixation.

Experiments from different parabolas (1 g and μg, resp.) and different flights were analyzed. The experiments were performed in a sequence of three consecutive μg and 1 g phases. A quadruple fluorescent staining was performed using TUNEL (rhodamine) for detection of apoptotic cells, DAPI for the nuclei, high content screening (HCS) CellMask deep red for the delineation of cells, and FITC-labeled anti ICAM-1 antibody for identification of cell surface expression of ICAM-1. Cells were imaged with a widefield microscope (Leica Microsystems, Wetzlar, Germany) using the uniform random sampling module and identified by an iso-surface calculation (Imaris, Bitplane AG, Zurich, Switzerland). This quadruple staining allowed the exclusion of apoptotic cells in a highly reliable fashion. An example of an apoptotic cell and a living cell is depicted in Figure 3(a). The mean intensity

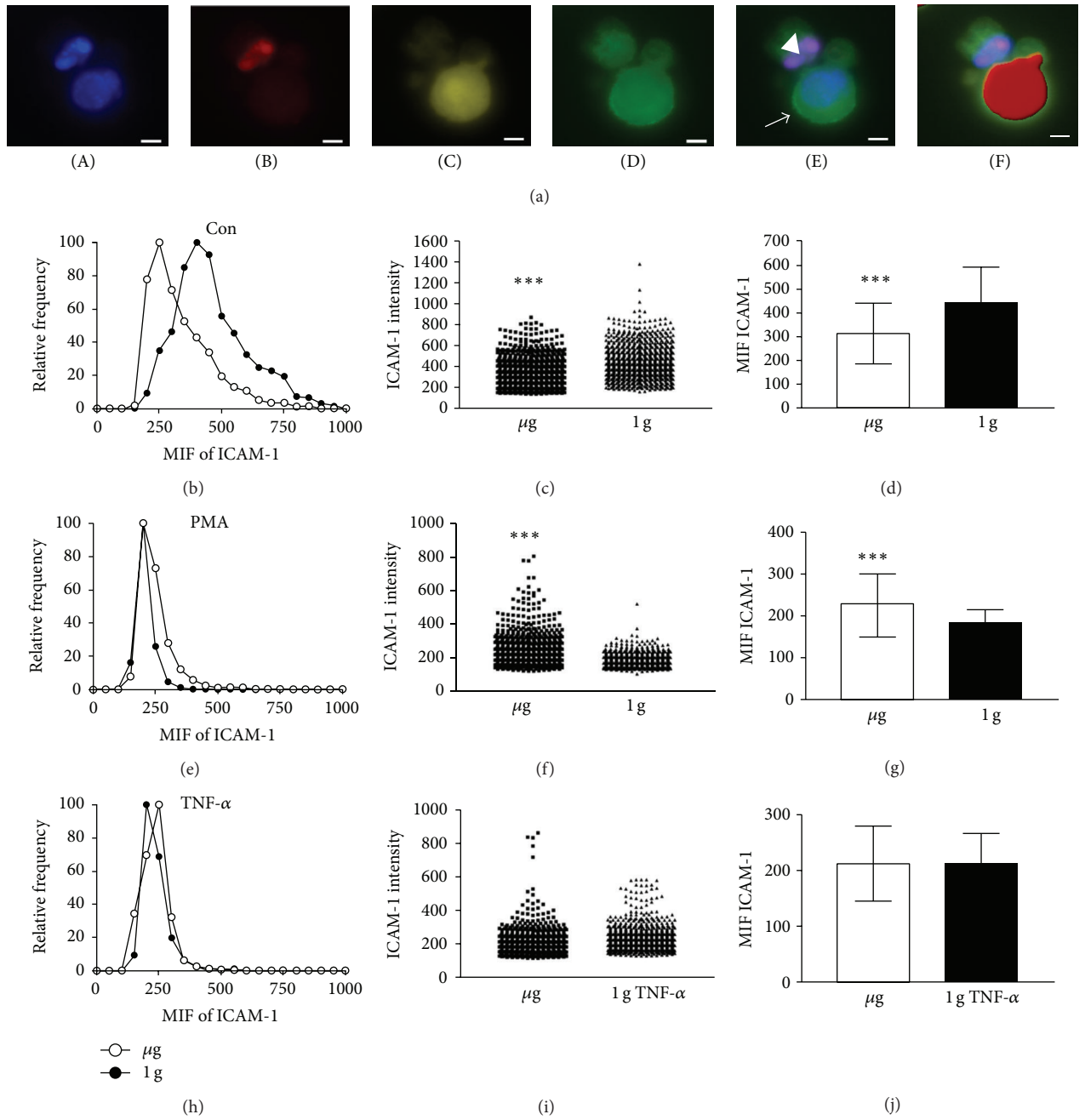

Figure 3: ICAM-1 surface expression reacts rapidly and reversibly to microgravity. (a) Microscopy of ICAM-1, TUNEL, HCS CellMask, and DAPI including surface calculation for HCS. In order to identify nuclei, cells were stained with DAPI (A). Apoptotic cells were identified by TUNEL reaction (B) and HCS CellMask label (C) which can be retained to a higher extend in nonapoptotic cells. ICAM-1 intensity is depicted in (D). A merge of TUNEL, DAPI, and ICAM-1 (E) shows an apoptotic cell (◂) and a living cell (→). The automated calculation of an iso-surface is exclusively done for living cells using the HCS CellMask channel as shown in the merge with TUNEL, DAPI, and ICAM-1 (F). (b)–(j) BV-2 microglial cells were treated with PMA ((e), (f), and (g)) or TNF-α ((h), (i), and (j)) at the onset of microgravity or during the 1 g in-flight control phase or left untreated ((b), (c), and (d)). Cells were fixed in flight after 20 sec normogravity (1 g) (-●-) or 20 sec microgravity (μg) (-○-). Cells were stained, imaged, and analyzed as described above. The mean intensity of the ICAM-1 signal was binned into mean intensity fluorescence (MIF) categories and the number of cells (frequency) is plotted against these intensity categories ((b), (e), and (h)). ICAM-1 fluorescence intensity of all analyzed cells ((c), (f), and (i)) is depicted for normogravity (triangles) and microgravity (squares). Mean ICAM-1 fluorescence intensity of all analyzed cells ((d), (g), and (j)) was pooled for normogravity (black bar) and microgravity (open bar). For automated imaging, the unified random sampling module was utilized and 63 randomized images of each sample were recorded and at least 500 single cells from 3 independent experiments from 3 different parabolas were analyzed. Mean intensity and SEM are shown and student's t-test showed highly significant difference of the fluorescence values of $^{***}P < 0.0001$, $n = 3$.

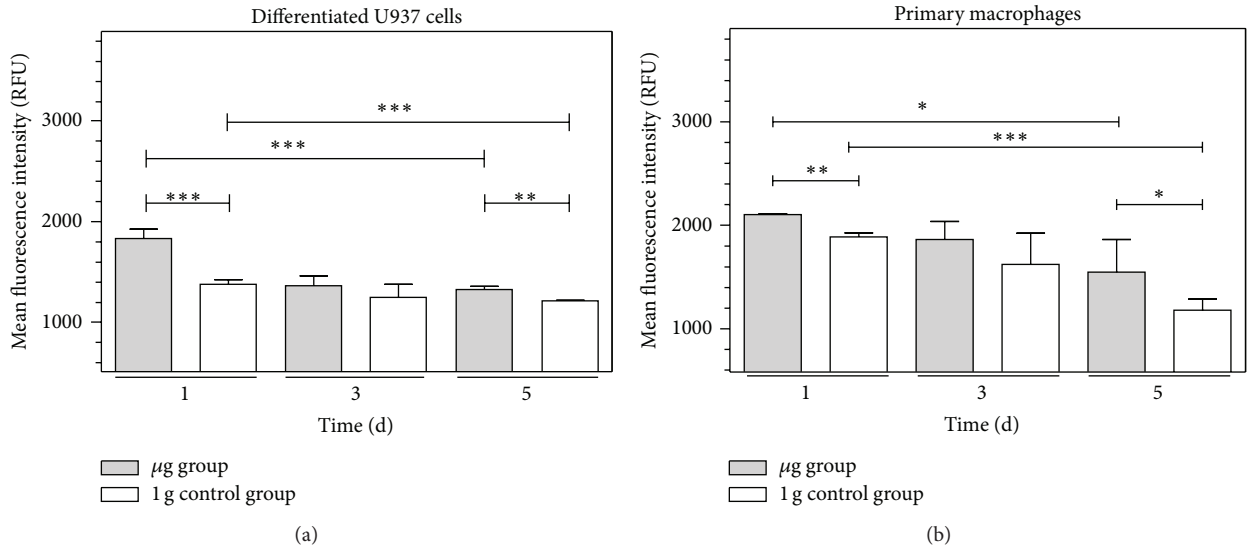

Figure 4: Cytometry analysis of ICAM-1 expression in macrophage-like differentiated U937 cells or primary human macrophages in simulated microgravity (2D clinorotation). Macrophage-like differentiated U937 cells (a) or primary human macrophages (b) were exposed to either clinorotation (μg), placed in the clinostat but not rotated (1 g control group), or cultured under standard cell culture conditions (incubator control). Cells were stained for ICAM-1 surface expression and analyzed by flow cytometry. The level of ICAM-1 surface expression is represented by the mean fluorescent intensity assessed by flow cytometry. (a) Quantification of ICAM-1 expression in macrophage-like differentiated U937 cells after exposure to different gravity conditions for 1 h, 3 h, or 5 h, $n = 6$. (b) Quantification of ICAM-1 expression in primary human macrophages after exposure to different gravity conditions for 1 h, 3 h, or 5 h, $n = 3$. Data are given as median ± SE ($^{*}P < 0.1$, $^{**}P < 0.05$, $^{***}P < 0.01$, according to one-way ANOVA followed by Wilcoxon or unpaired t-test).

of the ICAM-1 signal was analyzed in nondamaged and nonapoptotic cells only and binned into intensity categories. The relative frequency of these cells was plotted against the fluorescence intensity (Figures 3(b), 3(e), and 3(h)).

We found a rapid and reversible downregulation of ICAM-1 on the surface of BV-2 microglial cells after 20 sec of microgravity, apparent by the frequency of cells expressing ICAM-1 in various intensities (Figures 3(b) and 3(c)) and the mean of ICAM-1 expression intensity (Figure 3(d)) being only 70% in microgravity compared to normogravity. In the presence of PMA, ICAM-1 expression was upregulated (Figures 3(e), 3(f), and 3(g)), whereas the presence of the proinflammatory cytokine TNF-α abrogated the microgravity-induced ICAM-1 downregulation (Figures 3(h), 3(i), and 3(j)). Statistical analysis of all pooled data revealed downregulation of ICAM-1 expression in unstimulated microglia upon microgravity to be highly significantly different with $P < 0.001$ (Figure 3(d)). Changes of ICAM-1 expression in PMA stimulated cells were as well highly significant (Figure 3(g)), whereas TNF-α stimulation slightly ameliorated the gravity-dependent changes in ICAM-1 expression (Figure 3(j)). Thus, we found a rapid and reversible disappearance of ICAM-1 protein from the cell surface in microgravity.

3.3. Increase of ICAM-1 Expression in U937 Human Macrophage-Like Cells and Human Primary Macrophages in Simulated Microgravity. To corroborate the relevance of the results obtained with murine BV-2 microglial cells, we investigated a human macrophage-like cell system. Therefore, human monocytic U937 cells were differentiated into macrophage-like cells [23] and human M2 macrophages were differentiated from blood mononuclear cells. Before the experiment, differentiated macrophage-like cells were detached, resuspended in fresh medium, and filled into 1 mL standardized serological pipettes for the clinostat. Clinorotation was performed for 1 d, 3 d, and 5 d. The 1 g control group of differentiated U937 cells was filled into 1 mL serological pipettes in the same way as the clinorotation cell group but was not rotated. Cells were subsequently fixed and stained for cell surface ICAM-1 and apoptosis (TUNEL) to exclude apoptotic cells from the analysis and subjected to flow cytometry. We detected a highly significant increase of ICAM-1 expression in the clinorotated cells (μg group) compared to the nonrotated cells (1 g control group) after 1 d and 5 d in differentiated U937 cells (Figure 4(a)) and primary macrophages (Figure 4(b)). However, this increase receded after 3 and 5 days of clinorotation. Therefore, we conclude that ICAM-1 expression is increased in human macrophages after 1 and 5 days of simulated microgravity.

3.4. Increased ICAM-1 Expression in Differentiated U937 Cells in Real Microgravity during Parabolic Flight. During parabolic flight experiments, we investigated rapid effects of real microgravity on nondifferentiated and differentiated U937 cells and on primary human M2-differentiated macrophages. Nondifferentiated and differentiated myelomonocytic U937 cells were cultured and seeded into Nutrimix bags as described. During the parabolic maneuvers, cells were activated at the onset of μg or during 1 g for in-flight control experiments by the addition of PMA with medium in the

case of nondifferentiated U937 cells, or not activated by the addition of medium only in the case of differentiated U937 cells and primary macrophages. After 20 sec microgravity, cells were fixed by the addition of paraformaldehyde. A group of ground control cells was left in Nutrimix bags in the laboratory incubator and activated and fixed after landing in the same experimental equipment. Experiments from different parabolas (1 g and μg, resp.) and different flights were analyzed. A quadruple fluorescent staining was performed using TUNEL (rhodamine) for detection of apoptotic cells, DAPI for the nuclei, high content screening (HCS) CellMask deep red for the delineation of cells, and FITC-labeled anti ICAM-1 antibody for identification of cell surface expression of ICAM-1.

Nondifferentiated U937 Cells. Differentiation of U937 monocytic cells into macrophage-like cells significantly increased the cell surface expression of ICAM-1 (Figure 5(a)). Nondifferentiated U937 did not demonstrate differential expression of ICAM-1 in microgravity: neither in PMA-stimulated myelomonocytic U937 cells, nor in non-stimulated cells, any significant alteration of ICAM-1 expression could be detected in comparison between microgravity and 1 g conditions (Figure 5(b)). The only significant difference could be observed in nonstimulated U937 cells between the ground control group, the μg group, and the 1 g control group. Differences between 1 g ground and 1 g in-flight controls can be attributed to the flight itself (e.g., vibrations, handling of cell containers) and not to an altered gravity.

Differentiated U937 Cells. In contrast to nondifferentiated U937 cells, macrophage-like U937 cells displayed a highly significant gravity-dependent change in ICAM-1 expression (Figure 5(c)). In flight, cell surface ICAM-1 was reduced drastically compared to the ground control. In the microgravity group, ICAM-1 expression was enhanced. This finding is consistent with our experiments in simulated microgravity. We suppose that ICAM-1 is upregulated in differentiated macrophage-like cells in microgravity.

Primary Macrophages. For the analysis of primary human M2 macrophages, double fluorescence staining was performed using TUNEL (rhodamine) for detection of apoptotic cells and FITC-labeled anti ICAM-1 antibody for identification of cell surface expression of ICAM-1. Unfortunately, the 1 g incubator control was lost during the experiment procedures. Between the 1 g in-flight control and the microgravity group, no differences in ICAM-1 surface expression could be detected in primary human macrophages. However, due to the technical problems and low detected expression levels compared to primary macrophages in clinostat experiments (see Figure 4(b)), the informative value of these results may be limited and it is planned to repeat the parabolic flight experiment with primary human macrophages.

3.5. Increased ICAM-1 Expression in Differentiated U937 Cells during Long-Term Microgravity in the SIMBOX Experiment. During the SIMBOX (Science in Microgravity Box) mission on Shenzhou-8, we investigated microgravity-associated long-term alterations in macrophage-like differentiated U937 cells and analyzed the effect of long-term microgravity on the cytoskeleton and immunologically relevant surface molecules [23]. Human U937 cells were differentiated into a macrophage-like phenotype and exposed to microgravity or 1 g on a reference centrifuge on orbit for 5 days. The unmanned Shenzhou-8 spacecraft was launched with a Long March 2F (CZ-2F) rocket from the Jiuquan Satellite Launch Center (JSLC) and landed after a 17-day mission. After on-orbit fixation, the samples were analyzed with immunocytochemical staining and confocal microscopy after landing. Double fluorescent staining was performed using HCS CellMask deep red for the delineation of cells and FITC-labeled anti ICAM-1 antibody for identification of cell surface expression of ICAM-1. Cells were analyzed as described above. We detected a significant higher expression of ICAM-1 in long-term microgravity in comparison to the in-flight 1 g control group (Figure 6). Similar to the parabolic flight experiments, incubation of the macrophage-like differentiated U937 cells in the experiment hardware caused a significant downregulation of ICAM-1 expression. Thus, it can be excluded that the microgravity effects on ICAM-1 were caused by the experiment system itself.

3.6. No Influence of Altered Gravity on ICAM-1 mRNA. RNA samples were analyzed for their quantity and quality and further processed for the microarray hybridization on 12 × 135 K Roche NimbleGen arrays. Data from 46 single microarrays (19th DLR PFC: 8x μg, 6x H/W, 8x 1 g, and 6x 1.8 g; TEXUS-49: 7x μg, 6x H/W, and 5x BL) were collected, normalized, and further analyzed. The data tables were screened for ICAM-1 values and mean fluorescence intensities including standard deviations were calculated for all samples of one condition. ICAM-1 shows stable expression for all gravity conditions during the 19th DLR PFC and the TEXUS-49 campaign, as well as for the H/W controls (Figure 7), indicating that microgravity and hypergravity conditions did not have an influence on mRNA ICAM-1 level in the range of 20 seconds until 6 minutes.

3.7. Pathway Analysis Reveals an Influence of Real Microgravity on the Natural Killer Cell Mediated Cytotoxicity of Monocytic U937 Cells. Due to the wealth of data microarray analysis provides, we were able to perform a GeneSet enrichment analysis to identify any affected pathways or biological networks in connection with ICAM-1 (see Supplement 1 in the Supplementary Material available online at http://dx.doi.org/10.1155/2015/538786). For the experiments performed during the 19th DLR PFC with monocytic U937 cells, we identified one significantly influenced ICAM-1 related pathway during 20 sec of microgravity compared to the in-flight 1 g control, namely, the natural killer cell mediated cytotoxicity (enrichment P value 0.0203328). For the experiments performed on TEXUS-49 during 6 min of microgravity with monocytic U937 cells, we found two weakly altered pathways. Specifically, the NF-kappa B signaling pathway (enrichment P value 0.0632651) and the Epstein-Barr virus infection (enrichment P value

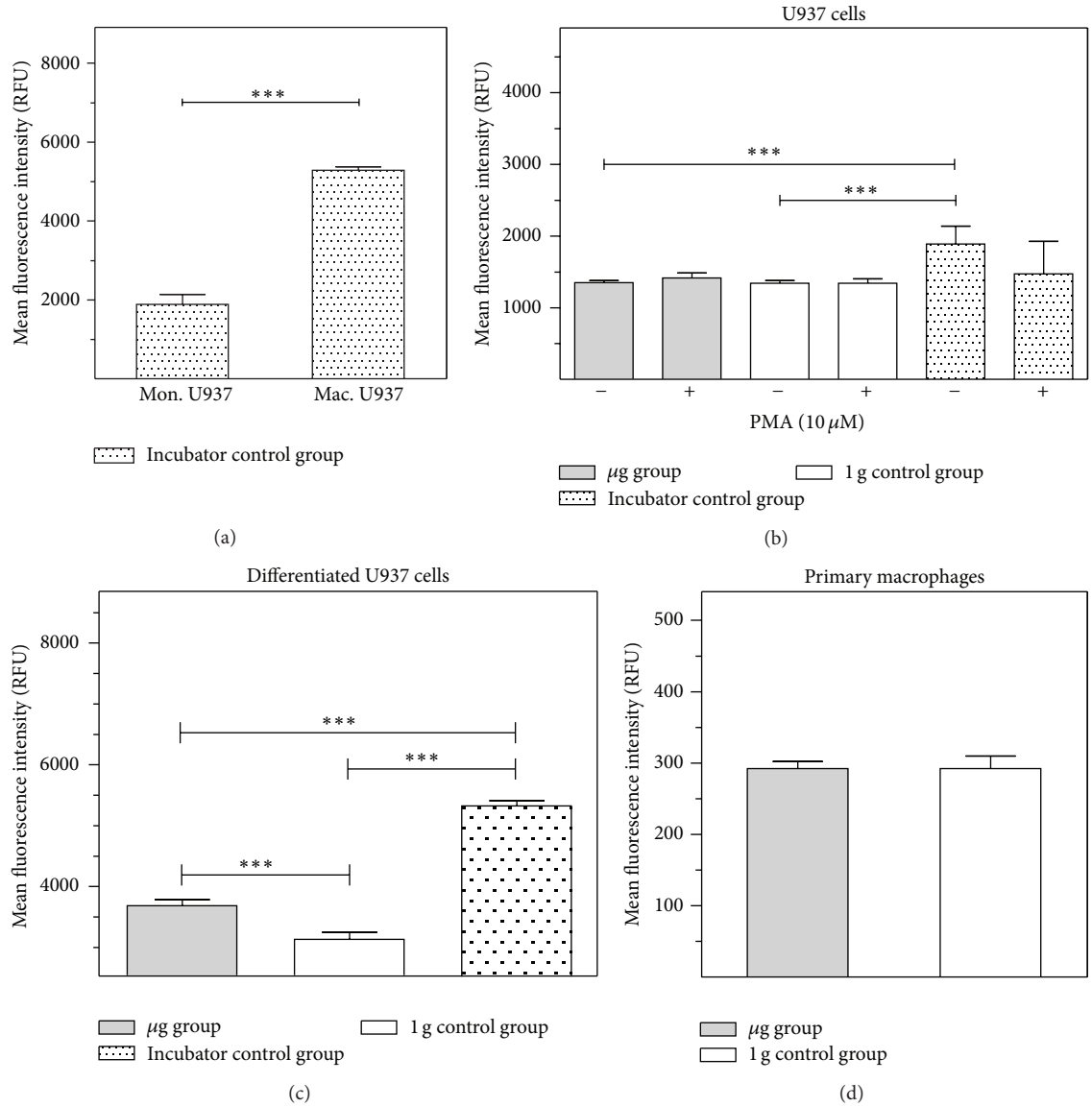

Figure 5: ICAM-1 expression in U937 cells, macrophage-like differentiated U937 cells, and primary human macrophages in different gravity conditions during parabolic flight experiment. ICAM-1 expression was assessed by flow cytometry and fluorescent microscopy following immunocytochemical staining. Cells were cultured under standard cell culture conditions (incubator control) or exposed to different gravity conditions during the 19th DLR parabolic flight campaign. U937 cells were fixed either after PMA-activation in microgravity (μg group) or in 1 g (1 g control group). Differentiated U937 and primary macrophages were fixed after the microgravity phases (μg group) or after the 1 g phases before and after the μg phase (1 g control group). The level of ICAM-1 surface expression is represented by the mean fluorescent intensity assessed by flow cytometry. (a) ICAM-1 surface expression in myelomonocytic U937 cells (mon. U937) and macrophage-like differentiated U937 cells (max. U937) under standard cell culture conditions. (b) ICAM-1 surface expression in U937 cells with and without activation by PMA in different gravity conditions. (c) ICAM-1 surface expression in macrophage-like differentiated U937 cells in different gravity conditions. (d) ICAM-1 surface expression in primary macrophages in different gravity conditions. Data are given as median ± SE ($^{*}P < 0.1$, $^{**}P < 0.05$, and $^{***}P < 0.01$, according to one-way ANOVA followed by Wilcoxon or unpaired t-test).

0.0641782) appeared sensitive to microgravity compared to baseline.

4. Discussion

In our study, we investigated the surface expression of ICAM-1 protein and expression of ICAM-1 mRNA in cells of the monocyte/macrophage system in microgravity during clinostat, parabolic flight, sounding rocket, and orbital experiments. In murine BV-2 microglial cells, we found a downregulation of ICAM-1 expression in clinorotation experiments and a rapid and reversible downregulation in the microgravity phase of parabolic flight experiments. In contrast, ICAM-1 expression increased in macrophage-like

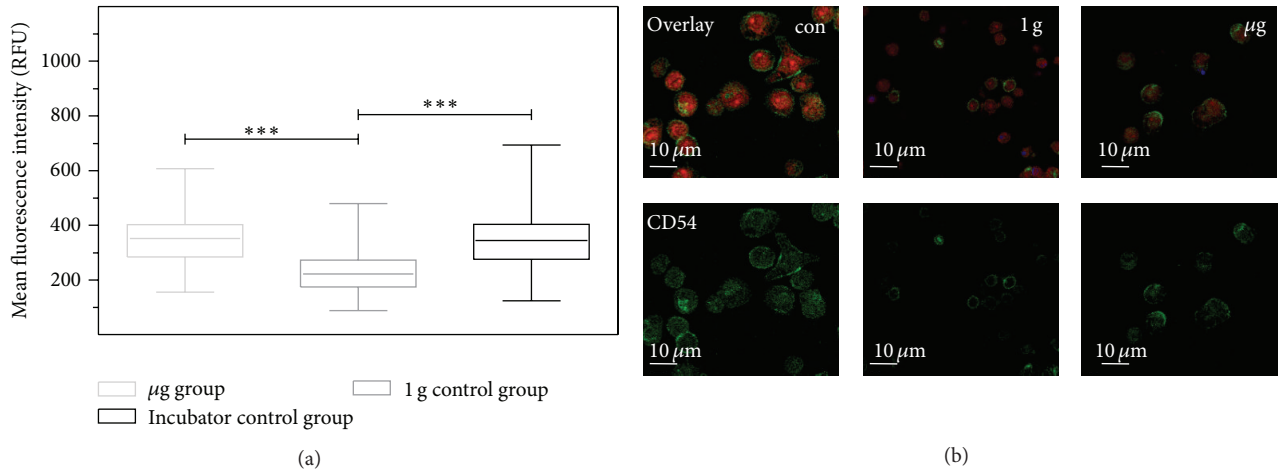

Figure 6: ICAM-1 expression in macrophage-like differentiated U937 cells after long-term exposure to microgravity during the SIMBOX/Shenzhou-8 mission. Cells were cultured under standard cell culture conditions (incubator control) or exposed to different gravity conditions during the SIMBOX/Shenzhou-8 mission. Differentiated U937 cells were fixed in microgravity (μg group) or in 1 g (1 g control group) after 5 days. Only CellMask-positive and TUNEL-negative cells were analyzed. (a) Each group represents analysis of the mean fluorescence of 200–1000 individual cells from one recovered slide. Data are expressed as the median of mean single cell fluorescence intensities with the smallest observation (sample minimum), lower quartile, median, upper quartile, and largest observation (sample maximum). Statistical analysis was performed with GraphPad Prism 5, Wilcoxon test, $^{*}P < 0.05$, $^{**}P < 0.01$, and $^{***}P < 0.001$. (b) Standard cell culture control (con), 1 g hardware control (1 g) and the microgravity sample (μg).

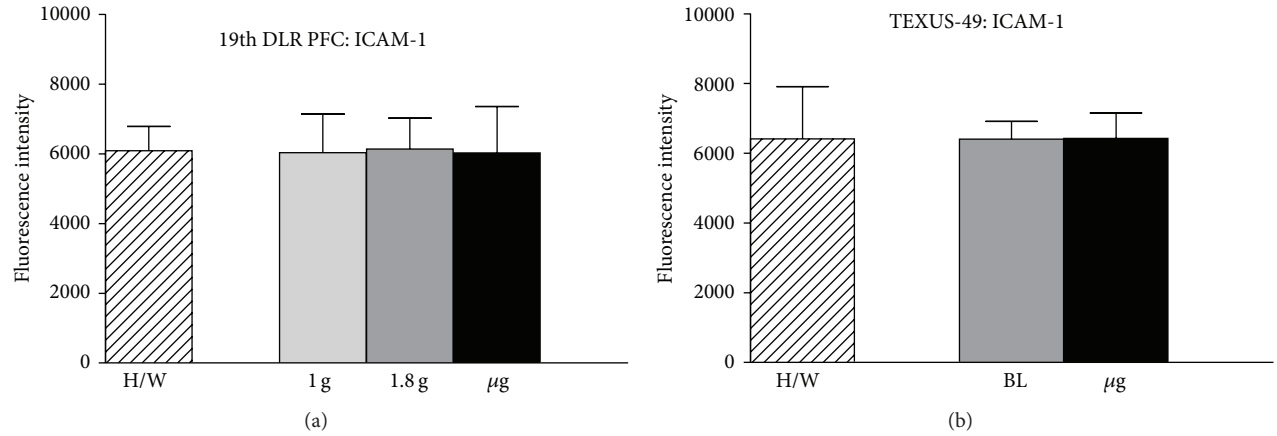

Figure 7: Influence of altered gravity during parabolic flight and sounding rocket flight on ICAM-1 mRNA expression levels. (a) ICAM-1 mRNA expression levels are demonstrated for samples of the 19th DLR parabolic flight campaign after 1 g (light gray), 1.8 g (dark gray), μg (black), and hardware ground controls (H/W, striped) exposure and (b) for samples of the TEXUS-49 campaign after launch and acceleration (BL, dark gray), μg (black), and hardware ground controls (H/W, striped). ICAM-1 fluorescence intensities do not show any significant differences for all compared conditions in both experimental setups. The number of analyzed arrays: 19th DLR PFC: 1 g ($n = 8$), 1.8 g ($n = 6$), μg ($n = 8$) and H/W ($n = 6$); TEXUS-49: H/W ($n = 6$), μg ($n = 7$), BL ($n = 5$).

differentiated human U937 cells during the microgravity phase of parabolic flights and in long-term microgravity provided by a 2D clinostat or during the orbital SIMBOX/Shenzhou-8 mission.

In nondifferentiated U937 cells, no effect of microgravity on ICAM-1 expression could be observed during parabolic flight experiments. A summarizing table, which presents an overview about the cell types tested, the platforms used, the experiment durations, analysis method, the number of experiments, and the detected effects on ICAM-1, is demonstrated in Table 1. In our study and according to previous investigations [26], we detected effects of the experimental hardware, which were controlled by the appropriate hardware control experiments.

In clinostat experiments, subtype of BV-2 microglial cells appeared in the FACS analysis of all clinostat samples (μg or 1 g controls), but not at all in the incubator controls. This subtype consisted of smaller cells and we suppose an "activated" phenotype of BV-2 microglial cells. It is well established that microglial form and function are linked and that cells can cycle reversibly from a simple rounded (activated and amoeboid) to a complex branched form (ramified and resting) [27].

Table 1: Regulation of ICAM-1 in cells of the monocyte/macrophage system in microgravity. Overview about cell types, microgravity platforms, the experiment durations, analysis methods, number of experiments, and effects on ICAM-1.

Experimental platform	Cell types	Experimental groups	Analysis method	Number of replicates	Time of μg exposal	Regulation of ICAM-1	
						μg/1 g	1 g/incubator control
Clinorotation	BV2 microglia cells	μg group 1 g control group	FACS (20.000 events/sample)	$N = 3$	24 h	↓	
	Primary macrophages	μg group 1 g control group	FACS (5.000 events/sample)	$N = 3$	1–5 d	↑	
	U937 macrophages	μg group 1 g control group	FACS (10.000 events/sample)	$N = 6$	1–5 d	↑	
Parabolic flight	BV2 microglia cells	μg group 1 g control group	Confocal microscopy/ random sampling module (>500 cells/sample)	$N = 3$ (w/o) $N = 3$ (with PMA) $N = 3$ (with TNF-a)	20 sec	↑ ↓ —	
	U937 macrophages	μg group 1 g control group Ground control	FACS (10.000 events/sample)	$N = 9$ $N = 9$ $N = 6$	20 sec	↑	↓
	U937 monocytes	μg group 1 g control group Ground control	FACS (10.000 events/sample)	$N = 9$ (w/o PMA) $N = 5$ (with PMA) $N = 12$ (w/o PMA) $N = 6$ (with PMA) $N = 2$ (w/o PMA) $N = 1$ (with PMA)	20 sec	—	—
		μg group 1 g control group 1.8 g control group Hardware control	Microarray	$N = 8$ $N = 8$ $N = 6$ $N = 6$	20 sec	—	—
	Primary macrophages	μg group 1 g control group	FACS (10.000 events/sample)	$N = 9$ $N = 9$	20 sec	—	
SIMBOX Shenzhou 8	U937 Macrophages	μg group 1 g control group Incubator control	Confocal microscopy (300 cells/sample) (650 cells/sample) (1000 cells/sample)	$N = 1$	5 d	↑	↓
TEXUS-49	U937 monocytes	μg group baseline group Hardware control	Microarray	$N = 7$ $N = 5$ $N = 6$	10 min	—	—

Thus, we assume that microgravity activates microglias cells but downregulates ICAM-1 expression (Figure 2). Control experiments revealed no influence of the serological pipette incubation system on the ICAM-1 expression compared to "normal" cell culture conditions between 1 and 5 d (data not shown).

In this study, we also developed a method that allowed a randomized screening of only those cells that were alive at the fixation time point after the parabola (Figure 3). This is of particular importance because of the damage caused to all cells subjected to a flight experiment. Until now, a method for analyzing only viable and nondamaged cells obtained from flight experiments was lacking. Due to the very limited number of samples during the experiment with BV-2 cells during the 13th DLR PFC, FACS analysis could not be utilized. We therefore developed a microscopy based method to analyze exclusively the living cell portion. Samples were imaged using the uniform random sampling module of Leica LAS AF software in order to fulfill all statistically necessary criteria of randomized sampling. Surface calculation of cells negative for TUNEL label under a certain threshold and positive for HCS CellMask allowed the exclusion of all apoptotic cells. The mean ICAM-1 intensity value of each analyzed cell was taken into account.

Modulation of the expression of surface adhesion molecules such as ICAM-1 has been reported as the consequence of long-term microgravity [28, 29]. In our study, we found that ICAM-1 surface expression responds to gravity changes in BV-2 microglial cells within 20 seconds. The rapid and reversible changes of ICAM-1 on the cell surface suggest a direct gravity-sensitive effect on the membrane compartment or on protein folding, whereas transcriptional or proteolytic processes are rather unlikely as they would be too slow. Interestingly, ICAM-1 cell surface expression in microgravity was upregulated in macrophage-like differentiated human U937 cells (Figures 4, 5, and 7) but downregulated in murine BV-2 microglial cells (Figure 2). In primary human macrophages, no clear conclusion is possible, because of the very low fluorescence levels in the analysis of parabolic flight samples (Figure 5). However, the clinostat experiments with primary human macrophages (Figure 4) suggest an upregulation of ICAM-1 in microgravity. The different ICAM-1 regulation between macrophage-like differentiated human U937 and murine BV-2 microglial cells in microgravity could be the consequence of the different species (murine and human) or different molecular and functional features of peripheral macrophages and CNS macrophages.

In our study, we detected no effect of microgravity on ICAM-1 mRNA expression, neither in a parabolic flight experiment, nor during the sounding rocket experiment (Figure 7). In a previous study, also no effect of simulated microgravity on ICAM-1 mRNA expression in endothelial cells could be found [15]. However, performing pathway analyses on ICAM-1 related pathways, we identified the natural killer cell mediated cytotoxicity being influenced significantly after 20 sec of microgravity. After 6 min of microgravity this effect appeared to be reversed and we found the NF-kappa B signaling pathway and the Epstein-Barr virus infection close to significant alteration. This observation is in line with findings in astronauts after long-term space missions where latent viruses persisting in a dormant state after primary infection were reactivated [30, 31]. Therefore, we hypothesize that these two pathways may be stronger affected over a longer period of microgravity. As we were not able to find an influence on the natural killer cell mediated cytotoxicity after 6 min of microgravity, we suppose this is one of the short-term reversible processes that can recover after an adaptation phase to microgravity.

Related to the regulation of surface ICAM-1 expression, internalization and receptor recycling of ICAM-1 are highly dynamic processes [32, 33] and linked to cytoskeletal function [34, 35].

Multiple investigators have reported that this complex network of fibers is sensitive to environmental factors such as microgravity and altered gravitational forces [36–38]. Several studies demonstrated modifications of the actin and microtubule cytoskeleton in real and simulated microgravity in lymphocytes, astrocytes, neurons, glial cells, mesenchymal stem cells, and thyroid carcinoma cells [36–41]. Morphological differences of both the microtubule and actin components of the cytoskeleton have been observed in cells grown in real and simulated microgravity [39–43]. During space flight, actin reorganization in response to the gravity level and abnormal assembly of actin stress fibers has been reported [44–46].

We conclude that disturbed immune function in microgravity could be a consequence of ICAM-1 modulation in the monocyte/macrophage system, which in turn could have a strong impact on the cells' interaction with T lymphocytes and migration. An experiment under real microgravity conditions on board of the ISS was conducted by Italian and Swiss investigators to test the hypothesis that lack of interaction might be the reason for the loss of activity of T cells in microgravity [14]. The investigation consisted of analyzing the cap formation of the adhesion proteins LFA-1 on T cells and ICAM-1 on monocytes. The data showed that LFA-1/ICAM-1 interactions occur in space but are dependent on activation time; they show differences in number, arrangement, and fluorescence intensity. Thus, LFA-1 and ICAM-1 adhesion proteins seem to be sensitive to real microgravity, without being altered in their interaction. Loss of functional ICAM-1 in the brain-resident microglial cells bears the risk of a significant impairment of the CNS immune system. Indeed, reactivation and shed of varicella-zoster virus (VZV) have been reported in astronauts [30, 31], a virus which becomes latent in the nervous system after primary infection, but is reactivated frequently in immune suppressed individuals.

In conclusion, we found that ICAM-1 can be downregulated rapidly and reversibly in BV-2 microglial cells and upregulated in macrophage-like differentiated U937 cells in response to microgravity. In both cell types, long-term effects up to several days could be detected. Thus, ICAM-1 can be considered as a rapid-reacting and sustained gravity-regulated molecule in mammalian cells.

Abbreviations

BL: Baseline
CC: Cell culture control
DLR: German Aerospace Center
ESA: European Space Agency
ESRANGE: European Space and Sounding Rocket Range
EUE: Experiment Unique Equipment
FACS: Fluorescence activated cell sorting
FCS: Fetal calf serum
GC: Ground control
H/W: Hardware
ICAM-1: Intercellular adhesion molecule 1
JSLC: Jiuquan Satellite Launch Center
LFA-1: Lymphocyte function-associated antigen 1
MAC-1: Myelomonocytic leukocyte integrin CD11b
μg: Microgravity
MMS: Monocyte-macrophage-system
PBMC: Peripheral blood mononuclear cell
PEEK: Polyether ether ketone
PFA: Paraformaldehyde
PFC: Parabolic flight campaign
PITC: Payload integration and test center
PMA: 12-O-Tetradecanoylphorbol-13-acetate
RCCS: Rotary Cell Culture Systems
RFI: Relative fluorescence intensity
RIN: RNA integrity number
RPM: Random positioning machine
SSC: Swedish Space Corporation
SIMBOX: Science in Microgravity Box
TUNEL: TdT-mediated dUTP-biotin nick end labeling.

Conflict of Interests

The authors declare that they have no competing interests.

Authors' Contribution

Oliver Ullrich developed the study idea, concept, and the overall study design in addition to planning, coordinating, and supervising the study. Katrin Paulsen and Oliver Ullrich wrote the paper. Svantje Tauber, Cora S. Thiel, and Liliana E. Layer contributed to the paper. Oliver Ullrich, Cora S. Thiel, Gesine Bradacs, Sonja Krammer, Josefine Biskup, Gabriela Rieder, Lisa Mutschler, Daniel Hofmänner, Isabell Buttron, and Hartwin Lier performed the experiments during the 13th DLR parabolic flight campaign. Liliana E. Layer, Cora S. Thiel, Oliver Ullrich, Svantje Tauber, Swantje Hauschild, Claudia Philpot, Annett Gutewort, Eva Hürlimann, Josefine Biskup, and Hartwin Lier performed the experiments during the 19th DLR parabolic flight campaign. Andreas Huge performed the pathway analysis. Svantje Tauber, Cora S. Thiel, and Oliver Ullrich performed the experiments during the TEXUS-49 mission and Katrin Paulsen, Svantje Tauber, Dana M. Simmet, Oliver Ullrich, Eva Hürlimann, and Nadine Gölz during the SIMBOX/Shenzhou-8 mission. Katrin Paulsen was responsible for the sample analysis from the 13th DLR and 19th DLR parabolic flight campaigns and the SIMBOX/Shenzhou-8 mission, and Cora S. Thiel was responsible for sample analysis from the TEXUS-49 mission. Nadine Gölz and Svantje Tauber contributed to the sample analysis. Frank Engelmann contributed to and supervised the technical procedures during the 13th and 19th DLR parabolic flight campaigns.

Acknowledgments

The authors gratefully acknowledge financial support by the German Aerospace Center DLR (Grant nos. 50WB0912 and 50WB1219). They also gratefully acknowledge the support of (in alphabetic order) Markus Braun, Miriam Christen, Giovanni Colacicco, Ulrike Friedrich, André Hilliger, Andreas Huge, Schirin Ibrahim, Otfried Joop, Andre Melik, Shirin Milani, Brice Moutett, Marianne Ott, Irina Rau, Frank Rühli, Chen Sang, Burkhard Schmitz, Andreas Schütte, Johanna Stahn, Marc Studer, Susanne Wolf, and Fengyuan Zhuang. They would like to thank the Swiss Air Force for the outstanding support of their study by providing daily air transports of in-flight cell samples from Zurich to Bordeaux and back during the 13th DLR parabolic flight campaign. Its reliable and rapid transport system guaranteed the recovery of flown samples in an outstanding quality for analysis.

References

[1] G. Sonnenfeld, "The immune system in space and microgravity," *Medicine and Science in Sports and Exercise*, vol. 34, no. 12, pp. 2021–2027, 2002.

[2] O. Ullrich, K. Huber, and K. Lang, "Signal transduction in cells of the immune system in microgravity," *Cell Communication and Signaling*, vol. 6, article 9, 2008.

[3] N. Guéguinou, C. Huin-Schohn, M. Bascove et al., "Could spaceflight-associated immune system weakening preclude the expansion of human presence beyond Earth's orbit?" *Journal of Leukocyte Biology*, vol. 86, no. 5, pp. 1027–1038, 2009.

[4] O. Ullrich and C. S. Thiel, "Gravitational force: triggered stress in cells of the immune system," in *Stress Challenges, and Immunity in Space: From Mechanisms to Monitoring and Preventive Strategies*, A. Choukèr, Ed., chapter 14, pp. 187–202, Springer, Berlin, Germany, 2012.

[5] I. V. Konstantinova, E. N. Antropova, V. I. Legen'kov, and V. D. Zazhireĭ, "Reactivity of lymphoid blood cells in the crew of "Soiuz-6", "Soiuz-7" and "Soiuz-8" spacecraft before and after flight," *Kosmicheskaia Biologiia i Aviakosmicheskaia Meditsina*, vol. 7, no. 6, pp. 35–40, 1973.

[6] S. Hauschild, S. Tauber, B. Lauber, C. S. Thiel, L. E. Layer, and O. Ullrich, "T cell regulation in microgravity—the current knowledge from in vitro experiments conducted in space, parabolic flights and ground-based facilities," *Acta Astronautica*, vol. 104, no. 1, pp. 365–377, 2014.

[7] B. Crucian, R. Stowe, H. Quiriarte, D. Pierson, and C. Sams, "Monocyte phenotype and cytokine production profiles are dysregulated by short-duration spaceflight," *Aviation, Space, and Environmental Medicine*, vol. 82, no. 9, pp. 857–862, 2011.

[8] M. Hughes-Fulford, T. Chang, and C. F. Li, "Effect of gravity on monocyte differentiation," in *Proceedings of the 10th ESA Life Sciences Symposium/29th Annual ISGP Meeting/24th Annual ASGSB Meeting/ELGRA Symposium "Life in Space for Life on Earth"*, Angers, France, June 2008.

[9] B. Bechler, A. Cogoli, M. Cogoli-Creuter, O. Muller, E. Hunzinger, and S. B. Criswell, "Activation of microcarrier-attached lymphocytes in microgravity," *Biotechnology and Bioengineering*, vol. 40, no. 8, pp. 991–996, 1992.

[10] J.-L. Wautier, H. Setiadi, D. Vilette, D. Weill, and M.-P. Wautier, "Leukocyte adhesion to endothelial cells," *Biorheology*, vol. 27, no. 3-4, pp. 425–432, 1990.

[11] W. A. Muller, "Mechanisms of leukocyte transendothelial migration," *Annual Review of Pathology: Mechanisms of Disease*, vol. 6, pp. 323–344, 2011.

[12] A. Grakoui, S. K. Bromley, C. Sumen et al., "The immunological synapse: a molecular machine controlling T cell activation," *Science*, vol. 285, no. 5425, pp. 221–227, 1999.

[13] T. Nagel, N. Resnick, W. J. Atkinson, C. F. Dewey Jr., and M. A. Gimbrone Jr., "Shear stress selectively upregulates intercellular adhesion molecule-1 expression in cultured human vascular endothelial cells," *The Journal of Clinical Investigation*, vol. 94, no. 2, pp. 885–889, 1994.

[14] M. A. Meloni, G. Galleri, G. Pani, A. Saba, P. Pippia, and M. Cogoli-Greuter, "Effects of real microgravity aboard international space station on monocytes motility and interaction with T-lymphocytes," in *Proceedings of the 10th ESA Life Sciences Symposium/29th Annual ISGP Meeting/24th Annual ASGSB Meeting/ELGRA Symposium "Life in Space for Life on Earth"*, Angers, France, 2008.

[15] Y. Zhang, C. Sang, K. Paulsen et al., "ICAM-1 expression and organization in human endothelial cells is sensitive to gravity," *Acta Astronautica*, vol. 67, no. 9-10, pp. 1073–1080, 2010.

[16] K. P. Murphy, *Janeway's Immunology*, Garland Science Taylor & Francis Group, LLC, New York, NY, USA, 8th edition, 2012.

[17] B. Alberts, A. Johnson, J. Lewis, M. Raff, K. Roberts, and P. Walter, *Molecular Biology of the Cell*, Garland Science, Taylor & Francis Group, LLC, New York, NY, USA, 5th edition, 2008.

[18] C. S. Thiel, K. Paulsen, G. Bradacs et al., "Rapid alterations of cell cycle control proteins in human T lymphocytes in microgravity," *Cell Communication and Signaling*, vol. 10, no. 1, article 1, 2012.

[19] K. Paulsen, C. Thiel, J. Timm et al., "Microgravity-induced alterations in signal transduction in cells of the immune system," *Acta Astronautica*, vol. 67, no. 9-10, pp. 1116–1125, 2010.

[20] E. Blasi, R. Barluzzi, V. Bocchini, R. Mazzolla, and F. Bistoni, "Immortalization of murine microglial cells by a v-*raf* / v-*myc* carrying retrovirus," *Journal of Neuroimmunology*, vol. 27, no. 2-3, pp. 229–237, 1990.

[21] S. J. Gerathewohl, Ed., *Zero-G Devices and Weightlessness Simulators, Report for the Armed Forces-NAS-NRC Committee on Bioastronautics Panel on Acceleration*, National Research Council, Publication 781, National Academy of Sciences, Washington, DC, USA, 1961.

[22] U. Kuebler, "SIMBOX Plunger," in *Astrium Space Biology Product Catalog*, chapter 7.18, pp. 153–157, Astrium Space Transportation, Department of New Business, Friedrichshafen, Germany, 2012.

[23] K. Paulsen, S. Tauber, N. Goelz et al., "Severe disruption of the cytoskeleton and immunologically relevant surface molecules in a human macrophageal cell line in microgravity—results of an in vitro experiment on board of the Shenzhou-8 space mission," *Acta Astronautica*, vol. 94, no. 1, pp. 277–292, 2014.

[24] M. Kanehisa, S. Goto, Y. Sato, M. Kawashima, M. Furumichi, and M. Tanabe, "Data, information, knowledge and principle: back to metabolism in KEGG," *Nucleic Acids Research*, vol. 42, no. 1, pp. D199–D205, 2014.

[25] M. Kanehisa and S. Goto, "KEGG: kyoto encyclopedia of genes and genomes," *Nucleic Acids Research*, vol. 28, no. 1, pp. 27–30, 2000.

[26] S. Tauber, S. Hauschild, C. Crescio et al., "Signal transduction in primary human T lymphocytes in altered gravity—results of the MASER-12 suborbital space flight mission," *Cell Communication and Signaling*, vol. 11, no. 1, article 32, 2013.

[27] A. Karperien, H. Ahammer, and H. F. Jelinek, "Quantitating the subtleties of microglial morphology with fractal analysis," *Frontiers in Cellular Neuroscience*, vol. 7, no. 3, 2013.

[28] L. Buravkova, Y. Romanov, M. Rykova, O. Grigorieva, and N. Merzlikina, "Cell-to-cell interactions in changed gravity: ground-based and flight experiments," *Acta Astronautica*, vol. 57, no. 2-8, pp. 67–74, 2005.

[29] Y. A. Romanov, L. B. Buravkova, M. P. Rikova, E. N. Antropova, N. N. Savchenko, and N. V. Kabaeva, "Expression of cell adhesion molecules and lymphocyte-endothelium interaction under simulated hypogravity in vitro," *Journal of Gravitational Physiology*, vol. 8, no. 1, pp. 5–8, 2001.

[30] R. J. Cohrs, S. K. Mehta, D. S. Schmid, D. H. Gilden, and D. L. Pierson, "Asymptomatic reactivation and shed of infectious varicella zoster virus in astronauts," *Journal of Medical Virology*, vol. 80, no. 6, pp. 1116–1122, 2008.

[31] S. K. Mehta, R. J. Cohrs, B. Forghani, G. Zerbe, D. H. Gilden, and D. L. Pierson, "Stress-induced subclinical reactivation of varicella zoster virus in astronauts," *Journal of Medical Virology*, vol. 72, no. 1, pp. 174–179, 2004.

[32] S. Muro, R. Wiewrodt, A. Thomas et al., "A novel endocytic pathway induced by clustering endothelial ICAM-1 or PECAM-1," *Journal of Cell Science*, vol. 116, no. 8, pp. 1599–1609, 2003.

[33] S. Muro, C. Gajewski, M. Koval, and V. R. Muzykantov, "ICAM-1 recycling in endothelial cells: A novel pathway for sustained intracellular delivery and prolonged effects of drugs," *Blood*, vol. 105, no. 2, pp. 650–658, 2005.

[34] O. Carpen, P. Pallai, D. E. Staunton, and T. A. Springer, "Association of intercellular adhesion molecule-1 (ICAM-1) with actin-containing cytoskeleton and α-actinin," *Journal of Cell Biology*, vol. 118, no. 5, pp. 1223–1234, 1992.

[35] E. VandenBerg, M. D. Reid, J. D. Edwards, and H. W. Davis, "The role of the cytoskeleton in cellular adhesion molecule expression in tumor necrosis factor-stimulated endothelial cells," *Journal of Cellular Biochemistry*, vol. 91, no. 5, pp. 926–937, 2004.

[36] H. Schatten, M. L. Lewis, and A. Chakrabarti, "Spaceflight and clinorotation cause cytoskeleton and mitochondria changes and increases in apoptosis in cultured cells," *Acta Astronautica*, vol. 49, no. 3-10, pp. 399–418, 2001.

[37] C. Papaseit, N. Pochon, and J. Tabony, "Microtubule self-organization is gravity-dependent," *Proceedings of the National Academy of Sciences of the United States of America*, vol. 97, no. 15, pp. 8364–8368, 2000.

[38] S. J. Crawford-Young, "Effects of microgravity on cell cytoskeleton and embryogenesis," *International Journal of Developmental Biology*, vol. 50, no. 2-3, pp. 183–191, 2006.

[39] B. M. Uva, M. A. Masini, M. Sturla et al., "Clinorotation-induced weightlessness influences the cytoskeleton of glial cells in culture," *Brain Research*, vol. 934, no. 2, pp. 132–139, 2002.

[40] B. M. Uva, F. Strollo, F. Ricci, M. Pastorino, J. I. Mason, and M. A. Masini, "Morpho-functional alterations in testicular and nervous cells submitted to modelled microgravity," *Journal of Endocrinological Investigation.*, vol. 28, no. 11, pp. 84–91, 2005.

[41] M. Infanger, P. Kossmehl, M. Shakibaei et al., "Simulated weightlessness changes the cytoskeleton and extracellular matrix proteins in papillary thyroid carcinoma cells," *Cell and Tissue Research*, vol. 324, no. 2, pp. 267–277, 2006.

[42] V. E. Meyers, M. Zayzafoon, J. T. Douglas, and J. M. McDonald, "RhoA and cytoskeletal disruption mediate reduced osteoblastogenesis and enhanced adipogenesis of human mesenchymal stem cells in modeled microgravity," *Journal of Bone and Mineral Research*, vol. 20, no. 10, pp. 1858–1866, 2005.

[43] M. L. Lewis, J. L. Reynolds, L. A. Cubano, J. P. Hatton, B. Desales Lawless, and E. H. Piepmeier, "Spaceflight alters microtubules and increases apoptosis in human lymphocytes (Jurkat)," *The FASEB Journal*, vol. 12, no. 11, pp. 1007–1018, 1998.

[44] M. Hughes-Fulford, "Review of the biological effects of weightlessness on the human endocrine system.," *Receptor*, vol. 3, no. 3, pp. 145–154, 1993.

[45] R. Gruener, R. Roberts, and R. Reitstetter, "Reduced receptor aggregation and altered cytoskeleton in cultured myocytes after space-flight," *Uchu Seibutsu Kagaku*, vol. 8, no. 2, pp. 79–93, 1994.

[46] M. Hughes-Fulford, "Function of the cytoskeleton in gravisensing during spaceflight," *Advances in Space Research*, vol. 32, no. 8, pp. 1585–1593, 2003.

Hindawi Publishing Corporation
BioMed Research International
Volume 2015, Article ID 976458, 10 pages
http://dx.doi.org/10.1155/2015/976458

Research Article

Genes Required for Survival in Microgravity Revealed by Genome-Wide Yeast Deletion Collections Cultured during Spaceflight

Corey Nislow,[1] Anna Y. Lee,[2] Patricia L. Allen,[3] Guri Giaever,[1] Andrew Smith,[2] Marinella Gebbia,[2] Louis S. Stodieck,[4] Jeffrey S. Hammond,[5] Holly H. Birdsall,[6,7] and Timothy G. Hammond[3,6,8,9]

[1]*Faculty of Pharmaceutical Sciences, The University of British Columbia, Vancouver, BC, Canada V6T 1Z3*
[2]*Donnelly CCBR, University of Toronto, Toronto, ON, Canada M5S 3E1*
[3]*Durham VA Medical Center, Research & Development Service, Durham, NC 27705, USA*
[4]*Bioserve Space Technologies, University of Colorado, Boulder, CO 80309, USA*
[5]*The Institute for Medical Research, Durham, NC 27705, USA*
[6]*Department of Veterans Affairs Office of Research and Development, Washington, DC 20420, USA*
[7]*Departments of Otorhinolaryngology, Immunology, and Psychiatry, Baylor College of Medicine, Houston, TX 77030, USA*
[8]*Nephrology Division, Department of Internal Medicine, Duke University School of Medicine, Durham, NC 27705, USA*
[9]*Nephrology Section, Department of Internal Medicine, George Washington University School of Medicine, Washington, DC 20052, USA*

Correspondence should be addressed to Timothy G. Hammond; grumpy70115@yahoo.com

Received 15 May 2014; Revised 30 September 2014; Accepted 15 October 2014

Academic Editor: Jack J. W. A. Van Loon

Spaceflight is a unique environment with profound effects on biological systems including tissue redistribution and musculoskeletal stresses. However, the more subtle biological effects of spaceflight on cells and organisms are difficult to measure in a systematic, unbiased manner. Here we test the utility of the molecularly barcoded yeast deletion collection to provide a quantitative assessment of the effects of microgravity on a model organism. We developed robust hardware to screen, in parallel, the complete collection of ~4800 homozygous and ~5900 heterozygous (including ~1100 single-copy deletions of essential genes) yeast deletion strains, each carrying unique DNA that acts as strain identifiers. We compared strain fitness for the homozygous and heterozygous yeast deletion collections grown in spaceflight and ground, as well as plus and minus hyperosmolar sodium chloride, providing a second additive stressor. The genome-wide sensitivity profiles obtained from these treatments were then queried for their similarity to a compendium of drugs whose effects on the yeast collection have been previously reported. We found that the effects of spaceflight have high concordance with the effects of DNA-damaging agents and changes in redox state, suggesting mechanisms by which spaceflight may negatively affect cell fitness.

1. Introduction

Physical effects of microgravity during spaceflight can often be described by equations that allow their quantification [1, 2]. For example, microgravity has well-defined effects on sedimentation in association with reduced terminal velocity and shear in suspension culture [3] and reduced gravity-dependent convection of gases [4]. Biological effects of spaceflight on cells and organisms, on the other hand, are much harder to define [1, 2]. For example, spaceflight also entails radiation exposure, which has been studied in diverse systems but whose effects are not fully understood [5]. What is needed is a robust, unbiased, quantifiable system that is relevant for translation to ground-based applications and that is able to clearly distinguish spaceflight effects. It is our premise that yeast deletion collections are ideally suited

for this type of analysis as yeast can be precisely controlled genetically and readily grown under spaceflight conditions. Biological responses of yeast strains during spaceflight can be quantified and compared to well-established databases of ground-based stressors and the comparisons can reveal features that are unique to microgravity as well as features that are shared with ground-based perturbations. While yeast cannot completely reflect the complexities of mammalian cells organized into tissues, the high degree of homology shared with human (~70% of all essential yeast genes have a significant human homolog) provides hypotheses for the mechanism of many responses of interest [6, 7].

Previous studies have attempted to identify, isolate, and offset the various physical factors changing during spaceflight to demonstrate their effects in an iterative fashion [8–10]. Earlier studies on the effects of space radiation on yeast failed to find any change in point mutation rates, DNA replication and/or repair, heritable damage, or colony morphology [5, 8, 11, 12]. However, those studies were limited by assay sensitivity. Here we applied the yeast deletion collection as a biological reporter to understand the metabolic pathways affecting survival during culture in spaceflight. In this fashion, we are able to make genome-wide comparisons and test for concordance against an extensive library of more than 3200 physical and pharmacological stressors [13].

Yeast is the first, and to date only, organism for which a complete, genome-wide knockdown collection is available. This collection is comprised of a genome-wide set of strains where each strain carries a precise deletion of a single gene [14]. Assembled over a four-year period by a consortium of 35 laboratories, this collection has been used by hundreds of laboratories to test thousands of different environmental stressors to define the genes required for survival in those conditions (see [15] for review). The molecular barcodes present in each strain allow the yeast deletion collection to be grown as a pool in the presence or absence of the stressor of interest after which the relative abundance of each strain is subsequently quantified [16]. Strains carrying a deletion of a gene required for survival in the presence of the stressor grow more slowly and thus exhibit a fitness defect reflected by their reduced abundance at the end of the culture period. In this manner, all genes required for growth can be readily identified in a single experiment, revealing the genes and associated pathways affected by the stressor.

To identify the metabolic and genomic pathways affected by spaceflight, the homozygous and heterozygous yeast deletion collections were grown in spaceflight and ground control conditions, with and without hyperosmolar sodium chloride, providing a second stressor. In spaceflight alone, the homozygous deletion collection revealed the importance of processes linked to mitochondria, while the heterozygous collection highlighted genes involved in regulating translation and ribosomal RNA transport. Both homozygous and heterozygous collections highlighted DNA repair. With the addition of NaCl, the homozygous collection also revealed the importance of RNA-related processes including ribosome assembly and biogenesis and mRNA processing and decay, as well as modification of tRNAs. Moreover, the NaCl addition highlighted replication processes more clearly (compared to the homozygous collection without NaCl), suggesting that spaceflight has measurable effects on these core and evolutionarily conserved processes. With the heterozygous collection, the addition of NaCl led to the identification of a nuclear pore organization gene, potentially providing additional insight into how RNA transport is affected by spaceflight. Taken together, the deletion collections identified several biological processes associated with spaceflight, and the additional hyperosmolar stress emphasized the importance of related processes.

In a follow-up analysis, we queried the effects of spaceflight against a database of drug effects on yeast to search for those that are most concordant, thereby suggesting similar mechanisms of perturbation. Not only do the effects of spaceflight have relatively high concordance with the effects of DNA-damaging agents, but also there is tight agreement amongst multiple therapeutic agents in this drug class, providing additional support for these findings.

2. Materials and Methods

2.1. Overall Design. The Opticell Processing Module, described below, was used to perform a series of ~21 generation pooled growth experiments on two yeast deletion collections: (i) ~4800 homozygous strains and (ii) ~5900 heterozygous strains (including ~1100 single-copy deletions of essential genes), each carrying unique DNA barcodes that act as strain identifiers. Experiments were performed in both rich media and rich media supplemented with 0.5 M NaCl to assess the additional effect of osmotic stress on survival. The samples flew sortie on space shuttle mission STS-135 to the International Space Station (ISS). Parallel control experiments were performed in static 1G terrestrial controls in the Orbital Environmental Simulator at Kennedy Space Center to match temperature, humidity, air composition, and volatile organic compounds. Ground controls were conducted in a 24-hour asynchronous fashion to allow matching of the experimental timelines on ISS as relayed through air-to-ground communication by the flight crew. At the end of the growth period, the fitness of each strain in each experimental pool was assessed as described [17]. Briefly, genomic DNA was extracted from each sample, the barcodes in each pool were amplified by PCR, and the abundance of each barcode was quantified by next generation sequencing. A barcode count reflects the abundance of the corresponding strain at the end of the experiment, that is, a quantification of the relative requirement of the deleted gene for growth in the tested condition. In total, the experiment results in a count for each gene resulting in a gene list rank ordered by their importance for growth in the tested condition.

2.2. Yeast Deletion Pool Construction. The yeast deletion collections were stored as individual strains in YPD containing 7% DMSO at −80°C, in 96-well plates. The plates were thawed, mixed, and robotically pinned onto YPD agar plates as an array of 384 strains. After two days of growth at 30°C, colonies were consolidated (four plates of 384 to one plate of 1536 colonies) and robotically pinned in triplicate. Cells were grown in 30°C for 2-3 days until colonies formed. Slow

growing strains were grown separately for 2-3 additional days. All plates were then flooded with 5–7 mL of media, scraped and pooled in YPD + 7% DMSO to a final concentration of OD_{600} = 0.84, and frozen at −80°C until use, as described [17].

2.3. Construction of Opticell Culture System and Spaceflight Experiment. In this study, we designed the Opticell Processing Module or OPM (Figure 1) that was capable of maintaining the yeast deletion collection as a pool grown in liquid culture for at least 20 generations in microgravity. The hardware comprised a liquid-sealed system of growth chambers (Opticells) that allowed for gas exchange across polystyrene membranes. Each OPM consisted of three Nunc Opticells held together with a common manifold and valve system that is autoclaved and attached with watertight O-ring seals. A 3 mL syringe connected to the manifold with a Luer fitting is used to transfer liquid between chambers and mix without breaking sterility and with minimal operator intervention. The valve on the manifold has four settings that connect the syringe to the following port locations 1: Off position, 2: Opticell A, 3: Opticell B, or 4: Opticell C. The OPM allows propagation of each deletion collection for a combined ~21 generations of growth when three chambers are used and the inoculum and transfer volumes are 0.5 mL.

To perform a growth assay in the OPM, each of the three chambers was prefilled with 7 mL of sterile growth media. Deletion collection aliquots were preloaded into each syringe and shipped to Kennedy Space Center, frozen in media containing 7% DMSO (v/v) as a cryoprotectant. During final integration at Kennedy Space Center, the OPMs were prechilled to 4°C. Each deletion collection aliquot was thawed, attached to an OPM manifold, injected, and mixed into chamber A. Cultures were maintained at 4°C and flown to the International Space Station (ISS). The growth experiment was initiated on orbit by warming the OPMs to 30°C. After 16–24 h at 30°C, a 0.5 mL sample was removed from chamber A using the same syringe and inoculated into chamber B. The process was repeated 16–24 hours later to inoculate 0.5 mL of sample from chamber B into chamber C. After an additional 16–24 hours, the OPMs were cooled back down to 4°C to greatly reduce any further growth and preserve the samples for return to Earth and postflight analysis. Exponential yeast growth leads to early depletion of growth media nutrients and significant retardation of further growth well before 16–24 hours. Growth is limited by media volume and strain distribution within the yeast deletion library reaches a steady state within that Opticell.

2.4. Next Generation Sequencing. The flight samples that returned from the ISS were handled in parallel with the ground control set. The OPM was disassembled into its three Opticells, and the entire contents were transferred to a storage tube using a blunt needle connected to a 20 mL syringe. One mL of each sample (at a final OD_{600} of 1.0-2.0) was processed to extract genomic DNA. Purified deletion pool DNA was amplified in two separate PCR reactions as described [17] and the amplicons purified prior to sequencing on an Illumina HiSeq2000. Each purified amplicon library was sequenced to a minimum depth of 500 counts/strain/sample as described [18]. Duplicate experiments were performed for all conditions, to ensure that at least one complete time course was collected for each pool (heterozygote and homozygote) and each condition. Due to failures in sample processing, several time points were not recovered or did not meet our in-house quality metrics (e.g., if sequence counts/strain were below threshold values). Accordingly, we focused on evaluating each experimental condition using singleton data as described in Table 1.

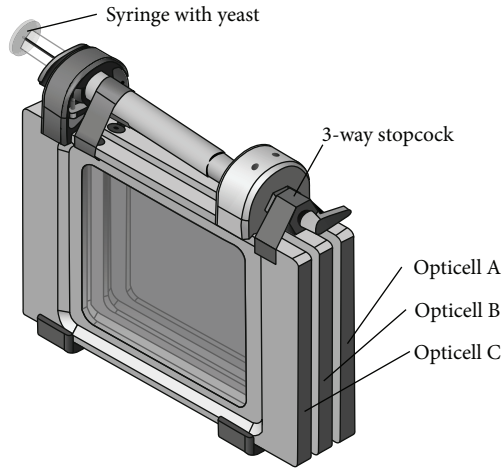

Figure 1: The Opticell Processing Module (OPM) designed for propagation of each deletion collection for ~21 generations of growth. The OPM comprises three commercially available optically clear chambers (Opticells, Nunc) that are joined by a manifold and scaffold that can be autoclaved and assembled rapidly. The manifold contains a multiway valve unit which mates to each Opticell or to an the off position using O-ring seals. The opposite side of the valve contains a Luer fitting into which a standard 3cc syringe is attached. To perform a growth assay in the OPM, each of the three chambers is filled with 7 mL of sterile growth media. Deletion pools are loaded into the inoculation syringe and then injected into Chamber A of the OPM, precooled to 4°C. Growth is initiated by warming the unit to 30°C. After 16–24 h, 0.5 mL is removed from Chamber A and injected and mixed into Chamber B using the same syringe. This is repeated to continue multigenerational growth in Chamber C.

2.5. Data Analysis. All computational analyses were performed using *R* [19] unless otherwise indicated.

2.5.1. Normalization of Sequence Counts. Sequence counts for each strain in each experiment were quantified and normalized according to [18]. Briefly, each 20-mer barcode was amplified with primers comprised of the common barcode primers in addition to the sequences required for cluster formation on the Illumina flow cell. For multiplexed Illumina sequencing, 5-mer tag sequences were incorporated into each primer between the Illumina and barcode primer sequences. This multiplexing tag allowed postsequencing assignment of each amplicon to a particular experiment. Results for the 7-generation time point of the heterozygous deletion pool grown in spaceflight without NaCl did not pass our quality

Table 1: Experimental samples collected and available for analysis.

Condition	Zygosity	Generations
Ground	Homozygous	7, 14, 21
Ground + 0.5 M NaCl	Homozygous	7, 14, 21
Flight	Homozygous	7, 14, 21
Flight + 0.5 M NaCl	Homozygous	7, 14, 21
Ground	Heterozygous	14, 21*
Ground + 0.5 M NaCl	Heterozygous	7, 14, 21
Flight	Heterozygous	14, 21*
Flight + 0.5 M NaCl	Heterozygous	7, 14, 21

*7-generation samples from the indicated condition were not available for analysis due to failures in sample processing or failure to meet in-house quality metrics as described in Methods.

control and, consequently, that time point was omitted from analyses of the heterozygous pool without NaCl. All other counts were mean-normalized between experiments such that each experiment had the same mean count. We added ten pseudocounts to all sequence tag tallies (and, thus, all subsequent gene tallies) to prevent division by zero during data analyses (see Table S1 and Table S2 for mean normalized counts in Supplementary Materials available online at http://dx.doi.org/10.1155/2014/976458).

2.5.2. Barcode Selection for Each Strain. For each strain, we used signal from only the upstream or the downstream barcode (relative to the deletion site). First, we assumed that barcode counts close to zero represent background noise (e.g., possibly due to incorrect mapping of reads to barcodes). We thus selected a background threshold (*bgThreshold* = 100; see Parameter Selection), assuming that counts below it do not accurately reflect strain abundance. Then, for each time course, we filtered out barcodes where the average (normalized) count for the first 14 generations (the earliest time point with usable data in all experiments) was below *bgThreshold*. This filtering removed all barcodes for ~650–3200 strains (depending on the time course), and these strains were omitted from subsequent analyses; see Supplementary Tables S3 (homozygous strains) and S4 (heterozygous strains).

For time courses that only had two time points (and thus an inefficient number to compute fits), strains that still had two barcodes after filtering were represented by their upstream barcodes due to their overall better behavior observed in a previous study [20]. For other time courses, linear fits (with and without the time logged) were computed for each remaining barcode. We defined the best fit as the fit with the lowest residual sum of squares (RSS) and used the F-test to compute a P value estimating the significance with which the fitted model is better than the null model (of a flat line at the average count value). The Benjamini and Hochberg method was used to correct the P for multiple comparisons and generate FDR values [21]. Strains with two remaining barcodes were represented by the barcode with the higher R^2 (a measure of the amount of variation in the data explained by the fitted model), because they manifest less noise and better fit the data.

2.5.3. Parameter Selection. The selected normalization method (tested mean and quartile normalization) and *bgThreshold* (tested 50, 100, and 150) is the combination that resulted in the most significant enrichment of slow growing strains identified in the heterozygous deletion pool, sampled every two generations for 20 generations (data not shown), with slow growers identified in a previous study [22]. Briefly, we defined slow growers as those exhibiting sizable decreases in abundance over time. The significance of the decrease was estimated with FDR values (see Barcode Selection for Each Strain), and the magnitude was estimated with $\Delta\text{AUC} = (\langle\text{area under the growth curve}\rangle - \langle\text{area under the flat growth curve}\rangle)/(t_{\max} - t_0)$, where the flat growth curve is fixed at the t_0 abundance level, and the area under a curve is estimated using the trapezoid method. Also, if at some time point the abundance of a strain is less than or equal to *bgThreshold* and remains at negligible levels for the rest of the time course, we identified the strain as slow growing.

2.5.4. Identification of Significant Fitness Defects in Time Point Comparisons. To identify strains that exhibited significant fitness defects at a later time point (14 or 21 generations) compared to the first time point (7 generations), normalized counts less than *bgThreshold* were first forced to equal *bgThreshold*. Then, for each strain, we computed $\log_2\text{ratio} = \log_2(\text{abundance}_{7G}/\text{abundance}_{14G/21G})$ where abundance_{yG} is the count of the strain at y generations. For a given time point, robust Z scores were computed from the set of $\log_2$ratios; for example, $Z_i = (\log_2\text{ratio}_i - \langle\log_2\text{ratio median}\rangle)/\langle\log_2\text{ratio MAD}\rangle$ for strain i. Each Z_i was then used to obtain P_i from the standard normal distribution, and we assume that strains with low P values are outliers in the distribution of $\log_2$ratios. Moreover, strains with counts above *bgThreshold* at the first time point and counts equivalent to *bgThreshold* at the later time point of interest are defined as having dropped out. Taken together, we define strains with significant fitness defects at a specific time point as strains with $\log_2\text{ratio} \geq 1$ and $P \leq 0.001$ and/or strains that dropped out (Table S5, Table S6).

2.5.5. Spaceflight versus Ground Comparisons. For comparisons involving specific time points, we identified the set of strains that exhibited significant fitness defects (relative to the first time point) in the flight condition but not in the ground condition. This set is then further restricted to the set of strains with useable data in both conditions.

2.5.6. Gene Ontology (GO) Enrichment Analysis. We obtained gene ontology (GO) annotations of yeast genes from the *Saccharomyces* Genome Database (downloaded on May 26, 2012). GO biological processes that were too specific (containing less than five genes) or too general (containing greater than 300 genes) were excluded from the analysis.

Given a query set of genes (e.g., genes deleted from a set of (flight-ground) strains), we used the hypergeometric test to obtain a P value estimating the significance with which the set is enriched with genes annotated to a given biological process, relative to a gene universe defined as the set of genes with usable data for both flight and ground conditions. Due to a

limited number of significantly enriched processes following correction for multiple comparisons (FDR ≤ 0.1), here we report significantly enriched processes prior to the correction ($P \leq 0.01$).

We visualized GO enrichment results with enrichment maps shown in Figures 2 and 3 that were generated using an approach similar to the Enrichment Map Cytoscape Plugin v1.1 [23, 24]. In contrast to the plugin, the nodes in each map were clustered with MCL (inflation = 2), using the overlap coefficient computed by the plugin as the similarity metric (coefficients less than 0.5 were set to zero). Nodes in the same cluster were assigned the same node color, and a cluster label was determined based on common themes in the processes within the cluster. Moreover, the size of a node was made to be proportional to the significance with which the corresponding process is enriched [$-\log_{10}(P)$]. Each bar plot summarizes the genes that contribute the most to the enrichment of processes with the same node color as the plot border. Specifically, a plot shows the flight-associated genes that are annotated to the largest number of relevant processes (if more than 10 genes, only the top 10 are shown). For each gene, the bar length is proportional to a fitness defect measure (i.e., $\log_2$ratio).

The enrichment maps also combine two sets of enrichment results, with the processes enriched in one set shown with circle nodes, the processes enriched in the second set shown with square nodes, and the processes enriched in both sets shown with diamond nodes.

2.5.7. Similarity between Flight-Associated Genes and Compound-Associated Genes. We previously treated pools of yeast deletion strains with ~3200 compounds separately [13]. Each compound was subsequently associated with a set of genes deleted from strains that exhibited significant fitness defects induced by the compound. Like sets of flight-associated genes in this study, sets of compound-associated genes were assessed for enrichment of genes annotated to specific biological processes (as described above), resulting in an "enrichment profile" for each condition of interest. In each profile, each process is associated with a P measuring the significance of enrichment. Similarity between a pair of enrichment profiles was computed by concordance of $-\log_{10}(P)$ across all processes common to both profiles, where concordance is like Pearson correlation except that scale is not ignored. Compounds with enrichment profiles that are most similar to a given flight enrichment profile may induce cellular responses that are most similar to the response induced by flight.

3. Results and Discussion

Because we cannot distinguish the individual parameters that include flight, lack of gravity, and increased radiation, for the purposes of this paper, these are referred to collectively as "spaceflight" throughout the text. To measure the effects of spaceflight on the rate of yeast growth in the Opticell, we inoculated 0.5 mL of a yeast deletion pool into 7 mL of YPD, resulting in a starting OD_{600} of ~0.06/mL and incubated at 30°C. Following growth for ~24 hr (~7 generations), 0.5 mL of the saturated culture was inoculated into the second chamber. This process was repeated for the final growth phase in the third chamber. Population doubling time was ~100 min in microgravity compared to ~90 min in ground-based controls. Each sample was grown for seven generations/Opticell for a total of 21 generations (Table 1). Doubling times were back-calculated using the OD_{600} of the samples collected at each time point.

The morphology of Opticell-grown yeast in spaceflight was indistinguishable from static controls when observed by light microscopy; for example, budding pattern, overall shape, and size were not detectably different in the two conditions. On scanning electron microscopy, there were budding polarity and ruffling changes in every field, but there were no consistent differences (data not shown).

We assessed the yeast deletion collection samples for patterns of strain sensitivity in the following manner: barcode counts for each strain in each sample were measured and normalized as described in Methods. The counts were used to rank each strain in each sample in order of their importance for growth. Four different samples were available from both spaceflight and ground cultures: (1) homozygous deletion collection in YPD, (2) homozygous deletion collection in YPD plus 0.5 M NaCl, (3) heterozygous deletion collection in YPD, and (4) heterozygous deletion collection in YPD plus 0.5 M NaCl. Each culture was sampled at three different time points, 7 generations, 14 generations, and 21 generations, and shown in Table 1. Samples from ground controls were compared to the corresponding samples grown in microgravity on the ISS.

We analyzed changes in strain abundance by comparing each time point to a later time point. Using this approach allowed us to capture those strains that became depleted in any seven-generation interval. Strains with sizable decreases in measured abundance or with abundances that drop to background levels (and remain there) were identified as exhibiting fitness defects (FDs). Moreover, strains with flight-specific FDs were identified by subtracting the strains with FDs in the ground condition.

For the purposes of our gene ontology (GO; http://amigo.geneontology.org) enrichment analysis, we considered the homozygous and heterozygous data separately. Based on a wealth of published data [14, 15], the homozygous, nonessential deletion collection tends to reveal a similar set of genes involved in pathways required for resistance to/survival in multiple environmental conditions, whereas the heterozygous collection of all strains tends to be more specific, identifying essential proteins uniquely required for growth in a specific condition [13].

For the homozygous deletion collection, strains that were depleted from the pool specifically in spaceflight conditions are significantly enriched for genes in biological processes related to different aspects of RNA metabolism and catabolism, including ribosome biogenesis, regulation of ribosomal protein transcription, cytoplasmic RNA translation, rRNA processing, tRNA modification, and mRNA decay (Table 2, Figure 2, and Table S5). We also found that processes related to DNA integrity were required for survival in spaceflight. In particular, the linked processes of DNA repair and DNA recombination and replication as well as

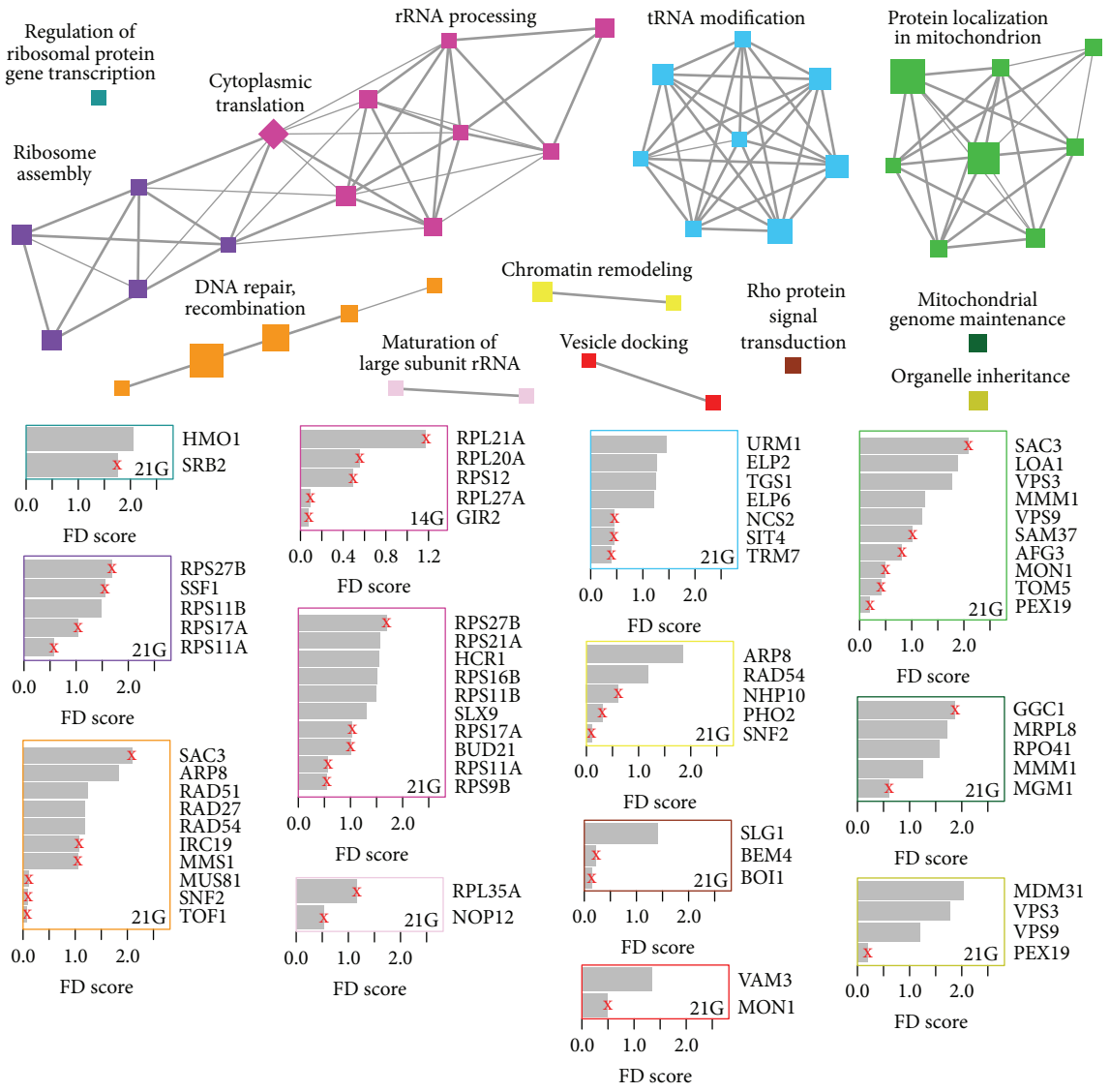

FIGURE 2: Biological processes enriched amongst genes associated with flight-specific fitness defects at different time points in the homozygous deletion series. Each node represents a significantly enriched gene ontology (GO) biological process (hypergeometric test $P \leq 0.01$). A circle node indicates enrichment at 14 generations compared to 7 generations (the first time point), a square node indicates enrichment at 21 generations compared to 7 generations, and a diamond node indicates enrichment at both 14 generations and 21 generations (see Methods). Node size is proportional to the significance of enrichment $[-\log_{10}(P)]$. Node color indicates processes that share genes (see Methods) and summary labels are shown for nodes of the same color. Edges indicate ≥ 50% gene overlap between connected processes; width is proportional to the degree of overlap. Each bar plot provides fitness defect (FD) scores for genes that contribute to the enrichment of processes with the same node color as the plot border. Specifically, the length of a bar is proportional to the $\log_2(\text{abundance}_{7G}/\text{abundance}_{14G/21G})$, where abundance_{yG} represents the abundance of the corresponding gene deletion strain at y generations (see Methods). An "x" on the bar indicates that the abundance of the strain lowers to background level at later time point.

chromatin remodeling were all required for resistance to the effects of spaceflight. Finally, these DNA repair requirements extend to the mitochondria, which, by virtue of its small genome, is hypersensitive to DNA damage. Consistent with this, we found that genes required for both mitochondrial maintenance and proper protein localization to the mitochondria were enriched in the homozygous samples.

The enrichment of these particular processes is consistent with a general induction of DNA damage, which, in turn, perturbs RNA biogenesis [25]. Interestingly we have previously observed this phenomenon with a class of therapeutics that act as nucleotide analogs, such as 5-fluorouridine and fluorocytosine (described in detail below). Additionally, it is particularly noteworthy that, although we do see evidence of a requirement for RNA and DNA processing genes in spaceflight alone, the requirement is exacerbated when spaceflight is combined with the additional hyperosmotic stress imposed by the addition of 0.5 M NaCl (Table S6).

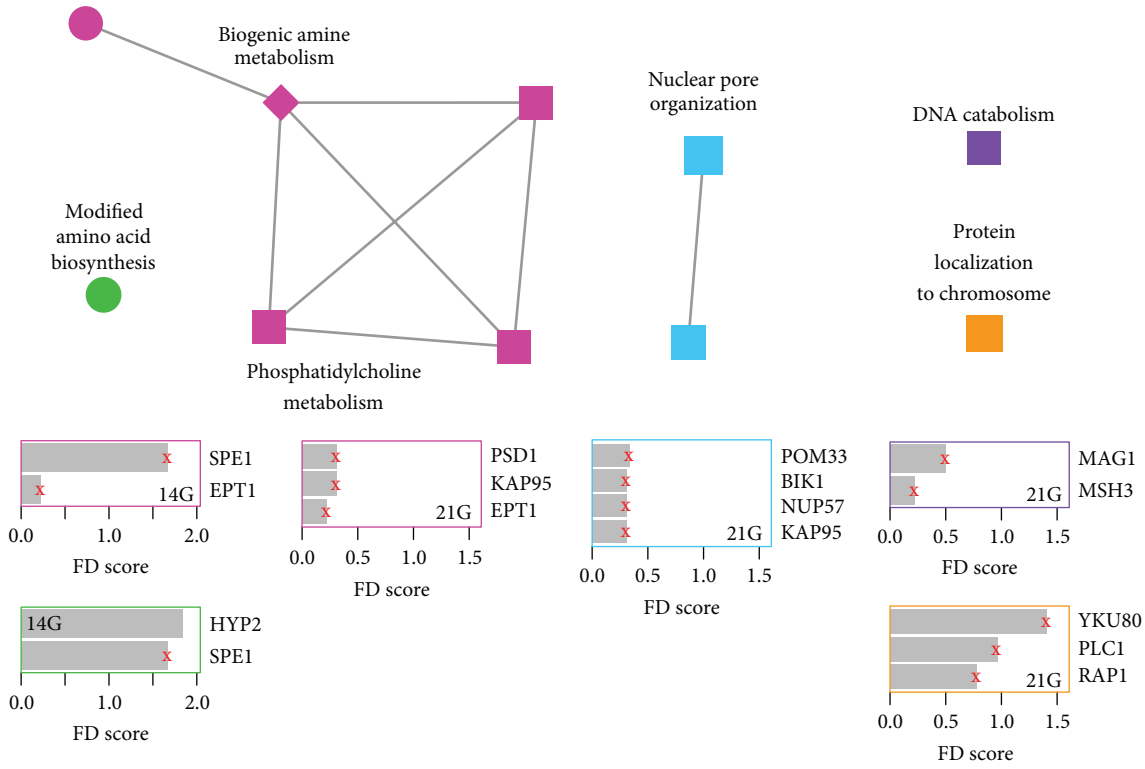

Figure 3: Biological processes enriched amongst genes associated with flight-specific fitness defects in the presence of NaCl, at different time points in heterozygous deletion samples. Each node represents a significantly enriched gene ontology (GO) biological process (hypergeometric test $P \leq 0.01$). Nodes, edges, and plots are as specified for Figure 2.

Table 2: Effects of spaceflight on yeast genome responses identified with the homozygous deletion series.

General pathway	GO biological process
RNA metabolism and catabolism	(i) Ribosome biogenesis (ii) Regulation of ribosomal protein transcription (iii) Cytoplasmic RNA translation (iv) rRNA processing (v) tRNA modification (vi) mRNA decay
DNA integrity	(i) DNA repair (ii) Recombination and replication (iii) Chromatin remodeling (iv) Mitochondrial maintenance (v) Proper protein localization to the mitochondria

We speculate that the added salt stress potentiates the DNA-damaging effects of spaceflight via the induction of reactive oxygen species (ROS). The ability of salt stress to induce ROS and subsequent DNA damage has been previously reported [26] and, in particular, the yeast mitochondria appears to be hypersensitive to this type of stress, consistent with its small genome being susceptible to the effects of DNA damage [27]. Furthermore, mitochondrial protein abundance has been shown to rapidly increase upon osmotic shock, and therefore the enrichment for mitochondrial protein localization we observe may reflect this requirement.

To gain further insight into the pathways that modulate the response to both microgravity stress and combined spaceflight and salt stress, we used the GO enrichment profiles to query a database of over 3200 distinct drug treatments of the yeast deletion collections [13]. Specifically we quantified the similarity between the GO enrichments by computing the concordance of $-\log_{10}(P)$ between any two profiles, where P measures the significance of enrichment of a single GO category. These concordance values are similar to Pearson correlation values; that is, values closer to one indicate greater similarity between profiles, except that high concordance also requires the scale of values to be similar between the profiles. When calculating concordance, we focused on GO biological process enrichment profiles (Table S7).

One of the strong concordances was observed with 5-fluorouridine (0.42), an FDA-approved anticancer drug that is thought to also act by two mechanisms: (i) inhibiting thymidylate synthetase and (ii) through metabolism into cytotoxic ribonucleotides and deoxyribonucleotides that can be incorporated into DNA and RNA (Table 3) [14]. In addition to being incorporated in DNA and RNA, we and others have shown that the drug has been shown to inhibit the essential ribonuclease activity of the exosome complex [28]. Similarly, carmofur, a derivative of 5-fluorouracil, displays a concordance of 0.34. A similar concordance is seen with

Table 3: Concordance between drug effects and spaceflight effects on yeast genome responses identified with the homozygous deletion series (+NaCl).

Drug (concordance)	Biological function
5-Fluorouridine (0.42) 5-Fluorouracil (0.36) Carmofur (0.34) 5-Fluorocytosine (0.35)	Pyrimidine analogs that inhibit thymidylate synthase and are metabolized into cytotoxic ribonucleotides and deoxyribonucleotides that can be incorporated into DNA and RNA
8-Methoxypsoralen (0.32)	DNA-damaging agent
Diallyl disulfide (0.4)	Increased glutathione-S-transferase changes redox state by binding electrophilic toxins

5-fluorocytosine (5-FC), whose activity is identical to 5-fluorouracil (5-FU). Finally, 8-methoxypsoralen, a DNA-damaging agent that, upon photoactivation, conjugates and forms covalent bonds with DNA, shows a congruence of 0.32. This compound causes the formation of both monofunctional (addition to a single strand of DNA) and bifunctional adducts (crosslinking of psoralen to both strands of DNA) that ultimately result in cell death.

We also found high concordance to the diallyl disulfide profile (0.40), an agent that has been demonstrated to be efficient for detoxification of a variety of cells. Diallyl disulfide and related garlic derivatives have been shown to significantly increase the production of the enzyme glutathione S-transferase (GST), which binds electrophilic toxins in the cell. Overloading the cell with inhibitory doses of diallyl disulfide reveals genes required for survival in the presence of increased reactive oxygen species (ROS) [29].

In the case of the heterozygous collection, we found significant GO enrichments for the following categories: lipid metabolism, DNA catabolism, and regulation of translation and posttranslational modification (specifically protein phosphorylation) (Figure 3). As expected (based on previous studies of the heterozygous collection), both the number of genes associated with FDs and the number of enriched categories are considerably smaller than those derived from the homozygous collection [30]. This likely reflects two related phenomena: first, genes that when deleted in heterozygotes are sensitive to spaceflight encode proteins that participate in the pathways identified in the homozygous collection, where the fitness defect is stronger because the gene is completely absent. Second, none of these heterozygote strains encode a direct target of the perturbation.

Interestingly, when we searched for drug profiles with high concordance with the spaceflight profiles derived from the heterozygous collection, we detected modest concordance with two human chemotherapeutics, mitoxantrone (concordance = 0.19), and Epirubicin (congruence 0.142). Both of these agents damage DNA by intercalating into the DNA double helix and also by stabilizing the cleavable complex that is the substrate of topoisomerase II [31–33].

4. Conclusions

The experiments presented here represent a proof of principle for conducting full genome environmental screens in spaceflight using robust hardware that can recapitulate a full automation suite with environmental control in the space of a small suitcase. The performance of this platform is significant for spaceflight studies and promises to enable terrestrial experiments in extreme environments that will have direct application to microbial bioprocessing for manufacturing, alternative fuel development, and basic research. The results from these experiments suggest that spaceflight has subtle but significant effects on core cellular processes including growth control via RNA and ribosomal biogenesis, metabolism, modification, and decay pathways. Furthermore, significant roles for DNA repair and replication, response to pH signaling, control of gene expression, and mitochondrial function were observed. The yeast chemogenetic analysis of spaceflight samples presented here strongly implicates DNA and RNA damage as the major ground-based analogs of spaceflight stress. Given the unique and substantial radiation exposure in space, this is consistent with major radiation-mediated effects. Unfortunately a 1 g control on ISS that might have allowed better discrimination between the contributions of space radiation versus the effects of microgravity on yeast responses was not available to us at this time. Current ongoing experiments are designed explore these effects and dissect them from other potentially confounding variables. The high concordance to the profile induced by diallyl disulfide suggests increased glutathione S-transferase, binding of electrophilic toxins, increased reactive oxygen species, and change in redox state. These pathways, which are required for survival in spaceflight, can guide future experiments in two fundamental ways: firstly by suggesting environmental modifications that can bolster cellular and organismal integrity by avoiding further stress to these pathways, and secondly, by identifying drug stresses that can exacerbate these pathway requirements in an effort to control pathological cell growth in the case of proliferative diseases.

Abbreviations

AUC: Area under the curve
BP: Biologic processes
DMSO: Dimethyl sulfoxide
FD: Fitness defect
FDR: False discovery rate
GO: Gene ontology
GST: Glutathione S-transferase
ISS: International Space Station
MAD: Median absolute deviation
MCL: Markov Clustering Algorithm
OD: Optical density
OPM: Opticell Processing Module
PCR: Polymerase chain reaction
ROS: Reactive oxygen species
RSS: Residual sum of squares
YPD: Yeast peptone dextrose.

Conflict of Interests

None of the authors have any commercial associations that might create a conflict of interests.

Acknowledgments

These studies were supported by NASA Grant no. NNX10AP01G. The authors thank NASA for spaceflight access under the auspices of the International Space Station National Lab Pathfinder program. This material is the result of work supported with resources and the use of facilities at the Durhan Veterans Affairs Medical Center and the Office of Research and Development, Department of Veterans Affairs, Veterans Health Administration. Sequencing was performed, in part at UBCSeq, Vancouver. Contents do not represent the views of the Department of Veterans Affairs or the United States of America.

References

[1] R. Herranz, R. Anken, J. Boonstra et al., "Ground-based facilities for simulation of microgravity: organism-specific recommendations for their use, and recommended terminology," *Astrobiology*, vol. 13, no. 1, pp. 1–17, 2013.

[2] J. J. van Loon, E. H. T. E. Folgering, C. V. C. Bouten, J. P. Veldhuijzen, and T. H. Smit, "Inertial shear forces and the use of centrifuges in gravity research. What is the proper control?" *Journal of Biomechanical Engineering*, vol. 125, no. 3, pp. 342–346, 2003.

[3] T. G. Hammond and J. M. Hammond, "Optimized suspension culture: the rotating-wall vessel," *American Journal of Physiology: Renal Physiology*, vol. 281, no. 1, pp. F12–F25, 2001.

[4] M. R. Benoit, R. B. Brown, P. Todd, E. S. Nelson, and D. M. Klaus, "Buoyant plumes from solute gradients generated by non-motile Escherichia coli," *Physical Biology*, vol. 5, no. 4, Article ID 046007, 2008.

[5] J. Kiefer and H. D. Pross, "Space radiation effects and microgravity," *Mutation Research*, vol. 430, no. 2, pp. 299–305, 1999.

[6] D. Botstein, S. A. Chervitz, and J. M. Cherry, "Yeast as a model organism," *Science*, vol. 277, no. 5330, pp. 1259–1260, 1997.

[7] D. Botstein and G. R. Fink, "Yeast: an experimental organism for 21st century biology," *Genetics*, vol. 189, no. 3, pp. 695–704, 2011.

[8] P. Todd, "Overview of the spaceflight radiation environment and its impact on cell biology experiments," *Journal of Gravitational Physiology*, vol. 11, no. 1, pp. 11–16, 2004.

[9] J. J. W. A. van Loon, "Micro-gravity and mechanomics," *Gravitational and Space Biology*, vol. 20, no. 2, pp. 3–18, 2007.

[10] M. Hughes-Fulford, "To infinity... and beyond! Human spaceflight and life science," *FASEB Journal*, vol. 25, no. 9, pp. 2858–2864, 2011.

[11] T. Fukuda, K. Fukuda, A. Takahashi et al., "Analysis of deletion mutations of the *rpsL* gene in the yeast *Saccharomyces cerevisiae* detected after long-term flight on the Russian space station Mir," *Mutation Research: Genetic Toxicology and Environmental Mutagenesis*, vol. 470, no. 2, pp. 125–132, 2000.

[12] A. Takahashi, K. Ohnishi, S. Takahashi et al., "The effects of microgravity on induced mutation in *Escherichia coli* and *Saccharomyces cerevisiae*," *Advances in Space Research*, vol. 28, no. 4, pp. 555–561, 2001.

[13] A. Y. Lee, R. P. St.Onge, M. J. Proctor et al., "Mapping the cellular response to small molecules using chemogenomic fitness signatures," *Science*, vol. 344, no. 6186, pp. 208–211, 2014.

[14] G. Giaever, P. Flaherty, J. Kumm et al., "Chemogenomic profiling: identifying the functional interactions of small molecules in yeast," *Proceedings of the National Academy of Sciences of the United States of America*, vol. 101, no. 3, pp. 793–798, 2004.

[15] G. Giaever and C. Nislow, "The yeast deletion collection: a decade of functional genomics," *Genetics*, vol. 197, no. 2, pp. 451–465, 2014.

[16] T. Roemer, J. Davies, G. Giaever, and C. Nislow, "Bugs, drugs and chemical genomics," *Nature Chemical Biology*, vol. 8, no. 1, pp. 46–56, 2012.

[17] S. E. Pierce, R. W. Davis, C. Nislow, and G. Giaever, "Genome-wide analysis of barcoded *Saccharomyces cerevisiae* gene-deletion mutants in pooled cultures," *Nature Protocols*, vol. 2, no. 11, pp. 2958–2974, 2007.

[18] A. M. Smith, L. E. Heisler, J. Mellor et al., "Quantitative phenotyping via deep barcode sequencing," *Genome Research*, vol. 19, no. 10, pp. 1836–1842, 2009.

[19] Development Core Team, *R: A Language and Environment for Statistical Computing*, R Foundation for Statistical Computing, Vienna, Austria, 2011.

[20] A. C. Douglas, A. M. Smith, S. Sharifpoor et al., "Functional analysis with a barcoder yeast gene overexpression system," *G3*, vol. 2, no. 10, pp. 1279–1289, 2012.

[21] Y. Benjamini and Y. Hochberg, "Controlling the false discovery rate: a practical and powerful approach to multiple testing," *Journal of the Royal Statistical Society Series B*, vol. 57, no. 1, pp. 289–300, 1995.

[22] A. M. Deutschbauer, D. F. Jaramillo, M. Proctor et al., "Mechanisms of haploinsufficiency revealed by genome-wide profiling in yeast," *Genetics*, vol. 169, no. 4, pp. 1915–1925, 2005.

[23] D. Merico, R. Isserlin, O. Stueker, A. Emili, and G. D. Bader, "Enrichment map: a network-based method for gene-set enrichment visualization and interpretation," *PLoS ONE*, vol. 5, no. 11, Article ID e13984, 2010.

[24] M. E. Smoot, K. Ono, J. Ruscheinski, P.-L. Wang, and T. Ideker, "Cytoscape 2.8: new features for data integration and network visualization," *Bioinformatics*, vol. 27, no. 3, pp. 431–432, 2011.

[25] S. Llanos and M. Serrano, "Depletion of ribosomal protein L37 occurs in response to DNA damage and activates p53 through the L11/MDM2 pathway," *Cell Cycle*, vol. 9, no. 19, pp. 4005–4012, 2010.

[26] G. F. Ribeiro, M. Côrte-Real, and B. Johansson, "Characterization of DNA damage in yeast apoptosis induced by hydrogen peroxide, acetic acid, and hyperosmotic shock," *Molecular Biology of the Cell*, vol. 17, no. 10, pp. 4584–4591, 2006.

[27] N. A. Doudican, B. Song, G. S. Shadel, and P. W. Doetsch, "Oxidative DNA damage causes mitochondrial genomic instability in *Saccharomyces cerevisiae*," *Molecular and Cellular Biology*, vol. 25, no. 12, pp. 5196–5204, 2005.

[28] F. Fang, J. Hoskins, and J. S. Butler, "5-fluorouracil enhances exosome-dependent accumulation of polyadenylated rRNAs," *Molecular and Cellular Biology*, vol. 24, no. 24, pp. 10766–10776, 2004.

[29] Y.-T. Lin, J.-S. Yang, S.-Y. Lin et al., "Diallyl disulfide (DADS) induces apoptosis in human cervical cancer Ca Ski cells via reactive oxygen species and Ca^{2+}-dependent mitochondria-dependent pathway," *Anticancer Research*, vol. 28, no. 5, pp. 2791–2799, 2008.

[30] M. E. Hillenmeyer, E. Fung, J. Wildenhain et al., "The chemical genomic portrait of yeast: uncovering a phenotype for all genes," *Science*, vol. 320, no. 5874, pp. 362–365, 2008.

[31] L. Capolongo, G. Belvedere, and M. D'Incalci, "DNA damage and cytotoxicity of mitoxantrone and doxorubicin in doxorubicin-sensitive and -resistant human colon carcinoma cells," *Cancer Chemotherapy and Pharmacology*, vol. 25, no. 6, pp. 430–434, 1990.

[32] B. Bellosillo, D. Colomer, G. Pons, and J. Gil, "Mitoxantrone, a topoisomerase II inhibitor, induces apoptosis of B-chronic lymphocytic leukaemia cells," *British Journal of Haematology*, vol. 100, no. 1, pp. 142–146, 1998.

[33] P. Vejpongsa and E. T. H. Yeh, "Topoisomerase 2β: a promising molecular target for primary prevention of anthracycline-induced cardiotoxicity," *Clinical Pharmacology and Therapeutics*, vol. 95, no. 1, pp. 45–52, 2014.

Hindawi Publishing Corporation
BioMed Research International
Volume 2015, Article ID 747693, 17 pages
http://dx.doi.org/10.1155/2015/747693

Review Article

RhoGTPases as Key Players in Mammalian Cell Adaptation to Microgravity

Fiona Louis,[1] Christophe Deroanne,[2] Betty Nusgens,[2] Laurence Vico,[1] and Alain Guignandon[1]

[1]*INSERM U1059, Laboratoire de Biologie du Tissu Osseux, Université Jean Monnet, 42023 Saint-Etienne Cedex, France*
[2]*Laboratoire de Biologie des Tissus Conjonctifs, GIGA, Université de Liège, 4000 Sart Tilman, Belgium*

Correspondence should be addressed to Alain Guignandon; guignand@univ-st-etienne.fr

Received 25 April 2014; Revised 14 August 2014; Accepted 9 September 2014

Academic Editor: Monica Monici

A growing number of studies are revealing that cells reorganize their cytoskeleton when exposed to conditions of microgravity. Most, if not all, of the structural changes observed on flown cells can be explained by modulation of RhoGTPases, which are mechanosensitive switches responsible for cytoskeletal dynamics control. This review identifies general principles defining cell sensitivity to gravitational stresses. We discuss what is known about changes in cell shape, nucleus, and focal adhesions and try to establish the relationship with specific RhoGTPase activities. We conclude by considering the potential relevance of live imaging of RhoGTPase activity or cytoskeletal structures in order to enhance our understanding of cell adaptation to microgravity-related conditions.

1. Introduction

Microgravity has been demonstrated to have profound effects on both cellular and molecular levels, including changes in cell morphology [1, 2], alterations of proliferation, growth or differentiation [3, 4], modification of gene expression [5–7], and changes in signal transduction cascades [5, 8]. Single undifferentiated cells *in vitro* respond to altered conditions of gravity, but not all sensors and upstream regulators are known, which limits our understanding of cell sensitivity to microgravity-related conditions and even more to microgravity per se.

There are numerous observations strengthening the idea that cytoskeletal structures and cell surface receptors connected to them play an important role in the regulation of the differentiation potential of stem cells [9]. As changes of shape and of the inner cytoskeletal architecture are common cell responses under conditions of real or simulated microgravity [2], the idea of cytoskeletal involvement in the cellular response to microgravity seems obvious. Moreover, stem cells or multipotent cells are recognized as being sensitive to mechanical stresses, which are known to influence cell commitment [10, 11]. The idea that not only terminally differentiated cells but also multipotent cells are sensitive to microgravity explains why even limited effects on cell commitment could have dramatic consequences. Small GTPases of the Rho family are known to control several aspects of cell dynamics (vesicular transport, traffic, cytoskeleton turnover) [12, 13] and appear to be the key players when trying to gain a better understanding of the effects of microgravity on differentiated and multipotent cells.

This review first attempts to highlight the fact that structures involved in mechanotransduction pathways are responsible for adaptation to microgravity: it will be explained that structural changes observed in cells exposed to real and simulated microgravity may result from specific RhoGTPase regulations. Then, the degree to which the effects of microgravity are important controllers of multipotent cell commitment will be discussed, highlighting the critical role of RhoGTPases in these regulations. The monitoring of RhoGTPase activities in conditions of microgravity is still a challenge as it is a dynamic process that controls other highly dynamic processes such as actin polymerization or focal adhesion turnover. In order to decipher cell adaptation in conditions

of microgravity, the community is in need of a live imaging technology, like the one from Pache et al. [15], but that can be set up in flight! We are conscious of all the difficulties of using Förster resonance energy transfer- (FRET-) based biosensors dedicated to RhoA (Ras homolog gene family member A) and Rac1 (Ras-related C3 botulinum toxin substrate 1), two important actors of this GTPases family, under conditions of microgravity, and we are convinced that research groups that are successful with these types of sensors will provide very exciting results that will eliminate many confounding factors related to conditions of microgravity, such as launch vibrations. We predict that many specific GAP and GEF (resp., RhoGTPases inhibitors and stimulators) will turn out to be key players in cell adaptation to microgravity-related conditions in the future.

2. Mechanotransductors as Gravity Sensors

Discussions of whether an *in vitro* single cell or a cell population can sense changes in the gravitational field are very controversial. The currently most unknown research area involves the mechanism by which the physical event of g-force susception (by invagination, sedimentation, or buoyancy) becomes the biological process of g-force perception. Despite this, an enormous body of experimental data undoubtedly indicates that several types of cultured cells are sensitive to gravity [16, 17]. If, in fact, cells do not fall (collapse), it is because they are supported in some way. This support takes the form of a mechanical stress, set up by the intermolecular forces in response to the distortion produced by gravity. In conditions where gravity is limited (microgravity) (such as those found in an orbiting vehicle) there is thus no distortion produced, and consequently, there is no (limited) mechanical stress.

It seems that undifferentiated cells have structural elements that may play the role of "gravitational sensors" and "sense" the intensity of a mechanical tension and that several intracellular processes can depend on the value of the gravitational force. Theoretical considerations suggest that the forces involved are too small to trigger any response to the changed environment. Several research teams think that these effects are mostly caused by changes at the tissue and organ level [17] and that such environmental changes are stronger and more diverse [18] (e.g., lung, heart, and kidney become larger while spleen or pancreas get smaller in rats [19]). In conclusion, gravitational effects have been considered significant for cells with a diameter of no less than 10 μm [20]. Thus, microgravity seems to alter mammalian cells as compared to bacterial cells which are normally too small.

Actors in the mechanotransduction chain represent key elements involved in microgravity adaptation. Nature provides clear examples of defined mechanoreceptors in eukaryotes such as the statoliths in plants and the otoliths of the inner ear in most species of vertebrates. Similar specialized cells of the sense organs detect pressure (touch) and vibrations and communicate these physical stimulations to the nerves of the afferent pathway up to the brain.

It thus seems that undifferentiated mammalian cells do indeed have structural elements that may play the role of a "gravitational sensor" and "sense" the intensity of a mechanical tension and that many intracellular processes (adhesion, proliferation, survival, contractility, migration, extracellular matrix (ECM) architecture, gene expression, etc.) can depend on the intensity of the gravitational force. The identification of cell structures capable of acting as gravisensors in *in vitro* cells still remains a problem. The general view of mechanosensing is that the overall cell is sensitive and is not a particular element.

In our opinion, the most significant element (*primum movens*) that may impact on cytoskeletal dynamics under microgravity is the displacement of the nucleus. The location of the nucleus is probably dictated by a tension equilibrium between the cyto- and nucleoskeletons and we can imagine that these tensions are constantly changing (in response to signals) and that the nucleus probably oscillates continuously [21]. A microgravity environment may influence the oscillating behavior of the nucleus [22] and then trigger a series of mechanical adjustments that may modulate cell shape and structures, as well as functions by way of transcription activities.

In response to changes in nucleus location, cytoskeletal structures and integrins might be solicited for cell adaptation. The cytoskeleton is a network of three interconnected systems of filaments: the actin microfilaments, the microtubules, and the intermediate filaments. They condition the shape of the cells and the major mechanical functions such as adhesion, polarization, directional migration, as well as proliferation, survival, or apoptosis, gene expression, and architectural organization of their supporting scaffold [12].

Experiments in real and simulated conditions of microgravity have shown that cytoskeletal modulations can occur quickly after variations in gravity have taken place. Numerousarticles have reported on changes within 30 min of the onset of a microgravity simulation, affecting from focal adhesions to signal transduction. Nevertheless cell response can be observed only after few seconds following gravitational changes, for example, in parabolic flight experiments. After only 22 seconds of microgravity, ML-1 thyroid cancer cells showed no sign of apoptosis or necrosis, but the F-actin and cytokeratin cytoskeleton was altered [23]. Endothelial cells also demonstrated no signs of death (after 31 parabolas of 22 seconds) but had a cytoplasmic rearrangement and an alteration of cytoskeleton gene expressions [24]. Concerning mesenchymal stem cells, morphologic characteristics of apoptosis cells (cell shrinkage, membrane blebbing, nuclear chromatin condensation, etc.) and decreased cell viability (rate of apoptosis up to 56.95%) were reported 12 h after parabolic flight experiment. The F-actin stress fibers and microtubules were disrupted and the expression of p53 (mRNA and protein levels) was upregulated [25]. So, gravity-induced response of cells can occur very early, within seconds.

The reorganization of the cytoskeleton is believed to govern the modifications in size and shape of cells and nuclei as well as the patterning, number, and maturation of focal adhesions. The structures of the cytoskeleton, nuclei, and integrins may claim, to varying degrees, to fulfill the role of gravisensors [26].

The most likely candidates to assume the role of these structures are various elements of the cytoskeleton, the nucleus, intracellular organelles, and also certain cell surface receptors (integrins), which interact both with cytoskeletal structures and the extracellular matrix. These structures are able to sense constraints and deformations in the matrix which are caused either by a gravitational or mechanical field and convert this signal into intracellular messengers, which then give rise to a cellular response to the changes in gravity [21, 27]. It is also noteworthy that the cytoskeleton and integrins are not the primary sensors but react in response to their regulatory proteins (controllers of polymerization/destabilization agent).

Numerous cellular processes are controlled by gravity, for example, calcium signaling, mechanotransduction, ligand-receptors interactions, and cell-cell communications, which are all linked [28]. During these mechanisms, cell density is important because force transmission is greatest at cell-cell and cell-substrate focal contacts where signaling molecules are concentrated or clustered (i.e., integrin clustering) [17]. Indeed, transmission of forces from outside the cell through cell-matrix and cell-cell contacts appears to control the maturation or disassembly of these adhesions which rearrange the organization and contractile activity of the cytoskeleton. The cytoskeletal tensions formed at adhesions mediate mechanical signalling [29]. Thus, vinculin phosphorylation determines whether cadherins transmit force and can produce biologically distinct functions [30].

In microgravity, gravity-induced breakage of cell-cell adhesions is reduced. So, cell-cell interaction was shown to be promoted in absence of gravity [31]. Cell adhesion protein expression, specifically proteins found in tight junctions and adherens junctions, was upregulated resulting in enhanced cell-cell contact between cells (endothelial cells [32]). Also, increased levels of E-cadherin were observed in 3D tumor constructs cultured in simulated microgravity [33].

In osteoblasts, a downregulation of cell-cell adhesion proteins, such as catenin, is observed [34] and also a reduction in adhesion proteins such as vinculin and extracellular matrix proteins such as fibronectin [35]. To explain this phenomenon, Levenberg et al. showed that there is an autoregulatory pathway that is activated by the presence of cell-cell or cell-substrate adhesion sites. So, when cell-cell adhesion is enhanced, cell-matrix adhesion is decreased [36]. These adhesion processes are also dependent on Ca^{2+} signaling pathways, such as cell-cell adhesion via E-cadherin. This Ca^{2+} dependence is through activation of the protein kinase C (PKC) second messenger system, as well as activation of phospholipase C (PLC), which in turn activates a signaling cascade, resulting in the release of intracellular Ca^{2+} [37]. This release of intracellular calcium, facilitating the binding of cadherins and β-catenin to the actin filaments comprising the cytoskeleton, resulted in increased strength of cell-cell contacts [38].

And several teams actually found a calcium release in vascular smooth muscle cells after 14 days of hindlimb unloading [39] and a downregulation of Calcium channel after 28 days [40]. Also, a reduction in intracellular calcium concentration is observed after 2 days of simulated microgravity in chondrocytes [41] as well as in neurons [42]. Moreover, in neutrophils, PKC pathway is inhibited under microgravity leading to a decrease in intracellular concentration of Ca^{2+} [43].

All the structural changes observed in cells subjected to microgravity-related conditions are dictated/controlled by dynamic molecular switches of the GTPase family (Figure 1). Small RhoGTPases mainly control the regulation of intracellular traffic and are responsible for cytoskeletal dynamics [44].

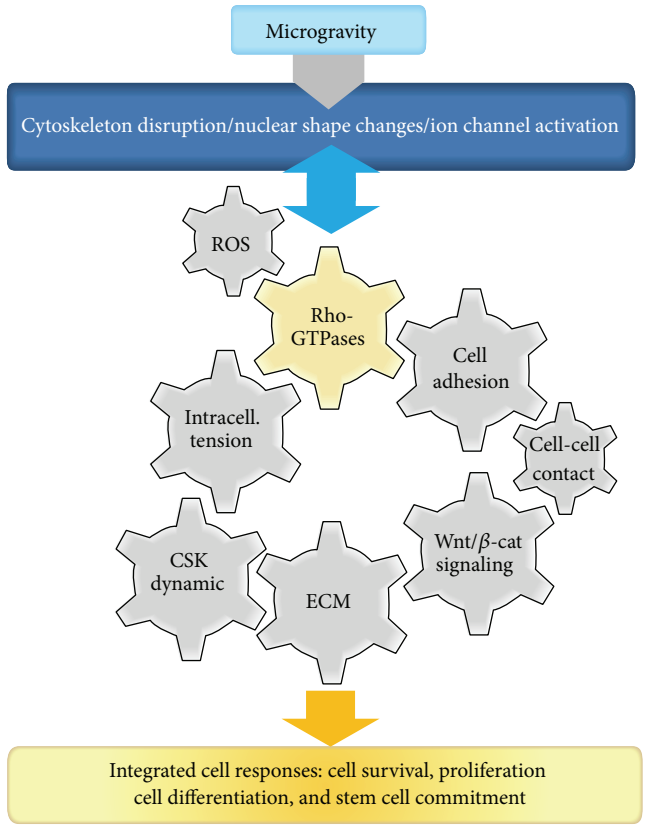

Figure 1: Central role of the RhoGTPases in the integrated response of mammalian cell to microgravity-related conditions. A growing number of studies are revealing that cells reorganize their cytoskeleton, modulate intracellular tension, and initiate nuclear shapes changes when exposed to conditions of microgravity. Most, if not all, of the structural changes observed on flown cells can be explained by modulation of RhoGTPases, which are mechanosensitive switches. RhoGTPases are known for cytoskeletal dynamics control; nevertheless they are also involved in many other aspects as discussed in this review. We identify general principles dependent on RhoGTPases and define cell sensitivity to gravitational stresses such as oxidative stress, intracellular tension, cell-cell and cell-ECM adhesions, and Wnt/β-catenin pathways. We will try to establish that integrated cellular responses in microgravity are related to specific RhoGTPase activities.

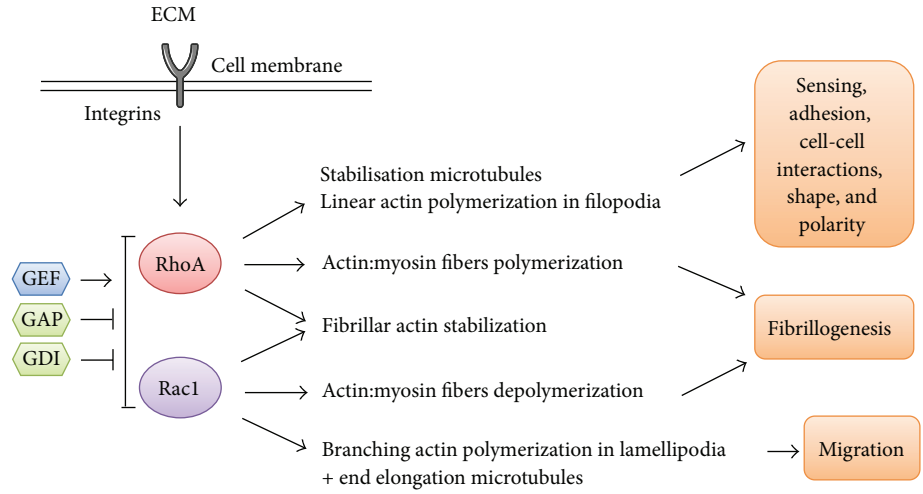

Figure 2: RhoGTPase actions on the cytoskeleton and cell dynamics (modified from [14]). Integrins are necessary for translating the mechanical properties of the extracellular environment into intracellular RhoGTPase-signaling pathways. RhoA influences filopodia formation and focal adhesion assembly and maturation, in addition to controlling stress fiber formation and intracellular tension. Rac1 primarily controls actin assembly and formation of lamellipodia to ensure cell migration. Fibrillogenesis is controlled positively by RhoA and negatively by Rac1. Both RhoA and Rac1 are controlled by specific activators (GEF) and inhibitors (GAP, GDI). Cell adaptation to mechanical/gravitational challenges triggers activation of pathways integrated by RhoGTPases.

3. RhoGTPases: Mechanosensitive Molecular Switches

RhoGTPases, found in all eukaryotic cells, are key regulatory molecules which link surface receptors to the organization and turnover of the cytoskeleton, govern the formation of cell-matrix adhesions, and uphold the transcriptional control of gene expression, cell survival, and proliferation [45]. They are members of the Ras superfamily of small GTP-binding proteins and are divided into three major classes: RhoA, Rac1, and Cdc42. GTPases are molecular switches that use a simple biochemical strategy to control complex cellular processes. They switch between two conformational states: a guanosine triphosphate- (GTP-) bound ("active") state and another ("inactive") state related to guanosine diphosphate (GDP). In their inactive forms, RhoGTPases are sequestrated in the cytoplasm, while upon signaling identified by integrins and growth factor receptors, they switch to their active forms and translocate to the cell membrane [46]. There, they activate distinct and specific effector molecules which in turn regulate the organization of the cytoskeleton and cell-matrix adhesions, thus controlling cellular activities such as adhesion, and also affect cell proliferation and the expression of specific genes (Figure 2) [12]. The cycle between the active and inactive forms is under the direct control of three groups of regulatory proteins. The guanine nucleotide exchange factors (GEFs) catalyze the exchange of GDP for GTP to activate Rho proteins. The Rho proteins are then deactivated by GTPase-activating proteins (GAPs) which increase the intrinsic GTPase activity of the Rho protein, leading to the hydrolysis of GTP to GDP. The third group of proteins involved in the cycle of Rho signaling is guanine dissociation inhibitors (RhoGDI), which hide the isoprenyl groups of GTPases, an action that promotes the sequestration of inactive GTPases in the cytosol. The RhoGDIs also inhibit the release of GDP from the GTPase and contribute to the maintenance of GTPases in an inactive state. The Rho protein cycle is stimulated by agonists acting through G protein-coupled receptors (GPCRs), tyrosine kinase receptors, cytokine receptor activation, and mechanical stresses that mainly govern the activity of the GEFs [47]. The best known actions of the RhoGTPases on mechanical parameters of the cytoskeleton can be underscored by the expression of constitutively active RhoA and Rac1 in cell lines. These modelsshow that RhoA activation leads to better cell spreading but lower mechanical properties, while Rac1 activation induces mechanotransduction [48]. As we assume that exposure to gravitational stress is a mechanical stimulation, Rac1 might be rapidly induced in microgravity-related conditions. These results reveal the importance of RhoGTPases on mechanosensing, cell shape adaptation, or signal transduction. We will summarize below the different controls they can have on cellular mechanisms and metabolism.

4. RhoGTPases Control Cytoskeleton Dynamic

In microgravity, a qualitative and quantitative analysis of the structures of F-actin, β-tubulin, and vinculin has revealed a higher density of filamentous actin and a decreased organization in stress fibers. Exposing mesenchymal stem cells (MSCs) to low gravity affected the distribution of the different filaments and more specifically led to a significant reduction of the F-actin fibers [49, 50], extended filopodia, increased perinuclear distribution, and decreased density [15, 51]. Moreover, other research groups have found evidence of an accumulation of actin at the cell border [52, 53]. This loss of

stress fibers is accompanied by an increase in monomeric G-actin content within the cells. The preceded alterations may be explained by a preferential reduction of RhoA activity.

Indeed, the activation of RhoA or Rac1 leads to the assembly of contractile actin:myosin filaments, protrusive actin-rich lamellipodia, and protrusive actin-rich filopodia, which in turn give rise to both the formation (actin polymerization) and the organization (filament bundling) of actin filaments. Thus, a number of studies (e.g., [54]) have shown that Rho kinase (ROCK) modulates the nonmuscle myosin II (NMM-II) activity by phosphorylation. Another protein, cofilin, regulates actin polymerization and filament elongation. Its phosphorylation leads to inactivation and occurs primarily through LIM kinases (LIMK), which are activated by Rac1-dependent kinases. Moreover, LIMK-dependent phosphorylation of cofilin can also be induced by RhoA acting through its target ROCK, which may be an important event in the stabilization of actin:myosin filaments [55]. Microgravity leads to an alteration of the actin cytoskeleton and consequently to a decrease of integrin signaling that may be caused by the inhibition of RhoA activity. The absence of gravity increases the G-actin form, which reduces cofilin phosphorylation, and is consistent with a decrease in focal adhesions and thus stress fibers [56].

Finally, if a constitutively active RhoA is overexpressed, a recovery stress of the fibers is enabled, similar to what can be observed under normal gravity, and integrin signaling is restored as shown in MSCs [57].

Microtubules play critical roles in eukaryotic cells. They are key structural elements of the mitotic spindle apparatus during mitosis and interphase and serve as tracks upon which motor proteins transport vesicles and other components move throughout the cell [58]. Several studies have mentioned perinuclear clustering in the microtubular network during microgravity [50, 59]. Also, the loss of the radial structure of microtubules has been observed after long stretches of time (4 h) in microgravity [60].

Microgravity has also been proposed to influence microtubules by affecting the self-organization of filaments. According to the theory on self-organization and in a series of *in vitro* studies with a change in gravity direction [61, 62] and microgravity [61], it was clearly shown that microtubule self-organization is sensitive to the direction and the magnitude of gravity, which may explain the results obtained under microgravity. Furthermore, the observed disorganization of microtubules may lead to a reduced rate of chromosome segregation during mitosis, while alterations of actin microfilaments and focal adhesions may also slow down cytokinesis and thus cell proliferation.

RhoGTPases regulate microtubule dynamics in different ways. Rac1 can phosphorylate at Ser16 of the microtubule plus-end-binding proteins (stathmins), which occurs in response to a number of extracellular stimuli [63]. The effect of RhoA on microtubule dynamics is likely to be context-dependent. For instance, in migrating fibroblasts, RhoA promotes the formation of stabilized microtubules. Also, microtubules play a major role in defining cell shape and polarity through the specific interaction of their plus-ends with proteins at the cell cortex. This plus-end capture of microtubules has been attributed to a number of plus-end-binding proteins, whose activities are influenced by RhoGTPases [12]. Altogether, results on microtubules observed in conditions of microgravity may be explained by an alteration of the RhoA and Rac1 activities.

Microgravity has also had an impact on intermediate filaments, which after 12 min in microgravity appeared as large bundles and aggregates in the vimentin network, that is, the most distributed of all intermediate filament proteins [64]. ROCK phosphorylates intermediate filament proteins, specifically at the cleavage furrow during cytokinesis. This cleavage furrow-specific phosphorylation plays an important role in the breakdown of local intermediate filaments and enables an efficient separation of intermediate filament networks [65]. In fact, RhoA and Rac1 induce phosphorylation and reorganization of vimentin through kinases such as RhoA-associated protein kinase 2 (ROCK2), p21-activated kinase (PAK), Src kinase (family of nonreceptor tyrosine kinases), and tyrosine kinases [66].

Concerning lamins, which are nuclear intermediate filaments, Uva et al. showed DNA fragmentation in glial cells after 30 min of microgravity and explained the phenomenon by caspases causing lamina to collapse and chromatin to condense [67]. Proteins linking nucleoskeleton and cytoskeleton complexes (LINC), thus connecting lamina to the cytoskeleton, have been found. When it comes to laminopathy models, in which this LINC complex is disrupted, they lead mostly to RhoA inhibition and lowered cytoplasmic elasticity, while actin and focal adhesion structures are mildly affected [68]. Changes in nuclear structures, that we identified earlier as an important initiator of microgravity effects [22], might explain the RhoA activity inhibition and changes in cell tension evoked under microgravity.

Rac1 was shown to accumulate in the nuclear envelope in addition to being expressed in the nucleoplasm and seemed to have the same pattern as that reported for lamin B [69]. This Rac1 accumulation was proven to promote cell division. In microgravity, the altered proliferation observed by Dai et al. or Damm et al. [70, 71] is controversial since Yuge et al. [72] rather found an increased proliferation in human mesenchymal stem cells. We thus suggest, based on our results obtained on rat osteosarcoma [73], that the lower proliferation might be explained by a reduced Rac1 activity in conditions of microgravity.

5. RhoGTPases as Regulators of Cell Adhesion and Matrix Remodeling

Integrins are transmembrane receptors that mediate the attachment between a cell and its surroundings, such as other cells or the ECM. In signal transduction, integrins convey information about the chemical composition and mechanical status of the environment into the cell. Therefore, in addition to transmitting mechanical forces, they are involved in cell signaling and the regulation of cell cycles, shapes, and motility [74].

Among the ligands of integrins can be mentioned fibronectin, vitronectin, collagen, and laminin. Then, adapter

proteins such as talin and vinculin link the cytoskeleton to integrins, which attach the cell to the substrate, forming a focal adhesion. A variety of signaling proteins are associated with focal adhesions, including focal adhesion kinase (FAK), which is an important mediator of signaling at these centers. Forces are also transmitted to the substrate at these sites. In fibroblasts, local forces correlate with the area of focal adhesions and actomyosin contractility blocking results in a rapid disruption of focal adhesions [75].

In conditions of microgravity, a reduced focal adhesion-related area (frequently reported [35, 76]) can be explained by the lower tension applied to the cytoskeleton. This situation can be associated with an inactivation of RhoA, and as a result by decreased fibrillogenesis (fibronectin collagen) dramatically limiting integrin signaling. The proof of a reduced integrin signaling is that MSCs have been observed to display changes in the expression levels of collagen-specific integrins after 7 days of cultivation in a rotational bioreactor [77]. In fact, activated expression of the α2-integrin has been seen during the course of MSC differentiation to osteogenesis [53]. In addition, Loesberg et al. found a downregulation of α1, β1, and β3 integrins after 48 h of simulated microgravity [78].

β1 integrin has been shown to be important for mediating the response of MSCs to mechanical stimulation [79]. Upon application of fluid shear stress, an increase in alkaline phosphatase (ALP) activity and expression of osteogenic markers is observed, along with the activation of FAK and extracellular signal-regulated kinase 1/2 (ERK1/2). But when β1 integrins are blocked, FAK and ERK1/2 activation becomes inhibited [79]. Phosphorylation of FAK has also been demonstrated to be important for osteogenic differentiation of human MSCs in response to tension [80]. In microgravity-related conditions, the limitation of integrin signaling can be a plausible explanation for the reduced osteogenesis.

In addition, limitation of the integrin-mediated response can also reduce important negative regulatory pathways. Thus, growth of preadipocytes on a fibronectin matrix inhibits adipocyte differentiation and this effect is overcome when actin filaments are disrupted and promotes a rounding-up of cells [81]. However, β1 in association with α5 binds to fibronectin, and Liu et al. [82] reported the presence of an expression switch from α5 to α6 at the growth arrest stage of differentiation, which is consistent with an ECM change observed during adipogenesis. This switch is necessary in order to go from proliferation to differentiation of preadipocytes and can be explained by integrins $\alpha 6\beta 1$ that bind to laminin and can thus interfere with chromatin and gene regulation.

These two integrins α5 and α6 are coordinately regulated by cyclic adenosine monophosphate (cAMP). Interestingly, cAMP has been shown to be activated in microgravity [83–85]. RhoA and cAMP have antagonistic roles in regulating cellular morphology [86]. Thus, the excessive production of cAMP in microgravity may explain the limitation of RhoA activation during adipogenesis followed by the integrin switch of α5 to α6 to promote adipogenesis. Also, it is well established that cAMP enhances the expression of both CCAAT-enhancer-binding proteins (C/EBP) α and β [87, 88] and initiates adipogenesis via the transcription factor CREB (cAMP response element binding protein) [89].

Concerning Rac1, cell adhesion to fibronectin (α5 integrin) but not to laminin (α6 integrin) is particularly efficient in activating Rac1 [90], leading to osteogenesis via β-catenin/Wnt pathways [91]. In microgravity, fibrillogenesis is rapidly limited [92, 93], which explains the delay or absence of osteogenesis in multipotent cells. The extracellular domains of cadherins and β-catenin provide a link to α-catenin and the actin cytoskeleton [94]. Upon tyrosine phosphorylation, β-catenin also plays a significant role in signaling when translocated to the nucleus to regulate cell proliferation [95].

Noritake et al. [96] have explained the increase in Rac1 during osteogenesis: until subconfluence, cell adhesions accumulate E-cadherins at the sites of cell-cell contacts which induce Rac1, and thus actin-meshwork formation and β-catenin, leading to osteogenesis. In fact, before E-cadherin-mediated cell-cell adhesion is established, GDP-Rac1 is sequestered in the cytosol by Rho GDI. When E-cadherins accumulate, GDP-Rac1 is converted to GTP-Rac1, through the action of a GEF, and is targeted to the plasma membrane releasing β-catenin linked to E-cadherin, which can go to the nucleus [97].

In addition, cell-to-cell physical contact via N-cadherin also plays a crucial role in regulating osteoblastic activity such as alkaline phosphatase activity and β-catenin signaling [98, 99]. Consequently, reduced cell-cell adhesion observed in microgravity, due to limited proliferation, may induce a decrease in Rac1 action and osteogenesis.

Moreover, it has been largely described that matrix rigidity affects osteogenesis. MSCs grown on collagen-I stiff gels (linking to α1 or $\alpha 2$-β1 integrins) have demonstrated activated osteogenesis, whereas softer collagen-I gels prime MSCs for a myogenic lineage [100]. However, cytoskeleton and the dynamic mechanical balance that exists between cells and their ECM support appear as major players in several mechanotransduction pathways [74]. Microgravity decreases the expression of collagen I [101–103], induces matrix metalloproteinases (MMP) production, and reduces the level of fibrillar collagen. Thus, it could be expected that altered conditions of gravity may change the mechanical properties of ECM (i.e., the stiffness). Several studies, for example, McBeath et al. or Shih et al. [104, 105], have shown that osteogenic differentiation becomes increased on stiffer matrices, as evident by type-I collagen, osteocalcin, Runx2 gene expressions, ROCK, FAK, and ERK1/2 induction and alizarin red S staining for mineralization. Consequently, FAK affects osteogenic differentiation through ERK1/2, whereas RhoA and ROCK regulate both FAK and ERK1/2 [105].

In microgravity, an initial modification of cytoskeletal dynamics might be at the origin of the following vicious circle: remodeling of a cytoskeleton is associated with a reduced internal tension (contractility) leading to the dispersion of FA. With such a reduction in FA, the cell tension cannot be restored and fibrillogenesis might be limited. Matrix deposition limitation and MMP activation (Rac1 dependent process [106, 107]) may further reduce the matrix stiffness, thus amplifying the dispersion of FA and reducing cell tension and fibrillogenesis. After a short exposure (from minutes to

hours) to microgravity-related conditions (before fibrillogenesis, MMP production), the matrix stiffness is not modified. We can thus speculate that the ability of the cells to detect the stiff matrix they are normally seeded on has become rapidly impaired. Mechanical information is normally conveyed by ECM and cells by FA adaptation following tensegrity principles (equilibrium of internal and external tension) [21]; in microgravity it seems that the displacement of the nucleus (sensitive to G) conveys the mechanical stimulus and from a tensegrity perspective, the cell adapts to the reduced tension by lowering the ECM tension (interruption of fibrillogenesis and MMP production). The short-term adaptation of the cell to microgravity that we have described up to now seems to be characterized by a rapid reduction of RhoA and an increased Rac1 activity. Altogether, these studies revealed that the control of cytoskeleton remodeling by RhoGTPases impacts on cell adhesion signaling, limiting internal cellular tension as well as ECM fibrillogenesis, and triggers MMP production, thus limiting cell-matrix adhesion and survival.

6. RhoGTPases in Stem Cell Commitment

In simulated microgravity, cellular morphology is drastically changed after 7 days. The MSCs appear rounder and less firmly attached to their substrate than under conditions of normal gravity. Rather, they are very spread out and display a fibroblastic morphology [53].

Since the work by McBeath et al., we know that the shape of a cell affects its differentiation potential [104]. Thus, MSCs that have been allowed to adhere over a larger area are able to differentiate towards the osteogenic lineage while cells adhering to a smaller area are restricted to the adipogenic lineage. These impacts on lineage commitment by mesenchymal stem cells seem to be regulated by shape-induced changes in the RhoGTPase activity and cytoskeletal tension [108]. Yao et al. [109] showed that the cell shape itself is an inherent cue to regulate stem cell differentiation, both with and without external chemical induction factors. Thus, according to McBeath et al. [104], expressing dominant-negative RhoA causes MSCs to become adipocytes, while constitutively active RhoA induces osteoblastic or myocytic differentiation [110, 111].

Concerning Rac1, it has been shown to promote cell adhesion and spreading and thereby to prevent the cell shape change and the establishment of the cortical actin structure necessary for adipocyte formation [109]. Adhering cells are characterized by an elaborate network of stress fibers and focal adhesions and are thus more prone to adopt a fibroblastic cell shape reflecting cytoskeleton tension [112, 113], which seems to be altered in conditions of microgravity.

The cell shape may also depend on the available substrate area and hence the cell density. However, if cellular growth is reduced in microgravity, the cell density will also be altered. Gao et al. [110] found that levels of RhoA activity did not vary substantially, but that the Rac1 activity was significantly higher in well-spread cells during early differentiation than in high-density cells.

They also demonstrated that Rac1 is necessary for osteogenesis and that constitutively active Rac1 inhibited adipogenesis, even if it is important for adipose commitment. Liu et al. [82] showed that an increase in preadipocyte density inhibited the RhoA activity and that a downregulation of the RhoA-ROCK pathway was required for both adipose lineage commitment and maturation [104, 111]. An increased cell density thus appeared to be critically important.

GTPases have also been shown to act in the cell cycle, mitosis, and cytokinesis. RhoGTPases influence the cyclin-dependent kinase (cdk) activity during the G1-Phase of the cell cycle. Thus, RhoGTPases control the organization of the microtubule and actin fibers during cell cycling. An inhibition of RhoA or Rac1 blocks the G1 progression in a variety of mammalian cell types [114, 115]. Also, Rac1 (but not RhoA) stimulates cyclin D1 transcription mediated by NF-κB (nuclear factor kappa-light-chain-enhancer of activated B cells) [116, 117]. Thus, the necessity to downmodulate the Rac1 activity in adipogenesis is that Rac1 may prolong proliferation of preadipocytes, which is consistent with the reported effects of Rac1 on cyclin D1 [90, 118, 119]. In fact, Rac1 accumulates in the nucleus during the G2 phase of the cell cycle and promotes cell division [69]. Concerning the cell division itself, it has been shown that actin:myosin filaments, under the control of ROCK, are required at the cortex to allow positioning of the centrosomes [120]. RhoA also plays a crucial role in the contractile ring function [121].

Microgravity affects the growth, proliferation, and differentiation of osteoblasts. Since the inhibition of RhoA, observed under microgravity, blocks G1 progression [114, 115], this may explain the altered proliferation and differentiation of osteoblastic cells and increased adipogenesis as summarized in Figure 3.

Furthermore, several cytoskeletal components, including Rac1 GTPase activating protein 1 (Rac-GAP1) and Tropomodulin 1, segregate asymmetrically during stem cell division, and overexpression of these proteins may enhance MSC commitment, as already proven with asymmetrical divisions of hematopoietic stem cells to progenitor cells [122].

7. RhoGTPases and Wnt/β-Catenin Signaling Crosstalk

Three Wnt signaling pathways have been characterized: the canonical Wnt pathway, the noncanonical planar cell polarity pathway, and the noncanonical Wnt/calcium pathway. The canonical Wnt pathway leads to regulation of gene transcription, the noncanonical planar cell polarity pathway regulates the cytoskeleton via a RhoGTPase regulation that is responsible for the shape of the cell, and the noncanonical Wnt/calcium pathway regulates calcium inside the cell [123].

Mellor et al. found that Wnt signaling was inhibited in conditions of microgravity [124] and mouse osteoblasts subjected to simulated microgravity were found to have lower levels of several components of the Wnt/β-catenin signaling pathway. This may indicate, even indirectly, the activation of an adipogenic program under microgravity [125]. Moreover, Wan et al. [126] recently demonstrated a changed RhoA and

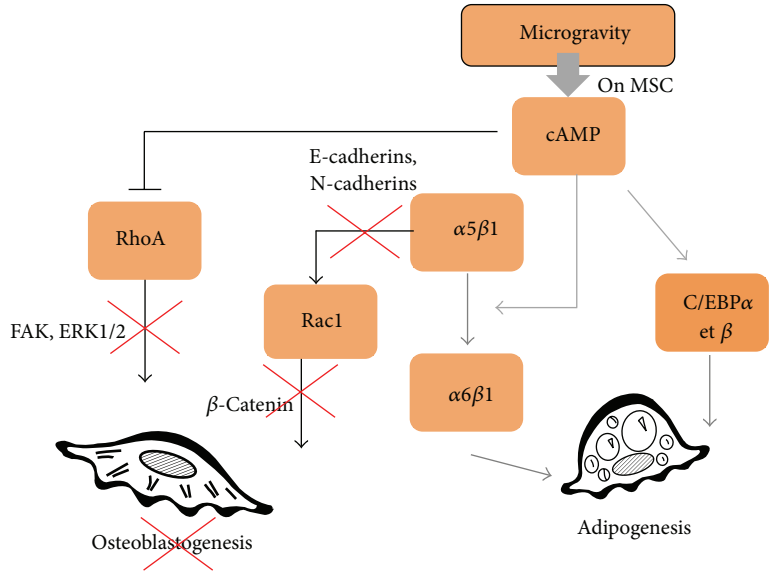

Figure 3: Role of AMPc on RhoGTPases activities and commitment of multipotent cells. Microgravity affects the growth, proliferation, and differentiation of multipotent cells by increasing AMPc production. AMPc contributes to cytoskeleton reorganization as it regulates negatively RhoA activity. Limitation of osteoblastogenesis might be linked to the ability of microgravity to reduce RhoA and Rac1 activities. RhoA and Rac1 activations support osteoblasts differentiation for their respective role in ERK activation and beta-catenin nuclear translocation. Sustained adipogenesis observed in microgravity-related condition might be linked to ability of AMPc to trigger integrin a5b1/a6b1 switch. Signaling through a6b1 integrin is known to support adipogenesis. A direct activation of adipogenic transcription factors (cEBPs) by AMPc has been also described.

β-catenin signaling after 1 and 2.5 h, respectively, in clinorotated osteoblasts. They revealed that both the RhoA activity and the TCF/LEF (T-cell factor-1 and lymphoid enhancing factor-1) activity, a β-catenin recruiter, were downregulated by unloading. However, the inhibition of β-catenin signaling blocked the unloading-induced RhoA suppression, and dominant negative RhoA inhibited the TCF/LEF suppression, revealing a regulation loop between β-catenin, RhoA, and TCF/LEF. Furthermore, while β-catenin signaling seemed to be required for microgravity regulation of RhoA, this response was not mediated by the actin cytoskeleton or intracellular tension [126]. The same was observed for Rac1/β-catenin signaling [91].

The Wnt canonical pathway involves the translocation of β-catenin to the nucleus, and β-catenin has been shown to promote osteogenic differentiation in early osteoblast progenitors *in vivo* [127]. In contrast, other studies have suggested that canonical Wnt signaling may actually promote stem cell renewal and inhibit osteogenic differentiation of osteoprogenitor cells *in vivo* [128], as well as promoting stem cell renewal in human MSCs derived from bone marrow [129]. Arnsdorf and colleagues [130] investigated the role of noncanonical Wnt signaling in mechanically induced osteogenic differentiation of MSCs. Exposure of MSCs to oscillatory fluid flow resulted in a translocation of β-catenin [131] and an upregulation of Wnt5a, which is capable of inducing both canonical and noncanonical pathways. Wnt5a is also necessary for the flow-induced activation of RhoA. However, the inhibition of Wnt5a did not affect the β-catenin translocation, which may instead be regulated by cadherin-catenin signaling. In addition, Santos et al. [132] showed that the activation of the RhoA/ROCK pathway by Wnt5a induced a downregulation of adipogenic markers. It was further reported that RhoA could also be activated by Wnt3a, one of the canonical Wnt family members [133], and that an inhibition of intracellular β-catenin decreased the RhoA activity [134].

Kim et al. [135] also found that Wnt signaling regulated the MSC differentiation into cardiomyocyte-like cells with a concomitant downregulation of RhoA and upregulation of Rac1. Concerning Rac1, it was shown to be a critical regulator in shear stress-driven β-catenin signaling in osteoblasts [91], and constitutively active Rac1 mutant caused a significant enhancement of the TCF/LEF activity.

These studies demonstrate that Wnt signaling is important for mechanically induced differentiation, through RhoA or Rac1 pathways. So, in conditions of microgravity, reduced RhoA, cell shape, and migratory behaviors can be explained by Wnt and β-catenin signaling. Finally, RhoGTPases are regulated by Wnt signaling, but in return, β-catenin location (translocation) is dependent on RhoGTPases. This intricate interplay between both regulatory elements makes them particularly important for the interpretation of microgravity effects.

8. RhoGTPases and Oxidative Stress

One of the first targets of Rac1 to be identified was p67phox, an essential structural component of the NADPH oxidase complex [136]. Since then, Rac1 has been reported to promote

reactive oxygen species (ROS) production in many cells and to mediate the activity of the Nox family [137, 138]. Consequently, Rac1 activation leads to the generation of ROS enabling adipogenesis commitment [139] and reducing osteoblastogenesis [140, 141]. Moreover, GTPases act on the antioxidant master gene Nrf2 (nuclear factor-like 2), which activates a protective adaptive response to oxidative stress through transcriptional activation of antioxidant defense genes [142].

RhoA is involved in Nrf2 phosphorylation, which is necessary for its activation [143]. Nrf2 is a transcription factor for Hace1 (HECT domain and ankyrin repeat containing E3 ubiquitin protein ligase 1), and Hace1 binds and ubiquitylates Rac1 when the latter is associated with NADPH oxidase, thus blocking ROS generation by NOX [143, 144]. So, RhoA activation may limit ROS production and adipogenesis while Rac1 activation may support it. However, several research groups have reported that ROS causes RhoA activation [145, 146], while Nimnual et al. demonstrated that Rac1-mediated ROS production results in the downregulation of the RhoA activity [147]. This is also required for Rac1-induced formation of membrane ruffles and integrin-mediated cell spreading. The GTPase regulation by oxidative cell status thus still remains unclear.

In line with these papers, several research groups, such as Versari et al., have found increased oxidative stress during space flight due to microgravity [148, 149] and cosmic radiations [150]. As RhoA is decreased in microgravity, this could explain the increased production of reactive oxygen species. According to this paper, we can assume that Rac1 activities are increased in microgravity. An upregulated Rac1 activity fits well with enhanced ROS production and improved adipogenesis.

However, a higher Rac1 activity is also consistent with a higher ability for cell migration [151, 152]. Nevertheless, results of migration in space are controversial. Bone marrow cells from rats and human embryonic brain cells show a facilitated cell migration [153, 154], while bone marrow CD34+ cells have a lower migration potential in simulated microgravity [155]. We can interpret the apparent discrepancies in migration results based on the time spent in microgravity: for short-term exposure (from minutes to hours), there are several reasons to believe that RhoA is decreased and Rac1 increased in line with their reciprocal inhibition [156], but for longer exposure (from hours to days), the Rac1-induced ROS production may increase RhoA activation [145, 146] and reduce the Rac1 activity limiting migration capabilities. The missing information in microgravity is related to the lack of measurements of specific RhoGTPase activities.

9. RhoGTPases Activities Monitoring in Microgravity

Meyers et al. showed a reduction in active RhoA (−88% (±2%)) and a decrease in phosphorylation of cofilin after 7 days in microgravity, in addition to the absence of stress fibers [56]. If overexpression of active RhoA is carried out, this enables a recovery of stress fibers and restored integrin signals, similar to those observed in normal gravity in MSC [57]. In simulated microgravity, a decrease in RhoA activity was also observed after 72 h [157, 158]. Unfortunately nothing is known about Rac1 activity. Zayzafoon et al. thus proposed a model in which the cytoskeleton is actually not the first sensor, but a secondary step affected by a gravity-sensitive sensor. In this model, it is the RhoA inactivation that is followed by cytoskeletal changes and transduction at FAs [57], which explains the alterations on MSC differentiations observed in microgravity. To our knowledge, our team is the first to perform RhoA and Rac1 monitoring during osteogenesis and adipogenesis in simulated microgravity using embryonic mesenchymal stem cells. C3H10T1/2 multipotent cells were cultured in modeled microgravity using NASA's rotating wall vessels (RWV) or in control cultures under conditions of earth gravity for up to 8 days, seeded on collagen-coated microbeads (Cytodex 3, Sigma). The results presented in Figure 4 show significant decreases in both RhoA and Rac1 after long-term exposure to simulated microgravity. To our knowledge no comparison can be made with data obtained in real microgravity, unfortunately. Regardless of the limitation of the model when it comes to simulated microgravity-related conditions, these results clearly showed that downregulations of RhoA and Rac1 were compatible with enhanced adipogenesis and limited osteogenesis.

As preservation of active RhoGTPases in flight condition might be challenging, the recent validation of biosensors for imaging of active RhoA, Rac1, and Cdc42 represents an important step in understanding cell responses to microgravity. Despite the critical role of RhoGTPases that we describe in this review, there is a dramatic lack of data concerning the monitoring of their activities during exposure to microgravity particularly in real microgravity. These data are of crucial importance since cell adaptation is a dynamic process; we need to use available technologies such as fused fluorescent proteins and biosensors dedicated to following RhoGTPase activities in order to decipher cell adaptation in conditions of microgravity. On ground experiments, extensive biochemical and profiling studies on mechanotransduction pathways can be performed. In an automated spaceflight, the use of biosensors specific to molecules integrating many pathways such as RhoGTPases should be presented as a simplified and integrated view of cell mechanics. The community is in need of a live imaging data (already validated on ground [159]) that can be now used in flight conditions. We believe that groups that are successful in providing this type of integrated data will surprise our community whose thinking is limited by analysis of fixed images of cells and the monitoring of individual parameters.

10. Conclusion

RhoGTPases represent a unique hub for integration of biochemical and mechanical signals. As such, they are probably very rapidly involved in a cell's adaptation to microgravity-related conditions. Published data describing this adaptation have reported on alterations of the cytoskeleton, adhesion, and fibrillogenesis as well as an enhancement of the ROS

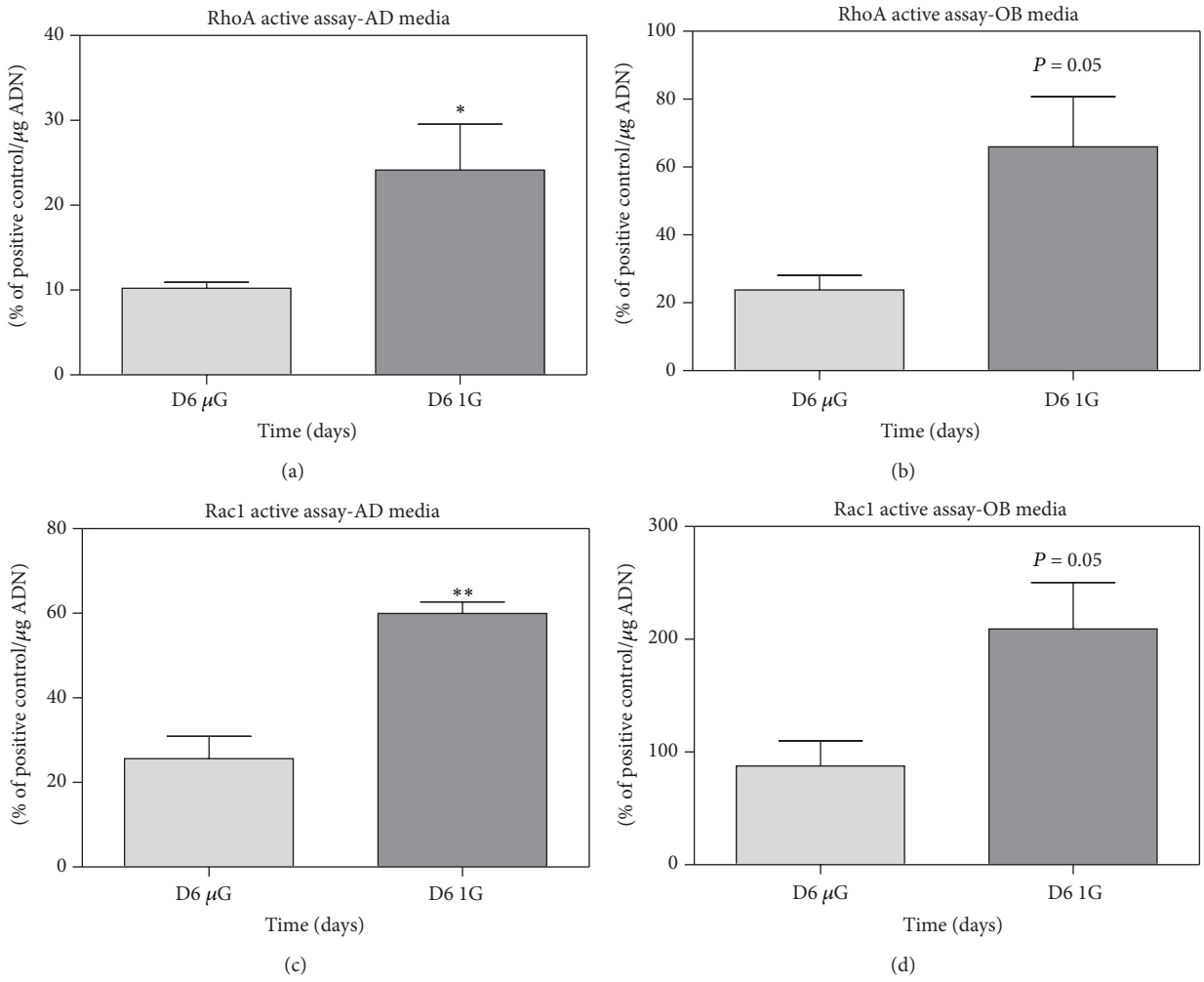

Figure 4: RhoA and Rac1 activities are downregulated after 6 days of culture in simulated-microgravity conditions. Cultures were performed with C3H10T1/2 (multipotent embryonic cells) on collagen-coated microbeads (Cytodex 3, Sigma) for adipogenic induction and on Cytodex 3 beads coated with apatite minerals complexed to collagen for an osteogenic one. The adipogenic media contained 1 μM of rosiglitazone and the osteogenic media 5 mg/mL of L-ascorbic acid, β-glycerophosphate at 10^{-3} M, and retinoic acid at 10^{-5} M, in αMEM. Microbeads with cells were cultured for 2 days in 90 mm petri dishes (untreated for culture) with 10 mL of proliferation media (αMEM), after which the cells were switched 2 days in differentiated media, and finally left for 6 days in a NASA rotating wall vessel (RWV). In parallel, controls were realized by culturing beads in petri dishes. RhoA and Rac1 active assays were performed with specific G-LISA kits (cytoskeleton). The positive controls were pure active proteins of RhoA and Rac1 provided with the kit. The results are expressed as percentage of the positive controls; they show standard error of the mean (SEM) of samples extracted from three independent experiments and are compared with Student's statistical t-test.

production and migration that can be explained by the specific regulation of RhoGTPases. To summarize the literature, we can speculate that after a short exposure of a cell to microgravity, the RhoA activity is depressed and the Rac1 activity increased. For long-term exposure, osteogenesis has been reported to be impaired and adipogenesis promoted. These changes in multipotent cell commitment fit nicely with prolonged depressed activities of both RhoA and Rac1 (Figure 5).

As we are convinced that focal adhesion and F-actin fibers are not the primary sensors of microgravity-related signals (but rather transducers or effectors of the response), many specific GAP and GEF (resp., RhoGTPase inhibitors and stimulators) will emerge as new players in the adaptation of cells to microgravity-related conditions. What are the mechanisms that explain the activation or inhibition of these GTPases regulators? As we try to establish that mechanosensors are involved in cell adaptation to microgravity we can predict that critical players identified in these extreme conditions will in return be recognized in the mechanobiology field.

Abbreviations

ALP: Alkaline phosphatase
C/EBP: CCAAT-enhancer-binding proteins
cAMP: Cyclic adenosine monophosphate
CREB: cAMP response element-binding protein

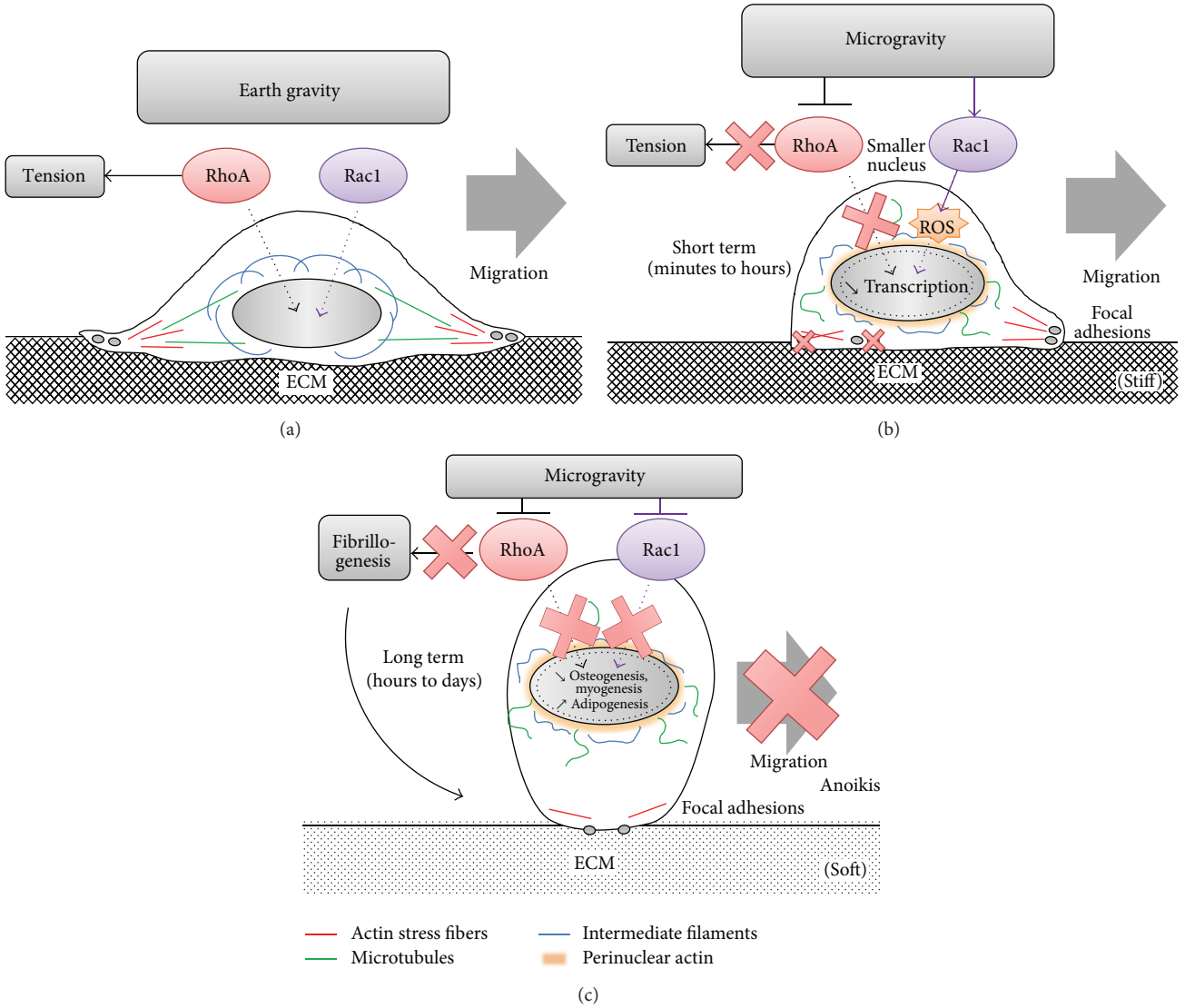

Figure 5: Proposed models describing the regulations of RhoA and Rac1 activities in space-related conditions. On Earth MSCs are well spread and exhibit a tensed cytoskeleton in particular of microtubules, intermediate filaments, and actin stress fibers associated with stable focal adhesions within the extracellular matrix. These elements are controlled by GTPases RhoA and Rac1. We hypothesize that during short-term exposure to microgravity, RhoA might be inhibited to allow cytoskeleton reorganization in respect to the new mechanical status. Cell tension reduction might be mandatory during this adaptation. At the same time, Rac1 is activated to control peripheral actin polymerization and induces ROS production. All these events lead rapidly to a rounder cell shape with disorganization of microtubules, stress fibers, intermediate filaments, and focal adhesions. Transcription may be also altered as nucleus shape is changed. In these conditions, cell is still able to migrate. When exposure to microgravity is prolonged both RhoA and Rac1 might be inhibited explaining decreases in osteogenesis and myogenesis and enhancement of adipogenesis of MSCs. In addition, RhoA inhibition limits fibrillogenesis (a tension-dependent process); extracellular matrix is not properly synthesized and lost its mechanical properties appearing softer for MSCs, reinforcing adipogenesis. At that time, migration is inhibited, consistent with cytoskeleton alterations and Rac1 decrease. MSCs become very round, have low adhesion, and may initiate anoikis.

CSK: Cytoskeleton
ECM: Extracellular matrix
ERK1/2: Extracellular signal-regulated kinase 1/2
FAK: Focal adhesion kinase
FRET: Förster resonance energy transfer
GAPs: GTPase-activating proteins
GDIs: Guanine dissociation inhibitors
GDP: Guanosine diphosphate
GEFs: Guanine nucleotide exchange factors
GPCR: G protein-coupled receptor
GTP: Guanosine triphosphate
Hace1: HECT domain and ankyrin repeat containing E3 ubiquitin protein ligase 1
LIMK: LIM kinases
LINC: Proteins linking nucleoskeleton and cytoskeleton complexes

MMPs:	Matrix metalloproteinases
MSC:	Mesenchymal stem cell
NF-κB:	Nuclear factor kappa-light-chain-enhancer of activated B cells
NMM-II:	Nonmuscle myosin II
Nrf2:	Nuclear factor (erythroid-derived 2-) like 2
PAK:	p21-activated kinase
Rac1:	Ras-related C3 botulinum toxin substrate 1
RhoA:	Ras homolog gene family, member A
ROCK:	Rho kinase
ROCK2:	RhoA-associated protein kinase 2
ROS:	Reactive oxygen species
RWV:	Rotating wall vessels
SEM:	Standard error of the mean
Src family kinase:	Family of nonreceptor tyrosine kinases
TCF/LEF:	T-cell factor-1 (Tcf-1) and lymphoid enhancing factor-1 (Lef-1).

Conflict of Interests

The authors declare that there is no conflict of interests regarding to the publication of this paper.

Acknowledgment

The study was partially funded by the European Space Agency (Microgravity Application Program, MAP "ERISTO") (European Research in Space and Terrestrial Osteoporosis, Contract no. 14232/00/NL/SH) and the French Centre National d'Etudes Spatiales (CNES).

References

[1] P. J. Rijken, R. P. de Groot, W. Briegleb et al., "Epidermal growth factor-induced cell rounding is sensitive to simulated microgravity," *Aviation Space & Environmental Medicine*, vol. 62, no. 1, pp. 32–36, 1991.

[2] M. Hughes-Fulford, "Function of the cytoskeleton in gravisensing during spaceflight," *Advances in Space Research*, vol. 32, no. 8, pp. 1585–1593, 2003.

[3] A. Cogoli, "Fundamentals of space biology: research on cells, animals, and plants in space," in *Cell Biology*, G. Clement, and K. Slenzka, Eds., pp. 121–170, Springer, New York, NY, USA, 2006.

[4] D. Grimm, P. Wise, M. Lebert, P. Richter, and S. Baatout, "How and why does the proteome respond to microgravity?" *Expert Review of Proteomics*, vol. 8, no. 1, pp. 13–27, 2011.

[5] R. P. de Groot, P. J. Rijken, J. Boonstra, A. J. Verkleij, S. W. de Laat, and W. Kruijer, "Epidermal growth factor-induced expression of c-fos is influenced by altered gravity conditions," *Aviation Space and Environmental Medicine*, vol. 62, no. 1, pp. 37–40, 1991.

[6] T. G. Hammond, F. C. Lewis, T. J. Goodwin et al., "Gene expression in space," *Nature Medicine*, vol. 5, no. 4, p. 359, 1999.

[7] Y. Liu and E. Wang, "Transcriptional analysis of normal human fibroblast responses to microgravity stress," *Genomics, Proteomics and Bioinformatics*, vol. 6, no. 1, pp. 29–41, 2008.

[8] O. Ullrich, K. Huber, and K. Lang, "Signal transduction in cells of the immune system in microgravity," *Cell Communication and Signaling*, vol. 6, article 9, 2008.

[9] P. S. Mathieu and E. G. Loboa, "Cytoskeletal and focal adhesion influences on mesenchymal stem cell shape, mechanical properties, and differentiation down osteogenic, adipogenic, and chondrogenic pathways," *Tissue Engineering—Part B: Reviews*, vol. 18, no. 6, pp. 436–444, 2012.

[10] J. C. Chen and C. R. Jacobs, "Mechanically induced osteogenic lineage commitment of stem cells," *Stem Cell Research and Therapy*, vol. 4, article 107, no. 5, 2013.

[11] J. Eyckmans, G. L. Lin, and C. S. Chen, "Adhesive and mechanical regulation of mesenchymal stem cell differentiation in human bone marrow and periosteum-derived progenitor cells," *Biology Open*, vol. 1, no. 11, pp. 1058–1068, 2012.

[12] A. B. Jaffe and A. Hall, "Rho GTPases: biochemistry and biology," *Annual Review of Cell and Developmental Biology*, vol. 21, pp. 247–269, 2005.

[13] A. Hall, "G proteins and small GTpases: distant relatives keep in touch," *Science*, vol. 280, no. 5372, pp. 2074–2075, 1998.

[14] M. Raftopoulou and A. Hall, "Cell migration: rho GTPases lead the way," *Developmental Biology*, vol. 265, no. 1, pp. 23–32, 2004.

[15] C. Pache, J. Kühn, K. Westphal et al., "Digital holographic microscopy real-time monitoring of cytoarchitectural alterations during simulated microgravity," *Journal of Biomedical Optics*, vol. 15, no. 2, Article ID 026021, 2010.

[16] L. B. Buravkova, "Problems of the gravitational physiology of a cell," *Human Physiology*, vol. 36, no. 7, pp. 746–753, 2010.

[17] D. Ingber, "How cells (might) sense microgravity," *The FASEB Journal*, vol. 13, pp. S3–S15, 1999.

[18] I. D. Pestov, "Fundamentals of gravitational biology," *Kosmicheskaia Biologiia i Meditsina*, vol. 2, no. 1, 9 pages, 1997.

[19] M. Miyake, M. Yamasaki, A. Hazama, S. Nielsen, and T. Shimizu, "Effects of microgravity on organ development of the neonatal rat," *Uchu Seibutsu Kagaku*, vol. 18, no. 3, pp. 126–127, 2004.

[20] E. C. Pollard, "Theoretical studies on living systems in the absence of mechanical stress," *Journal of Theoretical Biology*, vol. 8, no. 1, pp. 113–123, 1965.

[21] D. E. Ingber, N. Wang, and D. Stamenović, "Tensegrity, cellular biophysics, and the mechanics of living systems," *Reports on Progress in Physics*, vol. 77, no. 4, 2014.

[22] R. G. Bacabac, T. H. Smit, J. J. W. A. van Loon, B. Z. Doulabi, M. Helder, and J. Klein-Nulend, "Bone cell responses to high-frequency vibration stress: does the nucleus oscillate within the cytoplasm?" *The FASEB Journal*, vol. 20, no. 7, pp. 858–864, 2006.

[23] C. Ulbrich, J. Pietsch, J. Grosse et al., "Differential gene regulation under altered gravity conditions in follicular thyroid cancer cells: relationship between the extracellular matrix and the cytoskeleton," *Cellular Physiology and Biochemistry*, vol. 28, no. 2, pp. 185–198, 2011.

[24] J. Grosse, M. Wehland, J. Pietsch et al., "Short-term weightlessness produced by parabolic flight maneuvers altered gene expression patterns in human endothelial cells," *The FASEB Journal*, vol. 26, no. 2, pp. 639–655, 2012.

[25] R. Meng, H.-Y. Xu, S.-M. Di et al., "Human mesenchymal stem cells are sensitive to abnormal gravity and exhibit classic apoptotic features," *Acta Biochimica et Biophysica Sinica*, vol. 43, no. 2, pp. 133–142, 2011.

[26] M. G. Tairbekov, "Molekulyarnye i kletochnye osnovy gravitatsionnoi chuvstvitel'nosti (Molecular and Cellular Fundamentals of Gravitational Sensitivity)," 2002.

[27] C. A. Lambert, C. M. Lapière, and B. V. Nusgens, "Biology of adherent cells in microgravity," in *Biology in Space and Life on Earth*, R. N. Enno Brinckmann, Ed., pp. 123–155, Wiley-VCH, New York, NY, USA, 2007.

[28] T. B. Damm and M. Egli, "Calcium's role in mechanotransduction during muscle development," *Cellular Physiology and Biochemistry*, vol. 33, no. 2, pp. 249–272, 2014.

[29] C. S. Chen, J. Tan, and J. Tien, "Mechanotransduction at cell-matrix and cell-cell contacts," *Annual Review of Biomedical Engineering*, vol. 6, pp. 275–302, 2004.

[30] J. L. Bays, X. Peng, C. E. Tolbert et al., "Vinculin phosphorylation differentially regulates mechanotransduction at cell-cell and cell-matrix adhesions," *Journal of Cell Biology*, vol. 205, no. 2, pp. 251–263, 2014.

[31] N. L. Cowger, E. Benes, P. L. Allen, and T. G. Hammond, "Expression of renal cell protein markers is dependent on initial mechanical culture conditions," *Journal of Applied Physiology*, vol. 92, no. 2, pp. 691–700, 2002.

[32] G. L. Sanford, D. Ellerson, C. Melhado-Gardner, A. E. Sroufe, and S. Harris-Hooker, "Three-dimensional growth of endothelial cells in the microgravity-based rotating wall vessel bioreactor," *In Vitro Cellular & Developmental Biology: Animal*, vol. 38, no. 9, pp. 493–504, 2002.

[33] M. Ingram, G. B. Techy, R. Saroufeem et al., "Three-dimensional growth patterns of various human tumor cell lines in simulated microgravity of a NASA bioreactor," *In Vitro Cellular & Developmental Biology—Animal*, vol. 33, no. 6, pp. 459–466, 1997.

[34] H. L. Nichols, N. Zhang, and X. Wen, "Proteomics and genomics of microgravity," *Physiological Genomics*, vol. 26, no. 3, pp. 163–171, 2006.

[35] A. Guignandon, M. H. Lafage-Proust, Y. Usson et al., "Cell cycling determines integrin-mediated adhesion in osteoblastic ROS 17/2.8 cells exposed to space-related conditions," *The FASEB journal*, vol. 15, no. 11, pp. 2036–2038, 2001.

[36] S. Levenberg, B.-Z. Katz, K. M. Yamada, and B. Geiger, "Long-range and selective autoregulation of cell-cell or cell-matrix adhesions by cadherin or integrin ligands," *Journal of Cell Science*, vol. 111, no. 3, pp. 347–357, 1998.

[37] J. A. Felix, V. V. Chaban, M. L. Woodruff, and E. R. Dirksen, "Mechanical stimulation initiates intercellular Ca^{2+} signaling in intact tracheal epithelium maintained under normal gravity and simulated microgravity," *American Journal of Respiratory Cell and Molecular Biology*, vol. 18, no. 5, pp. 602–610, 1998.

[38] K. S. Ko, P. D. Arora, V. Bhide, A. Chen, and C. A. McCulloch, "Cell-cell adhesion in human fibroblasts requires calcium signaling," *Journal of Cell Science*, vol. 114, part 6, pp. 1155–1167, 2001.

[39] P. N. Colleran, B. J. Behnke, M. K. Wilkerson, A. J. Donato, and M. D. Delp, "Simulated microgravity alters rat mesenteric artery vasoconstrictor dynamics through an intracellular Ca^{2+} release mechanism," *American Journal of Physiology: Regulatory Integrative and Comparative Physiology*, vol. 294, no. 5, pp. R1577–R1585, 2008.

[40] M.-J. Xie, Y.-G. Ma, F. Gao et al., "Activation of BKCa channel is associated with increased apoptosis of cerebrovascular smooth muscle cells in simulated microgravity rats," *American Journal of Physiology: Cell Physiology*, vol. 298, no. 6, pp. C1489–C1500, 2010.

[41] X. Li, S. Yang, S. Li, P. Jiang, and Z. Lin, "Effects of simulated microgravity on the alkaline phosphatase activity and intracellular calcium concentration of cultured chondrocytes," *Chinese Science Bulletin*, vol. 44, no. 3, pp. 218–221, 1999.

[42] K. Meissner, J. R. Piqueira, and W. Hanke, "Fluorescent and dispersion experiments on biological membranes under microgravity," *Journal of Gravitational Physiology*, vol. 11, no. 2, pp. P195–P196, 2004.

[43] A. Sundaresan, D. Risin, and N. R. Pellis, "Loss of signal transduction and inhibition of lymphocyte locomotion in a ground-based model of microgravity," *In Vitro Cellular & Developmental Biology—Animal*, vol. 38, no. 2, pp. 118–122, 2002.

[44] A. Hall, "Rho GTpases and the actin cytoskeleton," *Science*, vol. 279, no. 5350, pp. 509–514, 1998.

[45] S. Etienne-Manneville and A. Hall, "Rho GTPases in cell biology," *Nature*, vol. 420, no. 6916, pp. 629–635, 2002.

[46] A. J. Ridley and A. Hall, "The small GTP-binding protein rho regulates the assembly of focal adhesions and actin stress fibers in response to growth factors," *Cell*, vol. 70, no. 3, pp. 389–399, 1992.

[47] M. Chiariello, J. P. Vaqué, P. Crespo, and J. S. Gutkind, "Activation of Ras and Rho GTPases and MAP Kinases by G-protein-coupled receptors," *Methods in Molecular Biology*, vol. 661, pp. 137–150, 2010.

[48] S. Servotte, Z. Zhang, C. A. Lambert et al., "Establishment of stable human fibroblast cell lines constitutively expressing active Rho-GTPases," *Protoplasma*, vol. 229, no. 2–4, pp. 215–220, 2006.

[49] M. Hughes-Fulford and M. L. Lewis, "Effects of microgravity on osteoblast growth activation," *Experimental Cell Research*, vol. 224, no. 1, pp. 103–109, 1996.

[50] M. A. Meloni, G. Galleri, G. Pani, A. Saba, P. Pippia, and M. Cogoli-Greuter, "Space flight affects motility and cytoskeletal structures in human monocyte cell line J-111," *Cytoskeleton*, vol. 68, no. 2, pp. 125–137, 2011.

[51] S. I. M. Carlsson, M. T. S. Bertilaccio, E. Ballabio, and J. A. M. Maier, "Endothelial stress by gravitational unloading: effects on cell growth and cytoskeletal organization," *Biochimica et Biophysica Acta—Molecular Cell Research*, vol. 1642, no. 3, pp. 173–179, 2003.

[52] L. B. Buravkova, P. M. Gershovich, J. G. Gershovich, and A. I. Grigor'ev, "Mechanisms of gravitational sensitivity of osteogenic precursor cells," *Acta Naturae*, vol. 2, no. 1, pp. 28–36, 2010.

[53] V. E. Meyers, M. Zayzafoon, S. R. Gonda, W. E. Gathings, and J. M. McDonald, "Modeled microgravity disrupts collagen I/integrin signaling during osteoblastic differentiation of human mesenchymal stem cells," *Journal of Cellular Biochemistry*, vol. 93, no. 4, pp. 697–707, 2004.

[54] F. Matsumura, "Regulation of myosin II during cytokinesis in higher eukaryotes," *Trends in Cell Biology*, vol. 15, no. 7, pp. 371–377, 2005.

[55] K. Ohashi, K. Nagata, M. Maekawa, T. Ishizaki, S. Narumiya, and K. Mizuno, "Rho-associated kinase ROCK activates LIM-kinase 1 by phosphorylation at threonine 508 within the activation loop," *The Journal of Biological Chemistry*, vol. 275, no. 5, pp. 3577–3582, 2000.

[56] V. E. Meyers, M. Zayzafoon, J. T. Douglas, and J. M. McDonald, "RhoA and cytoskeletal disruption mediate reduced osteoblastogenesis and enhanced adipogenesis of human mesenchymal stem cells in modeled microgravity," *Journal of Bone and Mineral Research*, vol. 20, no. 10, pp. 1858–1866, 2005.

[57] M. Zayzafoon, V. E. Meyers, and J. M. McDonald, "Microgravity: the immune response and bone," *Immunological Reviews*, vol. 208, no. 1, pp. 267–280, 2005.

[58] C. E. Walczak, "Microtubule dynamics and tubulin interacting proteins," *Current Opinion in Cell Biology*, vol. 12, no. 1, pp. 52–56, 2000.

[59] F. Yang, Z. Dai, Y. Tan, and Y. Li, "Effects of altered gravity on the cytoskeleton of neonatal rat cardiocytes," *Microgravity Science and Technology*, vol. 22, no. 1, pp. 45–52, 2010.

[60] M. L. Lewis, J. L. Reynolds, L. A. Cubano, J. P. Hatton, B. Desales Lawless, and E. H. Piepmeier, "Spaceflight alters microtubules and increases apoptosis in human lymphocytes (Jurkat)," *The FASEB Journal*, vol. 12, no. 11, pp. 1007–1018, 1998.

[61] J. Tabony, N. Rigotti, N. Glade, and S. Cortès, "Effect of weightlessness on colloidal particle transport and segregation in self-organising microtubule preparations," *Biophysical Chemistry*, vol. 127, no. 3, pp. 172–180, 2007.

[62] C. Papaseit, N. Pochon, and J. Tabony, "Microtubule self-organization is gravity-dependent," *Proceedings of the National Academy of Sciences of the United States of America*, vol. 97, no. 15, pp. 8364–8368, 2000.

[63] H. Daub, K. Gevaert, J. Vandekerckhove, A. Sobel, and A. Hall, "Rac/Cdc42 and p65PAK regulate the microtubule-destabilizing protein stathmin through phosphorylation at serine 16," *The Journal of Biological Chemistry*, vol. 276, no. 3, pp. 1677–1680, 2001.

[64] L. Sciola, M. Cogoli-Greuter, A. Cogoli, A. Spano, and P. Pippia, "Influence of microgravity on mitogen binding and cytoskeleton in Jurkat cells," *Advances in Space Research*, vol. 24, no. 6, pp. 801–805, 1999.

[65] H. Goto, H. Kosako, and M. Inagaki, "Regulation of intermediate filament organization during cytokinesis: possible roles of Rho-associated kinase," *Microscopy Research and Technique*, vol. 49, no. 2, pp. 173–182, 2000.

[66] L. Chang and R. D. Goldman, "Intermediate filaments mediate cytoskeletal crosstalk," *Nature Reviews Molecular Cell Biology*, vol. 5, no. 8, pp. 601–613, 2004.

[67] B. M. Uva, M. A. Masini, M. Sturla et al., "Microgravity-induced apoptosis in cultured glial cells," *European Journal of Histochemistry*, vol. 46, no. 3, pp. 209–214, 2002.

[68] C. M. Hale, A. L. Shrestha, S. B. Khatau et al., "Dysfunctional connections between the nucleus and the actin and microtubule networks in laminopathic models," *Biophysical Journal*, vol. 95, no. 11, pp. 5462–5475, 2008.

[69] D. Michaelson, W. Abidi, D. Guardavaccaro et al., "Rac1 accumulates in the nucleus during the G2 phase of the cell cycle and promotes cell division," *Journal of Cell Biology*, vol. 181, no. 3, pp. 485–496, 2008.

[70] Z. Q. Dai, R. Wang, S. K. Ling, Y. M. Wan, and Y. H. Li, "Simulated microgravity inhibits the proliferation and osteogenesis of rat bone marrow mesenchymal stem cells," *Cell Proliferation*, vol. 40, no. 5, pp. 671–684, 2007.

[71] T. B. Damm, A. Franco-Obregón, and M. Egli, "Gravitational force modulates G_2/M phase exit in mechanically unloaded myoblasts," *Cell Cycle*, vol. 12, no. 18, pp. 3001–3012, 2013.

[72] L. Yuge, T. Kajiume, H. Tahara et al., "Microgravity potentiates stem cell proliferation while sustaining the capability of differentiation," *Stem Cells and Development*, vol. 15, no. 6, pp. 921–929, 2006.

[73] A. Guignandon, C. Genty, L. Vico, M.-H. Lafage-Proust, S. Palle, and C. Alexandre, "Demonstration of feasibility of automated osteoblastic line culture in space flight," *Bone*, vol. 20, no. 2, pp. 109–116, 1997.

[74] F. J. Alenghat and D. E. Ingber, "Mechanotransduction: all signals point to cytoskeleton, matrix, and integrins," *Science's STKE: Signal Transduction Knowledge Environment*, vol. 2002, no. 119, article PE6, 2002.

[75] N. Q. Balaban, U. S. Schwarz, D. Riveline et al., "Force and focal adhesion assembly: a close relationship studied using elastic micropatterned substrates," *Nature Cell Biology*, vol. 3, no. 5, pp. 466–472, 2001.

[76] N. Nabavi, A. Khandani, A. Camirand, and R. E. Harrison, "Effects of microgravity on osteoclast bone resorption and osteoblast cytoskeletal organization and adhesion," *Bone*, vol. 49, no. 5, pp. 965–974, 2011.

[77] J. Gebken, B. Lüders, H. Notbohm et al., "Hypergravity stimulates collagen synthesis in human osteoblast-like cells: evidence for the involvement of p44/42 MAP-kinases (ERK 1/2)," *The Journal of Biochemistry*, vol. 126, no. 4, pp. 676–682, 1999.

[78] W. A. Loesberg, X. F. Walboomers, J. J. W. A. Van Loon, and J. A. Jansen, "Simulated microgravity activates MAPK pathways in fibroblasts cultured on microgrooved surface topography," *Cell Motility and the Cytoskeleton*, vol. 65, no. 2, pp. 116–129, 2008.

[79] L. Liu, C. Zong, B. Li et al., "The interaction between β1 integrins and ERK1/2 in osteogenic differentiation of human mesenchymal stem cells under fluid shear stress modelled by a perfusion system," *Journal of Tissue Engineering and Regenerative Medicine*, vol. 8, no. 2, pp. 85–96, 2014.

[80] D. F. Ward Jr., W. A. Williams, N. E. Schapiro et al., "Focal adhesion kinase signaling controls cyclic tensile strain enhanced collagen I-induced osteogenic differentiation of human mesenchymal stem cells," *Molecular and Cellular Biomechanics*, vol. 4, no. 4, pp. 177–188, 2007.

[81] B. M. Spiegelman and C. A. Ginty, "Fibronectin modulation of cell shape and lipogenic gene expression in 3T3-adipocytes," *Cell*, vol. 35, no. 3, part 2, pp. 657–666, 1983.

[82] J. Liu, S. M. DeYoung, M. Zhang, M. Zhang, A. Cheng, and A. R. Saltiel, "Changes in integrin expression during adipocyte differentiation," *Cell Metabolism*, vol. 2, no. 3, pp. 165–177, 2005.

[83] P. Barbe, J. Galitzky, I. de Glisezinski et al., "Simulated microgravity increases β-adrenergic lipolysis in human adipose tissue," *The Journal of Clinical Endocrinology & Metabolism*, vol. 83, no. 2, pp. 619–625, 1998.

[84] H. Maass, J. Transmontano, and F. Baisch, "Response of adrenergic receptors to 10 days head-down tilt bedrest," *Acta Physiologica Scandinavica, Supplement*, vol. 144, no. 604, pp. 61–68, 1992.

[85] V. A. Convertino, J. L. Polet, K. A. Engelke, G. W. Hoffler, L. D. Lane, and C. G. Blomqvist, "Evidence for increased β-adrenoreceptor responsiveness induced by 14 days of simulated microgravity in humans," *American Journal of Physiology*, vol. 273, no. 1, part 2, pp. R93–R99, 1997.

[86] J.-M. Dong, T. Leung, E. Manser, and L. Lim, "cAMP-induced morphological changes are counteracted by the activated RhoA small GTPase and the Rho kinase ROKα," *The Journal of Biological Chemistry*, vol. 273, no. 35, pp. 22554–22562, 1998.

[87] Z. Cao, R. M. Umek, and S. L. McKnight, "Regulated expression of three C/EBP isoforms during adipose conversion of 3T3-L1 cells," *Genes & Development*, vol. 5, no. 9, pp. 1538–1552, 1991.

[88] Q.-Q. Tang, M.-S. Jiang, and M. D. Lane, "Repressive effect of Sp1 on the C/EBPα gene promoter: role in adipocyte differentiation," *Molecular and Cellular Biology*, vol. 19, no. 7, pp. 4855–4865, 1999.

[89] J. E. Reusch, L. A. Colton, and D. J. Klemm, "CREB activation induces adipogenesis in 3T3-L1 cells," *Molecular & Cellular Biology*, vol. 20, no. 3, pp. 1008–1020, 2000.

[90] A. Mettouchi, S. Klein, W. Guo et al., "Integrin-specific activation of Rac controls progression through the G_1 phase of the cell cycle," *Molecular Cell*, vol. 8, no. 1, pp. 115–127, 2001.

[91] Q. Wan, E. Cho, H. Yokota, and S. Na, "Rac1 and Cdc42 GTPases regulate shear stress-driven β-catenin signaling in osteoblasts," *Biochemical and Biophysical Research Communications*, vol. 433, no. 4, pp. 502–507, 2013.

[92] M. Hughes-Fulford and V. Gilbertson, "Osteoblast fibronectin mRNA, protein synthesis, and matrix are unchanged after exposure to microgravity," *FASEB Journal*, vol. 13, no. 8, pp. S121–S127, 1999.

[93] A. Guignandon, C. Faure, T. Neutelings et al., "Rac1 GTPase silencing counteracts microgravity-induced effects on osteoblastic cells," *The FASEB Journal*, vol. 28, no. 9, pp. 4077–4087, 2014.

[94] F. H. Brembeck, M. Rosário, and W. Birchmeier, "Balancing cell adhesion and Wnt signaling, the key role of β-catenin," *Current Opinion in Genetics and Development*, vol. 16, no. 1, pp. 51–59, 2006.

[95] F. M. van Roy and P. D. McCrea, "A role for kaiso-p120ctn complexes in cancer?" *Nature Reviews Cancer*, vol. 5, no. 12, pp. 956–964, 2005.

[96] J. Noritake, M. Fukata, K. Sato et al., "Positive role of IQGAP1, an effector of Rac1, in actin-meshwork formation at sites of cell-cell contact," *Molecular Biology of the Cell*, vol. 15, no. 3, pp. 1065–1076, 2004.

[97] M. Fukata and K. Kaibuchi, "Rho-family GTPases in cadherin-mediated cell-cell adhesion," *Nature Reviews Molecular Cell Biology*, vol. 2, no. 12, pp. 887–897, 2001.

[98] C. H. M. Castro, C. S. Shin, J. P. Stains et al., "Targeted expression of a dominant-negative N-cadherin in vivo delays peak bone mass and increases adipogenesis," *Journal of Cell Science*, vol. 117, no. 13, pp. 2853–2864, 2004.

[99] S. L. Ferrari, K. Traianedes, M. Thorne et al., "Role for N-cadherin in the development of the differentiated osteoblastic phenotype," *Journal of Bone and Mineral Research*, vol. 15, no. 2, pp. 198–208, 2000.

[100] A. J. Engler, S. Sen, H. L. Sweeney, and D. E. Discher, "Matrix elasticity directs stem cell lineage specification," *Cell*, vol. 126, no. 4, pp. 677–689, 2006.

[101] T. P. Stein and C. E. Wade, "Metabolic consequences of muscle disuse atrophy," *The Journal of Nutrition*, vol. 135, no. 7, pp. 1824S–1828S, 2005.

[102] B. Nusgens, G. Chometon, A. Guignandon et al., "Role of the RhoGTPases in the cellular receptivity and reactivity to mechanical signals including microgravity," *Journal of Gravitational Physiology*, vol. 12, no. 1, pp. 269–270, 2005.

[103] Z.-G. Zhang, C. A. Lambert, S. Servotte et al., "Effects of constitutively active GTPases on fibroblast behavior," *Cellular and Molecular Life Sciences*, vol. 63, no. 1, pp. 82–91, 2006.

[104] R. McBeath, D. M. Pirone, C. M. Nelson, K. Bhadriraju, and C. S. Chen, "Cell shape, cytoskeletal tension, and RhoA regulate stem cell lineage commitment," *Developmental Cell*, vol. 6, no. 4, pp. 483–495, 2004.

[105] Y.-R. V. Shih, K.-F. Tseng, H.-Y. Lai, C.-H. Lin, and O. K. Lee, "Matrix stiffness regulation of integrin-mediated mechanotransduction during osteogenic differentiation of human mesenchymal stem cells," *Journal of Bone and Mineral Research*, vol. 26, no. 4, pp. 730–738, 2011.

[106] D. L. Long, J. S. Willey, and R. F. Loeser, "Rac1 is required for matrix metalloproteinase 13 production by chondrocytes in response to fibronectin fragments," *Arthritis and Rheumatism*, vol. 65, no. 6, pp. 1561–1568, 2013.

[107] D. C. Radisky, D. D. Levy, L. E. Littlepage et al., "Rac1b and reactive oxygen species mediate MMP-3-induced EMT and genomic instability," *Nature*, vol. 436, no. 7047, pp. 123–127, 2005.

[108] J. Settleman, "Tension precedes commitment—even for a stem cell," *Molecular Cell*, vol. 14, no. 2, pp. 148–150, 2004.

[109] X. Yao, R. Peng, and J. Ding, "Effects of aspect ratios of stem cells on lineage commitments with and without induction media," *Biomaterials*, vol. 34, no. 4, pp. 930–939, 2013.

[110] L. Gao, R. McBeath, and C. S. Chen, "Stem cell shape regulates a chondrogenic versus myogenic fate through Rac1 and N-cadherin," *Stem Cells*, vol. 28, no. 3, pp. 564–572, 2010.

[111] R. Sordella, W. Jiang, G.-C. Chen, M. Curto, and J. Settleman, "Modulation of Rho GTPase signaling regulates a switch between adipogenesis and myogenesis," *Cell*, vol. 113, no. 2, pp. 147–158, 2003.

[112] S. Huang, C. S. Chen, and D. E. Ingber, "Control of cyclin D1, $p27^{Kip1}$, and cell cycle progression in human capillary endothelial cells by cell shape and cytoskeletal tension," *Molecular Biology of the Cell*, vol. 9, no. 11, pp. 3179–3193, 1998.

[113] S. Huang and D. E. Ingber, "The structural and mechanical complexity of cell-growth control," *Nature Cell Biology*, vol. 1, no. 5, pp. E131–E138, 1999.

[114] M. F. Olson, A. Ashworth, and A. Hall, "An essential role for Rho, Rac, and Cdc42 GTPases in cell cycle progression through G1," *Science*, vol. 269, no. 5228, pp. 1270–1272, 1995.

[115] M. Yamamoto, N. Marui, T. Sakai et al., "ADP-ribosylation of the rhoA gene product by botulinum C3 exoenzyme causes Swiss 3T3 cells to accumulate in the G1 phase of the cell cycle," *Oncogene*, vol. 8, no. 6, pp. 1449–1455, 1993.

[116] D. Joyce, B. Bouzahzah, M. Fu et al., "Integration of Rac-dependent regulation of cyclin D1 transcription through a nuclear factor-κB-dependent pathway," *The Journal of Biological Chemistry*, vol. 274, no. 36, pp. 25245–25249, 1999.

[117] J. K. Westwick, Q. T. Lambert, G. J. Clark et al., "Rac regulation of transformation, gene expression, and actin organization by multiple, PAK-independent pathways," *Molecular & Cellular Biology*, vol. 17, no. 3, pp. 1324–1335, 1997.

[118] M. L. Coleman and C. J. Marshall, "A family outing: small GTPases cyclin' through G1," *Nature Cell Biology*, vol. 3, no. 11, pp. E250–E251, 2001.

[119] A. J. Ridley, "Cyclin' round the cell with Rac," *Developmental Cell*, vol. 1, no. 2, pp. 160–161, 2001.

[120] J. Rosenblatt, L. P. Cramer, B. Baum, and K. M. McGee, "Myosin II-dependent cortical movement is required for centrosome separation and positioning during mitotic spindle assembly," *Cell*, vol. 117, no. 3, pp. 361–372, 2004.

[121] M. Glotzer, "Animal cell cytokinesis," *Annual Review of Cell and Developmental Biology*, vol. 17, pp. 351–386, 2001.

[122] S. B. Ting, E. Deneault, K. Hope et al., "Asymmetric segregation and self-renewal of hematopoietic stem and progenitor cells with endocytic Ap2a2," *Blood*, vol. 119, no. 11, pp. 2510–2522, 2012.

[123] R. Nusse and H. Varmus, "Three decades of Wnts: a personal perspective on how a scientific field developed," *The EMBO Journal*, vol. 31, no. 12, pp. 2670–2684, 2012.

[124] L. Mellor, T. Bake, M. Hiremath, E. G. Loboa, and J. T. Oxford, "Simulated microgravity affects Wnt signaling in articular cartilage: possible implications for crosstalk between cartilage and subchondral bone," in *Proceedings of the 2014 NASA Human Research Program Investigators' Workshop*, Galveston, Tex, USA, February 2014.

[125] M. Capulli, A. Rufo, A. Teti, and N. Rucci, "Global transcriptome analysis in mouse calvarial osteoblasts highlights sets of genes regulated by modeled microgravity and identifies A "mechanoresponsive osteoblast gene signature"," *Journal of Cellular Biochemistry*, vol. 107, no. 2, pp. 240–252, 2009.

[126] Q. Wan, E. Cho, H. Yokota, and S. Na, "RhoA GTPase interacts with beta-catenin signaling in clinorotated osteoblasts," *Journal of Bone and Mineral Metabolism*, vol. 31, no. 5, pp. 520–532, 2013.

[127] S. J. Rodda and A. P. McMahon, "Distinct roles for Hedgehog and caronical Wnt signaling in specification, differentiation and maintenance of osteoblast progenitors," *Development*, vol. 133, no. 16, pp. 3231–3244, 2006.

[128] J.-B. Kim, P. Leucht, K. Lam et al., "Bone regeneration is regulated by Wnt signaling," *Journal of Bone and Mineral Research*, vol. 22, no. 12, pp. 1913–1923, 2007.

[129] D. Baksh and R. S. Tuan, "Canonical and non-canonical Wnts differentially affect the development potential of primary isolate of human bone marrow mesenchymal stem cells," *Journal of Cellular Physiology*, vol. 212, no. 3, pp. 817–826, 2007.

[130] E. J. Arnsdorf, P. Tummala, and C. R. Jacobs, "Non-canonical Wnt signalling and N-cadherin related β-catenin signalling play a role in mechanically induced osteogenic cell fate," *PLoS ONE*, vol. 4, no. 4, Article ID e5388, 2009.

[131] N. Case, M. Ma, B. Sen, Z. Xie, T. S. Gross, and J. Rubin, "β-Catenin levels influence rapid mechanical responses in osteoblasts," *The Journal of Biological Chemistry*, vol. 283, no. 43, pp. 29196–29205, 2008.

[132] A. Santos, A. D. Bakker, J. M. A. De Blieck-Hogervorst, and J. Klein-Nulend, "WNT5A induces osteogenic differentiation of human adipose stem cells via rho-associated kinase Rock," *Cytotherapy*, vol. 12, no. 7, pp. 924–932, 2010.

[133] J. Rossol-Allison, L. N. Stemmle, K. I. Swenson-Fields et al., "Rho GTPase activity modulates Wnt3a/β-catenin signaling," *Cellular Signalling*, vol. 21, no. 11, pp. 1559–1568, 2009.

[134] L. Peng, Y. Li, K. Shusterman, M. Kuehl, and C. W. Gibson, "Wnt-RhoA signaling is involved in dental enamel development," *European Journal of Oral Sciences*, vol. 119, supplement S1, pp. 41–49, 2011.

[135] M.-H. Kim, M. Kino-oka, N. Maruyama, A. Saito, Y. Sawa, and M. Taya, "Cardiomyogenic induction of human mesenchymal stem cells by altered Rho family GTPase expression on dendrimer-immobilized surface with d-glucose display," *Biomaterials*, vol. 31, no. 30, pp. 7666–7677, 2010.

[136] D. Diekmann, A. Abo, C. Johnston, A. W. Segal, and A. Hall, "Interaction of Rac with p67phox and regulation of phagocytic NADPH oxidase activity," *Science*, vol. 265, no. 5171, pp. 531–533, 1994.

[137] J. D. Lambeth, "Nox/Duox family of nicotinamide adenine dinucleotide (phosphate) oxidases," *Current Opinion in Hematology*, vol. 9, no. 1, pp. 11–17, 2002.

[138] R. Takeya and H. Sumimoto, "Molecular mechanism for activation of superoxide-producing NADPH oxidases," *Molecules and Cells*, vol. 16, no. 3, pp. 271–277, 2003.

[139] M. Almeida, E. Ambrogini, L. Han, S. C. Manolagas, and R. L. Jilka, "Increased lipid oxidation causes oxidative stress, increased peroxisome proliferator-activated receptor-γ expression, and diminished pro-osteogenic Wnt signaling in the skeleton," *The Journal of Biological Chemistry*, vol. 284, no. 40, pp. 27438–27448, 2009.

[140] C.-L. Kao, L.-K. Tai, S.-H. Chiou et al., "Resveratrol promotes osteogenic differentiation and protects against dexamethasone damage in murine induced pluripotent stem cells," *Stem Cells and Development*, vol. 19, no. 2, pp. 247–257, 2010.

[141] S. W. Lane, S. de Vita, K. A. Alexander et al., "Rac signaling in osteoblastic cells is required for normal bone development but is dispensable for hematopoietic development," *Blood*, vol. 119, no. 3, pp. 736–744, 2012.

[142] M.-K. Kwak, K. Itoh, M. Yamamoto, T. R. Sutter, and T. W. Kensler, "Role of transcription factor Nrf2 in the induction of hepatic phase 2 and antioxidative enzymes in vivo by the cancer chemoprotective agent, 3H-1, 2-dimethiole-3-thione," *Molecular Medicine*, vol. 7, no. 2, pp. 135–145, 2001.

[143] M. K. Cho, W. D. Kim, S. H. Ki et al., "Role of Gα_{12} and Gα_{13} as novel switches for the activity of Nrf2, a key antioxidative transcription factor," *Molecular & Cellular Biology*, vol. 27, no. 17, pp. 6195–6208, 2007.

[144] M. Daugaard, R. Nitsch, B. Razaghi et al., "Hace1 controls ROS generation of vertebrate Rac1-dependent NADPH oxidase complexes," *Nature Communications*, vol. 4, article 2180, 2013.

[145] A. Y. Chi, G. B. Waypa, P. T. Mungai, and P. T. Schumacker, "Prolonged hypoxia increases ros signaling and RhoA activation in pulmonary artery smooth muscle and endothelial cells," *Antioxidants and Redox Signaling*, vol. 12, no. 5, pp. 603–610, 2010.

[146] D. Kondrikov, R. B. Caldwell, Z. Dong, and Y. Su, "Reactive oxygen species-dependent RhoA activation mediates collagen synthesis in hyperoxic lung fibrosis," *Free Radical Biology and Medicine*, vol. 50, no. 11, pp. 1689–1698, 2011.

[147] A. S. Nimnual, L. J. Taylor, and D. Bar-Sagi, "Redox-dependent downregulation of Rho by Rac," *Nature Cell Biology*, vol. 5, no. 3, pp. 236–241, 2003.

[148] S. Versari, G. Longinotti, L. Barenghi, J. A. M. Maier, and S. Bradamante, "The challenging environment on board the International Space Station affects endothelial cell function by triggering oxidative stress through thioredoxin interacting protein overexpression: the ESA-SPHINX experiment," *The FASEB Journal*, vol. 27, no. 11, pp. 4466–4475, 2013.

[149] T. P. Stein, "Space flight and oxidative stress," *Nutrition*, vol. 18, no. 10, pp. 867–871, 2002.

[150] I. Testard, M. Ricoul, F. Hoffschir et al., "Radiation-induced chromosome damage in astronauts' lymphocytes," *International Journal of Radiation Biology*, vol. 70, no. 4, pp. 403–411, 1996.

[151] M. Fukata, M. Nakagawa, and K. Kaibuchi, "Roles of Rho-family GTPases in cell polarisation and directional migration," *Current Opinion in Cell Biology*, vol. 15, no. 5, pp. 590–597, 2003.

[152] C. D. Lawson and K. Burridge, "The on-off relationship of Rho and Rac during integrin-mediated adhesion and cell migration," *Small GTPases*, vol. 5, no. 1, Article ID e27958, 2014.

[153] T. Mitsuhara, M. Takeda, S. Yamaguchi et al., "Simulated microgravity facilitates cell migration and neuroprotection after bone marrow stromal cell transplantation in spinal cord injury," *Stem Cell Research and Therapy*, vol. 4, no. 2, article 35, 2013.

[154] P. A. Plett, R. Abonour, S. M. Frankovitz, and C. M. Orschell, "Impact of modeled microgravity on migration, differentiation, and cell cycle control of primitive human hematopoietic progenitor cells," *Experimental Hematology*, vol. 32, no. 8, pp. 773–781, 2004.

[155] A. Espinosa-Jeffrey, P. M. Paez, V. T. Cheli, V. Spreuer, I. Wanner, and J. De Vellis, "Impact of simulated microgravity on oligodendrocyte development: implications for central nervous system repair," *PLoS ONE*, vol. 8, no. 12, Article ID e76963, 2013.

[156] K. Burridge and K. Wennerberg, "Rho and Rac take center stage," *Cell*, vol. 116, no. 2, pp. 167–179, 2004.

[157] A. Higashibata, M. Imamizo-Sato, M. Seki, T. Yamazaki, and N. Ishioka, "Influence of simulated microgravity on the activation of the small GTPase Rho involved in cytoskeletal formation—molecular cloning and sequencing of bovine leukemia-associated guanine nucleotide exchange factor," *BMC Biochemistry*, vol. 7, article 19, 2006.

[158] X. Zhang, Y. Nan, H. Wang et al., "Model microgravity enhances endothelium differentiation of mesenchymal stem cells," *Naturwissenschaften*, vol. 100, no. 2, pp. 125–133, 2013.

[159] K. Hamamura, G. Swarnkar, N. Tanjung et al., "RhoA-mediated signaling in mechanotransduction of osteoblasts," *Connective Tissue Research*, vol. 53, no. 5, pp. 398–406, 2012.

Hindawi Publishing Corporation
BioMed Research International
Volume 2015, Article ID 475935, 12 pages
http://dx.doi.org/10.1155/2015/475935

Research Article

A Tissue Retrieval and Postharvest Processing Regimen for Rodent Reproductive Tissues Compatible with Long-Term Storage on the International Space Station and Postflight Biospecimen Sharing Program

Vijayalaxmi Gupta,[1] Lesya Holets-Bondar,[1] Katherine F. Roby,[2,3] George Enders,[2] and Joseph S. Tash[1]

[1]*Department of Molecular & Integrative Physiology, University of Kansas Medical Center, Mail Stop 3050, 3901 Rainbow Boulevard, HLSIC 3098, Kansas City, KS 66160, USA*
[2]*Department of Anatomy and Cell Biology, University of Kansas Medical Center, Kansas City, KS 66160, USA*
[3]*Institute for Reproductive Health and Regenerative Medicine, University of Kansas Medical Center, Kansas City, KS 66160, USA*

Correspondence should be addressed to Joseph S. Tash; jtash@kumc.edu

Received 6 June 2014; Revised 18 September 2014; Accepted 20 October 2014

Academic Editor: Jack J. W. A. Van Loon

Collection and processing of tissues to preserve space flight effects from animals after return to Earth is challenging. Specimens must be harvested with minimal time after landing to minimize postflight readaptation alterations in protein expression/translation, posttranslational modifications, and expression, as well as changes in gene expression and tissue histological degradation after euthanasia. We report the development of a widely applicable strategy for determining the window of optimal species-specific and tissue-specific posteuthanasia harvest that can be utilized to integrate into multi-investigator Biospecimen Sharing Programs. We also determined methods for ISS-compatible long-term tissue storage (10 months at −80°C) that yield recovery of high quality mRNA and protein for western analysis after sample return. Our focus was reproductive tissues. The time following euthanasia where tissues could be collected and histological integrity was maintained varied with tissue and species ranging between 1 and 3 hours. RNA quality was preserved in key reproductive tissues fixed in RNA*later* up to 40 min after euthanasia. Postfixation processing was also standardized for safe shipment back to our laboratory. Our strategy can be adapted for other tissues under NASA's Biospecimen Sharing Program or similar multi-investigator tissue sharing opportunities.

1. Introduction

With the current paucity of opportunities for studying whole animal mammalian physiology in space flight, the Biospecimen Sharing Program (BSP) for postflight tissue collection offers the opportunity to broaden access to biological samples shortly after return and maximize the data generated from flight animal payloads. The logistics of space flight experiments involving live animals often requires harvesting tissues at a remote site, followed by shipping the specimens to the Principle Investigators' laboratories for detailed analysis. Furthermore, as the capabilities to house rodent and other animals on the International Space station (ISS), and to conduct long-term space flight experiments using animals are enabled, the need to harvest and fix tissues for long-term storage on ISS that will retain high quality RNA and protein for subsequent analysis in laboratories on Earth is also required. These approaches to live animal experimentation in space flight that include tissue harvest for multiple investigators require determination of (1) tissue-specific windows of time between euthanasia and tissue fixation that retain quality of histology and (2) tissue-specific windows of time for tissue fixation that retain high quality protein and RNA for subsequent analysis. Determination of these windows provides a quantitative, logical approach to generate appropriately prioritized and optimized tissue harvest and fixation logistics in a multi-investigator Biospecimen Sharing Program scenario, be it on Earth or during tissue harvest on the ISS. In addition, tissue

storage methods should retain high sample quality under long-term storage, as samples may be harvested and stored on the ISS but may not be returned to Earth for many months, depending on ISS to Earth flight frequency and payload capacities. This issue has been addressed for preserving plant material for gene expression analysis [1], but there is no data available for animal tissues. Our participation in the BSP program involved tissue harvest from female mice at Kennedy Space Center, Florida, USA (KSC) for animals flown for 12–15 days in orbit on three space shuttle flights: STS-131, STS-133, and STS-135. In addition, we harvested tissues from male mice at the Institute for Biomedical Problems (IMBP) laboratory in Moscow, RU for animals flown for 30 days in orbit on the BION M1 satellite. Both the STS and BION series of flight experiments involved age- and time-matched ground control groups of animals. During the early flight planning phase of BION, there were possibilities that male or female mice would be flown and that male gerbil tissues may also be provided to the BSP. Thus, to be prepared for any of these possibilities, we undertook to determine the optimal tissue harvest windows for all of the species and reproductive tissues that we might be able to obtain. Our participation in these multi-investigator specimen sharing efforts covering four different primary flight PI experimental designs and harvest logistics necessitated a determination of the window of time between euthanasia and harvest and preservation of our tissues of interest that would allow us sufficient flexibility to obtain the highest possible quality of tissue for histopathology, RNA for gene-transcription analysis, and protein for expression and posttranslational modification analysis. A determination of these time windows is essential, since the tissues that are made available to the BSP investigators are provided after the primary flight PI's have obtained their tissues. Knowledge of the optimal windows for all of the tissues of interest aids in the preparation of targeted tissue harvest flow logistics that can provide each of the BSP team members the highest possible quality tissue, respectively. Therefore, as we report here, we developed a strategy to determine the window of time between euthanasia and fixation for retention of high quality histology for male and female reproductive organs. We also determined methods for long-term tissue storage for 10 months that provide for recovery of both high quality protein and RNA. These strategies are adaptable and can be applied to harvest and storage of other time-sensitive labile tissues from animals and plants. Furthermore, these methods can be used to optimize logistics and data collection under multi-investigator tissue harvest and sharing programs operated by any space agency, commercial entity, or flight platform.

2. Materials and Methods

2.1. Animals. Approximately 8 wk old male and female C57Bl/6J (Jackson Lab, Bar Harbor, ME) and ~10-month old male and female Mongolian gerbils (Charles River, Wilmington, MA) were used throughout this study. All animal use protocols were approved by the University of Kansas Institutional Animal Care and Use Committee (IACUC). Animals were maintained in standard cages with 12 : 12 h dark : light cycle, and standard food and water were provided ad libitum. All animals were euthanized using CO_2 asphyxiation followed by cervical dislocation prior to tissue harvest.

2.2. Determination of the Limit of Time and Temperature between Euthanasia and Tissue Fixation

2.2.1. Male Mice. Our protocol consisted of three groups of six mice each, with one mouse for each time point. In group A, all mice were euthanized at one time and the testes and epididymides were harvested and separated and then immediately placed in Ham's F-10 medium (Sigma Aldrich, St. Louis, MO) *on ice*. At time intervals of 0, 0.5, 1.0, 1.5, 2.0, and 2.5 hr each testis (one mouse per time point) and epididymis (2 mice per time point) were separated and then transferred from Ham's F-10 medium to Bouin's fixative (Sigma Aldrich, St. Louis, MO) at room temperature (RT; 21°C). In group B, the same procedure was followed, except that the testes and epididymides, separated, were placed in Ham's F-10 medium *at RT* until transfer to Bouin's at the same time interval as above. In group C, all mice were euthanized at one time, the *carcasses were maintained at (RT)*, and then at time 0, 0.5, 1.0, 1.5, 2.0, and 2.5 hr, the testis and epididymis were harvested from the carcasses, respectively. At each of the time points above, group C testes were placed in Bouin's solution and processed as per standard histology protocols, as detailed below. For all groups, the tissues fixed in Bouin's were processed as detailed in Section 2.3, below. At the same time point, group C epididymides were processed to obtain cauda sperm to assess sperm motility by computer assisted sperm analysis (CASA) [2]. For animals used for collection of cauda epididymal sperm for motility analysis, two animals were used at each time point.

2.2.2. Female Mice. Female mice were euthanized (carcasses maintained at RT as per group C, above) and their ovaries and uteri were harvested at 0, 0.5, 1.0, 1.5, 2.0, 2.5, and 3.0 hr after euthanasia (one animal per time point). At the times indicated, the tissues were fixed at RT in Bouin's overnight and then processed for histology as detailed below (Section 2.3).

2.2.3. Mongolian Gerbils. The six male gerbils were euthanized at one time, and the carcasses were kept at room temperature. At 0, 0.5, 1.0, 1.5, 2.0, and 3.0 hr after euthanasia, testis and epididymis were harvested from the carcasses and separated, respectively (one animal per time point). Similarly, all six female gerbils were euthanized and the carcasses were kept at RT. Ovaries and uterine horns were harvested from each carcass at the same time interval as the males. At the times indicated above, the tissues were placed in Bouin's fixative at RT and then processed for histology, as detailed below (Section 2.3). Sperm were immediately harvested from cauda epididymis as mentioned above, and sperm motility analysis was carried out using CASA, as described above [2].

2.3. Postharvest Processing of Mouse Testicular Tissues. Testes and epididymides from the mature mice were harvested, as

detailed above. Unless indicated otherwise, all procedures were done at RT. Tissues were fixed in Bouin's solution for 48 h, washed in 70% ethanol (ETOH) until the yellow color of Bouin's disappeared (~48 hr with frequent changes of 70% ETOH and gentle agitation), and divided into four groups: *Control group*: tissue was stored in 70% ETOH until paraffin embedding; *Rapid transition*: 70% ETOH was immediately replaced with PBS (Sigma Aldrich, St. Louis, MO), pH 7.4 for one wk, and then rapidly replaced with 70% ETOH; *Slow Re-ETOH only*: 70% ETOH was immediately replaced with PBS for one wk and then sequentially replaced at 2 hr intervals with each of 10%, 30%, 50%, and 70% ETOH; *Slow rehydration-dehydration*: 70% ETOH was sequentially (70%, 50%, 30%, 10%, then PBS, at 2 hr each) substituted with PBS for one wk and then replaced at 2 hr intervals with each of 10%, 30%, 50%, and 70% ETOH. To prevent contamination, we kept tissue in PBS at 4°C, and ETOH replacement was completed at RT with 2 hr intervals between changes, as detailed above. After each of the respective final dehydration steps above, the tissues were paraffin-embedded and processed for histology and hematoxylin and eosin staining (HE) using standard methods as performed previously [3].

2.4. Total RNA Extraction and Preservation. Freshly harvested mouse testes were immediately stabilized in 10 volumes of TRIzol reagent (Invitrogen, Carlsbad, CA) or RNA*later* solution (Ambion, Austin, TX). The samples placed in RNA*later* were stored for (1) two wks at 4°C; (2) one wk at RT and one wk at 4°C; or (3) two wks at RT. Before RNA extraction, tissues were retrieved from RNA*later* solution with sterile forceps and then submerged in TRIzol reagent. RNA was isolated with TRIzol reagent according to the manufacturer's instructions. Time of placement into RNA*later* was noted to determine if RNA quality was related to the duration of window from euthanasia to placement in RNA*later*. RNA integrity and quantity were determined using Agilent RNA kit and Agilent Bioanalyzer 2100 (Santa Clara, CA). One μg of RNA was subjected to RT PCR with the primers specific for mouse GAPDH (Forward: 5′CCTTCATTGACCTCAACTAC; Reverse: 5′ATGACAAGCTTCCCATTCTC), and interleukin-1alpha (IL-1α) (Forward: 5′ACTTGTTTGAAGACCTAAAG; Reverse: 5′GTTTCAGAGGTTCTCAGAG). Primers were designed using online Primer Design Tool Primer 3. Uteri and ovaries from STS-135 were harvested in RNA*later* solution and stored at −80°C for 10 months. Total RNA was isolated from ovaries and uterine horns with Gene Elute Mammalian RNA kit (Sigma Aldrich, St. Louis, MO). PCR products were verified on 3.0% agarose gels using standard procedures.

*2.5. Protein Extraction from Ovaries and Uterus Tissue Preserved in RNA*later*.* Ovaries stabilized in RNA*later* for one wk at RT and two wks at 4°C were used for protein extraction. The tissue was removed from RNA*later*, briefly rinsed with ice-cold PBS, pH 7.4, and then homogenized in RIPA buffer containing protease inhibitor cocktail (all from Sigma Aldrich, St. Louis, MO) or ProteoJet Mammalian Cell Lysis Reagent (Fermentas, Pittsburgh, PA). Uteri from STS-135 mission mice were preserved in RNA*later* for 10 months at −80°C, prior to processing in RIPA as described above. Protein concentration was determined using the DC Assay (Bio-Rad, Hercules, CA), and 15 μg protein was electrophoresed under denaturing conditions on 4–15% polyacrylamide gel and transferred to nitrocellulose membrane (Bio-Rad, Hercules, CA). The membranes were blocked for 1 hr with 5% nonfat milk in TBS-T (Tris buffered saline with Tween-20, Sigma Aldrich, St Louis, MO) and probed with 1 μg/mL rabbit anti-mouse estrogen receptor alpha (ERα) antibody (Santa Cruz Biotechnology, CA). To verify equal loading of proteins, membranes were stripped and reprobed with a goat anti-β-actin antibody (Santa Cruz Biotechnology, CA). Incubations with primary antibodies were carried out overnight at 4°C. After washing in TBS-T and probing with the corresponding horseradish peroxidase-labeled secondary antibody (Pierce Biotechnology, Rockford, IL), bound antibodies were identified using Amersham ACL Plus Western Blotting Detection Reagents (GE Healthcare, Pittsburgh, PA) and luminography. Western blots were quantitated by densitometric analysis.

3. Results

3.1. Effect of Delayed Processing on Quality of Mouse and Gerbil Reproductive Tissue Histology

3.1.1. Male Mouse. Testes harvested any time between time 0 after euthanasia up to 2.5 hr after euthanasia showed histological properties comparable to the time 0-harvested mice. For comparative purposes, the 0 min harvested testes represent the control for subsequent time points for each storage treatment, respectively. Histological quality of the testes was excellent in all postharvest treatment procedures; namely, tissues were kept in the carcass until fixation or fixed in Bouin's immediately or stored in Hams F10 on ice or RT before fixation. Testis tubules appeared normal in all treatment groups compared to the 0 min controls, with no shrinkage of tissue and complete retention of histologic architectural details (Figures 1(a), 1(b), and 1(c)).

Total motility and progressive motility of cauda epididymal mouse sperm at times 0, 0.5, 1.0, 1.5, 2.0, and 2.5 hr were not significantly different between any of the tissue harvest time points and also not significantly different between the three tissue harvest scenarios. Table 1 shows the percent progressive motility for each time point under all three tissue storage conditions. Table 2 shows the percent total motility for each time point under all three tissue storage conditions. Based on comparable results between the three tissue harvest regimens, we focused on the "tissue in carcass" at RT regimen for subsequent experiments with female mice, as well as male and female gerbils.

3.1.2. Male Gerbil. Testis showed normal distinct histological details with all spermatogenic cells arranged in a normal pattern in the tubule when collected up to 2.5 hr after euthanasia (Figure 2). Total motility of the gerbil cauda epididymal sperm harvested at each at time point was analyzed and is presented in Table 3. Since the data represent a single animal,

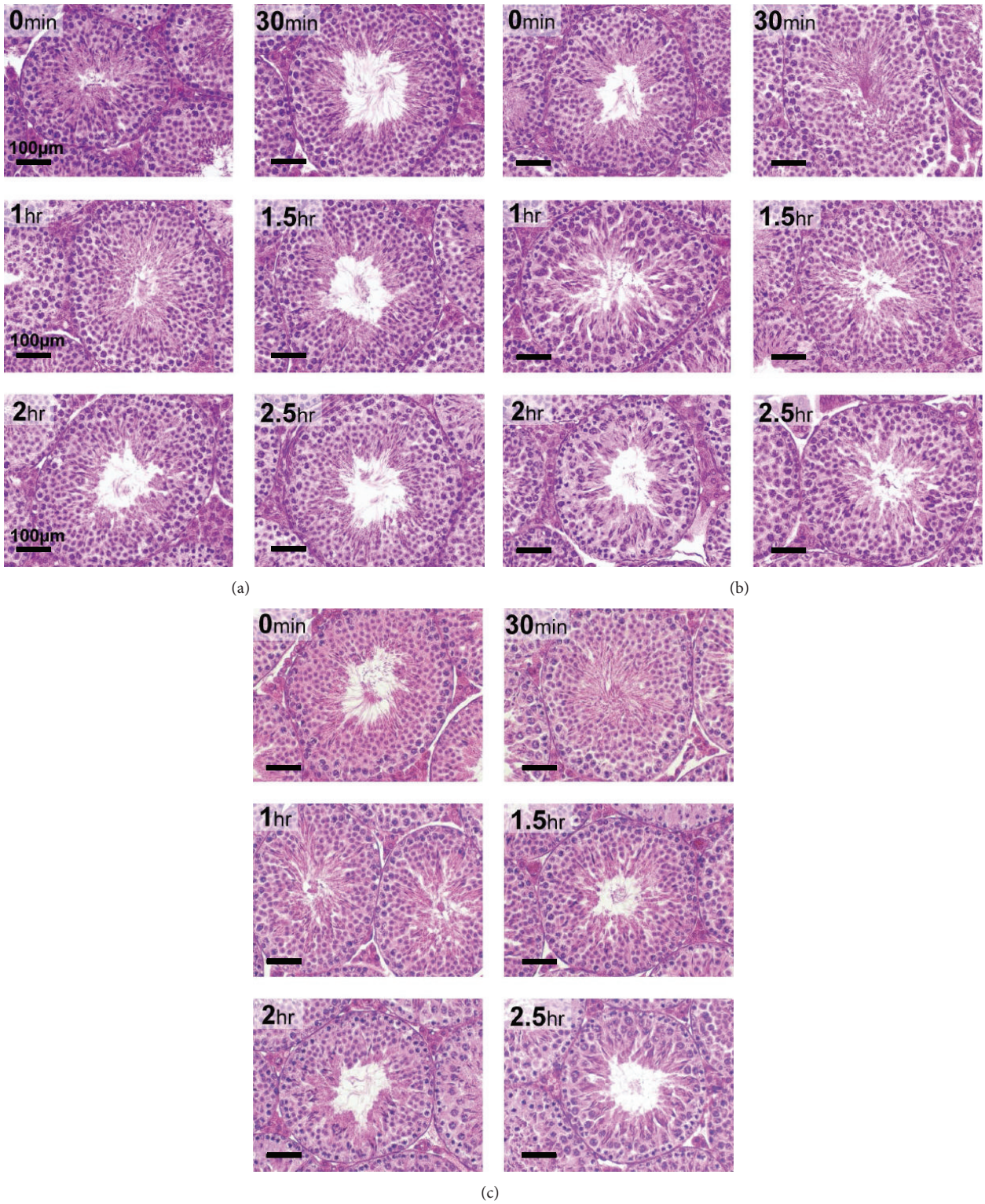

Figure 1: Effect of delayed processing on C57Bl/6J testicular morphology. Each panel represents light microscopy (40x objective) of sections of adult mouse testis stained with hematoxylin and eosin (HE) (magnification bar is 100 μm). (a) Tissues kept on ice for 0 to 2.5 hr after harvesting; (b) tissues allowed to remain in the carcass for 0 to 2.5 hr; (c) tissues removed and kept at RT for 0 to 2.5 hr in Ham's F10 after harvesting.

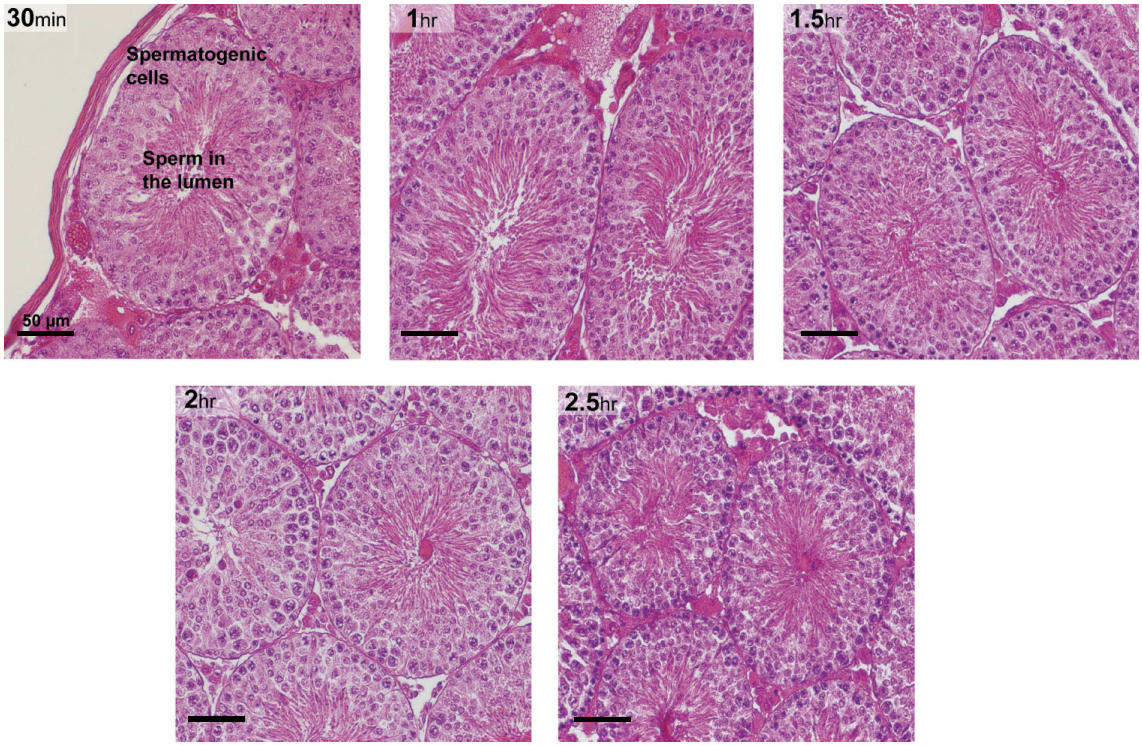

Figure 2: Gerbil testicular morphology (40x objective) at various time points after tissue harvest from the carcass (magnification bar is 50 μm). All gerbils were euthanized at once and tissues were harvested from the carcass at 0.5 hr interval from 0 to 2.5 hr. HE staining demonstrated the retention of histological features at every time point.

Table 1: Percent progressive motility (±SD) of mouse cauda epididymal sperm after exposure of epididymis to various conditions.

Time after euthanasia	In carcass	On ice*	*At room temperature
0 h	23 ± 18	25 ± 26	26 ± 19
0.5 h	28 ± 13	22 ± 13	27 ± 12
1.0 h	31 ± 3	32 ± 19	31 ± 9
1.5 h	27 ± 6	47 ± 9	30 ± 11
2.0 h	26 ± 7	18 ± 9	28 ± 14
2.5 h	26 ± 9	23 ± 12	25 ± 16

*Tissue was submerged in Ham's F-10 medium in a 15 mL tissue culture tube which was placed on ice or at room temperature. Values are mean ± standard deviation (n = 2 mice at each time point). There was no significant difference in motility between the three testing conditions at each time point.

Table 2: Percent total motility (±SD) of mouse cauda epididymal sperm after exposure of epididymis to various posteuthanasia conditions.

Time after euthanasia	In carcass	On ice*	*At room temperature
0 h	48 ± 18	49 ± 29	45 ± 21
0.5 h	51 ± 12	47 ± 11	50 ± 15
1.0 h	53 ± 6	60 ± 21	40 ± 9
1.5 h	57 ± 12	67 ± 16	54 ± 11
2.0 h	51 ± 14	46 ± 14	43 ± 14
2.5 h	50 ± 17	49 ± 18	52 ± 12

*Tissue was submerged in Ham's F-10 medium in a 15 mL culture tube which was placed on ice or at room temperature as indicated. Values are mean ± standard deviation (n = 2 mice at each time point). There was no significant difference in motility between the three testing conditions at each time point.

statistical analysis cannot be done. Given the variation in motility with time, the data suggest that motility was relatively stable at all time points, except with perhaps a drop at 2.5 hr.

3.1.3. Female Mouse. The *ovaries (Figure 3(a)) and uteri (Figure 3(b))* harvested from female mice up to 3 hr after euthanasia showed excellent histological properties devoid of apparent tissue degradation.

3.1.4. Female Gerbil. Gerbil *ovaries* (Figure 3(c)) harvested up to 1 hr after euthanasia showed normal healthy follicles and

Table 3: Percent total motility of gerbil cauda epididymal sperm recovered from the epididymis after storage in the carcass at RT for the times indicated (n = 1 at each time point).

Time after euthanasia	Total motility (%)	Progressive motility (%)
0 h	98.3	85.0
0.5 h	82.4	58.0
1.0 h	82.6	61.0
1.5 h	95.2	86.2
2.0 h	87.9	73.2
2.5 h	75.6	47.5

Since we used one animal per time point, standard deviation could not be determined.

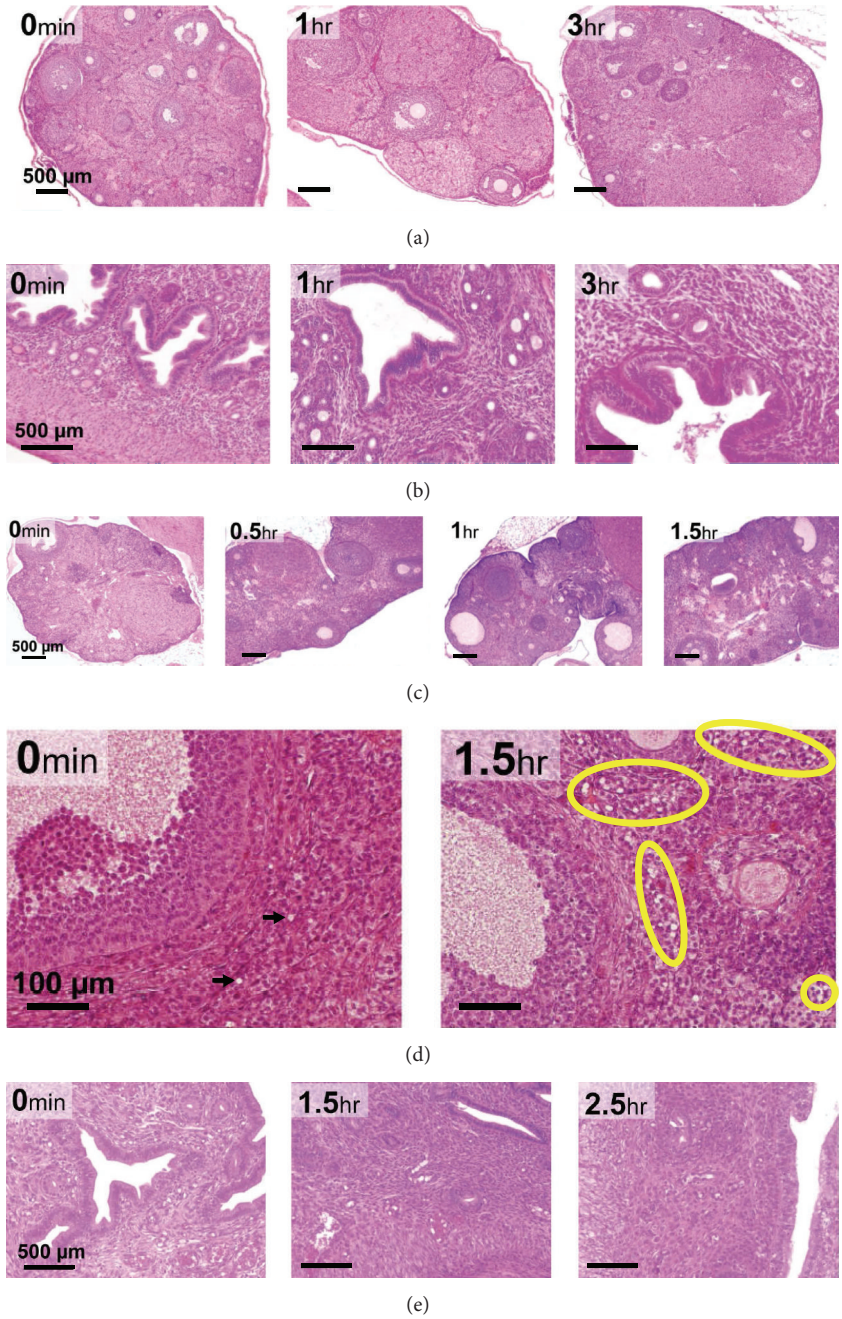

Figure 3: Mouse and gerbil ovarian and uterine horn histology. HE staining was used to evaluate quality of oocyte and follicles. Rows represent HE staining of: (a) mouse ovary up to 3 hr after euthanasia (4x objective, magnification bar is 500 μm); (b) mouse uteri up to 3 hr after euthanasia (10x objective, magnification bar is 500 μm); (c) gerbil ovary up to 1.5 hr after euthanasia (4x objective; magnification bar is 500 μm); (d) significantly high number of vacuoles are indicated in the yellow circles in gerbil ovaries from 1.5 h after euthanasia (40x objective, magnification bar is 100 μm); (e) gerbil uteri up to 2.5 hr after euthanasia (10x objective, magnification bar is 500 μm).

healthy oocytes devoid of signs of tissue degradation; however at 1.5 hr after euthanasia high numbers of unhealthy follicles and shrunken oocytes were seen, suggesting tissue deterioration due to the delay in fixation process after euthanasia. Significantly high numbers of "vacuoles-like" structures were also seen at 1.5 hr after euthanasia (Figure 3(d)), which is indicative of tissue degradation (indicated by the yellow circles). Control (0 min) gerbil ovaries had negligible "vacuoles" (indicated by two black arrows). The ovary harvested after 1.5 hr did not sustain the histological processing as they were too fragile and degraded, implying that gerbil ovaries were more sensitive and should be harvested within 1 hr of euthanasia. *Uterine* histology indicated tissues were intact and comparable to control at all tested time points (Figure 3(e)).

3.2. Effect of Different Postfixation Procedures on Quality of Testicular Histology. Testicular and epididymis morphology

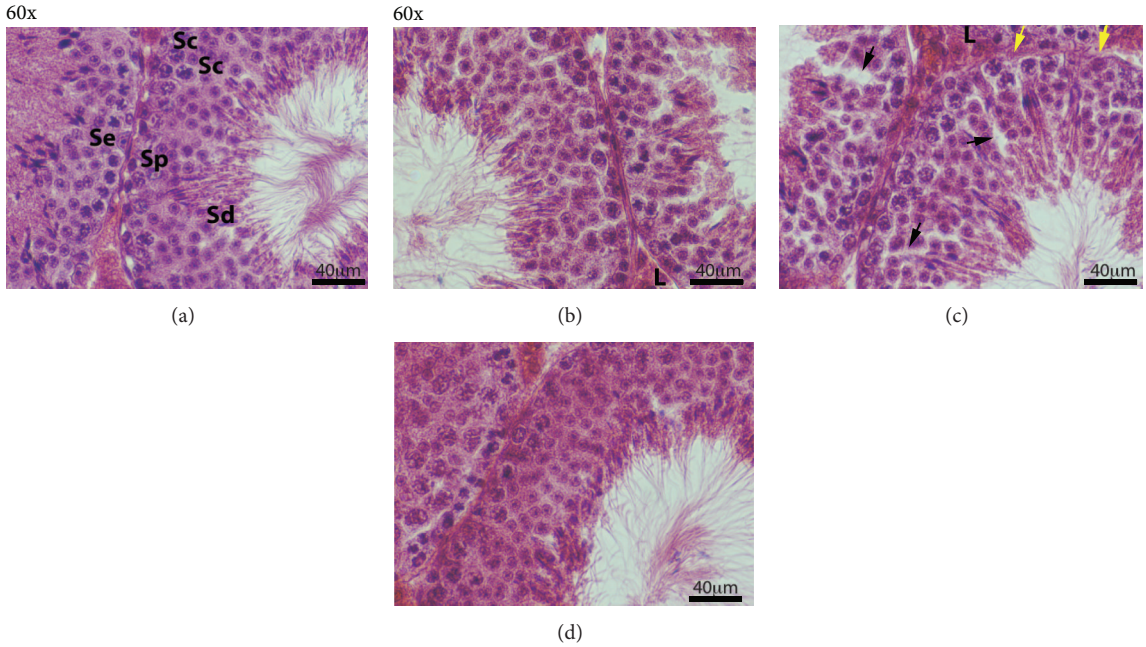

FIGURE 4: Morphological analysis of mouse testis after different postfixative manipulations. Sections of adult mouse testis were stained with HE (all at 60x; magnification bar is 40 μm). (a) Control; (b) slow rehydration-dehydration stepwise replacement of ETOH-PBS-ETOH; (c) slow Re-ETOH *only* stepwise replacement; (d) rapid ETOH-PBS-ETOH transition. Sertoli cell (Se), spermatogonia (Sp), spermatocytes (Sc), spermatids (Sd), and Leydig cell (L). *Black arrows*—abnormal open spaces in seminiferous epithelium; *yellow arrows*—abnormal wavy and thinner basement membrane.

was evaluated for histological changes after different postfixation processing (Figures 4 and 5). In control testicular tissue (Figure 4(a)), all types of spermatogenic cells, spermatogonia (Sp), Sertoli cells (Se), spermatocytes (Sc), and spermatids (Sd), were evident. Lymphatic spaces between seminiferous tubules and adjacent to Leydig cells (L) clusters are clearly defined. After the slow rehydration-dehydration stepwise replacement with ETOH, testis tubules appeared normal with histological architecture similar to the control group (Figure 4(b)). Although all types of spermatogenic cell were identified after slow rehydration-dehydration stepwise replacement, spermatogonia and Sertoli cell nuclei were more difficult to distinguish compared to control. The quality of testicular histology observed after slow Re-ETOH only (Figure 4(c)) was similar to that observed in the slow rehydration-dehydration stepwise replacement group. However, open spaces (black arrows) were observed within portions of seminiferous tubules in the slow Re-ETOH only group, and the seminiferous tubule basement membrane in this group often appeared wavy and thinner (yellow arrows) compared to the control (Figure 4(a)). The histologic quality was poor in the group treated by single step (rapid transition) change of solution (Figure 4(d)), as evidenced by a diffuse appearance of the tissue (not due to focus) and limited clarity of nuclear details in spermatogonia and Sertoli cells. In addition, the seminiferous tubule basement membrane was occasionally indistinct and some spermatid artifactual loss of residual bodies is also observed.

We found epididymal tissue to be sensitive to dehydration/rehydration shock (Figure 5). Slow rehydration-dehydration ETOH replacement had no visible negative effect on the quality of epididymal morphology (Figure 5(b)); however histological examination revealed differences in epididymal morphology after slow Re-ETOH only (Figure 5(c)) and rapid transition procedures (Figure 5(d)), compared to control (Figure 5(a)). The differences included alterations in the thickness of columnar epithelium, and basal and principal cells are not very sharp. The *slow rehydration-dehydration* caused less destruction of testicular and epididymal tissue than the rapid single-step changes of solution and has an overall better morphological detail preservation compared to the rapid ETOH-PBS solution change.

3.3. Total RNA and Protein Evaluation after Tissue Preservation in RNA*later* under Long-Term Storage

3.3.1. RNA Stability. We compared RNA integrity after preservation testicular tissue in TRIzol reagent and RNA*later* (Figure 6(a)). Total RNA integrity analysis demonstrated high quality RNA after storing tissue in RNA*later* for 1-2 wk at RT or 4°C compared to TRIzol preservation. Distinct 28S and 18S ribosomal RNA and absence of degraded RNA were observed on the gel. RT-PCR analysis of RNA with primers for GAPDH and IL-1α indicated high quality of expected PCR products in all analyzed samples (Figure 6(b)). Integrity analysis of total RNA isolated from STS-131 ground controls (G10, G11, and G12) and flight (F10, F11, and F12) mouse uteri after 30 to 40 min after euthanasia demonstrate high RNA quality in these samples (Figure 6(c)). We found no differences in RNA quality between all analyzed uteri and ovaries samples placed into RNA*later* from 15 min to 40 min after euthanasia.

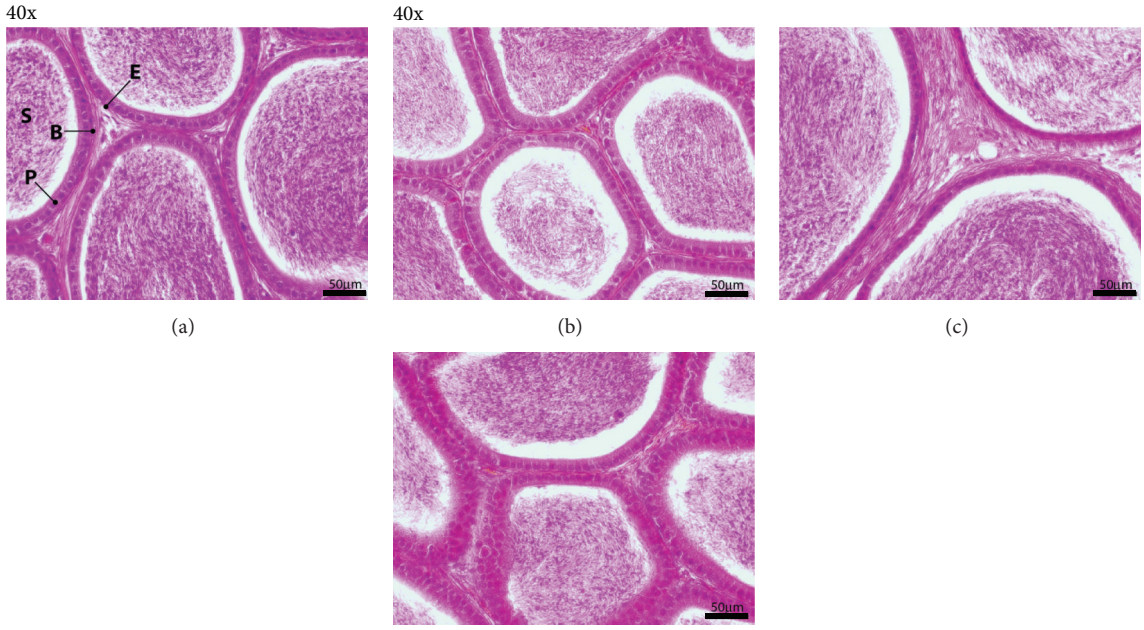

FIGURE 5: Morphological analysis of mouse epididymis after different postfixative modifications. Sections of adult mouse epididymis were stained with HE (all at 40x; magnification bar is 50 μm). (a) Control; (b) slow rehydration-dehydration stepwise replacement of ETOH-PBS-ETOH; (c) slow Re-ETOH *only* replacement; (d) rapid ETOH-PBS-ETOH transition. Epithelium (E), sperm (S), basal cell (B), and principal cell (P).

3.3.2. Long-Term Storage for RNA Analysis. Using ovary and uteri harvested from STS 135 mice, we also determined the effect of long-term (10 months) preservation in RNA*later* on RNA and protein quality (Figure 7). This time frame was chosen to mimic a possible storage scenario that could occur on the ISS. Ovaries and uterus from STS-135 ground controls stabilized in RNA*later* for 10 months showed excellent RNA quality (Figure 7(a)) and yield in range 6–8 μg.

3.3.3. Protein Stability. Although not commonly done, tissue stabilized in RNA*later* can be used for subsequent protein extraction. Protein obtained from samples stored in RNA*later* is suitable for western blotting or 2D gel electrophoresis, but not for applications that require native protein (Ambion Guideline for RNA*later*). We optimized the protocol for protein extraction from ovaries preserved in RNA*later* for one wk at RT or two wks at 4°C by using RIPA buffer or ProteoJet Lysis reagent (LR). Western analysis of β-actin integrity demonstrated that one wk ambient storage of testicular tissue in RNA*later* did not affect actin integrity as evidenced by the absence of proteolytic fragments and consistent signal intensity in replicate samples (Figure 6(d)).

3.3.4. Long-Term Storage for Protein Analysis. Protein from uteri stabilized in RNA*later* for 10 months after STS-135 mission was extracted with RIPA buffer. Immunoblot for ERα and β-actin verified excellent expression levels of both proteins with no evidence of proteolytic degradation of both proteins (Figure 7(b)). Quantitative densitometry analysis of western blots indicated reduced levels ERα in mostly flight animals. These results demonstrate that RNA*later* is an effective sample collection and stabilization reagent for protecting both RNA and protein under long-term conditions compatible for the ISS.

4. Discussion

We report here a logical method to determine the optimal time window of tissue harvest and fixation after euthanasia for use in multi-investigator tissue harvest programs that is compatible with processing of tissue sample obtained from space flight animals. We also demonstrate here a long-term storage regimen for animal tissues compatible with recovery of high quality RNA and protein under conditions similar to that on the ISS, when there may be many months between sample collection and return to Earth. The procedures set forth also include methods for tissue harvest at the site of return and for safe shipment to external laboratories for further processing for histopathology and recovery of protein and RNA. Several fixation/preservation studies have been carried out for plant samples [1, 4, 5]. One European Space Agency report included a brief discussion on fixation of mammalian cells in tissue culture for microscopy [6]. Freidin et al. [7] have demonstrated significant alterations on gene expression in lung carcinoma tissues collected about 30 minutes after harvest. Durrenberger et al. [8] reported that, in human brain samples collected from several brain banks, antemortem events appeared to negatively affect the RNA quality, but postmortem delays caused no significant deterioration. This observation supported earlier report that

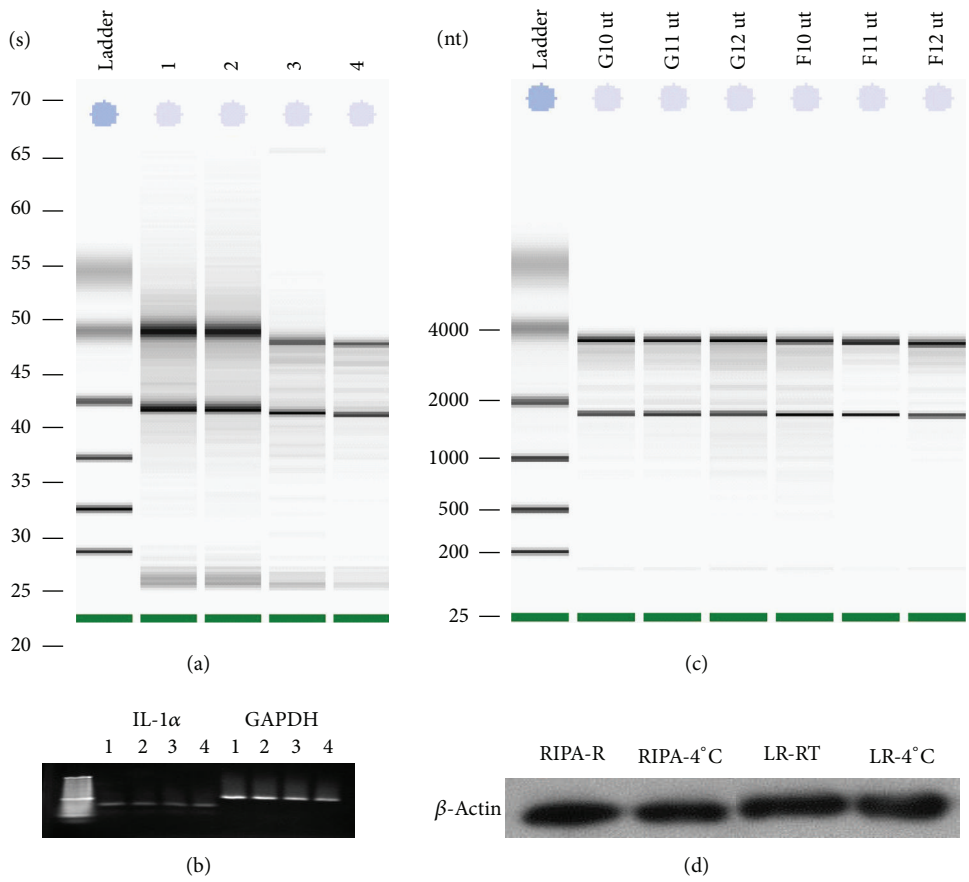

Figure 6: Effect of different extraction and storage methods on RNA and protein quality in ovaries, and testes extracted and/or stabilized in TRIzol or RNA*later*. (a) Total RNA integrity analysis. Total RNA was isolated from mouse testis and stabilized in TRIzol reagent (RNA yield and quality control (lane 1); RNA*later* for 2 wks at 4°C (lane 2); RNA*later* for 1 wk at room temperature and 1 wk at 4°C (lane 3); RNA*later* for 2 wks at RT (lane 4). (b) Agarose gel electrophoresis of PCR products with primers for IL-1α and GAPDH. For RT PCR total RNA was used after stabilization in TRIzol reagent (lane 1); RNA*later* for 2 wks at 4°C (lane 2); RNA*later* for 1 wk at RT and 1 wk at 4°C (lane 3); RNA*later* for 2 wks at RT (lane 4). (c) Total RNA integrity analysis STS-131 ground (G10, G11, and G12) and flight (F10, F11, and F12) uteri fixed in RNA*later* after 30–40 min after euthanasia. (d) Comparison of buffers to remove RNA*later* for subsequent western analysis of β-actin integrity in ovaries. Mouse ovaries were stored at RNA*later* for 1 wk at RT or 2 wk at 4°C; tissues were homogenized in RIPA lysis buffer (lanes 1, 2) or ProteoJET Lysis reagent (LR) (lanes 3, 4). Total cell lysates were prepared and subjected to SDS-PAGE. Western for β-actin is presented.

postmortem delay had negligible effect on RNA quality [9]. Human stomach has been described as the tissue showing the earliest sign of postmortem [10]. Presnell and Cina described stomach and pancreas as the earliest human tissues to deteriorate following death [11]. The significance of quick processing of histopathological specimen in a clinical setting has been identified by Rohr et al. [12]. However, we have not come across similar studies for animal tissues used in biomedical research. Prior to our study reported here, there was a significant knowledge gap in the literature for methods to process animal tissues compatible for multi-investigator Biospecimen Sharing Programs for space flight logistical scenarios. For our flight studies, using male and female mice on three different space shuttle flights and the BION M1 flight, it was critical to determine the optimum conditions of tissue harvest and processing for tissues of our interest, namely, testis, epididymis, ovary, and uteri.

Space flight studies usually comprise remotely dispersed multi-investigator collaborations. Thus, there is a need to ship tissue samples from the site of collection at the return-to-Earth laboratory facility for initial tissue harvest to the site of final processing and detailed data collection. With respect to collection of RNA samples, TRIzol reagent gives excellent RNA integrity; however it is a phenol-based solution and tissue preserved in TRIzol cannot be shipped internationally due to airline safety restrictions. Lyophilization of fresh tissue specimen has been shown to preserve RNA and protein quality and levels by Wu et al. [13]. Though lyophilization makes shipping easier, especially across international borders, it is not a viable option for preservation of highest quality histological analysis. To obtain optimum RNA and protein quality, our results demonstrate that mouse testicular tissue can be submerged in RNA*later* and stored successfully for analysis at a later time point, at least 10 months at −80°C. It should be noted that 10 months represents a minimum limit, and longer storage intervals would still need to be directly assessed. Given the current estimate for ISS SpaceX Dragon flights at approximately 3-month intervals, this would span

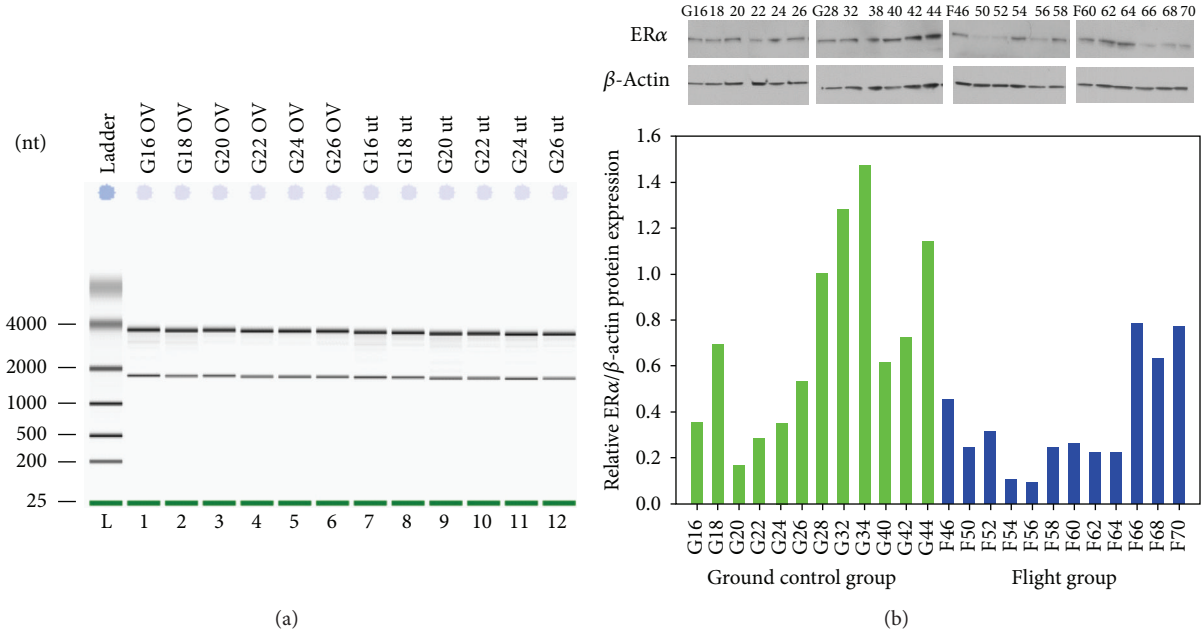

Figure 7: RNA and protein quality of STS-135 uteri and ovaries stabilized in RNA*later* for 10 months at −80°C. (a) STS-135 ground control (G16–G26) ovarian and uterine RNA integrity analysis. Total RNA was extracted and examined for RNA quality; (b) Western blot analysis of ERα and actin in STS-135 mouse uterus. Total cell lysates were prepared and subjected to SDS-PAGE (15 μg/lane). Western blot analysis was performed using the corresponding antibodies to check expression levels of the proteins. Representative Immunoblot (top) and its graphical presentation (bottom). Densitometric intensities of specific protein bands were digitally obtained and normalized to β-actin.

three opportunities for sample return after an experiment is terminated and ensure maintenance of RNA and protein sample quality. It is known that, in order to isolate high quality RNA and protein from mammalian tissue, the tissue must be processed directly after harvest. We determined, for our tissues of interest, that excellent RNA stability was achieved if the tissue samples were placed into RNA*later* up to 40 min after euthanasia. RNA*later* is a popular reagent that inactivates all cellular enzymes, including RNAses; thus RNA expression profiles can be preserved in situations when immediate RNA isolation is not feasible. The tissue can be stored in RNA*later* for a long time without nucleic acid degradation. RNA*later* has been used by investigators for collection of human tissue [14] and used in RNA expression microarrays [15]. Our results indicated that RNA*later* enables long-term tissue preservation for RNA and protein extraction compatible with delayed sample return from flight. This process should be evaluated for use on other tissues to maximize optimal histology and gene transcription data collection in the primary flight experiments as well as the Biospecimen Sharing Programs (BSP) investigators. Freidin et al. [7] have confirmed the significance of RNA*later* as a medium to preserve gene expression of lung tissues. Tissue processing methods should be standardized for best storage and analysis of harvested tissues. Our methods for tissue fixation, long-term storage, and recovery of protein and RNA are compatible for planned in-flight tissue harvest on ISS.

With regard to obtaining the best possible tissue fixation for histology collected under a multi-investigator Biospecimen Sharing Program, obtaining many tissues of interest to the participating investigators has to be considered in an integrated way to accommodate the scientific requirements of the overarching flight project, as well as the natural degradation process that tissues undergo as soon as euthanasia has occurred. Depending on the tissue and species, different windows of time from euthanasia to fixation may exist within which histological architecture (as well as RNA and protein integrity) is stable. In the study design reported here, we have determined the window of time and temperature for optimal postharvest maintenance of male and female tissue quality (testis, epididymis, ovary, and uterine horn) and sperm viability in mice and gerbils. These harvest protocols provide a logical method for integrating the tissue flow logistics for postflight animals for any project involving multiple investigators. Protocols compatible with investigators who require more rapid tissue retrieval can be identified and prioritized to ensure data preservation. We determined that mouse testes were able to retain excellent histological details when processed up to 3 hr after euthanasia. Sperm motility showed gradual decline with time. The authors would reiterate as mentioned in the Results section that sperm motility is a highly sensitive and variable parameter. It is normal to see major differences in motility of sperm obtained from not only one mouse to another, but also within samples obtained from the same mouse or gerbil. Nonetheless, even within the span of variability seen, our results indicate that, in case of mouse, there was no major difference in sperm motility between any of the time points, whereas in case of gerbil, we saw suggestions of a slight drop at 2.5 hr after harvest. Future studies for flight will require analysis of larger n's during definition

phase, if gerbils will be used. Of the tissues studied here, Mongolian gerbil ovaries appear most sensitive to delay in processing, and require more rapid posteuthanasia processing than mouse ovaries. Determining optimum conditions for tissue handling after harvest is very crucial and can help in maximizing tissue retrieval form animal models thereby maximizing data output. Based on the time-sensitivity, investigators may be able to plan the sequence in which the tissues are harvested starting with the most sensitive tissue to least sensitive.

Finally, with regard to the requirement to ship tissues fixed for histopathology, airline and ground transport providers (especially international carriers) have specific safety regulations that prohibit shipment of samples containing many widely used fixatives and preservatives of tissue histologic integrity. Science requirements may present challenges in using alternative fixatives. In this regard, Bouin's fixative (which contains picric acid) is the best fixative for the testis if the tissue is to be embedded in paraffin [16]. However, in space flight experiments, safety regulations prevent its use on flight platforms and its presence in tissue samples being shipped. Thus, we optimized protocols for fixative removal and storage of tissues in PBS for safe shipping, as well as reconstitution protocols for storing tissues in 70% ethanol to retain excellent histology.

5. Conclusion

Optimal time frames for harvesting testis, epididymis, ovary, and uteri without compromising the histological quality, sperm motility, and RNA quality have been determined. Differences in tissue-specific optimal fixation time windows were noted between mice and gerbils. We provide here new methods for (1) fixative removal and transfer of tissues into aqueous media for safe shipping and (2) reconstitution protocols into 70% ethanol that retains excellent histology. We conclude that stepwise replacement of ETOH-PBS-ETOH caused less degradation of histological quality of tissue than a single-step change of solution. Our results demonstrate that male and female mouse reproductive tissues stored in RNA*later* solution were stable and gave high quality RNA and protein after 10 months of storage at −80°C. Thus, we have determined methods for postharvest tissue processing to replace Bouin's with 70% ethanol for safe shipping across USA and also replace 70% ethanol with PBS to enable shipping of tissues across international borders. These protocols will facilitate integration of tissue harvest logistics in multi-investigator Biospecimen Sharing Programs for optimal tissue histology and retention of high quality RNA and protein recovery from animal tissues on long-term space flight experiments on ISS as well as other flight platforms.

Abbreviations

TBS-T: Tris buffered saline with 0.1% Tween 20
BSP: Biospecimen Sharing Program
ETOH: Ethyl alcohol
STS: Space Transport System
PBS: Phosphate buffered saline
ISS: International Space Station
CASA: Computer assisted sperm analysis
Wk: Week
RT: Room temperature
IACUC: Institutional Animal Care and Use Committee
KSC: Kennedy Space Center
RNA: Ribonucleic acid
CO_2: Carbon dioxide.

Conflict of Interests

The authors declare that there is no conflict of interests regarding the publication of this paper.

Acknowledgments

This study is supported by NASA Grant NNX09AP04G to Joseph S. Tash. The authors wish to acknowledge the excellent support for the project from Richard Boyle, Paula Dumars, Vera Vizir, Gwo-Shing, and Kenny Vassigh from Ames Research Center, NASA, and from Stacy Engel, Ashleigh Ruggles, and Ramona Bobber, at Kennedy Space Center, Florida. The authors thank Stanton Fernald of the KUMC Imaging Core for assistance in preparation of final figures.

References

[1] A.-L. Paul, H. G. Levine, W. McLamb et al., "Plant molecular biology in the space station era: utilization of KSC fixation tubes with RNAlater," *Acta Astronautica*, vol. 56, no. 6, pp. 623–628, 2005.

[2] J. Luo, V. Gupta, B. Kern et al., "Role of FYN kinase in spermatogenesis: defects characteristic of FYN-null sperm in mice," *Biology of Reproduction*, vol. 86, no. 1, article 22, 2012.

[3] J. S. Tash, B. Attardi, S. A. Hild, R. Chakrasali, S. R. Jakkaraj, and G. I. Georg, "A novel potent indazole carboxylic acid derivative blocks spermatogenesis and is contraceptive in rats after a single oral dose," *Biology of Reproduction*, vol. 78, no. 6, pp. 1127–1138, 2008.

[4] M. Braun, B. Buchen, and A. Sievers, "Fixation procedure for transmission electron microscopy of *Chara rhizoids* under microgravity in a Spacelab (IML-2)," *Journal of Biotechnology*, vol. 47, no. 2-3, pp. 245–251, 1996.

[5] V. D. Kern, F. D. Sack, N. J. White, K. Anderson, W. Wells, and C. Martin, "Spaceflight hardware allowing unilateral irradiation and chemical fixation in petri dishes.," *Advances in Space Research*, vol. 24, no. 6, pp. 775–778, 1999.

[6] F. J. Medina, A. Cogoli, C. Dournon et al., "Preservation of samples during space experiments," in *Topical Teams in the Life & Physical Sciences: Towards New Research Applications in Space*, pp. 200–208, European Space Agency, 2005.

[7] M. B. Freidin, N. Bhudia, E. Lim, A. G. Nicholson, W. O. Cookson, and M. F. Moffatt, "Impact of collection and storage of lung tumor tissue on whole genome expression profiling," *Journal of Molecular Diagnostics*, vol. 14, no. 2, pp. 140–148, 2012.

[8] P. F. Durrenberger, S. Fernando, S. N. Kashefi et al., "Effects of antemortem and postmortem variables on human brain mRNA quality: a brainNet Europe study," *Journal of Neuropathology & Experimental Neurology*, vol. 69, no. 1, pp. 70–81, 2010.

[9] J. F. Ervin, E. L. Heinzen, K. D. Cronin et al., "Postmortem delay has minimal effect on brain RNA integrity," *Journal of Neuropathology and Experimental Neurology*, vol. 66, no. 12, pp. 1093–1099, 2007.

[10] A. R. Thomas, *A Practical Guide for Making Post-Mortem Examinations*, BiblioBazaar, 2009.

[11] S. E. Presnell and S. J. Cina, "Postmortem changes," Medscape Drugs & Diseases, 2013, http://emedicine.medscape.com/article/1680032-overview.

[12] L. R. Rohr, L. J. Layfield, D. Wallin, and D. Hardy, "A comparison of routine and rapid microwave tissue processing in a surgical pathology laboratory: quality of histologic sections and advantages of microwave processing," *The American Journal of Clinical Pathology*, vol. 115, no. 5, pp. 703–708, 2001.

[13] Y. Wu, M. Wu, Y. Zhang et al., "Lyophilization is suitable for storage and shipment of fresh tissue samples without altering RNA and protein levels stored at room temperature," *Amino Acids*, vol. 43, no. 3, pp. 1383–1388, 2012.

[14] S. R. Florell, C. M. Coffin, J. A. Holden et al., "Preservation of RNA for functional genomic studies: a multidisciplinary tumor bank protocol," *Modern Pathology*, vol. 14, no. 2, pp. 116–128, 2001.

[15] G. L. Mutter, D. Zahrieh, C. Liu et al., "Comparison of frozen and RNALater solid tissue storage methods for use in RNA expression microarrays," *BMC Genomics*, vol. 5, article 88, 2004.

[16] L. D. Russell, R. A. Ettlin, H. A. Sinha, and E. D. Clegg, Eds., *Histological and Histopathological Evaluation of the Testis*, Cache River Press, Clearwater, Fla, USA, 1990.

Hindawi Publishing Corporation
BioMed Research International
Volume 2015, Article ID 342565, 7 pages
http://dx.doi.org/10.1155/2015/342565

Research Article

Large Artery Remodeling and Dynamics following Simulated Microgravity by Prolonged Head-Down Tilt Bed Rest in Humans

Carlo Palombo,[1] Carmela Morizzo,[1] Martino Baluci,[1] Daniela Lucini,[2] Stefano Ricci,[3] Gianni Biolo,[4] Piero Tortoli,[3] and Michaela Kozakova[1]

[1]*Department of Surgical, Medical, Molecular and Critical Area Pathology, University of Pisa, 56124 Pisa, Italy*
[2]*Department of Medical Biotechnologies and Translational Medicine, University of Milan, 20129 Milan, Italy*
[3]*Department of Information Engineering, University of Florence, 50139 Florence, Italy*
[4]*Department of Medicine, Surgery and Health Sciences, University of Trieste, 34127 Trieste, Italy*

Correspondence should be addressed to Carlo Palombo; carlo.palombo@med.unipi.it

Received 16 May 2014; Revised 26 October 2014; Accepted 27 October 2014

Academic Editor: Mariano Bizzarri

The effects of simulated microgravity on the static and dynamic properties of large arteries are still mostly unknown. The present study evaluated, using an integrated vascular approach, changes in structure and function of the common carotid and femoral arteries (CCA and CFA) after prolonged head-down tilt bed rest (HDTBR). Ten healthy men were enrolled in a 5-week HDTBR study endorsed by the Italian Space Agency (ASI). Arterial geometry, flow, stiffness, and shear rate were evaluated by ultrasound. Local carotid pulse pressure and wave reflection were studied by applanation tonometry. After five weeks of HDTBR, CFA showed a decrease in lumen diameter without significant changes in wall thickness (IMT), resulting in an inward remodeling. Local carotid pulse pressure decreased and carotid-to-brachial pressure amplification increased. The ratio of systolic-to-diastolic volumetric flow in CFA decreased, whereas in CCA it tended to increase. Indices of arterial stiffness and shear rate did not change during HDTBR, either in CCA or CFA. In summary, prolonged HDTBR has a different impact on CCA and CFA structure and flow, probably depending on the characteristics of the vascular bed perfused.

1. Introduction

Prolonged head-down tilt bed rest (HDTBR) represents an established experimental model allowing investigating the physiologic adaptations to microgravity conditions on the ground [1]. Studies evaluating the effect of simulated microgravity on cardiovascular system have demonstrated that the prolonged HDTBR is followed by a significant decrease in left ventricular (LV) mass accompanied by a reduction in LV performance [2]. Our group has previously demonstrated that a reduction in echocardiographic indices of LV systolic and diastolic performance after a 5-week period of HDTBR does not reflect an impairment in intrinsic myocardial function, but simply an adaptive response to circulatory unloading [3]. Data regarding response of the arterial system to bed rest are less clear. Prolonged unloading has been shown to induce an inward remodeling of the femoral artery with time-dependent decrease in arterial size, reaching 17% after 52 days of bed rest [4]. Eight weeks of physical inactivity have been also shown to increase carotid and femoral artery wall thickness and wall-to-lumen ratio [5]. Pathophysiologic mechanisms underlying these structural changes are supposed to include inactivity-related muscle atrophy associated with a reduced metabolic demand of the downstream muscle tissue [6], as well as an impact of altered hemodynamic stimuli on the arterial wall. It has been demonstrated that arteries are capable to respond to changes in hemodynamic stimuli (flow and shear rate) and mechanical forces (circumferential and pulsatile stress) by modification of their geometry [7]. However, previous studies did not provide definite evidence on bed rest induced changes in flow, shear rate, or wall stress, and data regarding impact

of deconditioning on arterial stiffness and wave reflection are sporadic [8]. In the present study, the common carotid and femoral arteries were investigated at baseline and after a 5-week HDTBR by an integrated vascular approach allowing evaluating impact of deconditioning on different structural and functional properties of the arterial system.

2. Methods

2.1. Subjects. Ten healthy young volunteers, all men, mean age 23 ± 2 years, were enrolled in a multidisciplinary HDTBR study endorsed by the Italian Space Agency (ASI) and taking place at the Orthopedic Hospital Valdoltra, Ankaran, Slovenia. None of the volunteers was a smoker. Medical history, physical examination, laboratory examinations, resting and stress ECG, and echocardiography have excluded any acute or chronic medical problem. The National Committee for Medical Ethics of the Slovene Ministry of Health (Ljubljana, Slovenia) approved the study. All participants were informed about the aim of the investigation, the procedures, and the methods and signed a written informed consent form according to the Declaration of Helsinki.

2.2. Study Protocol. All participants underwent a 5-week period of bed rest in a 6° head-down tilt position (HDTBR). During the bed rest period, participants were kept strictly in bed for 24 hours a day, and none of them took any medication or underwent any physical or pharmacological countermeasure. Dietary intake was 2300 kcal/day, and water intake was 1.0–1.5 L/day. Diuresis was monitored daily, and BP and heart rate were measured every 4 hours during daytime. Body composition and hematocrit were measured before and at the end of the bed rest. Carotid and femoral ultrasound, carotid applanation tonometry, carotid-femoral pulse wave velocity (PWV), and cardiac ultrasound were performed the day before entering bed rest and within 24 hours after its termination. Vascular and cardiac examinations were performed in a quiet room, three hours after a light breakfast and after an acclimatization period of 30 min in supine position. All vascular acquisitions and readings were performed by a single operator (CM).

2.3. Measurements

2.3.1. Body Composition Assessment. Body weight and fat-free mass were measured by electrical bioimpedance (BioScan 916S; Maltron International Ltd., Essex, UK).

2.3.2. Carotid and Femoral Ultrasound. On the right common carotid and femoral artery (CCA, CFA), two sequential acquisitions were performed using a modified commercially available equipment (MyLab30, Esaote, Firenze, Italy, with a 7.5–12 MHz broadband linear transducer, LA435), in order to obtain the following measures: (a) intima-media thickness (IMT), systolic, diastolic, and mean arterial luminal diameters; (b) centerline blood flow velocity (by conventional Duplex ultrasound); (c) shear rate values directly measured at the near and far arterial wall (by multigate Doppler system). For all ultrasound acquisitions, the angle of inclination for Doppler velocity measurements was consistently adjusted to 60°, whereas the vessel lumen was set parallel to the transducer.

(a) Longitudinal B-mode images of the right CCA and CFA with well-defined intima-media complex of the near and far wall were obtained and a loop over 5 cardiac cycles was stored. Brachial pressure and heart rate were measured during loop acquisition (Omron 705, Tokyo, Japan). Vascular ultrasound scans were analyzed by the computer-driven image analysis system MIP (Medical Image Processing; Institute of Clinical Physiology, CNR, Pisa, Italy); end-diastolic and end-systolic frames of the CCA or CFA were selected; end-diastolic far-wall IMT and minimum and maximum luminal diameters were measured within a region of interest. Arterial remodeling was assessed as a ratio of end-diastolic IMT and luminal radius (IMT/radius), where radius was calculated as minimum diameter/2. End-diastolic wall stress (kPa) was calculated as follows: diastolic BP (in kPa) ∗ end-diastolic radius/IMT. Delta diameter (Δ diameter) was calculated as the difference between maximum and minimum diameter, and the stiffness index beta was calculated as minimum diameter ∗ ln(Systolic BP/Diastolic BP)/Δ diameter. The values reported represent the average of three cardiac cycles. Intraindividual variability of IMT and arterial diameter measurement by MIP in our laboratory is 4.8 ± 2.8% and 3.1 ± 1.9%, respectively. To estimate mean volumetric flow per beat, CCA and CFA diameter averaged over the entire cardiac cycle was measured from the radiofrequency signal processed by a dedicated software tool (QIMT, Esaote Europe, Maastricht, Netherlands) in a 1 region of interest placed at the same area as flow-velocity integral was measured.

(b) In spectral Doppler recordings, peak systolic and diastolic velocities as well as systolic, diastolic and systo-diastolic flow-velocity integrals were measured, both for CCA and CFA. Resistive index was calculated as follows: (peak systolic velocity − peak diastolic velocity)/peak systolic velocity. Systolic and diastolic volumetric flows per beat were calculated as systolic and diastolic arterial area ($\Pi * \text{diameter}^2/4$) multiplied by the corresponding flow-velocity integral. Mean volumetric flow over cardiac cycle was calculated as systo-diastolic flow-velocity integral multiplied by area of luminal diameter averaged over cardiac cycle as obtained from radio-frequency signal (see above). All values are reported as the average of 3 cardiac cycles.

(c) Shear rate was assessed by a validated multigate Doppler system determining a flow velocity profile from a matrix of 128-point power spectral densities corresponding to 128 different depths along the Doppler beam [9]. A custom PC board based on a high-speed digital signal processor was used to process the quadrature demodulated echo signals derived from the MyLab30 and to display results in real time. A polynomial least-square fit is applied off-line on the 128 experimental velocity points, and the resulting profile is used to evaluate the gradient with respect to radius. The local peak shear rate at the near and far blood-wall interfaces was calculated.

2.3.3. Carotid Applanation Tonometry. Carotid applanation tonometry was performed on the right CCA using a validated system (PulsePen; Diatecne, Milan, Italy) [10]. Carotid pressure waveforms were calibrated according to brachial mean and diastolic pressure as previously described [11]. In the carotid pressure waveform, the following parameters were measured: local systolic BP, local pulse pressure, and augmentation index (AIx). Pulse pressure index was calculated as local pulse pressure divided by mean BP and pulse pressure amplification as the ratio of brachial to carotid pulse pressure [12]. The mean of 3 measurements was used for statistical analysis.

2.3.4. Carotid-Femoral Pulse Wave Velocity. Carotid-femoral PWV was measured according to current guidelines [13] using the Complior device (Alam Medical, Vincennes, France). Briefly, arterial waveforms were obtained transcutaneously over the right CCA and femoral artery, and the time delay (t) was measured between the feet of the two waveforms. The distance (D) covered by the waves was established as the distance between the two recording sites. PWV was then calculated as D (meters)/t (seconds). The measurement was performed three times and the mean value was used for statistical analysis. Simultaneous BP measurement was performed at the left brachial artery (Omron, Kyoto, Japan). In our laboratory, intraindividual variability of PWV measurement is 4.5 ± 2.8%.

2.3.5. Cardiac Ultrasound. Cardiac ultrasound was performed as previously described [3]. Stroke volume was measured as a product of aortic area and flow-velocity integral in aortic orifice [14]. Flow-velocity integral was obtained also in ascending aorta from the suprasternal notch. Results on changes in LV mass, performance, and loading conditions observed in the same study group were previously published in detail [3].

2.4. Statistical Analysis. Quantitative data are expressed as mean ± sd. Paired t-test was used to compare the measurements obtained before and after HDTBR. Linear univariate regression analysis was used to test the relationships between bed rest-induced changes in arterial diameter or flow and in FFM or stroke volume. Statistical significance was set at a value of P less than 0.05. Statistical analysis was performed by JMP software, version 8.0.2 (SAS Institute Inc., Cary, North Carolina, USA).

3. Results

During the bed rest period, body weight, BMI, fat FFM and Doppler-derived stroke volume, and flow-velocity integral in ascending aorta diminished, peripheral BP did not change significantly, and heart rate and hematocrit increased (Table 1).

After 5 weeks of HDTBR, no significant changes were observed in CCA geometry and stiffness (Table 2). CFA diameter significantly decreased (minimum diameter by 10 ± 4%), CFA intima-media thickness did not change, and therefore, the ratio end-diastolic CFA IMT/radius increased and circumferential wall stress decreased (Table 2). The changes in CFA minimum diameter showed a trend to correlate with changes in fat-free mass ($r = 0.49$; $P = 0.15$). CFA beta stiffness index remained unchanged after HDTBR (Table 2).

Table 1: Main anthropometric and hemodynamic characteristics and hematocrit in 10 healthy volunteers before and after HDTBR.

	Before	After	P
Weight (kg)	75 ± 10	73 ± 9	*<0.01*
BMI (kg/m^2)	23.3 ± 2.0	22.8 ± 1.6	*<0.05*
Fat-free mass (kg)	64 ± 5	61 ± 5	*<0.0001*
Hematocrit (%)	44.4 ± 2.9	47.9 ± 2.1	*0.001*
Systolic BP (mmHg)	115 ± 17	113 ± 10	*0.51*
Diastolic BP (mmHg)	62 ± 7	65 ± 4	*0.33*
Pulse pressure (mmHg)	53 ± 11	48 ± 10	*0.19*
Heart rate (bpm)	60 ± 10	71 ± 7	*<0.005*
Stroke volume (mL)	76 ± 11	63 ± 10	*<0.01*
FVI ascending aorta (cm)	21.7 ± 2.1	19.2 ± 2.8	*0.01*

BMI: body mass index; FFM: fat-free mass; BP: blood pressure; FVI: flow-velocity integral.

Responses in flow velocities and volumes differed between CCA and CFA. In CCA, peak systolic and diastolic velocity did not change significantly during the bed rest period. In CFA, both peak systolic and diastolic velocities increased, but the increase was higher for diastolic velocity and, consequently, the resistive index decreased. Systolic volumetric flow per beat remained stable both in CCA and in CFA. In contrast, diastolic volumetric flow showed a trend to decrease in CCA, whereas it increased in CFA (Table 2). Consequently, the ratio of systolic-to-diastolic flow in CCA tended to increase, while in CFA it significantly decreased. The relationships between volumetric flow per beat in CCA and stroke volume or ascending aorta flow-velocity integral (estimated by Doppler echocardiography) as well as the relationship between volumetric flow per beat in CFA and stroke volume were tested. In CCA, the mean and diastolic flow per beat at baseline were strongly related to baseline stroke volume ($r = 0.75$; $P = 0.01$ and $r = 0.82$; $P < 0.001$), and the changes in mean and diastolic flow per beat during HDTBR were related to changes in stroke volume ($r = 0.70$; $P < 0.05$ and $r = 0.54$; $P = 0.10$), as well as to changes in ascending aorta flow-velocity integral ($r = 0.78$; $P < 0.01$ and $r = 0.48$; $P = 0.15$). None of these relationships were observed for CFA.

Wall shear rate at near and far arterial wall did not change during HDTBR either in CCA or in CFA (Table 2). In CCA, the mean luminal diameter was positively related to wall shear rate at anterior ($r = 0.62$; $P = 0.05$) and posterior wall ($r = 0.63$; $P = 0.05$); however, this correlation was lost after the period of bed rest. No relationship between shear rate and luminal diameter was observed for CFA.

Carotid femoral PWV and AIx did not change after 5 weeks of HDTBR, while local carotid pulse pressure and pulse pressure index decreased and pressure amplification index

Table 2: Common carotid artery and common femoral artery structure, stiffness, and flow before and after HDTBR in 10 healthy volunteers.

	CCA		P	CFA		P
	Before	After		Before	After	
IMT (μm)	503 ± 48	520 ± 36	*0.27*	515 ± 79	523 ± 57	*0.58*
Diameter minimum (mm)	5.1 ± 0.3	5.0 ± 0.3	*0.12*	7.4 ± 0.9	6.7 ± 1.0	*<0.01*
Diameter maximum (mm)	5.9 ± 0.3	5.8 ± 0.3	*0.09*	8.1 ± 1.0	7.4 ± 1.0	*<0.01*
Δ diameter (mm)	0.80 ± 0.13	0.78 ± 0.11	*0.71*	0.74 ± 0.22	0.72 ± 0.23	*0.72*
End-diastolic IMT/radius	0.18 ± 0.02	0.19 ± 0.02	*0.14*	0.14 ± 0.03	0.16 ± 0.02	*<0.01*
End-diastolic wall stress (kPa)	42.4 ± 5.9	41.5 ± 5.6	*0.70*	60.7 ± 10.9	54.9 ± 7.9	*0.05*
Beta index	3.2 ± 0.7	2.9 ± 0.7	*0.29*	6.5 ± 1.9	5.6 ± 2.1	*0.20*
Peak velocity systolic (cm/s)	124 ± 25	125 ± 22	*0.83*	89 ± 15	116 ± 35	*0.09*
Peak velocity diastolic (cm/s)	25 ± 5	26 ± 6	*0.66*	6 ± 3	10 ± 5	*<0.05*
Resistive index	0.79 ± 0.04	0.79 ± 0.04	*0.88*	0.94 ± 0.02	0.91 ± 0.02	*0.05*
Mean flow per beat (mL)	9.3 ± 1.6	8.6 ± 1.3	*0.42*	9.4 ± 2.1	9.3 ± 2.4	*0.90*
Systolic flow per beat (mL)	4.9 ± 0.9	5.0 ± 0.6	*0.74*	7.8 ± 2.1	7.1 ± 2.3	*0.37*
Diastolic flow per beat (mL)	3.4 ± 0.7	2.9 ± 0.6	*0.08*	1.5 ± 0.5	1.9 ± 0.7	*0.05*
Ratio syst/diast flow per beat	1.5 ± 0.5	1.7 ± 0.4	*0.07*	5.8 ± 2.0	3.9 ± 0.6	*0.01*
WSR peak near wall (s^{-1})	524 ± 80	575 ± 120	*0.29*	569 ± 177	557 ± 197	*0.89*
WSR peak far wall (s^{-1})	460 ± 107	494 ± 95	*0.49*	357 ± 52	326 ± 69	*0.34*

IMT: intima-media thickness; WSR: wall shear rate.

Table 3: Carotid-femoral pulse wave velocity and carotid pressure waveform analysis before and after HDTBR in 10 healthy volunteers.

	Before	After	P
C-F PWV (m/s)	6.9 ± 1.0	6.9 ± 0.7	*0.53*
Local SBP (mmHg)	106 ± 11	101 ± 7	*0.23*
Local PP (mmHg)	44 ± 11	36 ± 7	*<0.05*
PPI	0.55 ± 0.11	0.46 ± 0.09	*0.05*
AIx	6.6 ± 5.9	5.4 ± 4.4	*0.50*
Pressure amplification	1.24 ± 0.11	1.31 ± 0.10	*<0.05*

C-F PWV: carotid-femoral pulse wave velocity; SBP: systolic blood pressure; PP: pulse pressure; PPI: pulse pressure index; AIx: augmentation index.

increased (Table 3). Changes in hematocrit were not related to changes in vascular measures.

4. Discussion

The present study compares the response of large elastic and muscular artery to prolonged HDTBR and provides some novel information about arterial mechanics and flow dynamics during deconditioning that are summarized in Figure 1. A complex vascular approach integrating established investigative modalities with new advanced techniques was exploited to this purpose.

4.1. Bed Rest Deconditioning and Vascular Geometry. In our young healthy volunteers, an inward remodeling of femoral artery, due to luminal diameter reduction, and a diminution of circumferential wall stress was observed after a 35-day bed rest. Carotid geometry, on the other hand, was not significantly influenced by deconditioning, a finding confirming the differences in response of carotid and femoral artery to bed rest. Observed reduction in femoral artery diameter is in agreement with results of the Berlin Bed Rest (BBR) study [4] and may reflect structural and/or functional changes, extensively discussed in a review paper of Thijssen et al. [7]. In our study, the changes in CFA diameter showed a trend to correlate directly with changes in fat-free mass. Such a correlation might suggest that the reduction in CFA lumen reflects a reduced metabolic demand in a downstream muscle tissue, as the gravitational unloading involves both artery and muscle. Yet, similar to the BBR study, femoral artery volumetric flow did not decrease after bed rest. This apparent discrepancy could be explained by the fact that conduit arteries adapt primarily to peak blood flow and oxygen demand during exercise [15]. The association between conduit artery diameter and muscle work has been suggested also in a recent study, in which a reduction in femoral artery diameter was demonstrated in subjects wearing a mechanical device (HEPHAISTOS) allowing an "unloaded orthosis" [16], that is, a reduction of muscle work with unchanged gravitational acceleration.

In contrast with results of the second BBR study [5] reporting an increment in CCA and femoral artery IMT after a 60-days bed rest period, we did not observe a significant change in carotid or femoral wall thickness; a shorter duration of bed rest in our study could explain the discrepancy.

4.2. Bed Rest Deconditioning and Blood Flow. Previous studies evaluating the effect of unloading on the blood flow in the lower extremity have produced inconclusive evidence. In the BBR study [4], the mean blood flow did not change in CFA and superficial femoral artery after bed rest; in the HEPHAISTOS study [16], blood flow volume in superficial

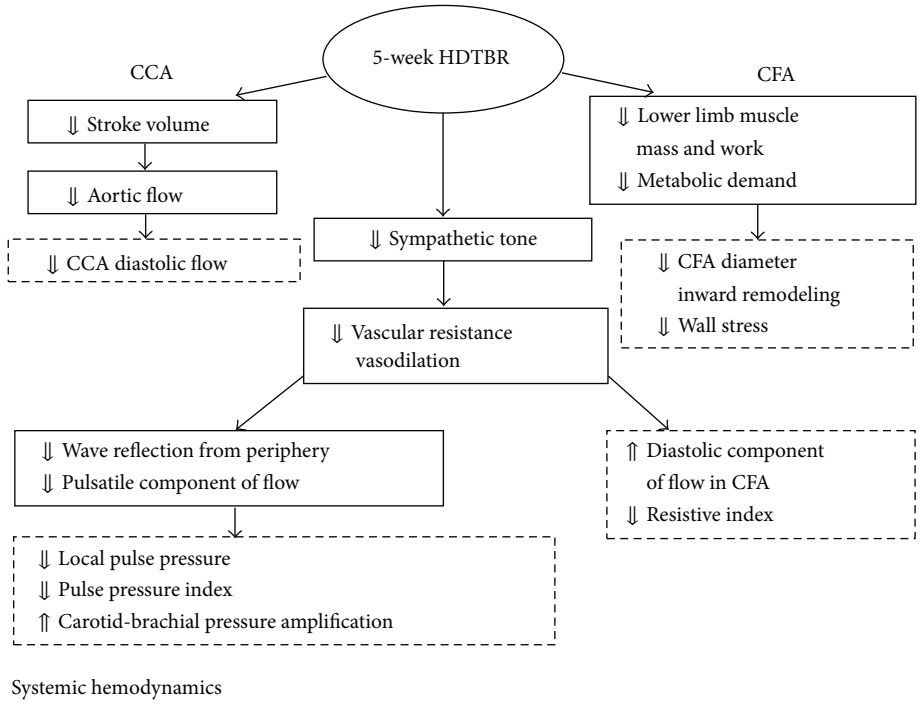

Figure 1: Schematic representation of changes observed at common carotid level, at femoral artery level, and in central hemodynamics after 35-days head-down tilt bed rest in 10 young healthy volunteers.

femoral artery remained unaffected by a reduction in muscle work while flow velocity increased by 17%; in studies using plethysmography, the blood flow at the arteriolar level decreased [17]. In a HDTBR study, a large portion of blood flow reduction as measured by plethysmography was observed already after the first day of unloading [18]. However, plethysmographic and Doppler measurements are hardly comparable.

Our study is the first to look separately at the systolic and diastolic flow velocities and volumes, both at CCA and CFA levels. In CCA, the diastolic component of volumetric flow after HDTBR showed trend to decrease, and the changes in both diastolic and mean volumetric flow were directly related to changes in stroke volume and in flow-velocity integral in ascending aorta. This observation suggests that carotid artery flow simply mirrors the changes occurring in aortic flow. In contrast, in CFA, the diastolic component of local blood flow significantly increased and, consequently, the resistive index and the ratio of systolic to diastolic flow volume decreased. This behavior may reflect a decrease in local vascular resistance at arteriolar level of the leg. Based upon evidence from previous HDTBR studies, a reduction of sympathetic firing to lower limb vessels could explain our finding. Stout et al. reported that during simulated microgravity, a cutaneous microcirculatory vasodilation is more marked in the lower than in the upper part of the body, being related to a baroreflex-mediated withdrawal of a sympathetic tone [19]. More recently, in healthy volunteers maintained for 90 days in HDTBR, Ferretti et al. demonstrated a significant reduction of the efferent muscle sympathetic nerve activity in the leg [20].

Wall shear rate, describing the tangential force exerted by the flow stream on the arterial wall, did not change during the study, either in elastic or muscular artery. A role of shear rate in arterial diameter control was suggested by a direct relationship between near- and far-wall shear rate and CCA luminal diameter at baseline conditions [21]. However such a relationship was not observed at femoral artery level.

4.3. Bed Rest Deconditioning, Large Artery Stiffness, and Central Pressure. The lack of bed rest induced changes in indices of either local carotid and femoral stiffness or segmental aortic stiffness (Table 3) further supports the premise that the changes in large artery geometry and flow depend upon functional instead of structural vascular changes. The significant reduction in the local carotid pulse pressure, a good surrogate of aortic pressure [22], together with the reduction in the pulse pressure index and the increase in the carotid-to-brachial pressure amplification estimated by means of carotid waveform analysis, reflect a significant decrease in the pulsatile component of central pressure compared to the steady one and, possibly, a reduction of wave reflection from a vasodilated periphery.

5. Study Limitations

This study has several limitations. First, the population studied is small and consists only of men. Second, all participants were young, and thus the results do not provide information on the effect of bed rest on arterial structure and function in older subjects. Third, vascular examinations were performed

only one day before and one day after HDTBR; consequently, we could not evaluate a sequence of changes over the bed rest period or after termination of bed rest. Fourth, plasma viscosity was not measured, so that only wall shear rate but not wall shear stress could be assessed. Furthermore, the experimental model used in this study, although established for simulating unloading conditions related to microgravity, does not allow separating the effects of a reduced muscle activity from those of a reduced gravitational acceleration. Finally, AIx values were not adjusted for heart rate. Due to the significant increase in heart rate observed after bed rest, we could have overestimated AIx and underestimated a reduction in wave reflection.

6. Conclusion

An integrated vascular approach combining established and experimental ultrasound, arterial contour wave analysis, and pulse wave velocity assessment was exploited to investigate the adaptation of large arteries to microgravity conditions simulated by HDTBR. Prolonged HDTBR showed a different impact on CCA and CFA structure and flow, probably depending on the characteristics of the vascular bed perfused. Changes in CCA blood flow seem to reflect bed rest induced decrease in stroke volume and aortic flow and did not alter CCA geometry. Reduction in CFA luminal diameter and inward remodeling may result from reduced metabolic demand in a downstream unloaded muscle tissue, and changes in CFA flow may reflect decrease in local vascular resistance secondary to withdrawal of a sympathetic tone. Observed changes in systemic hemodynamics that included decrease in local pulse pressure and pulse pressure index and increase in carotid-brachial pressure amplification suggest a reduction of wave reflection from a vasodilated periphery (Figure 1). Therefore, 5-week HDTBR results in a relative reduction of the pulsatile versus the steady component of blood flow and arterial pressure, possibly reflecting changes in systemic hemodynamics and in sympathetic control of the arteriolar tone.

In the prospect of improving the management of subjects undergoing real microgravity conditions, data obtained in this study confirm the indication to active counter-measurements aimed to prevent unloading-related sarcopenia as well as the possible usefulness of common carotid artery as a "window" to monitor central hemodynamic changes.

Conflict of Interests

The authors declare that there is no conflict of interests regarding the publication of this paper.

Acknowledgments

The authors are grateful to Dr. Bostjan Simunic, Institute of Kinesiology Research, University of Primorska, Koper, and to the personnel at the Valdoltra Orthopaedic Hospital in Ankaran (Slovenia) for their valuable medical assistance and technical support. This study was partly supported by grants of the Italian Space Agency (ASI), projects Disorders of Motor and Cardio-Respiratory Control (DMCR) and Osteoporosis and Muscle Atrophy (OSMA), and a Grant (PRIN 2010-2011) of the Italian Ministry of University and Research (MIUR).

References

[1] J.-O. Fortrat, D. Sigaudo, R. L. Hughson, A. Maillet, Y. Yamamoto, and C. Gharib, "Effect of prolonged head-down bed rest on complex cardiovascular dynamics," *Autonomic Neuroscience: Basic and Clinical*, vol. 86, no. 3, pp. 192–201, 2001.

[2] M. A. Perhonen, J. H. Zuckerman, and B. D. Levine, "Deterioration of left ventricular chamber performance after bed rest: "cardiovascular deconditioning" or hypovolemia?" *Circulation*, vol. 103, no. 14, pp. 1851–1857, 2001.

[3] M. Kozàkovà, E. Malshi, C. Morizzo et al., "Impact of prolonged cardiac unloading on left ventricular mass and longitudinal myocardial performance: an experimental bed rest study in humans," *Journal of Hypertension*, vol. 29, no. 1, pp. 137–143, 2011.

[4] M. W. P. Bleeker, P. C. E. de Groot, G. A. Rongen et al., "Vascular adaptation to deconditioning and the effect of an exercise countermeasure: results of the Berlin Bed Rest study," *Journal of Applied Physiology*, vol. 99, no. 4, pp. 1293–1300, 2005.

[5] N. T. L. van Duijnhoven, D. J. Green, D. Felsenberg, D. L. Belavý, M. T. E. Hopman, and D. H. J. Thijssen, "Impact of bed rest on conduit artery remodeling: effect of exercise countermeasures," *Hypertension*, vol. 56, no. 2, pp. 240–246, 2010.

[6] P. C. E. de Groot, M. W. P. Bleeker, and M. T. E. Hopman, "Magnitude and time course of arterial vascular adaptations to inactivity in humans," *Exercise and Sport Sciences Reviews*, vol. 34, no. 2, pp. 65–71, 2006.

[7] D. H. J. Thijssen, D. J. Green, and M. T. E. Hopman, "Blood vessel remodeling and physical inactivity in humans," *Journal of Applied Physiology*, vol. 111, no. 6, pp. 1836–1845, 2011.

[8] E. V. Nosova, P. Yen, K. C. Chong et al., "Short-term physical inactivity impairs vascular function," *Journal of Surgical Research*, vol. 190, pp. 672–682, 2014.

[9] P. Tortoli, T. Morganti, G. Bambi, C. Palombo, and K. V. Ramnarine, "Noninvasive simultaneous assessment of wall shear rate and wall distension in carotid arteries," *Ultrasound in Medicine & Biology*, vol. 32, no. 11, pp. 1661–1670, 2006.

[10] P. Salvi, G. Lio, C. Labat, E. Ricci, B. Pannier, and A. Benetos, "Validation of a new non-invasive portable tonometer for determining arterial pressure wave and pulse wave velocity: the PulsePen device," *Journal of Hypertension*, vol. 22, no. 12, pp. 2285–2293, 2004.

[11] L. M. Van Bortel, E. J. Balkestein, J. J. van der Heijden-Spek et al., "Non-invasive assessment of local arterial pulse pressure: comparison of applanation tonometry and echo-tracking," *Journal of Hypertension*, vol. 19, no. 6, pp. 1037–1044, 2001.

[12] A. P. Avolio, L. M. Van Bortel, P. Boutouyrie et al., "Role of pulse pressure amplification in arterial hypertension: experts' opinion and review of the data," *Hypertension*, vol. 54, pp. 375–383, 2009.

[13] P. Boutouyrie and S. J. Vermeersch, "Determinants of pulse wave velocity in healthy people and in the presence of cardiovascular risk factors: establishing normal and reference values," *European Heart Journal*, vol. 31, no. 19, pp. 2338–2350, 2010.

[14] J. F. Lewis, L. C. Kuo, J. G. Nelson, M. C. Limacher, and M. A. Quinones, "Pulsed Doppler echocardiographic determination of stroke volume and cardiac output: clinical validation of two

new methods using the apical window," *Circulation*, vol. 70, no. 3, pp. 425–431, 1984.

[15] F. A. Dinenno, H. Tanaka, K. D. Monahan et al., "Regular endurance exercise induces expansive arterial remodelling in the trained limbs of healthy men," *The Journal of Physiology*, vol. 534, no. 1, pp. 287–295, 2001.

[16] T. Weber, M. Ducos, E. Mulder et al., "The specific role of gravitational accelerations for arterial adaptations," *Journal of Applied Physiology*, vol. 114, no. 3, pp. 387–393, 2013.

[17] V. A. Convertino, D. F. Doerr, K. L. Mathes, S. L. Stein, and P. Buchanan, "Changes in volume, muscle compartment, and compliance of the lower extremities in man following 30 days of exposure to simulated microgravity," *Aviation, Space, and Environmental Medicine*, vol. 60, no. 7, pp. 653–658, 1989.

[18] F. Louisy, P. Schroiff, and A. Güell, "Changes in leg vein filling and emptying characteristics and leg volumes during long-term head-down bed rest," *Journal of Applied Physiology*, vol. 82, no. 6, pp. 1726–1733, 1997.

[19] M. S. Stout, D. E. Watenpaugh, G. A. Breit, and A. R. Hargens, "Simulated microgravity increases cutaneous blood flow in the head and leg of humans," *Aviation Space and Environmental Medicine*, vol. 66, no. 9, pp. 872–875, 1995.

[20] G. Ferretti, F. Iellamo, P. Pizzinelli et al., "Prolonged head down bed rest-induced inactivity impairs tonic autonomic regulation while sparing oscillatory cardiovascular rhythms in healthy humans," *Journal of Hypertension*, vol. 27, no. 3, pp. 551–561, 2009.

[21] S. K. Samijo, J. M. Willigers, R. Barkhuysen et al., "Wall shear stress in the human common carotid artery as function of age and gender," *Cardiovascular Research*, vol. 39, no. 2, pp. 515–522, 1998.

[22] T. Weber, S. Wassertheurer, B. Hametner et al., "Reference values for central blood pressure," *Journal of the American College of Cardiology*, vol. 63, no. 21, article 2299, 2014.

Hindawi Publishing Corporation
BioMed Research International
Volume 2015, Article ID 167642, 7 pages
http://dx.doi.org/10.1155/2015/167642

Research Article

Space Flight Effects on Antioxidant Molecules in Dry Tardigrades: The TARDIKISS Experiment

Angela Maria Rizzo,[1] Tiziana Altiero,[2] Paola Antonia Corsetto,[1] Gigliola Montorfano,[1] Roberto Guidetti,[3] and Lorena Rebecchi[3]

[1]*Department of Pharmacological and Biomolecular Sciences, Università degli Studi di Milano, Via D. Trentacoste 2, 20134 Milano, Italy*
[2]*Department of Education and Human Sciences, University of Modena and Reggio Emilia, Via A. Allegri 9, 42121 Reggio Emilia, Italy*
[3]*Department of Life Sciences, University of Modena and Reggio Emilia, Via G. Campi 213/D, 41125 Modena, Italy*

Correspondence should be addressed to Angela Maria Rizzo; angelamaria.rizzo@unimi.it and Lorena Rebecchi; lorena.rebecchi@unimore.it

Received 10 July 2014; Accepted 22 September 2014

Academic Editor: Monica Monici

The TARDIKISS (Tardigrades in Space) experiment was part of the Biokon in Space (BIOKIS) payload, a set of multidisciplinary experiments performed during the DAMA (Dark Matter) mission organized by Italian Space Agency and Italian Air Force in 2011. This mission supported the execution of experiments in short duration (16 days) taking the advantage of the microgravity environment on board of the Space Shuttle Endeavour (its last mission STS-134) docked to the International Space Station. TARDIKISS was composed of three sample sets: one flight sample and two ground control samples. These samples provided the biological material used to test as space stressors, including microgravity, affected animal survivability, life cycle, DNA integrity, and pathways of molecules working as antioxidants. In this paper we compared the molecular pathways of some antioxidant molecules, thiobarbituric acid reactive substances, and fatty acid composition between flight and control samples in two tardigrade species, namely, *Paramacrobiotus richtersi* and *Ramazzottius oberhaeuseri*. In both species, the activities of ROS scavenging enzymes, the total content of glutathione, and the fatty acids composition between flight and control samples showed few significant differences. TARDIKISS experiment, together with a previous space experiment (TARSE), further confirms that both desiccated and hydrated tardigrades represent useful animal tool for space research.

1. Introduction

As the interest in space exploration grows, it becomes of great importance to predict and know the response of uni- and multicellular organisms to unfavourable space conditions, including microgravity. This allows us to elaborate the opportune countermeasures to avoid the risks imposed by space environmental stressors. To date many studies for understanding physiological, biochemical, and molecular mechanisms against space stressors are performed on unicellular organisms or cultivated cells of multicellular organisms [1]. Although the experiments on cell cultures are useful, it is equally clear that cell cultures represent only the first level of life organization and they cannot be compared to the response of an entire multicellular living organism. The use of animals in space research allows us to conduct experiments with organisms characterized by a high level of hierarchical biological complexity and physiological processes, comparable to those of humans [2].

Even though animals could be useful models in space research, their use is often limited by the fact that many of them need specific rearing bioreactors of large volume [1, 3]. Tardigrades, or water bears, are little known and neglected animals that allow overcoming this problem. Their use in space research is supported by several reasons: (i) they are miniaturized animals (from 200 to 1000 μm in length) that can be kept and reared in small facilities/bioreactors; (ii) while having tissues and organs, they are simpler than several

other animals, having a limited cell number (about 1000); (iii) they can be easily reared under lab conditions; (iv) many of them are parthenogenetic, often apomictic, so clonal lineages can be obtained [1, 2]. Although all tardigrades are aquatic animals, they thrive in terrestrial habitats subjected to periodic desiccation thanks to their ability to enter a highly stable state of suspended metabolic activity called anhydrobiosis [4]. Entering in this physiological state, tardigrades lose up to 97% of their body water and shrivel into a desiccated structure about one-third of its original size. When rehydrated, tardigrades can return to their active metabolic state in a few minutes to a few hours [4, 5]. Desiccated tardigrades can persist in anhydrobiosis for several years, and a remarkable resilience to physical and chemical extremes has been documented [4–6]. By possessing the abilities to withstand complete desiccation, severe cold, microgravity, vacuum, and high levels of ionizing and UV radiations, anhydrobiotic tardigrades fulfill the most important criteria for tolerating exposure to natural space conditions including open space [2].

Tardigrades have already been exposed to space stressors on Low Earth Orbit during the FOTON-M3 mission in 2007 with different projects (TARDIS [7]; TARSE [1, 8]; RoTaRad [9]). With the TARSE (Tardigrade Resistance to Space Effect) project, we analyzed the responses of both desiccated and hydrated physiological state of the tardigrade *Paramacrobiotus richtersi* to spaceflight conditions within the spacecraft [1, 8]. Microgravity and radiation had no effect on animal survival and life history traits even though a higher number of laid eggs, a shorter egg development time, and a higher number of flight-born juveniles were recorded with respect to tardigrades reared on Earth [1, 10]. In addition, spaceflight induced in active tardigrades an increase of glutathione content, an increase of glutathione peroxidase activity, and a decrease of catalase, superoxide dismutase, and glutathione reductase activities [1]. Lastly, no change in thiobarbituric acid reactive substances was detected. On the basis of these results, we developed the new project TARDIKISS (Tardigrades in Space), with the aim to deepen the study of survivorship, life history traits, and regulation of antioxidant defences on alive desiccated tardigrades under space stressors including microgravity exposure. The flight tardigrades of the project TARDIKISS have had a very high survival (more than 91%) and females laid eggs which were able to hatch producing normal newborns able to reproduce in adulthood [11]. In this paper we compared the molecular pathways of molecules with antioxidant activity, thiobarbituric acid reactive substances, and fatty acid composition between flight tardigrades and ground control ones with the final aim to provide news about the biochemical mechanisms underlying resistance to space stress conditions.

2. Material and Methods

2.1. TARDIKISS Project. The TARDIKISS project was part of the BIOKIS (Biokon in Space) payload: a set of multidisciplinary experiments in the field of biology and dosimetry performed in microgravity condition during the DAMA (Dark Matter) mission organized by Italian Space Agency (ASI) and Italian Air Force in 2011. This mission supported the execution of experiments in short duration (16 days) taking the advantage of the microgravity environment on board of the last mission (STS-134) of Space Shuttle Endeavour docked to the International Space Station (ISS) [11].

TARDIKISS was composed of three sample sets: one flight sample (F) and two ground control samples. The former control (temperature control, TC) was a postflight control in which samples were exposed to the temperature profile experienced by tardigrades the days immediately before, during, and just after the flight mission; the latter (laboratory control, LC) was maintained in Modena laboratory for the duration of the flight at constant temperature. These samples provided the biological material used to test as space stressors, including microgravity, affected animal survivability, life cycle, DNA integrity, and changes of the pathways of molecules working as antioxidants.

Two anhydrobiotic eutardigrade species were considered, namely, *Paramacrobiotus richtersi* (Murray, 1911) (Macrobiotidae) and *Ramazzottius oberhaeuseri* (Doyère, 1840) (Ramazzottiidae). *Paramacrobiotus richtersi* is the model species already used in the FOTON mission [1]. *P. richtersi* was extracted from a hazel leaf litter (sample code C3499); it is carnivorous, white in colour, and the population here considered is bisexual and amphimictic. *R. oberhaeuseri* (Figure 1) was extracted from the lichen *Xanthoria parietina* (L.) Th. Fr. (1860) (sample code C3282); it is herbivorous, brown/red in colour, and the population considered in this study is unisexual and parthenogenetic. To extract tardigrades from their substrates, leaf litter and lichen were sprinkled with tap water and after 15 min submerged in water for 15 min at room temperature. Later, each substrate was sieved (mesh size of sieves: 250 μm and 37 μm) under running water; then animals were picked up from the sieved sediments with a glass pipette under a stereomicroscope.

For both tardigrade species, animals in desiccated (anhydrobiotic) physiological state were used. To obtain desiccated specimens, tardigrades were dehydrated in lab under controlled air relative humidity (RH) and temperature. After extraction from their substrates, tardigrades were kept in water for 24 h at 15°C without any food source. Then, they were forced into anhydrobiosis by placing groups of animals on a square (1 cm^2) blotting paper with natural mineral water (30 μL). The paper with tardigrades was initially exposed to 80% RH and 18°C for 4 h, then to 50% RH at 18°C for 4 h in a climatic chamber, and finally to 0–3% RH at room temperature for 12 h [1].

Papers with desiccated tardigrades were stored in twelve small plastic Petri dishes (1.8 cm × 1.0 cm) enveloped with parafilm and integrated within the Biokon facility (Kayser Italia), where a radiation dosimeter for neutrons and *i*-button data logger recorded temperature were also present [11]. During the entire flight mission the temperature profile was relatively constant ranging from 21°C to 25°C [11], while the dose equivalent rates due to space radiation exposure were 320 μSv (measured by TLD 100 and TLD 700) and 360 μSv (measured by TLD 600) [11].

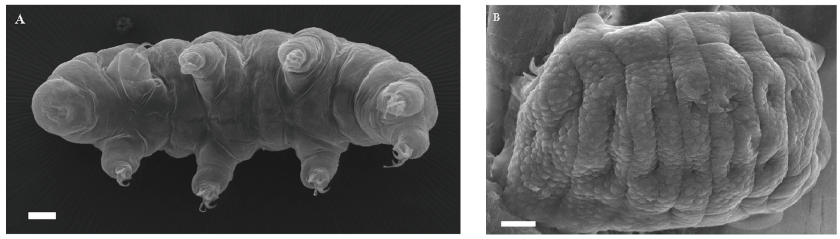

(a) (b)

Figure 1: Micrographs by scanning electron microscopy of the tardigrade *Ramazzottius oberhaeuseri* showing its two physiological states. (a) Hydrated and metabolically active specimen. (b) Desiccated and metabolically inactive specimen. Bars: a = 10 μm; b = 5 μm.

2.2. Biochemical Assays. Biochemical assays were performed on desiccated tardigrades comparing F samples with TC samples.

The activities of the enzymes superoxide dismutase (SOD total activity), catalase (CAT), glutathione peroxidase (GPx), and glutathione reductase (GR) were evaluated. The total glutathione (GSH) content, thiobarbituric acid reactive substances (TBARS), and fatty acid composition were also determined as previously described [12].

Substrates and reagents for enzyme determinations were NAD(P)H, DTNB, GSH, GSSG, glutathione reductase, and tert-butyl hydroperoxide; all of them were purchased from Sigma-Aldrich (St. Louis, Missouri, USA). For each sample set and each species, 6 or 8 (with the exception of SOD) replicates each made up by 10 *in toto* tardigrades were homogenized in water, on ice, with potter using 3 cycles of 30 sec each. The homogenate was assayed for protein content (according to [13]) and used for enzyme determination. For each enzyme, homogenates were analyzed in duplicate.

Briefly, the activity of the enzyme superoxide dismutase was assayed using the method based on NAD(P)H oxidation inhibition (according to [14]); the inhibition of NADPH oxidation by superoxide, which was chemically generated, was measured at 340 nm for 20 min, in the presence of tissue extracts. The incubation mixture included 213 μL of TDB (triethanolamine/diethanolamine 100 mM, pH 7.4), 10 μL of NADPH 7.5 μM, 7 μL of EDTA-$MnCl_2$ (100 mM–50 mM), and 20 μL of sample or blank. One unit of SOD activity was defined as the amount of enzyme required to inhibit the rate of NADPH oxidation by 50%.

To evaluate the activity of catalase, samples were assayed by measuring the consumption of H_2O_2 (according to [15]). Consumption of hydrogen peroxide by the tissue extracts was determined at 240 nm for 1 min at 30°C. The incubation mixture included 10 μL of H_2O_2 200 mM, 20 μL of homogenate, and 170 μL of Na-phosphate buffer (50 mM, pH 7.0). One unit of CAT activity was defined as the amount of enzyme required to catalyze the decomposition of 1 mmol of H_2O_2 min^{-1}.

The activity of the glutathione reductase was assayed following the oxidation of NADPH (according to [16]). Briefly, GSSG reduction and NADPH consumption were followed at 340 nm. The incubation mixture included 5 μL of GSSG 125 mM, 3 μL of NADPH 11 mM, animal homogenate from 20 to 50 μL, and K-phosphate buffer (100 mM, pH 7.0) to reach a final volume of 0.25 mL. One unit of GR activity was defined as the amount of enzyme required to catalyze the oxidation of 1 μmol NADPH min^{-1}.

To evaluate the activity of selenium-dependent glutathione peroxidase, the enzyme activity was assayed (according to [17]) following the decrease in the absorbance at 340 nm for 3 min, which corresponds to the rate of GSH oxidation to GSSG in the presence of NADPH and glutathione reductase. The incubation mixture included 5 μL of GSH 100 mM, 3 μL of NADPH 22 mM, GR 1 unit, 5 μL of tert-butyl hydroperoxide 20 mM, from 20 to 50 μL of animal homogenate, and EDTA-K phosphate buffer (3 mM–100 mM pH 7.0) to reach a final volume of 0.25 mL. One unit of GPx activity was defined as the amount of enzyme required to catalyze the oxidation of 1 μmol of NADPH min^{-1}.

To measure the total glutathione, tardigrades were homogenized on ice in 5% metaphosphoric acid; the homogenate was centrifuged at 5000 ×g for 10 min at 4°C, and the supernatant was assayed (according to [18]) with some slight modifications. Briefly, the sulfhydryl group of GSH, also generated from GSSG by adding GR, reacts with DTNB (5,5′-dithiobis-2-nitrobenzoic acid) and produces a yellow-coloured 5-thio-2-nitrobenzoic acid (TNB). The rate of TNB production is directly proportional to this reaction, which in turn is directly proportional to the concentration of GSH in the sample. The measurement of the absorbance of TNB at 412 nm provides an accurate estimation of the GSH level present in the sample.

To evaluate the thiobarbituric acid reactive substances (TBARS), tardigrade samples, standards (from 2.5 to 100 pmol TEP, 1,1-3,3 tetraethoxypropane), and blanks were assayed (according to [19]), both before and after induction of lipid peroxidation by $FeSO_4$ and ascorbic acid. TBARS were determined using a fluorescence spectrophotometer (Carly Eclipse, Varian, CA USA) at an excitation wavelength of 517 nm and an emission wavelength of 550 nm. For each sample set (F and TC) and species (*R. oberhaeuseri* and *P. richtersi*) 2 or 4 replicates were analyzed.

To evaluate the fatty acid composition, lipids were extracted from groups of 10 desiccated tardigrades with chloroform/methanol (according to [20]). The total extract was used for derivatization with sodium methoxide in methanol 3.33% w/v to obtain the fatty acid methylesters (FAME). FAME were injected into a gas chromatograph (Agilent Technologies 6850 Series II) equipped with a flame ionization detector (FID) under the following experimental

Table 1: Percentage of fatty acid composition in the tardigrades *Paramacrobiotus richtersi* and *Ramazzottius oberhaeuseri*.

Fatty acid	*Paramacrobiotus richtersi*		*Ramazzottius oberhaeuseri*	
	TC	F	TC	F
C16:0	28.86 (1.56)	29.41 (3.53)	29.65 (1.84)	32.64 (1.15)
C16:1	8.44 (1.98)	8.91 (0.79)	6.56 (1.68)	9.77 (0.23)
C18:0	14.53 (2.68)	17.86 (4.87)	16.22 (1.76)	18.56 (4.55)
C18:1	19.85 (3.43)	17.13 (4.55)	21.45 (1.71)	20.04 (6.21)
C18:2 n-6	9.75 (3.24)	13.18 (2.99)	12.11 (6.59)	12.97 (1.69)
C18:3 n-3	2.61 (2.05)	2.25 (1.69)	4.03 (3.48)	1.50 (0.30)
C20:3 n-6	1.11 (0.89)	1.03 (0.67)	0.22 (0.15)	0.24 (0.32)
C20:4 n-6	9.78 (7.56)	5.05 (5.20)	5.87 (1.74)	2.91 (2.02)
C20:5 n-3	1.17 (0.46)	1.99 (0.78)	1.30 (1.55)	0.57 (0.77)
C22:5 n-3	0.51 (0.51)	0.14 (0.19)	0.14 (0.23)	0.23 (0.33)
C22:6 n-3	4.00 (1.27)	3.03 (0.36)	2.45 (0.36)	0.56 (0.60)*
PUFA	28.92 (7.49)	26.68 (4.45)	26.12 (3.25)	18.99 (0.73)*
TBARS basal (pmoles/μg proteins)	2.81 (1.04)	2.51 (0.55)	2.77 (0.56)	2.60 (1.08)
TBARS induced (pmoles/μg proteins)	26.06 (3.65)	28.25 (1.27)	43.65 (1.61)	32.91 (2.58)

TC = ground temperature control samples; F = flight samples; PUFA = polyunsaturated fatty acids; TBARS = thiobarbituric reactive substances; $^*P < 0.05$; in brackets SD.

conditions: capillary column: AT Silar length 30 m, film thickness 0.25 μm: gas carrier: helium: temperatures: injector 250°C, detector 275°C, oven 50°C for 2 min, and rate of 10°C min^{-1} until 200°C for 20 min. A standard mixture containing methyl ester fatty acids was injected for calibration. For each sample set and species 2 or 4 replicates were analyzed.

2.3. Statistical Analysis. Data were analyzed with Mann-Whitney test and expressed as mean ± SD using the programme SPSS.

3. Results

The results of the enzyme activities in the tardigrades *Paramacrobiotus richtersi* and *Ramazzottius oberhaeuseri* are always indicated in relation to μg of proteins. It is worth noting that *R. oberhaeuseri* contains a lower amount of proteins compared to *P. richtersi* (Figure 2).

In both species, the comparative analysis of the enzyme activities and other antioxidant molecules between flight (F) and temperature control samples (TC) showed few significant differences (Figures 3 and 4). In particular, a significant decrease ($P < 0.05$) of the glutathione reductase activity was detected in *R. oberhaeuseri* F samples with respect to TC samples (Figure 4(b)). Although not statistically supported, in this species a tendency to decrease catalase, superoxide dismutase, and glutathione peroxidase activity and in glutathione content was detected. In *P. richtersi*, a tendency to decrease catalase, superoxide dismutase, and glutathione reductase activities and to increase the glutathione peroxidase activity was detected. Noteworthy, differences were recorded in the activities of ROS scavenging enzymes between the two species.

The total percentage fatty acid composition of F and TC samples is reported in Table 1. In *R. oberhaeuseri* a significant decrease ($P < 0.05$) was recorded for the fatty acid C22-6 n-3 and polyunsaturated fatty acids (PUFA) in the F samples with respect to the TC samples. Moreover, *R. oberhaeuseri* has significantly lower amount of C22-6 n-3 compared to *P. richtersi*. The amount of thiobarbituric acid reactive substances (TBARS) in tardigrades, both before and after induction of peroxidation *in vitro,* is also reported in Table 1. No differences were detected between F and TC samples in both species for basal levels and after induction of peroxidation.

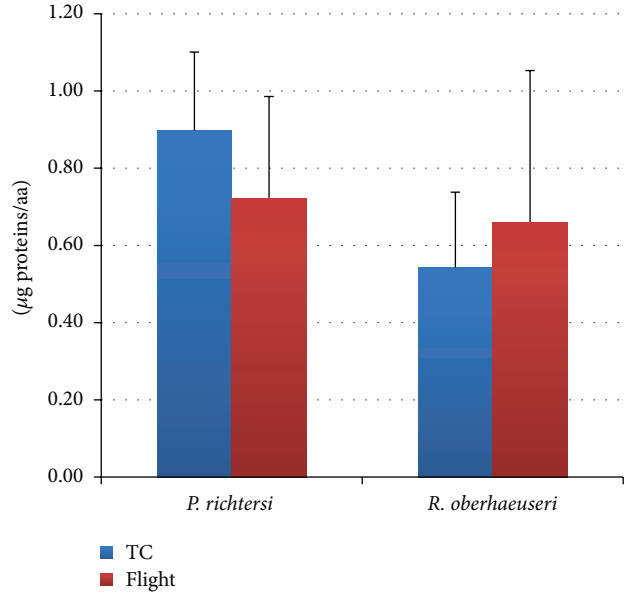

Figure 2: Total protein content in flight and ground temperature control (TC) samples in the tardigrades *Paramacrobiotus richtersi* and *Ramazzottius oberhaeuseri*. The bars show the mean with SD.

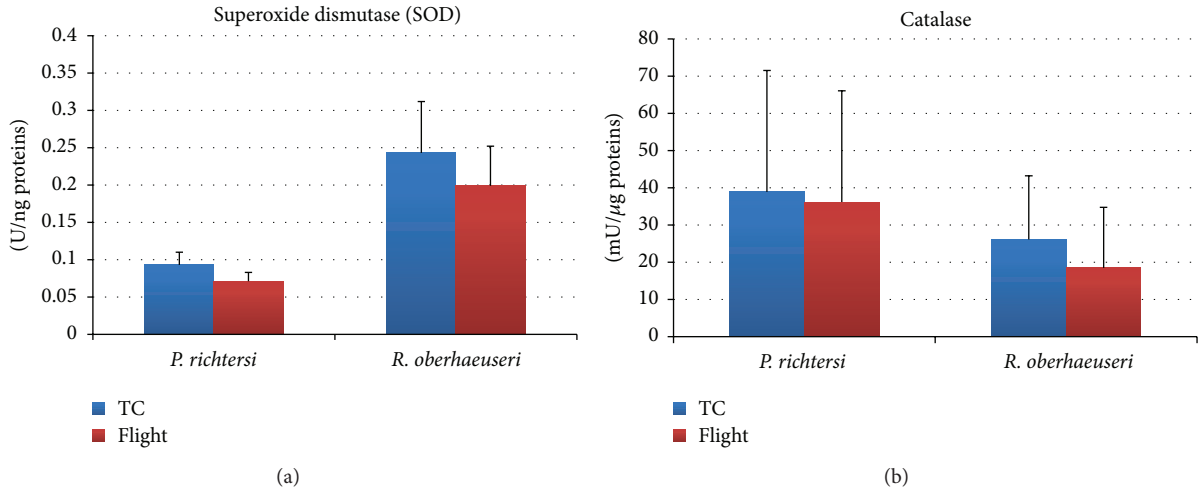

Figure 3: Superoxide dismutase (a) and catalase (b) activities in flight and ground temperature control (TC) samples in the tardigrades *Paramacrobiotus richtersi* and *Ramazzottius oberhaeuseri*. The bars show the mean with SD.

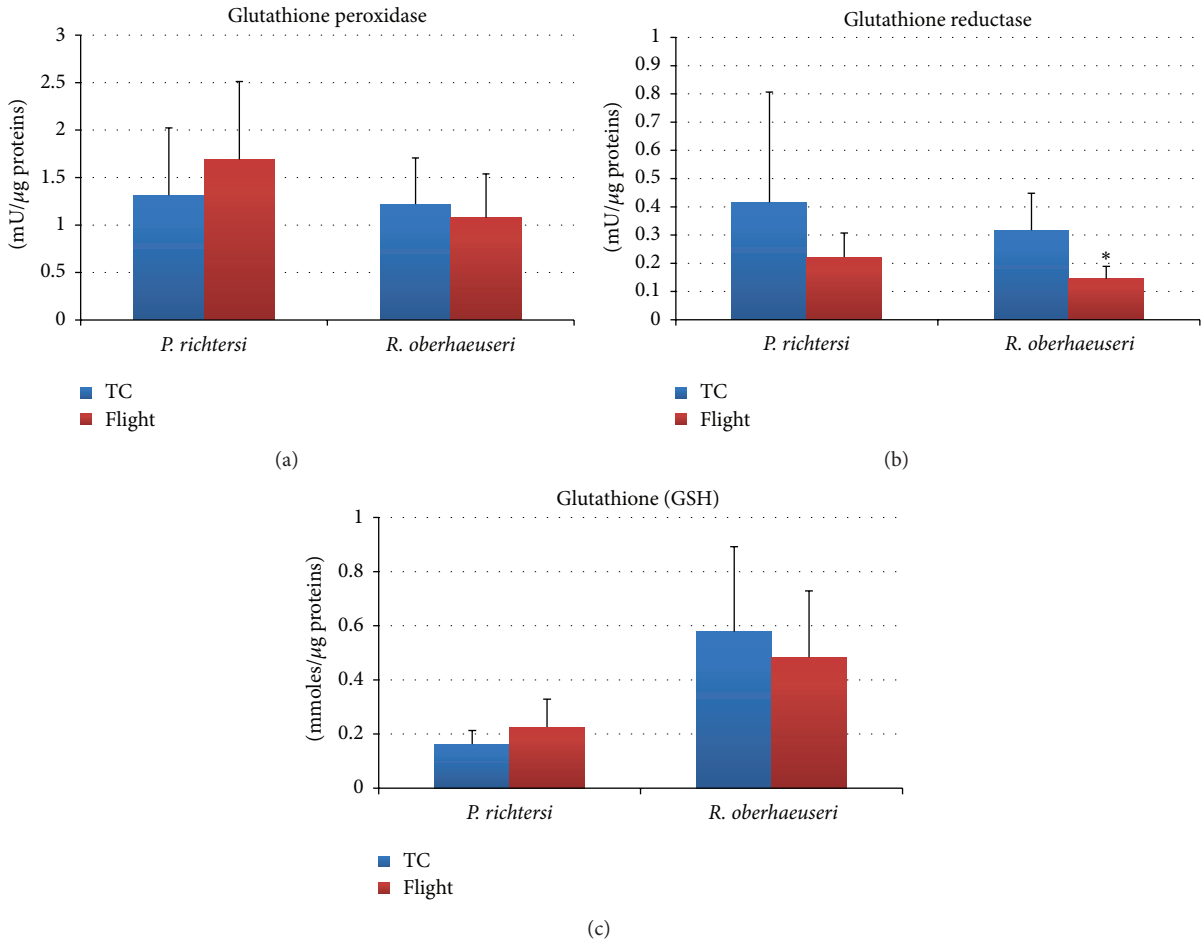

Figure 4: Glutathione peroxidase (a), glutathione reductase (b), and total glutathione content (c) in flight and ground temperature control (TC) samples in the tardigrades *Paramacrobiotus richtersi* and *Ramazzottius oberhaeuseri*. The bars show the mean with SD; $^{*}P < 0.05$.

4. Discussion

Exposure to space stress conditions induces oxidative stress. Oxidative stress resulting from an imbalance between the excessive production of reactive oxygen species (ROS) and limited action of antioxidant defences is implicated in the development of many important human pathologies including atherosclerosis, hypertension, inflammation, cancer, Parkinson, and Alzheimer diseases [21]. Oxidative stress may be highly destructive also in anhydrobiotic organisms even if the lower cellular water content decreases the production of ROS [21, 22]. Under normal conditions, antioxidant systems minimize the adverse effects caused by ROS, but desiccation stress could cause the loss or reduction of these defence control mechanisms since the metabolic activity is absent or reduced [21–24].

The ability of some animals, tardigrades among them, to survive extreme desiccation involves a complex array of factors working at structural, physiological, and molecular level. From a molecular/biochemical point of view, anhydrobiotic organisms synthesize molecules working as bioprotectants during entering, permanence, and leaving in a desiccated state [25]. For example, trehalose and sucrose stabilise the biological membrane avoiding protein unfolding and membrane disturbances; late embryogenesis abundant proteins and heat shock proteins work as chaperone systems repairing or eliminating damaged molecules, while antioxidant molecules counteract the negative effects of oxidative stress [25].

Since it is known that both hydrated and desiccated tardigrades have a good natural capability to overcome oxidative stress [26], they have been used in TARDIKISS experiments to evaluate the role of antioxidant defence in overcoming oxidative stress induced by exposure to space stress conditions such as ionizing and UV radiations.

The first space experiment (TARSE) conducted with hydrated starved specimens of the tardigrade *P. richtersi* demonstrated that some of the enzymes involved in antioxidant defences were significantly influenced by the flight stresses [1]. In particular, there was a significant decrease in catalase and SOD activities, the more active enzymes in *P. richtersi*. In addition, the glutathione system, the less active system in not stressed specimens of this species [26], was significantly induced during space flight [1]. These results could be related to the stresses experienced by the hydrated and metabolically active animals (microgravity, starvation, and radiations) during the flight. On the contrary the analysis of antioxidant defences in desiccated tardigrades of the TARDIKISS experiment showed fewer differences related to space flight even if the tendency was similar to that recorded in hydrated metabolically active animals of the TARSE experiment. A similar trend between TARSE and TARDIKISS experiments was also detected in regard to tardigrade survival since flight animals did not show significant differences in survival from temperature laboratory control ones [1, 11]. Only in *R. oberhaeuseri* (TARDIKISS experiment) a significant decrease in survival rate was recorded between F and TC samples, the species in which a significant decrease of the C22:6 n-3 fatty acid and of glutathione reductase activity and, even though not significant, of the activity of the other ROS scavenging enzymes were detected.

In conclusion, TARDIKISS experiment, together with previous space experiments using tardigrades [1, 7–9], further confirms that both desiccated and hydrated physiological states of tardigrades represent useful animal tool for space research. To further develop the space research using tardigrades, the setup of experiments with the possibility to change the exposition condition of metabolically hydrated animals, as well as the possibility to expose desiccated tardigrades to open space, is necessary. Experiments under true space condition provide a realistic evaluation of the mechanisms that could allow multicellular organisms, including tardigrades, to survive the combined and synergic effects of space stressors. Nevertheless, experiments on ground using simulators of microgravity, radiation, temperature, and other space stresses are an essential part of space research complementing experiments under true space conditions. The comparisons of two different sets of data (ground and space data) will allow better understanding of the physiological and molecular pathways of living organisms under space environment.

Conflict of Interests

The authors declare that there is no conflict of interests regarding the publication of this paper.

Acknowledgments

The authors are very grateful to the Italian Space Agency (ASI) and the Italian Air Force (AM) which funded the DAMA mission. The authors are also very grateful to Kayser Italia (KI) which developed and manufactured the hardware involved in the BIOKIS payload. They are grateful to anonymous reviewers for their constructive suggestions.

References

[1] L. Rebecchi, T. Altiero, R. Guidetti et al., "Tardigrade resistance to space effects: First results of experiments on the LIFE-TARSE Mission on FOTON-M3 (September 2007)," *Astrobiology*, vol. 9, no. 6, pp. 581–591, 2009.

[2] R. Guidetti, A. M. Rizzo, T. Altiero, and L. Rebecchi, "What can we learn from the toughest animals of the Earth? Water bears (tardigrades) as multicellular model organisms in order to perform scientific preparations for lunar exploration," *Planetary and Space Science*, vol. 74, no. 1, pp. 97–102, 2012.

[3] H. Marthy, "Developmental biology of animal models under varied gravity conditions: a review," *Vie et Milieu*, vol. 52, no. 4, pp. 149–189, 2002.

[4] N. Møbjerg, K. A. Halberg, A. Jørgensen et al., "Survival in extreme environments—on the current knowledge of adaptations in tardigrades," *Acta Physiologica*, vol. 202, no. 3, pp. 409–420, 2011.

[5] R. Guidetti, T. Altiero, and L. Rebecchi, "On dormancy strategies in tardigrades," *Journal of Insect Physiology*, vol. 57, no. 5, pp. 567–576, 2011.

[6] T. Altiero, R. Guidetti, V. Caselli, M. Cesari, and L. Rebecchi, "Ultraviolet radiation tolerance in hydrated and desiccated

eutardigrades," *Journal of Zoological Systematics and Evolutionary Research*, vol. 49, supplement 1, pp. 104–110, 2011.

[7] K. I. Jönsson, E. Rabbow, R. O. Schill, M. Harms-Ringdahl, and P. Rettberg, "Tardigrades survive exposure to space in low Earth orbit," *Current Biology*, vol. 18, no. 17, pp. R729–R731, 2008.

[8] L. Rebecchi, T. Altiero, M. Cesari et al., "Resistance of the anhydrobiotic eutardigrade *Paramacrobiotus richtersi* to space flight (LIFE-TARSE mission on FOTON-M3)," *Journal of Zoological Systematics and Evolutionary Research*, vol. 49, supplement 1, pp. 98–103, 2011.

[9] D. Persson, K. A. Halberg, A. Jørgensen, C. Ricci, N. Møbjerg, and R. M. Kristensen, "Extreme stress tolerance in tardigrades: surviving space conditions in low earth orbit," *Journal of Zoological Systematics and Evolutionary Research*, vol. 49, supplement 1, pp. 90–97, 2011.

[10] T. Altiero, L. Rebecchi, and R. Bertolani, "Phenotypic variations in the life history of two clones of *Macrobiotus richtersi* (Eutardigrada, Macrobiotidae)," *Hydrobiologia*, vol. 558, no. 1, pp. 33–40, 2006.

[11] M. Vukich, P. L. Ganga, D. Cavalieri et al., "BIOKIS: a model payload for multisciplinary experiments in microgravity," *Microgravity Science and Technology*, vol. 24, pp. 397–409, 2012.

[12] A. M. Rizzo, L. Adorni, G. Montorfano, F. Rossi, and B. Berra, "Antioxidant metabolism of *Xenopus laevis* embryos during the first days of development," *Comparative Biochemistry and Physiology—B Biochemistry and Molecular Biology*, vol. 146, no. 1, pp. 94–100, 2007.

[13] O. H. Lowry, N. J. Rosebrough, A. L. Farr, and R. J. Randall, "Protein measurement with the Folin phenol reagent," *The Journal of Biological Chemistry*, vol. 193, no. 1, pp. 265–275, 1951.

[14] F. Paoletti and A. Mocali, "Determination of superoxide dismutase activity by purely chemical system based on NAD(P)H oxidation," *Methods in Enzymology*, vol. 186, pp. 209–220, 1990.

[15] H. Aebi, "Catalase in vitro," *Methods in Enzymology*, vol. 105, pp. 121–126, 1984.

[16] M. C. Pinto, A. M. Mata, and J. Lopez-barea, "Reversible inactivation of *Saccharomyces cerevisiae* glutathione reductase under reducing conditions," *Archives of Biochemistry and Biophysics*, vol. 228, no. 1, pp. 1–12, 1984.

[17] J. R. Prohaska and H. E. Ganther, "Selenium and glutathione peroxidase in developing rat brain," *Journal of Neurochemistry*, vol. 27, no. 6, pp. 1379–1387, 1976.

[18] O. W. Griffith, "Glutathione and glutathione disulphide," in *Methods of Enzymatic Analysis*, H. U. Bergmeyer, Ed., vol. 3, pp. 521–529, Academic Press, New York, NY, USA, 1984.

[19] H. E. Wey, L. Pyron, and M. Woolery, "Essential fatty acid deficiency in cultured human keratinocytes attenuates toxicity due to lipid peroxidation," *Toxicology and Applied Pharmacology*, vol. 120, no. 1, pp. 72–79, 1993.

[20] J. Folch, M. Lees, and G. H. S. Stanley, "A simple method for the isolation and purification of total lipides from animal tissues," *The Journal of Biological Chemistry*, vol. 226, no. 1, pp. 497–509, 1957.

[21] M. B. França, A. D. Panek, and E. C. A. Eleutherio, "Oxidative stress and its effects during dehydration," *Comparative Biochemistry and Physiology—A Molecular and Integrative Physiology*, vol. 146, no. 4, pp. 621–631, 2007.

[22] R. Cruz de Carvalho, M. Catalá, J. Marques da Silva, C. Branquinho, and E. Barreno, "The impact of dehydration rate on the production and cellular location of reactive oxygen species in an aquatic moss," *Annals of Botany*, vol. 110, no. 5, pp. 1007–1016, 2012.

[23] I. Kranner and S. Birtić, "A modulating role for antioxidants in desiccation tolerance," *Integrative and Comparative Biology*, vol. 45, no. 5, pp. 734–740, 2005.

[24] R. Cornette and T. Kikawada, "The induction of anhydrobiosis in the sleeping chironomid: current status of our knowledge," *IUBMB Life*, vol. 63, no. 6, pp. 419–429, 2011.

[25] L. Rebecchi, "Dry up and survive: the role of antioxidant defences in anhydrobiotic organisms," *Journal of Limnology*, vol. 72, no. 1, pp. 62–72, 2013.

[26] A. M. Rizzo, M. Negroni, T. Altiero et al., "Antioxidant defences in hydrated and desiccated states of the tardigrade *Paramacrobiotus richtersi*," *Comparative Biochemistry and Physiology B: Biochemistry and Molecular Biology*, vol. 156, no. 2, pp. 115–121, 2010.

Hindawi Publishing Corporation
BioMed Research International
Volume 2015, Article ID 363575, 20 pages
http://dx.doi.org/10.1155/2015/363575

Research Article

Identification of Reference Genes in Human Myelomonocytic Cells for Gene Expression Studies in Altered Gravity

Cora S. Thiel,[1,2,3] Swantje Hauschild,[1,2,3] Svantje Tauber,[1,2,3] Katrin Paulsen,[1,2] Christiane Raig,[1] Arnold Raem,[4] Josefine Biskup,[1,2] Annett Gutewort,[1,2] Eva Hürlimann,[1] Felix Unverdorben,[1] Isabell Buttron,[1] Beatrice Lauber,[1] Claudia Philpot,[5] Hartwin Lier,[6] Frank Engelmann,[6,7] Liliana E. Layer,[1] and Oliver Ullrich[1,2,3,8]

[1] *Institute of Anatomy, Faculty of Medicine, University of Zurich, Winterthurerstraße 190, 8057 Zurich, Switzerland*
[2] *Department of Machine Design, Engineering Design and Product Development, Institute of Mechanical Engineering, Otto-von-Guericke-University Magdeburg, Universitätsplatz 2, 39106 Magdeburg, Germany*
[3] *Study Group "Magdeburger Arbeitsgemeinschaft für Forschung unter Raumfahrt- und Schwerelosigkeitsbedingungen" (MARS), Otto-von-Guericke-University Magdeburg, Universitätsplatz 2, 39106 Magdeburg, Germany*
[4] *Arrows Biomedical Deutschland GmbH, Center for Nanotechnology at the Westfälische Wilhelms-Universität Münster, Heisenbergstraße 11, 48149 Münster, Germany*
[5] *German Aerospace Center, Space Agency, Königswinterer Straße 522-524, 53227 Bonn, Germany*
[6] *KEK GmbH, Kemberger Straße 5, 06905 Bad Schmiedeberg, Germany*
[7] *University of Applied Science Jena, Carl-Zeiss-Promenade 2, 07745 Jena, Germany*
[8] *Zurich Center for Integrative Human Physiology (ZIHP), University of Zurich, Winterthurerstraße 190, 8057 Zurich, Switzerland*

Correspondence should be addressed to Oliver Ullrich; oliver.ullrich@uzh.ch

Received 14 May 2014; Accepted 4 September 2014

Academic Editor: Jack J. W. A. Van Loon

Gene expression studies are indispensable for investigation and elucidation of molecular mechanisms. For the process of normalization, reference genes ("housekeeping genes") are essential to verify gene expression analysis. Thus, it is assumed that these reference genes demonstrate similar expression levels over all experimental conditions. However, common recommendations about reference genes were established during 1 g conditions and therefore their applicability in studies with altered gravity has not been demonstrated yet. The microarray technology is frequently used to generate expression profiles under defined conditions and to determine the relative difference in expression levels between two or more different states. In our study, we searched for potential reference genes with stable expression during different gravitational conditions (microgravity, normogravity, and hypergravity) which are additionally not altered in different hardware systems. We were able to identify eight genes (ALB, B4GALT6, GAPDH, HMBS, YWHAZ, ABCA5, ABCA9, and ABCC1) which demonstrated no altered gene expression levels in all tested conditions and therefore represent good candidates for the standardization of gene expression studies in altered gravity.

1. Introduction

Since several limiting factors for human health and performance in microgravity have been clearly identified [1], it has been concluded that substantial research and development activities are required in order to provide the basic information for appropriate integrated risk management, including efficient countermeasures and tailored life support systems [2]. In particular, bone loss during long stays in weightlessness still remains an unacceptable risk for long-term and interplanetary flights [3], and serious concerns arose whether spaceflight-associated immune system weakening ultimately precludes the expansion of human presence beyond Earth's orbit [4]. The immune and skeletal systems are tightly linked by cytokine and chemokine networks and direct cell-cell interactions [5, 6], and the immune system influences metabolic, structural, and functional changes in bones directly [6]. Both systems share common cellular

players such as the osteoclasts, which are bone-resident macrophages and derivatives of monocytic cells. Therefore, knowing the cellular and molecular mechanisms of how gravity influences cell function is a valuable requirement to provide therapeutic or preventive targets for keeping important physiological systems fully functional during long-term space missions.

Since the first pioneering *in vitro* studies that revealed that cells of the immune system are sensitive to changes of gravitational force [7–10], several studies in real and simulated microgravity have confirmed microgravity-induced alterations in the molecular mechanisms and signal transduction processes in leukocytes, including the monocyte/macrophage system (MMS) [11, 12]. The MMS belongs to the innate immune system and is characterized by a fast but nonspecific immune reaction, the first line of defense against invading pathogens. Cells of the MMS in microgravity demonstrated disturbed cytokine release [13–15], reduced oxidative burst [16, 17], alteration of the cytoskeleton [18], and reduction in their locomotion ability [19]. Importantly, analysis of gene expression of monocytes during an ISS experiment revealed significant changes in gene expression associated with macrophageal differentiation [20].

Differential gene expression analyses are a widely used method to investigate the influence of different treatments or conditions on a cell system. The resulting changes on the molecular level can be investigated either by reverse transcription quantitative real-time PCR (RT-qPCR) as major technique for the sensitive and robust analysis of expression levels of specific genes [21–27] and microarrays for whole genome or transcriptome analyses [28].

After the genome sequencing era, when numerous genomes were completely decoded, the focus of interest shifted towards genome wide expression level analyses, so that a snapshot of the whole genome expression profile is obtained in a single experiment [28–30], offering also a possibility to obtain an insight into networks and pathways of biomolecular interactions on a large scale [29–33]. The technology behind microarray analysis developed fast, and different suppliers used different protocols for, for example, hybridization and data normalization. Therefore, it was and still is difficult to establish standards for the experimental procedure and processing of the raw data obtained [30]. Consequently, a concept for the development of standards for microarray experiments and data has been presented by the microarray gene expression database group (MGED) describing the minimum information about a microarray experiment (MIAME, [34]). This compilation covers (1) the experimental design, (2) the array design, (3) samples, (4) hybridizations, (5) measurements, and (6) normalization controls [34]. Also for RT-qPCR technique [35–38], standard guidelines (MIQE = minimum information for the publication of quantitative real-time PCR) were developed [27, 39–41].

One of the most crucial requirements of standardization are suitable internal controls so called reference genes that are used for data normalization, which are important to account for differences in the amount and quality of starting material as well as reaction efficiency [42]. GAPDH, HPRT, β-actin, tubulin, and ribosomal RNA genes are typical examples for frequently used reference genes [43–45]. However, reference genes have to be tested for their suitability as an endogenous control in each case prior to the experiment. This is of high importance substantiated by many studies reporting expression effects of classical "housekeeping genes" upon experimental treatments [46–49]. A selection of several reference genes used simultaneously can also be a good way to further increase reliability of the resulting data [50, 51]. In fact, recommendations state to identify three stable reference genes for each planned assay to assure a reliable outcome [50, 52]. The identification of stably expressed reference genes can be performed in a pilot study using dedicated algorithms like geNorm or BestKeeper or a combination hereof, where a minimum of eight potential reference genes are tested and ranked according to their stability being an indication for their suitability as control genes for normalization [50, 51]. Candidate reference genes for such a study may be, for example, chosen from the literature or from experimental data obtained from microarray analysis [27, 51].

However, common recommendations about reference genes were established during 1 g conditions and therefore their applicability in studies with altered gravity conditions has not been intensively demonstrated so far. Although, there are numerous publications describing differential gene expression analyses under simulated and real microgravity conditions in various cells types and tissues (supplementary Table 1 available online at http://dx.doi.org/10.1155/2014/363575), a systematic research on reference genes stable under altered gravity conditions has not been published yet.

In our study, we used microarray analyses to investigate the differential gene expression in U937 cells, a myelomonocytic human cell line, exposed to short-term (20 seconds) and middle-term (6 to 7 minutes) microgravity and hypergravity during parabolic flights and sounding rocket flights, two platforms commonly used by researchers to investigate the effects of real microgravity. Our experimental goal was to identify potential reference genes that can be recommended to the community of gravitational biology for differential expression analysis performed with cells of the immune system on those two frequently used platforms. Therefore, we chose 22 reference genes widely used throughout the literature and screened our microarray data for these particular genes evaluating their stability for possible application as control genes. Besides the highly conserved ribosomal RNA genes and others, ABC transporter and tRNA genes belong to evolutionary well-conserved genes as well. Since ribosomal RNA and tRNA genes are not represented on the array, we decided to adhere to tRNA related genes like tRNA synthetases, as these play a central role in basal cellular functions and should be robustly expressed to ensure cell survival. Therefore, our study comprised published reference genes, ABC transporters, and tRNA related genes.

2. Material and Methods

2.1. Cell Culture. U937 cells (ATCC CRL1593.2) originating from a diffuse histiocytic lymphoma, displaying many monocytic characteristics, were used as a model cell line to investigate the differential gene expression under altered gravity

conditions in monocytic/macrophageal cells. U937 cells were cultured in RPMI 1640 medium (Biochrom/Merck Millipore, Germany), supplemented with 10% fetal bovine serum (FBS Superior; Biochrom/Merck Millipore, Germany), 2 mM glutamine (Gibco/Life Technologies, Germany), and 100 U/mL penicillin as well as 100 μg/mL streptomycin (Gibco/Life Technologies, Germany). Cells were seeded with a density of 0.2×10^6 cells/mL and the medium was exchanged every 48 hours. Cells were harvested by centrifugation at 300 g for 5 min at room temperature, resuspended in fresh medium, and an aliquot was used for an adequate dilution with trypan blue to count the vital cell number. Cells were reseeded in fresh medium at a concentration of 0.2×10^6 cells/mL.

2.2. Parabolic Flight Experiments. We designed and constructed an experiment module suitable to perform cell culture experiments with living mammalian cells during parabolic flights on board the Airbus A300 ZERO-G. During the 19th DLR parabolic flight campaign (PFC), we focused on the analysis of differential gene expression in U937 cells considering the different gravity conditions: in-flight 1 g, 1.8 g, and 0 g. Experiments were only performed during the first parabola to assure that the investigated differential gene expressions are generated by a direct effect of gravitational change and not an accumulated long-term effect. During the 19th DLR PFC, experiments were reproduced on two independent flight days.

In search of rapidly responsive molecular alterations in mammalian cells, short-term microgravity provided by parabolic flight maneuvers is an ideal instrument to elucidate initial and primary effects, without the influence and interference of secondary signal cascades. Parabolic flights provide 1 g, 1.8 g, and microgravity (μg) with a quality of approximately 10^{-2} to 10^{-3} g. For the 19th DLR PFC, 1×10^7 U937 cells in 10 mL medium (RPMI 1640 supplemented with 100 U/mL penicillin, 100 μg/mL streptomycin, 250 ng/mL amphotericin B (Gibco/Life Technologies, Germany), 2 mM glutamine, and 2% FBS (i.e., serum starved)) were filled into 200 mL Nutrimix bags (B. Braun Melsungen, Germany) and transported from the home laboratory to the preflight preparation laboratories at the NOVESPACE premises in Bordeaux, France. After arrival, cells were destarved by addition of 0.8 mL FBS per Nutrimix bag and used for the flight experiment on the following day. For the flight day, the Nutrimix bags were placed in a solid plastic container to create a double containment to prevent spillage of fluids in the aircraft in case of leakage which is strictly prohibited by the NOVESPACE regulations. The rapid preservation of the effects of altered gravity on the gene expression in the U937 cells was achieved by injection of 50 mL of RLT buffer (Qiagen, Germany), a lysis buffer immediately lysing cells and tissues prior to RNA isolation. The 1 g in-flight controls were performed 5 min before the first parabola and the 1.8 g sample directly before the microgravity phase of the first parabola. The μg samples were fixed directly at the end of the microgravity phase of the first parabola. Samples were transported to the laboratory immediately after landing. 1 g ground controls were performed immediately after landing using the experimental module in the aircraft. In total, 30 samples were obtained during two parabolic flight days: 6x 1 g ground controls, 9x 1 g in-flight controls, 6x 1.8 g and 9x μg.

2.3. RNA Isolation after the Parabolic Flight Experiments. After landing of the aircraft and transport of the samples to the laboratory on site facilities, the containers were disassembled, the Nutrimix bags were gently agitated, and the lysed cell solution was filled into a T75 straight neck cell culture flask. The cell solution was vortexed for 10 sec and passed four times through a Ø 0.8 × 120 mm needle (B. Braun Melsungen, Germany) fitted to a 50 mL syringe. 50 mL of absolute ethanol was added and precipitates were resuspended by vigorous shaking. A valve and a sterile connective piece were placed on a QIAvac 24 plus vacuum system (Qiagen, Germany) and an RNA maxi column (Qiagen, Germany) was attached to the connective piece. A vacuum of −200 mbar was adjusted, and the column was loaded with the lysed cell suspension. Then, the valve was closed, and the column was centrifuged at 4000 g for 3 min. 15 mL of buffer RW1 (Qiagen, Germany) was applied for washing membrane bound RNA. After centrifugation at 4000 g for 7 min, the flow through was discarded and two washing steps with 10 mL RPE buffer (Qiagen, Germany) followed with centrifugation at 4000 g for 3 min and 10 min, respectively. The column bound RNA was eluted by application of 600 μL of RNase-free water (Qiagen, Germany), incubation for 1 min at room temperature, and centrifugation for 4 min at 4000 g. The elution step was repeated with the first eluate. The RNA was transported at approximately −150°C in a Cryo Express dry shipper (CX-100, Taylor-Wharton, USA) prepared with liquid nitrogen and stored at −80°C until the processing of the RNA for the microarray analysis.

2.4. Experiments during the TEXUS-49 Sounding Rocket Campaign. For the TEXUS-49 campaign at ESRANGE (European Space and Sounding Rocket Range, Kiruna, Sweden), U937 cells were cultured in the fully installed laboratories on site. Cells were seeded with a density of 0.2×10^6 cells/mL and the medium was exchanged every 48 hours as described above. On the launch day, cells were visually inspected, harvested, counted, and pooled to a concentration of 5×10^7 cells/mL. 0.5 mL of this cell suspension was filled in a sterile 3 mL plastic syringe shortly before the launch. Additionally, one syringe was filled with 0.3 mL of cell culture medium and another one with 1 mL Trizol LS (Life Technologies, Germany). The three syringes were mounted on a plastic block with a tubing system connecting them. This unit was finally integrated into the automatically operated experiment system. In total, 35 of these experiment units were prepared and were kept at 37°C until the integration into the payload of the rocket.

During the experimental run, firstly the 0.3 mL of medium, as a potential placeholder for an activation solution, and secondly the 1 mL of Trizol LS were injected to the cell suspension at defined time points to lyse the cells and preserve the current status of differential gene expression. This sequential injection of fluids was performed at 75 sec after launch to monitor the so-called baseline (BL) directly

before the μg phase and at 375 sec after launch shortly before the end of the μg phase. A group of 1 g ground controls were kept on ground in the incubator simultaneously to the μg sample group.

TEXUS-49 consisted of a VSB-30 engine (S-30 solid rocket stage with an S-31 second stage) and of the payload. The rocket was launched on March 29, 2011 at 06:01 a.m. from the ESRANGE Space Center near Kiruna, Sweden. During the ballistic suborbital flight, an altitude of 268 km and 378 sec of microgravity with a quality of 10^{-5} g were achieved. Further parameters include first stage peak thrust acceleration 6.3 g, mean thrust acceleration 5.03 g, burnout at 12.3 sec, and engine separation at 13.6 sec; second stage peak thrust acceleration 13.5 g, mean thrust acceleration 7.30 g, burnout at 43.0 sec, yo-yo despin at 56.0 sec, and engine separation at 59.0 sec.

2.5. RNA Isolation after the TEXUS-49 Sounding Rocket Campaign. Directly after landing, localization, and recovery of the payload, the experiment modules were dismantled and handed over to the scientists. The cell suspension was sheared three times with a 20 G needle (B. Braun Melsungen, Germany) and distributed in two 2.0 mL tubes. 0.1 mL of chloroform (Sigma-Aldrich, Germany) was added, and the homogenate was vortexed for 15 sec and incubated for 5 min at room temperature before a 15 min centrifugation step at 11000 g and 4°C. The upper phase of both 2.0 mL tubes was transferred into a 15 mL tube, and 4 mL of RLT buffer as well as 3 mL of absolute ethanol was added and mixed. 4 mL of this solution was pipetted on an RNA Midi column (Qiagen, Germany) and centrifuged for 30 sec at 3000 g and room temperature. The flow through was discarded and the residual 4 mL of RNA solution was loaded on the column and centrifuged for 5 min at 3000 g at room temperature. Then, the columns were washed twice with 2.5 mL of RPE buffer and centrifuged for 2 min and 5 min, respectively, at 3000 g at room temperature. The RNA was eluted by addition of 250 μL RNase-free water (Qiagen, Germany) to the column, incubation for 1 min at room temperature, and centrifugation for 3 min at 3000 g and room temperature. The eluate was loaded again onto the column, followed by a 1 min incubation and centrifugation for 5 min at 3000 g and room temperature. The isolated RNA was transferred into sterile cryotubes and stored until the return transport at approximately −150°C in a Cryo Express dry shipper (CX-100, Taylor-Wharton, USA) prepared with liquid nitrogen. After arrival in the home laboratory, samples were stored at −80°C until the processing of the RNA for the microarray analysis.

2.6. RNA Processing and Microarray Analysis. RNA quantity and purity were analyzed spectrophotometrically using a NanoDrop 1000 (Thermo Scientific, USA). Isolated RNA samples were all of high quality with 260/280 nm ratios between 1.9 and 2.1. The RNA integrity was measured using an Agilent 2100 Bioanalyzer (Agilent Technologies, USA). Only RNA with an RNA integrity number (RIN) > 8.7 was used for the following microarray analysis. 400 ng total RNA was applied to Cy3-labeling with the "Low RNA Input Linear Amplification Kit, PLUS, One-Color" (Agilent Technologies) and hybridized for 17.5 h to a NimbleGen expression microarray (12 × 135,000 features) employing the "Gene Expression Hybridization Kit" (Agilent Technologies). Afterwards, arrays were washed and scanned by the Microarray Scanner G2505B (Agilent Technologies).

The image files of the scanner were analyzed with the NimbleScan Software 2.6 using the robust multiarray analysis (RMA) with the default parameters. RMA, a probe-level summarization method, identifies probes that are outliers in the overall behavior of the expression measured for a given gene. The contribution of outlier probes is reduced in the reported gene expression level, which has been demonstrated to improve the sensitivity and reproducibility of microarray results. In addition to screening outlier probes, NimbleScan software's implementation of RMA [53] used quantile normalization and background correction.

The normalized microarray data were analyzed using Partek Genomics Suite 6.6. Statistical analysis was performed using the one-way ANOVA and the false discovery rate (FDR) [54] for multiple-testing correction. Further, the coefficient of variation (CV) expressed in percent was calculated, also known as "relative variability." It equals the standard deviation divided by the mean. An integration tool (available at http://www.leonxie.com/referencegene.php) [50, 51, 55] of four algorithms (geNorm, NormFinder, BestKeeper, and the comparative delta-CT method) was used to evaluate the expression stability of the reference genes. On the basis of the resulted rankings from the four algorithms, an overall ranking of the candidate genes was achieved.

2.7. Statistical Analysis of Selected Genes. Genes of interest were identified, and the log 2 values of the measured fluorescent intensities returned by the Partek software were back calculated to linear values. Then, means of all values of the same gene generated by different probes were calculated, if at least three values existed excluding outliers. Subsequently, standard deviations were calculated for the means and an unpaired t-test with Welch correction was performed using Excel 2011 (t-test, tails 2, type 3) to obtain statistical significance.

3. Results

The aim of our study was to identify a group of genes that show a stable, nonchanging expression profile in immune cells under altered gravity conditions over a time range of seconds until several minutes. Therefore, we performed experiments on the 19th DLR PFC and the sounding rocket mission TEXUS-49, two platforms that offer microgravity times of 20 seconds and 6 minutes, respectively. During both missions, U937 cells, a model for monocytic/macrophageal cells of the human immune system, were exposed to different gravity conditions for various time periods (see Table 1). During the 19th DLR PFC, cells were exposed only to the first parabola with the following sequence: 1 g in-flight control, 1.8 g, and microgravity (μg). Cells were subjected to altered gravity conditions of 1.8 g and μg for 20 seconds in each case and were immediately fixed and stored cooled until RNA isolation. In case of the TEXUS-49 campaign, cells underwent

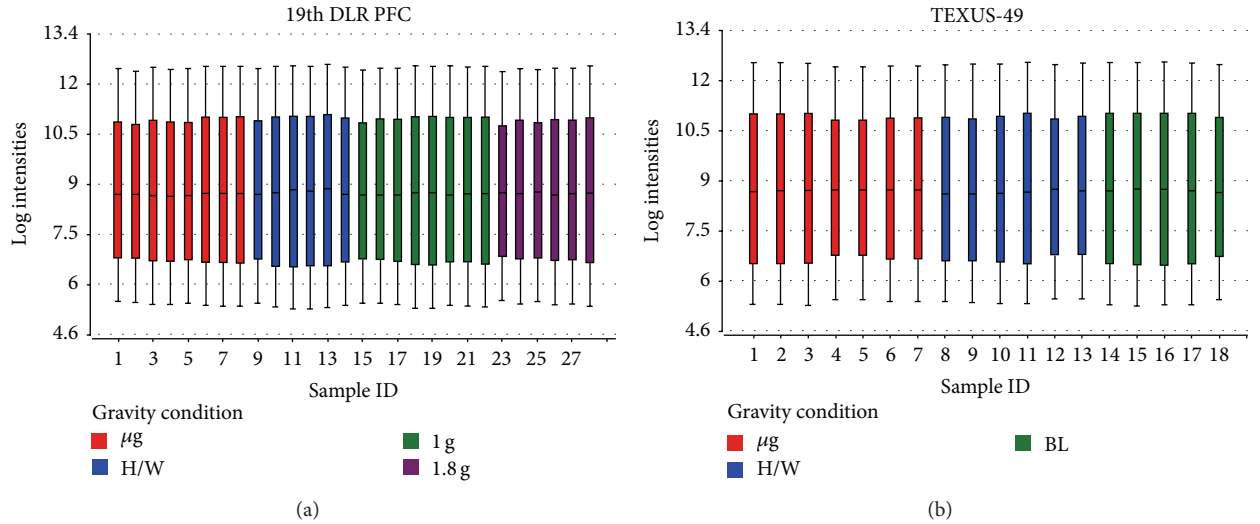

Figure 1: Boxplots showing the log expression values of individual microarrays. The central line represents the 50th percentile or median, whereas the upper and lower boundaries of the box display the 75th and 25th percentile, respectively. The upper and lower bars represent the 9th and the 91st percentile. Two experimental data sets are displayed, (a) 28 microarrays hybridized with samples from the 19th DLR PFC (8x μg, 6x H/W, 8x 1 g, 6x 1.8 g) and (b) 18 microarrays hybridized with samples originating from the TEXUS-49 campaign (7x μg, 6x H/W, 5x 1 g). The expression data show an even distribution for the displayed log intensities.

Table 1: Gravity conditions 19th DLR PFC and TEXUS-49.

Gravity condition	19th DLR PFC	TEXUS-49
1 g ground controls (hardware; H/W)	H/W	H/W
Microgravity	μg (20 sec)	μg (378 sec)
1 g in-flight control	1 g	—
In-flight baseline (hyper-g phase directly before μg; BL)	1.8 g (20 sec)	BL (1 g—max. 13.5 g; 75 sec)

the following sequence of altered gravity: hypergravity up to 13.5 g during the first 75 seconds after liftoff and μg for 378 seconds. Hypergravity is defined as the baseline (BL), because samples mirror the vibration and hypergravity effects directly before the microgravity phase. In both experimental setups, on ground 1 g hardware controls (H/W) were performed to be able to differentiate between the effects caused by the conditions experienced before hypergravity and μg and the altered gravity conditions themselves. After the campaigns, the RNA samples were analyzed for quantity and quality by NanoDrop spectrophotometry and a bioanalyzer analysis, and only samples with an RNA integrity number (RIN) higher than 8.7 were chosen for subsequent microarray analysis. 12 × 135 K Roche NimbleGen arrays were hybridized and data were collected after the normalization procedure. In total, we obtained data from 46 single microarrays (19th DLR PFC: 8x μg, 6x H/W, 8x 1 g, and 6x 1.8 g; TEXUS-49: 7x μg, 6x H/W, and 5x BL).

Data tables were compiled individually for the 19th DLR PFC and TEXUS-49 including all gravity conditions listed in Table 1, and a first overview of the datasets was provided by a boxplot diagram (Figures 1(a) and 1(b)). Boxplots are a useful tool to visualize the variation within a microarray and between microarrays. The central line shows the position of the median, while the upper and the lower boundaries represent the upper (75th percentile) and lower (25th percentile) quartile. The ends of the tails display the 9th and the 91st percentile. The boxplots of the microarray data show that there is only little variation within a single array and between the arrays that belong to the same gravity condition. Figure 1 shows that the quality of both data sets (19th DLR PFC and TEXUS-49) is sufficient to proceed with further analyses.

In search of potential reference genes for gravitational studies in this monocytic/macrophageal cell system, we first performed PubMed database search to identify commonly used reference genes in RNA expression analyses in human cells. We found 22 genes that were used in several reverse transcription quantitative real-time PCR (RT-qPCR) studies as control genes for normalization (Table 2, supplementary Table 2). The microarray data tables were screened for these 22 widely used reference genes, and 20 of them could be located on the Roche NimbleGen 12 × 135 K array that was used in our experiments. Two genes coding for 5s and 18s rRNAs could not be identified, since they are not spotted on the array. The PFC and TEXUS data sets were screened for those 20 selected potential reference genes, and fluorescence intensities were compiled for each gene and each gravity condition in heatmaps (Figures 2(a) and 2(b)). Overall fluorescence intensities for all samples showed only minor differences in the heatmaps. A more detailed visual inspection revealed completely equal fluorescence intensities for ACTB, ALB, B4GALT6, HMBS, HPRT1, PPIA, RPLP0, and YWHAZ for the gravity conditions prevailing during the 19th DLR PFC (Figure 2(a)). The gravity conditions investigated during the TEXUS-49 campaign showed stable expression values for the genes ACTB, ALB, B4GALT6, GUSB, PLA2G4A, POLR2A, PPIA, TBP, UBC, and YWHAZ (Figure 2(b)). For further characterization and identification of stable reference genes,

Table 2: List of potential reference genes.

Potential reference gene	Gene symbol	Citation
5s rRNA		[85]
18s rRNA		[86]
β-Actin	ACTB	[49, 51]
Albumin	ALB	[49]
β-2 microglobin	B2M	[49, 51, 56]
UDP-Gal:bGlcNAcb 1,4-galactosyl-transferase, polypeptide 6	B4GALT6	[86]
Glucose 6-phosphate dehydrogenase	G6PD	[49]
Glyceraldehyde-3-phosphate dehydrogenase	GAPDH	[49, 51, 56, 85, 87, 88]
Glucuronidase, beta	GUSB	[86]
Hydroxymethylbilane synthase (porphobilinogen deaminase)	HMBS	[49, 51, 56]
Hypoxanthine phosphoribosyltransferase 1	HPRT1	[49, 51, 56, 86]
Heat shock protein 90 kDa	HSP90AA1	[86]
Phospholipase A2	PLA2G4A	[49]
RNA polymerase II	POLR2A	[49, 86]
Peptidylprolyl isomerase A (Cyclophilin A)	PPIA	[49, 86]
Ribosomal protein L13	RPL13A	[49, 51, 56, 86]
Acidic ribosomal phosphoprotein P0	RPLP0	[89]
Succinate dehydrogenase complex, subunit A	SDHA	[51, 56, 86]
TATA box binding protein	TBP	[49, 51, 56, 86]
α-Tubulin	TUBA1	[49]
Ubiquitin C	UBC	[51, 56]
Tyrosine 3-monooxygenase tryptophan 5-monooxygenase activation protein	YWHAZ	[51, 56, 86]

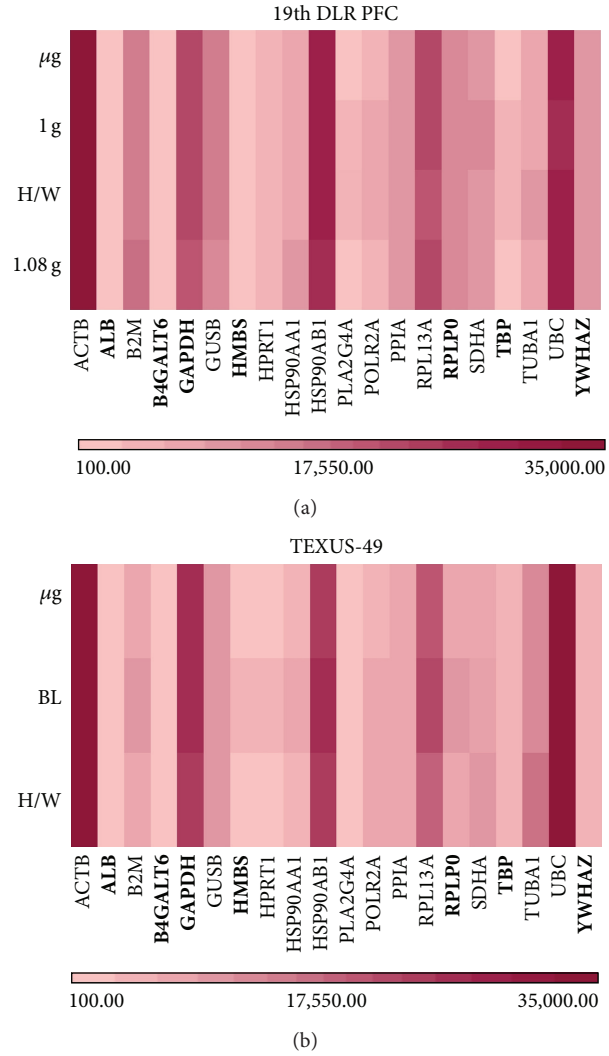

Figure 2: Heatmaps for selected reference genes. The graph illustrates fluorescent intensity levels of the 20 potential reference genes from Table 2 between the three and four different gravity conditions, respectively. Each gene is represented in one column, and each gravity condition is represented in one row. (a) μg, H/W, 1 g, and 1.8 g (19th DLR PFC) and (b) H/W, BL, and μg (TEXUS-49). The heatmap shows large variation in fluorescence intensities for the different genes. However, within the same gene, expression levels are similar for all tested conditions. The lower bar with the graduated red colors is the measure for the different fluorescence intensities.

we performed a geNorm pilot study [51] and calculated the coefficient of variation (CV) for all 20 potential reference genes (Figure 3). For homogeneous groups, CV values below 25%, and for heterogeneous groups, CV values below 50% are acceptable [56]. Rapid and extreme changes in gravity induce strong changes in cellular functions. Therefore, we classified our samples as heterogeneous groups. According to the set criteria, all analyzed potential reference genes showed CV values below 50% for the PFC and TEXUS data sets (Figures 3(a) and 3(b)). In the sample set of the 19th DLR PFC, all genes but HMBS fulfill even the more stringent criterion of a CV below 25% (Figure 3(a)). For the samples collected during the TEXUS-49 campaign, all genes but HPRT1 and PLA2G4A display CV values below 25% (Figure 3(b)).

To increase the number of potential reference genes that can be used as standards for differential expression analyses in gravitational studies, we extended our analysis to evolutionary highly conserved genes. We hypothesized that genes stable over time and taxonomic kingdoms should have very fundamental functions within a cell and thus be largely independent from external influences to ensure basic cellular functions. Besides ribosomal RNA genes, which are not represented on the microarray applied in this study, ABC transporters and tRNA genes are also evolutionary highly conserved over a wide variety of organisms. Unfortunately, the 12 × 135 K Roche NimbleGen array does also not contain probes for tRNA. Therefore, we had a look at expression profiles of ABC transporters and tRNA related genes (supplementary Tables 2 and 3). Since almost all fluorescence values of tRNA related genes showed a high variance making

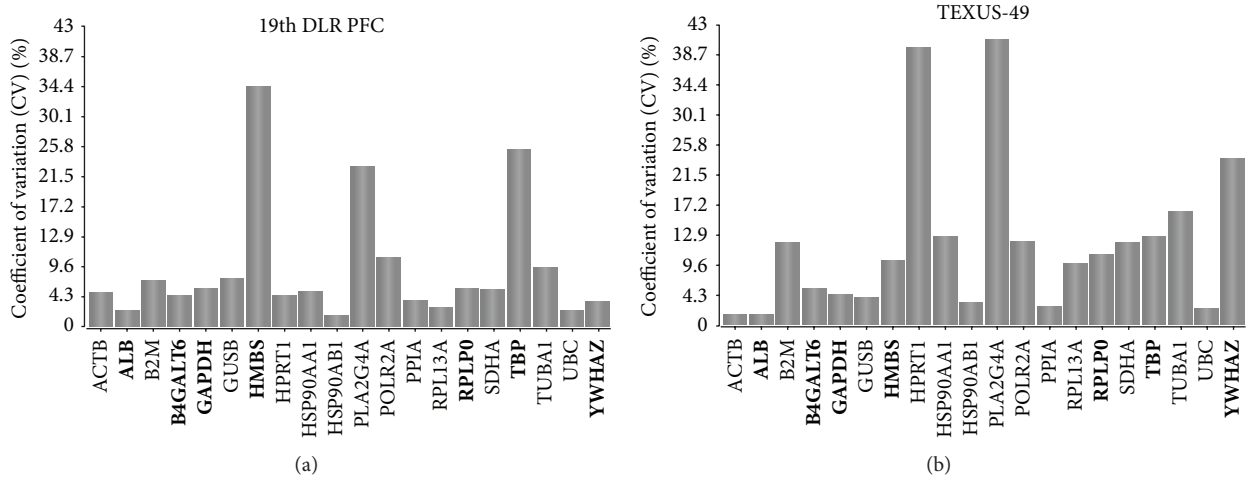

Figure 3: Coefficient of variation calculation for the potential reference genes. This bar chart displays the coefficient of variation (CV) in % of the 20 potential reference genes across the gravity conditions for the 19th DLR PFC (H/W, 1 g, 1.8 g, μg) and TEXUS-49 (H/W, BL, μg). A lower value corresponds to higher stability in gene expression. (a) 19th DLR PFC: All calculated CV values are below the threshold of 50%. (b) TEXUS-49: all CV values are below 50%, but in total more genes show higher coefficients of variation.

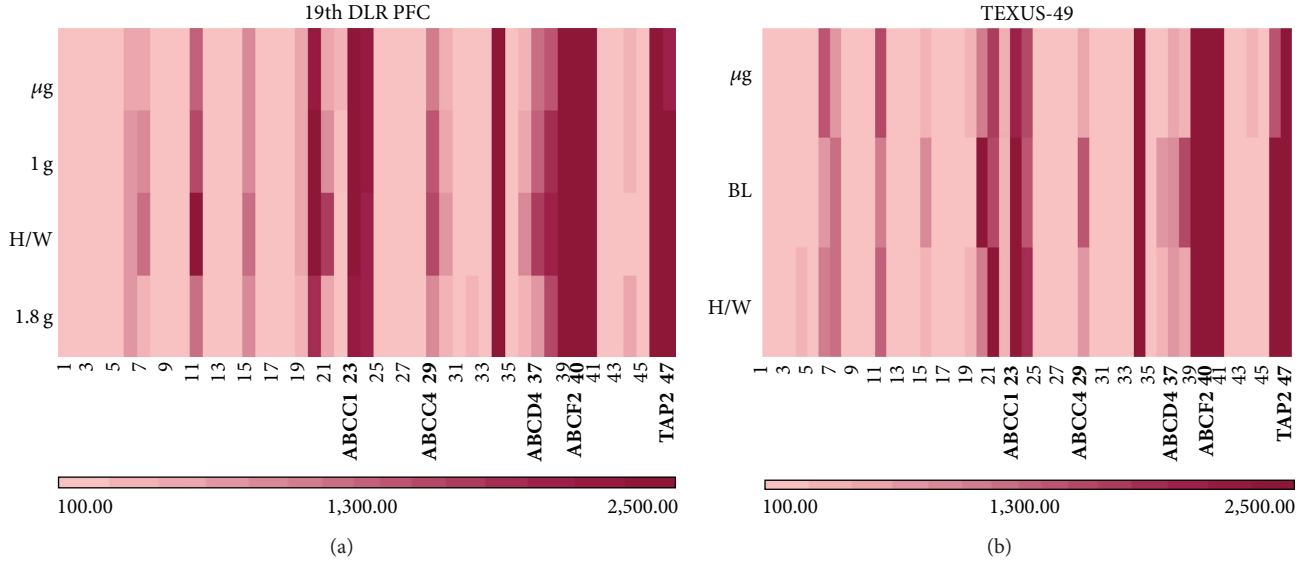

Figure 4: Heatmaps for highly conserved ABC transporters. The fluorescent intensity levels of the 47 ABC transporter genes shown in supplementary Table 2 were quantified for the different gravity conditions. Each gene is represented in one column, and each gravity condition is represented in one row. (a) μg, 1 g, H/W, and 1.8 g (19th DLR PFC) and (b) μg, BL, and H/W (TEXUS-49). The heatmaps show large variation in fluorescence intensities for the different genes. However, within the same gene, expression levels are mostly similar for all tested conditions. The lower bar with the graduated red colors is the measure for the different fluorescence intensities.

reasonable analysis impossible, we concentrated on the ABC transporters. Heatmap analyses were carried out to obtain a first impression on the gene stability (Figure 4). The samples from the 19th DLR PFC and TEXUS-49 mission also show a rather high variation in fluorescence intensities (Figures 4(a) and 4(b)). The calculation of the CV for these samples (Figure 5) displays higher values compared to the potential reference genes; however, taken together all analyzed samples of the 19th DLR PFC fulfill the criterion of CV values less than 50% in case of ABC transporter signals (Figure 5(a)). Out of 47 samples, 36 are also below 25% CV. Although three samples from TEXUS-49 showed values above 50% CV (Figure 5(b)), 37 samples stayed below the 25% threshold (Figure 5(b)). Selected reference genes and ABC transporters (marked in bold, Figures 4 and 5) were chosen for further detailed analysis of differential gene expression under altered gravity conditions.

For nine of the potential reference genes from the literature, there were at least three values returned by the microarray, generated by independent probes targeting the same gene. Two of these genes were excluded from further analysis due to high variance between their single values (HSP90AA1 and PPIA), and the remaining seven genes (ALB, B4GALT6, GAPDH, HMBS, RPLP0, TBP, and YWHAZ (see

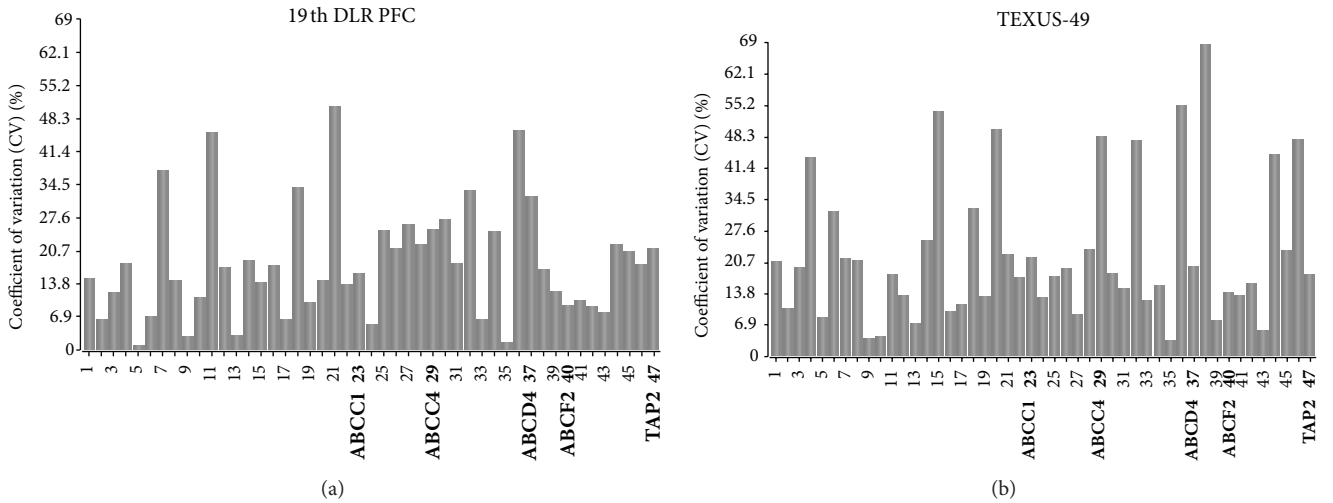

Figure 5: Coefficient of variation calculation for the ABC transporter genes. This bar chart displays the coefficient of variation (CV) in % of the 47 ABC transporter genes across the gravity conditions for the 19th DLR PFC (H/W, 1 g, 1.8 g, μg) and TEXUS-49 (H/W, BL, μg). A lower value corresponds to higher stability in gene expression. (a) 19th DLR PFC: all calculated CV values are below the threshold of 50% and fulfill the criterion. (b) TEXUS-49: three genes show CV values higher than 50% and were excluded from further analyses. The numbers correspond to the ABC transporters listed in supplementary Table 2. Genes that were further analyzed are labeled and marked in bold (ABCC1, ABCC4, ABCD4, ABCF2, and TAP2).

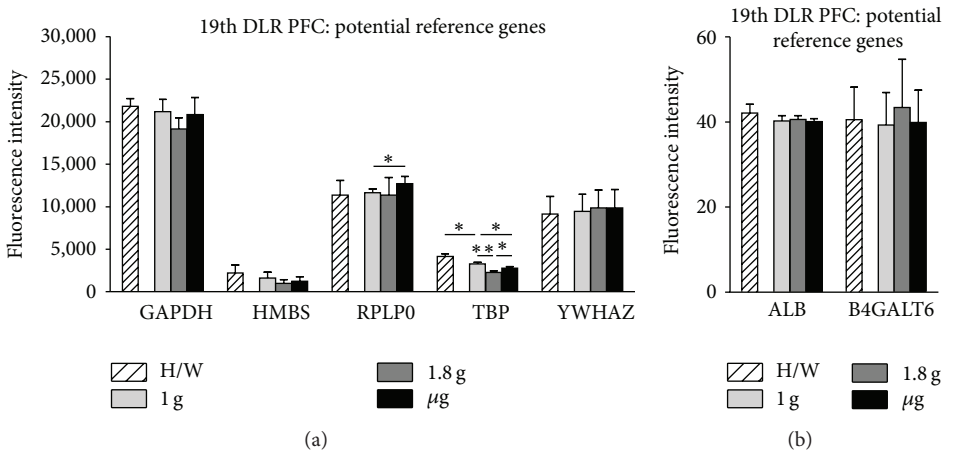

Figure 6: Influence of altered gravity during parabolic flight on potential reference genes. RNA expression levels after 1 g (light gray), 1.8 g (dark gray), and μg (black) conditions during the 19th DLR parabolic flight campaign. Hardware ground controls (H/W, striped) are shown for each experimental group. RNA expression levels are shown as fluorescence intensities. (a) The expression values for GAPDH, HMBS, RPLP0, TBP, and YWHAZ are displayed. (b) ALB and B4GALT6 show low but stable fluorescent intensities. GAPDH, HMBS, YWHAZ, ALB, and B4GALT6 show no significant change in RNA levels upon altered gravity for 20 sec, while RPLP0 displays μg sensitivity compared to 1 g and TBP reacts sensitively to all g conditions. Mean values of at least three measurements with standard deviations are shown. $^{*}P < 0.05$, $^{**}P < 0.005$.

Table 3)) were subjected to further statistics. The calculation of the mean fluorescence intensity levels revealed that different ranges of transcript abundance are present in both experimental setups. While ALB and B4GALT6 seem to be expressed rather low, GAPDH, HMBS, RPLP0, TBP, and YWHAZ are represented in much higher abundance (Figures 6 and 7). The comparison of mean fluorescence intensities of one gene under different g conditions revealed that GAPDH, HMBS, YWHAZ, ALB, and B4GALT6 are stably expressed with respect to all investigated gravity conditions during parabolic flight of the 19th DLR PFC (Figures 6(a) and 6(b)). RPLP0 is significantly upregulated by μg compared to 1 g, while TBP is initially downregulated by 1.8 g and recovers during μg (Figure 6(a)). Furthermore, comparison of in-flight 1 g controls to 1 g ground controls (H/W) shows a significantly reduced mRNA level of TBP portending that during the preexperimental phase a certain kind of stress was accumulated in the cells influencing its expression level.

The data analysis of the TEXUS-49 sounding rocket experiment reveals stable RNA expression levels throughout the different g levels for GAPDH, HMBS, RPLP0, YWHAZ, ALB, and B4GALT6 (Figures 7(a) and 7(b); Table 4, and

Table 3: Selected potential reference genes (19th DLR PFC).

Gene symbol	Accession number	19th DLR PFC: potential reference genes											
		H/W		1 g		1.8 g		μg		P values			
		Mean FI	SD	Mean FI	SD	Mean FI	SD	Mean FI	SD	H/W versus 1 g	1 g versus 1.8 g	1.8 g versus μg	1 g versus μg
ALB	NM_000477 BC035969 BC034023	2.13	2.04	40.28	1.22	40.62	0.88	40.10	0.71	0.2627	0.7154	0.4724	0.8383
B4GALT6	NM_004775 AF069054 BC074835	40.55	7.65	39.30	7.62	43.41	11.38	39.92	7.62	0.8506	0.6342	0.6847	0.9253
GAPDH	NM_002046 BC001601 BC009081	21,791.23	914.23	21,162.32	1,447.99	19,124.58	1,319.50	20,823.21	2,005.00	0.5652	0.1466	0.2971	0.8250
HMBS	NM_000190 NM_001024382 BC008149	2,184.20	973.77	1,612.83	677.49	998.73	443.39	1,226.98	531.59	0.4563	0.2695	0.5994	0.4833
RPLP0	NM_001002 BC001127 BC008594 BC000087 BC070194	11,352.34	1,728.26	11,633.77	426.19	11,380.89	2,060.50	12,714.95	837.10	0.7397	0.8004	0.2346	**0.0425**
TBP	NM_003194 X54993 BC109053	4,158.56	310.25	3,271.43	217.26	2,287.20	161.09	2,776.82	170.76	**0.0192**	**0.0042**	**0.0226**	**0.0390**
YWHAZ	NM_003406 BC068456 BC108281 BC101483 BC083508 BC072426 BC003623	9,136.31	2,070.39	9,445.22	1,990.27	9,843.30	2,125.25	9,853.06	2,184.44	0.7808	0.7239	0.9934	0.7214

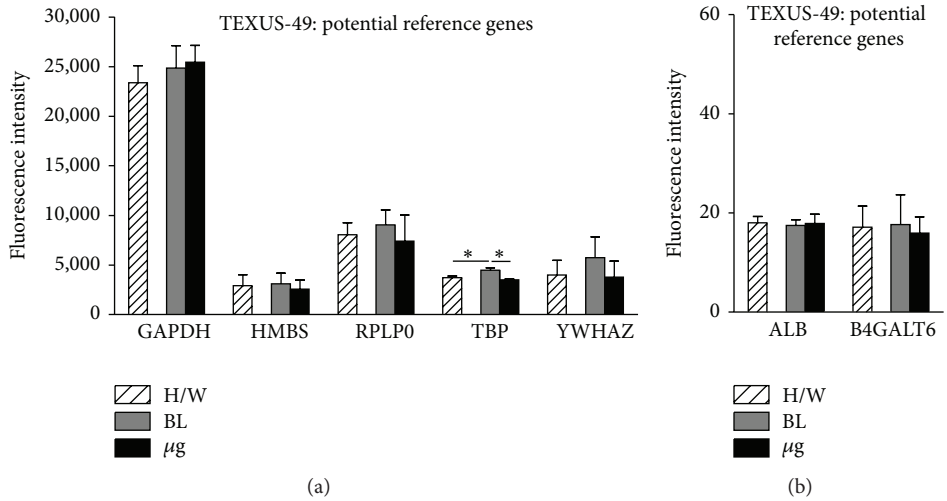

Figure 7: Influence of altered gravity during sounding rocket flight on potential reference genes. GAPDH, HMBS, RPLP0, TBP, and YWHAZ (a), ALB and B4GALT6 (b) RNA expression levels after launch and acceleration (BL, dark gray) and μg (black) conditions of TEXUS-49. Hardware ground controls (H/W, striped) are shown for each experimental group. RNA levels are displayed as fluorescence intensities. GAPDH, HMBS, RPLP0, YWHAZ, ALB, and B4GALT6 show no significant change in RNA levels upon altered gravity, while TBP reacts sensitively to all g conditions. Mean values of at least three measurements with standard deviations are shown. $^{*}P < 0.05$.

supplementary Table 1). TBP RNA levels were reduced in μg samples compared to the in-flight BL. Interestingly, comparisons between the H/W ground controls and BL revealed a postlaunch increase in RNA expression most likely induced by the launch vibrations or hypergravity (Figure 7(a)).

Only a very low number of tRNA related genes fulfilled our criterion of being represented by at least three probes (four out of 32). For three out of those four genes, fluorescent intensity showed a great variance between the single values as mentioned above. Only one tRNA synthetase (SARS) yielded reasonable results. The exposure of the cells to altered gravity conditions during the parabolic flight resulted in a decreased SARS expression in 1 g in-flight control and 1.8 g samples compared to the H/W ground control and 1 g control, respectively (supplementary Table 3). Although not significant, there is a visible increase of SARS mRNA upon μg compared to 1.8 g arguing for an immediate expression recovery after termination of 1.8 g. This is in line with the results from TEXUS-49 flight campaign where SARS shows no significant expression change in in-flight baseline control or in μg compared to H/W ground control. This could be due to fast expression recovery of the gene during g alterations, hyper-g phase, and μg.

The highly conserved ABC transporters were represented as a large group of genes on the applied microarray. We analyzed a total of 47 ABC transporters belonging to nine different sub-families (supplementary Table 2). 19 ABC transporter genes were represented by three or more individual probes on the microarray and 11 of them had similar fluorescent intensities meeting the requirements for a statistical analysis. Exemplarily, five of those 11 ABC transporters are shown in Figures 8 and 9.

During the short-term gravity alterations achieved by parabolic flights, ABCC1 and ABCF2 displayed no significant differential expression between all g conditions analyzed. TAP2 showed a significant reduction of RNA expression

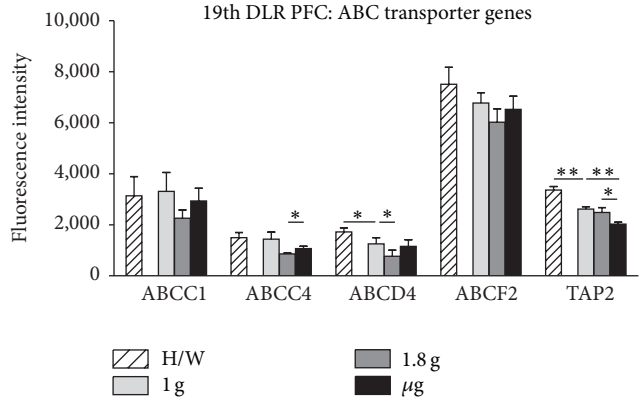

Figure 8: Influence of altered gravity during parabolic flight on ABC transporter genes. ABCC1, ABCC4, ABCD4, ABCF2, and TAP2 RNA levels after 1 g (light gray), 1.8 g (dark gray), and μg (black) conditions during the 19th DLR parabolic flight campaign. Hardware ground controls (H/W, striped) are shown for each experimental group. RNA expression levels are displayed as fluorescence intensities. ABCC1 and ABCF2 show no significant change in RNA expression levels upon altered gravity, while ABCC4 and TAP2 display μg sensitivity compared to 1.8 g and to 1.8 g and 1 g, respectively. ABCD4 reacts sensitively to 1.8 g compared to 1 g, and ABCD4 and TAP2 show vibration sensitivity comparing 1 g to H/W. Mean values of at least three measurements with standard deviations are shown. $^{*}P < 0.05$, $^{**}P < 0.005$.

comparing μg samples to 1.8 g samples, while ABCC4 showed an increase. ABCD4 revealed hyper-g sensitivity by reducing its RNA level during 1.8 g compared to 1 g. And ABCD4 and TAP2 displayed reduced expression during preflight phase compared to H/W control (Figure 8, Table 5).

A prolonged exposure of the cells to μg (378 sec versus 20 sec) during TEXUS-49 experiment led to significant reduction of mRNA levels of ABCC4, ABCD4, ABCF2, and

Table 4: Selected potential reference genes (TEXUS-49).

Gene symbol	Accession number	TEXUS-49: potential reference genes								
		H/W		BL		μg		*P* values		
		Mean FI	SD	Mean FI	SD	Mean FI	SD	H/W versus BL	BL versus μg	H/W versus μg
ALB	NM_000477 BC035969 BC034023	18.02	1.29	17.47	1.18	17.88	1.88	0.6184	0.7708	0.9215
B4GALT6	NM_004775 AF069054 BC074835	17.15	4.26	17.67	6.05	15.95	3.26	0.9093	0.6933	0.7197
GAPDH	NM_002046 BC001601 BC009081	23,385.82	1,721.78	24,862.07	2,271.02	25,451.17	1,692.90	0.4238	0.7383	0.2126
HMBS	NM_000190 NM_001024382 BC008149	2,921.40	1,084.02	3,087.49	1,094.22	2,568.23	899.65	0.8609	0.5612	0.6872
RPLP0	NM_001002 BC001127 BC008594 BC000087 BC070194	8,027.10	1,233.45	9,036.11	1,538.20	7,406.41	2,622.46	0.2871	0.2728	0.6499
TBP	NM_003194 X54993 BC109053	3,738.25	143.90	4,466.01	257.59	3,517.69	53.87	**0.0215**	**0.0201**	0.1037
YWHAZ	NM_003406 BC068456 BC108281 BC101483 BC083508 BC072426 BC003623	3,970.64	1,498.10	5,738.74	2,118.20	3,776.01	1,596.71	0.0993	0.0758	0.8180

Table 5: Selected ABC transporters (19th DLR PFC).

No.	Gene symbol	Accession Number	19th DLR PFC: ABC transporter genes											
			H/W		1 g		1.8 g		μg		*P* values			
			Mean FI	SD	Mean FI	SD	Mean FI	SD	Mean FI	SD	H/W versus 1 g	1 g versus 1.8 g	1.8 g versus μg	1 g versus μg
23	ABCC1	AB209120 NM_019900 NM_004996	3,140.46	751.71	3,309.29	743.99	2,258.45	325.89	2,934.79	496.93	0.7959	0.1193	0.1312	0.5141
29	ABCC4	BC041560 AY133678 NM_005845	1,497.37	199.75	1,437.84	279.45	857.05	30.65	1,067.01	91.26	0.7805	0.0676	**0.0459**	0.1380
37	ABCD4	NM_005050 BC012815 NM_020326 NM_020325	1,719.37	164.62	1,254.13	240.26	765.94	235.75	1,155.89	257.53	**0.0222**	**0.0273**	0.0673	0.5972
40	ABCF2	NM_005692 BC001661 AF091073	7,510.96	664.99	6,774.22	407.85	6,022.09	525.91	6,525.51	515.17	0.1916	0.1263	0.3019	0.5496
47	TAP2	NM_018833 BC002751 AF105151	3,365.61	136.24	2,614.83	94.54	2,485.22	190.87	2,027.84	74.61	**0.0023**	0.3711	**0.0394**	**0.0014**

Table 6: Selected ABC transporters (TEXUS-49).

No.	Gene symbol	Accession number	TEXUS-49: ABC transporter genes								
			H/W		BL		μg		*P* values		
			Mean FI	SD	Mean FI	SD	Mean FI	SD	H/W versus BL	BL versus μg	H/W versus μg
23	ABCC1	AB209120 NM_019900 NM_004996	2,405.02	686.83	3,096.07	634.60	2,020.76	398.49	0.2701	0.0797	0.4598
29	ABCC4	BC041560 AY133678 NM_005845	765.34	293.67	1,382.37	294.64	537.87	140.92	0.0620	**0.0228**	0.3164
37	ABCD4	NM_005050 BC012815 NM_020326 NM_020325	759.92	190.32	843.89	94.39	565.11	138.98	0.4697	**0.0194**	0.1539
40	ABCF2	NM_005692 BC001661 AF091073	8,382.41	751.10	7,963.43	721.46	6,373.22	573.28	0.5244	**0.0430**	**0.0238**
47	TAP2	NM_018833 BC002751 AF105151	4,902.84	12.08	4,000.89	35.26	3,430.97	49.27	**0.0001**	**0.0002**	**0.0002**

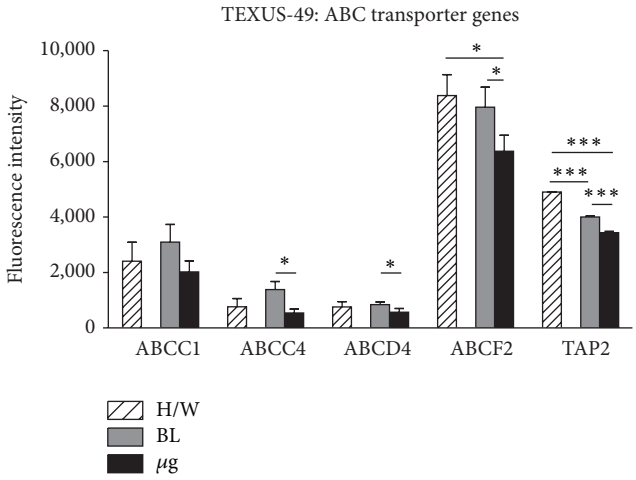

Figure 9: Influence of altered gravity during sounding rocket flight on ABC transporter genes. ABCC1, ABCC4, ABCD4, ABCF2, and TAP2 RNA expression levels after launch and acceleration (BL, dark gray) and μg (black) conditions of TEXUS-49. Hardware ground controls (H/W, striped) are shown for each experimental group. RNA levels are depicted as fluorescence intensities. Only ABCC1 expression is stable over all g conditions. ABCC4, ABCD4, ABCF2, and TAP2 display μg sensitivity compared to BL and to H/W in the case of ABCF2 and TAP2. TAP2 also shows vibration sensitivity comparing BL to H/W. Mean values of at least three measurements with standard deviations are shown. $^{*}P < 0.05$, $^{**}P < 0.005$, and $^{***}P < 0.0005$.

TAP2 in μg compared to in-flight BL. Furthermore, TAP2 expression already decreases in the first phase after launch (BL versus H/W), while the other ABC transporters' mRNA levels appeared stable (Figure 9, Table 6).

Taken together, in this study, we identified eight genes as nonchanging reference genes suitable for studies under altered gravity conditions, and nine genes as candidates for g-sensitivity and 83 genes could not be assigned to either group due to low probe number on the microarray or to great variance between the probe values (Table 7).

4. Discussion

Microarray expression data are intensely used to analyze differential gene expression in cells, tissues, and organisms that are exposed to various conditions [29, 30]. Even in the field of gravitational biology, gene expression analyses are utilized with increasing frequency. Recently, an article was released giving an overview of all published microarray based microgravity studies [57] describing the difficulties to combine and overlay the data from different experiments, study objects, microgravity platforms (simulated microgravity, sounding rocket, space shuttle, and ISS missions), and different microarray experimental designs [58–64]. The different analyses were done mostly in simulated microgravity and investigated various organisms and cell types like *Arabidopsis thaliana, Salmonella enterica*, and rat and mouse tissues, as well as human osteoblasts and T-cells [58–61, 65–70] (for the complete list see [57]). The goal was to screen the vast amount of data to identify a list of major "space genes" that are sensitive to microgravity throughout all involved platforms. The data inspection revealed a huge number of differentially expressed genes but with only little or no overlap between closely related studies on the level of single genes. In contrast, on the level of pathway analysis, it was possible to define major pathways like ECM-receptor interaction, focal adhesion, TGF-beta signaling, and glycolysis being affected in many species (human, mouse, rat, and *Xenopus*, in different combinations) by the exposure to microgravity [57]. Moreover, major "space genes" sensitive to microgravity were defined, if they were found to be differentially expressed in at least four of the examined studies. The results showed in total eight potential space genes (CD44, MARCKS, FN1, TUBA1, CTGF, CYR61, MT2, and MT1), which are involved in T-cell development, cell motility, extracellular matrix components, cytoskeleton, and oxidative stress protection [57]. The study describes in detail the difficulties of combining gene expression data from different groups due to varying experimental setups and conditions. It elucidates that it is of high relevance to be able to standardize gene expression data that arose from RT-qPCR or microarray studies. A key component for standardization within a single experiment and between different experiments is normalization. An important factor for normalization is the use of stable reference genes. There are numerous studies describing that commonly used reference genes could represent a pitfall, because they are often differentially expressed under specific experimental conditions and that they have to be considered carefully before the experiment [46–49]. Different guidelines have been published to facilitate standardized experimental design and increase comparability between analyses (MIQE, MIAME) [34, 39, 40]. It is, for example, highly recommended to perform a pilot study with programs like geNorm or BestKeeper prior to the experiment to identify several stable reference genes that can be used simultaneously as controls for normalization in the differential gene expression analysis [50, 51].

Alternatively, to microarrays a novel technique, RNA-Seq, is under development for whole genome expression analyses. It is reported that this method has advantages in detecting low abundance transcripts, genetic variants, and splice isoforms of genes as well as distinguishing biologically critical isoforms [71]. Despite the described technical advantages of RNA-Seq, microarrays remain popular for some reasons. The microarray platforms have a proven track record spanning nearly two decades in the lab. The arrays are generally considered easier to use with less complicated and less labor-intensive sample preparation than RNA-Seq. The same holds true for the data storage and data analysis. Moreover, despite the rapid drop in the cost associated with next-generation sequencing (NGS), arrays are still more economical and yield higher throughput, providing significant advantages when working with a large number of samples. Therefore, microarray analyses are still more commonly used for transcriptional profiling experiments [71].

Taking into account that many other studies throughout the last few years have reported a considerable portion of the traditionally used reference genes not being stably expressed under various experimental conditions, it becomes rather

Table 7: Overview of g-stable (+) and g-sensitive genes (−).

Gene symbol	Accession number	19th DLR PFC (H/W versus 1 g)	19th DLR PFC (1 g versus 1.8 g)	19th DLR PFC (1.8 g versus μg)	19th DLR PFC (1 g versus μg)	TEXUS-49 (H/W versus BL)	TEXUS-49 (BL versus μg)	TEXUS-49 (H/W versus μg)
		Potential reference genes						
ALB	NM_000477 BC035969 BC034023	+	+	+	+	+	+	+
B4GALT6	NM_004775 AF069054 BC074835	+	+	+	+	+	+	+
GAPDH	NM_002046 BC001601 BC009081	+	+	+	+	+	+	+
HMBS	NM_000190 NM_001024382 BC008149	+	+	+	+	+	+	+
RPLP0	NM_001002 BC001127 BC008594 BC000087 BC070194	+	+	+	−	+	+	+
TBP	NM_003194 X54993 BC109053	−	−	−	−	−	−	+
YWHAZ	NM_003406 BC068456 BC108281 BC101483 BC083508 BC072426 BC003623	+	+	+	+	+	+	+
		ABC transporter genes						
ABCA5	NM_018672 AJ275973 AY028897	+	+	+	+	+	+	+
ABCA9	NM_080283 BC062472 NM_172386 AB209120	+	+	+	+	+	+	+
ABCC1	NM_019900 NM_004996 BC041560	+	+	+	+	+	+	+
ABCC4	AY133678 NM_005845 AK127951	+	+	−	+	+	−	+
ABCC12	NM_145187 NM_033226 BC036378	−	+	+	+	−	−	+
ABCD4	NM_005050 BC012815 NM_020326 NM_020325	−	−	+	+	+	−	+
ABCF2	NM_005692 BC001661 AF091073	+	+	+	+	+	−	−
TAP2	NM_018833 BC002751 AF105151	−	+	−	−	−	−	−

apparent that a natural constant as 1 g might have even more an effect on the expression of genes than other test circumstances. Therefore, we focused in this study on the investigation of the expression qualities of several potential reference genes under 1 g compared to altered gravity conditions generated by two widely used platforms: parabolic flights and sounding rockets. These two platforms are of special interest because of the rather easy access compared to the extremely limited accessibilities of long-term microgravity experiments on satellites and the ISS. We present a microarray based analysis identifying stable reference genes in cells of the immune system exposed to short-term (several seconds) and middle-term (several minutes) altered gravity conditions on the two widely used platforms: parabolic flights and sounding rockets.

Our analyses of commonly used reference genes, ABC transporters and tRNA related genes, revealed that nine of the 17 genes suspected to be ubiquitously expressed are g-sensitive and therefore inappropriate for our purposes, amongst them being TATA box binding protein (TBP), a fundamental transcription factor for many genes, and seryl-tRNA synthetase (SARS), an essential enzyme for mRNA translation, also regulating vascular development (Table 7).

Two of the g-sensitive genes, that we identified in this study, are involved in multidrug resistance processes like the ABC transporters ABCC4 and transporter associated with antigen presenting 2 (TAP2). ABCC4 is of particular interest, because it has the ability to provide resistance to antiviral and anticancer nucleotide analogs and methotrexate [72, 73], acts as an independent regulator of intracellular cAMP, mediates cAMP dependent signal transduction to the nucleus, and controls human and rat smooth muscle cell (SMC) proliferation [74]. It is known that cAMP has largely inhibitory effects on components of macrophage activation and elevation of cAMP levels which suppresses FcgammaR-mediated phagocytosis [75]. Therefore, it would be interesting to look at this multidrug resistance-associated protein (ABCC4) in more detail in microgravity exposed cells to elucidate its role in the signaling cascades important for immune cell action and reaction under space conditions, as ABCC4 proved to be μg-sensitive during parabolic and sounding rocket flight (Figures 8 and 9). Furthermore, TAP2 seems to be even more g-sensitive because it shows significant differential gene expression under μg and hypergravity conditions during parabolic and sounding rocket flight (Figures 8 and 9). It will be interesting to further analyze the potential effects of differential gene expression of TAP2 because it is a key player in endogenous pathways for antigen presentation and involved in the cellular transport of antigens for subsequent association with MHC class I molecules [76]. An imbalance in its gene expression could lead to an impaired reactivity of cells of the immune system under altered gravity conditions.

Further standard genes as well as ABC transporters like RPLP0, ABCD4, and ABCF2 also turned out in our analysis to be g-sensitive. RPLP0 encodes for a ribosomal protein that is a component of the 60S subunit and interacts with P1 and P2 to form pentameric complexes [77]. It is involved, for example, in Chagas disease [78] as well as mixed connective tissue disease [79]. The ABC transporters ABCD4 and ABCF2 are involved in transport of molecules across extra- and intracellular membranes like in peroxisomal import of fatty acids and/or fatty acyl-CoAs in the organelle [80] and play a role in suppression of volume-sensitive outwardly rectifying Cl channel (VSOR), respectively [81]. Altered expression levels of those genes by microgravity or hypergravity could have an impact on the translational level or the supply of the cell with essential resources important for proper cellular function. Recently it was shown that during parabolic flights the activity of the MRP2-ABC-transporter was significantly reduced [82]. Furthermore, under short duration spaceflight missions certain ABC transporter genes in the medically relevant species *Salmonella* sp. and *Candida* sp. were upregulated [83, 84].

Interestingly, we identified many of the g-sensitive genes not only reacting on μg, but also on hypergravity indicating that not only the experimental g-conditions should be taken into account when selecting an appropriate reference gene, but also the accompanying g-conditions prevailing usually before μg is achieved. A detailed differential gene expression analysis of the parabolic flight and sounding rocket flight data sets for g-sensitive genes is currently ongoing.

Genes that proved to be stable over all g-conditions tested, were

(i) albumin (ALB), a protein comprising about one half of blood serum protein,

(ii) UDP-Gal:betaGlcNAc beta 1,4-galactosyltransferase, polypeptide 6 (B4GALT6), a type II membrane-bound glycoprotein important for glycolipid biosynthesis,

(iii) glyceraldehyde-3-phosphate dehydrogenase (GAPDH), a protein with several distinct functions, for example, the reversible oxidative phosphorylation of glyceraldehyde-3-phosphate,

(iv) hydroxymethylbilane synthase (HMBS), a protein catalyzing the head to tail condensation of four porphobilinogen molecules into the linear hydroxymethylbilane,

(v) tyrosine 3-monooxygenase/tryptophan 5-monooxygenase activation protein, zeta (YWHAZ), a gene product belonging to the 14-3-3 family of proteins that interacts with IRS1, suggesting a role in regulating insulin sensitivity,

(vi) ATP-binding cassette, subfamily A, member 5 (ABCA5), a membrane-associated protein belonging to the only major ABC subfamily found exclusively in multicellular eukaryotes with unknown function,

(vii) ATP-binding cassette, subfamily A, member 9 (ABCA9), another ABC1 family member induced during monocyte differentiation into macrophages, and

(viii) ATP-binding cassette, subfamily C, member 1 (ABCC1), a member of the MRP subfamily of ABC transporters involved in multidrug resistance and

functioning as a multispecific organic anion transporter.

Taken together, the compilation of genes that we present in Table 7 gives an overview about which genes are stably expressed during all investigated gravitational conditions lasting from seconds to minutes and can therefore be considered as suitable reference genes. Furthermore, Table 7 can be regarded as a tool for the community that can be easily adapted to select potential control genes in the design phase of a new, immune cell based, experiment on parabolic flights and sounding rocket flights because it provides valuable information about gene expression levels in μg, as well as in 1.8 g, in-flight 1 g and hardware ground control. Our results also allow for the identification of adaptation mechanisms by comparing short (parabolic flight) and intermediate (sounding rocket) microgravity periods and spot those genes that convert from sensitive into stable and vice versa. Our work should considerably facilitate identification of appropriate reference genes for individual experiments performed during parabolic flight and sounding rocket campaigns with immune cells, especially of the monocyte/macrophage system, in altered gravity.

Abbreviations

BL: Baseline
CEV: Centre d'essai en vol
CV: Coefficient of variation
ESA: European Space Agency
FBS: Fetal bovine serum
FDR: False discovery rate
DLR: German Aerospace Center
H/W: Hardware ground controls
HKG: Housekeeping genes
hyper-g: Hypergravity
IL: Interleukin
ISS: International Space Station
LPS: Lipopolysaccharide
μg: Microgravity
MMS: Monocyte-macrophage system
PFC: Parabolic flight campaign
qPCR: Quantitative real-time PCR
RIN: RNA integrity number
RPM: Random positioning machine
ROS: Reactive oxygen species
RWV: Rotating wall vessel
SD: Standard deviation
TNF-α: Tumor necrosis factor-alpha.

Conflict of Interests

The authors declare that there is no conflict of interests regarding the publication of this paper.

Authors' Contributions

Oliver Ullrich and Cora S. Thiel developed the study idea, concept, and the overall study design in addition to planning, coordinating, and supervising the study. Cora S. Thiel, Liliana E. Layer, and Swantje Hauschild wrote the paper. Oliver Ullrich edited the paper. Beatrice Lauber contributed to the paper. Liliana E. Layer, Cora S. Thiel, Oliver Ullrich, Svantje Tauber, Swantje Hauschild, Claudia Philpot, Annett Gutewort, Eva Hürlimann, Josefine Biskup, and Hartwin Lier performed the experiments during the 19th DLR parabolic flight campaign. Svantje Tauber, Cora S. Thiel, Felix Unverdorben, and Oliver Ullrich performed the experiments during the TEXUS-49 mission. Cora S. Thiel was responsible for sample analysis from the 19th DLR parabolic flight campaign and TEXUS-49 mission. Liliana E. Layer contributed to the sample analysis. Frank Engelmann contributed to and supervised the technical procedures during the 19th DLR parabolic flight campaign.

Acknowledgments

The authors gratefully acknowledge financial support by German Aerospace Center DLR (grants nos. 50WB0912 and 50WB1219). They also gratefully acknowledge the support of (in alphabetic order) Gesine Bradacs, Markus Braun, Miriam Christen, Giovanni Colacicco, Ulrike Friedrich, Nadine Gölz, André Hilliger, Andreas Huge, Schirin Ibrahim, Otfried Joop, Sonja Krammer, Andre Melik, Shirin Milani, Brice Mouttet, Marianne Ott, Irina Rau, Frank Rühli, Chen Sang, Burkhard Schmitz, Brita Scholte, Andreas Schütte, Johanna Stahn, Marc Studer, Susanne Wolf, and Fengyuan Zhuang.

References

[1] B. Comet, "Limiting factors for human health and performance: microgravity and reduced gravity. In: study on the survivability and adaptation of humans to long-duration interplanetary and planetary environments," Technical Note 2: Critical Assessments of the Limiting Factors for Human Health and Performance and Recommendation of Countermeasures HUMEX-TN-002, 2001.

[2] G. Horneck, R. Facius, M. Reichert et al., "HUMEX, a study on the survivability and adaptation of humans to long-duration exploratory missions, part II: missions to Mars," *Advances in Space Research*, vol. 38, no. 4, pp. 752–759, 2006.

[3] G. Horneck and B. Comet, "General human health issues for Moon and Mars missions: results from the HUMEX study," *Advances in Space Research*, vol. 37, no. 1, pp. 100–108, 2006.

[4] N. Guéguinou, C. Huin-Schohn, M. Bascove et al., "Could spaceflight-associated immune system weakening preclude the expansion of human presence beyond Earth's orbit?" *Journal of Leukocyte Biology*, vol. 86, no. 5, pp. 1027–1038, 2009.

[5] H. Takayanagi, "Osteoimmunology: shared mechanisms and crosstalk between the immune and bone systems," *Nature Reviews Immunology*, vol. 7, no. 4, pp. 292–304, 2007.

[6] J. Caetano-Lopes, J. E. Canhão, and H. Fonseca, "Osteoimmunology—the hidden immune regulation of bone," *Autoimmunity Reviews*, vol. 8, no. 3, pp. 250–255, 2009.

[7] A. Cogoli, B. Bechler, O. Müller, and E. Hunzinger, "Effect of microgravity on lymphocyte activation," in *Biorack on Spacelab D1*, pp. 89–100, European Space Agency, Paris, France, 1988.

[8] A. Cogoli and A. Tschopp, "Lymphocyte reactivity during spaceflight," *Immunology Today*, vol. 6, no. 1, pp. 1–4, 1985.

[9] A. Cogoli, A. Tschopp, and P. Fuchs-Bislin, "Cell sensitivity to gravity," *Science*, vol. 225, no. 4658, pp. 228–230, 1984.

[10] A. Cogoli, "Gravitational physiology of human immune cells: a review of in vivo, ex vivo and in vitro studies," *Journal of Gravitational Physiology*, vol. 3, no. 1, pp. 1–9, 1996.

[11] O. Ullrich, K. Huber, and K. Lang, "Signal transduction in cells of the immune system in microgravity," *Cell Communication and Signaling*, vol. 6, article 9, 2008.

[12] J. W. Armstrong, R. A. Gerren, and S. K. Chapes, "The effect of space and parabolic flight on macrophage hematopoiesis and function," *Experimental Cell Research*, vol. 216, no. 1, pp. 160–168, 1995.

[13] M. Limouse, S. Manie, I. Konstantinova, B. Ferrua, and L. Schaffar, "Inhibition of phorbol ester-induced cell activation in microgravity," *Experimental Cell Research*, vol. 197, no. 1, pp. 82–86, 1991.

[14] D. A. Schmitt, J. P. Hatton, C. Emond et al., "The distribution of protein kinase C in human leukocytes is altered in microgravity," *FASEB Journal*, vol. 10, no. 14, pp. 1627–1634, 1996.

[15] C.-L. Hsieh, P.-D. L. Chao, and S.-H. Fang, "Morin sulphates/glucuronides enhance macrophage function in microgravity culture system," *European Journal of Clinical Investigation*, vol. 35, no. 9, pp. 591–596, 2005.

[16] I. Kaur, E. R. Simons, V. A. Castro, C. M. Ott, and D. L. Pierson, "Changes in monocyte functions of astronauts," *Brain, Behavior, and Immunity*, vol. 19, no. 6, pp. 547–554, 2005.

[17] A. Adrian, K. Schoppmann, J. Sromicki et al., "The oxidative burst reaction in mammalian cells depends on gravity," *Cell Communication and Signaling*, vol. 11, no. 1, article 98, 2013.

[18] M. A. Meloni, G. Galleri, P. Pippia, and M. Cogoli-Greuter, "Cytoskeleton changes and impaired motility of monocytes at modelled low gravity," *Protoplasma*, vol. 229, no. 2–4, pp. 243–249, 2006.

[19] M. A. Meloni, G. Galleri, G. Pani, A. Saba, P. Pippia, and M. Cogoli-Greuter, "Space flight affects motility and cytoskeletal structures in human monocyte cell line J-111," *Cytoskeleton*, vol. 68, no. 2, pp. 125–137, 2011.

[20] M. Hughes-Fulford, T. Chang, and C.-F. Li, "Effect of gravity on monocyte differentiation," in *Proceedings of the 10th ESA Life Sciences Symposium/29th Annual ISGP Meeting/24th Annual ASGSB Meeting/ELGRA Symposium "Life in Space for Life on Earth"*, pp. 22–27, 2008.

[21] C. Porcher, M.-C. Malinge, C. Picat, and B. Grandchamp, "A simplified method for determination of specific DNA or RNA copy number using quantitative PCR and an automatic DNA sequencer," *BioTechniques*, vol. 13, no. 1, pp. 106–114, 1992.

[22] R. Higuchi, C. Fockler, G. Dollinger, and R. Watson, "Kinetic PCR analysis: real-time monitoring of DNA amplification reactions," *Nature Biotechnology*, vol. 11, no. 9, pp. 1026–1030, 1993.

[23] P.-W. Chiang, W.-J. Song, K.-Y. Wu et al., "Use of a fluorescent-PCR reaction to detect genomic sequence copy number and transcriptional abundance," *Genome Research*, vol. 6, no. 10, pp. 1013–1026, 1996.

[24] U. E. Gibson, C. A. Heid, and P. M. Williams, "A novel method for real time quantitative RT-PCR," *Genome Research*, vol. 6, no. 10, pp. 995–1001, 1996.

[25] C. A. Heid, J. Stevens, K. J. Livak, and P. M. Williams, "Real time quantitative PCR," *Genome Research*, vol. 6, no. 10, pp. 986–994, 1996.

[26] H. D. VanGuilder, K. E. Vrana, and W. M. Freeman, "Twenty-five years of quantitative PCR for gene expression analysis," *BioTechniques*, vol. 44, no. 5, pp. 619–626, 2008.

[27] R. Biassoni and A. Raso, Eds., *Quantitative Real-Time PCR: Methods and Protocols*, Humana Press, New York, NY, USA, 2014.

[28] W. M. Freeman, D. J. Robertson, and K. E. Vrana, "Fundamentals of DNA hybridization arrays for gene expression analysis," *BioTechniques*, vol. 29, no. 5, pp. 1042–1055, 2000.

[29] S. Drăghici, *Data Analysis for DNA Microarrays*, Chapman & Hall/CRC, Boca Raton, Fla, USA, 2003.

[30] H. C. Causton, J. Quackenbush, and A. Brazma, *Microarray Gene Expression Data Analysis: A Beginner's Guide*, Blackwell Publishing, Malden, Mass, USA, 2003.

[31] "The chipping forecast," *Nature Genetics*, vol. 21, pp. 1–60, 1999.

[32] P. O. Brown and D. Botstein, "Exploring the new world of the genome with DNA microarrays," *Nature Genetics*, vol. 21, no. 1, pp. 33–37, 1999.

[33] D. J. Lockhart and E. A. Winzeler, "Genomics, gene expression and DNA arrays," *Nature*, vol. 405, no. 6788, pp. 827–836, 2000.

[34] A. Brazma, P. Hingamp, J. Quackenbush et al., "Minimum information about a microarray experiment (MIAME)—toward standards for microarray data," *Nature Genetics*, vol. 29, no. 4, pp. 365–371, 2001.

[35] R. D. Canales, Y. Luo, J. C. Willey et al., "Evaluation of DNA microarray results with quantitative gene expression platforms," *Nature Biotechnology*, vol. 24, no. 9, pp. 1115–1122, 2006.

[36] S. Lefever, J. Vandesompele, F. Speleman, and F. Pattyn, "RTPrimerDB: the portal for real-time PCR primers and probes," *Nucleic Acids Research*, vol. 37, no. 1, pp. D942–D945, 2009.

[37] F. Pattyn, P. Robbrecht, A. de Paepe, F. Speleman, and J. Vandesompele, "RTPrimerDB: the real-time PCR primer and probe database, major update 2006," *Nucleic Acids Research*, vol. 34, supplement 1, pp. D684–D688, 2006.

[38] X. Wang and B. Seed, "A PCR primer bank for quantitative gene expression analysis," *Nucleic Acids Research*, vol. 31, no. 24, article e154, 2003.

[39] S. A. Bustin, V. Benes, J. A. Garson et al., "The MIQE guidelines: minimum information for publication of quantitative real-time PCR experiments," *Clinical Chemistry*, vol. 55, no. 4, pp. 611–622, 2009.

[40] S. Taylor, M. Wakem, G. Dijkman, M. Alsarraj, and M. Nguyen, "A practical approach to RT-qPCR-Publishing data that conform to the MIQE guidelines," *Methods*, vol. 50, no. 4, pp. S1–S5, 2010.

[41] V. Marx, "PCR: living life amplified and standardized," *Nature Methods*, vol. 10, no. 5, pp. 391–395, 2013.

[42] S. A. Bustin, "Absolute quantification of mrna using real-time reverse transcription polymerase chain reaction assays," *Journal of Molecular Endocrinology*, vol. 25, no. 2, pp. 169–193, 2000.

[43] T. Suzuki, P. J. Higgins, and D. R. Crawford, "Control selection for RNA quantitation," *BioTechniques*, vol. 29, no. 2, pp. 332–337, 2000.

[44] O. Thellin, W. Zorzi, B. Lakaye et al., "Housekeeping genes as internal standards: use and limits," *Journal of Biotechnology*, vol. 75, no. 2-3, pp. 291–295, 1999.

[45] N. Tanic, M. Perovic, A. Mladenovic, S. Ruzdijic, and S. Kanazir, "Effects of aging, dietary restriction and glucocorticoid treatment on housekeeping gene expression in rat cortex and hippocampus—evaluation by real time RT-PCR," *Journal of Molecular Neuroscience*, vol. 32, no. 1, pp. 38–46, 2007.

[46] T. D. Schmittgen and B. A. Zakrajsek, "Effect of experimental treatment on housekeeping gene expression: validation by real-time, quantitative RT-PCR," *Journal of Biochemical and Biophysical Methods*, vol. 46, no. 1-2, pp. 69–81, 2000.

[47] J. A. Warrington, A. Nair, M. Mahadevappa, and M. Tsyganskaya, "Comparison of human adult and fetal expression and identification of 535 housekeeping/maintenance genes," *Physiol Genomics*, vol. 2, no. 3, pp. 143–147, 2000.

[48] K. Dheda, J. F. Huggett, S. A. Bustin, M. A. Johnson, G. Rook, and A. Zumla, "Validation of housekeeping genes for normalizing RNA expression in real-time PCR," *BioTechniques*, vol. 37, no. 1, pp. 112–119, 2004.

[49] A. Radonić, S. Thulke, I. M. Mackay, O. Landt, W. Siegert, and A. Nitsche, "Guideline to reference gene selection for quantitative real-time PCR," *Biochemical and Biophysical Research Communications*, vol. 313, no. 4, pp. 856–862, 2004.

[50] M. W. Pfaffl, A. Tichopad, C. Prgomet, and T. P. Neuvians, "Determination of stable housekeeping genes, differentially regulated target genes and sample integrity: bestKeeper—excel-based tool using pair-wise correlations," *Biotechnology Letters*, vol. 26, no. 6, pp. 509–515, 2004.

[51] J. Vandesompele, K. De Preter, F. Pattyn et al., "Accurate normalization of real-time quantitative RT-PCR data by geometric averaging of multiple internal control genes," *Genome Biology*, vol. 3, no. 7, Article ID RESEARCH0034, 2002.

[52] J. H. Cai, S. Deng, S. W. Kumpf et al., "Validation of rat reference genes for improved quantitative gene expression analysis using low density arrays," *BioTechniques*, vol. 42, no. 4, pp. 503–512, 2007.

[53] R. A. Irizarry, B. Hobbs, F. Collin et al., "Exploration, normalization, and summaries of high density oligonucleotide array probe level data," *Biostatistics*, vol. 4, no. 2, pp. 249–264, 2003.

[54] Y. Benjamini and Y. Hochberg, "Controlling the false discovery rate: a practical and powerful approach to multiple testing," *Journal of the Royal Statistical Society Series B: Methodological*, vol. 57, no. 1, pp. 289–300, 1995.

[55] N. Silver, S. Best, J. Jiang, and S. L. Thein, "Selection of housekeeping genes for gene expression studies in human reticulocytes using real-time PCR," *BMC Molecular Biology*, vol. 7, article 33, 2006.

[56] J. Hellemans, G. Mortier, A. de Paepe, F. Speleman, and J. Vandesompele, "qBase relative quantification framework and software for management and automated analysis of real-time quantitative PCR data," *Genome biology*, vol. 8, no. 2, p. R19, 2007.

[57] J. Q. Clement, "Gene expression microarrays in microgravity research: toward the identification of major space genes," in *Innovations in Biotechnology*, E. C. Agbo, Ed., pp. 319–348, InTech, 2012.

[58] A.-I. Kittang, J. J. van Loon, O. Vorst, R. D. Hall, K. Fossum, and T.-H. Iversen, "Ground based studies of gene expression in Arabidopsis exposed to gravity stresses," *Journal of Gravitational Physiology*, vol. 11, no. 2, pp. P223–P224, 2004.

[59] M. Martzivanou, M. Babbick, M. Cogoli-Greuter, and R. Hampp, "Microgravity-related changes in gene expression after short-term exposure of *Arabidopsis thaliana* cell cultures," *Protoplasma*, vol. 229, no. 2–4, pp. 155–162, 2006.

[60] V. Chopra, A. A. Fadl, J. Sha, S. Chopra, C. L. Galindo, and A. K. Chopra, "Alterations in the virulence potential of enteric pathogens and bacterial-host cell interactions under simulated microgravity conditions," *Journal of Toxicology and Environmental Health Part A: Current Issues*, vol. 69, no. 14, pp. 1345–1370, 2006.

[61] S. Yamada, T. Ganno, N. Ohara, and Y. Hayashi, "Chitosan monomer accelerates alkaline phosphatase activity on human osteoblastic cells under hypofunctional conditions," *Journal of Biomedical Materials Research Part A*, vol. 83, no. 2, pp. 290–295, 2007.

[62] M. L. Lewis, L. A. Cubano, B. Zhao et al., "cDNA microarray reveals altered cytoskeletal gene expression in space-flown leukemic T lymphocytes (Jurkat)," *The FASEB Journal*, vol. 15, no. 10, pp. 1783–1785, 2001.

[63] M. A. Meloni, G. Galleri, S. Carta et al., "Preliminary study of gene expression levels in human T-cells exposed to cosmic radiations," *Journal of Gravitational Physiology*, vol. 9, no. 1, pp. P291–P292, 2002.

[64] S. J. Pardo, M. J. Patel, M. C. Sykes et al., "Simulated microgravity using the Random Positioning Machine inhibits differentiation and alters gene expression profiles of 2T3 preosteoblasts," *The American Journal of Physiology—Cell Physiology*, vol. 288, no. 6, pp. C1211–C1221, 2005.

[65] J. W. Wilson, R. Ramamurthy, S. Porwollik et al., "Microarray analysis identifies *Salmonella* genes belonging to the low-shear modeled microgravity regulon," *Proceedings of the National Academy of Sciences of the United States of America*, vol. 99, no. 21, pp. 13807–13812, 2002.

[66] M. Wittwer, M. Flück, H. Hoppeler, S. Müller, D. Desplanches, and R. Billeter, "Prolonged unloading of rat soleus muscle causes distinct adaptations of the gene profile," *The FASEB Journal*, vol. 16, no. 8, pp. 884–886, 2002.

[67] Z. Q. Dai, R. Wang, S. K. Ling, Y. M. Wan, and Y. H. Li, "Simulated microgravity inhibits the proliferation and osteogenesis of rat bone marrow mesenchymal stem cells," *Cell Proliferation*, vol. 40, no. 5, pp. 671–684, 2007.

[68] K. M. Fridley, I. Fernandez, M.-T. A. Li, R. B. Kettlewell, and K. Roy, "Unique differentiation profile of mouse embryonic stem cells in rotary and stirred tank bioreactors," *Tissue Engineering Part A*, vol. 16, no. 11, pp. 3285–3298, 2010.

[69] A. Qian, S. Di, X. Gao et al., "cDNA microarray reveals the alterations of cytoskeleton-related genes in osteoblast under high magneto-gravitational environment," *Acta Biochimica et Biophysica Sinica*, vol. 41, no. 7, pp. 561–577, 2009.

[70] N. E. Ward, N. R. Pellis, S. A. Risin, and D. Risin, "Gene expression alterations in activated human T-cells induced by modeled microgravity," *Journal of Cellular Biochemistry*, vol. 99, no. 4, pp. 1187–1202, 2006.

[71] S. Zhao, W.-P. Fung-Leung, A. Bittner, K. Ngo, and X. Liu, "Comparison of RNA-Seq and microarray in transcriptome profiling of activated T cells," *PLoS ONE*, vol. 9, no. 1, Article ID e78644, 2014.

[72] Z.-S. Chen, K. Lee, and G. D. Kruh, "Transport of cyclic nucleotides and estradiol 17-β-D-glucuronide by multidrug resistance protein 4. Resistance to 6-mercaptopurine and 6-thioguanine," *The Journal of Biological Chemistry*, vol. 276, no. 36, pp. 33747–33754, 2001.

[73] Z.-S. Chen, K. Lee, S. Walther et al., "Analysis of methotrexate and folate transport by multidrug resistance protein 4 (ABCC4): MRP4 is a component of the methotrexate efflux system," *Cancer Research*, vol. 62, no. 11, pp. 3144–3150, 2002.

[74] Y. Sassi, L. Lipskaia, G. Vandecasteele et al., "Multidrug resistance-associated protein 4 regulates cAMP-dependent signaling pathways and controls human and rat SMC proliferation,"

The Journal of Clinical Investigation, vol. 118, no. 8, pp. 2747–2757, 2008.

[75] D. M. Aronoff, C. Canetti, C. H. Serezani, M. Luo, and M. Peters-Golden, "Cutting edge: macrophage inhibition by cyclic AMP (cAMP): differential roles of protein kinase A and exchange protein directly activated by cAMP-1," *The The Journal of Immunology*, vol. 174, no. 2, pp. 595–599, 2005.

[76] E. Procko and R. Gaudet, "Antigen processing and presentation: TAPping into ABC transporters," *Current Opinion in Immunology*, vol. 21, no. 1, pp. 84–91, 2009.

[77] K.-M. Lee, C. W. Yu, D. S. Chan et al., "Solution structure of the dimerization domain of ribosomal protein P2 provides insights for the structural organization of eukaryotic stalk," *Nucleic Acids Research*, vol. 38, no. 15, pp. 5206–5216, 2010.

[78] I. Ferrari, M. J. Levin, G. Wallukat et al., "Molecular mimicry between the immunodominant ribosomal protein P0 of *Trypanosoma cruzi* and a functional epitope on the human β1-adrenergic receptor," *Journal of Experimental Medicine*, vol. 182, no. 1, pp. 59–65, 1995.

[79] R. W. Hoffman and M. E. Maldonado, "Immune pathogenesis of Mixed Connective Tissue Disease: a short analytical review," *Clinical Immunology*, vol. 128, no. 1, pp. 8–17, 2008.

[80] S. Kemp and R. J. A. Wanders, "X-linked adrenoleukodystrophy: very long-chain fatty acid metabolism, ABC half-transporters and the complicated route to treatment," *Molecular Genetics and Metabolism*, vol. 90, no. 3, pp. 268–276, 2007.

[81] Y. Ando-Akatsuka, T. Shimizu, T. Numata, and Y. Okada, "Involvements of the ABC protein ABCF2 and α-actinin-4 in regulation of cell volume and anion channels in human epithelial cells," *Journal of Cellular Physiology*, vol. 227, no. 10, pp. 3498–3510, 2012.

[82] S. Vaquer, E. Cuyàs, A. Rabadán, A. González, F. Fenollosa, and R. de la Torre, "Active transmembrane drug transport in microgravity: a validation study using an ABC transporter model," *F1000Research*, vol. 3, article 201, 2014.

[83] J. W. Wilson, C. M. Ott, K. Höner Zu Bentrup et al., "Space flight alters bacterial gene expression and virulence and reveals a role for global regulator Hfq," *Proceedings of the National Academy of Sciences of the United States of America*, vol. 104, no. 41, pp. 16299–16304, 2007.

[84] A. Crabbé, S. M. Nielsen-Preiss, C. M. Woolley et al., "Spaceflight enhances cell aggregation and random budding in *Candida albicans*," *PLoS ONE*, vol. 8, no. 12, Article ID e80677, 2013.

[85] C. K. Mantri, J. P. Dash, J. V. Mantri, and C. C. V. Dash, "Cocaine Enhances HIV-1 Replication in CD4+ T Cells by Down-Regulating MiR-125b," *PLoS ONE*, vol. 7, no. 12, Article ID e51387, 2012.

[86] F. Jacob, R. Guertler, S. Naim et al., "Careful selection of reference genes is required for reliable performance of RT-qPCR in human normal and cancer cell lines," *PLoS ONE*, vol. 8, no. 3, Article ID e59180, 2013.

[87] A. Marcant, A. Denys, A. Melchior et al., "Cyclophilin B attenuates the expression of TNF-α in lipopolysaccharide-stimulated macrophages through the induction of B cell lymphoma-3," *The Journal of Immunology*, vol. 189, no. 4, pp. 2023–2032, 2012.

[88] B. P. Barna, I. Huizar, A. Malur et al., "Carbon nanotube-induced pulmonary granulomatous disease: twist1 and alveolar macrophage M1 activation," *International Journal of Molecular Sciences*, vol. 14, no. 12, pp. 23858–23871, 2013.

[89] J. P. Chou, C. M. Ramirez, J. E. Wu, and R. B. Effros, "Accelerated aging in HIV/AIDS: novel Biomarkers of Senescent Human CD8+ T Cells," *PLoS ONE*, vol. 8, no. 5, Article ID e64702, 2013.

Hindawi Publishing Corporation
BioMed Research International
Volume 2015, Article ID 547495, 15 pages
http://dx.doi.org/10.1155/2015/547495

Research Article

A Whole-Genome Microarray Study of *Arabidopsis thaliana* Semisolid Callus Cultures Exposed to Microgravity and Nonmicrogravity Related Spaceflight Conditions for 5 Days on Board of Shenzhou 8

Svenja Fengler,[1] Ina Spirer,[1] Maren Neef,[1] Margret Ecke,[1] Kay Nieselt,[2] and Rüdiger Hampp[1]

[1]*Physiological Ecology of Plants, University of Tübingen, Auf der Morgenstelle 1, 72076 Tübingen, Germany*
[2]*Center for Bioinformatics, University of Tübingen, Sand 14, 72076 Tübingen, Germany*

Correspondence should be addressed to Svenja Fengler; svenja.fengler@uni-tuebingen.de

Received 8 May 2014; Revised 26 August 2014; Accepted 9 September 2014

Academic Editor: Monica Monici

The Simbox mission was the first joint space project between Germany and China in November 2011. Eleven-day-old *Arabidopsis thaliana* wild type semisolid callus cultures were integrated into fully automated plant cultivation containers and exposed to spaceflight conditions within the Simbox hardware on board of the spacecraft Shenzhou 8. The related ground experiment was conducted under similar conditions. The use of an in-flight centrifuge provided a 1 g gravitational field in space. The cells were metabolically quenched after 5 days via RNA*later* injection. The impact on the *Arabidopsis* transcriptome was investigated by means of whole-genome gene expression analysis. The results show a major impact of nonmicrogravity related spaceflight conditions. Genes that were significantly altered in transcript abundance are mainly involved in protein phosphorylation and MAPK cascade-related signaling processes, as well as in the cellular defense and stress responses. In contrast to short-term effects of microgravity (seconds, minutes), this mission identified only minor changes after 5 days of microgravity. These concerned genes coding for proteins involved in the plastid-associated translation machinery, mitochondrial electron transport, and energy production.

1. Introduction

Gravitation biology is a field of research which has made considerable progress within the last years, involving prokaryotes, fungi, plants, and animals. Plants are especially interesting, because, as sessile organisms, they possess high versatility in responding to environmental challenges and abiotic as well as biotic ones. In order to investigate responses to altered gravitation, a large range of methods is available that allows for modification of the Earth's gravitational field. These involve centrifugation (hypergravity), clinorotation, magnetic levitation, and random positioning (simulated microgravity), or parabolic flights of planes and sounding rockets, as well as satellites and spacecrafts (deliver microgravity). Experiments with plants show that not only tissues and organelles [1, 2] but also single-cell systems like characean rhizoids [3–7] as well as spores (*Ceratopteris richardii*, [8, 9]) and protoplasts [10–12] or homogeneous cell cultures (*Arabidopsis thaliana*) exhibit gravisensitivity [2, 13–16]. Experimental approaches that analyze the response to altered gravitation such as transcriptomics, proteomics, and metabolomics dominate recently. First molecular approaches were using transcriptomics, that is, the search for genes which change their expression under altered gravitation. In plants, like in other organisms, the improvement of gene expression quantification technologies, together with growing databases, supports this development considerably. To date, databases are available that exhibit plant datasets representing their response to diverse experimental stimuli [17–20]. They show that external signals are translated into biochemical ones, resulting in molecular signaling cascades which eventually result in a life-sustaining adaptation process.

For *Arabidopsis* (*Arabidopsis thaliana*) cell suspension cultures, the response to short-term microgravity was investigated intensely in our group by means of parabolic flights [21]. A combination of transcriptomics with phosphoproteomics showed that changes in gene expression and protein modification occur within seconds. The investigation of effects caused by longer-lasting microgravity depends on much scarcer availability of respective flight opportunities. However, data on cellular and molecular long-term responses of plants such as Brassicaceae (*Arabidopsis*), Fabaceae, and Poaceae has recently been published [2, 15, 22–31]. With regard to long-term experiments on gene expression, there are conflicting reports. Stutte et al. [30], for example, could not observe differentially expressed genes (DEGs) above a 2-fold cut-off in 24-day-old wheat leaves after a 21-day-space mission. In contrast, Paul et al. [15, 24] detected many DEGs in nearly 20-day-old *Arabidopsis* callus cultures and 18-day-old seedlings after a nearly 13-day-space mission. Furthermore, the set of altered genes detected in whole seedlings was different from that in callus cultures [15]. Thereby, the spaceflight-mediated upregulated expression of heat shock proteins appeared to be an age-independent cell culture specific response [15, 16]. Within the so-called TROPI-2 experiment, only 24 genes were altered in their abundance in *Arabidopsis* seedlings [2], due to possible microgravity effects after 4 days. In addition, these authors reported differences between the 1 g ground sample and the 1 g in-flight controls, with over 200 DEGs [2]. Also Zhang et al. [32] observed a greater difference between flight and ground samples with respect to 1 g in-flight conditions. These observations indicate that the differing results could be related to the organisms investigated, the time of exposure, hardware, experimental parameters, and set-up.

In this study, we report on results of a spaceflight experiment. This experiment was part of the Simbox (Science in Microgravity Box) mission, a joint project between the space agencies from Germany (Deutsches Zentrum für Luft- und Raumfahrt e. V.) and China (China Manned Space Engineering) in November 2011. As one out of 17 biological experiments, semisolid callus cultures of *Arabidopsis* were exposed to a 17-day spaceflight on board of the Chinese spacecraft Shenzhou 8. Due to reduced viability after longer periods of exposure within the flight hardware, the callus cultures were metabolically quenched after 5 days in space. Results of a whole-genome microarray screening (μg exposed samples, 1 g in-flight samples kept in a reference centrifuge, and 1 g ground samples) revealed major differences between both 1 g controls but a minor impact of microgravity.

2. Material and Methods

2.1. Experiment-Specific Hardware (HW). The Simbox was a modification of the Biobox-6 [33, 34] which was developed for unmanned recoverable capsules and space shuttle missions. Development and production were carried out by Astrium/EADS, Friedrichshafen, Germany [35]. This incubator (size of 461 × 551 × 273 mm, internal volume of 34 L, max. power consumption of 130 W, and empty mass of 17 kg) served as carrier for an experiment/static platform with an integrated centrifuge rotor (provides 1 g in-flight control). The Simbox incubator (Figure 1) enabled sample cultivation at 22–24°C (nominal temperature range) and 30–40% humidity throughout the mission. A duplicate model of the Simbox was constructed for the ground experiment. Our biological approach (experiment number 16) was realized by means of three fully automated type V Experiment Unit Envelopes (EUE, plant cultivation unit, without illumination). EUEs consisted of support housing made of polyetherketone with two culture chambers each (front and rear CC, 31.7 × 24 × 14.3 mm ± 0.15 mm). Our biological material was positioned on substrate holders (slides) with plastic spikes (Figure 2). The latter were needed to keep the cultures in place. In order to allow gas exchange, the CCs were sealed with a biofoil made of polysulfone (Tecason S Polysulfone, Ensinger Inc., Washington-Pennsylvania, USA). In addition, a peristaltic pump (flow rate of ≥2.43 mL/min) was used to

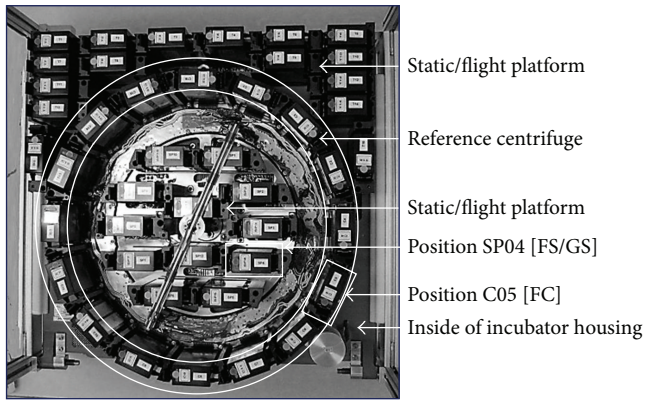

Figure 1: Photograph of the inside of the Simbox incubator used within the flight/ground experiment (housing removed). The rotor of the reference centrifuge (position C05 for sample group FC) is indicated by a circle. The static experimental platform is in the middle and outside of the centrifuge rotor (position SP04 for sample group FS within the flight experiment and GS within the ground experiment, resp.) (photograph: DLR/Astrium).

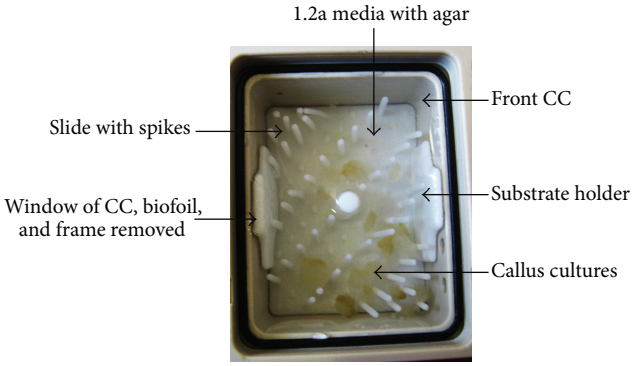

Figure 2: Photograph of the inside of one culture chamber (CC) (experiment container (EC), window, biofoil, and frame removed). The semisolid callus cultures were positioned on substrate holders (slides) with plastic spikes on 1.2a agar containing culture media.

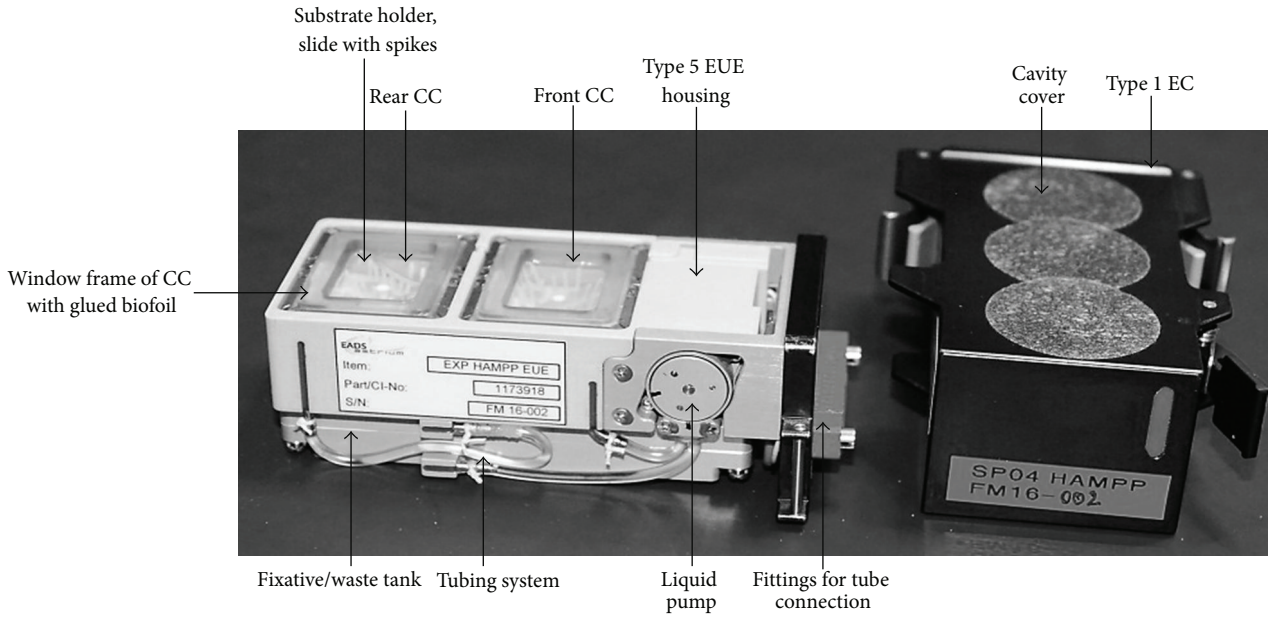

Figure 3: Photograph of the fully automated plant cultivation unit, type V EUE (left side), and EC removed (right side) (photograph: DLR/Astrium).

connect the CC to a fixative/waste unit (volume 20.3 mL ± 0.5 mL). EUEs were accommodated inside type I Experiment Containers (ECs) (Figure 3). Via sensors, parameters such as temperature, humidity, CO_2, and O_2 content as well as activation of the pump system were recorded and transmitted.

2.2. Cell Cultures. Sterile cuttings (about 50 mm long) of stems of wild type *Arabidopsis thaliana* (cv. Columbia Col-0) plants were used for callus formation on 1.2a media [36] containing 1% agar (Sigma-Aldrich, Germany). Calli were transferred to 500 mL Erlenmeyer flasks with 200 mL liquid 1.2a medium and cultivated under sterile conditions at 23°C in the dark on a rotary shaker (130 rpm, Infors, Bottmingen, Switzerland), as described previously [14]. New medium was added every week to the resulting cell suspension. Eight months before the Simbox mission, an aliquot of this culture (3 g) was spread on 6 cm Petri dishes (Greiner Bio-One, Frickenhausen, Germany) containing agar and 1.2a medium. Cell cultures were mailed to the Institute of Physiology and Ecology, Shanghai (Laboratory of Prof. Zheng), and the cultivation continued (as liquid suspension) as described above. These suspension cultures were transferred to the PITC (Payload Integration and Test Center, Beijing, China). The cultivation was then continued on agar plates (see above) and, finally these semisolid calli were brought to the launch site (Jiuquan Satellite Launch Center, Jiuquan, China) by plane.

2.3. Preparation of Final Experiment Configuration. One day before the launch, 11-day-old semisolid callus cultures were transferred into the CCs with 2 mL agar containing medium (Figures 2 and 3). Two ECs were used for the spaceflight (flight models: FM 16001 and FM 16002) and one for the ground experiment (FM 16003), respectively. One of the two ECs was contained in the centrifuge rotor, and the other one was fixed at the experiment/static platform (flight platform), respectively (Figure 1). Metabolic quenching of the samples was by the injection of RNA*later* (Ambion, Life Technologies, Darmstadt, Germany). This reagent is also used to stabilize nucleic acids. Twenty mL of this fixative was filled into the fixative/waste unit attached to the bottom of the EC. Between handover and integration into the Simbox flight/ground incubator, the ECs were stored at nominal laboratory temperature conditions (22–24°C). The Simbox incubator was unpowered for about 3 hours during transport to the spacecraft. During this time, the lowest temperature was 21°C (Figure 4).

2.4. The Experiment in Orbit. The Simbox was launched on board of the unmanned spacecraft Shenzhou 8 on October 31, 2011, at 21:58 UTC (universal time coordinated) with a Long March 2F rocket from the cosmodrome in JSLC. The precise mission timings including sample fixation time points are illustrated in Figure 5 (for a gravity-level profile, see Supplementary Material S1 available online at http://dx.doi.org/10.1155/2014/547495). Experiment zero time (EZT) was set when the spacecraft reached the orbit. At EZT, the centrifuge was activated to run with 74.40 rpm. Within the spacecraft, the oxygen partial pressure ranged from 18.04 to 27.32 kPa, and the carbon dioxide partial pressure was between −0.03 and 0.46 kPa. Radiation measurements yielded a total dose of 5.93 to 8.1 mSv and an equivalent dose of 0.37 to 0.51 mSv/d near the Simbox incubator (telemetry data: Chinese authorities, personal communication). The pump system was activated after 5 days in space and injected the fixative solution from the fixative/waste unit into the CC's

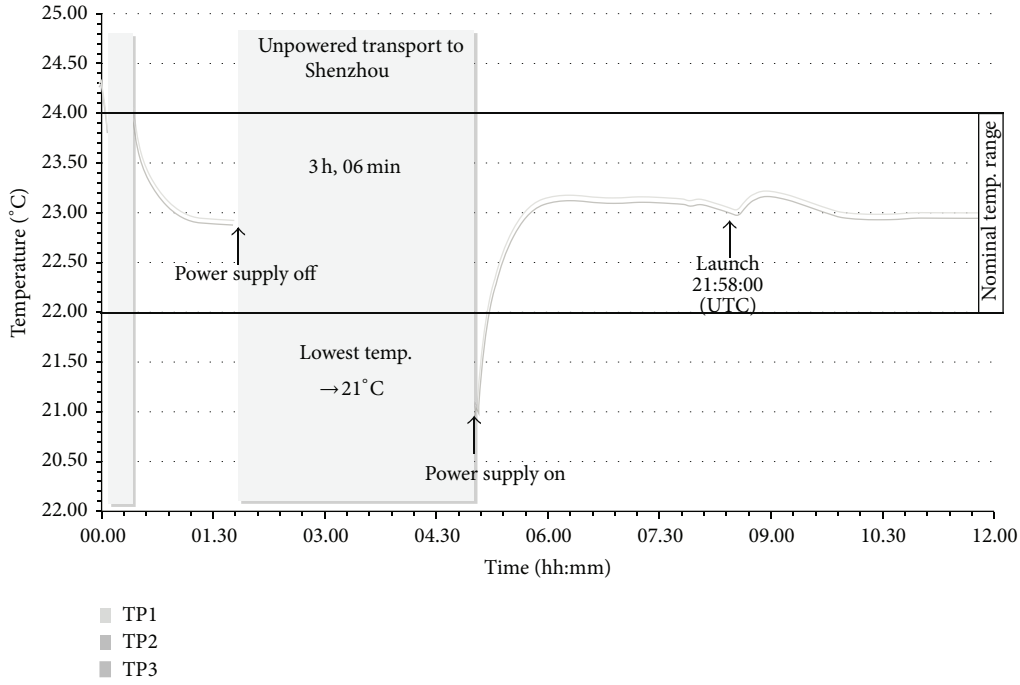

Figure 4: Temperature profile as recorded by 3 temperature sensors (TP1-3) attached to the Simbox incubator during integration of ECs into the incubator, transport to Shenzhou, and launch (data: Astrium).

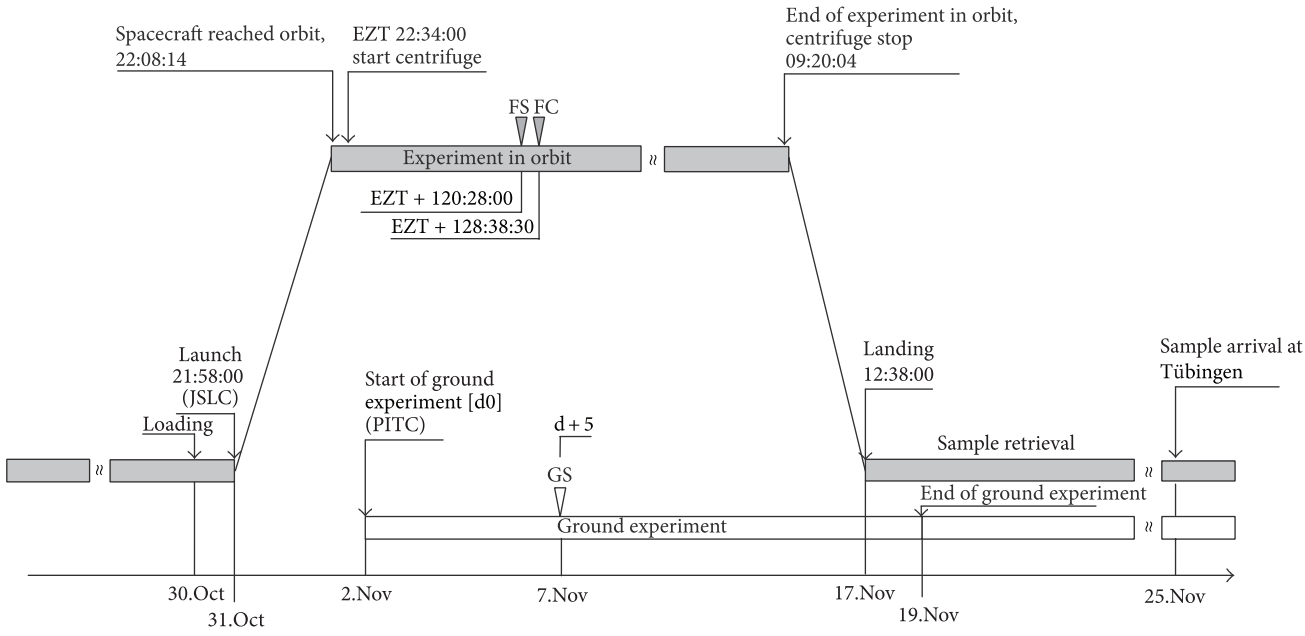

Figure 5: Precise mission timeline of the experiment in orbit (grey) and related ground experiment (white). Universal time coordinated (UTC), time units are given in hours:minutes: seconds, experimental zero time (EZT). Arrowheads (∇) indicate sample fixation time points of sample groups FS, FC, and GS, respectively.

of FMs. This yielded a final RNA*later* concentration of about 90% (v/v) after mixing. Temperature in CCs was kept at a nominal range of 22 to 24°C before, during, and after fixation (Figure 6). After 17 days in space, the spacecraft was separated from Tjangong-1 and touched ground on November 17, 2011. After landing and recovery of the capsule, samples were retrieved within 6 hours. The ECs were disassembled and stored around 4°C until they arrived in Tübingen on November 25, 2011. In the home laboratory, calli were harvested and stored at −80°C until processing.

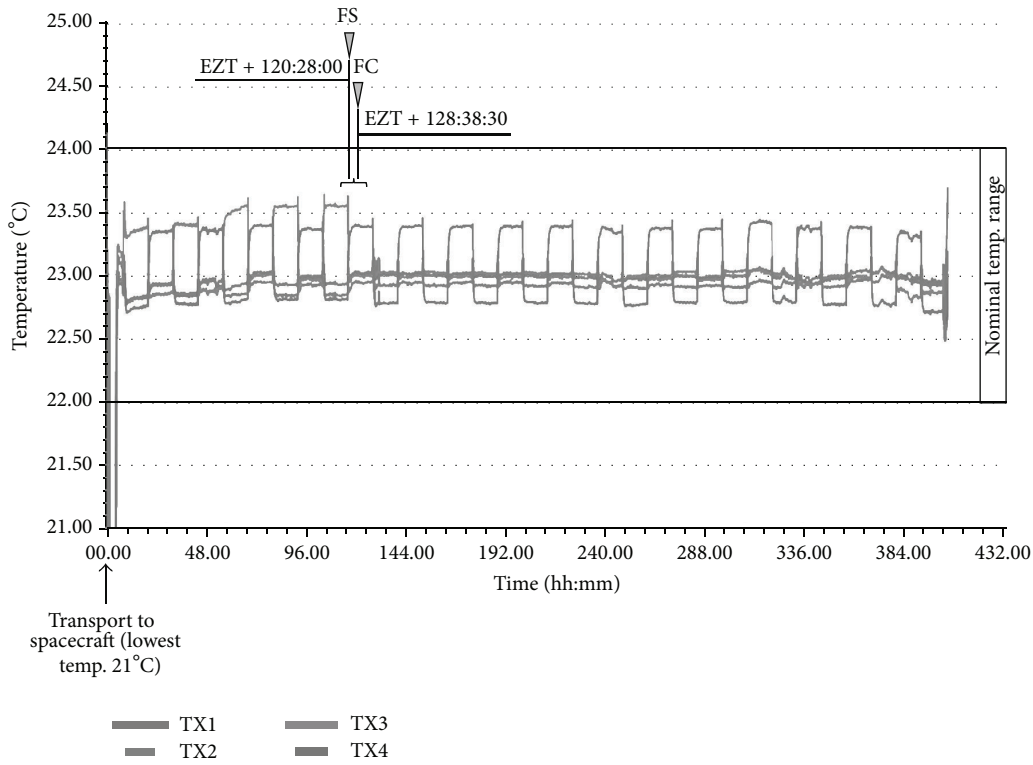

Figure 6: Temperature profile as recorded by 4 temperature sensors (TX1-4) attached to the Simbox incubator during the whole Simbox mission (data: Astrium). Sample fixation time points for the spaceflight samples (FS and FC) are indicated by arrowheads (grey triangle).

2.5. Ground Control. Immediately after the launch, the laboratory equipment and cell cultures were brought back to the PITC by Chinese scientists. The ground experiment started with a one-day delay on November 2, 2011 (Figure 5). The EUE was integrated into the Simbox duplicate, according to the position in the flight incubator (experiment/static platform), and kept at 23°C. As in the experiment in orbit, samples were metabolically quenched after 5 days (November 7). The ground experiment ended on November 19. The samples were handled as described for the experiment in orbit.

2.6. Experiment Conditions and Specification of Generated Samples. During the Simbox mission, the samples were exposed to different experimental conditions. In the experiment in orbit, FM 16002 was attached to the static platform of the Simbox incubator and experienced 5 days of microgravity (group FS, Flight Static). FM 16001 was centrifuged, resulting in a 1 g control (group FC, in-flight centrifugation). In the ground experiment, the same experimental design was used. FM 16003 was fixed to the static platform (group GS, ground static). In summary, we obtained one biological sample per CC, resulting in two replicates for each FM (front and rear CC) and for each experimental condition, respectively.

2.7. Isolation of Total RNA and High-Density Oligonucleotide Arrays. Total RNA was extracted using the RNeasy Plus kit (Qiagen, Hilden, Germany) according to the manufacturer's instructions. Quantity and quality controls were performed and samples were processed using the MessageAmp II-Biotin Enhanced, Single Round aRNA Amplification Kit (Ambion, Life Technologies, Darmstadt, Germany) as described earlier [21, 37]. Fragmented, biotin-labeled aRNA was then submitted to a high throughput microarray analysis (GeneChip Arabidopsis ATH1 Genome Array, Ref: 510690, LOT: 4155830, Affymetrix, Santa Clara, California, USA). Hybridization was performed according to the manufacturer's instructions (for details, see http://www.affymetrix.com/support/technical/manuals.affx). The Affymetrix protocol EukGE-WS2_V4 was used for washing and staining procedures.

2.8. Gene Expression Analysis. Expression data were calculated from raw values of the detected signal intensity of hybridization events of all spotted probe sets and saved as .CEL data files. Microarray data are available in the ArrayExpress database (http://www.ebi.ac.uk/arrayexpress, [38]) under accession number E-MTAB-2518. For integrative data analysis, we used the open-source software Mayday [39]. Normalization was performed using the robust multi-array average method of background-adjustment, quantile-normalization, and median-polish to ensure comparability of arrays and estimate $\log_2$ expression values [40–42]. Hierarchical clustering was performed by means of the neighbour joining method [43] in order to reconstruct and visualize relationships within expression values due to experiment conditions. The Pearson Correlation coefficient was used to

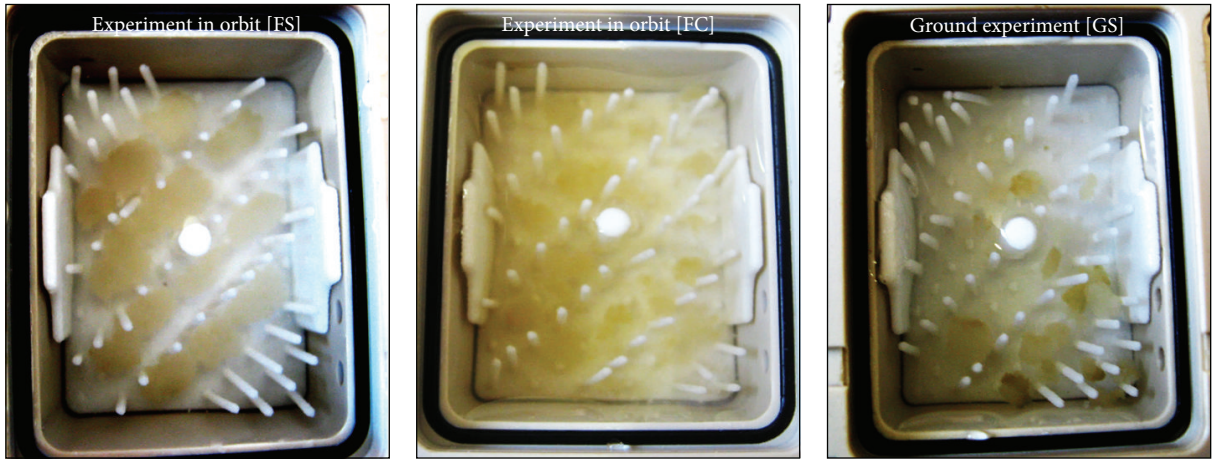

Figure 7: Photograph of *Arabidopsis thaliana* semisolidcallus cultures after a 5-day μg cultivation in orbit ((a), FS), 1 g in-flight cultivation ((b), FC) or on ground ((c), GS). The photographs were taken after fixation by RNA*later* and recovery of the spacecraft.

calculate the distance between each experimental condition (FS, FC, and GS) and biological replicates (front and rear CC). The matrix of variant genes was filtered and subjected to a Student's t-test ($P \leq 0.1$) with combined false discovery rate (FDR) correction to identify significantly altered transcripts ($P < 0.1$) between the sample groups FS and FC, FS, and GS, and FC and GS, respectively. Differentially expressed genes were determined by fold change (fc) calculation of $\log_2$ transformed expression data. Thereby, the threshold was set at $-1 \geq \log_2$ (fold change) ≥ 1 for at least 2-fold altered transcripts [40, 41, 44]. Additionally, the Affymetrix probe identifiers were tested by Gene Set Enrichment Analysis (GSEA, [45]) for enrichment of functional ontologies using Gene Ontology terms [46] within Mayday. Thereby, we focused on genes that share their function in identical biological processes for interpreting the genome-wide expression profiles.

3. Results

The aim of this experiment was to characterize the transcriptome of *Arabidopsis* semisolid callus cultures after 5 days in space. Due to the availability of an in-flight centrifuge, it was possible to compare expression data with (a) real microgravity samples (thought to yield the microgravity related alterations) and with (b) those from the ground controls (which should deliver effects of nonmicrogravity related spaceflight conditions). This was achieved with high-density oligonucleotide arrays.

3.1. Performance of Hardware and Biological Material. The hardware was thoroughly tested in order to retain viability of the callus cultures for as long as possible. These tests were focused on the biocompatibility of the used materials, gas-exchange properties of membranes, and viability of the cell cultures under the cultivation conditions within the EC. We also recorded the oxygen content within the CC [37]. As this declined from 8 to about 2 mg/L after 5 days, automated sample fixation was set at day 5 after take-off. Mission parameters, such as temperature, were within nominal range during the mission. Radiation measurements recorded increased values. After landing and return of the biological material to the University of Tübingen (Germany), the samples were visually checked. The fixed calli showed good morphology and had well grown during the initial culture of 5 days in space. The calli from the 1 g controls (flight and ground experiment) were smaller compared to those exposed to microgravity (Figure 7).

3.2. Biology of Samples and Gene Expression Analysis. The quality of the extracted total ribonucleic acid was satisfying for GeneChip hybridization (for RNA quality, see Supplementary Material S2) with clear bands representing the 28S and 18S rRNA. Whole-genome microarray screening was performed for each sample. Due to the limited amount of total RNA, the confirmation of expression data by quantitative real-time PCR was not possible. The data analysis revealed experiment-specific properties of biological replicates which were visualized by hierarchical clustering on the basis of the calculation of the Pearson Correlation coefficient (Figure 8). In this graph, a relatively short distance implies a high correlation between the samples. As obvious from Figure 8, the flight and ground experiment showed group-based clustering. The short distance between FS and FC (FS and FC boxes) in contrast to GS (GS boxes) indicates that nonmicrogravity related spaceflight conditions have major impact. The transcriptome of the biological replicates within the experiment groups (front and rear chamber of FS, FC, GS; $n = 2$) showed a high degree of similarity (Figure 8). This fact was confirmed by heat map generation based on calculated correlations (Figure 9). The Pearson Correlation was about 0.99 between front and rear CC for all three modules

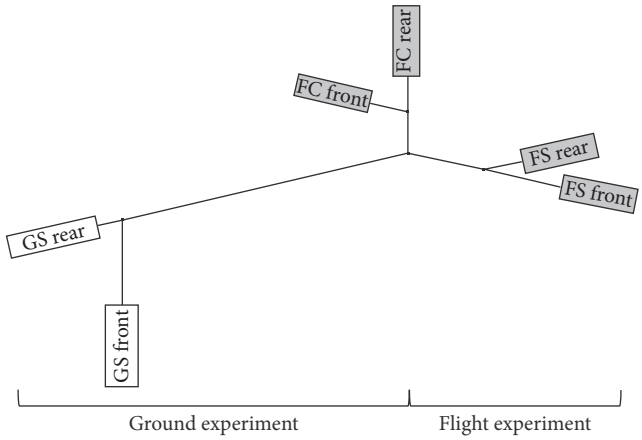

Figure 8: Hierarchical clustering by means of the neighbour joining method of generated sample groups (white: ground experiment; GS: ground static; grey: flight experiment; FS: flight space; FC: in-flight centrifugation). Each EUE consisted of two culture chambers (front and rear chambers, illustrated by boxes).

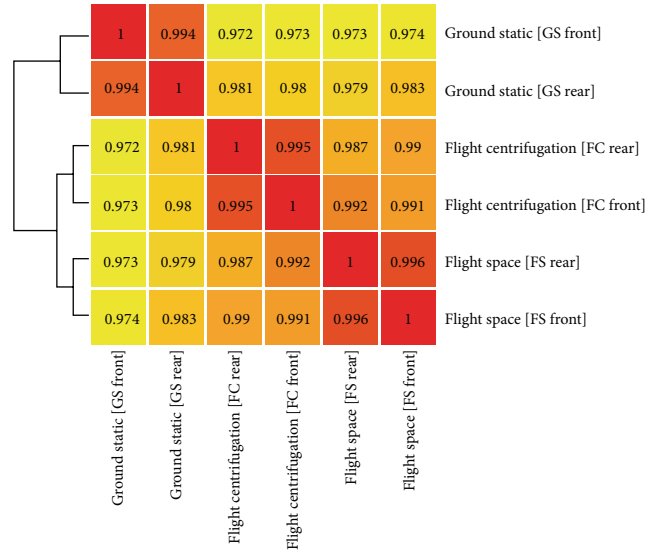

Figure 9: Pearson correlation heat map shows high degree of similarity between front and rear culture chamber of each sample within each sample group. Flight space (FS), in-flight centrifugation (FC), and ground static (GS).

(FS, FC, and GS, $n = 2$, Figure 9). Statistical (Student's t-test, $P < 0.1$, and FDR correction) and comparative analysis showed a relatively low response of semisolid callus cultures (Figure 10). Interestingly, microgravity conditions did not induce statistically significant changes ($P < 0.1$) at the gene expression level, although 298 genes were at least 2-fold differentially expressed (275 up- and 23 downregulated) within flight space (FS) samples. In contrast, nonmicrogravity related spaceflight conditions interfered with gene expression, considerably. Eight hundred ninety-seven genes were significantly and differentially expressed (at least 2-fold, $P < 0.1$) when 1 g ground and μg exposed flight samples were compared. Among them, 463 were upregulated and 434 genes were downregulated within FS (Figure 10). Comparison between both 1 g controls (in-flight, ground) resulted in 826 significantly ($P < 0.1$) differentially altered genes (543 up and 283 downregulated, Figure 10). Thereby, 573 significant DEGs ($P < 0.1$) were identical in both comparisons (Figure 10).

3.3. Identification of Altered Genes after Long-Term Microgravity. For detection of gene expression changes due to μg exposure, we compared data generated out of the sample groups flight space (FS) and in-flight centrifugation (FC). Two hundred seventy-five genes were at least 2-fold differentially upregulated and 23 downregulated (Figure 10). The application of statistics showed that there were no significant ($P < 0.1$) alterations at the expression level after 5 days in space. By means of a Gene Ontology [46] based Gene Set Enrichment Analysis (GSEA), the DEGs were related to common biological processes. In order to identify processes which are specifically influenced by microgravity conditions, we compared overrepresented processes that were identical between sample group FS versus FC and FS compared to GS (Table 1). Most prominent were effects on the translation machinery (Table 1, gene set number 24). Interestingly, all genes that were differentially upregulated and involved in translation processes were chloroplast-encoded. This gene set comprises genes coding for several protein subunits and components of ribosomes (e.g., ATCG00065, ATCG00660, ATCG00770, and ATCG00790) but also the nucleus-encoded translation initiation factor EIF-5A (AT1G13950) that is well known to regulate translation initiation and termination within the cytoplasma of eukaryotes (Table 2). The other part of identified differentially upregulated genes is involved in electron transport chains located within mitochondria (Table 1, gene sets number 4, 8 and 11) such as subunits of the NADH dehydrogenase multi-enzyme complex of the respiratory chain (ATMG00650, ATMG00070, ATMG00580) (Table 2). Mitochondrial electron transport is connected to the production of adenosine triphosphate (ATP). Thus, the gene set representative for ATP biosynthesis was also part of the DEGs (ATCG00120, ATMG00410, ATCG00480, and ATCG00150) (Table 2). Within the 23 downregulated genes (at least 2-fold), no special gene sets could be found, but the largest group codes for heat shock proteins (AT4G27670, AT2G29500, AT5G12020, AT5G59720, AT4G25200, AT1G53540, and AT5G12030).

3.4. Attempt to Distinguish between Effects of Microgravity and Nonmicrogravity Related Spaceflight Conditions on Gene Expression. One aim of this investigation was to separate responses to microgravity from those of nonmicrogravity related spaceflight conditions. Until today, only marginal data exist about these effects on plants in space. Thus, we screened for genes that were significantly ($P < 0.1$) altered within spaceflight samples (FS and FC) compared to the 1 g ground control and were identical between FS and FC compared to GS. This overlap yielded 573 significantly altered ($P < 0.1$) DEGs (Figure 10). The GSEA of these genes represented diverse biological processes (Table 1, bold font). The majority

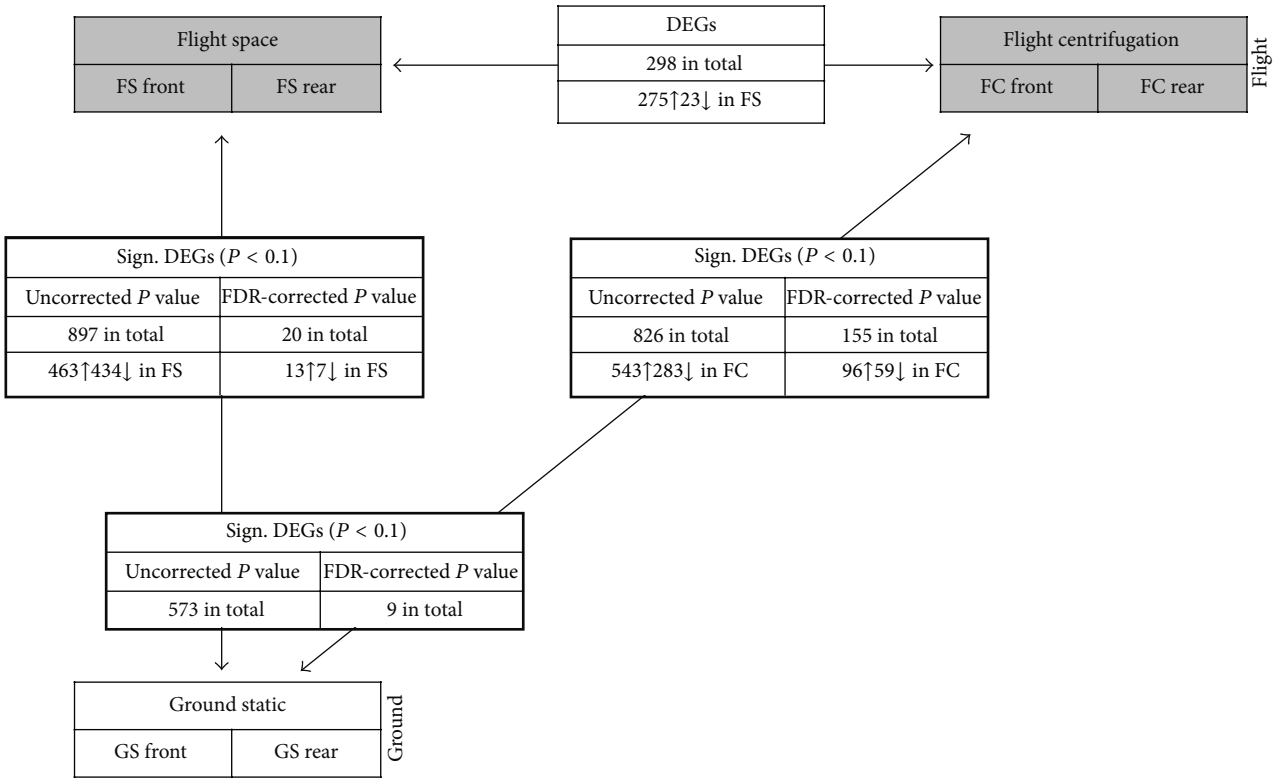

Figure 10: Overview of the number of differentially (fold change (fc) at least 2) and significantly expressed genes (DEGs, $P < 0.1$) within the flight (grey) and ground (white) experiment. The different sample groups are illustrated by boxes. Up- and downregulated transcripts are symbolized by arrows behind the number of altered genes. Genes that are significantly ($P < 0.1$) differentially expressed are shown in boxes framed in black (bold lines).

of these genes could be related to intracellular signaling pathways such as mitogen-activated protein kinase (MAPK) cascades and protein phosphorylation (Table 1, gene set number 6 and 12). Included were different MAP kinases (e.g., AT1G01560, AT1G73500), serine/threonine/tyrosine kinases (e.g., AT1G20650, AT5G16900, and AT4G38470), and many other kinases (Table 3). Furthermore, we identified genes coding for members of the calcium-binding EF-hand protein family (AT3G01830, AT3G47480) and the WRKY transcription factors 54, 70, and 38 (AT2G40750, AT3G56400, and AT5G22570) that have also transcription regulation activity (Table 3). Additionally, the spaceflight environment other than microgravity had a significant ($P < 0.1$) impact on general stress-responsive (gene set number 20) and defense-related genes (3), especially those involved in the response to oxidative stress and respiratory burst responses (21). These are peroxidases 21, 4, 52, and 25 (AT2G37130, AT1G14540, AT5G05340, and AT2G41480), catalase 3 (AT1G20620), and receptor-like kinases (AT5G46330, AT2G19190). The latter can be induced upon contact with the bacterial protein flagellin which is an important elicitor of the plant defense response. These kinases are also important members of the MAP kinase signaling cascade. Furthermore, general metabolic processes (gene set number 7), protein targeting (13), and rRNA processing (21) were overrep-resented due to nonmicrogravity related conditions in space.

4. Discussion

The expression data of *Arabidopsis* semisolid callus cultures show alterations in differential gene expression in response to microgravity. However, the influence of the spaceflight environment, in addition to microgravity, is significant.

4.1. Identification of Altered Genes after 5 Days of Microgravity. Comparison between microgravity and 1 g space controls revealed about 298 differentially (but not significantly) expressed genes. This number is low in comparison to short-term exposures to microgravity within a range of minutes (TEXUS 47, sounding rocket experiment, [47]) or seconds (14. DLR parabolic flight campaign, [21]). This finding could be due to the small number of biological replicates (2 biological replicates only due to limited material and hardware). However, similar observations are also reported by others. After 4 days in space, *Arabidopsis* plants exhibited only 27 transcripts which were at least 2-fold altered at their expression level [2]. This might indicate that plants respond immediately to a microgravity environment but then adapt to the new situation on the longer run. Also Zhang et al. [32] could also identify only 45 proteins changed in expression after 14 days in space (same mission). Genes with prolonged changes in expression could, however, provide important information about the physiological needs

Table 1: Visualization of enriched Gene Ontology categorization terms (GSEA, Gene Set Enrichment Analysis of biological processes). Gene sets identical in FS/FC and FS/GS are not colored; the ones identical in FS/GS, FC/GS and the overlap of both are in bold font (FS = flight space; FC = flight centrifugation, and GS = ground static).

Number	Enriched gene set (biological process)	FS/FC	FS/GS	FC/GS	Overlap
		Gene set size			
1	**ATP catabolic process**	0	**8**	**8**	**7**
2	ATP biosynthetic process	10	9	0	0
3	**Defense response**	0	**20**	**26**	**14**
4	Mitochondrial electron transport chain	7	7	0	0
5	**Lipid metabolic process**	0	**8**	**7**	**6**
6	**MAPK cascade**	0	**29**	**36**	**27**
7	**Metabolic process**	0	**25**	**20**	**16**
8	Mitochondrial electron transport	11	11	0	0
9	**Oxidation-reduction process**	0	**13**	**12**	**8**
10	**Photosynthesis, light harvesting**	0	**5**	**5**	**5**
11	Photosynthetic electron transport chain	5	5	0	0
12	**Protein phosphorylation**	0	**23**	**31**	**18**
13	**Protein targeting to membrane**	0	**12**	**13**	**10**
14	**Regulation of transcription, DNA-dependent**	0	**12**	**11**	**8**
15	**Respiratory burst involved in defense response**	0	**22**	**26**	**21**
16	**Response to chitin**	0	**7**	**6**	**6**
17	**Response to ethylene stimulus**	0	**5**	**6**	**5**
18	**Response to hypoxia**	0	**6**	**9**	**6**
19	**Response to oxidative stress**	0	**15**	**13**	**9**
20	**Response to stress**	0	**9**	**9**	**6**
21	**rRNA processing**	0	**16**	**15**	**14**
22	**Toxin catabolic process**	0	**7**	**7**	**6**
23	**Transition metal ion transport**	0	**10**	**12**	**8**
24	Translation	27	28	0	0
25	**Two-component signal transduction system**	0	**6**	**5**	**5**

after a few days in space. These include an upregulated group of genes which code for proteins that constitute the ribosomal complex within plastids. These are necessary for translation of mRNA. The upregulation of the mitochondrial electron transport chain could indicate an increased need for ATP. The upregulated expression of NADH dehydrogenase could have the same reason. Interestingly, gene products involved in processes like the response to stress, protein degradation, or programmed cell death appeared not to be altered in expression. The involvement of a series of genes with still unknown functions (not shown) suggests that the space environment induces also unknown cellular processes. Together with the fact that there were no significant changes in gene expression detectable after 5 days of microgravity, lets us suggest that at this stage the impact of a lack of gravitation on cell physiology was not too heavy. The space environment per se, however, causes possibly an increased energy demand, as shown by the upregulation of respiratory components. This aspect should be taken into consideration when plants will be used to provide nutrients, oxygen, and energy on long duration space missions.

Heat shock proteins (HSPs) dominate the group of transcripts which are reduced in amount (not shown). These proteins are involved in many forms of stress response. They enable the folding and membrane translocation of proteins and are thought to reconstitute the tertiary structure of proteins affected by stress events. This way they can increase the stress tolerance. A decreased expression (our study) should thus indicate a lower number of proteins affected in their structure and was also reported for *Arabidopsis in vitro* callus cultures under simulated microgravity conditions (magnetic levitation, magnetic field strength 10.1 Tesla) [48] as well as for the single-cell system of the fern *Ceratopteris richardii* [9]. There are, however, also reports on increased expression of HSPs [15, 16, 21, 24].

A group of plant genes which are always affected by altered gravity are those involved in cell wall modification [2, 49–51]. This reflects the need for increased stability

Table 2: Differentially expressed genes (fold change (fc) at least 2) within the sample group flight space (FS, front/rear CC) compared to in-flight centrifugation (FC). Samples taken after 5-day cultivation at microgravity and sorted according to the overrepresented biological processes identified by GSEA to be the most prominent.

Number	ATG number	Gene name/description	log (fc)	Enriched Gene set (biological process)
1	ATCG00065	Ribosomal protein S12	2.36	Translation
2	ATCG00660	Ribosomal protein L20	2.14	Translation
3	ATCG00770	30S ribosomal protein S8	1.96	Translation
4	ATCG00160	Ribosomal protein S2	1.84	Translation
5	ATCG00790	Ribosomal protein L16	1.8	Translation
6	ATCG00780	Ribosomal protein L14	1.63	Translation
7	AT1G13950	Eukaryotic translation initiation factor 5A-1	1.14	Translation
8	ATCG01120	Ribosomal protein S15	1.11	Translation
9	ATCG00750	Ribosomal protein S11	1.05	Translation
10	ATCG00800	Ribosomal protein S3	1.04	Translation
11	ATMG00650	NADH dehydrogenase subunit 4L	2.3	Mitochondrial electron transport
12	ATMG00060	NADH dehydrogenase subunit 5	1.84	Mitochondrial electron transport
13	AT2G07751	NADH-ubiquinone/plastochinone oxidoreductase	1.75	Mitochondrial electron transport
14	ATCG01050	Subunit of NAD(P)H dehydrogenase complex	1.74	Mitochondrial electron transport
15	ATMG00160	Cytochrome c oxidase subunit 2	1.66	Mitochondrial electron transport
16	ATMG00070	NADH dehydrogenase subunit 9	1.5	Mitochondrial electron transport
17	ATCG00420	NADH dehydrogenase subunit J	1.43	Mitochondrial electron transport
18	ATCG01250	NADH dehydrogenase ND2	1.25	Mitochondrial electron transport
19	ATMG00510	NADH dehydrogenase subunit 7	1.24	Mitochondrial electron transport
20	ATMG00270	NADH dehydrogenase subunit 6	1.24	Mitochondrial electron transport
21	ATMG00580	NADH dehydrogenase subunit 4	1.19	Mitochondrial electron transport
22	ATCG01070	NADH dehydrogenase ND4L	1.13	Mitochondrial electron transport
23	ATCG00120	ATPase α-subunit	2.15	ATP biosynthesis
24	ATCG00140	ATPase III subunit	1.59	ATP biosynthesis
25	ATMG00410	ATPase subunit 6	1.56	ATP biosynthesis
26	ATCG00130	ATPase F subunit	1.47	ATP biosynthesis
27	ATCG00480	β-Subunit of ATP synthase	1.33	ATP biosynthesis
28	ATCG00150	Subunit of ATPase complex CF0	1.12	ATP biosynthesis

(hypergravity) or more flexibility (microgravity). In the present study, expression of expansins (cell wall loosening) is increased (not shown). This might be the reason for the enhanced size of the microgravity cultures when compared to the 1 g controls (Figure 7).

4.2. Impact of the Nonmicrogravity Related Spaceflight Conditions on Gene Expression. The availability of a 1 g reference centrifuge enabled us to screen for genes affected by nonmicrogravity related spaceflight conditions in that we compared expression data between μg exposed and 1 g space with 1 g ground samples. This resulted in a considerable number of identical genes altered in mRNA abundance (573 genes) (Figure 10). We thus assume that this could be due to effects of spaceflight-related environmental conditions, including space radiation. Radiation measurements inside the capsule in a position close to our samples yielded a total dose of 5.9 to 8.1 mSV (milliSieverts) and an equivalent dose of 0.37 to 0.51 mSV/d (data: Chinese authorities). This is considerably more compared to terrestrial conditions (1 to 2 mSV/a) and could be one of the reasons for the alterations at transcript levels, obviously not related to μg. Also Zhang et al. [32] reported a greater difference on protein expression of non-μg conditions. Analysis showed that both experimental conditions (μg and non-μg spaceflight conditions) affect different biological processes (Table 1). Overrepresented processes should not be regarded separately, as they are closely linked together within a plant cell. For example, the formation of reactive oxygen species (ROS) is one of the initial responses upon most kinds of stresses. They are also produced as by-products of redox reactions. They are important second messengers, as well as toxic species, and their cellular levels are closely controlled by detoxification systems [52–54]. The role of ROS in response to environmental changes can, however, also be deduced from alterations in gene products, involved in ROS production and turnover. In this study, we observed that many ROS-related genes are significantly regulated (Table 3). These comprise peroxidases, catalase, and a glutathione S-transferase (Table 3). These proteins are suggested to be part of the stress-induced antioxidant system [55]. Glutathione S-transferases also possess peroxidase

Table 3: Differentially (at least 2-fold) and significantly expressed genes ($P < 0.1$, 573 in total) that are identical between flight space (FS) as well as in-flight centrifugation (FC) compared to ground static (GS). Changes are due to nonmicrogravity related spaceflight conditions. The genes are sorted according to the overrepresented biological processes identified by GSEA to be most prominent.

No	ATG number	Gene name/description	log (fc) (P value) FS versus GS	log (fc) (P value) FC versus GS	Biological process
1	AT1G01560	MAP kinase 11	1.83 (0.034)	2.13 (0.027)	MAPK cascade
2	AT1G73500	MAP kinase 9	1.34 (0.006)	1.37 (0.038)	MAPK cascade
3	AT3G01830	Calcium-binding EF-hand family protein	1.3 (0.032)	1.85 (0.027)	MAPK cascade
4	AT3G47480	Calcium-binding EF-hand family protein	1.24 (0.081)	1.87 (0.037)	MAPK cascade
5	AT2G40750	WRKY DNA-binding transcription factor 54	1.29 (0.008)	1.74 (0.006)	MAPK cascade
6	AT3G56400	WRKY DNA-binding transcription factor 70	1.85 (0.008)	2.19 (0.004)	MAPK cascade
7	AT5G22570	WRKY DNA-binding transcription factor 38	2.52 (0.006)	3.28 (0.004)	MAPK cascade
8	AT3G15500	NAC-domain containing transcription factor 3	2.98 ($5.72E-4$)	2.63 (0.003)	MAPK cascade
9	AT1G35670	Calcium-dependent calmodulin-independent protein kinase 2	1.2 (0.002)	1.23 (0.003)	Protein phosphorylation
10	AT1G20650	Serine/threonine protein kinase superfamily protein	−1.4 (0.024)	−1.5 (0.018)	Protein phosphorylation
11	AT3G61160	Serine/threonine protein kinase family protein	−1.22 (0.007)	−1.4 (0.008)	Protein phosphorylation
12	AT1G78290	Serine/threonine protein kinase family protein 2C	1.71 (0.019)	2.0 (0.034)	Protein phosphorylation
13	AT4G18640	Serine/threonine protein kinase family protein	1.08 (0.019)	1.07 (0.014)	Protein phosphorylation
14	AT4G18950	Serine/threonine/tyrosine protein kinase family protein	2.53 (0.031)	3.17 (0.02)	Protein phosphorylation
15	AT5G16900	Leucine-rich repeat protein kinase family protein	1.42 (0.023)	2.0 (0.012)	Protein phosphorylation
16	AT1G51890	Leucine-rich repeat protein kinase family protein	2.55 (0.05)	2.64 (0.047)	Protein phosphorylation
17	AT4G11480	Cysteine-rich receptor-like protein kinase family protein	1.56 (0.05)	1.89 (0.033)	Protein phosphorylation
18	AT4G23260	Cysteine-rich receptor-like protein kinase family protein	1.65 (0.068)	2.49 (0.041)	Protein phosphorylation
19	AT4G38470	Tyrosine kinase family protein 46	1.14 (0.008)	1.34 (0.015)	Protein phosphorylation
20	AT1G69790	Protein kinase superfamily protein	1.19 (0.038)	1.12 (0.009)	Protein phosphorylation
21	AT5G53450	Protein kinase	1.88 (0.088)	1.89 (0.075)	Protein phosphorylation
22	AT1G51620	Protein kinase family protein	1.8 (0.052)	2.31 (0.048)	Protein phosphorylation
23	AT3G04530	Phosphoenolpyruvate carboxylase kinase 2	−1.6 (0.06)	−1.19 (0.43)	Protein phosphorylation
24	AT5G63650	Protein kinase 2.5	−1.26 (0.028)	−1.01 (0.032)	Protein phosphorylation
25	AT1G16260	Cell-wall associated protein kinase family protein	1.73 (0.006)	2.13 (0.003)	Protein phosphorylation
26	AT1G68690	Proline-rich extension-like receptor kinase family protein	1.04 (0.002)	1.03 (0.04)	Protein phosphorylation

Table 3: Continued.

No	ATG number	Gene name/description	log (fc) (*P* value) FS versus GS	log (fc) (*P* value) FC versus GS	Biological process
27	AT5G46330	Flagellin 2-induced receptor-like kinase	−1.85 (0.043)	−2.38 (0.016)	Defense response
28	AT2G19190	Flagellin 22-induced receptor-like kinase	2.48 (0.065)	2.27 (0.075)	Defense response
29	AT2G15120	Disease-resistance family protein	2.68 (0.035)	2.53 (0.04)	Defense response
30	AT1G59780	Disease resistance protein	1.37 (0.092)	1.98 (0.052)	Defense response
31	AT1G63880	Disease resistance protein	−1.81 (0.003)	−1.79 (0.016)	Defense response
32	AT2G39200	Transmembrane domain-containing protein, similar to mildew resistance protein 12	2.6 (0.059)	2.55 (0.063)	Defense response
33	AT1G19610	Pathogenesis-related protein 1.4	−2.17 (0.002)	−2.14 (0.029)	Defense response
34	AT3G20600	Nonrace specific disease resistance protein	1.05 (0.037)	2.12 (0.011)	Defense response
35	AT1G02360	Chitinase family protein	2.6 (0.026)	2.87 (0.019)	Defense response
36	AT3G54420	Chitinase family protein class IV	1.73 (0.055)	2.53 (0.026)	Defense response
37	AT4G21390	Serine/threonine protein kinase family protein	1.5 (0.068)	1.86 (0.031)	Defense response
38	AT3G46280	Protein kinase family protein	1.83 (0.074)	2.3 (0.048)	Defense response
39	AT5G35750	Histidine kinase 2	−1.21 (0.042)	−1.35 (0.026)	Defense response
40	AT2G37130	Peroxidase 21	−3.06 (0.014)	−3.4 (0.008)	Response to oxidative stress
41	AT1G14540	Peroxidase 4	3.35 (0.018)	3.28 (0.02)	Response to oxidative stress
42	AT5G05340	Peroxidase 52	2.15 (0.014)	2.06 (0.019)	Response to oxidative stress
43	AT4G37530	Peroxidase family protein	2.17 (0.035)	2.15 (0.026)	Response to oxidative stress
44	AT2G41480	Peroxidase 25	−1.04 (0.011)	−1.06 (0.034)	Response to oxidative stress
45	AT1G20620	Catalase 3	−1.12 (0.07)	−1.39 (0.052)	Response to oxidative stress
46	AT2G29490	Glutathione S-transferase 19 class tau 1	1.75 (0.07)	1.7 (0.073)	Response to oxidative stress
47	AT3G22370	Oxidase family protein	1.3 (0.013)	1.0 (0.089)	Response to oxidative stress
48	AT4G37220	Stress-responsive protein	2.87 (0.004)	1.87 (0.049)	Response to stress
49	AT4G21870	Heat shock protein 26.5	−1.31 (0.002)	−1.43 (0.012)	Response to stress
50	AT2G38750	Calcium-dependent phospholipid binding protein	1.48 (0.02)	1.15 (0.032)	Response to stress

activity and can thus prevent cell damage by peroxides, such as hydrogen peroxide [56, 57]. The increase in detoxification-related transcripts appears reasonable, as radiation in orbit consists of highly energetic (HZE) particles from interplanetary galactic sources or results from solar particle events, which could have an impact on cells [58–62]. Wan et al. [63, 64] showed that X-rays, γ-rays, protons, and heavy charged particles increased oxidative stress in different cell types, and countermeasures for space radiation effects are the use of antioxidants [62]. Similar responses are probable for plant cells. Therefore, the impact of long-term space radiation on the transcriptome of *Arabidopsis* should be investigated in ground-based studies in simulation testbeds for the space environments [59].

In addition, a range of WRKY transcription factors and components of signaling chains (Ca^{2+}-dependent proteins, MAP kinases) were identified (Table 3). These responsive kinases (Table 3) are potentially also modulated by cytosolic fluctuations of H_2O_2 and can thus be part of signal transduction chains starting from hydrogen peroxide (for defense-related genes in tomato, see Orozco-Cárdenas et al. [65]). In contrast to other observations to altered gravitation [2, 15],

in this study, genes which are defense-, resistance-, and pathogen-related are significantly altered due to non-μg related spaceflight conditions.

5. Conclusions

In this study, gene expression changes within *Arabidopsis* wild type semisolid callus cultures were investigated after a 5-day spaceflight and compared to on-board and ground controls. Faced with limited HW capacities (only 3 EUEs) and small amounts of biological material ($n = 2$ for each sample group), high-density oligonucleotide arrays were used to screen for changes at the gene expression level. For future investigations, it would thus be desirable to have flight repetitions and an adequate amount of samples for additional analysis (e.g., qPCR). Unexpectedly, the response of callus cultures to long-term microgravity was less prominent compared to nonmicrogravity related spaceflight conditions. The latter, including space radiation, induced differential and significant expression changes of transcripts that are involved in the stress-induced antioxidant system, signalling chains, and defense-/resistance-related genes. These findings clearly highlight that the use of an in-flight reference centrifuge (1 g in-flight control) should be mandatory during space flight missions.

Conflict of Interests

The authors declare that there is no conflict of interests regarding the publication of this paper.

Acknowledgments

This work was supported by a grant of the Deutsches Zentrum für Luft- und Raumfahrt (DLR) (Grant no. 50WB0723) to Rüdiger Hampp. The authors are indebted to Dr. Markus Braun (DLR) for perfect campaign organization and to Achim Schwarzwälder, Dr. Astrid Horn, and the EADS Astrium team for hardware construction and technical support. They thank the China Manned Space Engineering and the Chinese scientists, especially Professor Zheng, for good cooperation at launch site. They are grateful to Margret Ecke for skilful production and maintenance of the cell cultures and Fabian Bergwitz for assistance in China, as well as Anne Hennig for ground-based experiments before the mission.

References

[1] G. Perbal and D. Driss-Ecole, "Mechanotransduction in gravisensing cells," *Trends in Plant Science*, vol. 8, no. 10, pp. 498–504, 2003.

[2] M. J. Correll, T. P. Pyle, K. D. L. Millar et al., "Transcriptome analyses of *Arabidopsis thaliana* seedlings grown in space: implications for gravity-responsive genes," *Planta*, vol. 238, no. 3, pp. 519–533, 2013.

[3] M. Braun, "Gravitropism in tip-growing cells," *Planta*, vol. 203, no. 1, pp. S11–S19, 1997.

[4] M. Braun, B. Buchen, and A. Sievers, "Electron microscopic analysis of gravisensing Chara rhizoids developed under microgravity conditions," *The FASEB Journal*, vol. 13, no. 8, pp. S113–S120, 1999.

[5] M. Braun, "Gravity perception requires statoliths settled on specific plasma membrane areas in characean rhizoids and protonemata," *Protoplasma*, vol. 219, no. 3-4, pp. 150–159, 2002.

[6] M. Braun, J. Hauslage, A. Czogalla, and C. Limbach, "Tip-localized actin polymerization and remodeling, reflected by the localization of ADF, profilin and villin, are fundamental for gravity-sensing and polar growth in characean rhizoids," *Planta*, vol. 219, no. 3, pp. 379–388, 2004.

[7] M. Braun and C. Limbach, "Rhizoids and protonemata of characean algae: model cells for research on polarized growth and plant gravity sensing," *Protoplasma*, vol. 229, no. 2–4, pp. 133–142, 2006.

[8] M. L. Salmi, T. J. Bushart, and S. J. Roux, "Autonomous gravity perception and responses of single plant cells," *Gravitational and Space Biology*, vol. 25, pp. 6–13, 2011.

[9] M. L. Salmi and S. J. Roux, "Gene expression changes induced by space flight in single-cells of the fern *Ceratopteris richardii*," *Planta*, vol. 229, no. 1, pp. 151–159, 2008.

[10] O. Rasmussen, D. A. Klimchuk, E. L. Kordyum et al., "The effect of exposure to microgravity on the development and structural organisation of plant protoplasts flown on Biokosmos 9," *Physiologia Plantarum*, vol. 84, no. 1, pp. 162–170, 1992.

[11] E. Hoffmann, K. Schönherr, and R. Hampp, "Regeneration of plant cell protoplasts under microgravity: investigation of protein patterns by SDS-PAGE and immunoblotting," *Plant Cell Reports*, vol. 15, no. 12, pp. 914–919, 1996.

[12] R. Hampp, E. Hoffmann, K. Schönherr, P. Johann, and L. De Filippis, "Fusion and metabolism of plant cells as affected by microgravity," *Planta*, vol. 203, pp. S42–S53, 1997.

[13] M. Martzivanou, M. Babbick, M. Cogoli-Greuter, and R. Hampp, "Microgravity-related changes in gene expression after short-term exposure of *Arabidopsis thaliana* cell cultures," *Protoplasma*, vol. 229, no. 2–4, pp. 155–162, 2006.

[14] M. Martzivanou and R. Hampp, "Hyper-gravity effects on the *Arabidopsis* transcriptome," *Physiologia Plantarum*, vol. 118, no. 2, pp. 221–231, 2003.

[15] A. L. Paul, A. K. Zupanska, D. T. Ostrow et al., "Spaceflight transcriptomes: Unique responses to a novel environment," *Astrobiology*, vol. 12, no. 1, pp. 40–56, 2012.

[16] A. K. Zupanska, F. C. Denison, R. J. Ferl, and A.-L. Paul, "Spaceflight engages heat shock protein and other molecular chaperone genes in tissue culture cells of *Arabidopsis Thaliana*," *The American Journal of Botany*, vol. 100, no. 1, pp. 235–248, 2013.

[17] R. Edgar, M. Domrachev, and A. E. Lash, "Gene Expression Omnibus: NCBI gene expression and hybridization array data repository," *Nucleic Acids Research*, vol. 30, no. 1, pp. 207–210, 2002.

[18] A. Brazma, H. Parkinson, U. Sarkans et al., "ArrayExpress—a public repository for microarray gene expression data at the EBI," *Nucleic Acids Research*, vol. 31, no. 1, pp. 68–71, 2003.

[19] J. Kilian, D. Whitehead, J. Horak et al., "The AtGenExpress global stress expression data set: protocols, evaluation and model data analysis of UV-B light, drought and cold stress responses," *Plant Journal*, vol. 50, no. 2, pp. 347–363, 2007.

[20] D. Swarbreck, C. Wilks, P. Lamesch et al., "The Arabidopsis Information Resource (TAIR): Gene structure and function

annotation," *Nucleic Acids Research*, vol. 36, no. 1, pp. D1009–D1014, 2008.

[21] N. Hausmann, S. Fengler, A. Hennig, M. Franz-Wachtel, R. Hampp, and M. Neef, "Cytosolic calcium, hydrogen peroxide and related gene expression and protein modulation in *Arabidopsis thaliana* cell cultures respond immediately to altered gravitation: parabolic flight data," *Plant Biology*, vol. 16, no. 1, pp. 120–128, 2014.

[22] J. Z. Kiss, W. J. Katembe, and R. E. Edelmann, "Gravitropism and development of wild-type and starch-deficient mutants of *Arabidopsis* during spaceflight," *Physiologia Plantarum*, vol. 102, no. 4, pp. 493–502, 1998.

[23] A. L. Paul, C. J. Daugherty, E. A. Bihn, D. K. Chapman, K. L. L. Norwood, and R. J. Ferl, "Transgene expression patterns indicate that spaceflight affects stress signal perception and transduction in Arabidopsis," *Plant Physiology*, vol. 126, no. 2, pp. 613–621, 2001.

[24] A.-L. Paul, M. P. Popp, W. B. Gurley, C. Guy, K. L. Norwood, and R. J. Ferl, "Arabidopsis gene expression patterns are altered during spaceflight," *Advances in Space Research*, vol. 36, no. 7, pp. 1175–1181, 2005.

[25] K. D. L. Millar, P. Kumar, M. J. Correll et al., "A novel phototropic response to red light is revealed in microgravity," *New Phytologist*, vol. 186, no. 3, pp. 648–656, 2010.

[26] J. Allen, P. A. Bisbee, R. L. Darnell et al., "Gravity control of growth form in *Brassica Rapa* and *Arabidopsis Thaliana* (Brassicaceae): consequences for secondary metabolism," *American Journal of Botany*, vol. 96, no. 3, pp. 652–660, 2009.

[27] M. E. Musgrave, A. Kuang, Y. Xiao et al., "Gravity independence of seed-to-seed cycling in *Brassica rapa*," *Planta*, vol. 210, no. 3, pp. 400–406, 2000.

[28] G. Perbal and D. Driss-Ecole, "Sensitivity to gravistimulus of lentil seedling roots grown in space during the IML 1 Mission of Spacelab," *Physiologia Plantarum*, vol. 90, no. 2, pp. 313–318, 1994.

[29] B. C. Tripathy, C. S. Brown, H. G. Levine, and A. D. Krikorian, "Growth and photosynthetic responses of wheat plants grown in space," *Plant Physiology*, vol. 110, no. 3, pp. 801–806, 1996.

[30] G. W. Stutte, O. Monje, R. D. Hatfield, A. L. Paul, R. J. Ferl, and C. G. Simone, "Microgravity effects on leaf morphology, cell structure, carbon metabolism and mRNA expression of dwarf wheat," *Planta*, vol. 224, no. 5, pp. 1038–1049, 2006.

[31] J. Ueda, K. Miyamoto, T. Yuda et al., "Growth and development, and auxin polar transport in higher plants under microgravity conditions in space: BRIC-AUX on STS-95 space experiment," *Journal of Plant Research*, vol. 112, no. 1108, pp. 487–492, 1999.

[32] Y. Zhang, L. Wang, J. Xie, and H. Zheng, "Differential protein expression profiling of *Arabidopsis thaliana* callus under microgravity on board the Chinese SZ-8 spacecraft," *Planta*. In press.

[33] M. Vukich, A. Donati, and V. Zolesi, "Kayser Italia hardware for radiation and microgravity experiments in space," *Rendiconti Lincei*, vol. 25, no. 1, pp. 7–11, 2014.

[34] E. Brinckmann, "Centrifuges and their application for biological experiments in space," *Microgravity Science and Technology*, vol. 24, no. 6, pp. 365–372, 2012.

[35] Astrium GmbH, *Astrium Space Transportation*, Astrium Space Biology Product Catalog, Friedrichshafen, Germany, 2012.

[36] H. Kleinig, "Pflanzliche Gewebekultur. Ein Praktikum," *Biologie in unserer Zeit*, vol. 16, no. 4, p. 128, 1986.

[37] S. Fengler, M. Neef, M. Ecke, and R. Hampp, "The Simbox experiment with *Arabidopsis thaliana* cell cultures: hardware tests and first results from the German-Chinese satellite mission Shenzhou 8," in *Proceedings of the Life in Space for Life on Earth Symposium*, vol. ESA SP-706, 2013.

[38] G. Rustici, N. Kolesnikov, M. Brandizi et al., "ArrayExpress update-trends in database growth and links to data analysis tools," *Nucleic Acids Research*, vol. 41, no. 1, pp. D987–D990, 2013.

[39] F. Battke, S. Symons, and K. Nieselt, "Mayday—integrative analytics for expression data," *BMC Bioinformatics*, vol. 11, article 121, 2010.

[40] R. A. Irizarry, B. M. Bolstad, F. Collin, L. M. Cope, B. Hobbs, and T. P. Speed, "Summaries of Affymetrix GeneChip probe level data," *Nucleic Acids Research*, vol. 31, no. 4, 2003.

[41] R. A. Irizarry, B. Hobbs, F. Collin et al., "Exploration, normalization, and summaries of high density oligonucleotide array probe level data," *Biostatistics*, vol. 4, no. 2, pp. 249–264, 2003.

[42] B. M. Bolstad, R. A. Irizarry, M. Åstrand, and T. P. Speed, "A comparison of normalization methods for high density oligonucleotide array data based on variance and bias," *Bioinformatics*, vol. 19, no. 2, pp. 185–193, 2003.

[43] M. Simonsen, T. Mailund, and C. N. Pedersen, "Rapid neighbour-joining," in *Algorithms in Bioinformatics*, vol. 5251 of *Lecture Notes in Computer Science*, pp. 113–122, Springer, Berlin, Germany, 2008.

[44] D. M. Mutch, A. Berger, R. Mansourian, A. Rytz, and M.-A. Roberts, "The limit fold change model: a practical approach for selecting differentially expressed genes from microarray data," *BMC Bioinformatics*, vol. 3, article 17, 2002.

[45] A. Subramanian, P. Tamayo, V. K. Mootha et al., "Gene set enrichment analysis: a knowledge-based approach for interpreting genome-wide expression profiles," *Proceedings of the National Academy of Sciences of the United States of America*, vol. 102, no. 43, pp. 15545–15550, 2005.

[46] M. Ashburner, C. A. Ball, J. A. Blake et al., "Gene ontology: tool for the unification of biology," *Nature Genetics*, vol. 25, no. 1, pp. 25–29, 2000.

[47] M. Babbick, Ž. Barjaktarović, and R. Hampp, "Alterations in the expression of transcription factors in *Arabidopsis thaliana* cell cultures during sounding rocket μG," in *Proceedings of the 18th ESA Symposium on European Rocket and Balloon Programmes*, pp. 473–477, June 2007.

[48] A. I. Manzano, J. J. W. A. van Loon, P. C. M. Christianen, J. M. Gonzalez-Rubio, F. J. Medina, and R. Herranz, "Gravitational and magnetic field variations synergize to cause subtle variations in the global transcriptional state of *Arabidopsis in vitro* callus cultures," *BMC Genomics*, vol. 13, no. 1, article 105, 2012.

[49] H. Wang, Q. Z. Hui, W. Sha, R. Zeng, and C. X. Qi, "A proteomic approach to analysing responses of *Arabidopsis thaliana* callus cells to clinostat rotation," *Journal of Experimental Botany*, vol. 57, no. 4, pp. 827–835, 2006.

[50] T. Hoson, K. Soga, R. Mori et al., "Stimulation of elongation growth and cell wall loosening in rice coleoptiles under microgravity conditions in space," *Plant and Cell Physiology*, vol. 43, no. 9, pp. 1067–1071, 2002.

[51] A. Nasir, S. M. Strauch, I. Becker et al., "The influence of microgravity on *Euglena gracilis* as studied on Shenzhou 8," *Plant Biology*, vol. 16, no. supplement 1, pp. 113–119, 2014.

[52] K. Apel and H. Hirt, "Reactive oxygen species: metabolism, oxidative stress, and signal transduction," *Annual Review of Plant Biology*, vol. 55, pp. 373–399, 2004.

[53] S. Davletova, K. Schlauch, J. Coutu, and R. Mittler, "The zinc-finger protein Zat12 plays a central role in reactive oxygen and abiotic stress signaling in Arabidopsis," *Plant Physiology*, vol. 139, no. 2, pp. 847–856, 2005.

[54] R. Mittler, "Abiotic stress, the field environment and stress combination," *Trends in Plant Science*, vol. 11, no. 1, pp. 15–19, 2006.

[55] P. G. Sappl, A. J. Carroll, R. Clifton et al., "The *Arabidopsis glutathione* transferase gene family displays complex stress regulation and co-silencing multiple genes results in altered metabolic sensitivity to oxidative stress," *The Plant Journal*, vol. 58, no. 1, pp. 53–68, 2009.

[56] V. P. Roxas, R. K. Smith Jr., E. R. Allen, and R. D. Allen, "Over-expression of glutathione S-transferase/glutathione peroxidase enhances the growth of transgenic tobacco seedlings during stress," *Nature Biotechnology*, vol. 15, no. 10, pp. 988–991, 1997.

[57] V. P. Roxas, S. A. Lodhi, D. K. Garrett, J. R. Mahan, and R. D. Allen, "Stress tolerance in transgenic tobacco seedlings that overexpress glutathione S-transferase/glutathione peroxidase," *Plant and Cell Physiology*, vol. 41, no. 11, pp. 1229–1234, 2000.

[58] G. Horneck, "Radiobiological experiments in space: a review," *Nuclear Tracks and Radiation Measurements*, vol. 20, no. 1, pp. 185–205, 1992.

[59] G. Horneck, "Astrobiology studies of microbes in simulated interplanetary space," in *Laboratory Astrophysics and Space Research*, pp. 667–685, 1999.

[60] C. Baumstark-Khan, C. E. Hellweg, A. Arenz, and M. M. Meier, "Cellular monitoring of the nuclear factor κB pathway for assessment of space environmental radiation," *Radiation Research*, vol. 164, no. 4, pp. 527–530, 2005.

[61] C. E. Hellweg and C. Baumstark-Khan, "Getting ready for the manned mission to Mars: the astronauts' risk from space radiation," *Naturwissenschaften*, vol. 94, no. 7, pp. 517–526, 2007.

[62] A. R. Kennedy, "Biological effects of space radiation and development of effective countermeasures," *Life Sciences in Space Research*, vol. 1, no. 1, pp. 10–43, 2014.

[63] X. S. Wan, Z. Zhou, and A. R. Kennedy, "Adaptation of the dichlorofluorescein assay for detection of radiation-induced oxidative stress in cultured cells," *Radiation Research*, vol. 160, no. 6, pp. 622–630, 2003.

[64] X. S. Wan, Z. Zhou, J. H. Ware, and A. R. Kennedy, "Standardization of a fluorometric assay for measuring oxidative stress in irradiated cells," *Radiation Research*, vol. 163, no. 2, pp. 232–240, 2005.

[65] M. L. Orozco-Cárdenas, J. Narváez-Vásquez, and C. A. Ryan, "Hydrogen peroxide acts as a second messenger for the induction of defense genes in tomato plants in response to wounding, systemin, and methyl jasmonate," *The Plant Cell*, vol. 13, no. 1, pp. 179–191, 2001.

Hindawi Publishing Corporation
BioMed Research International
Volume 2015, Article ID 754283, 14 pages
http://dx.doi.org/10.1155/2015/754283

Research Article

RCCS Bioreactor-Based Modelled Microgravity Induces Significant Changes on *In Vitro* 3D Neuroglial Cell Cultures

Caterina Morabito,[1,2] Nathalie Steimberg,[2,3] Giovanna Mazzoleni,[2,3] Simone Guarnieri,[1,2] Giorgio Fanò-Illic,[1,2] and Maria A. Mariggiò[1,2,4]

[1] *Department of Neuroscience, Imaging and Clinical Sciences, Unit of Functional Biotechnology, Aging Research Center (Ce.S.I.), "G. d'Annunzio" University of Chieti-Pescara, Via dei Vestini 29, 66100 Chieti, Italy*
[2] *Interuniversity Institute of Myology, Italy*
[3] *Laboratory of Tissue Engineering, Department of Clinical and Experimental Sciences, School of Medicine, University of Brescia, Viale Europa 11, 25123 Brescia, Italy*
[4] *Section of Physiology and Physiopathology, Department of Neuroscience, Imaging and Clinical Sciences, "G. d'Annunzio" University of Chieti-Pescara, Via dei Vestini 31, 66013 Chieti, Italy*

Correspondence should be addressed to Maria A. Mariggiò; mariggio@unich.it

Received 24 April 2014; Revised 10 September 2014; Accepted 10 September 2014

Academic Editor: Mariano Bizzarri

We propose a human-derived neuro-/glial cell three-dimensional *in vitro* model to investigate the effects of microgravity on cell-cell interactions. A rotary cell-culture system (RCCS) bioreactor was used to generate a modelled microgravity environment, and morphofunctional features of glial-like GL15 and neuronal-like SH-SY5Y cells in three-dimensional individual cultures (monotypic aggregates) and cocultures (heterotypic aggregates) were analysed. Cell survival was maintained within all cell aggregates over 2 weeks of culture. Moreover, compared to cells as traditional static monolayers, cell aggregates cultured under modelled microgravity showed increased expression of specific differentiation markers (e.g., GL15 cells: GFAP, S100B; SH-SY5Y cells: GAP43) and modulation of functional cell-cell interactions (e.g., N-CAM and Cx43 expression and localisation). In conclusion, this culture model opens a wide range of specific investigations at the molecular, biochemical, and morphological levels, and it represents an important tool for *in vitro* studies into dynamic interactions and responses of nervous system cell components to microgravity environmental conditions.

1. Introduction

Microgravity modulates numerous features and functions of biological organisms through its effects on physical phenomena, such as hydrostatic pressure in fluid-filled compartments, sedimentation of organelles, and convection processes of flow and heat. These physical parameters can, in turn, directly and indirectly influence cellular and tissue morphology, metabolism and signalling, and, consequently, a wide range of cell functions [1]. Several years ago, it was proposed that gravity is involved in embryonic development, through effects on morphogenesis and organogenesis of the central nervous system and on sensory organs in invertebrates and vertebrates. In particular, when amphibian eggs were fertilised *in vivo* or *in vitro* under microgravity conditions, some abnormalities during embryonic development were observed, even if compensatory mechanisms produced nearly normal larvae [2]. Also, during space flight, signs of neurophysiological impairment have been observed for astronauts, although few studies have been carried out to investigate such effects on the nervous system, in particular at the cellular level [3].

Recently Pani and colleagues reported that neuronal monolayers showed alterations in morphology and viability when exposed to short- and middle-term simulated microgravity in the random positioning machine, while long-term exposures revealed high adaptation of single neurons to the new gravity conditions [4]. Also other neuronal cell models

showed morphological and/or cytoskeletal alterations when exposed to simulated weightlessness or during changing gravity [5, 6]. These effects appeared conditioned by the presence of microgravity conditions, and after short-term exposures, under ground-conditions, the cells were able to fully recover their features and the ability to form adherent monolayer cultures [4, 7].

Traditional monolayer cell cultures that are kept under static conditions (two-dimensional (2D) cell culture) have provided great advances in our understanding of the physiological regulatory processes of single cells. On the other hand, the intrinsic complexity of cell-cell extracellular signalling and the remarkable plasticity in the composition and structure of the extracellular matrix have made it very difficult to study these interactions using conventional cell-culture techniques. For these reasons, advanced methods are needed to grow cells while maintaining their native three-dimensional (3D) cytoarchitecture and the specific tissue-like microenvironment. Interestingly, 3D cultures have been shown to favour the maintenance of tissue-specific phenotypes and tissue-like cytoarchitecture. However, an important limitation for long-term culture in three dimensions is the low diffusion of oxygen and nutrients and the absence of a blood supply to the deeper parts of the tissue construct. This is particularly the case for neural cells, and it can result in the appearance of a central core of dead cells [8, 9].

In the 1990s, after the beginning of the many international space programmes, attempts were made to grow 3D cell cultures or tissue explants in particular microenvironments, to test the effects of reduced gravity. Major efforts have been addressed to the building of a system that can reproduce a tissue-like microenvironment *in vitro* and to study the cytoskeletal and nuclear matrix protein interactions during cell exposure to simulated microgravity, as is present in space [10]. Engineers at the US National Aeronautics and Space Administration (NASA) devised a rotating bioreactor, which is a useful device for culturing cells on Earth, as well as in space. Briefly, this monoaxial clinostat (the rotary cell-culture system (RCCS) bioreactor) is a horizontally rotating and fluid-filled culture vessel that is equipped with a gas-exchange membrane that optimises the oxygen supply to the biological samples. Without air bubbles or air-liquid interface, the fluid dynamic conditions inside the culture chamber generate a laminar flow state that greatly reduces shear stress and turbulence, which are hazardous for cell survival. These dynamic conditions provided by the RCCS bioreactor favour spatial colocalisation and three-dimensional assembly of single cells into aggregates [11]. The rotational speed of the culture chamber can be modified to set conditions in which the 3D cell constructs/aggregates also rotate around their own axes, further providing an efficient high mass transfer of nutrient and wastes. When cultured cell aggregates grow in size, the rotational speed of the culture vessel can be increased, to compensate for the increased sedimentation rates. The operational conditions of the RCCS bioreactor can also be adjusted so that the gravitational vectors are randomised up, to reach a modelled microgravity state [12, 13]. In this way, 3D biological samples can remain in a constant orientation, with respect to the chamber wall, and move in near-solid body rotation with the fluid, thus fulfilling the requirements needed to successfully model microgravity conditions [14].

In the present study, we aimed to develop a 3D dynamic *in vitro* neuroglial coculture system, to evaluate the capacity of the cells to reproduce, at least in part, neuronal features. To this end, we used two well-characterised cell lines, GL15 and SH-SY5Y cells, which are astrocyte-like and neuronal-like cells, respectively. The human glioblastoma GL15 cell line is an established *in vitro* astrocyte model that has been functionally characterised by our group and others [15, 16], and these express a typical astroglial phenotype and functions. The human neuroblastoma-derived SH-SY5Y cells are a widely used and well-characterised neuronal cell model that has been extensively used for *in vitro* neurotoxicity testing and has been shown to differentiate towards either adrenergic or cholinergic phenotypes [17–20]. In addition, the human origin of these cell lines makes them an appealing model for basic *in vitro* research studies. Thus, to develop astrocyte-like or neuronal-like *in vitro* models, 3D monotypic cultures (GL15 cells only or SH-SY5Y cells only) were established in a RCCS bioreactor. Of note, it has been demonstrated that cell-cell interactions, as for example, those between glial cells and neurons, are crucial for both glial and neuronal differentiation and developmental processes, as well as for response to neural injury [21, 22]. For these reasons, we also established 3D neuronal/glial heterotypic cultures (cocultures), to more closely reproduce the *in vivo* microenvironment of the nervous tissue and to bridge the gap between *in vitro* systems and animal models. These analyses were also performed under modelled microgravity when the 3D cell aggregates were sufficiently grown in size to adjust to the operational conditions of the RCCS bioreactor, so as to reach a state of vector-averaged microgravity. Under such conditions, their cell morphology, viability, and functional features were analysed and compared.

2. Materials and Methods

All of the reagents for cell culture were from Life Technologies (Milan, Italy). The plasticware was from BD Falcon (Sacco, Milan, Italy).

2.1. Cell Culture. The SH-SY5Y cell line (from the European Collection of Cell Cultures, supplied through Sigma-Aldrich, UK) and the GL15 cell line were both cultured in Dulbecco's modified Eagle's medium (DMEM) with 10% foetal bovine serum, 100 IU/mL penicillin, 100 μg/mL streptomycin, and 1 mM glutamine. The cells were amplified in monolayers and detached for subculturing using 0.05% trypsin and 0.02% EDTA. SH-SY5Y and GL15 cell cultures, used for experimental assays, were prepared by seeding cells in T75 Falcon flasks, to form 2D static monolayer cultures, or in the RCCS bioreactor to establish 3D cultures subjected to microgravity. Both culture models were cultured in DMEM with 10% foetal bovine serum, 100 IU/mL penicillin, 100 μg/mL streptomycin, and 1 mM glutamine and maintained in the same incubator (5% CO_2, at 95% humidity) for the same times, and the medium was refreshed twice a week.

2.2. 3D Culture in the RCCS Bioreactor. The RCCS bioreactor (Synthecon, Houston, USA) can generate a special microenvironment where high mass transfer is achieved with low shear stress. It is equipped with a cylindrical growth chamber that contains an inner corotating cylinder with a gas-exchange membrane (a 55 mL autoclavable slow-turning lateral vessel) where specific hydrodynamic and physical conditions are attained. The culture of cell spheroids was performed in this device in a 5% CO_2 incubator at 95% humidity. The horizontally rotating culture vessel was filled with the complete medium (without air-liquid interface to reduce the shear stress). After a defined rotational speed was reached, the cells were cultured under Earth gravity, in a near laminar fluid flow environment (i.e., a free-fall state). Under such conditions, the cells grew in the form of 3D multicellular aggregates [23, 24].

The cell-density seeding for both GL15 and SH-SY5Y cells was approximately 1.5×10^6 cells/mL. The medium was refreshed twice a week. For cocultures, the SH-SY5Y and the GL15 cells were each seeded at a density of 0.75×10^6 cells/mL. The rotational speed of the culture chamber was initially set at between 6 rpm and 8 rpm, and then it was gradually increased as the multicellular aggregates increased in size, to maintain the aggregates in constant equilibrium (i.e., under free-fall conditions).

At the indicated times, the cells were harvested, and according to the experimental conditions required, the multicellular aggregates were either included in Tissue-Tek OCT compound (VWR International Srl, USA) (for *in situ* analysis) or centrifuged at 2300 rpm for 5 min at 4°C, and the resulting cell pellets were kept at −80°C until Western blotting was carried out.

For the embedded aggregates, slices (6 μm to 10 μm) were prepared with a CM1900 cryostat (Leica, Milan, Italy) and processed for cell viability assays or frozen at −20°C for further investigations.

2.3. Morphological Analysis. The frozen sections were left to warm up to room temperature and were subsequently incubated for 12 min in Harris' haematoxylin solution, washed twice in water, and incubated for 15 s in Eosin solution. After washing, the sections were dehydrated and mounted with Eukitt mounting medium (Electron Microscopy Sciences). The sections were examined under a Vanox optical microscope (Olympus, Opera Zerbo, Italy).

2.4. Cell Viability Assay. The sections were incubated for 15 min at room temperature in a solution containing recombinant Annexin V conjugated to the Alexa 488 fluorophore and propidium iodide (Vybrant kit #2, Life Technologies, Italy) as described by the manufacturer. Moreover, to quantify the total number of cells in the aggregates, 4′-6-diamidino-2-phenylindole (DAPI) was added to this solution at a final concentration of 0.10 μg/mL. The sections were mounted in Prolong antifade medium (Life Technologies) and examined under an inverted fluorescence microscope (Axiovert; Zeiss, Arese, Italy) equipped with an image analyser. Photomicrographs were analysed with the ProImage+ and Scion Image software (http://proimage.software.informer.com/ and http://scion-image.software.informer.com/), to determine the cell viability.

2.5. Immunostaining Assay. The frozen GL15 and SH-SY5Y cells in OCT sections were fixed with 3.7% paraformaldehyde at room temperature for 30 min. Slices were then permeabilised with 0.1% Triton X-100 at room temperature for 15 min and incubated for 1 h in 10% bovine serum albumin at room temperature and then for 1 h at 37°C with the primary antibody, followed by 1 h at 37°C with either an Alexa 488- or an Alexa 633-conjugated secondary antibody (Molecular Probes, Milan, Italy). For double staining, the second primary antibody was incubated with the constructs after removal of the first, Alexa 488-conjugated secondary antibody. After the antibody incubation, the cells were washed three times with 0.1% Tween 20, each for 5 min at room temperature. Finally, the nuclei were stained with 1 μg/mL propidium iodide for 30 min. After three washes with phosphate-buffered saline, they were mounted on coverslips and examined.

Primary monoclonal mouse antibodies, neuronal cell adhesion molecule (N-CAM), tyrosine hydroxylase, growth associated protein 43 (GAP43), glial fibrillary acidic protein (GFAP), and S100B were from Sigma-Aldrich (Milan, Italy), and connexin 43 (Cx43) was from Chemicon International Inc. (Temecula, CA, USA).

The fluorescence images were obtained using a Zeiss LSM510 META confocal system (Jena, Germany) connected to an inverted Zeiss Axiovert 200 microscope equipped with a Plan Neofluar oil-immersion objective (40x/1.3 NA).

2.6. Western Blotting. Frozen pellets of the GL15 and SH-SY5Y cell aggregates were lysed in cell lysis buffer (50 mM Tris-HCl, 100 mM NaCl, 50 mM NaF, 40 mM β-glycerophosphate, 5 mM EDTA, 1% Triton X-100, 200 μM sodium orthovanadate, 100 μg/mL phenylmethylsulfonyl fluoride, 10 μg/mL leupeptin, 5 μg/mL pepstatin A, 10 μg/mL benzamidine, and pH 7.4). After vortexing for 5 min, the samples were centrifuged at 1000 rpm for 10 min at 4°C in a microcentrifuge. The protein content of each supernatant was quantified colorimetrically (Bio-Rad Laboratories Srl, Milan, Italy), and aliquots containing 40 μg protein were added to Laemmli buffer (8% SDS, 10% glycerol, 5% β-mercaptoethanol, 25 mM Tris-HCl, 0.003% bromophenol blue, and pH 6.5) and applied to and separated by SDS-PAGE on 7% to 10% SDS polyacrylamide slab gels. Proteins were electroblotted onto hydrophobic polyvinylidene difluoride membranes (Immobilon, Millipore, Milan, Italy) using a tank transfer system (Bio-Rad Laboratories Srl). Transfer efficiency was verified by Ponceau red staining of the blots and Coomassie blue staining of the gels. The SH-SY5Y cell blots were incubated with the following mouse monoclonal antibodies: anti-N-CAM (1 : 100 dilution; Sigma-Aldrich), anti-tyrosine hydroxylase (1 : 1000 dilution; Sigma-Aldrich), anti-GAP43 (1 : 1000 dilution; Sigma-Aldrich), and/or anti-Cx43 (1 : 1000 dilution; Chemicon). The GL15 cell blots were incubated with the following mouse monoclonal antibodies: anti-glial fibrillary acidic protein (GFAP; 1 : 500 dilution; Sigma-Aldrich), anti-S100B (1 : 500 dilution; Sigma-Aldrich), and/or also Cx43 (1 : 1000 dilution; Chemicon). These were

then detected by chemiluminescence (ECL plus; GE Healthcare). Moreover, after a membrane-stripping procedure, the GL15 and SH-SY5Y cell membranes were immunostained with a mouse monoclonal anti-actin antibody (1 : 1000 dilution; Sigma-Aldrich).

3. Results

3.1. Cell Aggregates in the RCCS Bioreactor: Morphology and Viability

3.1.1. GL15 Cells. Initial experiments were performed to establish the most suitable protocol to prepare the cell aggregates. GL15 cells were incubated in the RCCS bioreactor as preinduced cell clusters or as homogeneous cell suspensions that were left to spontaneously aggregate. The preinduced aggregates were obtained using the hanging drop method (see [24]). Both types of aggregates were maintained under conditions of microgravity in the RCCS bioreactor for up to 2 weeks. The single cells spontaneously aggregated within 48 h of culture, although some features of the spontaneous cell aggregates were different compared to the preinduced aggregates.

The preinduced aggregates provided relatively uniform clusters, while the spontaneously formed aggregates appeared more irregular in shape. In addition, after 2 weeks in the RCCS bioreactor, the spontaneously formed aggregates showed a trend (not significant) towards a greater mean area ($2.98 \pm 0.26\,mm^2$), compared to that of the preinduced aggregates ($1.89 \pm 1.28\,mm^2$) (Figure 1).

The cell viability in the preinduced aggregates and the spontaneously formed aggregates was also assessed after 2 weeks in the RCCS bioreactor, to determine the apoptotic or the necrotic cells (Figure 2). To this aim, the cells were tested to measure early apoptosis by detecting phosphatidylserine expression revealed by Annexin V binding or necrosis by membrane permeability to the propidium iodide (PI) vital dye. Cells positive to Annexin V green fluorescence signal are known to be apoptotic cells, while those positive to PI red fluorescence signal are necrotic cells; the absence of green or red signal and the nuclear staining with DAPI revealed viable cells. The image analyses of stained cells revealed that some apoptotic cells (Figure 2(a), green fluorescence) were evident at a similar extent in preinduced and spontaneous GL15 aggregates (Figure 2(b)). A relevant amount of necrotic cells (Figure 2(a), red fluorescence) was present in preinduced aggregates compared to spontaneous ones in which necrotic cells were nearly absent (Figure 2(b)). These data revealed the presence of possible stress conditions in the preinduced aggregates, while the spontaneously formed aggregates showed cells that were in a more healthy state. This cell stress might be the result of hypoxic processes in the central core of the preinduced aggregates in particular, potentially due to the static conditions encountered in the hanging drops. For this reason, the rest of the investigations used only the spontaneously formed cell aggregates, and those formed by the GL15 cells are henceforth referred to as the G-aggregates.

3.1.2. SH-SY5Y Cells. Following the same procedure described above for the formation of the G-aggregates, the SH-SY5Y cells were cultured to form spontaneous aggregates in the RCCS bioreactor for up to 2 weeks, and their cell morphology and viability were then assessed. These aggregates formed by the SH-SY5Y cells are henceforth referred to as the S-aggregates.

At the end of the incubation period, the S-aggregates showed variable and irregular shapes, with a mean area of $2.68 \pm 0.13\,mm^2$. In addition, there were very low levels of apoptotic and necrotic cells (Figure 2(b)), which indicated that these 3D dynamic culture conditions are a suitable method to sustain cell viability also for neuronal-like cells.

3.2. Qualitative Analysis of Phenotype-Specific Markers

3.2.1. GL15 Cells. To analyse the expression of the GL15 cell specific phenotype in the G-aggregates cultured in the RCCS bioreactor for up to 2 weeks, immunostaining for glial markers was carried out. The G-aggregates showed glial-cell-specific protein expression similar to that observed in the GL15 cells cultured as monolayers under 2D conditions (Figure 3). The G-aggregates and the GL15 cells cultured as monolayers both showed cytoplasmic localisation of GFAP and S100B, as two markers of the glial cytoskeleton (Figures 3(a)–3(d)).

Cell interactions due to gap-junction-mediated intercellular communication have been shown to have crucial roles in the regulation of the glial-cell network and nervous system functions [25]. For this reason, the expression of Cx43 was also investigated, as Cx43 is the main gap-junction protein expressed by astrocytes. As shown in Figure 3(e), the GL15 cells grown in two dimensions expressed Cx43 near the plasmalemma, at cell-cell contact areas, and in the cytoplasm. A similar distribution was also seen for Cx43 in the G-aggregates (Figure 3(f)).

3.2.2. SH-SY5Y Cells. We characterised the phenotype expressed by the SH-SY5Y cells in the S-aggregates maintained in the dynamic 3D culture in the RCCS bioreactor for 2 weeks, by determining the expression of the neuronal specific markers N-CAM, GAP43, and tyrosine hydroxylase. Immunofluorescence analysis revealed that N-CAM in the S-aggregates was localised towards the plasma membrane and near cell-cell contact areas, thus resembling its distribution in the SH-SY5Y cells cultured in 2D monolayers (Figures 4(a) and 4(b)), which showed cell-cell adhesion interactions. GAP43 is involved in neurite outgrowth and neuronal plasticity [26], and in SH-SY5Y cell monolayers it was localised into neurite-like processes (Figure 4(c)). In the S-aggregates, GAP43 was localised in the cytoplasmic compartment (Figure 4(d)). The distribution of tyrosine hydroxylase (TH), which is a rate-limiting enzyme in dopamine/norepinephrine synthesis [27], was in the cytoplasm under both of these cell-culture conditions (Figures 4(e) and 4(f)).

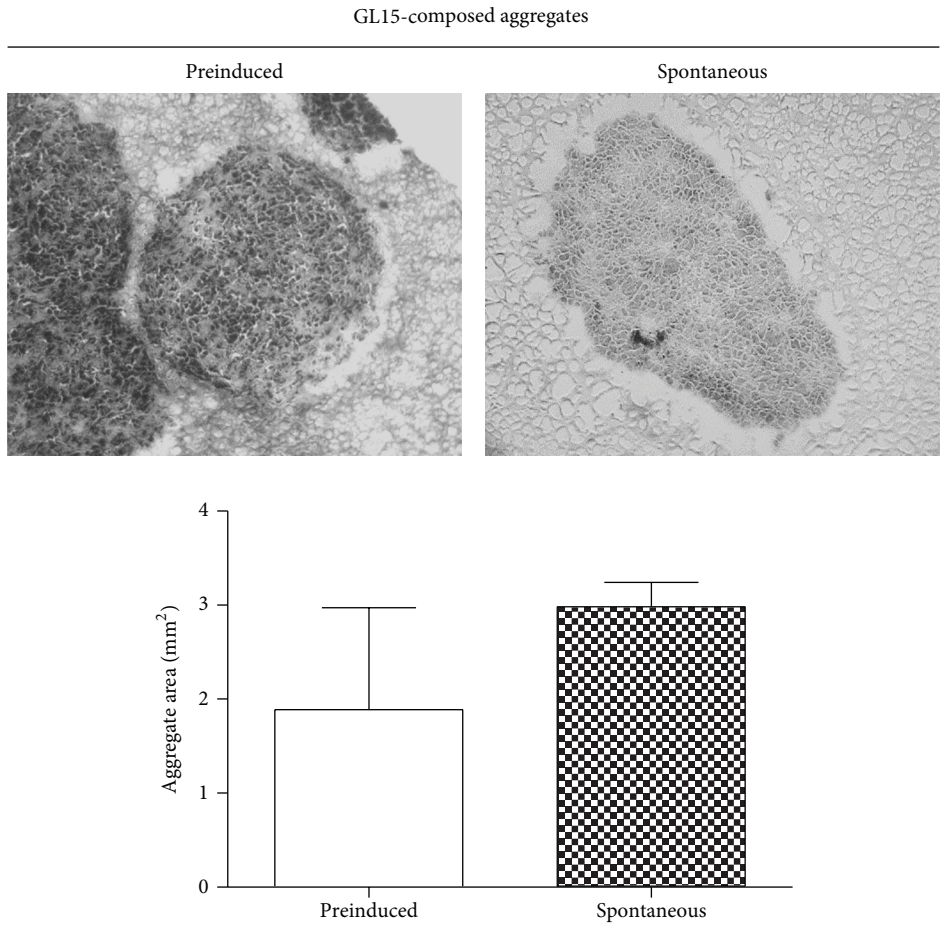

Figure 1: GL15 cell aggregate morphology. Representative images and quantification of sections from preinduced and spontaneously formed GL15 aggregates (as indicated). Data are means ± SEM. $n = 15$ for the averaged areas of the aggregate sections, calculated using the ImageJ software (http://imagej.nih.gov/ij/).

3.3. Quantitative Analysis of Phenotype-Specific Markers

3.3.1. GL15 Cells. The differentiation status of cells is characterised not only by marker localisation but also by marker expression levels. To evaluate potential quantitative differences between the G-aggregate modelled microgravity-exposed cultures and the GL15 cells as 2D static monolayer cultures, the expression levels of the GFAP, S100B, and Cx43 proteins were determined by Western blotting (Figure 5). The G-aggregates showed increased levels of GFAP, S100B, and Cx43 after the first 48 h of culture. These levels gradually decreased over the following 2 weeks, when those of S100B and Cx43 were similar to those observed in the GL15 cells as 2D static cultures, while those of GFAP remained increased in the G-aggregates (Figure 5).

3.3.2. SH-SY5Y Cells. Western blotting carried out for the S-aggregates showed that N-CAM-140 and GAP43 expression levels were increased during the incubation, compared to the SH-SY5Y cells as 2D static monolayer cultures (Figure 6). In particular, for the S-aggregates, N-CAM-140 reached a peak after 2 weeks, while GAP43 peaked after 48 h. Conversely, N-CAM-180 and tyrosine hydroxylase did not significantly change in the S-aggregates compared to SH-SY5Y cells as 2D static cultures (Figure 6).

3.4. Coculture of GL15 and SH-SY5Y Cells in the RCCS Bioreactor. The SH-SY5Y cells were also cocultured with the GL15 cells in the RCCS bioreactor with the aim to reestablish a more neural-like microenvironment and thus to be closer to *in vivo* conditions. Initial experiments were carried out to determine if it was possible to establish viable GL15 plus SH-SY5Y cocultures in the RCCS bioreactor, henceforth referred to as GS-aggregates. GL15 and SH-SY5Y cells were thus cocultured in the RCCS bioreactor at a 1 : 1 ratio for up to 2 weeks. At the end of this period, the sizes of the GS-aggregates were similar to those of the monotypic G-aggregates and S-aggregates (Figure 7), and although the S-aggregates appeared smaller than the others, these differences did not reach significance. Cell viability assays also showed that the GS-aggregates had low levels of apoptotic and necrotic cells (data not shown).

To characterise the cell phenotype in these GS-aggregates, immunostaining was carried out for N-CAM, GFAP, and Cx43. These coculture conditions induced the establishment

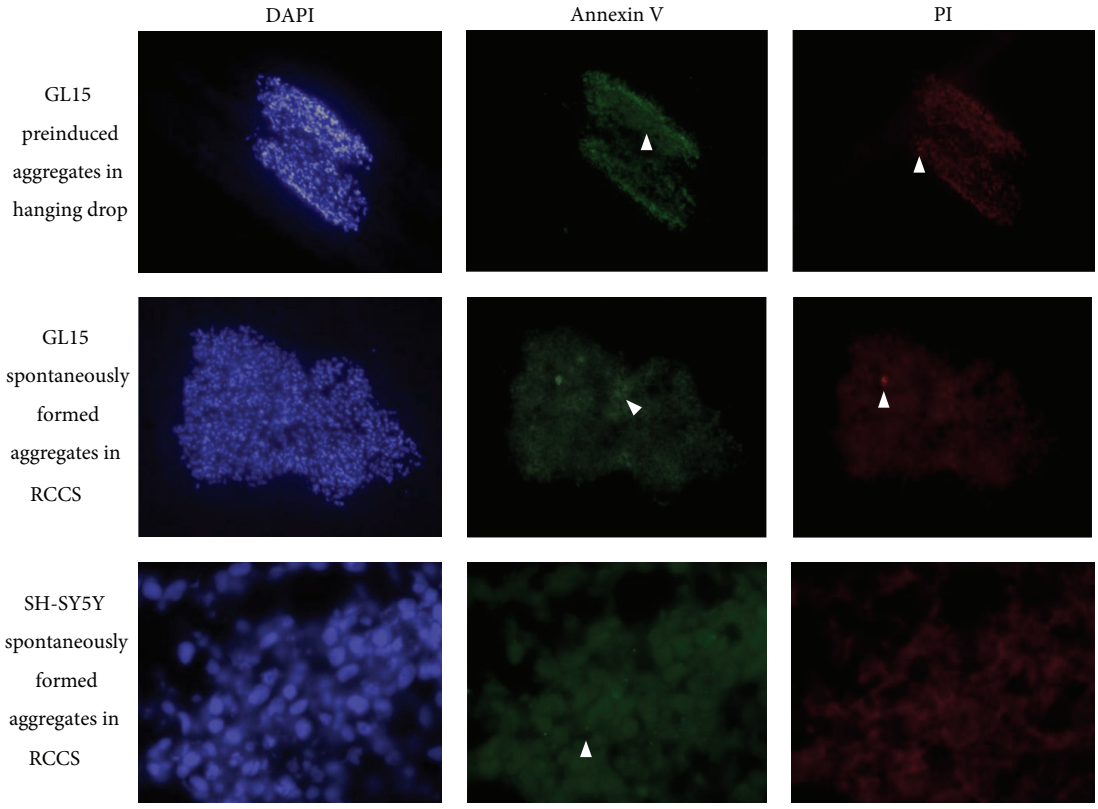

(a)

	Total cell number	Apoptotic cells (%)	Necrotic cells (%)
GL15 preinduced aggregates in hanging drop	512	16	19
GL15 spontaneously formed aggregates in RCCS	914	14	0.07
SH-SY5Y spontaneously formed aggregates in RCCS	491	7	1

(b)

Figure 2: Cell viability assay. (a) Representative images of preinduced and spontaneously formed GL15 aggregates and spontaneously formed SH-SY5Y aggregates (as indicated). Aggregates were stained with DAPI (blue), Annexin V-Alexa 488 (green), and propidium iodide (PI; red). DAPI-positive/Annexin V-Alexa 488-negative/PI-negative cells are healthy; DAPI-positive/Annexin V-Alexa 488-positive/PI-negative and PI-positive cells are considered apoptotic (Annexin V, arrowheads); DAPI-positive/Annexin V-Alexa 488-negative/PI-positive cells are necrotic (PI, arrowheads). (b) Quantification of apoptotic and necrotic cells in aggregate sections. Data derived from 3 independent experiments.

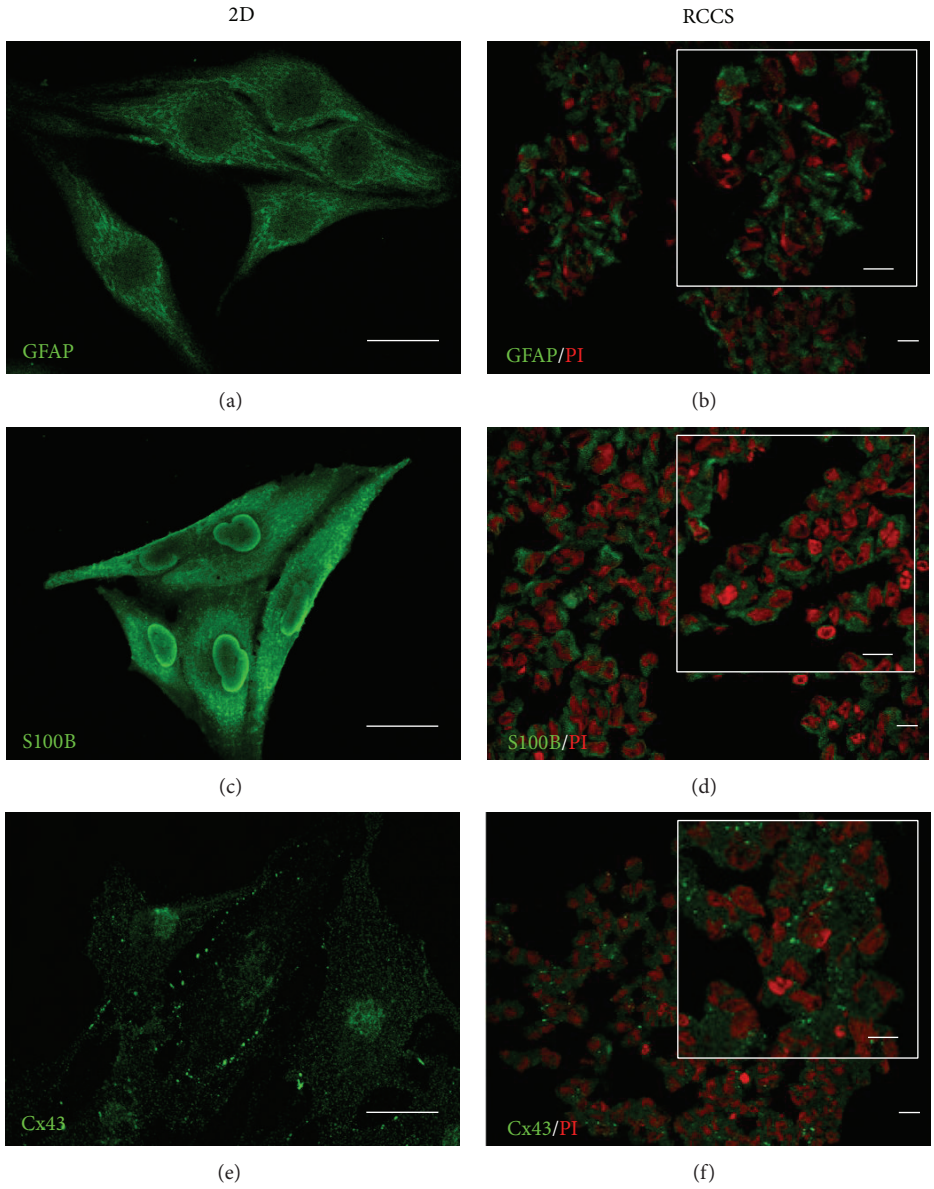

Figure 3: Glial marker localisation in GL15 cells. Representative confocal images of GL15 cells cultured as a monolayer (2D, (a), (c), and (e)) and under the modelled microgravity (RCCS bioreactor, (b), (d), and (f)) and immunostained with anti-GFAP ((a) and (b)), anti-S100B ((c) and (d)), and anti-Cx43 ((e) and (f)) antibodies (as indicated). The RCCS G-aggregate sections were also stained with propidium iodide (PI). Insets in (b), (d), and (f) show image magnification. Scale bars, 25 μm.

of GS-aggregates that contained both glial-like and neuronal-like cell phenotypes. After the 2 weeks of culture in the RCCS bioreactor, these GS-aggregates showed specific fluorescence signals for astrocyte (GFAP-positive) and neuronal (N-CAM-positive) phenotypes (Figure 8).

The GS-aggregates were double-stained for N-CAM and Cx43. These N-CAM-specific and Cx43-specific fluorescent signals revealed a particular distribution of these proteins, whereby even if colocalisation of the N-CAM and Cx43 patterns was not evident, possible heterotypic cell-cell interactions could not be excluded. In particular, within the GS-aggregates, N-CAM localised to the peripheral areas of the cells, while Cx43-specific fluorescent spots appeared to be sparsely distributed, which indicated a low level of cell-cell functional interactions (Figure 9). In addition, in the same GS-aggregates, there were also evident N-CAM-negative and/or Cx43-negative cells, which indicated potential different cell activities due to different protein expression levels.

Western blotting of N-CAM and Cx43 expression levels revealed that, in the GS-aggregates, the monomeric Cx43 protein (43 kDa) was downregulated during the RCCS bioreactor incubation. Interestingly, homogenates from the GS-aggregates showed a Cx43-positive band at 86 kDa, which demonstrates the presence of a dimeric form of Cx43, which was highly expressed in the initial phases of the coculture (over the first 24 h), and which significantly decreased over

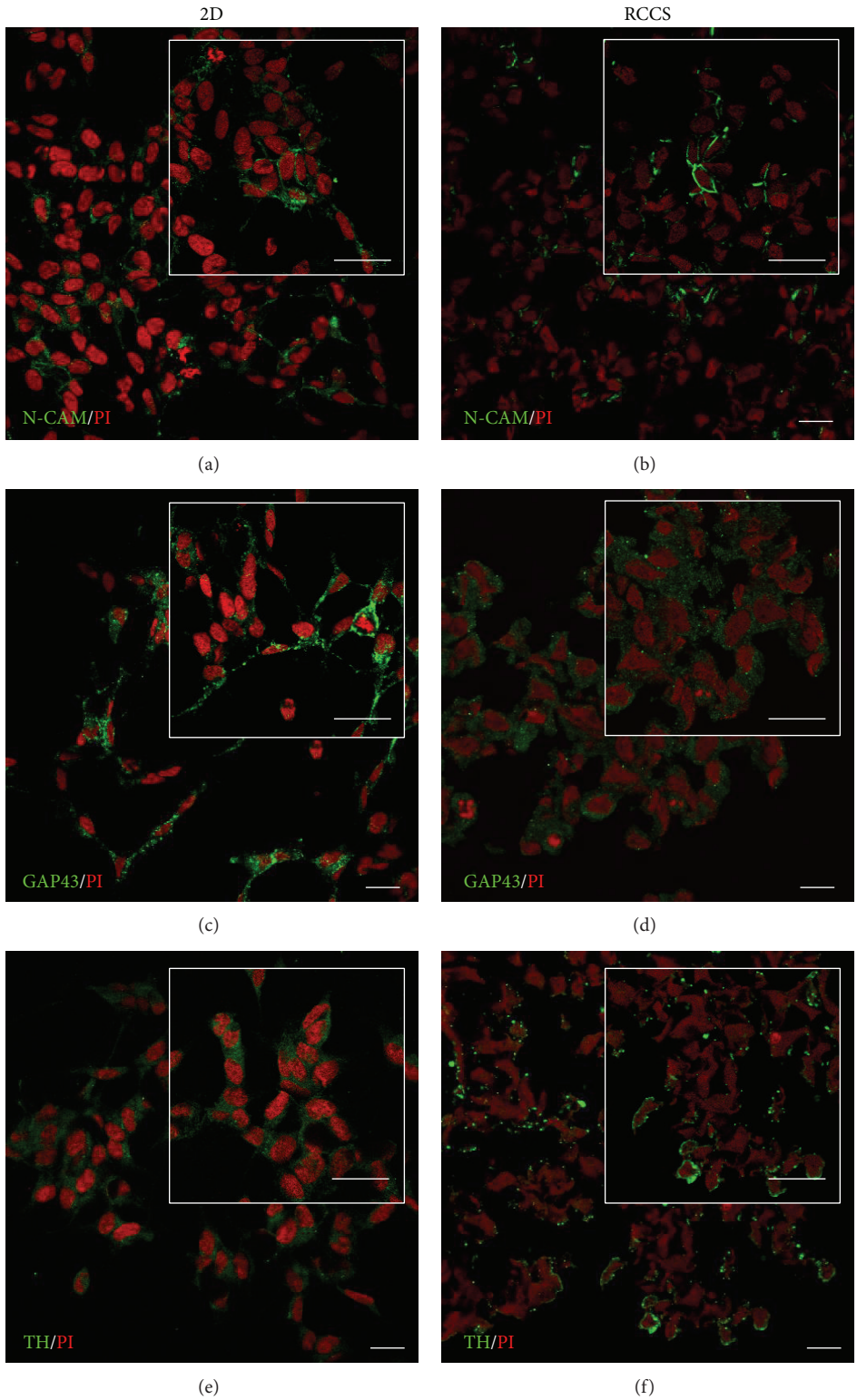

Figure 4: Neuronal marker localisation in SH-SY5Y cells. Representative confocal images of SH-SY5Y cells cultured as a monolayer (2D, (a), (c), and (e)) and under the modelled microgravity (RCCS bioreactor, (b), (d), and (f)) and immunostained with anti-N-CAM ((a) and (b)), anti-GAP43 ((c) and (d)), and anti-tyrosine hydroxylase (TH) ((e) and (f)) antibodies (as indicated). All of the cells were also stained with propidium iodide (PI). Insets show image magnification. Scale bars, 20 μm.

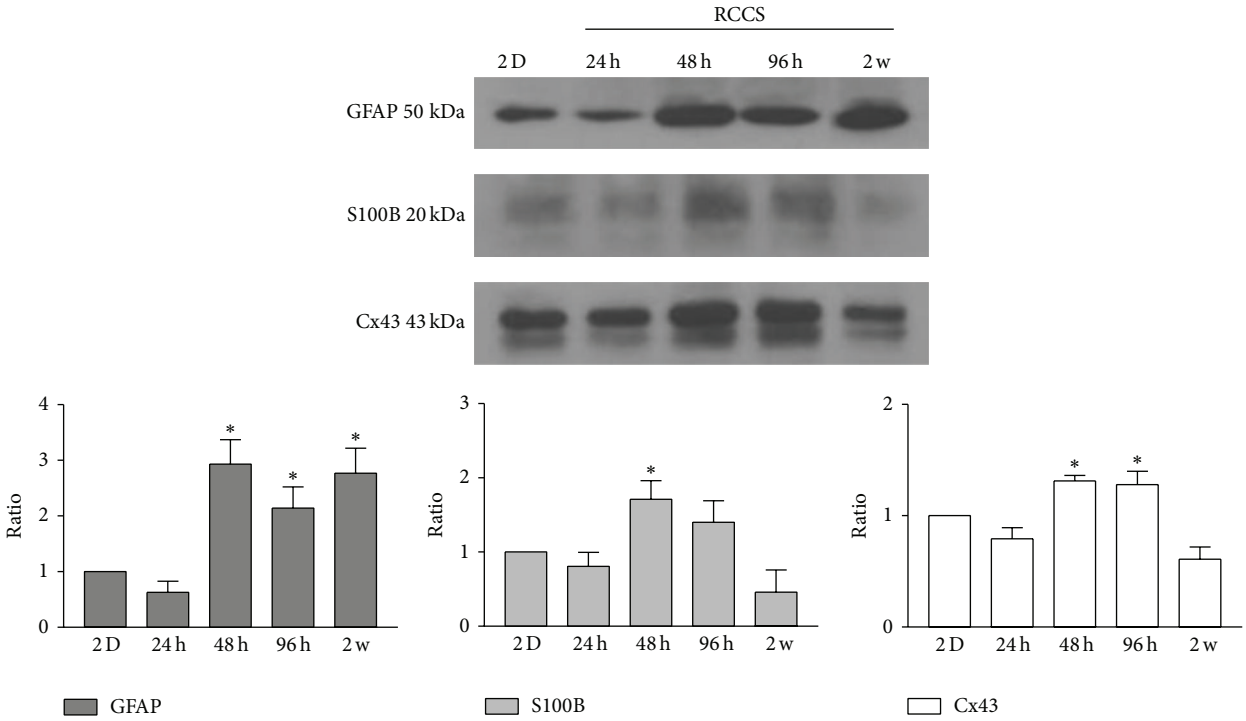

Figure 5: Expression of glial cell markers. Representative Western blotting and quantification of the levels of GFAP, S100B, and Cx43 in GL15 cells cultured in 2D monolayers and in the RCCS bioreactor for 24 h, 48 h, 96 h, and 2 weeks (2 w). Data are from densitometric ratio analyses as means ± SEM from 3 independent experiments. $^{*}P < 0.05$ versus 2D monolayers.

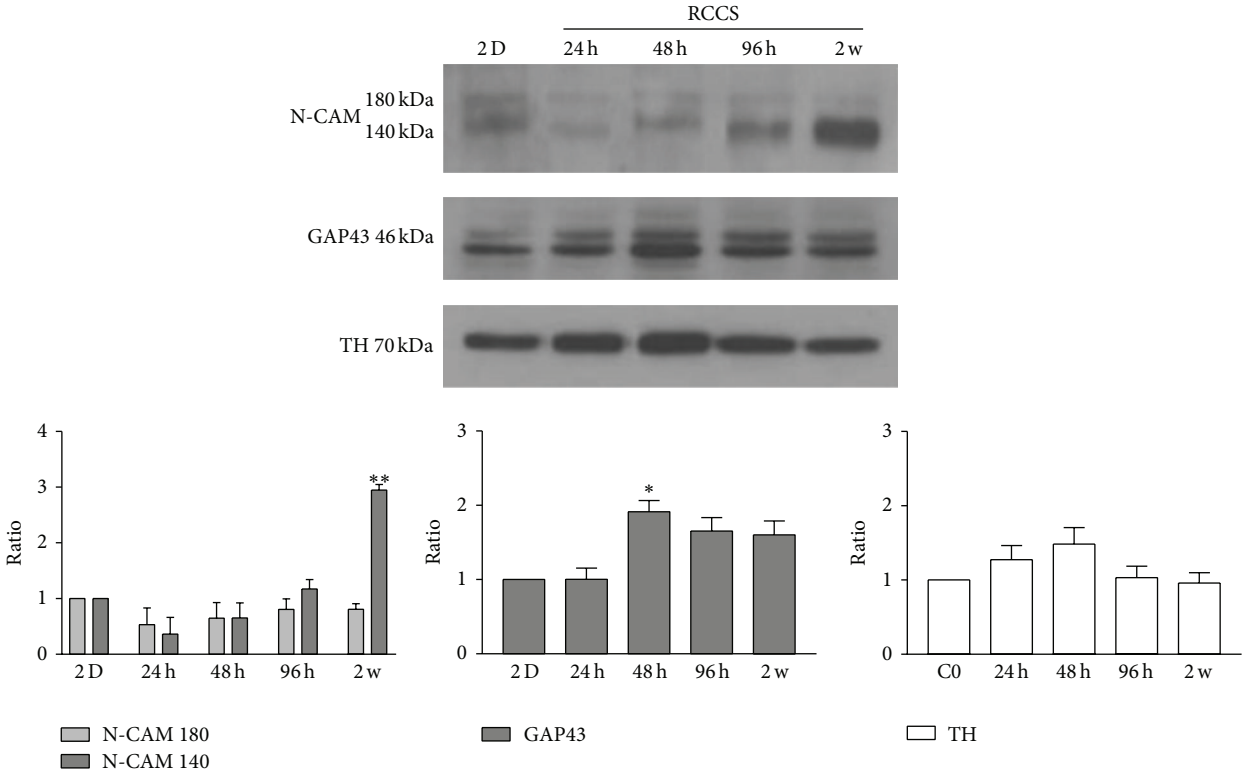

Figure 6: Expression of neuronal cell markers. Representative Western blotting and quantification of the levels of N-CAM, GAP43, and tyrosine hydroxylase (TH) in SH-SY5Y cells cultured in 2D monolayers and in the RCCS bioreactor for 24 h, 48 h, 96 h, and 2 weeks (2 w). Data are densitometric ratio analyses as means ± SEM from 3 independent experiments. $^{*}P < 0.05$ and $^{**}P < 0.01$ versus 2D monolayers.

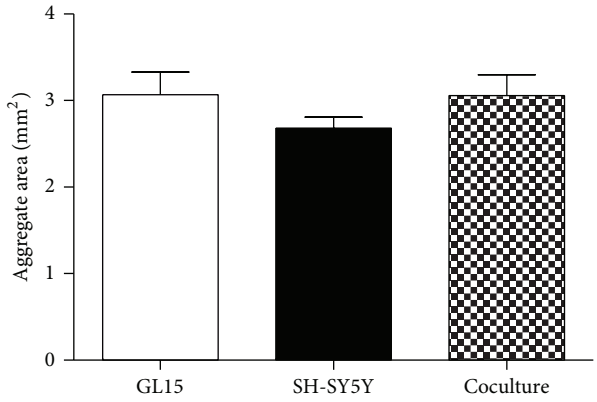

Figure 7: Cell aggregate sizes. Quantification of section area of GL15, SH-SY5Y, and cocultured (GL15 plus SH-SY5Y) cell aggregates (as indicated). Data are means ± SEM ($n = 15$) for the averaged areas of the aggregate sections, calculated using the ImageJ software (http://imagej.nih.gov/ij/).

the 2 weeks of the GS-aggregates in the RCCS bioreactor (Figure 10). The N-CAM isoform expression pattern showed a slight, but not significant, decrease in N-CAM-180 levels and a significant increase in N-CAM-140 levels (Figure 10), which resembled the N-CAM-140 increase observed in the S-aggregate homogenates.

4. Discussion

There are evidences available showing that microgravity can affect the functioning of the nervous system, although the possible physiological mechanisms of these effects remain difficult to determine [7, 28]. Such difficulties in investigations into microgravity effects are mainly due to the poor models that are available, either because of their high cost and low availability (e.g., spaceflight) or because they are little representative of true microgravity conditions (e.g., hindlimb suspension/disuse model). Among the ground-based models, *in vitro* culture of cells/tissues within clinorotation-based systems (e.g., random positioning machine, RCCS bioreactor) represents a reasonable alternative to spaceflight. The RCCS bioreactor, in particular, was initially developed by NASA engineers to maintain cells in culture during space missions and to counteract the forces faced during shuttle launch and landing. The RCCS bioreactor was further used to maintain cells in dynamic 3D culture on the ground, and because of its particular properties, the RCCS bioreactor also allows the modelling of microgravity on the ground. Setting standardised parameters, it is possible to also promote the colocalisation of cells, the establishment of cell-cell contacts, and, consequently, the spontaneous formation of multicellular aggregates [11, 13]. Moreover, the rotation speed can also be regulated in such a way that it is possible to reach a vector-averaged gravity that simulates low-gravity conditions [14].

In the present study, we designed and investigated a powerful human-derived 3D organotypic-like model of nervous system tissue. The experimental strategy was to study this 3D cell aggregation in terms of the cell phenotypes following short-term culture (up to 48 h, as a time that allows the formation of multicellular aggregates) and long-term (up to 2 weeks) culture, to analyse the effects of this modelled microgravity system on cell behaviour. However, apart from the effects related to microgravity, the development of a reliable neuro/glia cell *in vitro* model is of great interest for basic and clinical research in the field of the nervous system. Thus, we developed astrocyte-like and neuron-like *in vitro* models here, as 3D monotypic (GL15 cells only; SH-SY5Y cells only) and heterotypic (cocultures of both GL15 and SH-SY5Y cells) cell cultures in the RCCS bioreactor.

The particular dynamic conditions in the RCCS bioreactor have been shown to favour the differentiated phenotype expression for numerous cell and tissue types [13, 24, 29–31]. In our hands, over 48 h of culture, these optimal dynamic conditions favoured spontaneous formation of healthy multicellular aggregates according to the cell type considered, as demonstrated by the low cell death in these spontaneous cell aggregates. The survival of these G-aggregates and S-aggregates and also of the GS-aggregates was assessed for up to 2 weeks in the RCCS bioreactor cultures, and the data confirm the absence of significant necrosis in their central cores, in contrast to what has been reported in the literature for similar static culture conditions [32]. This evidence supported our choice to use the spontaneously formed aggregate method, as this allowed the random distribution of the cells inside the aggregates, which is a feature that is particularly important for the establishment of the heterotypic coculture model.

Under our 3D cell culture conditions in growth medium, the GL15 cells showed an astrocyte-like phenotype, with the expression of the glial-specific markers GFAP [33] and S100B. Interestingly, under these conditions, Cx43 expression was also evident in these G-aggregates. These data confirm the importance of cell-cell interactions in the regulation of phenotypic expression. The modulation of Cx43 expression might be related to the formation of these G-aggregates in the 3D culture. During the first phase of G-aggregate formation, there was upregulation of Cx43 expression. In a previous study, we showed that these GL15 cells express Cx43 and form junctional channels where the permeability is directly related to the cell proliferation rate, as it decreased when their differentiated status was reached [16]. In the present study, this transient upregulation of Cx43 during G-aggregate formation might support the hypothesis that Cx43 has a crucial role and function in cellular aggregation in addition to its well-known involvement in differentiation processes [34]. This hypothesis was also supported by Cotrina and colleagues, who demonstrated a role for Cx43 hemichannels in cellular adhesion of C6 glioma cells [35].

The optimal dynamic culture conditions provided by the RCCS bioreactor were also demonstrated by the favoured expression of neuronal-specific markers by the SH-SY5Y cells in the S-aggregates, such as tyrosine hydroxylase, GAP43, and N-CAM. The expression levels of tyrosine hydroxylase appeared similar in both the 2D and the 3D cultures at all of the times tested, which demonstrated the adrenergic phenotype that was expressed by these S-aggregates.

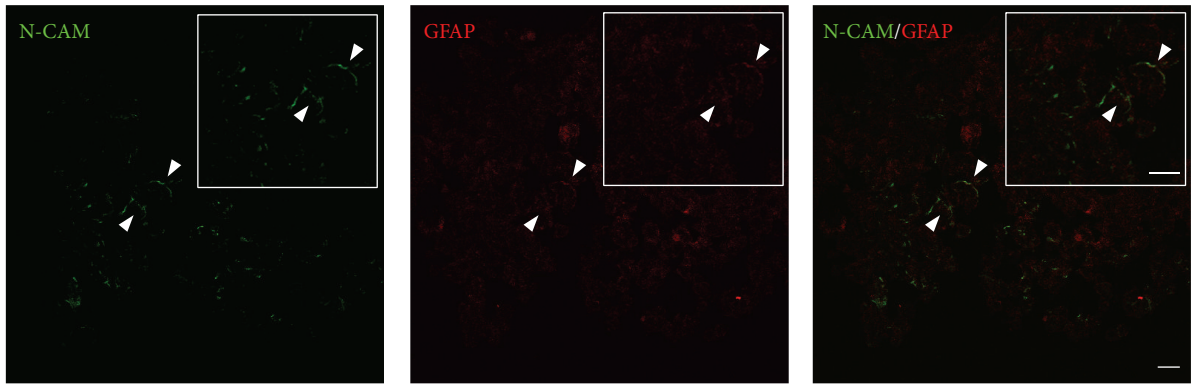

Figure 8: Localisation of glial and neuronal cell markers in the GS-aggregates. Representative confocal images of GS-aggregates cultured under the modelled microgravity, for 2 weeks, and immunostained with anti-N-CAM and anti-GFAP antibodies (as indicated). Insets show image magnification. Scale bars, 20 μm.

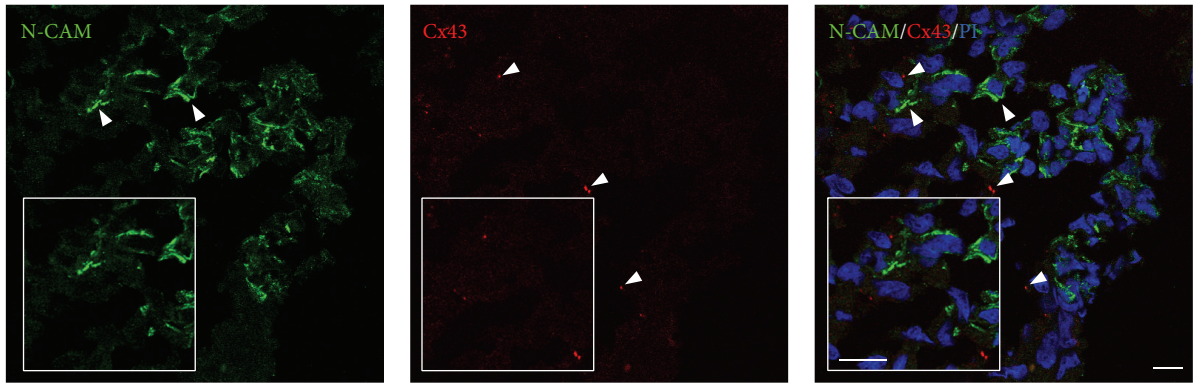

Figure 9: Localisation of cell-cell interaction markers in the GS-aggregates. Representative confocal images of GS-aggregates cultured under modelled microgravity, for 2 weeks, and immunostained with anti-N-CAM and anti-Cx43 antibodies (as indicated). The GS-aggregate sections were also stained with propidium iodide (PI; right). Insets show image magnification. Scale bars, 10 μm.

GAP43 expression increased during the cell aggregation (48 h), which confirms active cell-cell interactions, with the cytoskeletal modifications shown by GAP43 regulation. The stabilisation of these cell aggregates is supported by the increase in N-CAM expression.

During the long-term exposure to modelled microgravity, specific protein expression was differently regulated in the cell aggregates. Even after 2 weeks under culture in the modelled microgravity, in the G-aggregates the glial-specific and functional markers (i.e., GFAP, S100B, and Cx43) showed localisation patterns that were similar to those observed in the monolayers under normal gravity conditions. Interestingly, under microgravity, S100B and Cx43 expression levels in the G-aggregates were downregulated over two weeks, as compared to those in the G-aggregate cultures at 48 h exposure, whereas there was a slight transient, although not significant, effect on GFAP expression.

The exact physiological roles of GFAP in astrocytes remain incompletely understood, although they appear to be involved in cell-shape maintenance, nervous system cytoarchitecture, mechanical stability, and synaptic function [36]. On the other hand, it is well-known that Cx43 modulation is involved in neuronal development and plasticity [37] and that S100B is expressed and also secreted by astrocytes and can thus be an extracellular mediator of cell signalling [38]. This evidence supports the hypotheses that the microgravity can affect not only cell shape but also cell function.

In the S-aggregates, the modelled microgravity conditions did not have any significant effects on the localisation of N-CAM and tyrosine hydroxylase, but they were shown to induce a switch of the GAP43 protein from the neurite-like processes to the cytoplasmic compartment. In addition, the microgravity induced a slight, although not significant, decrease in the expression levels of GAP43 and tyrosine hydroxylase, while it had no effect on the expression of the N-CAM-180 isoform but significantly increased the expression of the N-CAM-140 isoform, which has been shown to have a key role in neuronal survival and signal transduction [39, 40]. This suggests the involvement of N-CAM-140 during this modelled microgravity exposure that could promote a significant degree of neuronal remodelling and survival.

It has been previously reported that, in neuro/glial cocultures, the neurons induce a reduction in astrocyte proliferation [41]. In particular, this effect was mediated by membrane-membrane interactions between the neurons and the astroglia *in vitro* and raised the possibility that membrane

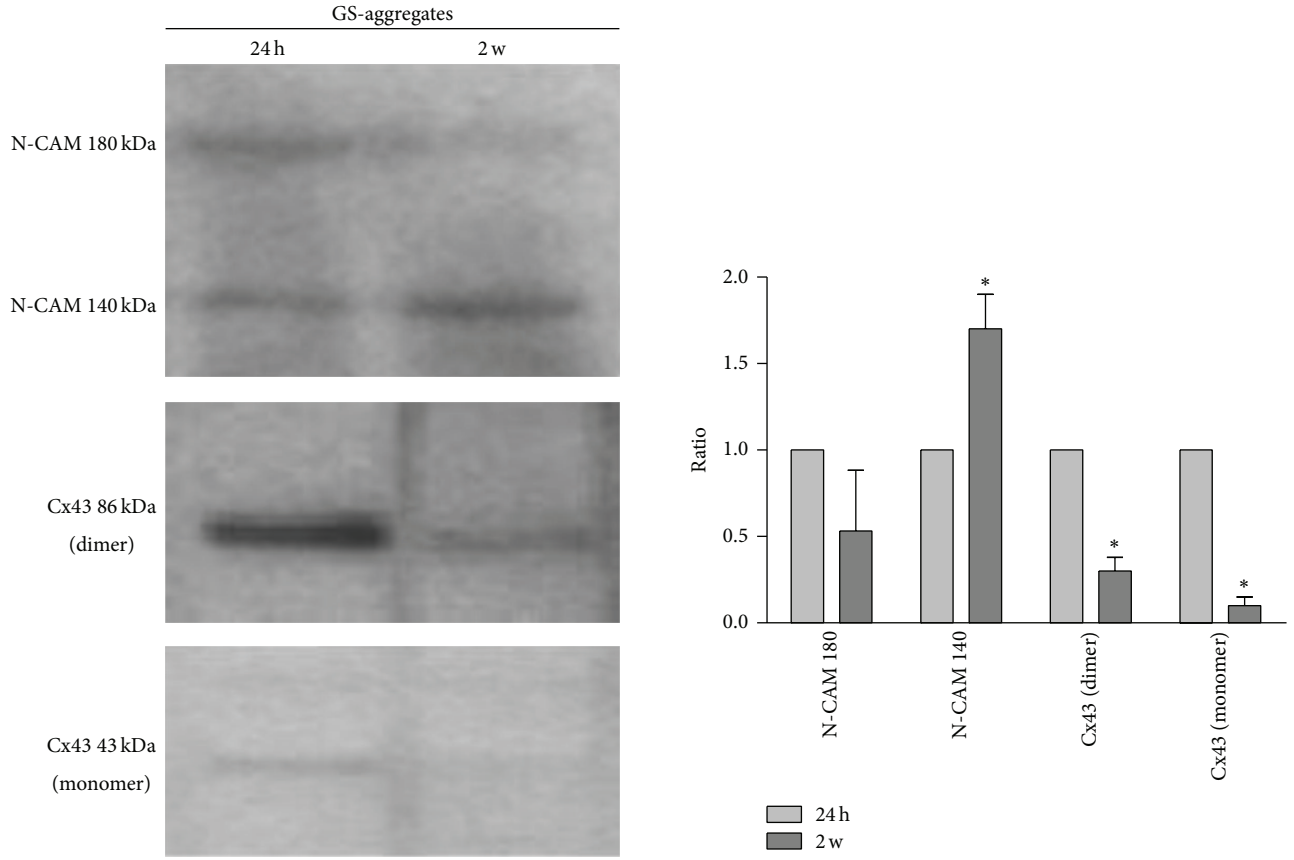

Figure 10: Expression levels of functional markers in the GS-aggregates. Representative Western blotting and quantification of the levels of N-CAM and Cx43 in GS-aggregates cultured in the RCCS bioreactor for 24 h and 2 weeks (2 w). Data are densitometric ratio analyses as means ± SEM from 3 independent experiments. $^{*}P < 0.05$, for 2-week versus respective 24 h cultures.

elements involved in glial cell growth regulation include neuron-glial interaction molecules [41]. In our neuron-like and glial-cell-like coculture, we focused our attention on N-CAM and Cx43 expression, as these participate in important intercellular signal interactions. The GL15 cells used here did not express N-CAM isoforms (data not shown), and the immunofluorescence signals might reveal SH-SY5Y homotypic interactions, even if N-CAM heterotypic interactions could not be excluded (such as N-CAM-integrins). However the N-CAM expression pattern in homogenates from GS-aggregates resembled that for the S-aggregates, with an increase in the expression of N-CAM-140, one of the three main isoforms of N-CAM that is implicated in regeneration and remodelling of the nervous system [42].

Gap-junction-mediated intercellular communication among astrocytes has long been thought to contribute to tissue homeostasis in the brain [43]. Cx43 has been used as a marker to investigate neuron-glia interactions [22]. Astrocytes express Cx30 and Cx43, which can form homotypic (Cx43/Cx43 and Cx30/Cx30), but not heterotypic, junctions [44]. Interestingly, in the homogenates from the GS-aggregates, in addition to the classical 43 kDa form of Cx43, a dimeric form of Cx43 (i.e., 86 kDa) was also expressed. This Cx43 dimeric form has been related to stress conditions. In other models, oxidative stress status has been related to the appearance of such a higher molecular weight band for Cx43, which suggests that this represents an aggregated form of Cx43 [45]. Under our conditions, the presence of this dimeric form of Cx43 might reveal a first phase of impact between the neuronal-like and the glial-like phenotypes; subsequently, these Cx43 forms significantly decreased when the GS-aggregates reached dynamic adaptive conditions.

5. Conclusions

In conclusion, the evidence presented here suggests that the 3D laminar flow, the high mass transfer, and the low shear-stress microenvironment generated by the RCCS bioreactor represent optimal conditions for the well-being of monotypic neural-like and glial-like cells, as well as for heterotypic aggregates, and for long-term culture. Moreover, such model system can reproduce 3D cell-cell interactions that are similar to those under *in vivo* conditions [46] and can mimic the microgravity conditions of exposure. Our data highlight how some phenotypic markers of monotypic and heterotypic neuro/glia culture models can be influenced by microgravity.

The data presented here open a wide range of specific investigations in terms of cell transduction pathways, cell-cell interactions and signalling, and heterotypic culture biology, and the cell models we have described and analysed here represent important tools in the study of *in vitro* biological and pathological processes of the nervous system.

Conflict of Interests

The authors declare that there is no conflict of interests regarding the publication of this paper.

Authors' Contribution

Caterina Morabito and Nathalie Steimberg equally contributed to this study.

Acknowledgments

The authors wish to thank Jennifer Boniotti (UNIBS) for technical support. This study was supported by ASI 2013 Dec 134/2013 to MAM and by G. d'Annunzio University research funds to MAM.

References

[1] G. Vunjak-Novakovic, N. Searby, J. de Luis, and L. E. Freed, "Microgravity studies of cells and tissues," *Annals of the New York Academy of Sciences*, vol. 974, pp. 504–517, 2002.

[2] A.-M. Duprat, D. Husson, and L. Gualandris-Parisot, "Does gravity influence the early stages of the development of the nervous system in an amphibian?" *Brain Research Reviews*, vol. 28, no. 1-2, pp. 19–24, 1998.

[3] B. M. Uva, M. A. Masini, M. Sturla et al., "Microgravity-induced apoptosis in cultured glial cells," *European Journal of Histochemistry*, vol. 46, no. 3, pp. 209–214, 2002.

[4] G. Pani, N. Samari, R. Quintens et al., " Morphological and physiological changes in mature in vitro neuronal networks towards exposure to short-, middle- or long-term simulated microgravity," *PLOS ONE*, vol. 8, no. 9, Article ID e73857, 2013.

[5] R. Gruener and G. Hoeger, "Vector-averaged gravity alters myocyte and neuron properties in cell culture," *Aviation Space and Environmental Medicine*, vol. 62, no. 12, pp. 1159–1165, 1991.

[6] H. Rösner, T. Wassermann, W. Möller, and W. Hanke, "Effects of altered gravity on the actin and microtubule cytoskeleton of human SH-SY5Y neuroblastoma cells," *Protoplasma*, vol. 229, no. 2–4, pp. 225–234, 2006.

[7] A. Crestini, C. Zona, P. Sebastiani et al., "Effects of simulated microgravity on the development and maturation of dissociated cortical neurons," *In Vitro Cellular & Developmental Biology–Animal*, vol. 40, no. 5-6, pp. 159–165, 2004.

[8] L. Lossi, S. Alasia, C. Salio, and A. Merighi, "Cell death and proliferation in acute slices and organotypic cultures of mammalian CNS," *Progress in Neurobiology*, vol. 88, no. 4, pp. 221–245, 2009.

[9] K. Rambani, J. Vukasinovic, A. Glezer, and S. M. Potter, "Culturing thick brain slices: an interstitial 3D microperfusion system for enhanced viability," *Journal of Neuroscience Methods*, vol. 180, no. 2, pp. 243–254, 2009.

[10] L. E. Freed and G. Vunjak-Novakovic, "Spaceflight bioreactor studies of cells and tissues," *Advances in Space Biology and Medicine*, vol. 8, pp. 177–195, 2002.

[11] D. A. Wolf and R. P. Schwarz, "RP: analysis of gravity-induced particle motion and fluid perfusion flow in the NASA-designed rotating zero-heaed-space tissue culture vessel," NASA Technical Paper 3143, 1991.

[12] C. M. Begley and S. J. Kleis, "The fluid dynamic and shear environment in the NASA/JSC rotating-wall perfused-vessel bioreactor," *Biotechnology and Bioengineering*, vol. 70, no. 1, pp. 32–40, 2000.

[13] T. G. Hammond and J. M. Hammond, "Optimized suspension culture: the rotating-wall vessel," *The American Journal of Physiology—Renal Physiology*, vol. 281, no. 1, pp. F12–F25, 2001.

[14] P. S. Ayyaswamy and K. Mukundakrishnan, "Optimal conditions for simulating microgravity employing NASA designed rotating wall vessels," *Acta Astronautica*, vol. 60, no. 4–7, pp. 397–405, 2007.

[15] V. Bocchini, T. Beccari, C. Arcuri, L. Bruyere, C. Fages, and M. Tardy, "Glial fibrillary acidic protein and its encoding mRNA exhibit mosaic expression in a glioblastoma multiform cell line of clonal origin," *International Journal of Developmental Neuroscience*, vol. 11, no. 4, pp. 485–492, 1993.

[16] M. A. Mariggio, G. Mazzoleni, T. Pietrangelo et al., "Calcium-mediated transductive systems and functionally active gap junctions in astrocyte-like GL15 cells," *BMC Physiology*, vol. 1, no. 1, article 4, 2001.

[17] Y.-T. Cheung, W. K.-W. Lau, M.-S. Yu et al., "Effects of all-*trans*-retinoic acid on human SH-SY5Y neuroblastoma as *in vitro* model in neurotoxicity research," *NeuroToxicology*, vol. 30, no. 1, pp. 127–135, 2009.

[18] S. Guarnieri, R. Pilla, C. Morabito et al., "Extracellular guanosine and GTP promote expression of differentiation markers and induce S-phase cell-cycle arrest in human SH-SY5Y neuroblastoma cells," *International Journal of Developmental Neuroscience*, vol. 27, no. 2, pp. 135–147, 2009.

[19] M. Miloso, D. Villa, M. Crimi et al., "Retinoic acid-induced neuritogenesis of human neuroblastoma SH-SY5Y cells is ERK independent and PKC dependent," *Journal of Neuroscience Research*, vol. 75, no. 2, pp. 241–252, 2004.

[20] S. Pahlman, J. C. Hoehner, E. Nanberg et al., "Differentiation and survival influences of growth factors in human neuroblastoma," *European Journal of Cancer Part A: General Topics*, vol. 31, no. 4, pp. 453–458, 1995.

[21] T. Fellin, "Communication between neurons and astrocytes: relevance to the modulation of synaptic and network activity," *Journal of Neurochemistry*, vol. 108, no. 3, pp. 533–544, 2009.

[22] A. Vernadakis, "Glia-neuron intercommunications and synaptic plasticity," *Progress in Neurobiology*, vol. 49, no. 3, pp. 185–214, 1996.

[23] G. Mazzoleni, D. Di Lorenzo, and N. Steimberg, "Modelling tissues in 3D: the next future of pharmaco-toxicology and food research?" *Genes and Nutrition*, vol. 4, no. 1, pp. 13–22, 2009.

[24] N. Steimberg, J. Boniotti, and G. Mazzoleni, "3D culture of primary chondrocytes and bone/cartilage tissue explants in simulated microgravity," in *Methods in Bioengineering: Alternative Technologies to Animal Testing*, M. Yarmush and R. Langer, Eds., Artech House, 2010.

[25] D. A. Goodenough and D. L. Paul, "Gap junctions," *Cold Spring Harbor Perspectives in Biology*, vol. 1, no. 1, Article ID a002576, 2009.

[26] M. I. Mosevitsky, "Nerve ending "signal" proteins GAP-43, MARCKS, and BASP1," *International Review of Cytology*, vol. 245, pp. 245–325, 2005.

[27] D. A. Lewis, D. S. Melchitzky, and J. W. Haycock, "Four isoforms of tyrosine hydroxylase are expressed in human brain," *Neuroscience*, vol. 54, no. 2, pp. 477–492, 1993.

[28] I. B. Krasnov, "Gravitational neuromorphology," *Advances in Space Biology and Medicine*, vol. 4, pp. 85–110, 1994.

[29] X. Chen, H. Xu, C. Wan, M. McCaigue, and G. Li, "Bioreactor expansion of human adult bone marrow-derived mesenchymal stem cells," *Stem Cells*, vol. 24, no. 9, pp. 2052–2059, 2006.

[30] G. Mazzoleni, F. Boukhechba, N. Steimberg, J. Boniotti, J. M. Bouler, and N. Rochet, "Impact of dynamic culture in the RCCSTM bioreactor on a three-dimensional model of bone matrix formation," *Procedia Engineering*, vol. 10, pp. 3670–3675, 2011.

[31] B. R. Unsworth and P. I. Lelkes, "Growing tissues in microgravity," *Nature Medicine*, vol. 4, no. 8, pp. 901–907, 1998.

[32] P. Humphreys, S. Jones, and W. Hendelman, "Three-dimensional cultures of fetal mouse cerebral cortex in a collagen matrix," *Journal of Neuroscience Methods*, vol. 66, no. 1, pp. 23–33, 1996.

[33] G. Moretto, N. Brutti, V. de Angelis, C. Arcuri, and V. Bocchini, "A time-dependent increase in glial fibrillary acidic protein expression and glutamine synthetase activity in long-term subculture of the GL15 glioma cell line," *Cellular and Molecular Neurobiology*, vol. 17, no. 5, pp. 509–519, 1997.

[34] T. Nakase and C. C. G. Naus, "Gap junctions and neurological disorders of the central nervous system," *Biochimica et Biophysica Acta—Biomembranes*, vol. 1662, no. 1-2, pp. 149–158, 2004.

[35] M. L. Cotrina, J. H.-C. LIN, and M. Nedergaard, "Adhesive properties of connexin hemichannels," *Glia*, vol. 56, no. 16, pp. 1791–1798, 2008.

[36] V. Menet, M. Gimenez Y Ribotta, N. Chauvet et al., "Inactivation of the glial fibrillary acidic protein gene, but not that of vimentin, improves neuronal survival and neurite growth by modifying adhesion molecule expression," *Journal of Neuroscience*, vol. 21, no. 16, pp. 6147–6158, 2001.

[37] R. Rozental, M. Srinivas, S. Gökhan et al., "Temporal expression of neuronal connexins during hippocampal ontogeny," *Brain Research Reviews*, vol. 32, no. 1, pp. 57–71, 2000.

[38] R. Donato, G. Sorci, F. Riuzzi et al., "S100B's double life: intracellular regulator and extracellular signal," *Biochimica et Biophysica Acta*, vol. 1793, no. 6, pp. 1008–1022, 2009.

[39] M. A. Mariggiò, C. Morabito, S. Guarnieri, A. Gentile, K. Kolkova, and G. Fanò, "IgIII (270-280)-fragment-like H_2N-DDSDEEN-COOH peptide modulates N-CAM expression via Ca^{2+}-dependent ERK signaling during "in vitro neurogenesis"," *Peptides*, vol. 29, no. 9, pp. 1486–1497, 2008.

[40] P. S. Walmod, K. Kolkova, V. Berezin, and E. Bock, "Zippers make signals: NCAM-mediated molecular interactions and signal transduction," *Neurochemical Research*, vol. 29, no. 11, pp. 2015–2035, 2004.

[41] M. E. Hatten, "Neuronal inhibition of astroglial cell proliferation is membrane mediated," *Journal of Cell Biology*, vol. 104, no. 5, pp. 1353–1360, 1987.

[42] L. C. B. Rønn, V. Berezin, and E. Bock, "The neural cell adhesion molecule in synaptic plasticity and ageing," *International Journal of Developmental Neuroscience*, vol. 18, no. 2-3, pp. 193–199, 2000.

[43] M. Theis, G. Sohl, J. Eiberger, and K. Willecke, "Emerging complexities in identity and function of glial connexins," *Trends in Neurosciences*, vol. 28, no. 4, pp. 188–195, 2005.

[44] J. L. Orthmann-Murphy, M. Freidin, E. Fischer, S. S. Scherer, and C. K. Abrams, "Two distinct heterotypic channels mediate gap junction coupling between astrocyte and oligodendrocyte connexins," *Journal of Neuroscience*, vol. 27, no. 51, pp. 13949–13957, 2007.

[45] C. M. L. Hutnik, C. E. Pocrnich, H. Liu, D. W. Laird, and Q. Shao, "The protective effect of functional connexin43 channels on a human epithelial cell line exposed to oxidative stress," *Investigative Ophthalmology and Visual Science*, vol. 49, no. 2, pp. 800–806, 2008.

[46] E. Fennema, N. Rivron, J. Rouwkema, C. van Blitterswijk, and J. de Boer, "Spheroid culture as a tool for creating 3D complex tissues," *Trends in Biotechnology*, vol. 31, no. 2, pp. 108–115, 2013.

Hindawi Publishing Corporation
BioMed Research International
Volume 2015, Article ID 434803, 13 pages
http://dx.doi.org/10.1155/2015/434803

Review Article

The Impact of Microgravity and Hypergravity on Endothelial Cells

Jeanette A. M. Maier,[1] Francesca Cialdai,[2] Monica Monici,[2] and Lucia Morbidelli[3]

[1] *Department of Biomedical and Clinical Sciences "L. Sacco", Università di Milano, Via Gian Battista Grassi 74, 20157 Milan, Italy*
[2] *ASAcampus Joint Laboratory, ASA Research Division, Department of Experimental and Clinical Biomedical Sciences "M. Serio", University of Florence, Viale Pieraccini 6, 50139 Florence, Italy*
[3] *Department of Life Sciences, University of Siena, Via A. Moro 2, 53100 Siena, Italy*

Correspondence should be addressed to Lucia Morbidelli; morbidelli@unisi.it

Received 4 July 2014; Revised 20 October 2014; Accepted 4 November 2014

Academic Editor: Jack J. W. A. Van Loon

The endothelial cells (ECs), which line the inner surface of vessels, play a fundamental role in maintaining vascular integrity and tissue homeostasis, since they regulate local blood flow and other physiological processes. ECs are highly sensitive to mechanical stress, including hypergravity and microgravity. Indeed, they undergo morphological and functional changes in response to alterations of gravity. In particular microgravity leads to changes in the production and expression of vasoactive and inflammatory mediators and adhesion molecules, which mainly result from changes in the remodelling of the cytoskeleton and the distribution of caveolae. These molecular modifications finely control cell survival, proliferation, apoptosis, migration, and angiogenesis. This review summarizes the state of the art on how microgravity and hypergravity affect cultured ECs functions and discusses some controversial issues reported in the literature.

1. The Endothelium

The concept of endothelium as an inert barrier lining the inner side of blood vessels has been overcome by the finding that the endothelium is a dynamic, heterogeneous, and disseminated organ which orchestrates blood vessel and circulatory functions, thus exerting a critical role for tissue homeostasis. Indeed, the endothelial cells (ECs) possess essential secretory, synthetic, metabolic, and immunologic activities [1, 2].

The endothelium is semipermeable and regulates the transport of various molecules between the blood and underlying interstitial space by expressing specific carriers. ECs also control vascular permeability, especially in microvascular districts. Moreover, ECs importantly contribute to maintaining a nonthrombogenic blood-tissue interface since they release various antithrombotic and fibrinolytic factors as well as molecules that impact on platelets [1, 2].

The endothelium is an immunocompetent organ because it exposes histocompatibility and blood group antigens can be induced to express adhesion molecules for leukocytes and produce cytokines. Finally, a functional relation exists between endothelial and smooth muscle cells, as a consequence of the presence of junctions allowing the passage of electric charges and metabolites, and the production and release of vasoactive mediators [1, 2]. Indeed, ECs finely control vasomotor responses through the production and metabolism of vasoactive molecules acting on smooth muscle cells, as endothelin-1 (ET-1), nitric oxide (NO), and angiotensin II (AngII). They also tightly control smooth muscle cells proliferation [1, 2]. ECs are protagonists in angiogenesis, that is, the formation of new blood vessels from preexisting ones. Angiogenesis involves the most dynamic functions of the endothelium, since it requires the migration of ECs, their ability to degrade the extracellular matrix, their proliferation and differentiation, ultimately leading to functional capillaries [3]. This highly organised process is modulated by the balance between stimulators and inhibitors of angiogenesis.

Vascular endothelium is structurally and functionally heterogeneous [4]. This heterogeneity is detectable at

different levels, that is, markers of cell activation, gene expression, responsiveness to growth factors, and antigen composition, and differentiates the behaviour between micro- and macrovascular ECs, as well as between cells isolated from different organs and from different vascular districts of the same organ. In fact, the arteriolar endothelium is different from the venous one, as well as from the micro- and macrovessel derived ECs. The endothelium of the cerebral circulation—which is the main component of the blood-brain barrier to protect the brain from toxic substances—deserves special consideration. It is continuous, has tight junctions, and differs both from fenestrated endothelium, where cells have pores, and from discontinuous endothelium, where cells have intracellular and transcellular discontinuities [2].

ECs are normally quiescent *in vivo* with a turnover rate of approximately once every three years [5]. Most of ECs in the adult have a cell cycle variable from months to years, unless injury to the vessel wall or angiogenesis occurs. Only endothelium from endometrium and corpus luteum has a doubling time of weeks.

ECs act as mechanotransducers, whereby the transmission of external forces induces various cytoskeletal changes and activates second messenger cascades, which, in turn, may act on specific response elements of promoter genes. Therefore, it is not surprising that ECs are sensitive to variations of gravity.

2. Methods to Simulate Microgravity and Hypergravity on Earth

Gravity is exerted permanently on organisms which are in constant orientation in the gravity field (static stimulation) and if their orientation is changed with respect to the gravity vector (dynamic stimulation) [6].

The only way to achieve real microgravity is to use parabolic flights, rockets, space crafts, or space labs as available on the International Space Station (ISS). However, the possibility to perform experiments in real microgravity is limited because of high costs and the limited number of missions. On the other hand, the short duration of microgravity conditions achieved by using parabolic flights or rockets limits the studies of many complex and prolonged biological processes. Therefore, many efforts have been made to establish methods to simulate microgravity on Earth. All the devices available, however, mimic only some aspects of real microgravity.

2.1. Clinostat. Clinostats are considered reasonably effective ground-based tools for simulating microgravity [7–10] and have been used to study the effects of microgravity [11–19].

The clinostat randomizes motion and theoretically reduces the uniform gravity influence. In the more widely diffuse design, that is, the random positioning machine (RPM), the clinostat consists of an inner chamber containing the samples which rotate clockwise, anticlockwise, vertically, and horizontally. The horizontal and vertical motions are provided by an outer chamber. All the chambers are operated by small motors under computer control. The cells are grown in cell chambers or in flasks filled completely with media, thus diminishing the likelihood of turbulence and shear forces during culture rotation. When using the clinostat to simulate microgravity, the shear stress and vibrations generated by the clinostat must be taken into account. Shear stress can be limited by completely filling the chamber with the culture medium. Parallel controls are necessary to eliminate the effects of vibrations. It is also important to consider the distance of the samples from the centre of the platform, where the maximal reduction of gravity occurs. Another important parameter to monitor is the speed of rotation. It has been verified that the effects of clinostat-determined microgravity are similar to those obtained in space labs [8–19].

2.2. Rotating Wall Vessel Bioreactor. This device was developed at NASA's Johnson Space Center to simulate the effects of microgravity on cells in a ground-based culture system. The bioreactor, the rotating wall vessel (RWV)/rotating cell culture system (RCCS) from Synthecon (http://www.synthecon.com/), is a cylindrical vessel that maintains cells in suspension by slow rotation around its horizontal axis with a coaxial tubular silicon membrane for oxygenation. Adherent cells need to be cultured on beads. This system represents a new cell culture technology developed for 3D cultures of different cell types and biotechnological applications. The vessel wall and the medium containing cells bound to microcarrier beads or 3D cultures rotate at the same speed, producing a vector-averaged gravity comparable with that of near-Earth free-fall orbit [20]. Most results obtained using the RWV were confirmed by experiments in real microgravity [12, 21–23].

2.3. Magnetic Levitation. This is a relatively novel Earth-based simulation technique used to investigate the biological response to weightlessness. Magnetic levitation takes place when the magnetic force counterbalances the gravitational force. Under this condition, a diamagnetic sample is in a simulated microgravity environment. However, the magnetic field which is generated affects cell behaviour, therefore confounding the effects of simulated microgravity. Mouse osteoblastic MC3T3-E1 cultured in a superconducting magnet for 2 days showed marked alterations of gene expression [24]. Random rotation and magnetic levitation induced similar changes in the actin of A431 cells that were also described in real microgravity [25]. At the moment, however, no studies are available on ECs under magnetic levitation, but they should be fostered as levitation as an alternative to simulate microgravity might yield novel information or confirm previous data, thereby helping in designing successful experiments in real microgravity.

2.4. Models to Generate Hypergravity. Variation in gravity exposure is also related to hypergravity, as the one to which the astronauts are transiently exposed during launch and return to Earth. Also military pilots and subjects engaged

in certain sports such as motor racing, motorcycling, bobsledding, and the luge experience hypergravity. The comparison among the conditions of microgravity, normogravity (1 ×g), and hypergravity may be helpful to understand the mechanisms underlying the effects of gravitational alterations on endothelial function and to understand what happens when humans quickly pass from hypergravity to microgravity conditions and vice versa.

Centrifuges constructed for research under hypergravity conditions are characterized by high precision control of rpm. Their speed and the angle of inclination of the sample can be regulated to obtain the desired hypergravity in a range from 1 to many g. Centrifuges are also used to perform 1 ×g control experiments on board of the ISS and spacecraft. Studies on endothelial cells in hypergravity are available [12, 26, 27].

3. The Effects of Microgravity on ECs

Exposure to microgravity during space missions impacts on various systems. In humans microgravity-induced alterations include bone loss, muscle atrophy, cardiovascular deconditioning, impairment of pulmonary function, and immune response [50, 51]. The cardiovascular system is affected by spaceflight, with changes manifesting as cardiac dysrhythmias, cardiac atrophy, orthostatic intolerance, and reduced aerobic capacity [52]. These changes can cause adaptation problems when astronauts return back to Earth, especially after long-duration spaceflights [53].

Because ECs are key players in the maintenance of vascular integrity, inflammation, and angiogenesis, several studies have been devoted to the mechanisms by which microgravity affects EC functions.

Various reports have indicated that ECs are highly sensitive to microgravity and undergo morphological, functional, and biochemical changes under these conditions [11, 12, 23, 28, 29, 37, 38, 46, 49, 54]. These studies have used a variety of *in vitro* cell models with divergent results. One of the reasons for these discrepancies can be EC heterogeneity or the isolation from different species. Indeed, human, bovine, murine, and porcine endothelial cells have been investigated under gravitational unloading. With concern to human cells, studies are available on human ECs from the umbilical vein (HUVEC), widely considered a model of macrovascular endothelial cells, as well as on human microvascular ECs (HMEC). Moreover, studies have been performed on EA.hy926 cells, a fusion of HUVEC with the lung carcinoma cell line A549 [55]. Although immortalized cell lines offer significant logistical advantages over primary cells in *in vitro* studies, they exhibit important differences when compared to their primary cell counterparts. Indeed, microarrays used for a genome-wide comparison between HUVEC and EA.hy926 in their baseline properties have shown that EA.hy926 cells are useful in studies on genes encoding molecules involved in regulating thrombohemorrhagic features, while they appear to be less suited for studies on the regulation of cell proliferation and apoptosis [56]. Moreover, immortalized endothelial cell lines show different expression pattern of biomarkers when compared to primary cells [57]. The controversial results reported about the response of ECs to microgravity could be due also to the diverse experimental approaches utilized, such as the device simulating microgravity, the duration of exposure to simulated microgravity, and the degree of reduction of the gravity that can be reached operating these devices differently (see above). Nevertheless, altered EC morphology, cell membrane permeability and senescence are documented by spaceflight experiments on cultured endothelium [21, 30, 58].

Several aspects of endothelial behaviour have been studied in simulated and real microgravity. Table 1 summarizes the published findings.

3.1. Migration. Controversy exists on this topic. No significant modulation of cell migration under basal condition and in response to the angiogenic factor hepatocyte growth factor (HGF) was observed in HUVEC as well as in HMEC cultured in the RPM [12, 46]. Shi et al. [39] demonstrated that, after 24 h of exposure to simulated microgravity in a clinostat, HUVEC migration was significantly promoted through the eNOS pathway upregulation by means of PI3K-Akt signalling. On the contrary, the endothelial cell line EA.hy926 in simulated microgravity migrated more than controls [31], while in a study on porcine aortic endothelial cells (PAEC), microgravity modelled by a RPM caused a marked impairment of cell migration induced by serum or the angiogenic factors vascular endothelial growth factor (VEGF) and fibroblast growth factor-2 (FGF-2) [11].

3.2. Proliferation and Formation of 3D Structures. Carlsson and Versari, using the RWV and the RPM, respectively, found that the proliferation rate of HUVECs was reversibly increased under simulated microgravity [12, 28]. Also bovine aortic ECs (BAEC) grew faster in the RWV than controls [35]. On the contrary, simulated microgravity inhibited the growth of HMEC and murine microvascular ECs [23, 46]. The results obtained using microvascular EC are reinforced by the *in vivo* finding showing an impairment of angiogenesis in space. Wound healing, in which neovascularization is an early and fundamental step, is retarded in space-flown animal models [59], and the development of vascular channels in a rat fibular osteotomy model is inhibited after flight, as shown by an experiment carried out during a shuttle mission [60].

Also in PAECs a marked impairment of EC responsiveness to angiogenic factors and a reduced ability to proliferate were reported [11]. Using the endothelial cell line EA.hy926, Grimm et al. [43] showed the formation of 3D tubular structures in clinorotation. After two weeks, a subtype of 3D aggregates was observed with a central lumen surrounded by one layer of ECs. These single-layered tubular structures resembled the intimas of blood vessels. Characterization of these tubular structures revealed that they might originate from double-row cell assemblies formed between the fifth and seventh day of culture under simulated microgravity [43].

3.3. Apoptosis. Increased apoptosis after culture in the RPM has been observed in PAEC and the endothelial cell line

Table 1: The effects of real or simulated microgravity on different endothelial cell types.

Experimental model	Experimental conditions	Effects	Authors
Primary human umbilical vein ECs (HUVEC)	Rotating wall vessel (RWV) Random positioning machine (RPM) 48 or 96 h	Growth stimulation ↑ NO production Actin remodelling ↓ Actin ↑ Thioredoxin-interacting protein ↓ hsp-70 and 90	Versari et al., 2007 [12]
	Spaceflight (Progress 40P mission) 10 d	↑ secretion of IL-1α and IL-1β Ion channels (TPCN1, KCNG2, KCNJ14, KCNG1, KCNT1, TRPM1, CLCN4, CLCA2), mitochondrial oxidative phosphorylation, and focal adhesion were widely affected	Versari et al., 2013 [21]
	RWV 72 h or 96 h	↑ PGI2 and NO	Carlsson et al., 2002 [22]
	RPM 24–48 h	↑ NO ↑ Cav-1 phosphorylation (Tyr 14) ↑↑ hsp70	Spisni et al., 2006 [26]
	RWV 4, 24, 48, 96, 144 h	↓ IL-1α Remodelling of cytoskeleton ↓ actin	Carlsson et al., 2003 [28]
	RPM 24 h	↑ eNOS, Cav-1 and -2 ↓ of the length and width of the cells ↓ ICAM-1, VCAM-1, E-selectin, and IL-6 and TNF-α	Grenon et al., 2013 [29]
	Spaceflight 12 d	Cytoskeletal damage ↑ cell membrane permeability In readapted cells: persisting cytoskeletal changes ↓ metabolism and cell growth	Kapitonova et al., 2012 [30]
	2D-Clinostat (developed by China Astronaut Research and Training Center) 30 rpm, 24 h	↑ HUVEC tube formation and migration ↓ number of caveolae in the membrane ↑ eNOS activity by phosphorylation of Akt and eNOS ↑ ICAM-1 expression	Siamwala et al., 2010 [31]
	RWV 5 min, 30 min, 1 h, and 24 h	Depolymerization of F-actin and clustering of ICAM-1 on cell membrane (short term) Actin fiber rearrangement and stable clustering of ICAM-1 (after 24 h) ↑ ICAM-1 and VCAM-1 RNA after 30 min	Zhang et al., 2010 [32]
	RPM 96 h	Alteration of proteins regulating cytoskeleton assembly ↓ IL-1α, IL-8, and bFGF ↑ chemokines Rantes and Eotaxin, involved in leukocytes recruitment	Griffoni et al., 2011 [33]
	RPM 24 h	↑ iNOS by a mechanism dependent on suppression of AP-1	Wang et al., 2009 [34]

Table 1: Continued.

Experimental model	Experimental conditions	Effects	Authors
Bovine aortic ECs (BAEC)	RWV for up to 30 d	Growth stimulation ↑ NO Production of NO dependent on the RWV rotation rate: 73% increase at 8 rpm, 262% increase at 15 rpm, and 500% increase at 20 rpm	Sanford et al., 2002 [35]
Porcine aortic ECs (PAEC)	RPM 72 h	↑ proapoptotic genes (p53, FAS-L, BAX) ↓ antiapoptotic genes (Bcl-2) Dissolution of mitochondrial membrane integrity Impairment of cell responsiveness to exogenous stimuli	Morbidelli et al., 2005 [11]
Bovine coronary venular ECs (CVEC)	RPM 72 h	↑ Fibronectin (formation of intricate network of FN fibers) ↑ Laminin ↑ β-Actin (formation of stress fibers) ↑ $\alpha\beta$-Integrin (formation of clusters)	Monici et al., 2011 [36]
Human EC line EA.hy926	RPM 10 days	↑ Caspase-3, Bax, and Bcl-2 ↑ collagen types I and III Alterations of the cytoskeletal α- and β-tubulins and F-actin ↓ brain-derived neurotrophic factor, platelet tissue factor, VEGF, and ET-1	Infanger et al., 2007 [37]
	RPM 7 days	Modulation of genes encoding for signal transduction and angiogenic factors, cell adhesion, membrane transport proteins, or enzymes involved in serine biosynthesis	Ma et al., 2013 [38]
	RPM 2 h	↑ cellular migration ↑ filopodia and lamellipodia Actin rearrangements	Shi et al., 2012 [39]
	RPM 4, 12, 24, 48, and 72 h	↑ NO ↑ extracellular matrix (ECM) proteins Alteration in cytoskeletal components ↑ expression of ECM proteins (collagen type I, fibronectin, osteopontin, laminin) and flk-1 protein Morphological and biochemical signs of apoptosis after 4 h, further increasing after 72 h	Infanger et al., 2006 [40]
	Parabolic flight (22 s microgravity, 1.8 xg 2 periods of 20 s)	*Parabolic flight* ↓ COL4A5, COL8A1, ITGA6, ITGA10, and ITGB3 mRNAs after P1 (first parabolas) ↑ EDN1 and TNFRSF12A mRNAs after P1 ↓ ADAM19, CARD8, CD40, GSN, PRKCA mRNAs ↑ PRKAA1 (AMPKα1) mRNAs cytoplasmic rearrangement ↑↑ ABL2 after P1 and P31	Grosse et al., 2012 [41]
	Parabolic flight (22 s microgravity, 1.8 xg 2 periods of 20 s)	*Parabolic flight* Actin network rearrangement ↑ CCNA2, CCND1, CDC6, CDKN1A, EZR, MSN, OPN, VEGFA, CASP3, CASP8, ANXA1, ANXA2, and BIRC5 ↓ FLK1 ↑ EZR, MSN, OPN, ANXA2, and BIRC5 after 31P	Wehland et al., 2013 [42]

Table 1: Continued.

Experimental model	Experimental conditions	Effects	Authors
	RPM 7, 14, 21, and 28 d	Different responsiveness to VEGF and bFGF added exogenously Altered gene and protein expression of phosphokinase A catalytic subunit, phosphokinase C alpha, and ERK-1 and 2 ↓ VEGF, bFGF, soluble TNFRSF5, TNFSF5, ICAM-1, TNFR 2, IL-18, complement C3, and von Willebrand factor	Grimm et al., 2010 [43]
	RPM 7 and 28 d	Delayed 3D cell growth; ↑ beta(1)-integrin, laminin, fibronectin, α-tubulin in tube-like structures after 4 weeks of culturing	Grimm et al., 2009 [44]
Human EC line EA.hy926 Bovine lung microvascular ECS Bovine pulmonary aortic ECs Porcine ventricular endocardial ECs	RPM 2 h	Results indicate that iNOS is a molecular switch for the effects of microgravity on different kinds of endothelial cells ↑ angiogenesis via the cyclic guanosine monophosphate (cGMP-) PKG dependent pathway	Siamwala et al., 2010 [45]
Human dermal microvascular cells (HMEC)	RWV, RPM 48 or 96 or 168 h	↑ TIMP-2 ↑ NO ↓ proteasome activity	Mariotti and Maier, 2008 [46]
Murine lung capillary ECs (1G11 cells)	RWV 72 h	↓ endothelial growth ↑ p21 ↓ IL-6 ↑ eNOS and NO	Cotrupi et al., 2005 [23]
Human pulmonary microvascular ECs (HPMECs)	MG-3 clinostat (developed by the Institute of Biophysics Chinese Academy of Sciences)	↑ apoptosis ↓ PI3K/Akt pathway ↑ NF-κB and depolymerization of F-actin	Kang et al., 2011 [47]
Human and bovine microvascular ECs	RWV 96 h	↑ hsp70 in cells which maintained the capability to proliferate in microgravity	Cotrupi and Maier 2004 [48]
Cocultures of endothelial monolayers, human lymphocytes, immune cells, and myeloleucemic (K-560) cells	Spaceflight (ISS)	↑ adhesion of PMA-activated lymphocytes Retained ability of immune cells to contact, recognize, and destroy oncogenic cells *in vitro*	Buravkova et al., 2005 [49]

Legend: ↑, increased; ↓, decreased.

EA.hy926 [11, 40]. In particular, following exposure to simulated hypogravity, PAEC change their morphology and gene expression pattern, triggering proapoptotic signals. The gene expression profile demonstrated the upregulation of p53, FAS-L, and BAX genes, and the concomitant downregulation of the antiapoptotic protein Bcl-2 and proliferation marker PCNA. The induction of apoptosis was accompanied by mitochondrial disassembly, thus suggesting the activation of the mitochondrial intrinsic pathways [11].

In pulmonary HMEC simulated microgravity-induced apoptosis by downregulating the PI3K/Akt pathways and increasing the expression of NFκB [47]. On the contrary, no apoptosis was observed in HUVEC and dermal HMEC cultured for various times in the RWV or in the RPM, and this has been linked to the rapid induction of heat shock protein (hsp)-70 [28, 46, 48]. Indeed, hsp-70 protects endothelial cells from apoptotic stimuli acting downstream of cytochrome c release and upstream of caspase 3.

3.4. Alterations of Cytoskeleton and Extracellular Matrix. The cytoskeleton plays a key role in the adaptation to mechanical stress, including alterations of gravity [61, 62]. Therefore, the changes that cytoskeletal components, such as microtubules, undergo in microgravity can be a key to explaining the effects of weightlessness on cells [63, 64].

Carlsson et al. [28] studied actin microfilaments in HUVEC exposed to microgravity simulated by the RWV. In comparison with controls, the cells showed elongated and extended podia, disorganization of actin microfilaments that clustered in the perinuclear area, and decrease in stress fibers. Moreover, after 96 h exposure, actin RNA levels were downregulated and total actin amounts were reduced. The cytoskeletal modifications were reversible upon return to normal growth conditions (1 ×g). The authors speculated that the reduction in actin amount could be an adaptive mechanism to avoid the accumulation of redundant actin fibers. The same results were obtained when the experiment was replicated by using a RPM to model the microgravity conditions [12]. More recently, in HUVEC exposed to mechanical unloading by RPM, Grenon et al. [29] found disorganization of the actin network with clustering of the fibers around the nucleus. Moreover, they observed that caveolin-1 was less associated with the plasma membrane and adopted a perinuclear localization. Thus the authors advanced the hypothesis that disruption of the actin cytoskeleton organization could impair the translocation of caveolin-1 to the caveolae.

After spaceflight (Soyuz TMA-11), readapted HUVEC cells with subsequent passages exhibited persisting changes in the organization of microtubules, with prominent bundles that occupied the peripheral cytoplasm [30].

In a study carried out by Zhang et al. [32] HUVEC activated with TNF-α and exposed to microgravity modelled by RWV demonstrated that, after 30 min, depolymerization of F-actin and clustering of ICAM-1 on cell membrane occurred. Moreover, ICAM-1 and VCAM-1 RNA were upregulated. After 24 h, actin fiber rearrangement was initiated, clustering of ICAM-1 became stable, and the mRNAs of ICAM-1 and VCAM-1 returned to levels comparable with the controls. The authors speculated that actin cytoskeleton rearrangement and changes in levels and distribution of surface adhesion molecules could significantly affect transendothelial migration processes.

Grosse et al. [41] studied the effect of parabolic flight on the cytoskeleton of the endothelial cell line EA.hy926. Every parabola (P) included two hypergravity (1.8 g) periods of 20 s, separated by a 22 s microgravity period. After P1, they observed a rearrangement of β-tubulin that accumulated around the nucleus. After P31, β-tubulin and vimentin were downregulated. Using the EA.hy926 cell line exposed to parabolic flight, Wehland et al. [42] reported that the actin network underwent a drastic rearrangement, mostly affected by vibration.

Grimm et al. [44] studied the walls of tube-like structures spontaneously formed by the endothelial cell line EA.hy926 cultured in a RPM. They found that the walls consisted of single-layered endothelial-like cells which had produced significantly more β_1-integrin, laminin (LM), fibronectin (FN), and α-tubulin than controls. Microgravity-induced upregulation of proteins involved in the extracellular matrix building was confirmed in studies carried out by Monici et al. [36] on cultured bovine coronary venular endothelial cells (CVECs) exposed for 72 h to microgravity modelled by a RPM. The authors observed an increase in actin content and impressive production of actin stress fibers, accompanied by the overexpression and clustering of β_1-integrin, 40% increase in LM, 111% increase in FN content, and formation of a tight and intricate network of FN fibrils.

Since FN and LM are strongly involved in the regulation of cell adhesion/migration, their upregulation and altered networking, together with the changes in actin and integrin patterns induced the authors to hypothesize that the exposure to microgravity causes a dysregulation in cell motility and adhesion to the substrate.

In summary, all of the studies carried out so far demonstrated that microgravity strongly affects cytoskeleton organization and induces a rearrangement of the actin network with clustering of the fibers in the perinuclear area. A similar behaviour has been observed also analysing the microtubule network. Moreover, clustering of adhesion molecules on the plasma membrane and overexpression of proteins of the extracellular matrix have been reported by some authors.

The results are less consistent when considering the expression of cytoskeleton proteins or their RNA. Probably the discrepancies are due to differences in experimental models (different cell populations), protocols, and analytical procedures.

However, it is widely accepted that the microgravity-induced changes in the cytoskeleton can strongly affect the behaviour of endothelial cells in terms of adhesion, migration, and production of extracellular matrix and can interfere with other processes such as translocation of molecules inside the cells, transendothelial migration, and even inflammation and angiogenesis.

3.5. Synthesis of Vasoactive Molecules. The levels of vasoactive molecules, such as NO, and ET-1 are modified under microgravity conditions, which also indicates that microgravity may influence both hemodynamic changes and angiogenesis [33, 37]. In particular, HUVEC and HMEC exposed to simulated microgravity using RWV and RPM produce more NO than controls as the result of increased levels of endothelial-nitric oxide synthase (e-NOS) [12], which correlates with the increase of caveolins [26, 29]. In particular, Grenon et al. suggested that the alterations in NO production are mediated by changes in the cytoskeleton detected in all the endothelial types studied [29]. Wang et al. [34] explained the increased amounts of NO in HUVEC after 24 h in simulated microgravity as the results of the upregulation of inducible NOS through a mechanism dependent on the suppression of the activity of the transcription factor AP-1. Also in BAEC NO production was increased [35].

In the endothelial cell line EA.hy926, a reduced release of ET-1 and VEGF was reported [37], while the production of NO was increased via the iNOS-cGMP-PKG pathway [39, 45]. If confirmed *in vivo* in space, these results might, in part, explain the hemodynamic changes and the redistribution of blood flows induced by microgravity.

3.6. Genomic and Proteomic Analysis. Microgravity affects several molecular features of ECs markedly modulating gene expression. In HUVEC cultured in the RPM, the secretome was evaluated by a 2D proteomic approach [33]. The proangiogenic factor FGF-2 and the proinflammatory cytokines interleukin-1 (IL-1) and IL-8 were decreased in simulated microgravity, whereas two chemokines involved in leukocyte recruitment, Rantes and Eotaxin, were increased [33]. The unprecedented gene profile analysis on HUVEC cultured on the ISS for 10 days was performed by Versari et al. [21]. 1023 genes were significantly modulated, the majority of which are involved in cell adhesion, oxidative phosphorylation, stress responses, cell cycle, and apoptosis, thioredoxin-interacting protein being the most upregulated. Briefly, in cultured HUVEC, real microgravity affects the same molecular machinery which senses alterations of flow and generates a prooxidative environment that alters endothelial function and promotes senescence [21]. Similar conclusions were reached by Kapitonova et al. [30, 58], who described premature senescence in space-flown HUVEC. By accelerating some aspects of senescence, microgravity offers a big challenge to study the mechanisms implicated in the onset of aging.

Looking at the endothelial cell line EA.hy926, a short term lack of gravity (22 s) generated by parabolic flights significantly influences the signalling pathways [41]. When these cells are cultured for various times from 4 to 72 h on the RPM, a number of proteins of the extracellular matrix implicated in apoptosis are modulated when compared to control cells [40]. In the RPM some EA.hy926 cells form tube-like 3D aggregates, while others continue to grow adherently. 3D aggregates and adherent cells were analyzed by gene array and PCR techniques and compared to controls [38]. 1625 differentially expressed genes were identified and, in particular, the levels of expression of 27 genes changed at least 4-fold in RPM-cultured cells when compared to controls. These genes code for angiogenic factors and proteins implicated in signal transduction, cell adhesion, membrane transport, or enzymes. Fifteen of them, with IL-8 and von Willebrand factor being the most affected, showed linkages to genes of 20 proteins that are important in the maintenance of cell structure and in angiogenesis.

EA.hy926 cell line and human dermal microvascular ECs (HMVECs) were then compared after culture on the RPM for 5 and 7 days [54]. A total of 1175 types of proteins were found in EA.hy926 cells and 846 in HMVECs, 584 of which were common and included metabolic enzymes, structure-related and stress proteins. This proteomic study also highlights that HMVECs develop tube-like 3D structures faster than EA.hy926 possibly through a transient augmentation of ribosomal proteins during the 3D assembling of ECs.

4. The Effects of Hypergravity on ECs

A summary of published data on endothelial cell behaviour is reported in Table 2. HUVECs exposed to hypergravity (3 ×g) for 24–48 h showed inhibition of cell growth but unaltered apoptosis, increased COX-2, eNOS, and Cav-1, suggesting a possible role of caveolae in mechanotransduction. Also an increased synthesis of PGI2 and NO, which are also proangiogenic, was observed. However, surprisingly, the formation of capillary-like structure was inhibited [65]. Versari et al. [12], studying the same cells exposed to 3.5 ×g, found increased NO production, enhanced cell migration, but no effects on proliferation. Moreover, altered distribution of actin fibers without modifications of the total amounts of actin was detected [12]. In the same conditions, HUVEC showed a time-dependent decrease in occludin correlating with an increase in paracellular permeability and a decrease in transendothelial electrical resistance, indicating a decrease in EC barrier function [66, 67], with exactly opposing results in BAEC cultured under hypogravity in RWV where increased barrier properties were detected [35].

Koyama et al. [69] reported that, after a few minutes of exposure to 3 ×g in a centrifuge, BAECs showed actin reorganization via Rho activation and FAK phosphorylation, increased cell proliferation, and ATP release. A daily exposure of 1-2 h repeated for 5 consecutive days promoted cell migration. Wehland et al. [42] investigated short term (s) effects of hypergravity (1.8 ×g) on EA.hy926 cells and found that the cells were weakly affected by loading in the conditions used for the experiment. On the contrary, short term effects of microgravity were much more evident.

In order to evaluate these results two considerations have to be made.

(1) Very different protocols and parameters have been used for EC exposure to hypergravity: continuous versus discontinuous exposure, different g force value, and exposure times ranging from minutes to days.

(2) ECs, both derived from the microvasculature and macrocirculation, are very sensitive to mechanical stress. It should be underscored that, in physiological

Table 2: The effects of hypergravity conditions on different endothelial cell types.

Experimental model	Experimental conditions	Effects	Authors
Primary human umbilical vein ECs (HUVEC)	Hypergravity conditions (generated by a MidiCAR centrifuge at 3.5 xg) for 24–48 h	↑ migration ↑ NO Altered distribution of actin fibers	Versari et al., 2007 [12]
	Hypergravity conditions (generated by a centrifuge at 3 xg) for 24–48 h	↑ cav-1 ↑ distribution of caveolae in the cell interior ↑ COX-2, NO, and PGI2 production ↓ angiogenesis (through a pathway not involving apoptosis)	Spisni et al., 2003 [65]
	Liftoff simulation by centrifuge (7.5 min simulation of the pattern of g forces experienced during liftoff of the NASA space shuttle)	↓ MAPK phosphorylation ↑ occludin expression	Sumanasekera et al., 2006 [66]
	Liftoff simulation by centrifuge (7.5 min simulation of the pattern of g forces experienced during liftoff of the NASA space shuttle)	↑ Paracellular permeability ↓ Occludin ↓ Transendothelial electrical resistance ↓ MAPK activation ↓ EC barrier function	Sumanasekera et al., 2007 [67]
Bovine aortic ECs (BAEC)	Hypergravity (thermostated 3-18K Sigma Zentrifugen, 5 periods of 10 min exposure to 10 xg spaced with 10 min at 1 xg)	Modified integrin distribution Reorganization of cytoskeletal network ↓ genes controlling vasoconstriction and inflammation ↓ Proapoptotic signals	Morbidelli et al., 2009 [68]
	Hypergravity (3 xg) applied by low speed centrifuge	↑ ATP release ↑ actin reorganization via RhoA activation and FAK phosphorylation ↑ cell proliferation and migration	Koyama et al., 2009 [69]
Bovine coronary venular ECs (CVEC)	Hypergravity (thermostated 3-18K Sigma Zentrifugen, 5 periods of 10 min exposure to 10 xg spaced with 10 min at 1 xg)	↓ proapoptotic genes (FADD, Fas, Fas-L) ↑ antiapoptotic gene NFκBChange in cytoskeleton organization Alteration of cell energy metabolism	Monici et al., 2006 [27]
Human EC line EA.hy926	Hypergravity Experiments (MuSIC, DLR, Cologne, Germany centrifuge 1.8 xg) Vibration experiments (Vibraplex vibration platform frequency range 0.2–14 kHz)	↓ CARD8, NOS3, VASH1, SERPINH1 (all P1), CAV2, ADAM19, TNFRSF12A, CD40, and ITGA6 (P31) mRNAs No significant changes on gene expression and morphology of the cells	Grosse et al., 2012 [41]
	Hypergravity Experiments (MuSIC, DLR, Cologne, Germany centrifuge 1.8 xg) Vibration experiments (Vibraplex vibration platform frequency range 0.2–14 kHz)	↓ Pan-actin, tubulin, and Moesin ↓ gene expression of CCND1, MSN, RDX, OPN, BIRC5, and ACTB ↑ Pan-actin, tubulin, and ezrin ↓ β-Actin and Moesin ↓ ACTB, CCND1, CDC6, CDKN1A, VEGFA, FLK-1, EZR, ITBG1, OPN, CASP3, CASP8, ANXA2, and BIRC5	Wehland et al., 2013 [42]

Legend: ↑, increased; ↓, decreased.

Table 3: Summary of the principal parameters influenced by simulated microgravity and hypergravity in different types of ECs.

	Microgravity					Hypergravity			
	Endothelial cell line EA.hy926	Dermal HMEC	HUVEC	PAEC	BAEC	Endothelial cell line EA.hy926	HUVEC	CVEC	BAEC
Migration	↓	=	=/↑	↓	ND	ND	↑	ND	↑
Proliferation	ND	↓	↑	↓	↑	ND (=/↑)	=	ND	↑
Apoptosis	↑	=	=	↑	=	=/↓	=	=	=
NO synthesis	↑	↑	↑	ND	↑	ND	↑	ND	ND
Cytoskeletal rearrangements	+++	+++	+++	+++	+++	+++	++	+++	+++

Legend: ↑, increased; ↓, decreased; =, no change; ND, not determined; ++ and +++, highly and strongly upregulated.

conditions, the quality and intensity of mechanical stimulation to which the endothelium is exposed depend on the vascular district.

Following the latter consideration, we hypothesized that EC response to gravitational alteration could depend on the district from which the cell population derives and could be different in cells derived from macro- or microcirculation. To verify this hypothesis, we studied and compared the behaviour of coronary venular endothelial cells (CVEC) [27] and BAEC [68] exposed to 10 ×g for 5 periods of 10 minutes each spaced with four recovery periods of the same duration. Following exposure, both the cell types showed similar changes in cytoskeleton organization and $\alpha v\beta 3$ integrin distribution. The peripheral ring of actin microfilaments was substituted by trans-cytoplasmic stress fibers, microtubules, and intermediate filaments gathered in the perinuclear area, focal contacts in the protruding lamellipodia disappeared, and $\alpha v\beta 3$ integrin molecules clustered in the central body of the cells. Both in CVEC and in BAEC the expression of the cytoskeletal proteins β-actin and vimentin increased. In BAEC the transcripts for the matrix proteins LM and FN decreased. In both the cell types exposure to hypergravity decreased the transcription of genes encoding for the proapoptotic factors Fas and FasL, Bcl-XL [27, 68].

Cell energy metabolism, assessed by autofluorescence spectroscopy and imaging, did not change significantly in BAECs. On the contrary, CVECs exposed to hypergravity showed an increase of the anaerobic metabolism, in comparison with 1 ×g controls [27].

The phenotypic expression of molecules involved in inflammation and angiogenesis such as eNOS, FGF-2, and COX-2, which is not expressed in basal conditions, did not significantly change as assessed by immunofluorescence microscopy in CVECs. Nevertheless, in BAECs the expression of *COX-2* and other genes controlling the calibre of the vessels, that is, renin, ET processing enzyme, and inflammation, such as TNFα and its receptor CD40, P and E selectins, CD54, was downregulated. Briefly, hypergravity does not seem to affect significantly the survival of both macro- and microvascular ECs. However, significant changes have been observed in cytoskeleton and integrin distribution in all the ECs studied, and changes in cell energy metabolism have been observed only in CVECs, while the downregulation of some genes involved in inflammation and vasoconstriction has been found only in BAECs. Considering the expression of growth modulators, hypergravity increased VEGF expression while it decreased a series of interleukins acting as inhibitors of EC proliferation [27, 68]. These results are consistent with the hypothesis that the EC response to gravitational alterations depends, at least in part, on the vascular district from which the cells are derived.

5. Concluding Remarks

The effects of simulated gravity changes on endothelial cells described in various papers are rather discordant but all converge in the indication that endothelial behaviour is significantly altered (Table 3). Briefly, from studies on different types of ECs exposed to simulated microgravity we can summarize the following.

(i) Impact on cell proliferation and survival: all the studies indicate alterations of cell proliferation. Only HUVEC and BAEC have been reproducibly found to proliferate faster in microgravity than controls. Microvascular EC and other endothelial cells are growth inhibited or induced to apoptosis.

(ii) Impact on NO synthesis: most studies agree on the increased production of NO through the modulation of NOS isoforms.

(iii) Impact on cytoskeleton: all the studies described important cytoskeletal remodelling in all the different EC analyzed.

(iv) Impact on gene expression: no doubt exists about the profound modifications of gene expression by exposure to simulated or real microgravity.

The impact of hypergravity on ECs is less defined. Due to the different experimental approaches adopted on various cell types the findings are not consistent and deserve further consideration.

The effects of gravitational forces on mechanotransduction in ECs responses have been the matter of only a few investigations and remain largely unknown. The plausible mechanosensing targets for gravity changes appear to be the cytoskeletal structure and particularly caveolae [26, 29, 65].

In conclusion, because (i) endothelial cells are crucial for the integrity of the vessel wall and (ii) vessels are responsible for the homeostasis of all the tissues, it is pivotal to continue studies on this topic since the modulation of endothelial

functions can contribute to cardiovascular deconditioning and other disorders observed in space, from bone loss to muscle atrophy. However, it would be recommended to clearly define the experimental models to use. A clear cut definition of endothelial cell models to be used and the conditions to model gravity need to be standardized.

Conflict of Interests

The authors declare that there is no conflict of interests regarding the publication of this paper.

Acknowledgments

Part of this work has been funded by Agenzia Spaziale Italiana (ASI) and European Spatial Agency (ESA).

References

[1] D. B. Cines, E. S. Pollak, C. A. Buck et al., "Endothelial cells in physiology and in the pathophysiology of vascular disorders," *Blood*, vol. 91, no. 10, pp. 3527–3561, 1998.

[2] H. F. Galley and N. R. Webster, "Physiology of the endothelium," *British Journal of Anaesthesia*, vol. 93, no. 1, pp. 105–113, 2004.

[3] S. P. Herbert and D. Y. R. Stainier, "Molecular control of endothelial cell behaviour during blood vessel morphogenesis," *Nature Reviews Molecular Cell Biology*, vol. 12, no. 9, pp. 551–564, 2011.

[4] E. R. Regan and W. C. Aird, "Dynamical systems approach to endothelial heterogeneity," *Circulation Research*, vol. 111, no. 1, pp. 110–130, 2012.

[5] K. E. Foreman and J. Tang, "Molecular mechanisms of replicative senescence in endothelial cells," *Experimental Gerontology*, vol. 38, no. 11-12, pp. 1251–1257, 2003.

[6] B. Buchen, M. Braun, Z. Hejnowicz, and A. Sievers, "Statoliths pull on microfilaments—experiments under microgravity," *Protoplasma*, vol. 172, no. 1, pp. 38–42, 1993.

[7] W. Briegleb, "Some qualitative and quantitative aspects of the fast-rotating clinostat as a research tool," *ASGSB Bulletin: Publication of the American Society for Gravitational and Space Biology*, vol. 5, no. 2, pp. 23–30, 1992.

[8] T. F. B. Kraft, J. J. W. A. van Loon, and J. Z. Kiss, "Plastid position in *Arabidopsis* columella cells is similar in microgravity and on a random-positioning machine," *Planta*, vol. 211, no. 3, pp. 415–422, 2000.

[9] M. A. Kacena, P. Todd, L. C. Gerstenfeld, and W. J. Landis, "Experiments with osteoblasts cultured under varying orientations with respect to the gravity vector," *Cytotechnology*, vol. 39, no. 3, pp. 147–154, 2002.

[10] Ž. Barjaktarović, A. Nordheim, T. Lamkemeyer, C. Fladerer, J. Madlung, and R. Hampp, "Time-course of changes in amounts of specific proteins upon exposure to hyper-g, 2-D clinorotation, and 3-D random positioning of *Arabidopsis* cell cultures," *Journal of Experimental Botany*, vol. 58, no. 15-16, pp. 4357–4363, 2007.

[11] L. Morbidelli, M. Monici, N. Marziliano et al., "Simulated hypogravity impairs the angiogenic response of endothelium by up-regulating apoptotic signals," *Biochemical and Biophysical Research Communications*, vol. 334, no. 2, pp. 491–499, 2005.

[12] S. Versari, A. Villa, S. Bradamante, and J. A. M. Maier, "Alterations of the actin cytoskeleton and increased nitric oxide synthesis are common features in human primary endothelial cell response to changes in gravity," *Biochimica et Biophysica Acta*, vol. 1773, no. 11, pp. 1645–1652, 2007.

[13] R. Gruener, R. Roberts, and R. Reitstetter, "Reduced receptor aggregation and altered cytoskeleton in cultured myocytes after space-flight," *Biological Sciences in Space*, vol. 8, no. 2, pp. 79–93, 1994.

[14] D. Grimm, P. Kossmehl, M. Shakibaei et al., "Effects of simulated microgravity on thyroid carcinoma cells," *Journal of Gravitational Physiology*, vol. 9, no. 1, pp. P253–P256, 2002.

[15] K. Hirasaka, T. Nikawa, L. Yuge et al., "Clinorotation prevents differentiation of rat myoblastic L6 cells in association with reduced NF-κB signaling," *Biochimica et Biophysica Acta*, vol. 1743, no. 1-2, pp. 130–140, 2005.

[16] Z. Li, Y. Song, M. Yuzhong et al., "Influence of simulated microgravity on avian primordial germ cell migration and reproductive capacity," *Journal of Experimental Zoology*, vol. 292, no. 7, pp. 672–676, 2002.

[17] D. Sarkar, T. Nagaya, K. Koga, F. Kambe, Y. Nomura, and H. Seo, "Rotation in clinostat results in apoptosis of osteoblastic ROS 17/2.8 cells," *Journal of Gravitational Physiology*, vol. 7, no. 2, pp. P71–P72, 2000.

[18] B. M. Uva, M. A. Masini, M. Sturla et al., "Clinorotation-induced weightlessness influences the cytoskeleton of glial cells in culture," *Brain Research*, vol. 934, no. 2, pp. 132–139, 2002.

[19] C. C. Woods, K. E. Banks, R. Gruener, and D. DeLuca, "Loss of T cell precursors after spaceflight and exposure to vector-averaged gravity," *The FASEB Journal*, vol. 17, no. 11, pp. 1526–1528, 2003.

[20] B. R. Unsworth and P. I. Lelkes, "Growing tissues in microgravity," *Nature Medicine*, vol. 4, no. 8, pp. 901–907, 1998.

[21] S. Versari, G. Longinotti, L. Barenghi, J. A. M. Maier, and S. Bradamante, "The challenging environment on board the International Space Station affects endothelial cell function by triggering oxidative stress through thioredoxin interacting protein overexpression: the ESA-SPHINX experiment," *FASEB Journal*, vol. 27, no. 11, pp. 4466–4475, 2013.

[22] S. I. Carlsson, M. T. Bertilaccio, I. Ascari, S. Bradamante, and J. A. Maier, "Modulation of human endothelial cell behaviour in simulated microgravity," *Journal of Gravitational Physiology*, vol. 9, no. 1, pp. P273–P274, 2002.

[23] S. Cotrupi, D. Ranzani, and J. A. M. Maier, "Impact of modeled microgravity on microvascular endothelial cells," *Biochimica et Biophysica Acta—Molecular Cell Research*, vol. 1746, no. 2, pp. 163–168, 2005.

[24] B. E. Hammer, L. S. Kidder, P. C. Williams, and W. W. Xu, "Magnetic levitation of MC3T3 osteoblast cells as a ground-based simulation of microgravity," *Microgravity Science and Technology*, vol. 21, no. 4, pp. 311–318, 2009.

[25] M. J. A. Moes, J. C. Gielen, R.-J. Bleichrodt, J. J. W. A. Van Loon, P. C. M. Christianen, and J. Boonstra, "Simulation of microgravity by magnetic levitation and random positioning: effect on human A431 Cell morphology," *Microgravity Science and Technology*, vol. 23, no. 2, pp. 249–261, 2011.

[26] E. Spisni, M. Toni, A. Strillacci et al., "Caveolae and caveolae constituents in mechanosensing: effect of modeled microgravity on cultured human endothelial cells," *Cell Biochemistry and Biophysics*, vol. 46, no. 2, pp. 155–164, 2006.

[27] M. Monici, N. Marziliano, V. Basile et al., "Hypergravity affects morphology and function in microvascular endothelial cells,"

Microgravity Science and Technology, vol. 18, no. 3-4, pp. 234–238, 2006.

[28] S. I. M. Carlsson, M. T. S. Bertilaccio, E. Ballabio, and J. A. M. Maier, "Endothelial stress by gravitational unloading: effects on cell growth and cytoskeletal organization," *Biochimica et Biophysica Acta: Molecular Cell Research*, vol. 1642, no. 3, pp. 173–179, 2003.

[29] S. M. Grenon, M. Jeanne, J. Aguado-Zuniga, M. S. Conte, and M. Hughes-Fulford, "Effects of gravitational mechanical unloading in endothelial cells: association between caveolins, inflammation and adhesion molecules," *Scientific reports*, vol. 3, p. 1494, 2013.

[30] M. Y. Kapitonova, S. Muid, G. R. A. Froemming et al., "Real space flight travel is associated with ultrastructural changes, cytoskeletal disruption and premature senescence of HUVEC," *Malaysian Journal of Pathology*, vol. 34, no. 2, pp. 103–113, 2012.

[31] J. H. Siamwala, S. H. Reddy, S. Majumder et al., "Simulated microgravity perturbs actin polymerization to promote nitric oxide-associated migration in human immortalized Eahy926 cells," *Protoplasma*, vol. 242, no. 1, pp. 3–12, 2010.

[32] Y. Zhang, C. Sang, K. Paulsen et al., "ICAM-1 expression and organization in human endothelial cells is sensitive to gravity," *Acta Astronautica*, vol. 67, no. 9-10, pp. 1073–1080, 2010.

[33] C. Griffoni, S. di Molfetta, L. Fantozzi et al., "Modification of proteins secreted by endothelial cells during modeled low gravity exposure," *Journal of Cellular Biochemistry*, vol. 112, no. 1, pp. 265–272, 2011.

[34] Y.-C. Wang, S. Zhang, T.-Y. Du, B. Wang, and X.-Q. Sun, "Clinorotation upregulates inducible nitric oxide synthase by inhibiting AP-1 activation in human umbilical vein endothelial cells," *Journal of Cellular Biochemistry*, vol. 107, no. 2, pp. 357–363, 2009.

[35] G. L. Sanford, D. Ellerson, C. Melhado-Gardner, A. E. Sroufe, and S. Harris-Hooker, "Three-dimensional growth of endothelial cells in the microgravity-based rotating wall vessel bioreactor," *In Vitro Cellular and Developmental Biology-Animal*, vol. 38, no. 9, pp. 493–504, 2002.

[36] M. Monici, F. Cialdai, G. Romano et al., "An in vitro study on tissue repair: impact of unloading on cells involved in the remodelling phase," *Microgravity Science and Technology*, vol. 23, no. 4, pp. 391–401, 2011.

[37] M. Infanger, C. Ulbrich, S. Baatout et al., "Modeled gravitational unloading induced downregulation of endothelin-1 in human endothelial cells," *Journal of Cellular Biochemistry*, vol. 101, no. 6, pp. 1439–1455, 2007.

[38] X. Ma, M. Wehland, H. Schulz et al., "Genomic approach to identify factors that drive the formation of three-dimensional structures by EA.hy926 endothelial cells," *PLoS ONE*, vol. 8, no. 5, Article ID e64402, 2013.

[39] F. Shi, Y.-C. Wang, T.-Z. Zhao et al., "Effects of simulated microgravity on human umbilical vein endothelial cell angiogenesis and role of the PI3K-Akt-eNOS signal pathway," *PLoS ONE*, vol. 7, no. 7, Article ID e40365, 2012.

[40] M. Infanger, P. Kossmehl, M. Shakibaei et al., "Induction of three-dimensional assembly and increase in apoptosis of human endothelial cells by simulated microgravity: impact of vascular endothelial growth factor," *Apoptosis*, vol. 11, no. 5, pp. 749–764, 2006.

[41] J. Grosse, M. Wehland, J. Pietsch et al., "Short-term weightlessness produced by parabolic flight maneuvers altered gene expression patterns in human endothelial cells," *FASEB Journal*, vol. 26, no. 2, pp. 639–655, 2012.

[42] M. Wehland, X. Ma, M. Braun et al., "The impact of altered gravity and vibration on endothelial cells during a parabolic flight," *Cellular Physiology and Biochemistry*, vol. 31, no. 2-3, pp. 432–451, 2013.

[43] D. Grimm, J. Bauer, C. Ulbrich et al., "Different responsiveness of endothelial cells to vascular endothelial growth factor and basic fibroblast growth factor added to culture media under gravity and simulated microgravity," *Tissue Engineering A*, vol. 16, no. 5, pp. 1559–1573, 2010.

[44] D. Grimm, M. Infanger, K. Westphal et al., "A delayed type of three-dimensional growth of human endothelial cells under simulated weightlessness," *Tissue Engineering A*, vol. 15, no. 8, pp. 2267–2275, 2009.

[45] J. H. Siamwala, S. Majumder, K. P. Tamilarasan et al., "Simulated microgravity promotes nitric oxide-supported angiogenesis via the iNOS-cGMP-PKG pathway in macrovascular endothelial cells," *FEBS Letters*, vol. 584, no. 15, pp. 3415–3423, 2010.

[46] M. Mariotti and J. A. M. Maier, "Gravitational unloading induces an anti-angiogenic phenotype in human microvascular endothelial cells," *Journal of Cellular Biochemistry*, vol. 104, no. 1, pp. 129–135, 2008.

[47] C.-Y. Kang, L. Zou, M. Yuan et al., "Impact of simulated microgravity on microvascular endothelial cell apoptosis," *European Journal of Applied Physiology*, vol. 111, no. 9, pp. 2131–2138, 2011.

[48] S. Cotrupi and J. A. M. Maier, "Is HSP70 upregulation crucial for cellular proliferative response in simulated microgravity?" *Journal of Gravitational Physiology*, vol. 11, no. 2, pp. P173–176, 2004.

[49] L. Buravkova, Y. Romanov, M. Rykova, O. Grigorieva, and N. Merzlikina, "Cell-to-cell interactions in changed gravity: ground-based and flight experiments," *Acta Astronautica*, vol. 57, no. 2–8, pp. 67–74, 2005.

[50] S. J. Crawford-Young, "Effects of microgravity on cell cytoskeleton and embryogenesis," *International Journal of Developmental Biology*, vol. 50, no. 2-3, pp. 183–191, 2006.

[51] J. Pietsch, J. Bauer, M. Egli et al., "The effects of weightlessness on the human organism and mammalian cells," *Current Molecular Medicine*, vol. 11, no. 5, pp. 350–364, 2011.

[52] V. A. Convertino, "Status of cardiovascular issues related to space flight: implications for future research directions," *Respiratory Physiology and Neurobiology*, vol. 169, supplement 1, pp. S34–S37, 2009.

[53] B. J. Yates and I. A. Kerman, "Post-spaceflight orthostatic intolerance: possible relationship to microgravity-induced plasticity in the vestibular system," *Brain Research Reviews*, vol. 28, no. 1-2, pp. 73–82, 1998.

[54] X. Ma, A. Sickmann, J. Pietsch et al., "Proteomic differences between microvascular endothelial cells and the EA.hy926 cell line forming three-dimensional structures," *Proteomics*, vol. 14, no. 6, pp. 689–698, 2014.

[55] C. J. S. Edgell, C. C. McDonald, and J. B. Graham, "Permanent cell line expressing human factor VIII-related antigen established by hybridization," *Proceedings of the National Academy of Sciences of the United States of America*, vol. 80, no. 12, pp. 3734–3737, 1983.

[56] M. Boerma, G. R. Burton, J. Wang, L. M. Fink, R. E. McGehee Jr., and M. Hauer-Jensen, "Comparative expression profiling in primary and immortalized endothelial cells: changes in gene expression in response to hydroxy methylglutaryl-coenzyme A reductase inhibition," *Blood Coagulation and Fibrinolysis*, vol. 17, no. 3, pp. 173–180, 2006.

[57] H. F. Galley, M. G. Blaylock, A. M. Dubbels, and N. R. Webster, "Variability in E-selectin expression, mRNA levels and sE-selectin release between endothelial cell lines and primary endothelial cells," *Cell Biology International*, vol. 24, no. 2, pp. 91–99, 2000.

[58] M. Y. Kapitonova, S. L. Kuznetsov, G. R. A. Froemming et al., "Effects of space mission factors on the morphology and function of endothelial cells," *Bulletin of Experimental Biology and Medicine*, vol. 154, no. 6, pp. 796–801, 2013.

[59] J. M. Davidson, A. M. Aquino, S. C. Woodward, and W. W. Wilfinger, "Sustained microgravity reduces intrinsic wound healing and growth factor responses in the rat," *FASEB Journal*, vol. 13, no. 2, pp. 325–329, 1999.

[60] M. E. Kirchen, K. M. O'Connor, H. E. Gruber et al., "Effects of microgravity on bone healing in a rat fibular osteotomy model," *Clinical Orthopaedics and Related Research*, vol. 318, pp. 231–242, 1995.

[61] D. Ingber, "How cells (might) sense microgravity," *The FASEB Journal*, vol. 13, no. 8, pp. S3–S15, 1999.

[62] M. Hughes-Fulford and J. Boonstra, "Cell mechanotransduction: cytoskeleton and related signalling pathways," in *Cell Mechanochemistry. Biological Systems and Factors Inducing Mechanical Stress, such as Light, Pressure and Gravity*, M. Monici and J. W. A. van Loon, Eds., pp. 75–95, Transworld Research Network, Trivandrum, India, 2010.

[63] C. Papaseit, N. Pochon, and J. Tabony, "Microtubule self-organization is gravity-dependent," *Proceedings of the National Academy of Sciences of the United States of America*, vol. 97, no. 15, pp. 8364–8368, 2000.

[64] R. G. Bacabac, D. Mizuno, and G. H. Koenderink, "Mechanical properties of living cells: on mechanosensing and microgravity," in *Cell Mechanochemistry. Biological Systems and Factors Inducing Mechanical Stress, Such as Light, Pressure and Gravity*, M. Monici and J. W. A. van Loon, Eds., pp. 23–54, Transworld Research Network, Trivandrum, India, 2010.

[65] E. Spisni, M. C. Blanco, C. Griffoni et al., "Mechanosensing role of caveolae and caveolar constituents in human endothelial cells," *Journal of Cellular Physiology*, vol. 197, no. 2, pp. 198–204, 2003.

[66] W. K. Sumanasekera, L. Zhao, M. Ivanova et al., "Effect of estradiol and dihydrotestosterone on hypergravity-induced MAPK signaling and occludin expression in human umbilical vein endothelial cells," *Cell and Tissue Research*, vol. 324, no. 2, pp. 243–253, 2006.

[67] W. K. Sumanasekera, G. U. Sumanasekera, K. A. Mattingly, S. M. Dougherty, R. S. Keynton, and C. M. Klinge, "Estradiol and dihydrotestosterone regulate endothelial cell barrier function after hypergravity-induced alterations in MAPK activity," *American Journal of Physiology: Cell Physiology*, vol. 293, no. 2, pp. C566–C573, 2007.

[68] L. Morbidelli, N. Marziliano, V. Basile et al., "Effect of hypergravity on endothelial cell function and gene expression," *Microgravity Science and Technology*, vol. 21, no. 1-2, pp. 135–140, 2009.

[69] T. Koyama, C. Kimura, M. Hayashi, M. Watanabe, Y. Karashima, and M. Oike, "Hypergravity induces ATP release and actin reorganization via tyrosine phosphorylation and RhoA activation in bovine endothelial cells," *Pflugers Archiv European Journal of Physiology*, vol. 457, no. 4, pp. 711–719, 2009.

Hindawi Publishing Corporation
BioMed Research International
Volume 2014, Article ID 782390, 10 pages
http://dx.doi.org/10.1155/2014/782390

Research Article

A Functional Interplay between 5-Lipoxygenase and μ-Calpain Affects Survival and Cytokine Profile of Human Jurkat T Lymphocyte Exposed to Simulated Microgravity

Valeria Gasperi,[1] Cinzia Rapino,[2,3] Natalia Battista,[4,5] Monica Bari,[1] Nicolina Mastrangelo,[1] Silvia Angeletti,[6] Enrico Dainese,[4,5] and Mauro Maccarrone[5,6]

[1] *Department of Experimental Medicine & Surgery, Tor Vergata University of Rome, Via Montpellier 1, 00133 Rome, Italy*
[2] *Faculty of Veterinary Medicine, University of Teramo, Piazza A. Moro 45, 64100 Teramo, Italy*
[3] *StemTeCh Group, Via Colle dell'Ara, 66100 Chieti, Italy*
[4] *Faculty of Bioscience, Technology for Food Agriculture and Environment, University of Teramo, Piazza A. Moro 45, 64100 Teramo, Italy*
[5] *European Center for Brain Research (CERC), IRCCS Santa Lucia Foundation, Via del Fosso di Fiorano 64-65, 00143 Rome, Italy*
[6] *Center of Integrated Research, Campus Bio-Medico University of Rome, Via Alvaro del Portillo 21, 00128 Rome, Italy*

Correspondence should be addressed to Valeria Gasperi; valeria.gasperi@uniroma2.it, Enrico Dainese; edainese@unite.it, and Mauro Maccarrone; m.maccarrone@unicampus.it

Received 15 May 2014; Accepted 18 August 2014; Published 16 September 2014

Academic Editor: Jack J. W. A. Van Loon

A growing body of evidence strongly indicates that both simulated and authentic weightlessness exert a broad range of effects on mammalian tissues and cells, including impairment of immune cell function and increased apoptotic death. We previously reported that microgravity-dependent activation of 5-lipoxygenase (5-LOX) might play a central role in the initiation of apoptosis in human T lymphocytes, suggesting that the upregulation of this enzyme might be (at least in part) responsible for immunodepression observed in astronauts during space flights. Herein, we supplement novel information about the molecular mechanisms underlying microgravity-triggered apoptotic cell death and immune system deregulation, demonstrating that under simulated microgravity human Jurkat T cells increase the content of cytosolic DNA fragments and cytochrome c (typical hallmarks of apoptosis) and have an upregulated expression and activity of μ-calpain. These events were paralleled by the unbalance of interleukin- (IL-) 2 and interferon- (INF-) γ, anti- and proapoptotic cytokines, respectively, that seemed to be dependent on the functional interplay between 5-LOX and μ-calpain. Indeed, we report unprecedented evidence that 5-LOX inhibition reduced apoptotic death, restored the initial IL-2/INF-γ ratio, and more importantly reverted μ-calpain activation induced by simulated microgravity.

1. Introduction

Several studies have shown that authentic space conditions markedly alter physiological processes, thus leading to cardiovascular changes [1], loss of bone density [2, 3], muscle atrophy [2, 4], and immunodepression [5, 6]. To date, it is well established that cells of the immune system are severely affected by microgravity conditions [5–8]. In particular, alterations observed in astronauts and rodents flown in space included altered distribution and function of circulating leukocytes [9–11], lymphocytopenia [12–14], and impaired T cell activation [9, 14–16]. In addition, several *in vivo* and *in vitro* studies reported a weightlessness-dependent alteration of cytokine secretion from T-helper 1 (Th1) and T-helper 2 (Th2) cells that in turn results in a deregulation of cell-to-cell crosstalk as well as of inflammatory responses [9–11, 17].

It has been reported that several proinflammatory Th1 cytokines, including interferon- (INF-) γ, tumor necrosis factor- (TNF-) β and interleukin- (IL-) 2, and anti-inflammatory Th2 cytokines like IL-4 and IL-10, as well as leukaemia inhibitory factor (LIF), are related to programmed

cell death (PCD). These glycoproteins, indeed, are able to induce or protect cells from apoptosis [18–23], so that an alternative classification distinguishes them as anti-(LIF, IL-2, IL-4, IL-10) or proapoptotic (INF-γ) substances. A hot topic is the study of the effect of microgravity (be it real or simulated) on apoptosis of different mammalian cell types, including cerebral vascular smooth muscle [24], thyroid cancer [25], endothelial cells [26], cultured glial cells [27], spermatozoa [28], B lymphocytes [29], and T cells [6, 30]. In particular, 5-lipoxygenase (5-LOX) has been proposed as a "gravity responder," which executes the apoptotic events induced by microgravity in human lymphocytes [6, 30].

Evidence is accumulating that the execution of PCD is finely regulated by a distinct set of signal transduction pathways and catabolic mechanisms (e.g., mitochondrial, lysosomal, and nuclear alterations, lipid modifications, and cytosolic calcium accumulation), and recent data provided first hints that lipid hydroperoxides impact on PCD [31]. Indeed, LOX-catalyzed lipid peroxidation has been reported to be a specific downstream event that triggers apoptosis-inducing factor- (AIF) mediated PCD in primary neurons in culture and in mice [31]. In the same context, calpains cleave multiple substrates potentially involved in PCD and including cyclin-dependent kinase-5 [32], plasma membrane Ca^{2+} ATPase isoform-1 [33], and calcineurin [34]. Also AIF is a calpain substrate implicated in neuronal death, because its proteolysis activates PCD through a translocation of AIF itself from the mitochondria to the nucleus [35, 36].

Against this background, the present study aimed at better defining the influence of the space environment on survival and cytokine profile of human lymphocytes, in order to identify a possible link between these events. In this context, we report an unprecedented functional interplay between 5-LOX and μ-calpain in modulating PCD induced by simulated microgravity.

2. Materials and Methods

2.1. Reagents. Chemicals were of the purest analytical grade. Human recombinants IL-2, IL-4, IL-6, IL-10, INF-γ, and LIF, calpain substrate [N-Suc-Leu-Tyr-AMC (7-amido-4-methylcoumarin)], AA861 (specific inhibitor of 5-LOX), and E64D (specific inhibitor of calpain) were purchased from Sigma Chemical Co. (St. Louis, MO, USA). Mouse anti-cytochrome c antibody was from Cell Signalling Technology Inc. (Danvers, MA, USA); mouse anti-calpain-1 was from Calbiochem (Merck Darmstadt, Germany). Rabbit anti-LIF, anti-IL-2, anti-IL-4, anti-IL-6, anti-IL-10, anti-INF-γ, secondary antibodies conjugated to horseradish peroxidase (HRP), and enhanced chemiluminescence (ECL) kit were from Santa Cruz Biotechnology Inc. (Santa Cruz, CA, USA). Goat anti-rabbit conjugated to alkaline phosphatase (GAR-AP) was from Bio-Rad (Hercules, CA, USA).

2.2. Simulated Microgravity Cell Cultures. To simulate space conditions, the rotary cell culture system (RCCS), developed by the National Aeronautics and Space Administration (Washington, DC, USA) and manufactured by Synthecon (Houston, TX, USA), was used. Human Jurkat T cells (Clone E6-1) (ATCC, Manassas, VA, USA) were grown in RPMI 1640 medium supplemented with 2 mM glutamine, 2.5 mM sodium pyruvate, 100 U/mL penicillin, 100 μg/mL streptomycin, and 10% heat-inactivated foetal bovine serum. Cells were placed in completely filled 50 mL vessels, to avoid the presence of air bubbles that could lead to shear force damage of cells on the RCCS. Vessels were rotated at a speed of 7.2 rpm (simulated microgravity and referred to as sim-μg), as reported [30, 37], or cultured at ground gravity (1 g), as controls. Incubation of 1 g and sim-μg cells with different compounds was performed at 37°C in an atmosphere of 5% CO_2, at the indicated concentrations and for the indicated periods of time.

2.3. Evaluation of PCD. PCD was estimated by the cell-death detection enzyme-linked immunosorbent assay (ELISA) kit (Boehringer Mannheim, Germany), based on evaluation of histone-associated DNA fragments in the cytoplasm, as previously reported [30].

Cytochrome c release from mitochondria was analyzed as reported [38]. Briefly, cells were lysed in HB buffer (5 mM Tris-HCl pH 7.4, 10 mM KCl, 1 mM $MgCl_2$, and 1 mM DTT), containing protease inhibitor cocktail, and centrifuged at 1000 ×g for 10 min to completely remove nuclei and whole cells. The resulting supernatant was centrifuged at 3000 ×g for 10 min; then the pellet was saved as membrane-bound organellar fraction enriched with mitochondria, while the supernatant, after centrifugation at 100000 ×g for 40 min, was collected as cytosolic fraction. These two fractions were analyzed for cytochrome c localization by means of ELISA: mitochondrial and cytosolic proteins (20 μg/well) were incubated with anti-cytochrome c antibody (diluted 1 : 500), and after incubation with a GAR-AP (diluted 1 : 2000), colour development of the alkaline phosphatase reaction was measured at 405 nm ($A_{405\,nm}$), by using *p*-nitrophenyl phosphate as substrate.

2.4. Analysis of μ-Calpain Activity and Expression. Detection of μ-calpain mRNA was performed by quantitative reverse transcriptase-polymerase chain reaction (q-RT-PCR), as previously reported [6]. Briefly, total RNA was extracted from Jurkat cells using the RNeasy extraction kit (Qiagen, Crawley, UK), following the manufacturer's instructions. RT-PCR reactions were performed using the RT-PCR SuperScript III Platinum Two-Step qRT-PCR Kit (Invitrogen, Carlsbad, CA, USA). One μg total RNA was used to synthesize cDNA with 10 U/μL SuperScript III reverse transcriptase, in the presence of 2 U/μL RNaseOUT, 1.25 μM oligo (dT), 1.25 ng/μL random hexamers, 5 mM $MgCl_2$, 0.5 mM dNTP mix, and DEPC-treated water. The reaction was performed using the following RT-PCR program: 25°C for 10 min, 42°C for 50 min, 85°C for 5 min, and then, after addition of 0.1 U/μL of *E. coli* RNase H, the product was incubated at 37°C for 20 min. For expression studies, target transcripts were amplified in ABI PRISM 7700 sequence detector system (Applied Biosystems, Foster City, CA, USA). Thermal cycling involved 40 cycles of 95°C for 15 sec and 60°C for 30 sec, after initial denaturation for 10 min

at 95°C. TaqMan MGB probe was synthesized by Applied Biosystems (Foster City, CA, USA). The probe was labelled with the fluorescent dye 6-carboxyfluorescein at the 5′ end and a dark quencher at the 3′ end (Applied Biosystems). Fluorescence was measured after each cycle of PCR and, to confirm the quality of isolated RNA and to standardize the amount of RNA applied, glyceraldehyde-3-phosphate dehydrogenase (GAPDH) was used as endogenous control with FAMTM dye label and MGB. Real-time PCR mixtures contained template cDNA, 20x Primer/Probe Mix, TaqMan MGB Probe with FAMTM dye label, no primer limitation, Minor Groove Binder and Nonfluorescent Quencher, Universal PCR Master Mix, no AmpErase UNG Applied Biosystems (Foster City, CA, USA) in a total volume of 25 μL in a 96-well plate. Relative μ-calpain expression levels were measured by $\Delta\Delta$CT method (PE-Applied Biosystems; Sequence Detector User Bulletin).

Calpain protein expression was evaluated by Western blot analysis. Briefly, cell lysates (20 μg/well) were subjected to SDS-PAGE, electroblotted onto PVDF membranes, incubated with mouse anti-μ-calpain antibody (1 : 4000), which detects both the full-length (large subunit) and the autoproteolytically cleaved forms of μ-calpain, and detected with ECL. Calpain quantification was also evaluated through ELISA method, by incubating protein lysates (20 μg/well) with mouse anti-μ-calpain-1 (1 : 2000) as primary antibody and HRP-conjugated antibody (1 : 5000) as secondary antibody. The HRP enzymatic activity was determined by adding 100 μL/well of tetramethylbenzidine containing 0.002% H_2O_2, and the absorbance was read on a microplate reader (ELISA Ascent Software per Multiskan) at 450 nm. Absorbance values of the samples were within the linearity range of the ELISA test, assessed by calibration curves with known amounts of μ-calpain (in the range of 7.5–60.0 ng/well).

The enzymatic activity of μ-calpain was measured as reported [39]. Briefly, cell lysates (40 μg/test) were incubated with 150 μM calpain substrate (N-Suc-Leu-Tyr-AMC) in 10 mM Hepes, pH 7.4, 1% Triton X-100, and 100 μM $CaCl_2$, for 2 hours at 37°C. After incubation, hydrolyzed AMC groups were measured on a fluorimeter LS50B (Perkin-Elmer Life Sciences Inc., Boston, MA, USA) with an excitation filter of 380 nm and emission filter of 460 nm.

2.5. 5-LOX Activity. The activity of 5-LOX (arachidonate:oxygen 5-oxidoreductase; E.C. 1.13.11.34) was determined as previously reported [6]. Briefly, the end product leukotriene (LT) B_4 was extracted from Jurkat cells (5×10^6 cell/test) and quantified at 405 nm by using the Leukotriene B_4 EIA Kit (Cayman Chemical Company, Ann Arbor, MA, USA) and calibration curves drawn according to the customer's instructions.

2.6. Cytokine Profile Analysis. Jurkat cells harvested after 48 hours were centrifuged at 200 ×g for 10 min to collect cells and culture medium. Cells were lysed in 50 mM Tris-HCl (pH 7.4), containing protease inhibitors, and cytokine content was quantified by coating proteins (20 μg/well) from whole lysates overnight in a 96-well ELISA microplate, as reported [40]. Rabbit anti-LIF, anti-IL-2, anti-IL-4, anti-IL-6, anti-IL-10, and anti-INFγ (diluted 1 : 500) were used as primary antibodies; GAR-AP (diluted 1 : 2000) was used as secondary antibody and absorbance values were read at 405 nm. Release of LIF and other cytokines from Jurkat cells into the medium was quantified through Quantikine Immunoassay kit (R&D System, Minneapolis, MN, USA) and a specific Multiprotein Profiling ELISA Kit (SuperArray Bioscience Co., Germany), respectively, according to the manufacturer's instructions. To this aim, 50 μL of culture medium was used, and the content of each protein was evaluated by comparing $A_{405\,nm}$ values to those of antigen standard curves (positive controls).

2.7. Statistical Analysis. All values were expressed as means ± SEM of at least three independent experiments. Student's unpaired t-test or one-way ANOVA (followed by Bonferroni *post hoc* analysis) was used to compare quantitative data with normal distributions and equal variance. The statistical InStat 3 program (GraphPAD Software for Science, San Diego, California) was used, and a value of $P < 0.05$ was considered statistically significant.

3. Results

3.1. Prolonged Exposure to Simulated Microgravity Induces Apoptosis in Human Jurkat T Cells. Jurkat T cells were exposed to simulated microgravity for different times (from 0 to 48 hours) and the hallmarks of apoptosis DNA fragmentation and cytochrome c release were analyzed. In agreement with previously reported data [30], RCCS treatment led to a time-dependent increase of cytosolic DNA fragments that were undetectable after a brief exposure (4 hours) to simulated microgravity, increased after 24 hours (~2-fold over 1 g cells), and reached a maximum level of ~3-fold over controls 24 hours later (Table 1). Then, the subcellular localization of cytochrome c upon simulated microgravity was checked. Jurkat cells exposed to weightlessness showed a loss of mitochondrial cytochrome c and a parallel increase in the cytosolic content, with a time-dependence comparable to that observed for DNA fragmentation (Table 1). Conversely, Jurkat cells incubated at 1 g under the same experimental conditions did not show significant signs of PCD (Table 1). Since RCCS treatment for 48 hours yielded a significant increase in PCD, we chose to perform all subsequent experiments using this time point.

3.2. Prolonged Exposure to Simulated Microgravity Upregulates μ-Calpain Expression and Activity in Human Jurkat T Cells. We have previously reported that after 48 hours of exposure to authentic microgravity, human lymphocytes show increased mRNA levels of μ-calpain [6], a Ca^{2+}-dependent intracellular cysteine protease that is implicated in different physiological functions, including cell growth and apoptosis [41]. Therefore, once established that under our experimental conditions Jurkat cells underwent apoptosis, we checked whether RCCS treatment might engage μ-calpain. In agreement with our previous data [6], RT-qPCR experiments

Table 1: Time-dependent effect of simulated microgravity on apoptotic markers in Jurkat T cells exposed to simulated microgravity (sim-μg) or kept at normal gravity (1g).

Parameter	1g	4-hour sim-μg	24-hour sim-μg	48-hour sim-μg
DNA fragmentation	100 ± 8	107 ± 8	270 ±18*	342 ±21**
Cytochrome c release (cytosol/mitochondria ratio)	100 ± 9	111 ± 7	347 ±41*	450 ±47**

Results are expressed as percentage of 1g cells set to 100. For DNA fragmentation, 100% = 0.300 ± 0.030 $A_{405\,nm}$; for cytochrome c release, 100% = 0.074 ± 0.005. * denotes $P < 0.01$ versus 1g cells; ** denotes $P < 0.001$ versus 1g cells.

demonstrated a significant increase of μ-calpain mRNA in sim-μg Jurkat cells (~2-fold over 1 g cells) (Figure 1(a)). Interestingly, upregulation of *capn* 1 gene, which encodes μ-calpain, was paralleled by increased protein content (Figures 1(b) and 1(c)). Western blot analysis, indeed, showed that 48 hours of RCCS treatment dramatically increased μ-calpain protein levels; in particular, larger amounts of autocleaved and active fragment of μ-calpain (~75 kDa) [42] were found in sim-μg, whereas no active enzyme was observed in 1 g cells (Figure 1(b)). Such a result was further corroborated by ELISA, revealing that RCCS almost doubled μ-calpain protein content after 48 hours (Figure 1(c)). We next determined whether increased mRNA and protein content might result in increased enzyme activity. By analysing the cleavage of a fluorogenic μ-calpain substrate, we observed an enhanced protease activity in sim-μg T cells (~2-fold over 1 g cells) (Figure 1(d)). Specific proteolytic activity of calpain was confirmed by the addition of 5 μM calpastatin (Figure 1(d)), the natural calpain inhibitor [43]. Since calpain activation seemed to be implicated in DNA fragmentation [44, 45], we analyzed the effect of E64D, a cell permeable and selective inhibitor of the same protease [46], on simulated microgravity-induced PCD. As shown in Figure 1(e), inhibition of calpain activity significantly lowered internucleosomal DNA fragmentation, thus preventing weightlessness-induced cell death of T cells.

3.3. Prolonged Exposure to Simulated Microgravity Affects the Balance between Proapoptotic and Antiapoptotic Cytokines in Jurkat Cells. Then, we characterized the cytokine profile in Jurkat T cells exposed to simulated microgravity. As demonstrated by ELISA assay, 48 hours of RCCS treatment significantly reduced the synthesis and release of antiapoptotic cytokines like LIF, IL-4, and IL-2, while increasing protein levels of the proapoptotic cytokine INF-γ (Figure 2). Instead, no change in IL-6 and IL-10 content was observed upon simulated microgravity treatment (Figure 2).

Next, we went further by investigating whether RCCS-induced PCD might be related to the unbalance between proapoptotic and antiapoptotic cytokines. To this aim, we analyzed apoptosis in Jurkat cells cultured under simulated microgravity for 48 hours, in the presence of the cytokines that changed upon RCCS exposure. Neither LIF nor IL-4 (both at 10 ng/mL) reduced cytosolic DNA fragments (Figure 3(a)) and cytochrome c content (Figure 3(b)); on the other hand, 10 ng/mL IL-2 was able to protect Jurkat cells from simulated microgravity-triggered cell death, since it significantly reduced both DNA fragmentation and cytochrome c release (Figures 3(a) and 3(b)). To validate our hypothesis, we also analyzed the effect of INF-γ (10 ng/mL). In agreement with the previous data (Figure 2), the latter cytokine drastically enhanced RCCS-induced PCD of Jurkat cells (~ 4.5- and 2.5-fold over 1 g cells and sim-μg cells, resp.) (Figures 3(a) and 3(b)).

Table 2: Time-dependent effect of simulated microgravity on 5-LOX activity in Jurkat cells.

Sample	LOX activity (% of 1g cells)[a]
1g cells	100 ± 11
4-hour sim-μg cells	213 ±18*
24-hour sim-μg cells	249 ±23*
48-hour sim-μg cells	235 ±21*

[a]100% of 5-LOX activity = 89 ± 7 pg of $LTB_4/1 \times 10^6$ cells. * denotes $P < 0.01$ versus 1g cells.

To gain further insights on the evaluation of a possible relationship between altered IL-2/INF-γ content and calpain activation, we measured the activity of the latter enzyme in the presence of these two cytokines. Interestingly, IL-2 reduced calpain activation due to simulated microgravity, while INF-γ did not significantly affect enzyme activity (Figure 3(c)).

3.4. Effect of Inhibition of μ-Calpain and 5-LOX on Apoptosis and Cytokine Release. Since we observed that simulated microgravity triggers apoptosis by altering the content of IL-2 and INF-γ, we asked whether such an event might engage 5-LOX, which has been proposed as a "gravity responder" [30]. First, we analyzed 5-LOX activity by quantifying the content of its LTB_4 product upon RCCS exposure. In agreement with previous data, we found an early increase of 5-LOX activity (~2 fold over 1 g cells), with values that remained unchanged over the whole time period tested (Table 2). Hence, we subjected Jurkat cells to simulated microgravity in the presence of 10 μM AA861, a specific 5-LOX inhibitor [47]. As shown in Table 3, we observed that 5-LOX inhibition reduced DNA fragmentation and cytochrome c release and reverted calpain activation. More interestingly, it was able to restore the balance between IL-2/and INF-γ that was altered by RCCS treatment. These data seem to suggest that increased 5-LOX activity might be (at least in part) responsible for altered cytokine levels.

4. Discussion

The effects of LTs on the secretion of cytokines have been reported both *in vitro* and *in vivo* [46]. Here, we demonstrated that increased LTB_4 synthesis upon simulated

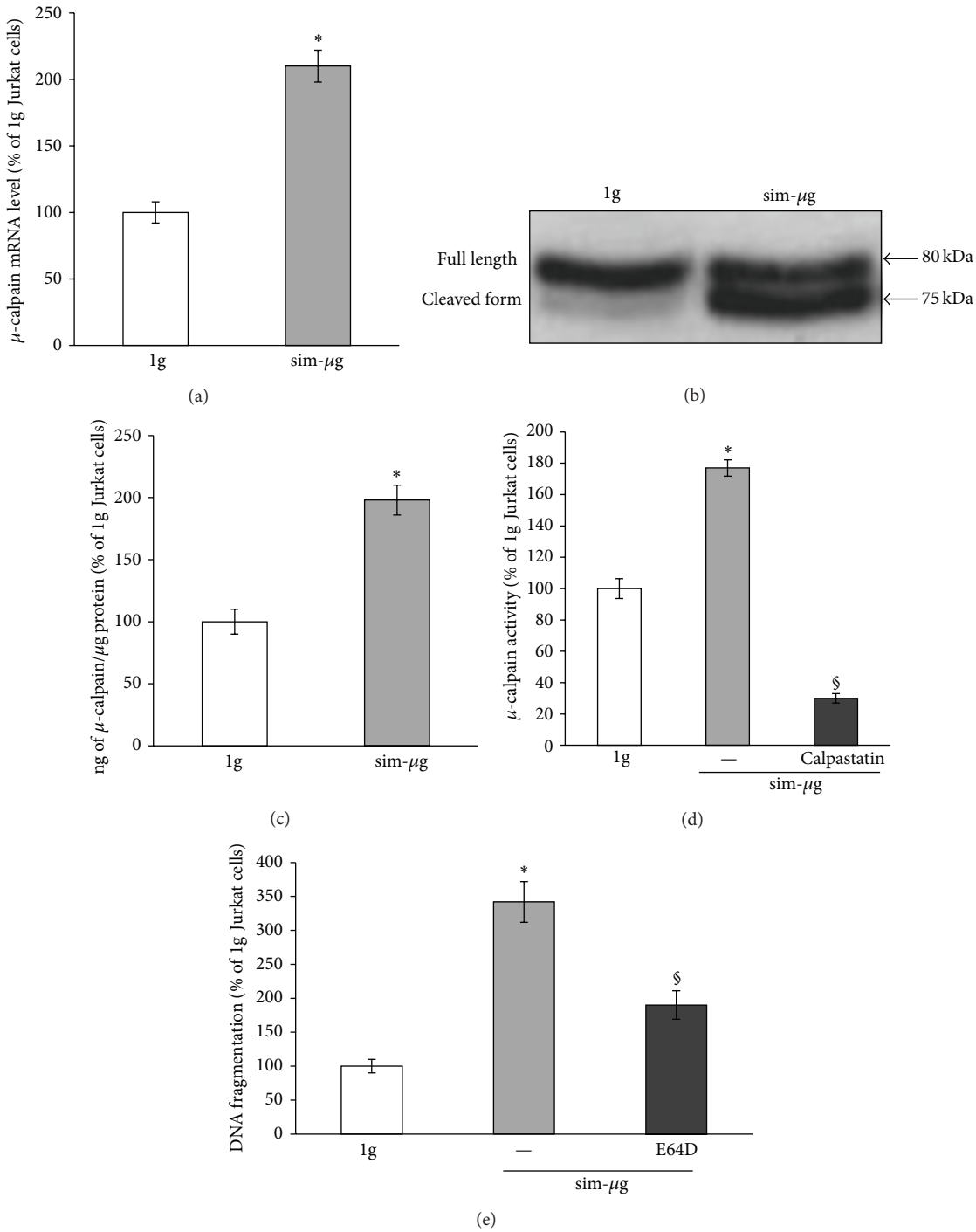

Figure 1: Effect of simulated microgravity on μ-calpain expression and activity in Jurkat T cells. (a) RT-qPCR analysis of *μ-calpain* gene expression in Jurkat cells exposed to simulated microgravity (sim-μg) at 37°C for 48 hours. Gene levels were normalized to the housekeeping GAPDH and expressed as percentage of 1 g cells considered as control, set to 100 (b). Western blot analysis of protein expression in Jurkat cells treated as in (a). (c) ELISA analysis of μ-calpain protein content in Jurkat cells treated as in (a). Results are expressed as percentage of 1 g cells considered as control, set to 100 (= 9.48 ± 0.50 ng/per μg protein) (d) μ-calpain activity analysis in Jurkat cells treated as in (a) in absence (−) or in presence of 5 μM of calpastatin. Results are expressed as percentage of 1 g cells considered as control, set to 100 (= 66.26 ± 3.65 pmol/min per mg protein). (e) DNA fragmentation in Jurkat cells exposed to simulated microgravity for 48 hours in absence (−) or in presence of 10 μM E64D. Values are expressed as percentage of 1 g cells considered as control. *denotes $P < 0.001$ versus 1 g cells; §denotes $P < 0.05$ versus sim-μg cells.

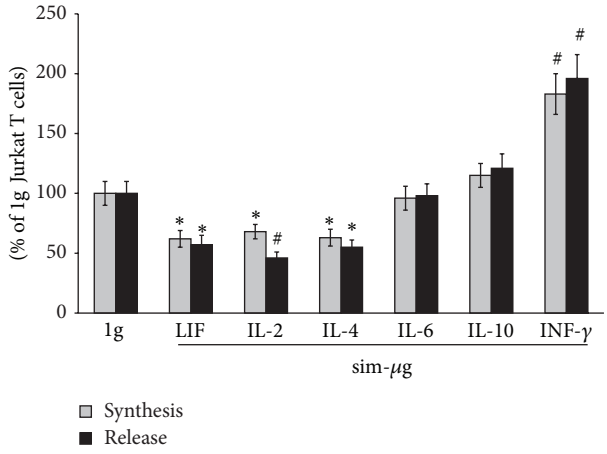

Figure 2: Effect of simulated microgravity on cytokine profile of Jurkat T cells. Cells were exposed (sim-μg) or not exposed (1 g) to simulated microgravity at 37°C for 48 hours and cytokine synthesis (gray bars) and release (black bars) were analyzed as reported in Section 2.6. Results are reported as percentage of 1 g cells set to 100. For synthesis, 100% of IL-2 = 0.27 ± 0.01 $A_{405\,nm}$; 100% of IL-4 = 0.34 ± 0.02 $A_{405\,nm}$; 100% of LIF = 0.22 ± 0.02 $A_{405\,nm}$; 100% of IL-6 = 0.18 ± 0.01 $A_{405\,nm}$; 100% of IL-10 = 0.34 ± 0.02 $A_{405\,nm}$; 100% of INF-γ 0.25 ± 0.02 $A_{405\,nm}$. For release, 100% of LIF = 0.42 ± 0.03 $Abs_{405\,nm}$; 100% of IL-2 = 6.6 ± 0.5 pg/mL; 100% of IL-4 = 1.2 ± 0.1 pg/mL; 100% of IL-6 = 20 ± 2 pg/mL; 100% of IL-10 = 2.5 ± 0.3 pg/mL; 100% INF-γ = 12.2 ± 0.1 pg/mL. *denotes $P < 0.05$ versus 1 g cells; $^{\#}$denotes $P < 0.01$ versus 1 g cells.

Table 3: Effect of 5-LOX inhibition on Jurkat T cells exposed for 48 hours to simulated microgravity (sim-μg) or kept at normal gravity (1g).

Parameter	1g	sim-μg	sim-μg + 10 μM AA861
DNA fragmentation	100 ± 10	342 ±21***	250 ±11$^{\#}$
Cytochrome c release (cytosol/mitochondria ratio)	100 ± 9	450 ±47***	230 ±24$^{\#}$
Calpain activity	100 ± 11	177 ±9***	31 ±2$^{\#}$
IL-2 protein content	100 ± 9	67 ±5*	93 ±8$^{\#}$
INF-γ protein content	100 ± 9	179 ±15**	120 ±4$^{\#}$

Values are reported as percentage of relative control set to 100. For DNA fragmentation, 100% = 0.30 ± 0.03 $A_{405\,nm}$; for cytochrome c release, 100% = 0.074 ± 0.005; for calpain activity, 100% = 66.26 ± 3.65 pmol/min per mg protein; for IL-2 synthesis, 100% = 0.27 ± 0.01 $A_{405\,nm}$; for INF-γ synthesis, 100% = 0.25 ± 0.02 $A_{405\,nm}$. *denotes = $P < 0.05$ versus 1g cells; **denotes $P < 0.01$ versus 1g cells; ***denotes $P < 0.001$ versus 1g cells; $^{\#}$denotes $P < 0.01$ versus sim-μg cells.

microgravity exposure is paralleled by a reduced release of antiapoptotic cytokines, such as LIF, IL-4, and IL-2 [19–23], as well as by a significant increase of the production of the proapoptotic cytokine INF-γ [18, 23]. These data are in line with the immunomodulatory role postulated for 5-LOX metabolites, and especially for LTB_4. Indeed, the latter substance is a powerful chemoattractant for inflammatory cells and induces degranulation, superoxide anion production, and adherence of neutrophils to vascular endothelial cells [48]. LTB_4 has been already demonstrated to affect the production of several cytokines, including IL-1β [49, 50], IL-2 [51, 52], IL-6 [53], INF-γ [54], IL-4 [55], and IL-10 [56]. Moreover, LTB_4 has been also demonstrated to modulate the expression of the IL-2 receptor β-chain in natural killer cells and in $CD8^{+}$ lymphocytes [57].

In this context, our data add further information on the mechanism of PCD activation, suggesting a crosstalk between 5-LOX and μ-calpain signalling. In particular, we demonstrate that exposure of Jurkat T cells to simulated microgravity induced activation of μ-calpain and 5-LOX. Our results suggest that the functional interplay between these two enzymes could be related to the synthesis of a specific pattern of cytokines. In line with this, our results show that 5-LOX inhibition (i) reduced DNA fragmentation and cytochrome c release (typical apoptotic markers); (ii) reestablished the initial IL-2/INF-γ ratio; and (iii) more importantly reverted μ-calpain activation induced by simulated microgravity (Table 3). Furthermore, we showed that treatment of Jurkat T cell with IL-2, whose levels are downregulated upon simulated microgravity exposure (Figure 2), significantly reduced μ-calpain activation upon RCCS treatment. Remarkably, the latter result is in agreement with the well-known antiapoptotic effect of IL-2 [21, 23]. It should be noted that the lack of any increase in μ-calpain activity in the presence of 5-LOX inhibitors might be suggestive that additional and as-yet-unknown 5-LOX products are able to directly activate μ-calpain. Thus, in addition to a specific role of distinct cytokines in modulating the crosstalk between 5-LOX and μ-calpain, we can speculate that 5-LOX activation could also induce the formation of specific lipid hydroperoxides that could trigger PCD *via* μ-calpain activation. In line with the latter hypothesis, hydroperoxides of cardiolipin and phosphatidylserine have been detected as byproducts upon PCD [58]. Consistently, it has been demonstrated that LOX-induced lipid peroxidation triggers AIF-mediated PCD [31]. Indeed, although a finely regulated lipid peroxidation may have beneficial effects for the cells and the whole organism, leading to different physiological roles of LOXs (such as eicosanoid synthesis, cell maturation, and lipid mobilization), when the lipid bilayer of biological membranes is oxidized in an uncontrolled manner (as in the case of external stimuli like microgravity), it may lose its barrier function and thus harm the integrity of subcellular organelles or of the whole cell [59]. Consistently, an overactivated 5-LOX can open pore-like structures in mitochondrial membranes [60, 61], thus forming the basis for a converging role of this enzyme in the induction of PCD by unrelated stimuli [59].

Overall, our results demonstrate that simulated microgravity-dependent increase in 5-LOX activity regulates survival and cytokine release of human T lymphocytes by engaging μ-calpain.

5. Conclusions

Our findings seem to add biochemical support to the immunodepression observed in astronauts exposed to authentic

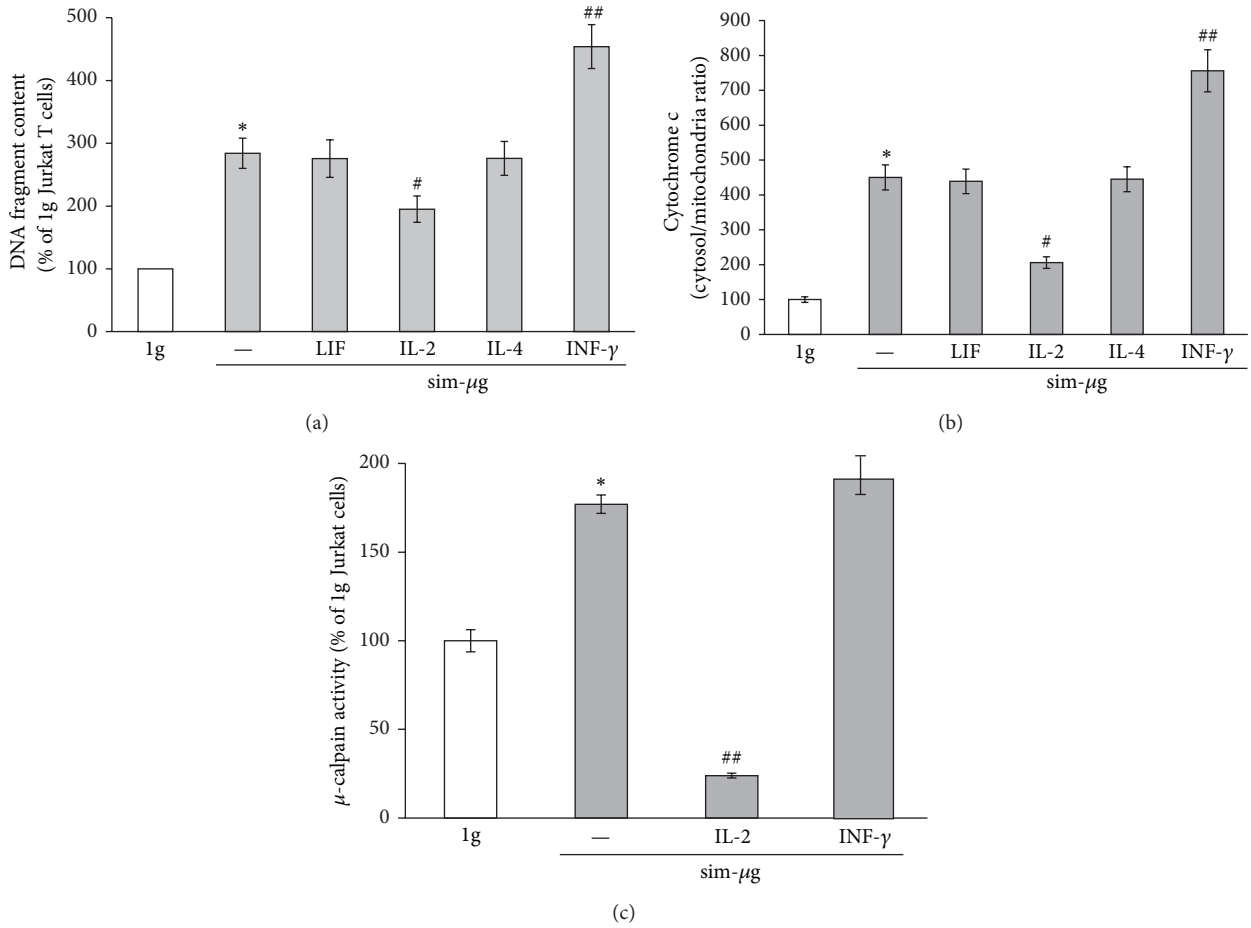

Figure 3: Cytokine effects on Jurkat cell apoptosis under simulated microgravity conditions. Jurkat T cells were exposed (sim-μg) or not exposed (1 g) to simulated microgravity in absence (−) or in presence of the indicated cytokines (10 ng/mL), and DNA fragmentation (a), cytochrome c release (b), and μ-calpain activity (c) were evaluated as reported in Section 2. Results are reported as percentage of 1 g cells set to 100. For DNA fragmentation, 100% = 0.300 ± 0.030 $A_{405\,nm}$; for cytochrome c release, 100% = 0.074 ± 0.005; for μ-calpain activity, 100% = 66.26 ± 3.65 pmol/min per mg protein. *denotes $P < 0.001$ versus1 g cells; $^{\#}$denotes $P < 0.05$ versus sim-μg cells; $^{\#\#}$denotes $P < 0.01$ versus sim-μg cells.

microgravity for long periods of time (e.g., International Space Station crew members or astronauts travelling to Mars). Taking into account that Jurkat E6.1 cells are somewhat different from normal human T cells [61], nonetheless, they are considered a valid experimental model, especially in the light of their exaggerated signaling, making changes much easier to detect. Therefore, only authentic space conditions will give a conclusive answer on whether or not the unbalance between proapoptotic and antiapoptotic cytokines due to impaired 5-LOX and μ-calpain activities can affect immune response, helping to design countermeasures against apoptosis observed in space.

Abbreviations

LOX: Lipoxygenase
AMC: 7-Amido-4-methyl-coumarin
AIF: Apoptosis-inducing factor
RCCS: Rotary cell culture system
ECL: Enhanced chemiluminescence
ELISA: Enzyme-linked immunosorbent assay
GAPDH: Glyceraldehyde-3-phosphate dehydrogenase
GAR-AP: Goat anti-rabbit conjugated to alkaline phosphatase
1 g: Ground gravity
HRP: Horseradish peroxidase
INF-γ: Interferon-γ
IL-2: Interleukin-2
LIF: Leukaemia inhibitory factor
(LT)B_4: Leukotriene B_4
sim-μg: Simulated microgravity
PCD: Programmed cell death
q-RT-PCR: Quantitative reverse transcriptase-polymerase chain reaction
Th1: T-helper 1
Th2: T-helper 2
TNF-β: Tumor necrosis factor-β.

Conflict of Interests

The authors declare that there is no conflict of interests.

Acknowledgment

This investigation was supported under contracts from "Disturbi del Controllo Motorio e Cardiorespiratorio" and "From Molecules to Man," 2006–2009, to Mauro Maccarrone.

References

[1] R. M. Baevsky, V. M. Baranov, I. I. Funtova et al., "Autonomic cardiovascular and respiratory control during prolonged spaceflights aboard the International Space Station," *Journal of Applied Physiology*, vol. 103, no. 1, pp. 156–161, 2007.

[2] L. C. Shackelford, "Musculoskeletal response to space flight," in *Principles of Clinical Medicine for Space Flight*, M. R. Barratt and S. L. Pool, Eds., pp. 293–306, Springer Science and Business Media, New York, NY, USA, 2008.

[3] J. H. Keyak, A. K. Koyama, A. LeBlanc, Y. Lu, and T. F. Lang, "Reduction in proximal femoral strength due to long-duration spaceflight," *Bone*, vol. 44, no. 3, pp. 449–453, 2009.

[4] E. Wang, "Age-dependent atrophy and microgravity travel: what do they have in common?" *The FASEB Journal*, vol. 13, no. 8, pp. S167–S174, 1999.

[5] D. Williams, A. Kuipers, C. Mukai, and R. Thirsk, "Acclimation during space flight: effects on human physiology," *Canadian Medical Association Journal*, vol. 180, no. 13, pp. 1317–1323, 2009.

[6] N. Battista, M. A. Meloni, M. Bari et al., "5-Lipoxygenase-dependent apoptosis of human lymphocytes in the International Space Station: data from the ROALD experiment," *The FASEB Journal*, vol. 26, no. 5, pp. 1791–1798, 2012.

[7] N. Guéguinou, C. Huin-Schohn, M. Bascove et al., "Could spaceflight-associated immune system weakening preclude the expansion of human presence beyond Earth's orbit?" *Journal of Leukocyte Biology*, vol. 86, no. 5, pp. 1027–1038, 2009.

[8] J. Pietsch, J. Bauer, M. Egli et al., "The effects of weightlessness on the human organism and mammalian cells," *Current Molecular Medicine*, vol. 11, no. 5, pp. 350–364, 2011.

[9] B. E. Crucian, R. P. Stowe, D. L. Pierson, and C. F. Sams, "Immune system dysregulation following short- vs long-duration spaceflight," *Aviation Space and Environmental Medicine*, vol. 79, no. 9, pp. 835–843, 2008.

[10] B. Crucian, R. Stowe, S. Mehta et al., "Immune system dysregulation occurs during short duration spaceflight on board the space shuttle," *Journal of Clinical Immunology*, vol. 33, no. 2, pp. 456–465, 2013.

[11] B. S. Crucian, S. R. Zwart, S. Mehta et al., "Plasma cytokine concentrations indicate that in vivo hormonal regulation of immunity is altered during long-duration spaceflight," *Journal of Interferon & Cytokine Research*, 2014.

[12] S. K. Chapes, S. J. Simske, A. D. Forsman, T. A. Bateman, and R. J. Zimmerman, "Effects of space flight and IGF-1 on immune function," *Advances in Space Research*, vol. 23, no. 12, pp. 1955–1964, 1999.

[13] S. K. Chapes, S. J. Simske, G. Sonnenfeld, E. S. Miller, and R. J. Zimmerman, "Effects of spaceflight and PEG-IL-2 on rat physiological and immunological responses," *Journal of Applied Physiology*, vol. 86, no. 6, pp. 2065–2076, 1999.

[14] A. T. Ichiki, L. A. Gibson, T. L. Jago et al., "Effects of spaceflight on rat peripheral blood leukocytes and bone marrow progenitor cells," *Journal of Leukocyte Biology*, vol. 60, no. 1, pp. 37–43, 1996.

[15] Z. Allebban, A. T. Ichiki, L. A. Gibson, J. B. Jones, C. C. Congdon, and R. D. Lange, "Effects of spaceflight on the number of rat peripheral blood leukocytes and lymphocyte subsets," *Journal of Leukocyte Biology*, vol. 55, no. 2, pp. 209–213, 1994.

[16] D. S. Gridley, J. M. Slater, X. Luo-Owen et al., "Spaceflight effects on T lymphocyte distribution, function and gene expression," *Journal of Applied Physiology*, vol. 106, no. 1, pp. 194–202, 2009.

[17] K. Felix, K. Wise, S. Manna et al., "Altered cytokine expression in tissues of mice subjected to simulated microgravity," *Molecular and Cellular Biochemistry*, vol. 266, no. 1-2, pp. 79–85, 2004.

[18] S. P. Tu, M. Quante, G. Bhagat et al., "IFN-γ inhibits gastric carcinogenesis by inducing epithelial cell autophagy and T-cell apoptosis," *Cancer Research*, vol. 71, no. 12, pp. 4247–4259, 2011.

[19] D. Duval, B. Reinhardt, C. Kedinger, and H. Boeuf, "Role of suppressors of cytokine signaling (Socs) in leukemia inhibitory factor (LIF) -dependent embryonic stem cell survival," *The FASEB Journal*, vol. 14, no. 11, pp. 1577–1584, 2000.

[20] H. Slaets, D. Dumont, J. Vanderlocht et al., "Leukemia inhibitory factor induces an antiapoptotic response in oligodendrocytes through Akt-phosphorylation and up-regulation of 14-3-3," *Proteomics*, vol. 8, no. 6, pp. 1237–1247, 2008.

[21] L. R. Devireddy and M. R. Green, "Transcriptional program of apoptosis induction following interleukin 2 deprivation: identification of RC3, a calcium/calmodulin binding protein, as a novel proapoptotic factor," *Molecular and Cellular Biology*, vol. 23, no. 13, pp. 4532–4541, 2003.

[22] L. M. Minter and B. A. Osborne, "Notch and the survival of regulatory T cells: location is everything!," *Science Signaling*, vol. 5, no. 234, article pe31, 2012.

[23] F. C. H. Pinto, G. B. Menezes, S. A. L. Moura, G. D. Cassali, M. M. Teixeira, and D. C. Cara, "Induction of apoptosis in tumor cells as a mechanism of tumor growth reduction in allergic mice," *Pathology Research and Practice*, vol. 205, no. 8, pp. 559–567, 2009.

[24] M.-J. Xie, Y.-G. Ma, F. Gao et al., "Activation of BK_{Ca} channel is associated with increased apoptosis of cerebrovascular smooth muscle cells in simulated microgravity rats," *American Journal of Physiology: Cell Physiology*, vol. 298, no. 6, pp. C1489–C1500, 2010.

[25] D. Grimm, J. Bauer, P. Kossmehl et al., "Simulated microgravity alters differentiation and increases apoptosis in human follicular thyroid carcinoma cells," *The FASEB Journal*, vol. 16, no. 6, pp. 604–606, 2002.

[26] C. Y. Kang, L. Zou, M. Yuan et al., "Impact of simulated microgravity on microvascular endothelial cell apoptosis," *European Journal of Applied Physiology*, vol. 111, no. 9, pp. 2131–2138, 2011.

[27] B. M. Uva, M. A. Masini, M. Sturla et al., "Microgravity-induced apoptosis in cultured glial cells," *European Journal of Histochemistry*, vol. 46, no. 3, pp. 209–214, 2002.

[28] L. H. Yan, Z. Hong, M. G. Ying et al., "Simulated microgravity conditions and carbon ion irradiation induce spermatogenic cell apoptosis and sperm DNA damage," *Biomedical and Environmental Sciences*, vol. 26, no. 9, pp. 726–734, 2013.

[29] B. Dang, Y. Yang, E. Zhang et al., "Simulated microgravity increases heavy ion radiation-induced apoptosis in human B lymphoblasts," *Life Sciences*, vol. 97, no. 2, pp. 123–128, 2014.

[30] M. Maccarrone, N. Battista, M. Meloni et al., "Creating conditions similar to those that occur during exposure of cells to microgravity induces apoptosis in human lymphocytes by 5-lipoxygenase-mediated mitochondrial uncoupling and cytochrome c release," *Journal of Leukocyte Biology*, vol. 73, no. 4, pp. 472–481, 2003.

[31] A. Seiler, M. Schneider, H. Förster et al., "Glutathione peroxidase 4 senses and translates oxidative stress into 12/15-lipoxygenase dependent- and AIF-mediated cell death," *Cell Metabolism*, vol. 8, no. 3, pp. 237–248, 2008.

[32] M.-S. Lee, Y. T. Kwon, M. Li, J. Peng, R. M. Friedlander, and L.-H. Tsai, "Neurotoxicity induces cleavage of p35 to p25 by calpain," *Nature*, vol. 405, no. 6784, pp. 360–364, 2000.

[33] D. Guerini, B. Pan, and E. Carafoli, "Expression, purification, and characterization of isoform 1 of the plasma membrane $Ca2^{+}$ pump: Focus on calpain sensitivity," *The Journal of Biological Chemistry*, vol. 278, no. 40, pp. 38141–38148, 2003.

[34] H.-Y. Wu, K. Tomizawa, Y. Oda et al., "Critical role of calpain-mediated cleavage of calcineurin in excitotoxic neurodegeneration," *The Journal of Biological Chemistry*, vol. 279, no. 6, pp. 4929–4940, 2004.

[35] B. M. Polster, G. Basañez, A. Etxebarria, J. M. Hardwick, and D. G. Nicholls, "Calpain I induces cleavage and release of apoptosis-inducing factor from isolated mitochondria," *Journal of Biological Chemistry*, vol. 280, no. 8, pp. 6447–6454, 2005.

[36] S. A. Susin, H. K. Lorenzo, N. Zamzami et al., "Molecular characterization of mitochodrial apoptosis-inducing factor," *Nature*, vol. 397, no. 6718, pp. 441–446, 1999.

[37] R. Mitteregger, G. Vogt, E. Rossmanith, and D. Falkenhagen, "Rotary cell culture system (RCCS): a new method for cultivating hepatocytes on microcarriers," *The International Journal of Artificial Organs*, vol. 22, no. 12, pp. 816–822, 1999.

[38] M. V. Catani, V. Gasperi, D. Evangelista, A. F. Agrò, L. Avigliano, and M. MacCarrone, "Anandamide extends platelets survival through CB1-dependent Akt signaling," *Cellular and Molecular Life Sciences*, vol. 67, no. 4, pp. 601–610, 2010.

[39] K. G. Daniel, J. S. Anderson, Q. Zhong, A. Kazi, P. Gupta, and Q. P. Dou, "Association of mitochondrial calpain activation with increased expression and autolysis of calpain small subunit in an early stage of apoptosis," *International Journal of Molecular Medicine*, vol. 12, no. 2, pp. 247–252, 2003.

[40] V. Gasperi, F. Fezza, N. Pasquariello et al., "Endocannabinoids in adipocytes during differentiation and their role in glucose uptake," *Cellular and Molecular Life Sciences*, vol. 64, no. 2, pp. 219–229, 2007.

[41] P. Łopatniuk and J. M. Witkowski, "Conventional calpains and programmed cell death," *Acta Biochimica Polonica*, vol. 58, no. 3, pp. 287–296, 2011.

[42] H. Sorimachi, S. Ishiura, and K. Suzuki, "Structure and physiological function of calpains," *Biochemical Journal*, vol. 328, article 3, pp. 721–732, 1997.

[43] T. Uemori, T. Shimojo, K. Asada et al., "Characterization of a functional domain of human calpastatin," *Biochemical and Biophysical Research Communications*, vol. 166, no. 3, pp. 1485–1493, 1990.

[44] J. Takano, M. Tomioka, S. Tsubuki et al., "Calpain mediates excitotoxic DNA fragmentation via mitochondrial pathways in adult brains: evidence from calpastatin mutant mice," *The Journal of Biological Chemistry*, vol. 280, no. 16, pp. 16175–16184, 2005.

[45] A. Rami, R. Agarwal, G. Botez, and J. Winckler, "μ-Calpain activation, DNA fragmentation, and synergistic effects of caspase and calpain inhibitors in protecting hippocampal neurons from ischemic damage," *Brain Research*, vol. 866, no. 1-2, pp. 299–312, 2000.

[46] Y. Yang, Z. H. Liu, C. F. Ware, and J. D. Ashwell, "A cysteine protease inhibitor prevents activation-induced T-cell apoptosis and death of peripheral blood cells from human immunodeficiency virus-infected individuals by inhibiting upregulation of Fas ligand," *Blood*, vol. 89, no. 2, pp. 550–557, 1997.

[47] Y. Tanihiro, Y. Chieko, O. Kenkichi et al., "2,3,5-Trimethyl-6-(12-hydroxy-5,10-dodecadiynyl)-l,4-benzoquinone (AA861), a selective inhibitor of the 5-lipoxygenase reaction and the biosynthesis of slow-reacting substance of anaphylaxis," *Biochimica et Biophysica Acta: Lipids and Lipid Metabolism*, vol. 713, no. 2, pp. 470–473, 1982.

[48] J. C. Eun, E. E. Moore, A. Banerjee et al., "Leukotriene B4 and its metabolites prime the neutrophil oxidase and induce proinflammatory activation of human pulmonary microvascular endothelial cells," *Shock*, vol. 35, no. 3, pp. 240–244, 2011.

[49] G. Bonizzi, J. Piette, M. P. Merville, and V. Bours, "Distinct signal transduction pathways mediate nuclear factor- κB induction by IL-1beta in epithelial and lymphoid cells," *Journal of Immunology*, vol. 159, no. 11, pp. 5264–5272, 1997.

[50] J. Marcinkiewicz, A. Grabowska, K. Bryniarski, and B. M. Chain, "Enhancement of $CD4^{+}$ T-cell-dependent interleukin-2 production in vitro by murine alveolar macrophages: the role of leukotriene B4," *Immunology*, vol. 91, no. 3, pp. 369–374, 1997.

[51] M. Los, H. Schenk, K. Hexel, P. A. Baeuerle, W. Droge, and K. Schulze-Osthoff, "IL-2 gene expression and NF-κB activation through CD28 requires reactive oxygen production by 5-lipoxygenase," *The EMBO Journal*, vol. 14, no. 15, pp. 3731–3740, 1995.

[52] J. Dornand, C. Sekkat, J.-C. Mani, and M. Gerber, "Lipoxygenase inhibitors suppress IL-2 synthesis: relationship with rise of $[Ca^{++}]$i and the events dependent on protein kinase C activation," *Immunology Letters*, vol. 16, no. 2, pp. 101–106, 1987.

[53] M. A. Brach, S. de Vos, C. Arnold, H.-J. Gruß, R. Mertelsmann, and F. Herrmann, "Leukotriene B4 transcriptionally activates interleukin-6 expression involving NK-NB and NF-IL6," *European Journal of Immunology*, vol. 22, no. 10, pp. 2705–2711, 1992.

[54] H. M. Johnson and B. A. Torres, "Leukotrienes: Positive signals for regulation of γ-interferon production," *Journal of Immunology*, vol. 132, no. 1, pp. 413–416, 1984.

[55] N. Dugas, B. Dugas, J.-P. Kolb, K. Yamaoka, J. F. Delfraiss, and C. Damais, "Role of leukotriene B4 in the interleukin-4-induced human mononuclear phagocyte activation," *Immunology*, vol. 88, no. 3, pp. 384–388, 1996.

[56] S. Jozefowski, R. Biedroń, M. Bobek, and J. Marcinkiewicz, "Leukotrienes modulate cytokine release from dendritic cells," *Immunology*, vol. 116, no. 4, pp. 418–428, 2005.

[57] J. Stankova, N. Gagnon, and M. Rola-Pleszczynski, "Leukotriene B4 augments interleukin-2 receptor-beta (IL-2Rβ) expression and IL-2Rβ-mediated cytotoxic response in human peripheral blood lymphocytes," *Immunology*, vol. 76, no. 2, pp. 258–263, 1992.

[58] V. E. Kagan, V. A. Tyurin, J. Jiang et al., "Cytochrome c acts as a cardiolipin oxygenase required for release of proapoptotic factors," *Nature Chemical Biology*, vol. 1, no. 4, pp. 223–232, 2005.

[59] M. Maccarrone, G. Melino, and A. Finazzi-Agrò, "Lipoxygenases and their involvement in programmed cell death," *Cell Death and Differentiation*, vol. 8, no. 8, pp. 776–784, 2001.

[60] K. van Leyen, R. M. Duvoisin, H. Engelhardt, and M. Wiedmann, "A function for lipoxygenase in programmed organelle degradation," *Nature*, vol. 395, no. 6700, pp. 392–395, 1998.

[61] R. R. Bartelt, N. Cruz-Orcutt, M. Collins, and J. C. D. Houtman, "Comparison of T cell receptor-induced proximal signaling and downstream functions in immortalized and primary T cells," *PLoS ONE*, vol. 4, no. 5, Article ID e5430, 2009.

Hindawi Publishing Corporation
BioMed Research International
Volume 2014, Article ID 652863, 5 pages
http://dx.doi.org/10.1155/2014/652863

Research Article

How Microgravity Changes Galectin-3 in Thyroid Follicles

Elisabetta Albi,[1] Francesco Curcio,[2] Andrea Lazzarini,[1,2] Alessandro Floridi,[1] Samuela Cataldi,[1] Remo Lazzarini,[1] Elisabetta Loreti,[3] Ivana Ferri,[3] and Francesco Saverio Ambesi-Impiombato[2]

[1] *Laboratory of Nuclear Lipid BioPathology, CRABiON, 06100 Perugia, Italy*
[2] *Department of Medical and Biological Sciences, University of Udine, 33100 Udine, Italy*
[3] *Institute of Pathologic Anatomy and Histology, University of Perugia, 06100 Perugia, Italy*

Correspondence should be addressed to Elisabetta Albi; elisabetta.albi@yahoo.com

Received 22 April 2014; Revised 7 August 2014; Accepted 28 August 2014; Published 11 September 2014

Academic Editor: Monica Monici

After long-term exposure to real microgravity thyroid gland *in vivo* undergoes specific changes, follicles are made up of larger thyrocytes that produce more cAMP and express more thyrotropin-receptor, caveolin-1, and sphingomyelinase and sphingomyelin-synthase; parafollicular spaces lose C cells with consequent reduction of calcitonin production. Here we studied four immunohistochemical tumor markers (HBME-1, MIB-1, CK19, and Galectin-3) in thyroid of mice housed in the Mouse Drawer System and maintained for 90 days in the International Space Station. Results showed that MIB-1 proliferative index and CK19 are negative whereas HBME-1 and Galectin-3 are overexpressed. The positivity of Galectin-3 deserves attention not only for its expression but also and especially for its localization. Our results highlighted that, in microgravity conditions, Galectin-3 leaves thyrocytes and diffuses in colloid. It is possible that the gravity force contributes to the maintenance of the distribution of the molecules in both basal membrane side and apical membrane side and that the microgravity facilitates slippage of Galectin-3 in colloid probably due to membrane remodelling-microgravity induced.

1. Introduction

Galectins are endogenous lectins which constitute a galactoside-binding protein family of 15 members [1]. All members share close sequence homology in their carbohydrate recognition domain but exhibit different affinities for different saccharide ligands and can be bi- or multivalent in terms of their ligand-binding activity in cell surface [2]. Eukaryotic cell surfaces are dominated by the glycocalyx, a ~100 nm wide macromolecular structure consisting of glycans attached to proteins and lipids and N-glycans appear to be the major ligand for galectins [3]. Each member of the galectin family contains at least one domain of about 130 amino acids; this domain binds to saccharides and is designated the carbohydrate recognition domain (CRD). Based on the number and organization of domains in the polypeptides, the galectins have been classified into subfamilies: (a) the prototype group contains one domain, the CRD; (b) the chimera group contains a proline- (P-) and glycine- (G-) rich domain (also about 130 amino acids) which fused amino terminal to the CRD; and (c) the tandem repeat group contains two CRDs [4].

Galectin-3 (Gal-3), the only representative of the chimera group, was first discovered as an IgE-binding protein and characterized as a 32 kDa antigen on the surface of murine macrophages [5]. It is mainly a cytosolic protein but can easily traverse the intracellular and plasma membranes to translocate into the nucleus or mitochondria or get externalized [6]. The protein shuttles between the cytoplasm and nucleus on the basis of targeting signals that are recognized by importins for nuclear localization and exportin-1 for nuclear export. Depending on the cell type, specific experimental conditions *in vitro*, or tissue location, Gal-3 has been reported to be exclusively cytoplasmic, predominantly nuclear, or distributed between the two compartments [7]. The presence of Gal-3 in the nucleus is dependent on the integrity

of ribonucleoprotein complexes [8] and a Gal-3-U1 small nuclear ribonucleoprotein (snRNP) complex has been identified, which provides a mechanism of incorporation of the Gal-3 into the pre-mRNA splicing substrate [9]. In addition, Gal-3 is secreted via nonclassical pathway outside of the cell independent on the classical secretory pathway through the endoplasmic reticulum/Golgi network thus being found on the cell surface or in the extracellular space [10]. Thus, Gal-3 is a multifunctional protein, which regulates pleiotropic biological functions such as cell growth, cell adhesion, cell-cell interactions, apoptosis, angiogenesis, and mRNA processing. Its unique structure enables interacting with a plethora of ligands in a carbohydrate dependent or independent manner [6].

In thyroid gland, Gal-3 plays a role in the pathogenesis of well-differentiated carcinoma, particularly in papillary carcinoma [11]. Therefore, it is one of the markers most commonly used to assist in distinguishing thyroid lesions together to human bone marrow endothelial cell-1 (HBME-1) as a tumor marker of follicular origin and cytokeratin-19 (CK-19) with general intense and diffuse expression in papillary carcinoma and heterogeneous labeling in carcinoma and in follicular adenoma [12]. In addition MIB-1 is useful in evaluating proliferative activity and in predicting the aggressiveness of thyroid carcinoma [13].

We have previously demonstrated that microgravity induces changes in the physiology of the thyroid gland. In fact, in comparison with control animals, thyroids of spaceflight animals have a more homogenous structure, produce more cAMP, and overexpress thyrotropin-receptor (TSHR), caveolin-1 [14], and sphingomyelinase and sphingomyelin-synthase [15] and are characterized by a loss of parafollicular cells with reduction of calcitonin production [16].

Data are not available at the time regarding the evaluation of thyroid tumor markers in microgravity. We report for the first time the effect of long-term exposure to real microgravity environment on thyroid HBME-1, MIB-1, CK19, and Gal-3.

2. Materials and Methods

2.1. Experimental Design and Animal Care. All experimental procedures were authorized by the Public Veterinary Health Department of the Italian Ministry of Health. The experiment was also conducted in accordance with the regulations for the care and use of laboratory animals and with the guidelines of the Japanese Physiological Society. Furthermore, this study was also approved by the Committee on Animal Care and Use at Graduate School of Medicine, Osaka University (no. 22-071). Finally, the protocol utilized in the study has been authorized by the Public Veterinary Health Department of the Italian Ministry of Health. All experiments were carried out using male C57BL/10J mice (8 weeks old).

2.2. Microgravity Experiment. 3 mice were individually housed in the Mouse Drawer System (MDS), a 11.6 × 9.8 × 8.4 cm payload developed by Thales-Alenia Space Italy and all treatments were performed as previously reported [14]. Food and water were supplied *ad libitum*. The MDS was launched in the Space Shuttle Discovery, within the Space Transport System (STS)-128 mission, on August 28, 2009. It was then housed in Japanese Experimental Module (Kibou) on the ISS until its return to the Earth by Space Shuttle Atlantis (STS-129 mission) on November 27, 2009. Only 1 mouse returned to the Earth alive after 91 days of space flight.

Thyroids were sampled bilaterally from each mouse killed by inhalation of carbon dioxide at the Life Sciences Support Facility of Kennedy Space Center within 3-4 hours after landing and either processed or frozen immediately, according to the various experimental protocols. The procedure was approved by the IACUC protocol n° FLT-09-070(KSC).

After the spaceflight experiment, the on-ground experiment was also carried out at the Vivarium of the Advanced Biotechnology Center in Genoa, Italy. One group of 3 mice with the same species, sex, and age was housed in normal vivarium cage as the laboratory control. Amount of food and water supplementation and environmental conditions were simulated as the flight group. After 3 months, thyroids were sampled bilaterally and treated for spaceflight mice.

2.3. Thyroid Tissue Treatment. The thyroid lobes were fixed in 4% neutral phosphate-buffered formaldehyde solution for 24 h as previously reported [14]. Thyroids were dropped with essentially random orientation in paraffin. The paraffin blocks were sectioned into 4-μm-thick sections. All sections were mounted on silane-coated glass slides. Each slide contained a pair of sections at a distance equal to 140 μm. Between 5 and 14 pairs of sections were sampled excluding the first and the last; sections 2, 6, and 10 were used for HBME-1 detection, sections 3, 7, and 11 for MIB-1 detection, sections 4, 8, and 12 for CK19 detection, and sections 5, 9, and 13 for Gal-3 detection. Tissue sections were deparaffinized and rehydrated through a series of xylene and ethanol washes.

2.4. Immunohistochemical Analysis. For immunohistochemical analysis Bond Dewax solution was used for removal of paraffin from tissue sections before rehydration and immunostaining on the Bond automated system (Leica Biosystems Newcastle Ltd, UK) as previously reported [17]. Immunostaining detection was performed according to Bancroft and Stevens [18] by using HBME-1 and Ki-67 (MIB-1 clone) from Dako (Milano, Italy) and CK19 and Gal-3 antibodies and Bond Polymer Refine Detection from Leica Biosystems (Newcastle Ltd, UK). The observations were performed by using inverted microscopy EUROMEX FE 2935 (ED Amhem, The Netherlands) equipped with a CMEX 5000 camera system (40x magnification). The analysis of the tissue section size was performed by ImageFocus software.

2.5. Statistical Analysis. The experiments have been conducted on the thyroid of 1 animal for the microgravity experiment (the only ones that returned alive from the mission) and 3 control animals for the microgravity experiment (vivarium 1). Median and range of sections 2, 6, and 10 (HBME-1), of sections 3, 7, and 11 (MIB-1), of sections 4, 8, and 12 (CK19), and of sections 5, 9, and 13 (Gal-3) were given.

3. Results and Discussion

Prolonged space flights are known to elicit changes in human cardiovascular, musculoskeletal, immune, and nervous systems whose functions are regulated by the thyroid gland [14]. The structure of thyroid shows the presence of follicles, containing colloid and surrounded by a single layer of thyroid epithelial cells or thyrocytes that produce the metabolically active iodothyronines, and parafollicular spaces with thyroid C cells that produce calcitonin [19]. We have previously reported that thyrocyte cells in culture delay cell growth and enter into a proapoptotic state after long stay on the International Space Station (ISS) [20]. *In vivo* experiments on the board of ISS showed that thyroid of spaceflight mice has more ordered follicles with thicker thyrocytes containing increased nuclear volume [14] and reduction of interfollicular space with loss of C cells [16] in comparison with thyroid gland of ground mice. In order to verify whether the structural changes of the thyroid gland in microgravity conditions could lead to pathological conditions, in this study we investigated the immunoexpression of markers known to be related to clinical outcome. The limitation of the present paper is that only 1 mouse survived to the 91-day spaceflight. However the MDS experiment was a unique opportunity to study the microgravity long-term exposure effects on several tissues of an animal model and to collect interesting observations that could prepare the field to future experiments. The results showed that microgravity gives a nonspecific staining in the colloid during MIB-1, CK19, and Gal-3 immunohistochemistry analysis, absent in control samples. It is really hard to pinpoint the reason but it is possible to hypothesize an increase of membrane permeability microgravity-dependent on the basis of the observation that, at the end of the spaceflight, endothelial cells display profound changes indicating cytoskeletal lesions and increased cell membrane permeability [21]. MIB-1 and CK19 immunopositivity do not show changes in thyroid of spaceflight mice in comparison with control animals (Figure 1(a)). Differently, the immunostaining is present for HBME-1 and it is very strong for Gal-3 (Figure 1(a)). Alshenawy demonstrated that no single marker is completely sensitive and specific for diagnosis of thyroid lesions but only their combination [22] with Gal-3 + HBME-1 was considered the best combination for distinguishing benign from malignant lesions [23]. In thyroid of spaceflight mice the structure of thyroid follicles is more organized than that of the control animals [14] and thyrocytes delay their growth [20] and MIB-1 is negative. So it is very difficult at the moment to consider that the expression of HBME-1 and Gal-3 markers is linked to tumor transformation. However, the possibility that HBME-1 and Gal-3 overexpression might indicate a premaligne state of thyroid tissue cannot be excluded by considering that in microgravity follicles are made up of cells 2 times larger and colloid darker [14] similar to those of papillary carcinoma [24]. Our result showed that HBME-1 is present only in trace in thyroid of control mice maintained in the vivarium whereas it appears evident after space flight with well-defined localization in thyrocytes (Figure 1(a)). Median and range value of immunopositive surface area is 4,62 (5,51–4,57) mm^2, and its ratio in relation

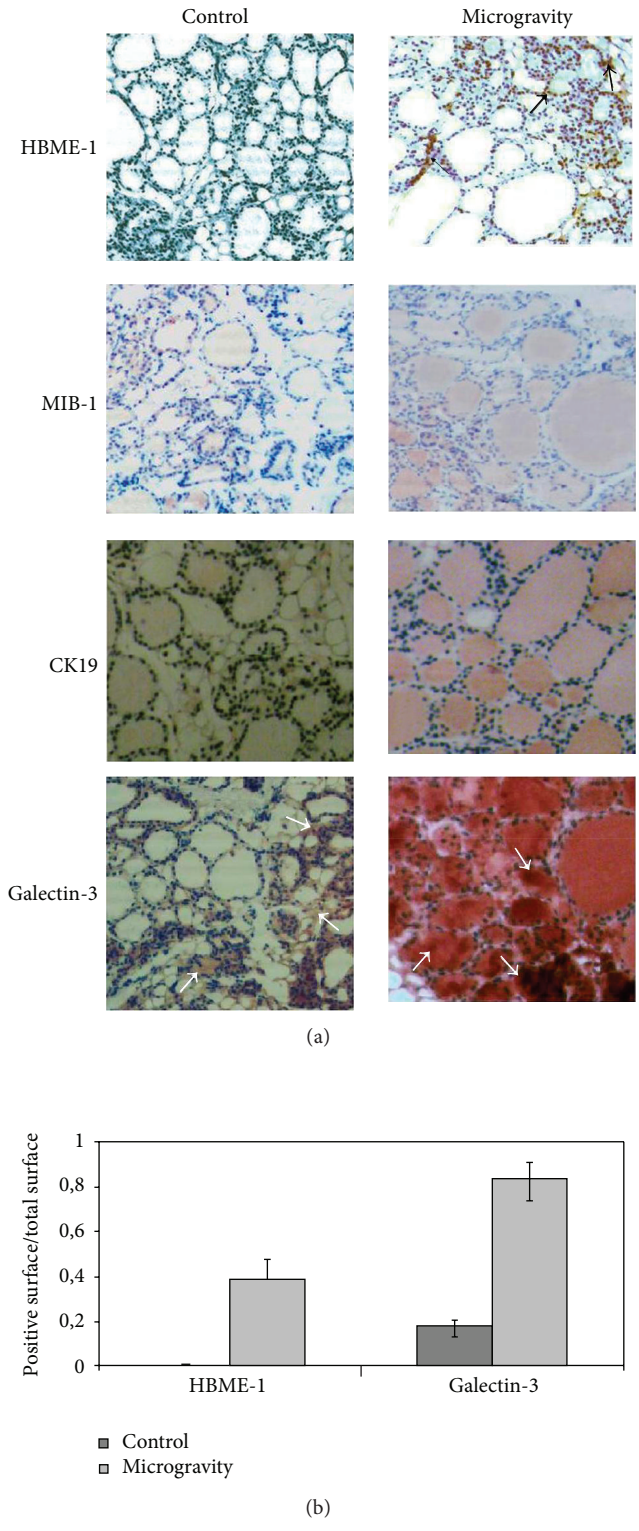

Figure 1: Effect of microgravity on HBME-1, MIB-1, CK19, and Galectin-3. (a) Marker detection in thyroid tissue by immunohistochemical staining. "Control," mice maintained in vivarium cages; "microgravity," experimental mice in space environment. (b) Ratio between the immunopositive surface and total surface of thyroid lobe. The values are expressed as median and range of two sections as reported in Material and Methods, 40x magnification. The arrows indicate positive areas.

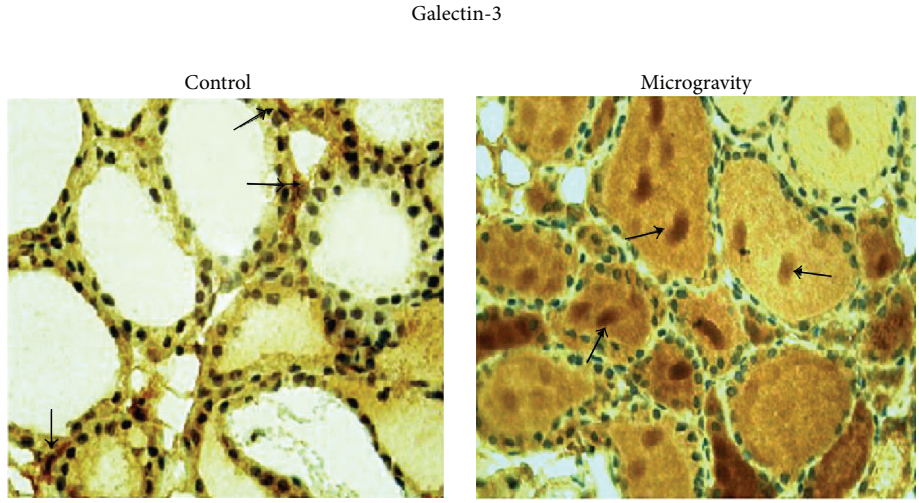

Figure 2: Localization of Galectin-3 in colloid. Gal-3 immunohistochemical staining. "Control," mice maintained in vivarium cages; "microgravity," experimental mice in space environment, 40x magnification. The arrows indicate positive areas.

to total surface is reported in Figure 1(b). Gal-3 labelling is present in some of follicular thyrocytes of control animals and it increases strongly in spaceflight mice (Figure 1(a)). Median and range value of immunopositive surface area is 1,72 (1,99–1,25) mm^2 in the control and 7,94 (8,59–7,00) in microgravity by increasing 4,67 times the positive surface/total surface ratio (Figure 1(b)). The presence of Gal-3 in normal thyroid tissue has already been demonstrated [25]. Our data show an overexpression in microgravity. We do not have support in the literature since this is the first study on observation of the behavior of thyroid pathological markers in microgravity. Nevertheless Grosse et al. demonstrated that NF-κB is overexpressed and different factors that interact with it are differentially regulated under altered gravity conditions [26]. In addition spaceflight conditions change gene expression profile in thyroid cancer cells [27]. Therefore microgravity influences gene expression and consequently protein content. However, the positivity of Gal-3 deserves attention not only for its expression but also and especially for its localization. Our results highlighted that, in microgravity conditions, Gal-3 leaves thyrocytes and diffuses in colloid (Figure 2). It is possible that microgravity induces changes of cell membrane that in turn facilitates the escape of Gal-3 accumulated in thyrocytes. We have previously demonstrated that thyrocytes in culture (FTRL-5 cell line) release thyrotropin receptor, linked to cholesterol and sphingomyelin, in culture medium during space missions by indicating a depletion of lipid rafts and consequently cell membrane remodelling [20]. Clarke et al. told about microgravity-induced decrease in membrane order [28] and Hsu et al. localized Gal-3 in membrane lipid rafts [29]. It is possible to suppose that Gal-3 overexpressed in thyrocytes moves into colloid due to the modification of the cell membrane following the variation of gravity force. It has been demonstrated that Gal-3 is mainly a cytosolic protein but it shuttles to the nucleus or extracellular space the basis of targeting signals [6]. Here we do not have specific staining in these locations but the molecules move in the opposite direction; they do not protrude from the basal membrane of thyrocytes towards the extracellular space but from the apical membrane to the colloid. On the other hand, Delacour et al. suggested a direct role of Gal-3 in apical sorting as a sorting receptor [30]. It is possible that the gravity force contributes to the maintenance of the distribution of the molecules in both basal membrane side and apical membrane side and that the microgravity facilitates slippage of Gal-3 in colloid.

4. Conclusion

To our knowledge this is the first study correlating thyroid tumor markers with long stay mice in microgravity conditions. Here we found higher expression of HBME-1 and Gal-3 in comparison with ground gravity. However MIB-1 proliferative index and CK19 are negative. Gal-3, usually present in cytoplasm, nuclei, and extracellular space, leaves thyrocytes and diffuses in colloid probably due to membrane remodelling-microgravity induced.

Conflict of Interests

The authors declare that there is no conflict of interests regarding the publication of this paper.

Acknowledgment

This work has been partially supported by grants from Agenzia Spaziale Italiana (ASI).

References

[1] S. H. Barondes, V. Castronovo, D. N. W. Cooper et al., "Galectins: a family of animal β-galactoside-binding lectins," *Cell*, vol. 76, no. 4, pp. 597–598, 1994.

[2] S. Di Lella, V. Sundblad, J. P. Cerliani et al., "When galectins recognize glycans: from biochemistry to physiology and back again," *Biochemistry*, vol. 50, no. 37, pp. 7842–7857, 2011.

[3] A. Grigorian, S. Torossian, and M. Demetriou, "T-cell growth, cell surface organization, and the galectin-glycoprotein lattice," *Immunological Reviews*, vol. 230, no. 1, pp. 232–246, 2009.

[4] J. Hirabayashi and K.-I. Kasai, "The family of metazoan metal-independent β-galactoside-binding lectins: structure, function and molecular evolution," *Glycobiology*, vol. 3, no. 4, pp. 297–304, 1993.

[5] M. K. Ho and T. A. Springer, "Mac-2, a novel 32,000 Mr mouse macrophage subpopulation-specific antigen defined by monoclonal antibodies," *Journal of Immunology*, vol. 14, pp. 1221–1228, 1982.

[6] T. Funasaka, A. Raz, and P. Nangia-Makker, "Nuclear transport of galectin-3 and its therapeutic implications," *Seminars in Cancer Biology*, vol. 27C, pp. 30–38, 2014.

[7] K. C. Haudek, P. G. Voss, L. E. Locascio, J. L. Wang, and R. J. Patterson, "A mechanism for incorporation of galectin-3 into the spliceosome through its association with U1 snRNP," *Biochemistry*, vol. 48, no. 32, pp. 7705–7712, 2009.

[8] J. G. Laing and J. L. Wang, "Identification of carbohydrate binding protein 35 in heterogeneous nuclear ribonucleoprotein complex," *Biochemistry*, vol. 27, no. 14, pp. 5329–5334, 1988.

[9] K. C. Haudek, K. J. Spronk, P. G. Voss, R. J. Patterson, J. L. Wang, and E. J. Arnoys, "Dynamics of galectin-3 in the nucleus and cytoplasm," *Biochimica et Biophysica Acta*, vol. 1800, no. 2, pp. 181–189, 2010.

[10] J. Dumic, S. Dabelic, and M. Flögel, "Galectin-3: an open-ended story," *Biochimica et Biophysica Acta*, vol. 1760, no. 4, pp. 616–635, 2006.

[11] T. Yoshii, H. Inohara, Y. Takenaka et al., "Galectin-3 maintains the transformed phenotype of thyroid papillary carcinoma cells," *International Journal of Oncology*, vol. 18, no. 4, pp. 787–792, 2001.

[12] L. L. de Matos, A. B. del Giglio, C. O. Matsubayashi, M. de Lima Farah, and M. A. da Silva Pinhal, "Expression of ck-19, galectin-3 and hbme-1 in the differentiation of thyroid lesions: systematic review and diagnostic meta-analysis," *Diagnostic Pathology*, vol. 7, no. 1, article 97, 2012.

[13] P. Kjellman, G. Wallin, A. Höög, G. Auer, C. Larsson, and J. Zedenius, "MIB-1 index in thyroid tumors: a predictor of the clinical course in papillary thyroid carcinoma?" *Thyroid*, vol. 13, no. 4, pp. 371–380, 2003.

[14] M. A. Masini, E. Albi, C. Barmo et al., "The impact of long-term exposure to space environment on adult mammalian organisms: a study on mouse thyroid and testis," *PLoS ONE*, vol. 7, no. 4, Article ID e35418, 2012.

[15] E. Albi, F. Curcio, R. Spelat et al., "Observing the mouse thyroid sphingomyelin under space conditions: a case study from the MDS mission in comparison with hypergravity conditions," *Astrobiology*, vol. 12, no. 11, pp. 1035–1041, 2012.

[16] E. Albi, F. Curcio, R. Spelat et al., "Loss of parafollicular cells during gravitational changes (microgravity, hypergravity) and the secret effect of pleiotrophin," *PLoS ONE*, vol. 7, no. 12, Article ID e48518, 2012.

[17] E. Albi, F. Curcio, R. Spelat et al., "The thyroid lobes: the different twins," *Archives of Biochemistry and Biophysics*, vol. 518, no. 1, pp. 16–22, 2012.

[18] J. D. Bancroft and A. Stevens, Eds., *Theory and Practice of Histological Techniques*, Churchill Livingstone, New York, NY, USA, 1996.

[19] C. C. Capen and S. L. Martin, "The effects of xenobiotics on the structure and function of thyroid follicular and C-cells," *Toxicologic Pathology*, vol. 17, no. 2, pp. 266–293, 1989.

[20] E. Albi, F. S. Ambesi-Impiombato, M. Peverini et al., "Thyrotropin receptor and membrane interactions in FRTL-5 thyroid cell strain in microgravity," *Astrobiology*, vol. 11, no. 1, pp. 57–64, 2011.

[21] M. Y. Kapitonova, S. Muid, G. R. A. Froemming et al., "Real space flight travel is associated with ultrastructural changes, cytoskeletal disruption and premature senescence of HUVEC," *Malaysian Journal of Pathology*, vol. 34, no. 2, pp. 103–113, 2012.

[22] H. A. Alshenawy, "Utility of immunohistochemical markers in diagnosis of follicular cell derived thyroid lesions," *Pathology & Oncology Research*, 2014.

[23] H. A. Saleh, J. Feng, F. Tabassum, O. Al-Zohaili, M. Husain, and T. Giorgadze, "Differential expression of galectin-3, CK19, HBME1, and Ret oncoprotein in the diagnosis of thyroid neoplasms by fine needle aspiration biopsy," *CytoJournal*, vol. 6, article 18, 2009.

[24] R. V. Lloyd, D. Buehler, and E. Khanafshar, "Papillary thyroid carcinoma variants," *Head and Neck Pathology*, vol. 5, no. 1, pp. 51–56, 2011.

[25] J. Feilchenfeldt, M. Tötsch, S.-Y. Sheu et al., "Expression of galectin-3 in normal and malignant thyroid tissue by quantitative PCR and immunohistochemistry," *Modern Pathology*, vol. 16, no. 11, pp. 1117–1123, 2003.

[26] J. Grosse, M. Wehland, J. Pietsch et al., "Gravity-sensitive signaling drives 3-dimensional formation of multicellular thyroid cancer spheroids," *The FASEB Journal*, vol. 26, no. 12, pp. 5124–5140, 2012.

[27] X. Ma, J. Pietsch, M. Wehland et al., "Differential gene expression profile and altered cytokine secretion of thyroid cancer cells in space," *FASEB Journal*, vol. 28, no. 2, pp. 813–835, 2014.

[28] M. S. Clarke, C. R. Vanderburg, and D. L. Feeback, "The effect of acute microgravity on mechanically-induced membrane damage and membrane-membrane fusion events," *The Journal of Gravitational Physiology*, vol. 8, no. 2, pp. 37–47, 2001.

[29] D. K. Hsu, A. I. Chernyavsky, H.-Y. Chen, L. Yu, S. A. Grando, and F.-T. Liu, "Endogenous galectin-3 is localized in membrane lipid rafts and regulates migration of dendritic cells," *Journal of Investigative Dermatology*, vol. 129, no. 3, pp. 573–583, 2009.

[30] D. Delacour, C. I. Cramm-Behrens, H. Drobecq, A. Le Bivic, H. Y. Naim, and R. Jacob, "Requirement for galectin-3 in apical protein sorting," *Current Biology*, vol. 16, no. 4, pp. 408–414, 2006.

Hindawi Publishing Corporation
BioMed Research International
Volume 2014, Article ID 413708, 11 pages
http://dx.doi.org/10.1155/2014/413708

Research Article

The Influence of Simulated Microgravity on Purinergic Signaling Is Different between Individual Culture and Endothelial and Smooth Muscle Cell Coculture

Yu Zhang,[1,2] Patrick Lau,[3] Andreas Pansky,[1] Matthias Kassack,[2] Ruth Hemmersbach,[3] and Edda Tobiasch[1]

[1] *Department of Natural Sciences, Bonn-Rhine-Sieg University of Applied Sciences, 53359 Rheinbach, Germany*
[2] *Institute of Pharmacology and Medical Chemistry, University of Dusseldorf, 40225 Dusseldorf, Germany*
[3] *Institute of Aerospace Medicine, German Aerospace Center, 51147 Cologne, Germany*

Correspondence should be addressed to Edda Tobiasch; edda.tobiasch@h-brs.de

Received 25 April 2014; Revised 30 June 2014; Accepted 23 July 2014; Published 28 August 2014

Academic Editor: Monica Monici

Exposure to microgravity conditions causes cardiovascular deconditioning in astronauts during spaceflight. Until now, no specific drugs are available for countermeasure, since the underlying mechanism is largely unknown. Endothelial cells (ECs) and smooth muscle cells (SMCs) play key roles in various vascular functions, many of which are regulated by purinergic 2 (P2) receptors. However, their function in ECs and SMCs under microgravity conditions is still unclear. In this study, primary ECs and SMCs were isolated from bovine aorta and verified with specific markers. We show for the first time that the P2 receptor expression pattern is altered in ECs and SMCs after 24 h exposure to simulated microgravity using a clinostat. However, conditioned medium compensates this change in specific P2 receptors, for example, P2X7. Notably, P2 receptors such as P2X7 might be the important players during the paracrine interaction. Additionally, ECs and SMCs secreted different cytokines under simulated microgravity, leading into a pathogenic proliferation and migration. In conclusion, our data indicate P2 receptors might be important players responding to gravity changes in ECs and SMCs. Since some artificial P2 receptor ligands are applied as drugs, it is reasonable to assume that they might be promising candidates against cardiovascular deconditioning in the future.

1. Introduction

Exposure to microgravity conditions during space missions induces a variety of health issues in astronauts, including bone loss, muscle atrophy, decreased immune activity, and cardiovascular deconditioning [1–3]. The cardiovascular deconditioning is very likely caused by the dysfunction of the major vascular cells: endothelial cells (ECs) and smooth muscle cells (SMCs). ECs build up the monolayer coating inner surface of blood vessels. Layers of SMCs arranged in fibers support the EC monolayer by providing contraction and relaxation of vessels [4]. Importantly, the interaction between ECs and SMCs has been shown to be a key player in human cardiovascular physiology [5]. ECs are sensitive to mechanical stress, and they secret cytokines inhibiting SMC proliferation [6]. Purinergic receptors can bind extracellular nucleotides such as ATP [7, 8] and they are crucial players in regulating a series of physiological and pathological cardiovascular processes such as atherosclerosis, hypertension, and vascular pain [9, 10]. Purinergic receptors are divided into P1 receptors and P2 receptors [11]. P2 receptors can be subdivided into P2X receptors that are ion channels and P2Y receptors that are G protein-coupled receptors [12]. Until now, seven P2X (P2X1-7) and eight P2Y (P2Y1, 2, 4, 6, 11, 12, 13, and 14) have been characterized. However, the role of extracellular nucleotides on vascular cell function under microgravity condition is still unknown.

Recent publications have shown that cytoskeleton arrangement, gene expression of extracellular matrix, and cell surface adhesion molecules in ECs were altered after 22 seconds and 24 h exposure to microgravity [13–16]. ECs formed tubes after culturing for longer term (7 days)

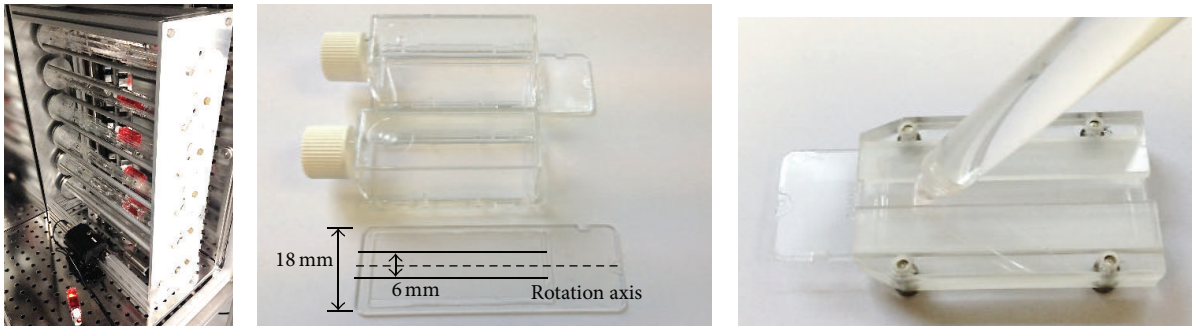

(a) (b) (c)

Figure 1: Cell Culture in a Clinostat to Simulate Microgravity Conditions. The clinostat (a) was used to simulate the microgravity environment by rotating cells. Only cells grown in the 6 mm area in the middle of culture slide (b) received the optimal simulated microgravity and were thus harvested using a special cell scraper (c).

under simulated microgravity conditions using a Random Positioning Machine (RPM) [17]. On the other hand SMCs showed suppressed proliferation and an enhanced rate of apoptosis after 72 h exposure to simulated microgravity using a rotating wall vessel (RWV) [18]. However, these findings were encountered when single cell type such as endothelial or smooth muscle cells was cultured under real or simulated microgravity. Considering ECs already showed to secrete different cytokines under simulated microgravity using RPM [19], the important interactions between ECs and SMCs under microgravity condition should be evaluated and thus require investigations.

In this study, an indirect cell coculture model was established by culturing SMCs with EC-conditioned medium and vice versa. The P2 receptor expression pattern was analyzed and compared under three conditions: normal gravity control (1 g), simulated microgravity (MG), and simulated microgravity with conditioned medium. For the simulation of microgravity a fast rotating clinostat was used, in which the cells were quickly rotated around one axis perpendicular to the direction of gravity [20]. The influence of conditioned medium collected from normal gravity and simulated microgravity on cell proliferation and migration was also investigated.

2. Methods

2.1. Isolation and Characterization of Bovine Aortic Endothelial and Smooth Muscle Cells. Bovine aorta was cut longitudinal into 5 cm sections and divided again into rectangles after removing residual and connective tissues. The cut aorta into type I collagenase (10 mg/mL in PBS) coated cell culture dishes, with the inner layer (endothelium) attached to the collagenase, and incubated for 60 min at 37°C. The aortic endothelial cells were slightly scraped with a cell scraper and put onto gelatin (in PBS (1% v/v)) coated culture plates [21]. Medium was added to the freshly scraped cells and the plates were then incubated at 37°C, 5% CO_2 under humidified conditions. Aortic smooth muscle cells were isolated by obtaining the media layer through removal of the outer layer and scraping off the endothelial cells. The media layer was cut into 2 mm × 2 mm sections and put into cell culture dish for 2 h without medium to allow these sections adhering tightly to the surface [22]. The medium was added and the pieces were incubated at 37°C, 5% CO_2 under humidified conditions for up to a week to let SMCs migrate and proliferate from the tissue pieces to the surface of culture dish.

2.2. Cell Culture. The cells were cultured in DMEM medium (Merck Millipore, Berlin, Germany) supplied with 10% FCS and 1% penicillin/streptomycin. ECs and SMCs were split and seeded at a density of 5000 cells/cm^2, after they reached a level of 80–90% confluence. ECs and SMCs with passage number 2–4 were used. The cell line human microvascular endothelial cell-1 (HMEC-1), C2C12 (ATCC number: CRL-1772) and MG-63 (ATCC number: CRL-1427), and U-87 MG (ATCC number: HTB-14) were cultured in DMEM medium and subsequently used as positive control.

2.3. Clinostat Experiments. The fast-rotating 2D clinostat used in this study was originally developed by the Institute of Aerospace Medicine, German Aerospace Center (DLR) (see Figure 1(a)). It has 6 parallel horizontal axes, each for fixation for up to 4 slide flasks. ECs and SMCs were seeded at a density of 10,000 cells/cm^2 onto 9 cm^2 cell culture slide flasks (Nunc, Thermo Fisher Scientific, Langenselbold, Germany). When they reached a confluence level of 60%–70%, the culture flasks were filled up completely with DMEM medium. To avoid shear stress and thus the induction of respective metabolic changes in signal transduction pathways, for example, apoptosis, air bubbles were removed carefully. The flasks were inserted on the clinostat and rotated at 60 rpm for 24 h in the CO_2 incubator at 37°C. Controls were also filled with medium and placed simultaneously under normal gravity.

Cells from the whole flask were first used to analyze the P2 receptor expression pattern that altered subtypes could be distinguished from unaffected. Later, according to the clinostat principle, only cells exposed to minimal *g*-forces were taken for further analysis. This means that only cells from the middle of the flask were taken (see Figure 1(b)).

Under a defined constant speed of 60 rpm the maximal residual acceleration at an area of 6 mm provided an optimal quality of simulated microgravity (≤0.0121 g) [23]. Thus, only cells within this 6 mm area were isolated to evaluate altered P2 subtypes for both gene and protein expression in detail. To maintain the cells accurately and consistently in the center, a special chamber consisting of two cover plates, attached to a bottom plate [23], was used to allow slide insertion without wiping off the cell layer. A corresponding cell scraper was used to scratch the cells from the specific 6 mm width area in the center (Figure 1(c)).

2.4. Conditioned Medium. To investigate a possible paracrine influence on P2 receptor expression, ECs and SMCs were seeded in a density of 2500 cells/cm^2. Cell growth medium was collected when they were 80%–90% confluent. The conditioned medium (CM) was composed out of cell growth medium and normal DMEM medium in a ratio of 1 : 2 on respective cell type. The SMC-conditioned medium was subsequently fully added into the culture slide with ECs and set of a 24 h clinorotation as a group of EC MG + CM. The ECs in normal gravity group (EC 1 g) and in clinorotation but filled with normal DMEM medium (EC MG) were set simultaneously. The similar experiments were set for SMCs with normal gravity (SMC 1 g), clinorotation (SMC MG), and clinorotation filled with EC-conditioned medium (SMC MG + CM).

To evaluate a possible paracrine effect on cell proliferation and migration, cell growth medium was collected from cells cultured 24 h in normal gravity and cultured 24 h under clinorotation, respectively. The used conditioned medium (CM) was composed out of cell growth medium and normal DMEM medium in a ratio of 1 : 2 on respective cell type. The ECs were subsequently treated with normal DMEM medium, SMC-conditioned medium from normal gravity (CM SMC + 1 g), and clinorotation (CM SMC + MG) separately for proliferation or migration assays. Similar experiments were set and performed with SMCs as well. All experiments were performed with samples from three cows.

2.5. RNA Isolation and Semiquantitative PCR. RNA was extracted after clinorotation using a Ribozol RNA reagent (Amresco, OH, USA). cDNAs were synthesized from 2.0 μg total RNA by using Revert Aid Reverse Transcriptase and oligo-dT primer (Thermo Fisher Scientific, MA, USA). Primers for P2 receptors, EC, and SMC specific markers in the human and bovine system were designed and shown in the supplementary data available at http://dx.doi.org/10.1155/2014/413708. The RT-PCR conditions such as annealing temperature and magnesium concentration are given in the supplementary data as well. 1% of agarose gels were set up to evaluate the RT-PCR products. As positive control, RNA extracts from the cell lines HMEC-1, MG-63, C2C12, and U-87 MG were used for respective P2 receptor subtypes given in the supplementary data.

2.6. Western Blot Analysis. The proteins were extracted from the cells in a protein lysis buffer (Cell Signaling Technology, MA, USA) and subsequently centrifuged at 22,000 g for 5 min at 4°C to remove cellular debris. After boiling for 5 min, the lysate samples were separated by a 12% SDS-PAGE electrophoresis and electrotransferred to a PVDF membrane. The membrane was blocked in TBST containing 5% BSA and incubated with anti-P2X7, P2Y1, P2Y2, P2Y11, VEGFR2, VE-cadherin, PECAM-1, calponin, SMA-α, MYH-11 (1 : 500), or GAPDH antibodies (1 : 5,000) (Santa Cruz Biotechnology, CA, USA) overnight at 4°C. The membranes were washed three times with TBST and incubated with the secondary antibodies (1 : 5,000) (CALBIOCHEM, CA, USA) for 60 min at RT. After washing with TBST, immune-detection was accomplished by using the Luminata Forte Western HRP substrate (Merck Millipore, MA, USA) and images were taken using Bio-Rad Chemidoc system.

2.7. Immunofluorescence. The cells were fixed in 4% paraformaldehyde for 15 min. Cells were incubated with primary anti-VEGFR2, VE-cadherin, PECAM-1, calponin, SMA-α, MHY-11, P2X7, P2Y1, P2Y2, and P2Y11 (Santa Cruz Biotechnology, CA, USA) diluted in a ratio of 1 : 100 in antibody dilution buffer containing 1% BSA and 0.2% Triton-X-100 in PBS at 4°C overnight. After rinsing with PBS 3 times, cells were stained with FITC-labeled anti-goat or rabbit antibody, respectively (1 : 100) (Southern Biotech, AL, USA), at RT for 60 min. Cell nuclei were stained with DAPI (Sigma, MO, USA), and the cell cytoskeleton was labeled using rhodamine (1 : 2,000) (Life Technologies, CA, USA). After washing with PBS, fluorescent signals were analyzed with an Axio Observer D1 fluorescence microscope (Carl Zeiss, Germany) or a FW300 confocal fluorescent microscope (Olympus, Japan), respectively.

2.8. DiI-ac-LDL Uptake. ECs were incubated with 10 μg/mL DiI-labeled acetylated-low density lipoprotein (DiI-ac-LDL) (Biomedical Technologies Inc. MA, USA) for 4 hours at 37°C and investigated with a fluorescent microscope (Carl Zeiss, Germany) at a wavelength of 565 nm. After staining with LDL, cells were fixed with 4% formaldehyde for 15 min and subsequently incubated with DAPI (1 : 10000 in PBS) and rinsed with PBS. Images were taken with an Axio Observer D1 fluorescent microscopy (Carl Zeiss, Germany).

2.9. Proliferation and Wound Assay. For the proliferation assay 20,000 ECs were seeded separately in each well of 12-well plates. ECs were grown in DMEM medium, in a SMC-conditioned medium in normal gravity (SMC CM + 1 g) and in a SMC-conditioned medium in simulated microgravity (SMC CM + MG) (see Section 2.4 for conditioned medium details). ECs incubated with the respective medium were subsequently obtained after 24 h and 48 h under normal gravity incubation and numbers were calculated. Similarly experiments were set for SMCs: SMCs were cultured in DMEM medium, in an EC-conditioned medium in normal gravity (EC CM + 1 g), and EC-conditioned medium in simulated microgravity (EC CM + MG) for 24 h and 48 h. Cell number in each well was counted.

For the wound assay ECs and SMCs (10,000/cm^2) were seeded and grown to 80%–90% confluence. A straight scratch injury was made using a sterile 1 mL pipette tip on 6-well plates. The ECs were incubated for 24 h at 37°C in a CO_2 incubator with normal DMEM medium, SMC-conditioned medium in normal gravity (SMC CM + 1 g), and SMC-conditioned medium in simulated microgravity (SMC CM + MG). On the other hand SMCs were cultured in DMEM medium, EC-conditioned medium in normal gravity (EC CM + 1 g), and EC-conditioned medium in simulated microgravity (EC CM+MG). Hydroxyurea (5 mM) was added to inhibit cell proliferation. Images were taken using a phase contrast microscope (Carl Zeiss, Germany). The numbers of migrated cells in three individual areas were calculated and quantified using Image J software (NIH).

2.10. Statistical Analysis. Statistical analysis was applied for the experiments using the Microsoft Office program Excel 2010 and SPSS 12.0. Data are shown as means ± standard deviation. Experiments were repeated at least three times for three donors, which are given as n = number of experiments. The probability (P) value was calculated using LSH test to assess differences between two groups. Levels of significance were labeled as follows: $^{*}P \leq 0.05$, $^{**}P \leq 0.01$, and $^{***}P \leq 0.001$. Significance was given with the appropriate number of asterisks or in numbers.

3. Results

3.1. Characterization of Primary ECs and SMCs from Bovine Aorta. The isolated ECs showed positive gene expression of endothelial cell markers VEGFR2, VE-cadherin, and PECAM-1, whereas SMCs positively expressed smooth muscle cell markers SMA-α, calponin, and MYH-11 (Figure 2(a)). Western blot experiments confirmed the gene expression data on the protein level. ECs positively expressed VEGFR2, VE-cadherin, and PECAM-1, while SMCs were positive for calponin, SMA-α, and MYH-11 (Figure 2(b)). Importantly both gene and protein data showed that ECs were negative for SMC markers except a weak band found in calponin. SMCs were negative for the three tested endothelial cell markers. These results indicate that isolated ECs and SMCs were without major cross contaminations. The fluorescent staining data further confirmed the results from the RT-PCR and Western blot analysis (Figures 2(c) and 2(d)). In addition, isolated ECs also showed the typical endothelial activity by uptaking LDL (Figure 2(e)).

3.2. P2 Receptor Expression in ECs after 24 h Simulated Microgravity with and without SMC-Conditioned Medium. All fifteen P2 receptors were analyzed for their gene expression by RT-PCR. In the first experiment, RNA was collected in one set of clinorotation experiments from the whole culture flask. All P2 receptors were expressed in ECs with the exception of P2X3 and P2Y6. Next to this P2X5, P2Y4, P2Y11, and P2Y14 were upregulated, while P2X7, P2Y1, and P2Y4 were downregulated on the gene expression level in ECs under 24 h simulated microgravity condition (MG) induced by clinorotation if compared to ECs under normal gravity (1 g) (Figure 3(a)). In a further set of clinorotation experiments, the conditioned medium collected from SMCs grown under normal gravity condition (see Section 2.4) was added to ECs. For this experiment, only cells grown in the 6 mm diameter area of the center were taken to isolate RNA and protein. RT-PCR data showed that although the expression of P2X7 and P2Y1 was decreased after clinorotation P2X7 in ECs showed an increase on the gene level when cultured in SMC-conditioned medium. P2Y11 protein expression in ECs was upregulated and further increased also on the SMC conditioned medium compared to P2X7 (Figure 3(b)). Western blot and fluorescence confirmed the change of P2X7 on protein level (Figures 3(c) and 3(d)).

3.3. P2 Receptor Expression in SMCs after 24 h Simulated Microgravity with and without EC-Conditioned Medium. Identical operational steps were undertaken to investigate SMCs under simulated microgravity. In SMCs, all P2 receptors were expressed except P2X3, P2X7, P2Y6, and P2Y11. After 24 h clinorotation, RT-PCR showed an increased gene expression of P2X4, P2X7, and P2Y2, whereas P2X2, P2Y1, and P2Y14 were downregulated in SMCs under simulated microgravity condition (MG) if compared to the SMCs under normal gravity (1 g) (Figure 4(a)). After adding EC-conditioned medium (see Section 2.4) within clinostat experiment, clinorotation induced an upregulation of P2X7 gene expression in SMCs as revealed by RT-PCR (Figure 4(b)). Interestingly, P2X7 showed a decreased gene expression after adding EC-conditioned medium compared to its increase without EC-conditioned medium under 24 h clinorotation. P2Y1 was upregulated in SMCs under simulated microgravity; however conditioned medium showed no effect on its expression. Gene level alterations of P2X7 and P2Y2 were confirmed on the protein level by Western blot or fluorescent staining; however, P2Y1 showed an increasing protein expression in simulated microgravity and with EC-conditioned medium (Figures 4(c) and 4(d)).

3.4. Proliferation and Migration of ECs Cultured with SMC-Conditioned Medium Collected under Normal Gravity and Simulated Microgravity. Conditioned medium from SMCs collected after 24 h normal gravity and after 24 h simulated microgravity was used to culture ECs evaluating the paracrine influence of SMCs on EC proliferation and migration. SMC-conditioned medium from normal gravity (SMC CM + 1 g) did not have a significant influence on EC proliferation after 24 h but caused a decrease of EC numbers after 48 h. SMC-conditioned medium collected after simulated microgravity (SMC CM + MG) inhibited EC proliferation significantly after both 24 h and 48 h, respectively (Figure 5(a)). To mimic a wound in the endothelium a straight scratch through the cells was set. The SMC-conditioned medium cultured under normal gravity (SMC CM + 1 g) and simulated microgravity (SMC CM + MG) condition was added to study EC migration capacity. The conditioned medium from MG enhanced EC migration after 24 h, and even more significantly after 48 h in the presence of hydroxyurea (Figures 5(b)

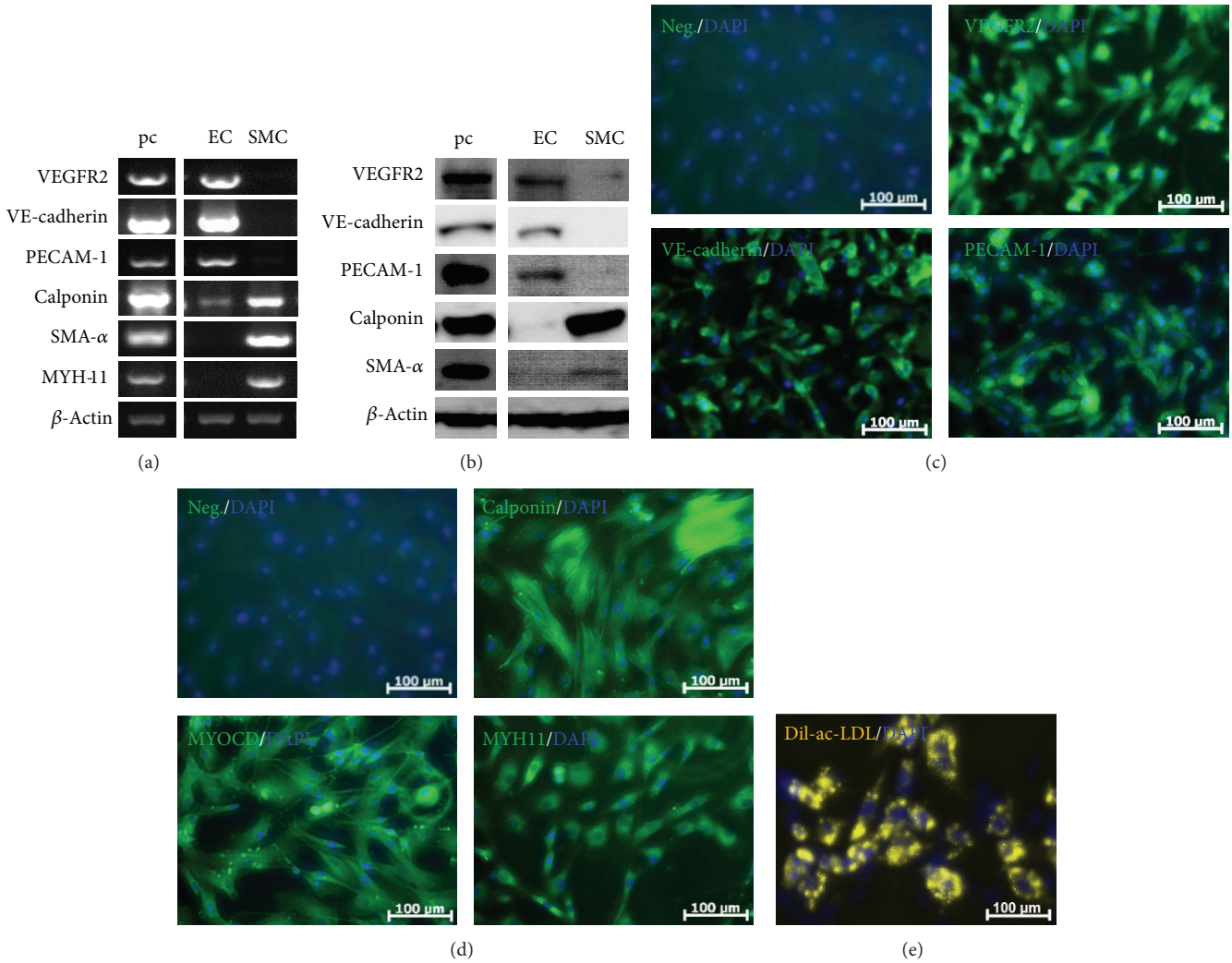

Figure 2: Characterization of Bovine Endothelial and Smooth Muscle Cells. The isolated cells were verified with the EC specific markers VEGFR2, VE-cadherin, PECAM-1 and the SMC specific markers calponin, SMA-α, MYH-11 by RT-PCR (a) and Western blot (b). GAPDH served as internal control. The endothelial (c) and smooth muscle cells (d) were also identified with the above-mentioned markers via fluorescent staining. The isolated endothelial cells were further examined for the typical endothelial activity of LDL up-take (e). All pictures are representative of one cow sample out of three.

and 5(c)). Figure 5 is a representative of example one of three cows. The numbers of proliferating and migrating ECs from the three individual cows are given in the supplementary data.

3.5. Proliferation and Migration of SMCs Grown in EC Derived Conditioned Medium Collected after 24 h under Normal Gravity and Simulated Microgravity. Experiments with SMCs were performed in a comparable manner as described for ECs. The conditioned medium collected from EC grown under normal gravity (EC CM + 1 g) reduced the proliferation of SMCs. However, the conditioned medium collected from EC grown under simulated microgravity condition (EC CM + MG) compensated this effect (Figure 6(a)). Conditioned medium under simulated microgravity induced SMC migration after 48 h but inhibited it after 24 h (Figures 6(b) and 6(c)). Figure 6 is a representative of example one of three individual cows. The numbers of proliferating and migrating SMCs from the three individual cows are given in the supplementary data.

4. Discussion

In this study, we showed for the first time that several specific P2 receptor expressions were altered on gene and protein level after 24 h under simulated microgravity condition as shown in Figure 7. Culturing ECs with SMC-conditioned medium under normal gravity and vice versa can compensate the P2 receptor expression change such as P2X7.

Similar to the findings of Wang and colleagues [24], our data showed that ECs and SMCs expressed different P2 receptors on cell membrane. P2X4, P2Y1, P2Y2, and P2Y11 were predominantly expressed in ECs, while P2X1 and P2Y2 were strongly expressed in SMCs. Macrovascular and

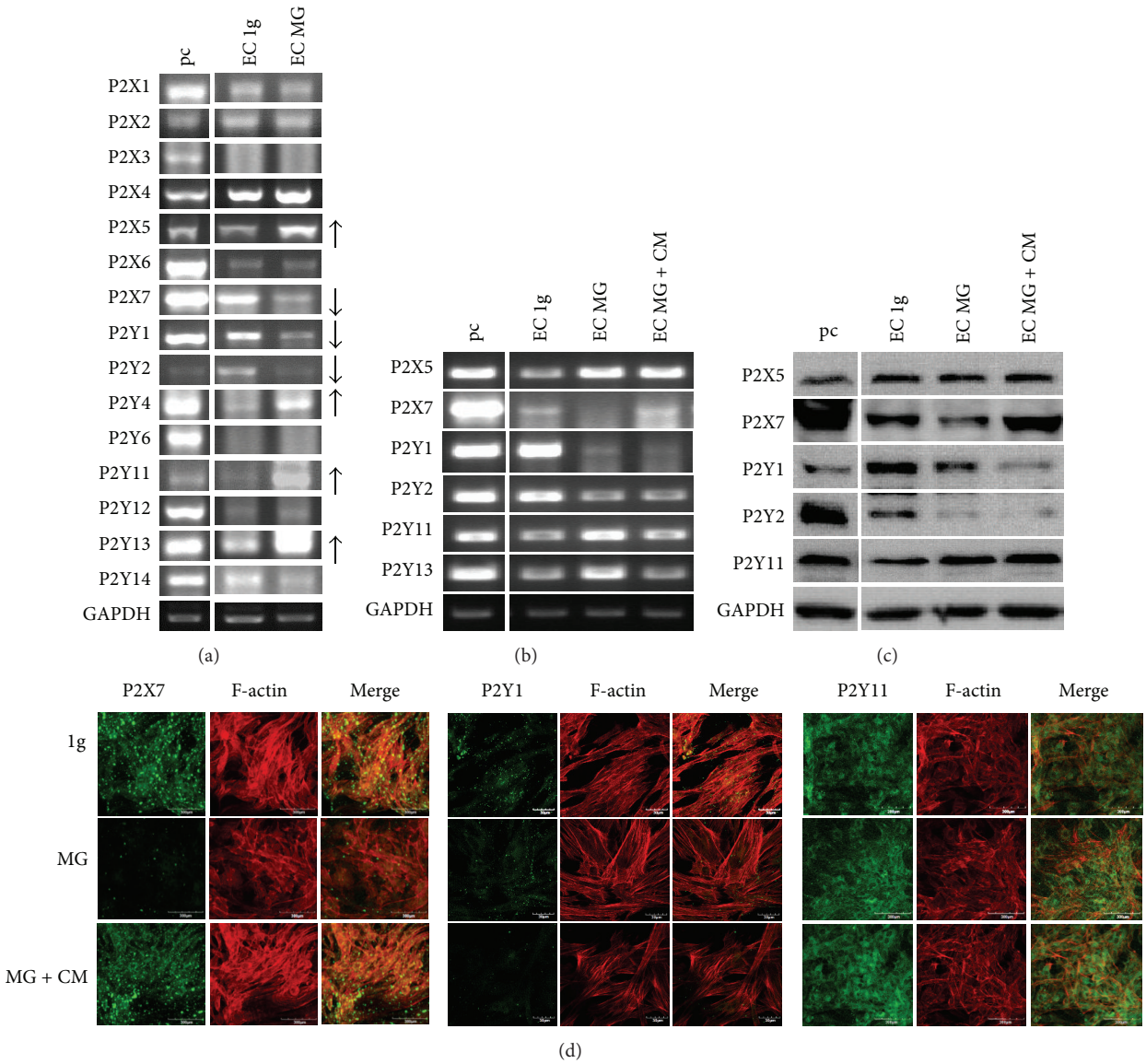

Figure 3: P2 Receptor Expression in Endothelial Cells after 24 h under Normal Gravity and Simulated Microgravity. All cells on the surface of flasks were isolated for RT-PCR. P2X5, P2Y4, P2Y11, P2Y13 were up-regulated and P2X7, P2Y1 and P2Y2 were down-regulated in the ECs after 24 h in the clinostat (a). Cells grown within 6 mm of the center had the optimal simulated microgravity condition and were therefore isolated to confirm the above P2 receptor alteration on the RNA (b) and protein (c) level after 24 h simulated microgravity with and without SMC-conditioned medium collected under normal gravity. P2X5 and P2Y11 were up-regulated in ECs but P2X5 up-regulation was not significant on protein level. P2X7, P2Y1, P2Y2 were down-regulated on both gene and protein level. The SMC-conditioned medium can compensate the decrease of P2X7 expression but cause no significant effect on the alteration of P2Y1, P2Y2 and P2Y11. The fluorescent staining confirmed the protein change of P2X7, P2Y1 and P2Y11 (d).

microvascular ECs have shown the several functional differences such as matrix metalloproteinase expression [25] and beta-adrenergic regulation of transendothelial permeability [26]. The expression of P2X3 and P2Y4 is low in bovine aortic ECs if compared to the control HMEC-1 which suggests that macrovascular ECs might differ in the P2 receptor expression pattern compared to microvascular ECs.

The P2 receptor expression patterns of ECs and SMCs have already been shown to play an important role in various cardiovascular functions. For example, in controlling vascular tone, ATP and UTP released from ECs act on P2Y1, P2Y2, and P2Y4 leading to the production of NO and subsequent vasodilatation. Simultaneously, ATP released by the sympathetic nerve acts on P2X1, P2X2, and P2X4, resulting in vasoconstriction [9]. We found that the expression of P2X2 and P2X4 in SMCs was significantly increased after clinorotation indicating to maybe more vasoconstriction. Next to this P2Y1 and P2Y2 expressions were decreased, which suggests NO production might decrease and cause less vasodilatation. Kang and colleagues found that 72 h exposure

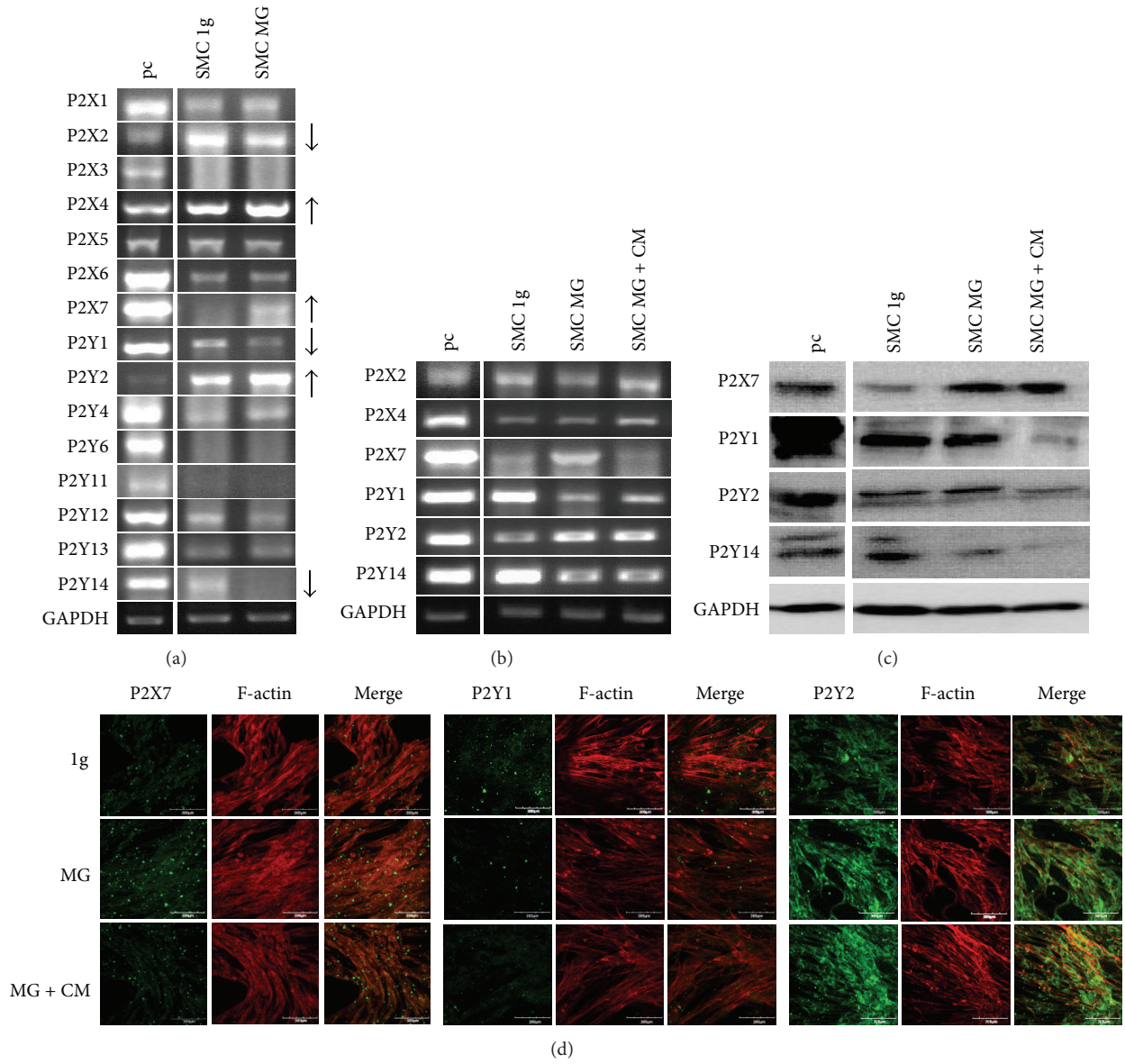

Figure 4: P2 Receptor Expression in Smooth Muscle Cells after 24 h under Normal Gravity and Simulated Microgravity. The experiments for SMC were performed similarly to those for the endothelial cells above. All cells on the surface of flasks were isolated for RT-PCR. P2X4, P2X7 and P2Y2 were up-regulated whereas P2X2, P2Y1 and P2Y14 were down-regulated in the SMCs after 24 h clinorotation (a). Cells grown within 6 mm of the center had the optimal simulated microgravity condition and were thus isolated to confirm the above P2 receptor alteration on both, RNA (b) and protein (c) level after 24 h clinorotation with and without EC-conditioned medium from normal gravity. P2X2 and P2X4 showed no significantly changed. P2X7 and P2Y2 was up-regulated, P2Y1 and P2Y14 were down-regulated. The EC-conditioned medium can compensate for the increase of P2X7 and P2Y2 expression, but no significant effect was observed on P2Y1 and P2Y14 (d).

to clinorotation led to a decreased proliferation but increased the rate of apoptotic SMCs. Additionally, the SMC phenotype was induced and transferred from the contractive to the synthetic type [18]. Our data showed that the expression of P2X7 and P2Y2 was altered differentially between ECs and SMCs under simulated microgravity, which indicates that they could be the key P2 receptor subtypes responding to the change of gravity. To point out, P2X7 has an important role in cell apoptosis and can activate a series of downstream signals due to several protein kinase binding sites on its long intracellular tail [10]. A mechanical force such as shear stress can induce endothelial cell apoptosis that might be regulated through P2X7. It is of interest that P2X7, which was downregulated in ECs, was upregulated in SMCs. This change could be compensated by adding conditioned medium from the other cell type. Such compensation was not found in the other P2 receptor subtypes which might point to P2X7 as a major player in the interaction between ECs and SMCs in simulated microgravity with respect to apoptosis regulation.

Various proteins of endothelial cells are altered under real or simulated microgravity, such as F-actin [27], tubulin [28], cell adhesion molecules [16], integrins [27], eNOS [29], and

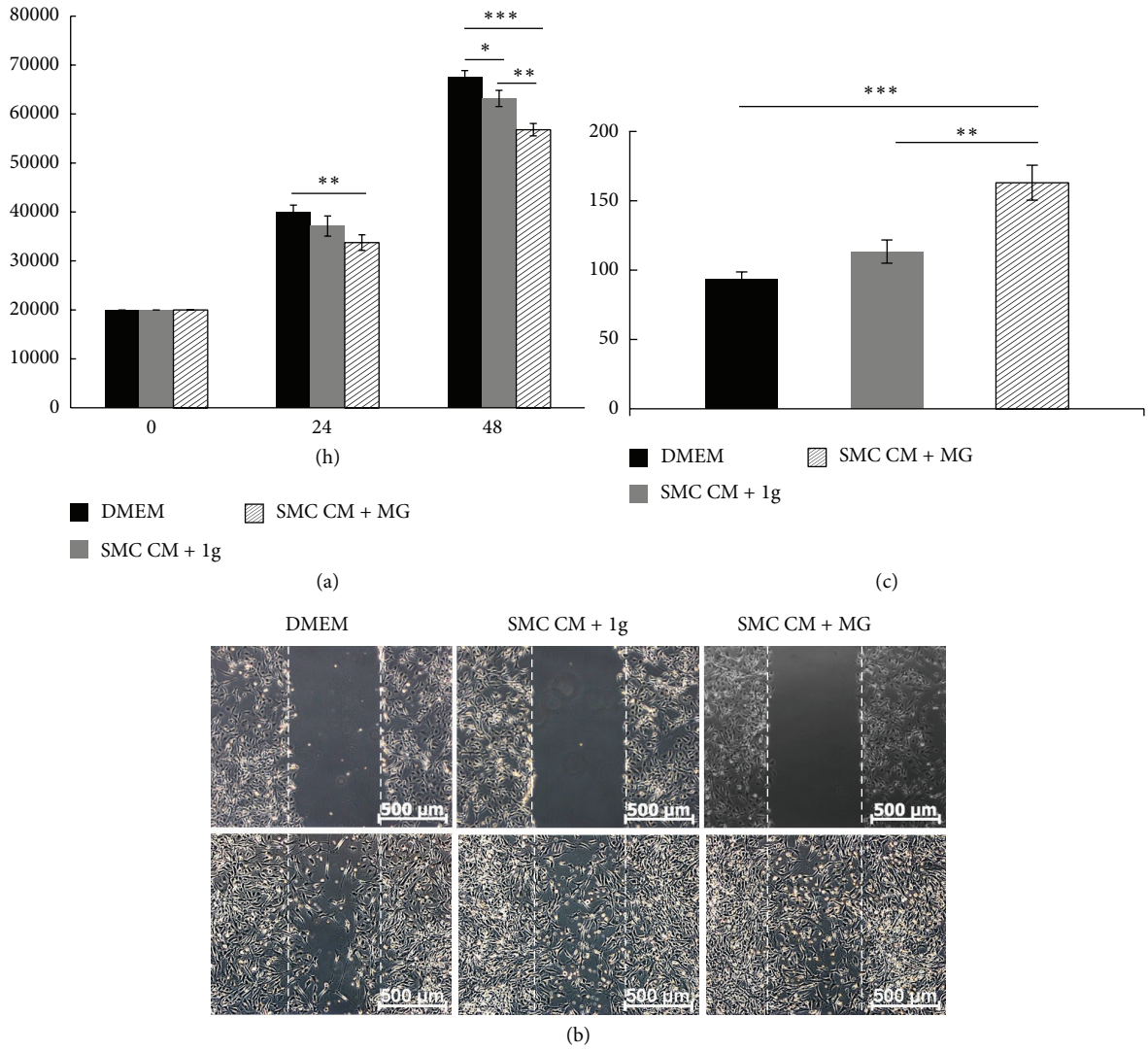

Figure 5: Effect of SMC-Conditioned Medium on EC Proliferation and Migration. To evaluate the EC proliferation, normal DMEM medium, and conditioned medium of SMCs after normal gravity (SMC CM + 1 g) and simulated microgravity (SMC CM + MG), was added for a 24 h and 48 h culture period. The conditioned medium from SMCs after normal gravity showed a decrease of EC numbers after 48 h. SMC-conditioned medium under simulated microgravity inhibited EC proliferation significantly after 24 h and 48 h incubation (a). To evaluate EC migration, ECs were scratched and normal DMEM medium, SMC-conditioned medium under normal gravity and under simulated microgravity was added for a 24 h culture period (b). Conditioned medium from SMCs under simulated microgravity (SMC CM + MG) enhanced EC migration significantly if compared to the normal DMEM medium and SMC-conditioned medium under normal gravity (c).

iNOS [30]. In line with that ECs also showed a decreased proliferation rate, increased apoptosis [28, 31], and migration [29] in simulated microgravity. However, these data were observed based on cultured ECs as single cell type, either under real or simulated microgravity. An EC and SMC coculture model was successfully created via EC-conditioned medium culturing SMCs and vice versa. In addition to the paracrine effect on P2 receptor expression such as P2X7, our results showed that this effect found under simulated microgravity could influence EC or SMC behavior for cell proliferation and migration. SMC proliferation has been demonstrated to be a crucial process in atherosclerosis since migrated and proliferating SMCs form a major cell type in the plaque [32].

In healthy vessels ECs secrete cytokines that inhibit SMC proliferation and form a monolayer to block small molecules from blood that might cause SMC proliferation. We found that conditioned medium collected from ECs in normal gravity inhibited SMC proliferation, but conditioned medium collected from ECs after clinorotation was not able to do so. On the other hand, EC damage or dysfunction is one of the first steps during the development of pathological change in atherosclerosis. The conditioned medium of SMC grown in simulated microgravity reduced EC proliferation. Enhanced apoptosis was observed when only ECs were cultured in simulated microgravity by Infanger and coauthors [28]. They found several caspases such as caspase-3 and caspase-9 activated after simulated microgravity treatment.

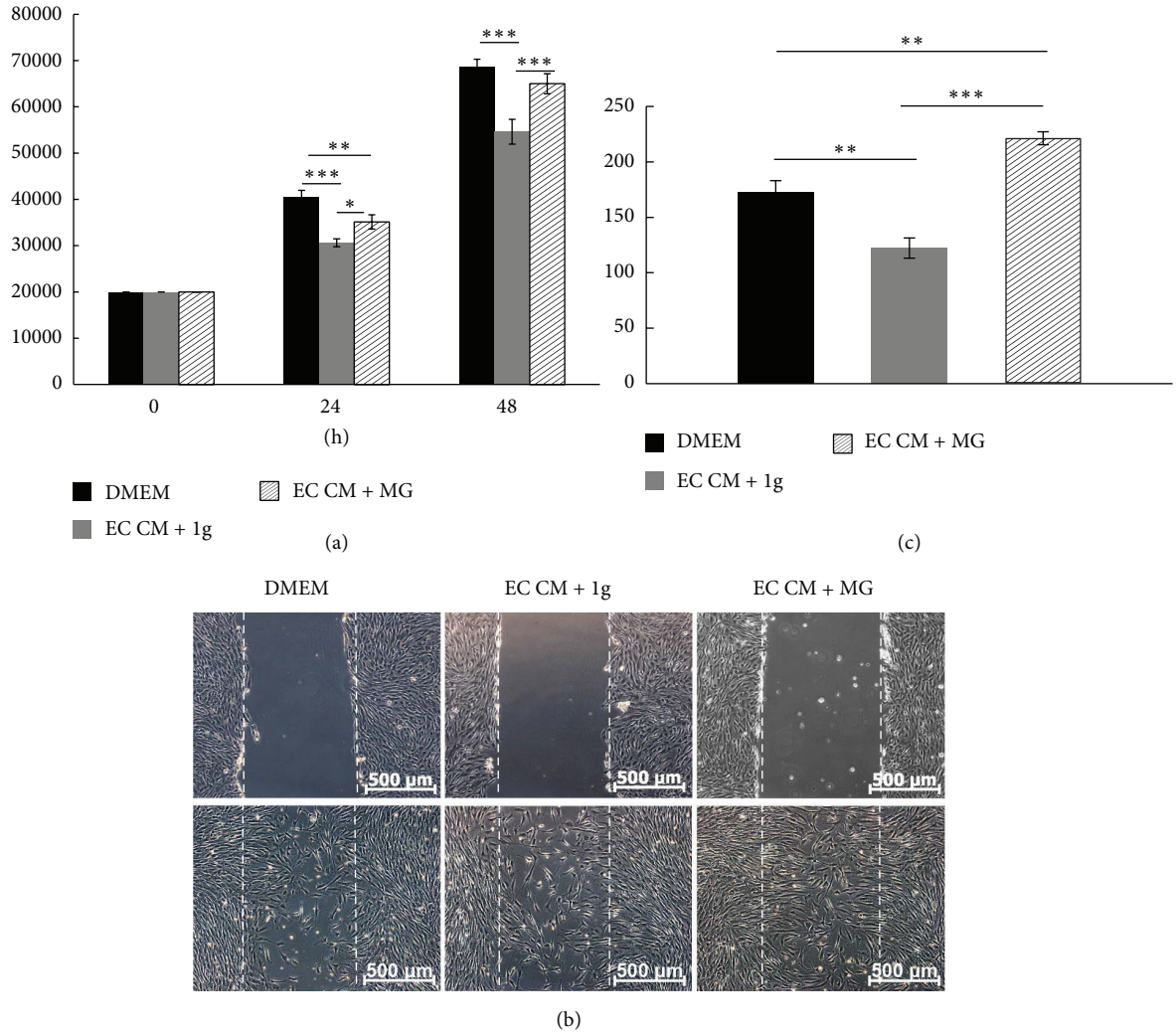

Figure 6: Effect of EC-Conditioned Medium on SMC Proliferation and Migration. To investigate the SMC proliferation, normal DMEM medium, and EC-conditioned medium under normal gravity (EC CM + 1 g) and simulated microgravity (EC CM + MG), was added and SMCs were subsequently incubated for 24 h and 48 h. Conditioned medium from EC grown under normal gravity (EC CM + 1 g) significantly inhibited SMC proliferation after 24 h and 48 h incubation and conditioned medium from EC grown under simulated microgravity (EC CM + MG) led to a significant decrease of SMC numbers after 24 h, which is not obvious after 48 h (a). To evaluate SMC migration, SMCs were scratched and cultured under normal DMEM medium, EC-conditioned medium under normal gravity and under simulated microgravity for 24 h (b). EC-conditioned medium under normal gravity (EC CM + 1 g) inhibited the SMC migration significantly. Whereas EC-conditioned medium under simulated microgravity (EC CM + MG) enhanced migrated SMC numbers (c).

Apoptosis might be induced by activation of NF-κB via the PI3K/Akt pathway [28, 31]. These data suggest that astronauts may be more prone to suffer from cardiovascular diseases such as atherosclerosis during space missions and paracrine effects between ECs and SMCs might be the key factors in this process. On the other hand migration of ECs is the first step in angiogenesis and a major factor in metastasis. In addition, it also plays an important role in restenosis in the vascular system after application of a stent. There are evidences that microgravity can promote angiogenesis in both macrovascular and microvascular ECs when only ECs were cultured under simulated microgravity [29, 30]. Our data showed an enhanced number of migrated ECs when cultured with SMC-conditioned medium derived after clinostat application, compared to the DMEM control and SMC-conditioned medium collected after 24 h exposure to normal gravity. This indicates the effect of microgravity might enhance the angiogenesis via both autocrine and paracrine signals.

Contradictory observations have been demonstrated in several publications; for example, EC migration increased in simulated microgravity both in this study and in the study of Siamwala and colleagues [30] while Versari and colleagues found a decreased EC migration under simulated microgravity [33]. One explanation for these findings might be that different endothelial cells were used such as primary endothelial cells from an artery or umbilical vein, or an endothelial cell line (EAhy926), which might give a different

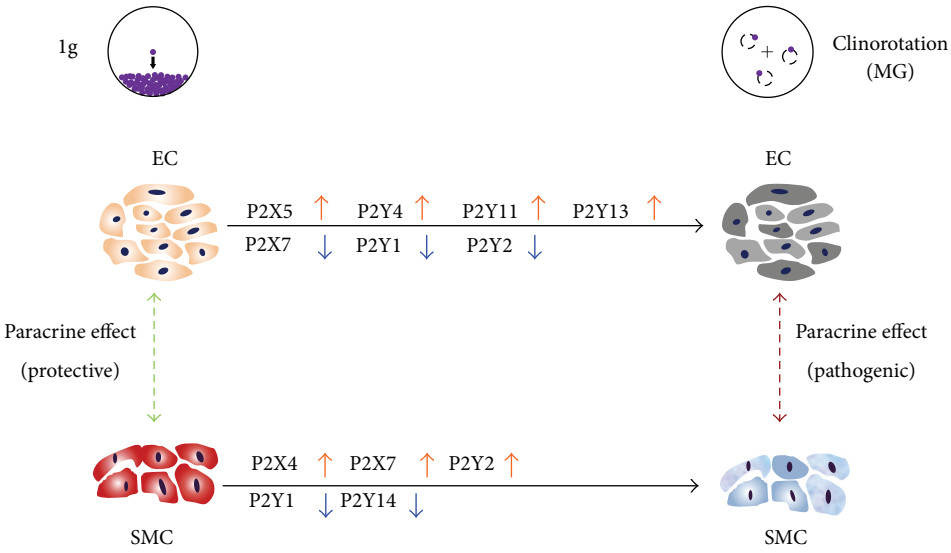

Figure 7: Scheme of P2 Receptor Alteration and the Postulated Paracrine Effect in ECs and SMCs under Simulated Microgravity. Several P2 receptor expressions were altered in ECs and SMCs under 24 h simulated microgravity condition using a clinostat. To point out that the expression P2X7 and P2Y2 was altered differentially between ECs and SMCs under simulated microgravity. Especially, the change of P2X7 in ECs was compensated under SMC-conditioned medium and vice versa. The conditioned medium collected under simulated microgravity showed the pathogenic influence of EC and SMC proliferation and migration if compared to condition medium from normal gravity.

response due to its immortalization and thus prolonged time in culture. Another explanation could be that different devices were applied to simulate microgravity conditions such as the clinostat, the RPM, and the RWV. Different equipment might produce different qualities of microgravity as well as a different amount and quality of shear stress during rotation [20]. Clinorotation was shown to produce the lowest shear forces and the central area used in our study has an optimized simulated microgravity environment [23]. Furthermore, different ECs from different body parts were used. Macrovascular and microvascular ECs already revealed a difference in promoting angiogenesis under real/simulated microgravity conditions, which is regulated via the iNOS-cGMP-PKG pathway in macrovascular ECs but via eNOS-PI3K-Akt in microvascular ECs [29, 30]. Taken together, the simulated microgravity data independently of ground-based facility we use have to be approved and verified in real microgravity for a final statement on the outcome.

5. Conclusion

Our data show for the first time that P2 receptor gene and protein expression in both ECs and SMCs were altered under simulated microgravity. SMC-conditioned medium collected under simulated microgravity influenced some P2 receptor expressions as well as proliferation and migration of ECs and vice versa. Additionally, proliferation and migration of ECs and SMCs differed between conditioned medium collected under normal gravity and under simulated microgravity. These data suggest that the extracellular environment such as paracrine signals is an important factor and cannot be ignored considering the impact of microgravity on vascular cells. Since some P2 receptor artificial ligands are already applied as drugs for cardiovascular patients, specific P2 receptor ligands might be reasonable candidates to investigating their function for cardiovascular deconditioning under microgravity in the future.

Conflict of Interests

All authors declare that there are no conflicts of interest and agree with the contents of the paper.

Acknowledgments

This work was supported by the Bundesministerium für Bildung und Forschung- (BMBF-) FHprofUnt, [FKZ: 03FH012PB2 to E.T], NRW FH-Extra, [FKZ: z1112fh012 to E.T], DAAD PPP Vigoni, [FKZ: 314-vigoni-dr and FKZ: 54669218 to E.T], and BMBF-AIF, [FKZ: 1720X06 to E.T]; the fellowship of YZ was funded by China Scholarship Council [no. 20100602024] and the Helmholtz Space Life Sciences Research School (SpaceLife). SpaceLife is funded in equal parts by the Helmholtz Association and the German Aerospace Center (DLR).

References

[1] J. Pietsch, J. Bauer, M. Egli et al., "The effects of weightlessness on the human organism and mammalian cells," *Current Molecular Medicine*, vol. 11, no. 5, pp. 350–364, 2011.

[2] A. R. Hargens and S. Richardson, "Cardiovascular adaptations, fluid shifts, and countermeasures related to space flight," *Respiratory Physiology and Neurobiology*, vol. 169, pp. S30–S33, 2009.

[3] M. Coupé, J. O. Fortrat, I. Larina, G. Gauquelin-Koch, C. Gharib, and M. A. Custaud, "Cardiovascular deconditioning:

from autonomic nervous system to microvascular dysfunctions," *Respiratory Physiology and Neurobiology*, vol. 169, pp. S10–S12, 2009.

[4] E. L. Schiffrin, "The endothelium and control of blood vessel function in health and disease," *Clinical and Investigative Medicine*, vol. 17, no. 6, pp. 602–620, 1994.

[5] D. B. Cines, E. S. Pollak, C. A. Buck et al., "Endothelial cells in physiology and in the pathophysiology of vascular disorders," *Blood*, vol. 91, no. 10, pp. 3527–3561, 1998.

[6] C. A. Limbach, M. Lange, M. Schulze, and E. Tobiasch, "Recent patents on biomedical applications for the treatment of atherosclerosis," *Recent Patents on Regenerative Medicine*, vol. 2, no. 2, pp. 75–102, 2012.

[7] N. Zippel, C. A. Limbach, N. Ratajski et al., "Purinergic receptors influence the differentiation of human mesenchymal stem cells," *Stem Cells and Development*, vol. 21, no. 6, pp. 884–900, 2012.

[8] Y. Zhang, D. Khan, J. Delling, and E. Tobiasch, "Mechanisms underlying the osteo- and adipo-differentiation of human mesenchymal stem cells," *The Scientific World Journal*, vol. 2012, Article ID 793823, 14 pages, 2012.

[9] G. Burnstock, "Control of vascular tone by purines and pyrimidines," *The British Journal of Pharmacology*, vol. 161, no. 3, pp. 527–529, 2010.

[10] G. Burnstock, "Purinergic signalling," *British Journal of Pharmacology*, vol. 147, no. 1, pp. S172–S181, 2006.

[11] G. Burnstock, "Purine and pyrimidine receptors," *Cellular and Molecular Life Sciences*, vol. 64, no. 12, pp. 1471–1483, 2007.

[12] Y. Zhang and E. Y. Tobiasch, "The role of purinergic receptors in stem cells in their derived consecutive tissues," in *Adult Stem Cell Standardization*, P. di Nardo, Ed., pp. 73–98, River Publishers, 2011.

[13] M. Wehland, X. Ma, M. Braun et al., "The impact of altered gravity and vibration on endothelial cells during a parabolic flight," *Cellular Physiology and Biochemistry*, vol. 31, no. 2-3, pp. 432–451, 2013.

[14] J. Grosse, M. Wehland, J. Pietsch et al., "Short-term weightlessness produced by parabolic flight maneuvers altered gene expression patterns in human endothelial cells," *The FASEB Journal*, vol. 26, no. 2, pp. 639–655, 2012.

[15] Y. Zhang, C. Sang, K. Paulsen et al., "ICAM-1 expression and organization in human endothelial cells is sensitive to gravity," *Acta Astronautica*, vol. 67, no. 9-10, pp. 1073–1080, 2010.

[16] D. Grimm, J. Bauer, C. Ulbrich et al., "Different responsiveness of endothelial cells to vascular endothelial growth factor and basic fibroblast growth factor added to culture media under gravity and simulated microgravity," *Tissue Engineering A*, vol. 16, no. 5, pp. 1559–1573, 2010.

[17] D. Grimm, M. Infanger, K. Westphal et al., "A delayed type of three-dimensional growth of human endothelial cells under simulated weightlessness," *Tissue Engineering A*, vol. 15, no. 8, pp. 2267–2275, 2009.

[18] H. Y. Kang, Y. B. Fan, A. Q. Sun, X. L. Jia, and X. Y. Deng, "Simulated microgravity exposure modulates the phenotype of cultured vascular smooth muscle cells," *Cell Biochemistry and Biophysics*, vol. 66, no. 1, pp. 121–130, 2013.

[19] C. Griffoni, S. Di Molfetta, L. Fantozzi et al., "Modification of proteins secreted by endothelial cells during modeled low gravity exposure," *Journal of Cellular Biochemistry*, vol. 112, no. 1, pp. 265–272, 2011.

[20] R. Herranz, R. Anken, J. Boonstra et al., "Ground-based facilities for simulation of microgravity: organism-specific recommendations for their use, and recommended terminology," *Astrobiology*, vol. 13, no. 1, pp. 1–17, 2013.

[21] S. M. Schwartz, "Selection and characterization of bovine aortic endothelial cells," *In Vitro*, vol. 14, no. 12, pp. 966–980, 1978.

[22] M. A. Stepp, M. S. Kindy, C. Franzblau, and G. E. Sonenshein, "Complex regulation of collagen gene expression in cultured bovine aortic smooth muscle cells," *The Journal of Biological Chemistry*, vol. 261, no. 14, pp. 6542–6547, 1986.

[23] P. Eiermann, S. Kopp, J. Hauslage, R. Hemmersbach, R. Gerzer, and K. Ivanova, "Adaptation of a 2-D clinostat for simulated microgravity experiments with adherent cells," *Microgravity Science and Technology*, vol. 25, pp. 153–159, 2013.

[24] L. Wang, L. Karlsson, S. Moses et al., "P2 receptor expression profiles in human vascular smooth muscle and endothelial cells," *Journal of Cardiovascular Pharmacology*, vol. 40, no. 6, pp. 841–853, 2002.

[25] C. J. Jackson and M. Nguyen, "Human microvascular endothelial cells differ from macrovascular endothelial cells in their expression of matrix metalloproteinases," *International Journal of Biochemistry and Cell Biology*, vol. 29, no. 10, pp. 1167–1177, 1997.

[26] S. Zink, P. Rösen, and H. Lemoine, "Micro- and macrovascular endothelial cells in β-adrenergic regulation of transendothelial permeability," *The American Journal of Physiology—Cell Physiology*, vol. 269, no. 5, pp. C1209–C1218, 1995.

[27] M. Infanger, C. Ulbrich, S. Baatout et al., "Modeled gravitational unloading induced downregulation of endothelin-1 in human endothelial cells," *Journal of Cellular Biochemistry*, vol. 101, no. 6, pp. 1439–1455, 2007.

[28] M. Infanger, P. Kossmehl, M. Shakibaei et al., "Induction of three-dimensional assembly and increase in apoptosis of human endothelial cells by simulated microgravity: impact of vascular endothelial growth factor," *Apoptosis*, vol. 11, no. 5, pp. 749–764, 2006.

[29] F. Shi, Y. C. Wang, T. Z. Zhao et al., "Effects of simulated microgravity on human umbilical vein endothelial cell angiogenesis and role of the PI3K-Akt-eNOS signal pathway," *PLoS ONE*, vol. 7, no. 7, Article ID e40365, 2012.

[30] J. H. Siamwala, S. Majumder, K. P. Tamilarasan et al., "Simulated microgravity promotes nitric oxide-supported angiogenesis via the iNOS-cGMP-PKG pathway in macrovascular endothelial cells," *FEBS Letters*, vol. 584, no. 15, pp. 3415–3423, 2010.

[31] C. Kang, L. Zou, M. Yuan et al., "Impact of simulated microgravity on microvascular endothelial cell apoptosis," *European Journal of Applied Physiology*, vol. 111, no. 9, pp. 2131–2138, 2011.

[32] V. J. Dzau, R. C. Braun-Dullaeus, and D. G. Sedding, "Vascular proliferation and atherosclerosis: new perspectives and therapeutic strategies," *Nature Medicine*, vol. 8, no. 11, pp. 1249–1256, 2002.

[33] S. Versari, A. Villa, S. Bradamante, and J. A. M. Maier, "Alterations of the actin cytoskeleton and increased nitric oxide synthesis are common features in human primary endothelial cell response to changes in gravity," *Biochimica et Biophysica Acta*, vol. 1773, no. 11, pp. 1645–1652, 2007.

Hindawi Publishing Corporation
BioMed Research International
Volume 2014, Article ID 547242, 12 pages
http://dx.doi.org/10.1155/2014/547242

Review Article

Human Locomotion under Reduced Gravity Conditions: Biomechanical and Neurophysiological Considerations

Francesca Sylos-Labini,[1,2] Francesco Lacquaniti,[1,2,3] and Yuri P. Ivanenko[2]

[1] *Centre of Space Bio-Medicine, University of Rome Tor Vergata, Via Montpellier 1, 00133 Rome, Italy*
[2] *Laboratory of Neuromotor Physiology, IRCCS Santa Lucia Foundation, Via Ardeatina 306, 00179 Rome, Italy*
[3] *Department of Systems Medicine, University of Rome Tor Vergata, Via Montpellier 1, 00133 Rome, Italy*

Correspondence should be addressed to Yuri P. Ivanenko; y.ivanenko@hsantalucia.it

Received 24 April 2014; Accepted 12 June 2014; Published 28 August 2014

Academic Editor: Mariano Bizzarri

Reduced gravity offers unique opportunities to study motor behavior. This paper aims at providing a review on current issues of the known tools and techniques used for hypogravity simulation and their effects on human locomotion. Walking and running rely on the limb oscillatory mechanics, and one way to change its dynamic properties is to modify the level of gravity. Gravity has a strong effect on the optimal rate of limb oscillations, optimal walking speed, and muscle activity patterns, and gait transitions occur smoothly and at slower speeds at lower gravity levels. Altered center of mass movements and interplay between stance and swing leg dynamics may challenge new forms of locomotion in a heterogravity environment. Furthermore, observations in the lack of gravity effects help to reveal the intrinsic properties of locomotor pattern generators and make evident facilitation of nonvoluntary limb stepping. In view of that, space neurosciences research has participated in the development of new technologies that can be used as an effective tool for gait rehabilitation.

1. Introduction

Life evolved in the presence of gravity, which has two major impacts on motor functions: specific body orientation in space and antigravity muscle tone and specific rules of motion in the gravity field. Gravity plays an essential role in terrestrial locomotion. The dominant hypothesis regarding templates for bipedal walking in the gravity field is the pendular mechanism of walking, up to intermediate speeds, and the bouncing mechanism of running, up to the highest speeds attainable [1]. The inverted pendulum-like mechanism of energy exchange taking place during walking would be optimized at slower speeds in reduced gravity [2, 3]. Despite our intuitive appreciation for the influence of gravity, we do not fully understand how gravity interacts with other forces, such as inertia, to affect many biological and physical processes and what type of gait and/or limb synchronization (trot, gallop, lateral sequence walk, pace, skipping, etc.) would evolve at other gravity levels.

Understanding locomotion characteristics is critical for those working in the area of gait biomechanics and neurophysiology f pattern generation networks and of exercise countermeasures for astronauts. Many researchers have investigated the effects of reducing and eliminating gravity on locomotive kinematics and kinetics [4–8]. Others have studied locomotion in actual weightlessness or hypogravity [9, 10]. The techniques have included supine and erect cable suspension, parabolic aircraft flights, water immersion, and centrifugal methods [6]. Increased knowledge of locomotion kinematics, kinetics, muscular activity patterns, and sensory feedback modulation may help to facilitate more effective exercise countermeasures, develop innovative technologies for gait rehabilitation, and provide new insights into our understanding of the physiological effects of gravity. In this review, we will consider the known tools and techniques used for hypogravity simulation and their effects on human locomotion.

2. Methods and Apparatuses for Reduced Gravity Simulation

Spaceflights are the more direct way to assess the effect of gravity on locomotion, but studying locomotion in actual hypogravity is demanding and expensive [6]. The drawbacks to spaceflight experiments include difficulty in using necessary data collection hardware and performing an experiment with adequate sample size. Parabolic flight offers a viable alternative, but periods of weightlessness are limited to ~20 s, which only allows for acute locomotion investigations [11].

There are several apparatuses that have been used in the past to simulate reduced gravity locomotion. One of the more used systems is the vertical body weight support (BWS) (Figures 1(a) and 1(b)). These kinds of simulators are usually obtained supporting the subjects in a harness that applies a controlled upward force. For example, the WARD [12] mechanism consists of a mechanical gear driven by a pneumatic cylinder (Figure 1(b)). It is held in a cart that slides forward and backward over a track. Low-friction sliding of the mechanism ensures that only vertical forces are applied to the subject. Vertical BWS systems may also make use of a small increase in air pressure around the user's lower body to create a lifting force approximately at the person's center of mass [13]. Other vertical systems [8, 14] use a series of compliant rubber spring elements that are stretched to create the upward (to simulate gravity less than 1 g) or downward (to simulate gravity greater than 1 g) force (Figure 1(a)). The main limitation of these reduced gravity simulators (in addition to high local skin pressure via a harness) is that each supporting limb experiences a simulated reduction of gravity proportional to the applied force, while the swinging limb experiences 1 g.

The tilted BWS systems (Figures 1(c) and 1(d)) are constructed to simulate more realistic effects of gravity changes on both the stance and swing legs in the sagittal plane. These simulators, that have been used in the past by both Roscosmos (Russian Federal Space Agency) and NASA to train astronauts before space flights [15–17], are based on the idea of neutralizing the component of the gravity force normal to the lying surface [$mg \cdot \cos(\alpha)$, where α is the angle of inclination], while the component of the gravity force acting on the body and swinging limbs in the sagittal plane is reduced in relation to the tilt angle [$mg \cdot \sin(\alpha)$]. A similar concept has been used in the reduced gravity simulator (Figure 1(d)) designed by Ivanenko et al. (Italian patent number Rm2007A000489): the subject lies on the side on a tilted couch (up to 40° from the horizontal position) with both legs suspended in the exoskeleton and steps on the treadmill, which is tilted to the same angle [7, 18, 19]. This simulator included additional mass of the tilted chassis (~15 kg) and exoskeleton (1.5 kg for each leg). Thus the entire assembly had a mass of ~18 kg that increased both gravitational and inertial forces during walking.

Another class of gravity-related manipulations is "subject load device" (SLD) that applies a gravity replacement force in the direction down to the surface. This type of SLD can be used in the vertical systems to increase the gravity [8] or in the lying position (Figure 1(e)). When an astronaut walks or runs on a treadmill in weightlessness, a subject load device is used to return him or her back to the treadmill belt and to load the limbs. The gravity replacement load is transferred, via a harness, to the pelvis and/or the shoulders. Gravity simulators can simulate active treadmill running in weightlessness and provide a method of testing proposed improvements in SLD design and exercise protocols [20, 21]. In supine suspension systems (Figure 1(e)), subjects are suspended horizontally attached to latex rubber cords. A cloth sleeve and rubber cord are attached each to the upper and lower arms and legs (eight total) [20]. The limitation of this system is a local pressure on some parts of the body (e.g., shoulders) and modifications in the swing phase dynamics due to nonconstant forces of rubber cords and gravity acting in the anterioposterior direction of leg movements (Figure 1(e)).

Based on the passive gravity balancing technology, Ma et al. [22, 23] proposed a design concept of a passive reduced gravity simulator to simulate human walking or other activities in a reduced-gravity environment for potential applications of training astronauts and space travelers (Figure 1(f)). The system consists of a 3-DOF dual parallelogram mechanism, a 2-DOF torso support assembly, and a pair of 3-DOF leg exoskeletons. The weight of the body and the legs is compensated by the spring-balanced dual-parallelogram mechanism and torso-support assembly, and the weight of each leg is compensated by a leg exoskeleton. The system is capable of simulating human walking and jumping in a hypogravity environment [24]. Hardware prototyping and experimental study of the new system are currently underway.

In the following section we discuss the basic principles of adaptation of locomotion to different gravity values using the technologies described here.

3. Biomechanical Aspects of Locomotion in Reduced Gravity

Despite some differences, all reduced gravity simulation approaches show a reasonable approximation of the reduction in the gravitational force acting on the center of body mass (COM) and similar results concerning the speed of gait transitions. An important consequence of the pendulum-like behavior of the limbs in the gravity field is the principle of dynamic similarity [29], which states that geometrically similar bodies that rely on pendulum-like mechanics of movement have similar gait dynamics at the same Froude number:

$$\mathrm{Fr} \sim \frac{V^2}{gL}, \tag{1}$$

where V is the speed of locomotion, g is the acceleration of gravity, and L is a characteristic leg length. That is, all lengths, times, and forces scale by the same factors. In order to optimize the recovery of mechanical energy, the kinetic energy and the potential energy curves must be equal in amplitude and opposite in phase, as in a pendulum. Assuming that the change in kinetic energy within each step

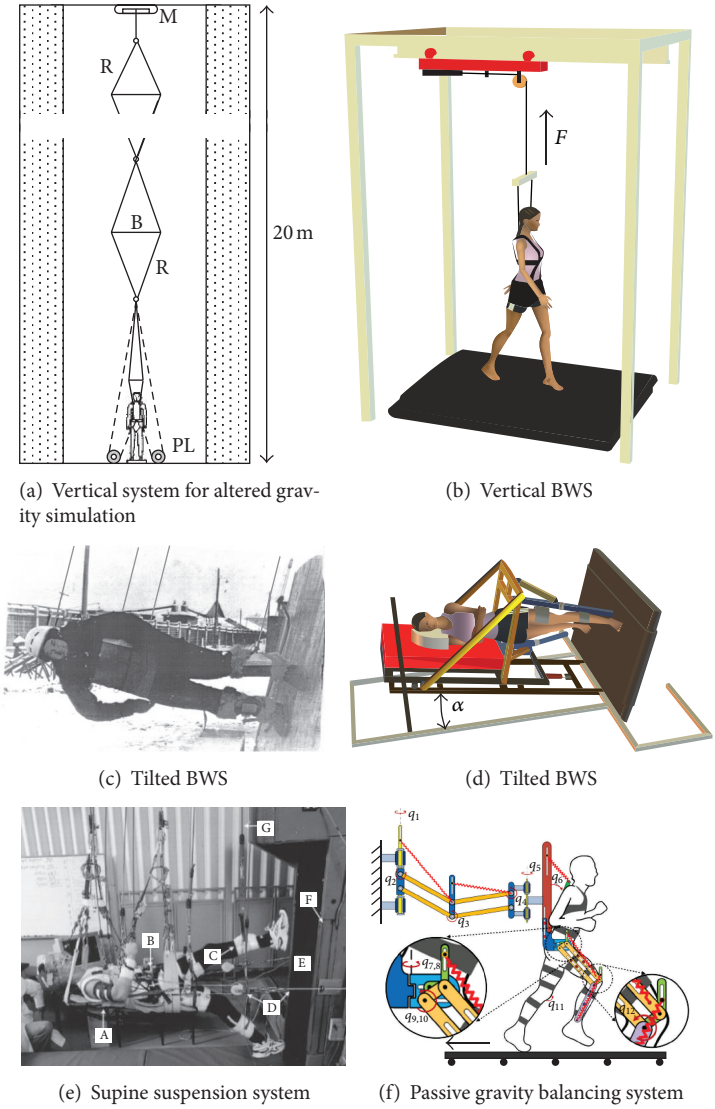

(a) Vertical system for altered gravity simulation

(b) Vertical BWS

(c) Tilted BWS

(d) Tilted BWS

(e) Supine suspension system

(f) Passive gravity balancing system

Figure 1: Reduced gravity simulators for locomotion. (a) Schema of the vertical system used to simulate different gravity values (redrawn from [8]). R: rubber bands, B: light metal bars, M: electric motor to stretch the elastic band system, PL: pulleys to invert the direction of the pull on the subject (dashed lines). (b) Vertical body weight support (BWS) system: subject walks on a treadmill with different levels of BWS while being supported in a harness, pulled upwards by a preset unloading force F. (c) Tilted BWS system used by Roscosmos (Russian Federal Space Agency) to train astronauts before space flights [15]: the subject walks on a truncated cone (60 m height, 9.2° inclination relative to the vertical), supported by five ropes sustaining the head, trunk, and legs (picture portraying Professor Gurfinkel reproduced with his kind permission). (d) Tilted unloading system for stepping on a treadmill: the subject lies on the side on a tilted couch (up to 40° from the horizontal position) with both legs suspended in the exoskeleton and steps on the treadmill, which is tilted to the same angle. The component of the gravity force acting on the stance and swing limb segments is proportional to the tilting angle α [18]. (e) Supine suspension system (adapted from [20], courtesy of Professor Peter Cavanagh): the subject is suspended horizontally attached to latex rubber cords. A cloth sleeve and rubber cord are attached each to the upper and lower arms and legs (eight total). The subject is actively pulled toward the treadmill by a gravity replacement load through cables attached to a load splitter. (f) Passive reduced gravity walking simulator (courtesy of Dr. Ou Ma). The system consists of a 3-DOF dual parallelogram mechanism, a 2-DOF torso support assembly, and a pair of 3-DOF leg exoskeletons. The weight of the body and the legs is compensated by the spring-balanced dual-parallelogram mechanism and torso-support assembly, and the weight of each leg is compensated by a leg exoskeleton [22–24].

is an increasing function of the walking speed (while the change in the potential energy is proportional to gravity), the hypothesis was proposed that the inverted pendulum-like mechanism of energy exchange during walking would be optimized at slower speeds in reduced gravity [3, 10]. An optimal exchange between potential and kinetic energies of the COM occurs at Fr ~ 0.25 [2] (Figure 2(a)). Even though specific limb segment proportions may play an essential role in the kinematics and energetics of walking [30], animal anatomy and individualized limb segment dimensions are

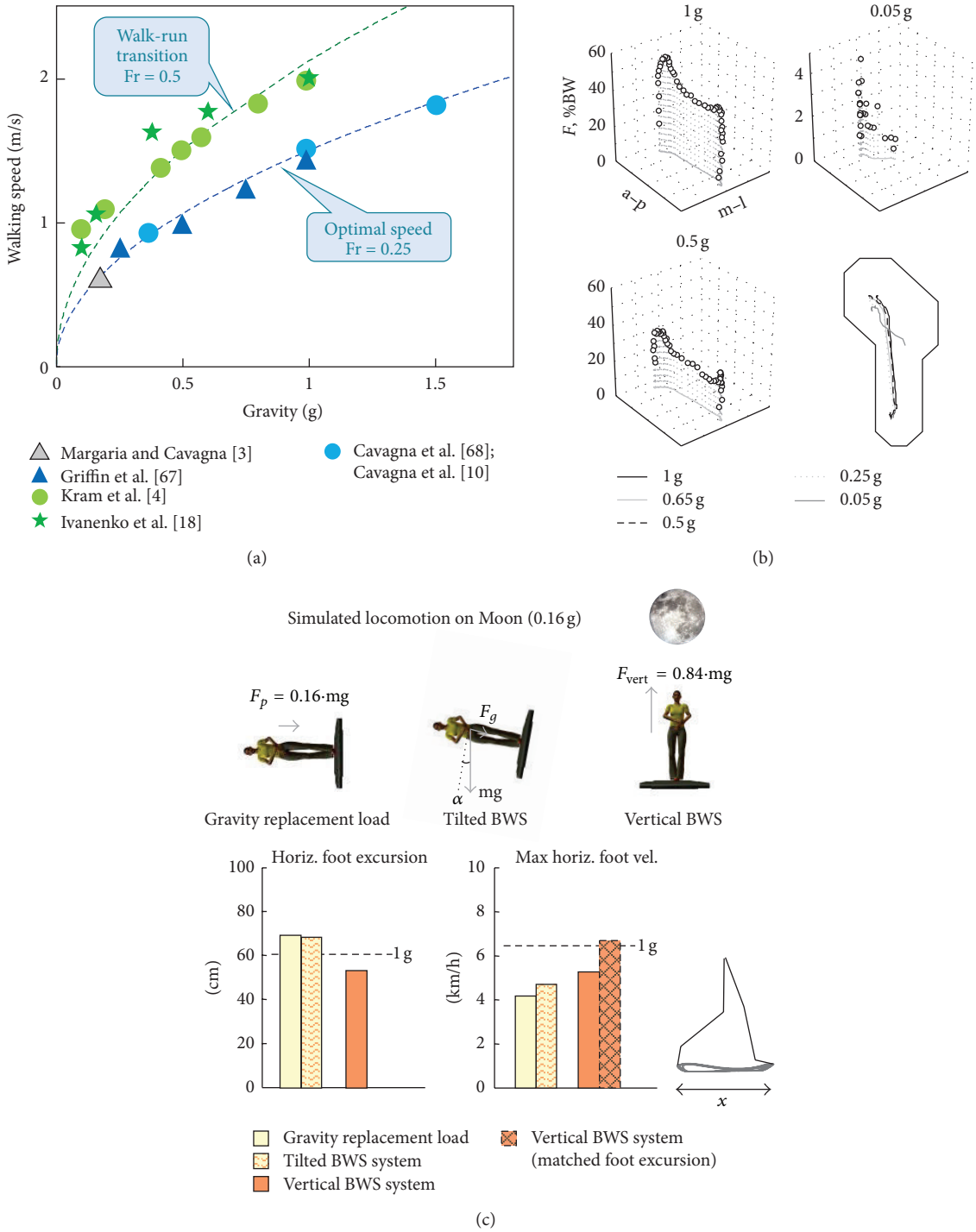

Figure 2: Biomechanical features of locomotion in reduced gravity conditions. (a) Optimal (blue) and walk-to-run transition (green) speeds as a function of gravity. Dynamically similar speeds predicted by Fr = 0.25 and Fr = 0.5 are indicated by blue and green dashed curves, respectively [25]. Green circles and stars refer to measurements of optimal walk-to-run transition speeds in simulated low-gravity conditions [5, 18]. The grey triangle indicates an earlier estimate of optimal walking speed predicted for the Moon gravitational environment by Margaria and Cavagna [3]. Blue triangles refer to the optimal speeds (at which most of the mechanical exchange between potential and kinetic energy of the body center of mass occurs) obtained in a simulation study of Griffin et al. [26]. Blue circles represent measurements of optimal speed obtained during parabolic flight [10, 27]. (b) Time course of the net vertical component of in-shoe reaction forces plotted as a function of the spatial coordinates of the foot at different reduced gravity levels. Note change in vertical scale in the 0.05 g condition. The lower right panel shows the trajectories of the center of pressure superimposed on a foot outline (adapted from [28]). (c) Maximum longitudinal foot velocity and foot excursion (x) during walking at 2 km/h at 0.16 g using three different reduced gravity simulators (represented schematically in the upper panels). Horizontal dashed lines indicate values for walking at 1 g. The hatched bar (right panel) corresponds to the maximal foot velocity for the vertical BWS system approximated by matching the foot excursion to that of the tilted BWS system [7]. Note significantly lower foot velocities during swing using tilted BWS systems.

optimized in such a way that the Froude number can explain optimal walking velocity.

On Earth, walking and running gaits are usually adopted for different speeds of locomotion, with a preferred transition occurring at ~2 m/s for human adults and at slow speeds for children (Fr ~ 0.5), in accordance with the dynamic similarity theory [29]. Different studies [4, 18] demonstrated that, at lower levels of gravity, the walk-run transition occurred at progressively slower absolute speeds but at approximately the same Froude number (Figure 2(a)).

Despite similarities in approximating reduced gravity, there are nevertheless essential differences between different simulation approaches. The variables that showed the greatest differences between vertical and tilted reduced gravity systems (Figure 1) were maximal longitudinal foot velocity and longitudinal foot excursion (Figure 2(c)), in agreement with significant influences of gravity on swing leg dynamics [7]. Even though the maximal longitudinal foot velocity for the tilted BWS condition decreased only slightly relative to the vertical BWS, however, the actual decrement was much more obvious if one takes into account that it was significantly compensated for or masked by increments in the stride length [7]. A previous modeling study also predicted differential effects of gravity during stance and swing phases [31]. In fact, the changes in the longitudinal foot excursion were basically opposite for the vertical and tilted BWS systems (Figure 2(c)). For the former system the amplitude of longitudinal foot motion decreased, while for the latter system it increased relative to the 1 g condition. Considering a monotonic (presumably proportional [32]) relationship between the stride length and the maximal foot velocity at a given gravity level (1 g), the peak foot velocity would be expected to be ~1.5 times higher for the vertical than for tilted BWS condition if the stride lengths were similar (Figure 2(c)). The previous studies on parabolic flights investigating the effect of gravity on walking mechanics demonstrated increments in the swing phase duration (by 29% at 0.25 g [33]; see also [11]), in line with the substantial contribution of gravity to the swing leg. Overall, the findings demonstrate that gravity acting on both stance and swing legs plays an important role in shaping locomotor patterns.

4. Nonlinear Reorganization of EMG Patterns

It is known that load plays a crucial role in shaping patterned motor output during stepping [34–36], and humans produce a specific heel-to-toe rolling pattern during stance in normal gravity conditions. Ground contact forces reflect the net vertical and shear forces acting on the contact surface and result from the sum of the mass-acceleration products of all body segments while the foot is in contact with ground [37]. Simulating reduced gravity between 0.05 and 1 g reveals drastic changes of kinetic parameters but limited changes of the kinematic coordination [28]. The reported accurate control of limb/foot kinematics [28] may depend on load- and displacement-compensation mechanisms working effectively throughout a wide range of ground contact forces, from full body weight up to <5% of its value. The peak vertical contact forces decrease proportionally to gravity, but at 0.05 g they are applied at the forefoot only (Figure 2(b)). During lower limb loading, a variety of receptors can be activated, such as Golgi tendon organs, cutaneous receptors of the foot, and spindles from stretched muscles [36]. These sensory signals interact with central rhythm-generating centers and help in shaping the motor patterns, controlling phase-transitions, and reinforcing ongoing activity [38, 39]. For instance, loading of the limb enhances the activity in antigravity muscles during stance and delays the onset of the next flexion [40]. It is important to understand the mechanisms of sensorimotor adaptation to the biomechanics of locomotion and foot placement/loading in heterogravity, especially to longer-term changes of load.

A key feature of adaptation to hypogravity is a remarkable nonlinear scaling of muscle activity patterns contrary to monotonic changes in foot loading. The simplest kind of change with simulated reduced gravity [28] was seen in ankle extensors: the mean amplitude of activity decreased systematically with decreasing simulated gravity, consistent with their antigravity function [35, 41]. By contrast, the behavior of other muscles could not be predicted simply on the basis of the static load during stance. The amplitude and pattern of muscle activity generally depended on speed and could vary nonmonotonically with body unloading. There was also a complex reorganization of the pattern of activity of thigh muscles with decreasing simulated gravity, as well as noteworthy individual differences [28]. Figure 3(a) illustrates an example of nonlinear reorganization of EMG patterns in one subject walking at 3 km/h. With body weight unloading, gluteus maximus and distal leg extensors decreased their activity, while other muscles demonstrated a "paradoxical" increment of activation (e.g., quadriceps) or considerable changes in the activation waveforms (hamstring muscles). Note also the absence of the typical burst of RF at the beginning of the swing phase at low simulated gravity levels (Figure 3(a)), consistent with other studies on the effect of body weight unloading [42] and walking speed [43]. It is unlikely that these changes are due to the order of trials or the consequence of learning the hypogravity condition since presentation order of speeds and BWS was randomized across sessions and experiments [28]. Also, the duration of each trial was ~1 min, with at least 2 min rest between trials, and a short (~30 s) training period of walking at different speeds was allowed for each simulated reduced gravity level before the actual data collection was begun (the walking patterns typically adapt rapidly to simulated reduced gravity [4, 5]). This reorganization is presumably related to the multifunctional (biarticular) action of these muscles and to the need to repartition the joint torque contributions across different muscles as a function of the changes induced by gravity. At 1 g, the main peak of m. biceps femoris activity occurring before heel-contact serves to decelerate the swinging limb [37]. However, as gravity is decreased, its main activity occurs in mid-stance and late stance, presumably in relation to the need to assist vaulting over an inverted pendulum of the stance limb and swing initiation.

There might be various factors accounting for the nonlinear reorganization of muscle activity patterns with gravity. To start with, nonlinear scaling also occurs during walking

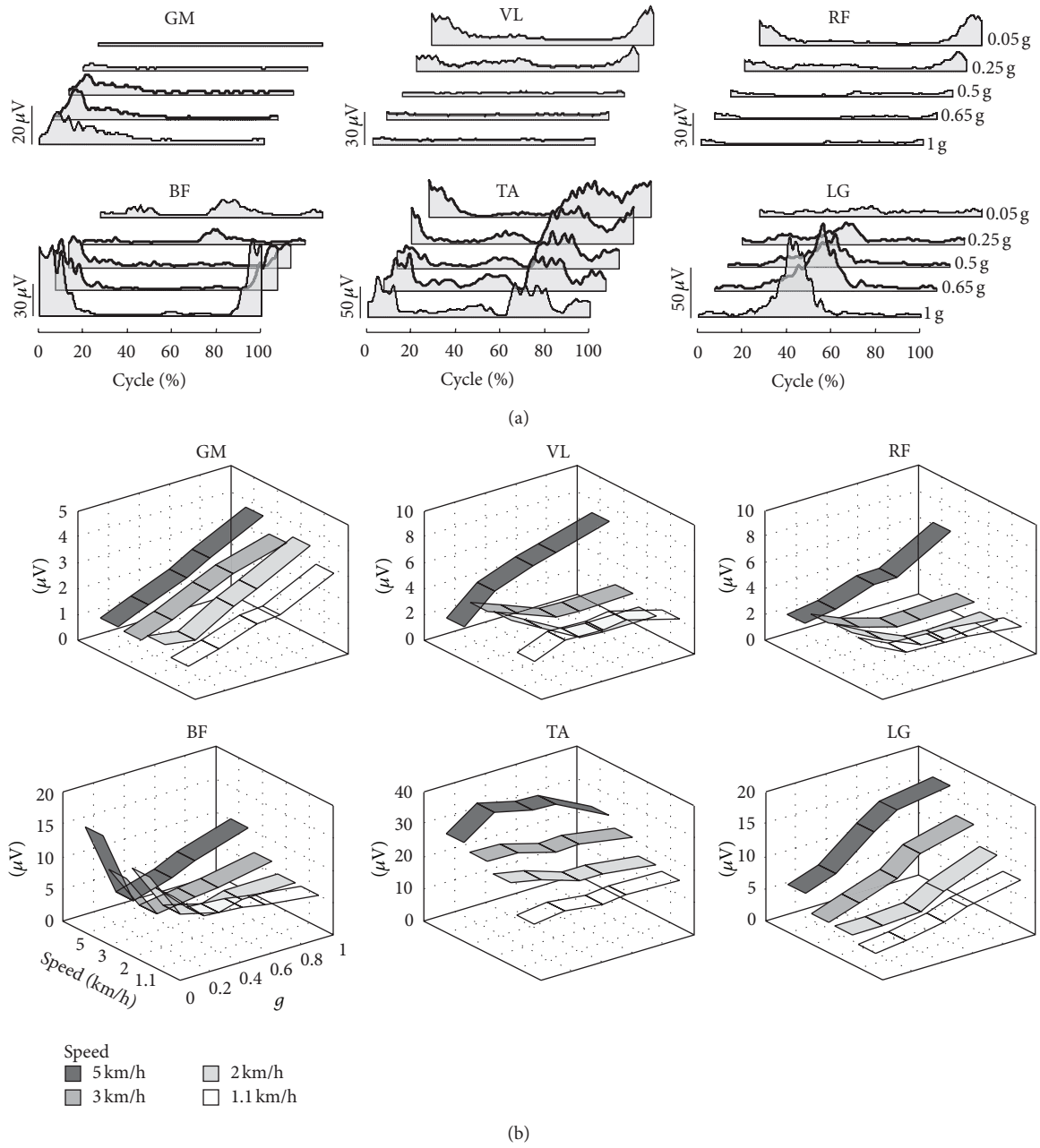

Figure 3: Nonlinear reorganization of muscle activity patterns. (a) An example of ensemble-averaged electromyographic (EMG) activity of lower limb muscles versus the normalized gait cycle is shown for a subject walking at 3 km/h at different simulated reduced gravity levels [28]. (b) Mean EMG activity computed over the gait cycle and averaged across all cycles and subjects ($n = 8$). For each muscle, values for trials performed at each speed are plotted as a function of simulated reduced gravity (adapted from [28]). GM, gluteus maximus, VL, vastus lateralis, RF, rectus femoris, BF, biceps femoris, TA, tibialis anterior, LG, and lateral gastrocnemius.

at different speeds at 1 g. For instance, VL and RF activity is quite small at low speeds (less than ~3 km/h) but becomes prominent at higher speeds (>4 km/h) (Figure 3(b)), a speed effect consistent with that reported in the literature [28, 43, 45, 46]. Given that, it should be stressed that walking at lower gravity levels at the same speed (Figure 3(a)) corresponds to walking at higher speeds if one uses the Froude number as a dimensionless parameter (e.g., walk-run transition at 0.25 g occurs at ~4 km/h, Figure 2(a)), so that "paradoxical" increments of VL and RF EMG activity in Figure 3(a) may reflect higher biomechanical demands on proximal leg muscles at higher dimensionless speeds. Nonlinear reorganization of EMG patterns was also observed when using exoskeleton robotic devices that provide body weight support [42, 47]. Changes in the body reference configuration during stance (slightly flexed posture [48, 49]) may contribute to a greater

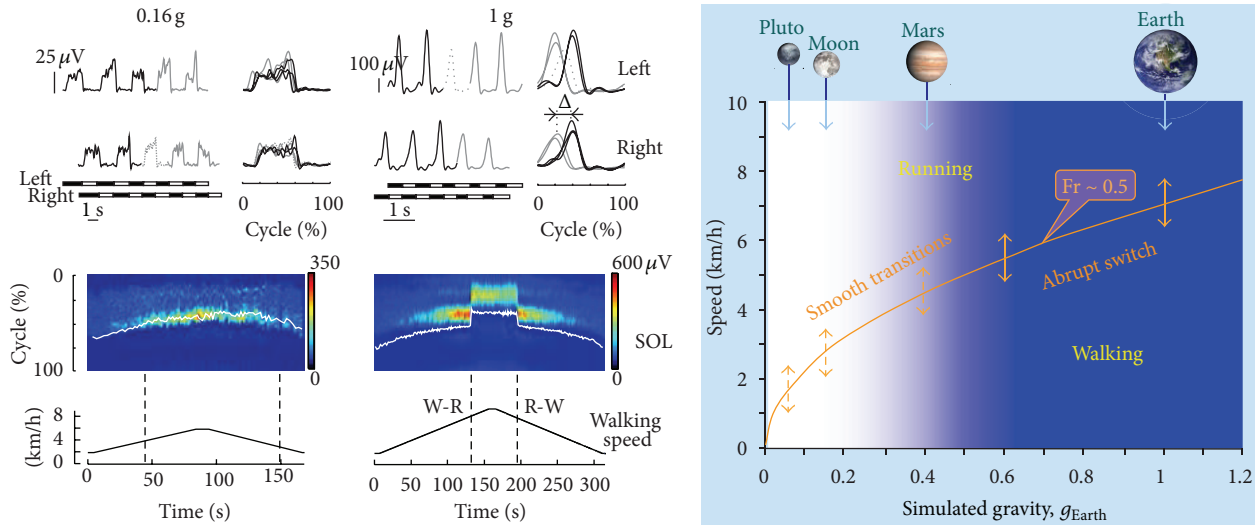

FIGURE 4: Smoothness/abruptness of gait transitions at different gravity levels. (a) Soleus (SOL) EMG patterns during slow changes in treadmill belt speed (lower panels) in one representative subject at 0.16 g (left) and 1 g (right). *Upper panels*: examples of SOL EMG waveforms (left, plotted versus time; right, plotted versus normalized cycle) during 5 consecutive strides of both legs around the transition from walking (black lines) to running (gray lines). Dotted curves denote the (transition) stride of the leg in which the swing phase first exceeded 50% gait cycle. Bottom horizontal bars denote stance (black) and swing (white) phases. *Lower panels*: the color maps represent a sequence of discrete activation waveforms (vertical slices). x-axis indicates the number of the gait cycles (corresponding to the appropriate timing of the trial), y-axis indicates normalized gait cycle (from touchdown to another touchdown), and color indicates EMG amplitude. The white line indicates when toe off occurred. Vertical dashed lines indicate walk-to-run (W-R) and run-to-walk (R-W) transitions. Note abrupt changes in the relative stance duration and muscle activation patterns at gait transitions at 1 g and no obvious distinction in these parameters at the transition from walking to running at 0.16 g. (b) Schematic representation of the smoothness of gait transitions as a function of gravity. The orange curve symbolizes the dimensionless walk-run transition speed consistent with the theory of dynamic similarity (Fr ~ 0.5) [19, 29, 44]. The blue color range of gravitational levels represents a discontinuous switch from walk to run, whereas the white region indicates smooth transitions.

activity of proximal extensors as well. Finally, there is a differential effect of speed on quadriceps muscle activity at reduced gravity levels: VL and RF activity increases at low speeds (<3 km/h) while it decreases at a high speed (5 km/h) (Figure 3(b)). Potential nonlinear scaling of muscle activity for most whole body movements in microgravity should also be taken into account for exercise countermeasures for astronauts.

5. Different Gaits

Considering complex, high-dimensional, dynamically coupled interactions between an organism and gravitational environment, in principle, one challenging solution is to adopt different coordination patterns and not only an optimal speed of locomotion. Are different gaits possible on other planets?

One approach to study locomotor adaptations is to look at the effect of gravity on gait transitions. A gait has been defined as "a pattern of locomotion characteristic of a limited range of speeds described by quantities of which one or more change discontinuously at transitions to other gaits" [29]. An important aspect of gait transitions is a discontinuous switch that occurs at some point while varying the speed of progression (although some exceptions may exist [50–52]). As already discussed (Figure 2(a)), gravity has a strong effect on the speed at which gait transitions occur (Fr ~ 0.5). Surprisingly, however, we found [18, 19] that at lower levels of simulated gravity the transition between walking and running was generally gradual, without any noticeable abrupt change in gait parameters or EMG bursts (Figure 4(a)). This was associated with a significant prolongation of the swing phase, whose duration became virtually equal to that of stance in the vicinity of the walk-run transition speed, and with a gradual shift from inverted-pendulum gait (walking) to bouncing gait (running). A lack of discontinuous changes in the pattern of speed-dependent locomotor characteristics in a hypogravity environment (Figure 4(b)) is consistent with the idea of a continuous shift in the state of a given set of central pattern generators, rather than the activation of a separate set of central pattern generators for each distinct gait [19].

Interestingly, the smoothness of gait transitions is accompanied by a gradual shift from inverted-pendulum gait to bouncing gait, resulting in a "paradoxical" inverted-pendulum running in the vicinity of run-walk and walk-run transitions [18]. The swing phase may have more influence on gait than it was previously thought. For instance, relatively slower swing and longer foot excursions (tilted BWS condition, Figure 2(c)) may raise questions about optimality or comfort of walking and could account for potentially different preferred gaits, such as loping on the Moon observed in Apollo astronauts (though the Lunar suit limits the range

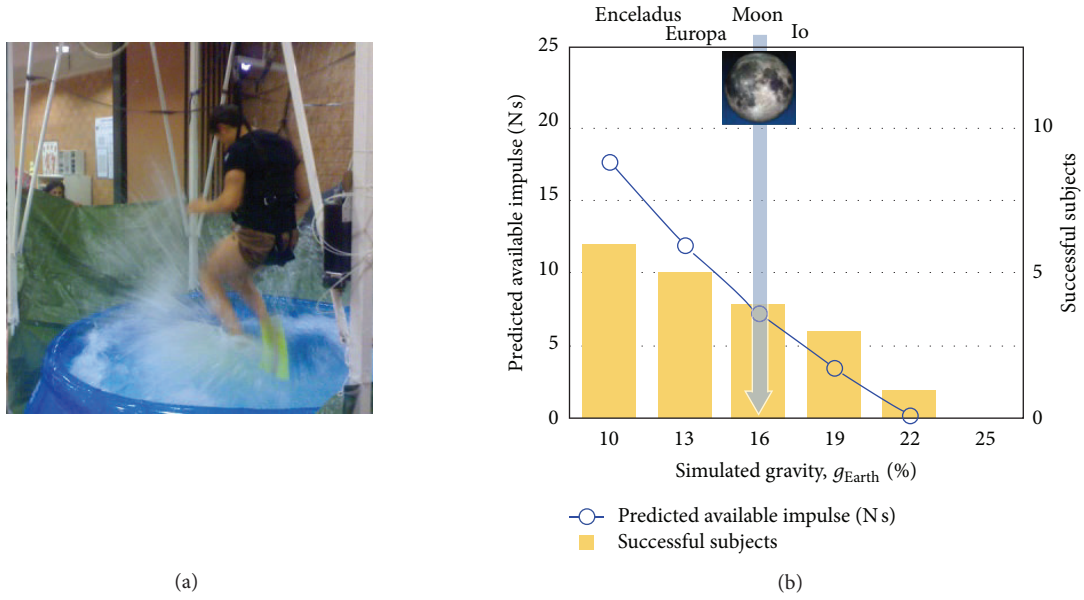

FIGURE 5: Running on water at simulated reduced gravity. The blue curve represents the net vertical impulse available to run on water, as predicted by the model used by Minetti et al. [53]. Bars represent the number of subjects, out of 6, capable of avoiding sinking at different simulated gravity values. Both variables show that 22% of Earth gravity (g_{EARTH}) is the maximum gravity at which humans can run on water, when assisted by a small rigid fin (as illustrated in the left panel).

of motion in the leg joints and may also contribute to the loping gait on the Moon [9]). The resulting changes in the intersegmental and interlimb coordination may in turn affect the COM motion. Overall, the results support the idea of looking for new forms of locomotion (both bipedal and quadrupedal) in a heterogravity environment [54] based on the interplay between stance and swing leg dynamics, altered interlimb coupling, and altered center of mass movements.

Other significant influences of gravity on short-term and long-term gait adaptations may be related to its effects on the body reference configuration [48, 49] and anticipatory mechanisms of limb and body movements [55, 56]. For instance, the basis of habitual human posture is postural tone of the skeletal muscles and microgravity elicits substantial changes in muscle tone and posture [48, 49]. Based on clinical observations, it has been recently argued that any reflection on the nature and choice of preferred gait (e.g., bipedal versus quadrupedal) should include a consideration of the mechanisms determining the choice of unconscious habitual posture [57]. Also, in analogy with the results based on upper-limb movements related to time-to-contact [55] or movement planning [58], anticipatory postural and locomotor adjustments for lower limb movements (e.g., for the control of heel strike or accurate foot placement) should take gravity into consideration. Therefore, altered gravity conditions may also affect locomotor-related tasks such as the negotiation of stationary and moving obstructions during walking or gait initiation/termination [56, 59, 60].

Finally, the repertoire of known gaits can be expanded to a variety of animals. For instance, on Earth only a few legged species, such as water strider insects and some aquatic birds and lizards, can run on water. For most other species, including humans, this is precluded by body size and proportions, lack of appropriate appendages, and limited muscle power. However, if gravity is reduced to less than Earth's gravity, running on water should require less muscle power. Recently, Minetti et al. [53] used this hydrodynamic model of Glasheen and McMahon [61] to predict the gravity levels at which humans should be able to run on water and tested the hypothesis in the laboratory using a reduced gravity simulator (Figure 5). The results showed that a hydrodynamic model of Basilisk lizards running on water [61] can also be applied to humans, despite the enormous difference in body size and morphology. Particularly, 22% of Earth's gravity is the maximum at which humans can run on water, when assisted by a small rigid fin (Figure 5) [53]. It is also worth noting the limitations for our musculoskeletal system for producing force/power (endurance); for instance, the stride frequency in humans is limited to about 2 Hz, whatever the planet is. On Earth, the biggest animal that can run on water is likely Western Grebes, and even these birds can run only for several seconds since the force production is basically anaerobic (participants in [53] could run at simulated "Moon" gravity only for ~10 s). In contrast, at reduced gravity (Moon), these birds could run on water in a charming manner for much longer time.

6. Clinical Implications

Reduced gravity also offers unique opportunities for adjusting the basic patterns to altered locomotor conditions for gait rehabilitation. Body weight support systems coupled with robotic devices or pharmacologic treatments are now often used in the rehabilitation practice to assist physical therapy of

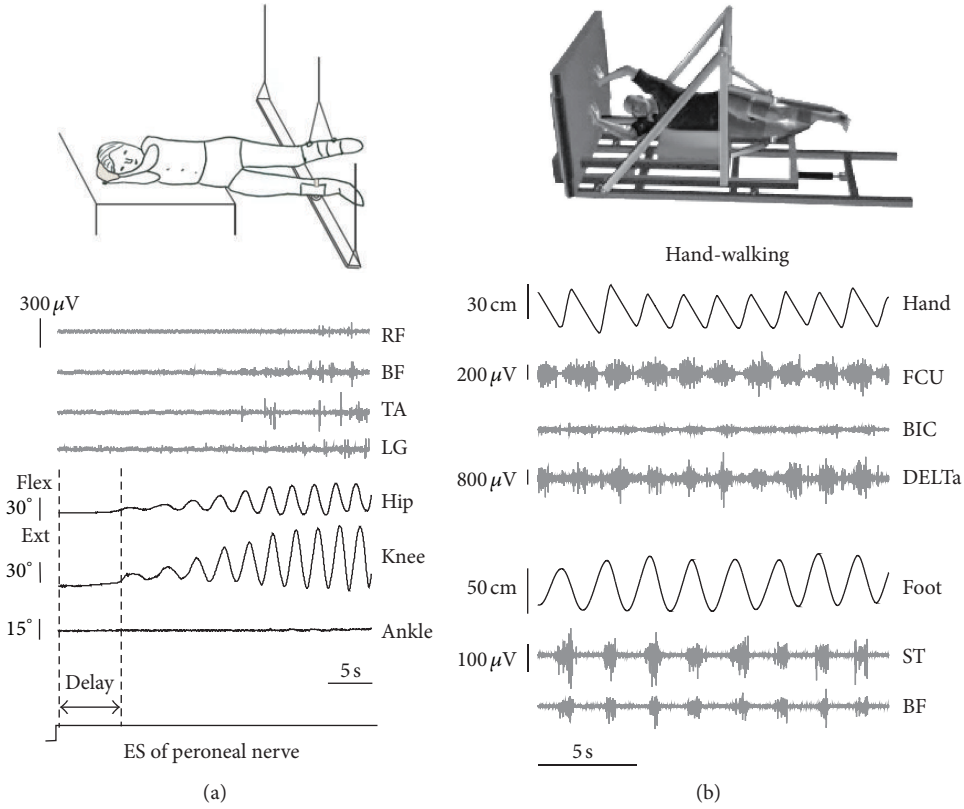

Figure 6: Eliciting nonvoluntary limb stepping movements in simulated weightlessness (gravity neutral) conditions. (a) An example of nonvoluntary rhythmic movements of the suspended legs induced by electrical stimulation (ES) of peroneal nerve from the study of Selionov et al. [62]. Note the absence of ankle joint rotations during evoked air-stepping. (b) An example of evoked rhythmic leg movements during hand walking in one subject from the study of Sylos-Labini et al. [63]. RF, rectus femoris, BF, biceps femoris, TA, tibialis anterior, LG, lateral gastrocnemius, FCU, flexor carpi ulnaris, BIC, biceps brachii, DELTa, anterior deltoid, ST, and semitendinosus. Hand and foot denote anterior-posterior displacements of the left hand and foot.

individuals with neurological disorders. We will not review any detailed analysis of clinical outcomes for ambulation when using locomotor training with body weight support systems and refer to other reviews [64]. Nevertheless, it is worth emphasizing a facilitatory effect of the lack of gravity on rhythmogenesis and its potential for gait recovery.

Novel pharmacological strategies [65] and electromagnetic stimulation techniques [62, 66–68] are being developed aimed at modulating spinal activity and restoring the locomotor function. The spinal central pattern generator (CPG) circuitry can be easily activated in healthy humans in a gravity neutral position by applying tonic central and peripheral sensory inputs. To minimize interference with the ongoing task of body weight and balance control, stepping movements are elicited during air-stepping in the absence of gravity influences and external resistance. Figure 6 illustrates examples of nonvoluntary rhythmic movements of the suspended legs induced by electrical stimulation of peroneal nerve [62] and during hand walking [63]. It has been suggested that functional multisensory stimulations and a functional neural coupling between arm and legs can inspect CPG access by sensory and central activations and entrain locomotor neural networks and promote gait recovery. Such investigations may contribute to the clinical development of central pattern generator-modulating therapies and neuroprosthetic technologies [65, 69].

7. Concluding Remarks

This perspective outlines an interdisciplinary approach to extend our knowledge on adaptation of human locomotion to a hypogravity environment, including biomechanical, neurophysiological, and comparative aspects, effective exercise countermeasures for astronauts, and even exobiology of new forms of locomotion on different planets. The tools and techniques used for hypogravity simulation and their effects on human locomotion provide new insights into our understanding of the physiological effects of gravity. The beneficial effect of weightlessness on rhythmogenesis would further enhance the utility of this approach and developments of innovative technologies for gait rehabilitation.

Conflict of Interests

The authors declare that there is no conflict of interests regarding the publication of this paper.

Acknowledgments

This work was supported by the Italian Health Ministry, Italian Ministry of University and Research (PRIN project), and Italian Space Agency (DCMC, CRUSOE, and COREA grants).

References

[1] R. J. Full and D. E. Koditschek, "Templates and anchors: neuromechanical hypotheses of legged locomotion on land," *The Journal of Experimental Biology*, vol. 202, no. 23, pp. 3325–3332, 1999.

[2] A. E. Minetti, "Invariant aspects of human locomotion in different gravitational environments," *Acta Astronautica*, vol. 49, no. 3–10, pp. 191–198, 2001.

[3] R. Margaria and G. A. Cavagna, "Human locomotion in subgravity," *Aerospace Medicine*, vol. 35, pp. 1140–1146, 1964.

[4] R. Kram, A. Domingo, and D. P. Ferris, "Effect of reduced gravity on the preferred walk-run transition speed," *The Journal of Experimental Biology*, vol. 200, no. 4, pp. 821–826, 1997.

[5] J. M. Donelan and R. Kram, "The effect of reduced gravity on the kinematics of human walking: a test of the dynamic similarity hypothesis for locomotion," *The Journal of Experimental Biology*, vol. 200, no. 24, pp. 3193–3201, 1997.

[6] B. L. Davis and P. R. Cavanagh, "Simulating reduced gravity: a review of biomechanical issues pertaining to human locomotion," *Aviation Space and Environmental Medicine*, vol. 64, no. 6, pp. 557–566, 1993.

[7] F. Sylos-Labini, Y. P. Ivanenko, G. Cappellini, A. Portone, M. J. Maclellan, and F. Lacquaniti, "Changes of gait kinematics in different simulators of reduced gravity," *Journal of Motor Behavior*, vol. 45, no. 6, pp. 495–505, 2013.

[8] G. A. Cavagna, A. Zamboni, T. Faraggiana, and R. Margaria, "Jumping on the moon: power output at different gravity values," *Aerospace Medicine*, vol. 43, no. 4, pp. 408–414, 1972.

[9] C. E. Carr and J. McGee, "The apollo number: space suits, self-support, and the walk-run transition," *PLoS ONE*, vol. 4, no. 8, Article ID e6614, 2009.

[10] G. A. Cavagna, P. A. Willems, and N. C. Heglund, "The role of gravity in human walking: pendular energy exchange, external work and optimal speed," *Journal of Physiology*, vol. 528, part 3, pp. 657–668, 2000.

[11] J. K. De Witt, G. P. Perusek, B. E. Lewandowski et al., "Locomotion in simulated and real microgravity: horizontal Suspension vs. parabolic flight," *Aviation Space and Environmental Medicine*, vol. 81, no. 12, pp. 1092–1099, 2010.

[12] F. Gazzani, A. Fadda, M. Torre, and V. Macellari, "WARD: a pneumatic system for body weight relief in gait rehabilitation," *IEEE Transactions on Rehabilitation Engineering*, vol. 8, no. 4, pp. 506–513, 2000.

[13] A. M. Grabowski and R. Kram, "Effects of velocity and weight support on ground reaction forces and metabolic power during running," *Journal of Applied Biomechanics*, vol. 24, no. 3, pp. 288–297, 2008.

[14] J. P. He, R. Kram, and T. A. McMahon, "Mechanics of running under simulated low gravity," *Journal of Applied Physiology*, vol. 71, no. 3, pp. 863–870, 1991.

[15] V. A. Bogdanov, V. S. Gurfinkel, and V. E. Panfilov, "Human motion under lunar gravity conditions (Human performance in various locomotive tasks under simulated lunar reduced gravity conditions, classifying test stands and equipment)," *Kosmicheskaya Biologiya i Meditsina*, vol. 5, pp. 3–13, 1971.

[16] J. R. Hansen, *Spaceflight Revolution: NASA Langley Research Center from Sputnik to Apollo*, National Aeronautics and Space Administration, Washington, DC, USA, 1995.

[17] D. E. Hewes, "Reduced-gravity simulators for studies of man's mobility in space and on the moon," *Human Factors*, vol. 11, no. 5, pp. 419–431, 1969.

[18] Y. P. Ivanenko, F. Sylos-Labini, G. Cappellini, V. Macellari, J. McIntyre, and F. Lacquaniti, "Gait transitions in simulated reduced gravity," *Journal of Applied Physiology*, vol. 110, no. 3, pp. 781–788, 2011.

[19] F. Sylos-Labini, Y. P. Ivanenko, G. Cappellini, S. Gravano, and F. Lacquaniti, "Smooth changes in the EMG patterns during gait transitions under body weight unloading," *Journal of Neurophysiology*, vol. 106, no. 3, pp. 1525–1536, 2011.

[20] K. O. Genc, V. E. Mandes, and P. R. Cavanagh, "Gravity replacement during running in simulated microgravity," *Aviation Space and Environmental Medicine*, vol. 77, no. 11, pp. 1117–1124, 2006.

[21] J. L. McCrory, H. A. Baron, S. Balkin, and P. R. Cavanagh, "Locomotion in simulated microgravity: gravity replacement loads," *Aviation Space and Environmental Medicine*, vol. 73, no. 7, pp. 625–631, 2002.

[22] Q. Lu, C. Ortega, and O. Ma, "Passive gravity compensation mechanisms: technologies and applications," *Recent Patents on Engineering*, vol. 5, no. 1, pp. 32–44, 2011.

[23] O. Ma and J. Wang, "Apparatus and method for reduced-gravity simulation," 2012.

[24] Q. Lu, J. McAvoy, and O. Ma, "A simulation study of a reduced-gravity simulator for simulating human jumping and walking in a reduced-gravity environment," in *Proceedings of the ASME Dynamic Systems and Control Conference*, 2009.

[25] A. E. Minetti, "Walking on other planets," *Nature*, vol. 409, no. 6819, pp. 467–469, 2001.

[26] T. M. Griffin, N. A. Tolani, and R. Kram, "Walking in simulated reduced gravity: mechanical energy fluctuations and exchange," *Journal of Applied Physiology*, vol. 86, no. 1, pp. 383–390, 1999.

[27] G. A. Cavagna, P. A. Willams, and N. C. Heglund, "Walking on mars," *Nature*, vol. 393, no. 6686, article 636, 1998.

[28] Y. P. Ivanenko, R. Grasso, V. Macellari, and F. Lacquaniti, "Control of foot trajectory in human locomotion: role of ground contact forces in simulated reduced gravity," *Journal of Neurophysiology*, vol. 87, no. 6, pp. 3070–3089, 2002.

[29] R. Alexander McN., "Optimization and gaits in the locomotion of vertebrates," *Physiological Reviews*, vol. 69, no. 4, pp. 1199–1227, 1989.

[30] F. Leurs, Y. P. Ivanenko, A. Bengoetxea et al., "Optimal walking speed following changes in limb geometry," *The Journal of Experimental Biology*, vol. 214, part 13, pp. 2276–2282, 2011.

[31] D. A. Raichlen, "The effects of gravity on human walking: a new test of the dynamic similarity hypothesis using a predictive model," *The Journal of Experimental Biology*, vol. 211, no. 17, pp. 2767–2772, 2008.

[32] Y. Osaki, M. Kunin, B. Cohen, and T. Raphan, "Three-dimensional kinematics and dynamics of the foot during walking: a model of central control mechanisms," *Experimental Brain Research*, vol. 176, no. 3, pp. 476–496, 2007.

[33] J. F. Roberts, "Walking responses under lunar and low gravity conditions," AMRL-TR 6570th, Aerospace Medical Research Laboratory, 1963.

[34] S. H. Scott and D. A. Winter, "Biomechanical model of the human foot: kinematics and kinetics during the stance phase of walking," *Journal of Biomechanics*, vol. 26, no. 9, pp. 1091–1104, 1993.

[35] S. J. Harkema, S. L. Hurley, U. K. Patel, P. S. Requejo, B. H. Dobkin, and V. R. Edgerton, "Human lumbosacral spinal cord interprets loading during stepping," *Journal of Neurophysiology*, vol. 77, no. 2, pp. 797–811, 1997.

[36] J. Duysens, F. Clarac, and H. Cruse, "Load-regulating mechanisms in gait and posture: comparative aspects," *Physiological Reviews*, vol. 80, no. 1, pp. 83–133, 2000.

[37] D. A. Winter, *The Biomechanics and Motor Control of Human Gait: Normal, Elderly and Pathological*, University of Waterloo Press, Waterloo, Canada, 1991.

[38] K. G. Pearson, "Common principles of motor control in vertebrates and invertebrates," *Annual Review of Neuroscience*, vol. 16, pp. 265–297, 1993.

[39] K. G. Pearson, "Proprioceptive regulation of locomotion," *Current Opinion in Neurobiology*, vol. 5, no. 6, pp. 786–791, 1995.

[40] J. Duysens, B. M. H. van Wezel, H. W. A. A. van de Crommert, M. Faist, and J. G. M. Kooloos, "The role of afferent feedback in the control of hamstrings activity during human gait," *European Journal of Morphology*, vol. 36, no. 4-5, pp. 293–299, 1998.

[41] L. Finch, H. Barbeau, and B. Arsenault, "Influence of body weight support on normal human gait: development of a gait retraining strategy," *Physical Therapy*, vol. 71, no. 11, pp. 842–855, 1991.

[42] J. C. Moreno, F. Barroso, D. Farina et al., "Effects of robotic guidance on the coordination of locomotion," *Journal of NeuroEngineering and Rehabilitation*, vol. 10, no. 1, article 79, 2013.

[43] A. R. den Otter, A. C. H. Geurts, T. Mulder, and J. Duysens, "Speed related changes in muscle activity from normal to very slow walking speeds," *Gait and Posture*, vol. 19, no. 3, pp. 270–278, 2004.

[44] F. Saibene and A. E. Minetti, "Biomechanical and physiological aspects of legged locomotion in humans," *European Journal of Applied Physiology*, vol. 88, no. 4-5, pp. 297–316, 2003.

[45] Y. P. Ivanenko, R. E. Poppele, and F. Lacquaniti, "Spinal cord maps of spatiotemporal alpha-motoneuron activation in humans walking at different speeds," *Journal of Neurophysiology*, vol. 95, no. 2, pp. 602–618, 2006.

[46] A. Pépin, K. E. Norman, and H. Barbeau, "Treadmill walking in incomplete spinal-cord-injured subjects: 1. Adaptation to changes in speed," *Spinal Cord*, vol. 41, no. 5, pp. 257–270, 2003.

[47] F. Sylos-Labini, V. La Scaleia, I. Pisotta et al., "EMG patterns during assisted walking in the exoskeleton," *Frontiers in Human Neuroscience*, vol. 8, article 423, 2014.

[48] J. Massion, K. Popov, J.-C. Fabre, P. Rage, and V. Gurfinkel, "Is the erect posture in microgravity based on the control of trunk orientation or center of mass position?" *Experimental Brain Research*, vol. 114, no. 2, pp. 384–389, 1997.

[49] G. Andreoni, C. Rigotti, G. Baroni, G. Ferrigno, N. A. Colford, and A. Pedotti, "Quantitative analysis of neutral body posture in prolonged microgravity," *Gait & Posture*, vol. 12, no. 3, pp. 235–242, 2000.

[50] S. M. Gatesy and A. A. Biewener, "Bipedal locomotion: effects of speed, size and limb posture in birds and humans," *Journal of Zoology*, vol. 224, no. 1, pp. 127–147, 1991.

[51] J. Rubenson, D. B. Heliams, D. G. Lloyd, and P. A. Fournier, "Gait selection in the ostrich: mechanical and metabolic characteristics of walking and running with and without an aerial phase," *Proceedings of the Royal Society B: Biological Sciences*, vol. 271, no. 1543, pp. 1091–1099, 2004.

[52] L. Ren and J. R. Hutchinson, "The three-dimensional locomotor dynamics of African (*Loxodonta africana*) and Asian (*Elephas maximus*) elephants reveal a smooth gait transition at moderate speed," *Journal of the Royal Society Interface*, vol. 5, no. 19, pp. 195–211, 2008.

[53] A. E. Minetti, Y. P. Ivanenko, G. Cappellini, N. Dominici, and F. Lacquaniti, "Humans running in place on water at simulated reduced gravity," *PLoS ONE*, vol. 7, no. 7, Article ID e37300, 2012.

[54] M. Srinivasan and A. Ruina, "Computer optimization of a minimal biped model discovers walking and running," *Nature*, vol. 439, no. 7072, pp. 72–75, 2006.

[55] J. McIntyre, M. Zago, A. Berthoz, and F. Lacquaniti, "Does the brain model Newton's laws?" *Nature Neuroscience*, vol. 4, no. 7, pp. 693–694, 2001.

[56] G. Clément, V. S. Gurfinkel, F. Lestienne, M. I. Lipshits, and K. E. Popov, "Adaptation of postural control to weightlessness," *Experimental Brain Research*, vol. 57, no. 1, pp. 61–72, 1984.

[57] Y. P. Ivanenko, W. G. Wright, R. J. St George, and V. S. Gurfinkel, "Trunk orientation, stability, and quadrupedalism," *Frontiers in Neurology*, vol. 4, article 20, 2013.

[58] C. Papaxanthis, T. Pozzo, K. E. Popov, and J. McIntyre, "Hand trajectories of vertical arm movements in one-G and zero-G environments. Evidence for a central representation of gravitational force," *Experimental Brain Research*, vol. 120, no. 4, pp. 496–502, 1998.

[59] P. Crenna, D. M. Cuong, and Y. Brénière, "Motor programmes for the termination of gait in humans: organisation and velocity-dependent adaptation," *Journal of Physiology*, vol. 537, no. 3, pp. 1059–1072, 2001.

[60] B. J. McFadyen and H. Carnahan, "Anticipatory locomotor adjustments for accommodating versus avoiding level changes in humans," *Experimental Brain Research*, vol. 114, no. 3, pp. 500–506, 1997.

[61] J. W. Glasheen and T. A. McMahon, "Size-dependence of water-running ability in basilisk lizards (*Basiliscus basiliscus*)," *The Journal of Experimental Biology*, vol. 199, no. 12, pp. 2611–2618, 1996.

[62] V. A. Selionov, Y. P. Ivanenko, I. A. Solopova, and V. S. Gurfinkel, "Tonic central and sensory stimuli facilitate involuntary air-stepping in humans," *Journal of Neurophysiology*, vol. 101, no. 6, pp. 2847–2858, 2009.

[63] F. Sylos-Labini, Y. P. Ivanenko, M. J. Maclellan, G. Cappellini, R. E. Poppele, and F. Lacquaniti, "Locomotor-like leg movements evoked by rhythmic arm movements in humans," *PloS ONE*, vol. 9, no. 3, Article ID e90775, 2014.

[64] P. Sale, M. Franceschini, A. Waldner, and S. Hesse, "Use of the robot assisted gait therapy in rehabilitation of patients with stroke and spinal cord injury," *European Journal of Physical and Rehabilitation Medicine*, vol. 48, no. 1, pp. 111–121, 2012.

[65] P. A. Guertin, "Preclinical evidence supporting the clinical development of central pattern generator-modulating therapies for chronic spinal cord-injured patients," 2014.

[66] Y. Gerasimenko, P. Musienko, I. Bogacheva et al., "Propriospinal bypass of the serotonergic system that can facilitate stepping," *Journal of Neuroscience*, vol. 29, no. 17, pp. 5681–5689, 2009.

[67] V. A. Selionov, I. A. Solopova, D. S. Zhvansky et al., "Lack of non-voluntary stepping responses in Parkinson's disease," *Neuroscience*, vol. 235, pp. 96–108, 2013.

[68] C. A. Angeli, V. R. Edgerton, Y. P. Gerasimenko, and S. J. Harkema, "Altering spinal cord excitability enables voluntary movements after chronic complete paralysis in humans," *Brain*, 2014.

[69] D. Borton, M. Bonizzato, J. Beauparlant et al., "Corticospinal neuroprostheses to restore locomotion after spinal cord injury," *Neuroscience Research*, vol. 78, pp. 21–29, 2014.

Hindawi Publishing Corporation
BioMed Research International
Volume 2014, Article ID 857934, 9 pages
http://dx.doi.org/10.1155/2014/857934

Research Article

Conditioned Media from Microvascular Endothelial Cells Cultured in Simulated Microgravity Inhibit Osteoblast Activity

Alessandra Cazzaniga, Sara Castiglioni, and Jeanette A. M. Maier

Dipartimento di Scienze Biomediche e Cliniche Luigi Sacco, Università di Milano, Via GB Grassi 74, Milano, Italy

Correspondence should be addressed to Jeanette A. M. Maier; jeanette.maier@unimi.it

Received 23 April 2014; Revised 9 July 2014; Accepted 9 July 2014; Published 19 August 2014

Academic Editor: Mariano Bizzarri

Background and Aims. Gravity contributes to the maintenance of bone integrity. Accordingly, weightlessness conditions during space flight accelerate bone loss and experimental models in real and simulated microgravity show decreased osteoblastic and increased osteoclastic activities. It is well known that the endothelium and bone cells cross-talk and this intercellular communication is vital to regulate bone homeostasis. Because microgravity promotes microvascular endothelial dysfunction, we anticipated that the molecular cross-talk between endothelial cells exposed to simulated microgravity and osteoblasts might be altered. *Results*. We cultured human microvascular endothelial cells in simulated microgravity using the rotating wall vessel device developed by NASA. Endothelial cells in microgravity show growth inhibition and release higher amounts of matrix metalloproteases type 2 and interleukin-6 than controls. Conditioned media collected from microvascular endothelial cells in simulated microgravity were used to culture human osteoblasts and were shown to retard osteoblast proliferation and inhibit their activity. *Discussion*. Microvascular endothelial cells in microgravity are growth retarded and release high amounts of matrix metalloproteases type 2 and interleukin-6, which might play a role in retarding the growth of osteoblasts and impairing their osteogenic activity. *Conclusions*. We demonstrate that since simulated microgravity modulates microvascular endothelial cell function, it indirectly impairs osteoblastic function.

1. Introduction

Bone development and remodeling depend mainly upon complex interactions between osteoblasts and osteoclasts. Indeed, an intimate communication exists between osteoblasts and osteoclasts since osteoclasts control osteoblastic growth and function, while osteoblasts regulate the differentiation and the activity of osteoclasts [1]. Recently, other cells of the bone microenvironment are emerging as implicated in bone health. Among others, endothelial cells are players of the communication network in the bone [2]. In embryonic skeletal tissue, osteogenesis and angiogenesis are temporally related [3] and, in the adults, osteoblasts are always located adjacent to endothelial cells in blood vessels at sites of new bone formation [4]. The fact that older subjects with osteoporosis have decreased blood vessels in their skeletal tissue, accompanied by a parallel decrease in osteoblasts, further highlights this close relation [5]. Several lines of evidence indicate that a mutual communication system exists between the endothelium and the osteoblasts. At the cellular and molecular levels, vascular endothelial cells have been shown to regulate bone remodelling via cell signalling networks of ligand-receptor complexes and osteoblasts release growth factors that influence endothelial cells [3].

In long duration space missions, astronauts experience considerable bone loss, about 1-2% of bone mass per month in the weight-bearing regions of the leg and the spine, mainly because of an uncoupling between osteoblasts and osteoclasts [6–8]. We anticipate that endothelial-osteoblast communication might be impaired in space and contributes to bone loss. Indeed, dysfunctions in human endothelial cells cultured in simulated microgravity have been described [9–15], and alterations in the capillaries of the epiphyses and metaphyses of femoral bones of rats flown aboard the US laboratory SLS-2 were detected [16].

Cross-talk between endothelial cells and osteoblasts in simulated microgravity has not been deciphered yet. As

a first approach to investigate this issue, we exposed osteoblasts to conditioned media (CM) from microvascular endothelial cells (HMEC) cultured in the rotating wall vessel (RWV), which simulates some aspects of microgravity. Studies utilizing CM are considered a successful strategy for the identification of soluble factors interconnecting different cell types and candidate biomarkers for further validation in clinical samples [17]. Indeed, CM reveal the cell secretome, that is, the collection of proteins that are released through the classical and nonclassical secretion pathways, and also proteins shed from the cell surface. These secreted proteins include enzymes, growth factors, cytokines, and other soluble mediators and are important contributors to cell survival, growth, and differentiation [17]. We here show that CM from HMEC grown in simulated microgravity impair the proliferation and activity of cultured primary osteoblasts and osteoblast-like Saos-2 cells.

2. Materials and Methods

2.1. Cell Culture. HMEC were obtained from CDC (Atlanta, USA) and grown in MCDB131 containing epidermal growth factor (10 ng/mL) and 10% fetal bovine serum (FBS) on 2% gelatin-coated dishes. Normal human osteoblasts (NHOst) were maintained in osteoblast growth media (OGM) as indicated by the manufacturer (Lonza, Basel, Switzerland) at 37°C in a humidified atmosphere containing 5% CO_2 [18]. Saos-2 cells (American Type Culture Collection) were cultured in DMEM containing 10% FBS. Before beginning the experiments with CM from HMEC, NHOst and Saos-2 cells were gradually adapted to be cultured in 1 : 1 HMEC growth medium and OGM or DMEM, respectively. To simulate microgravity, we utilized the RWV (Synthecom Inc, Houston, TX, USA). HMEC were seeded on beads (Cytodex 3, Sigma Aldrich, St. Louis, MO, USA); as controls (CTR), HMEC grown on beads were cultured in the vessels not undergoing rotation [11]. In the RWV, the vessel rotates around a horizontal axis (28 rpm) and allows diffusion of oxygen and carbon dioxide across a semipermeable membrane. The vessel wall and the medium containing cells bound to microcarrier beads rotate at the same speed, producing a vector-averaged gravity comparable with that of near-earth free-fall orbit [19]. The beads do not form aggregates in the RWV and tend to be evenly distributed throughout the vessel. Such a rotation reduces gravity to approximately 3×10^{-2} g [10]. After 72 h in the RWV or in the vessels without rotation, the media from HMEC were collected, centrifuged, filtered through 0.2 μm filter, diluted 1 : 1 with fresh culture medium to replenish nutrients, and used to culture NHOst and Saos-2 cells. In these experiments, the medium was changed every 48 h.

2.2. DNA Fragmentation. HMEC cell death was evaluated using the cell death detection ELISA (Roche) which determines cytoplasmic histone-associated DNA fragments. Briefly, after 48 and 72 h in the RWV or under control conditions, the cells were lyzed and centrifuged and the supernatant was analyzed according to the manufacturer's instruction. As a positive control, we used HMEC exposed for 30 min to H_2O_2 (10 μM) and cultured for additional 48 h in their growth medium.

2.3. Cell Proliferation. For MTT assay, NHOst and Saos-2 at 50% confluence were cultured in 96-well plates for 24 h before being exposed for different times to the media collected from HMEC. MTT measures the reduction of yellow tetrazolium salt MTT to dark purple formazan by succinate dehydrogenase, mainly in mitochondria and it is now widely accepted as a reliable way to examine cell viability and proliferation [20]. Briefly, at the end of the experiment, the media were replaced with medium containing 3-(4,5-Dimethyl-2-thiazolyl)-2,5-diphenyl-2H-tetrazolium bromide (MTT, 0.5 mg/mL) (Sigma Aldrich, St. Louis, MO, USA). Formazan crystals generated by the cellular reduction activity were dissolved in DMSO. Absorbance was measured at 550 nm.

Neutral red uptake assay was also used to estimate NHOst viability. Briefly, 24 h after seeding in 96-well dishes, the cells were exposed to CM from HMEC. After 3 days, neutral red was added to the medium to a final concentration of 50 μg/mL. 2 h later, the wells were washed with PBS and fixed. Absorbance was measured at 550 nm [21].

HMEC and Saos-2 cells were trypsinized and stained with trypan blue solution (0.4%) and the viable cells were counted using a Burker chamber.

2.4. Osteoblast Activity. NHOst and Saos-2 cells at 80% confluence were cultured in 24-well plates with conditioned media from HMEC added with 100 nM dexamethasone, 50 μM L-ascorbate-2-phosphate, and 10 mM glycerophosphate, at 37°C in a 5% CO_2 for 7 and 14 days. Osteoblast activity was evaluated quantifying alkaline phosphatase (ALP) enzymatic activity in the medium by a colorimetric assay based on the hydrolysis of P-nitrophenyl phosphate. The absorbance was measured at 405 nm [18]. To analyze calcium deposition, the cells were rinsed with PBS, fixed (70% ethanol, 1 h), and stained for 10 min with 2% Alizarin Red S (pH 4.2). Cultures were photographed with a digital camera. Alizarin Red was then released from the cell matrix by incubation for 15 min in 10% cetylpyridinium chloride in 10 mM sodium phosphate (pH 7.0). The absorbance was measured at 562 nm [18].

2.5. Measurements of TIMP-2 and IL-6 by ELISA. Conditioned media were centrifuged and filtered. The amounts of tissue inhibitor of matrix metalloprotease (TIMP)-2 and interleukin (IL)-6 were measured using a double-antibody sandwich ELISA (GE Healthcare) according to the manufacturer's instructions. The concentrations of TIMP-2 and IL-6 were determined by interpolation from a standard curve.

2.6. Western Blot. HMEC cells were lysed, separated on SDS-PAGE, and transferred to nitrocellulose sheets. Western analysis was performed using antibodies against p21, p53, and GAPDH (Tebu Bio-Santa Cruz). Secondary antibodies were labelled with horseradish peroxidase (Amersham Pharmacia Biotech). The SuperSignal chemiluminescence kit (Pierce) was used to detect immunoreactive proteins.

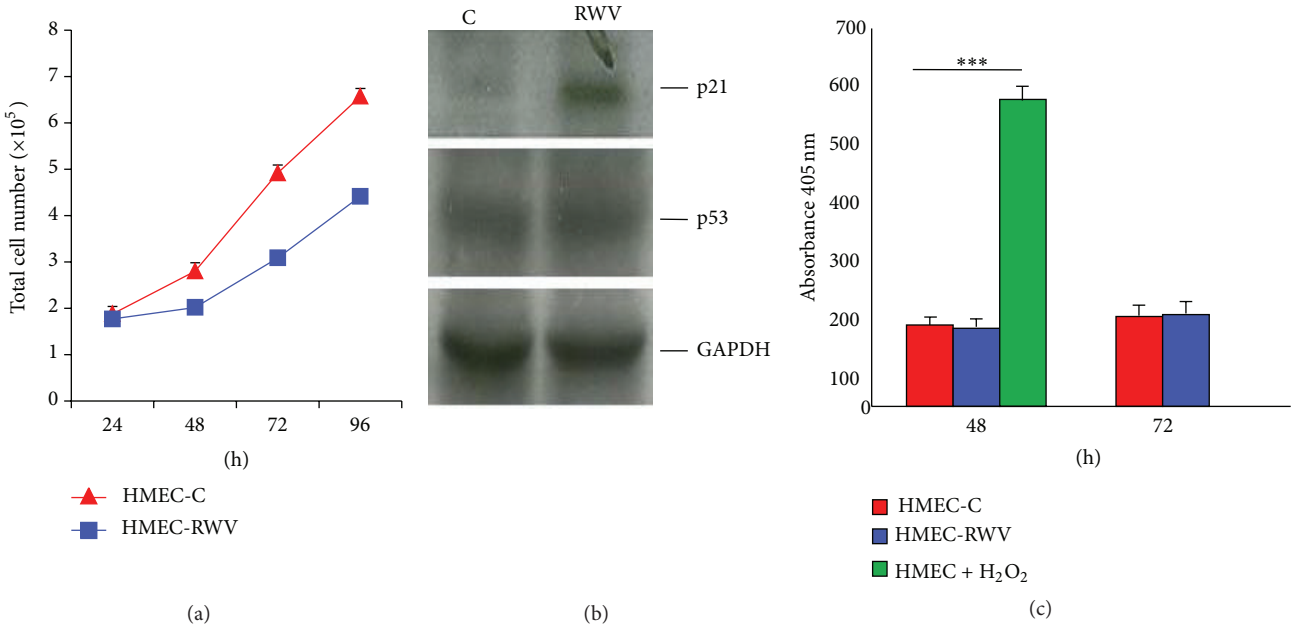

Figure 1: Simulated microgravity inhibits HMEC growth. (a) HMEC were cultured for different times in the RWV (HMEC-RWV) and trypsinized and viable cells were counted. HMEC-C: control. (b) Cell extracts (50 μg/lane) were loaded on a 15% SDS-PAGE, blotted into nitrocellulose filter, incubated with anti-p21 and anti-p53 antibodies, and visualized by chemiluminescence as described. After stripping, the blot was incubated with an anti-GAPDH antibody to show that comparable amounts of proteins were loaded per lane. (c) Apoptosis was evaluated by ELISA on HMEC lysates after 48 and 72 h in the RWV or under control conditions. Our positive control is represented by HMEC exposed to H_2O_2 for 30 min and then cultured for additional 48 h.

2.7. Statistical Analysis. All experiments were repeated at least three times in triplicate. Data are presented as means ± standard deviation. Statistical differences were determined using the unpaired two-tailed Student's t test. Consider $^{*}P < 0.05$, $^{**}P < 0.01$.

3. Results

3.1. Simulated Microgravity Alters HMEC Behaviour. Figure 1(a) shows that culture in the RWV retarded HMEC proliferation. Accordingly, growth inhibition correlated with the upregulation of p21 (WAF1), an inhibitor of cyclin-dependent kinases, as detected by western blot, and this event seems to be p53-independent since no modulation of p53 was observed in HMEC (Figure 1(b)). We also show that no cell death is detectable after 48 and 72 h culture in the RWV (Figure 1(c)). It is noteworthy that similar results were obtained when microgravity was simulated using the random positioning machine (RPM) (data not shown). On the basis of results obtained by protein array on 40 proteins involved in inflammation, we validated the increase of IL-6 and TIMP-2 in the CM from HMEC cultured for 48 and 72 h in the RWV and relative controls by ELISA. Figure 2(a) shows that TIMP-2 is significantly increased in the media collected from HMEC after 48 and 72 h in the RWV, while secreted IL-6 was increased after 72 h culture in simulated microgravity (Figure 2(b)). On these bases, we decided to use 72 h conditioned media from HMEC for the experiments on bone cells.

3.2. HMEC Secreted Factors Impact on NHOst Cell Proliferation and Osteogenic Activity. We evaluated the effects of CM from HMEC on NHOst cell proliferation. MTT assay revealed a significant reduction of NHOst cell proliferation cultured in the presence of CM from HMEC in simulated microgravity (Figure 3(a)). These results were confirmed by neutral red assay, which estimates the number of viable cells in a culture on the basis of their ability to incorporate and bind the supravital dye neutral red in the lysosomes (Figure 3(b)). We did not detect any significant difference in cell death in NHOst exposed to the conditioned media from HMEC cultured for 72 h in the RWV and relative controls (not shown).

To evaluate osteoblastic activity, NHOst cells were cultured for 7 and 14 days in a 24-well plate with CM from HMEC added with an osteogenic cocktail containing 100 nM dexamethasone, 50 μM L-ascorbate-2-phosphate, and 10 mM glycerophosphate. Two parameters were evaluated, that is, ALP activity, which has long been recognised as a reliable indicator of osteoblastic activity, and calcium deposition by Alizarin Red Staining.

ALP enzymatic activity was measured after 7 and 14 days by a colorimetric assay. Figure 4(a) shows that media from HMEC in simulated microgravity inhibited ALP activity. To analyze calcium deposition, we used the Alizarin Red S Staining. Figure 4(b) shows that CM from HMEC exposed to simulated microgravity markedly inhibited the deposition of mineral matrix.

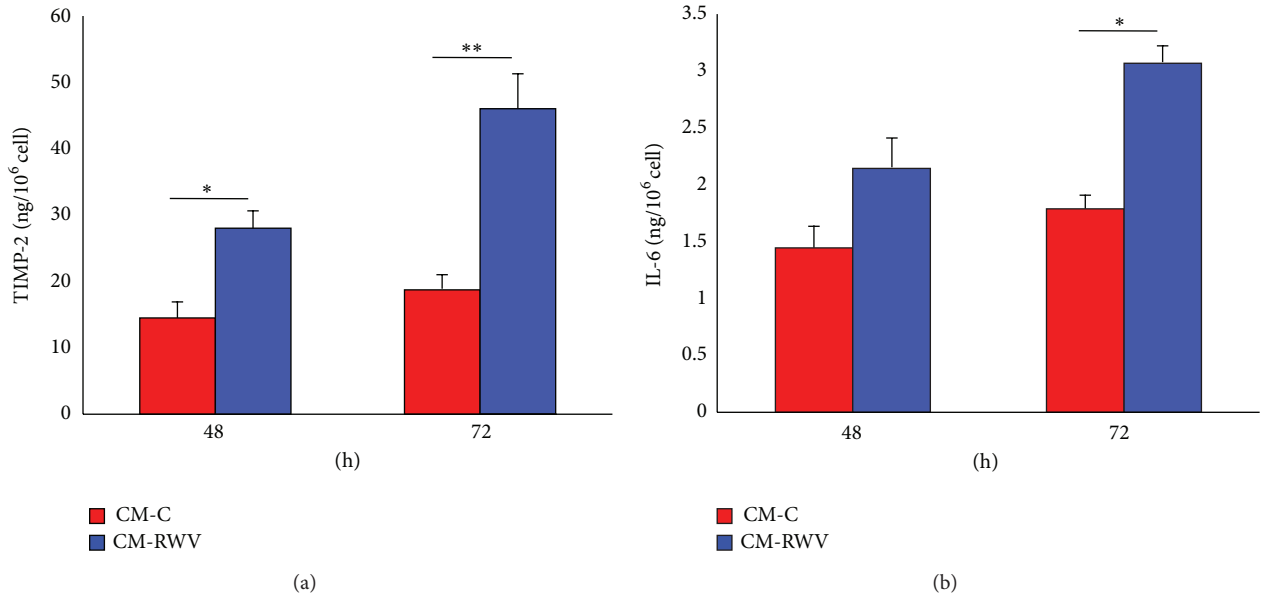

Figure 2: Simulated microgravity induces TIMP-2 and IL-6 secretion by HMEC. TIMP-2 (a) and IL-6 (b) were measured by ELISA in media collected after different times of culture in the RWV (CM-RWV) or from relative controls (CM-C).

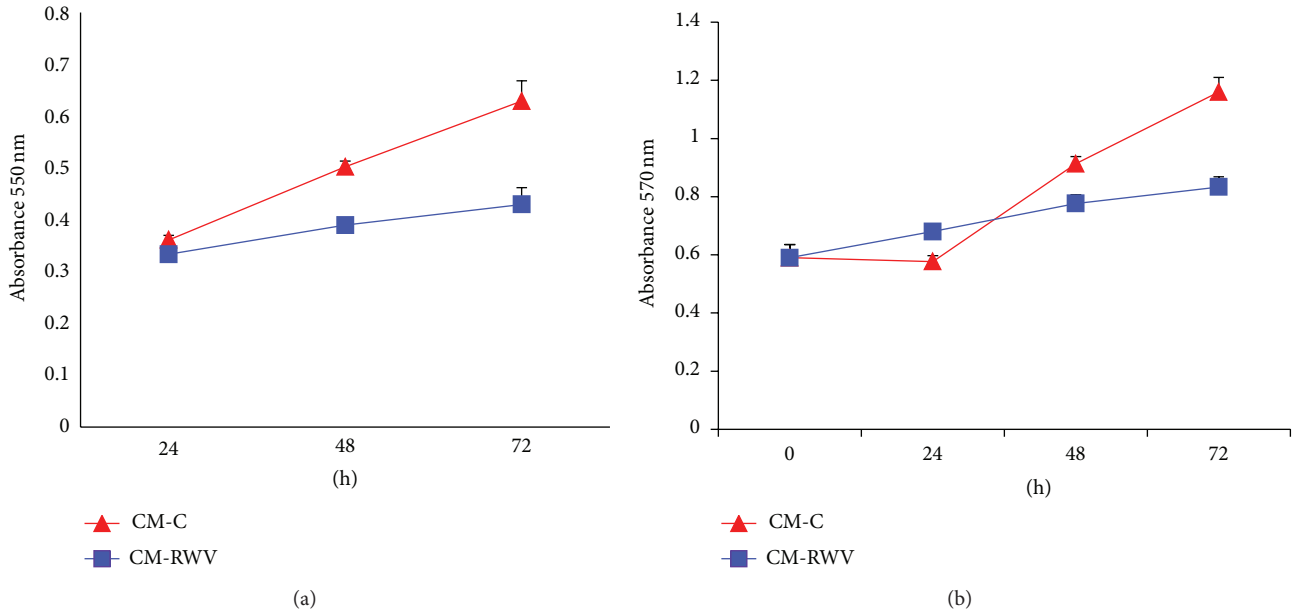

Figure 3: CM from HMEC in simulated microgravity inhibit NHOst proliferation. NHOst were cultured for different times with CM from HMEC in simulated microgravity (CM-RWV) or by HMEC controls (CM-C). Viable cells were evaluated by MTT assay (a) and neutral red (b) and the absolute absorbance values are shown. Data are expressed as the mean ± standard deviation of three different experiments performed in triplicate.

3.3. HMEC Secreted Factors Impact on Saos-2 Cell Proliferation and Osteogenic Activity. Many factors, such as age, gender, and site of isolation, influence the behavior of primary osteoblasts [22]. We therefore performed experiments also on an immortalized cell line to reproduce the results obtained in NHOst and we chose Saos-2 cells because they closely resemble primary osteoblasts [22]. Indeed, Saos-2 cells are used as representative of primary osteoblasts when standard tests are evaluated [23].

Saos-2 cells were exposed to CM from HMEC in the RWV and relative controls for different times. MTT assay shows that media from HMEC in the RWV impair cell proliferation (Figure 5(a)). These results were confirmed when the cells were counted (Figure 5(b)).

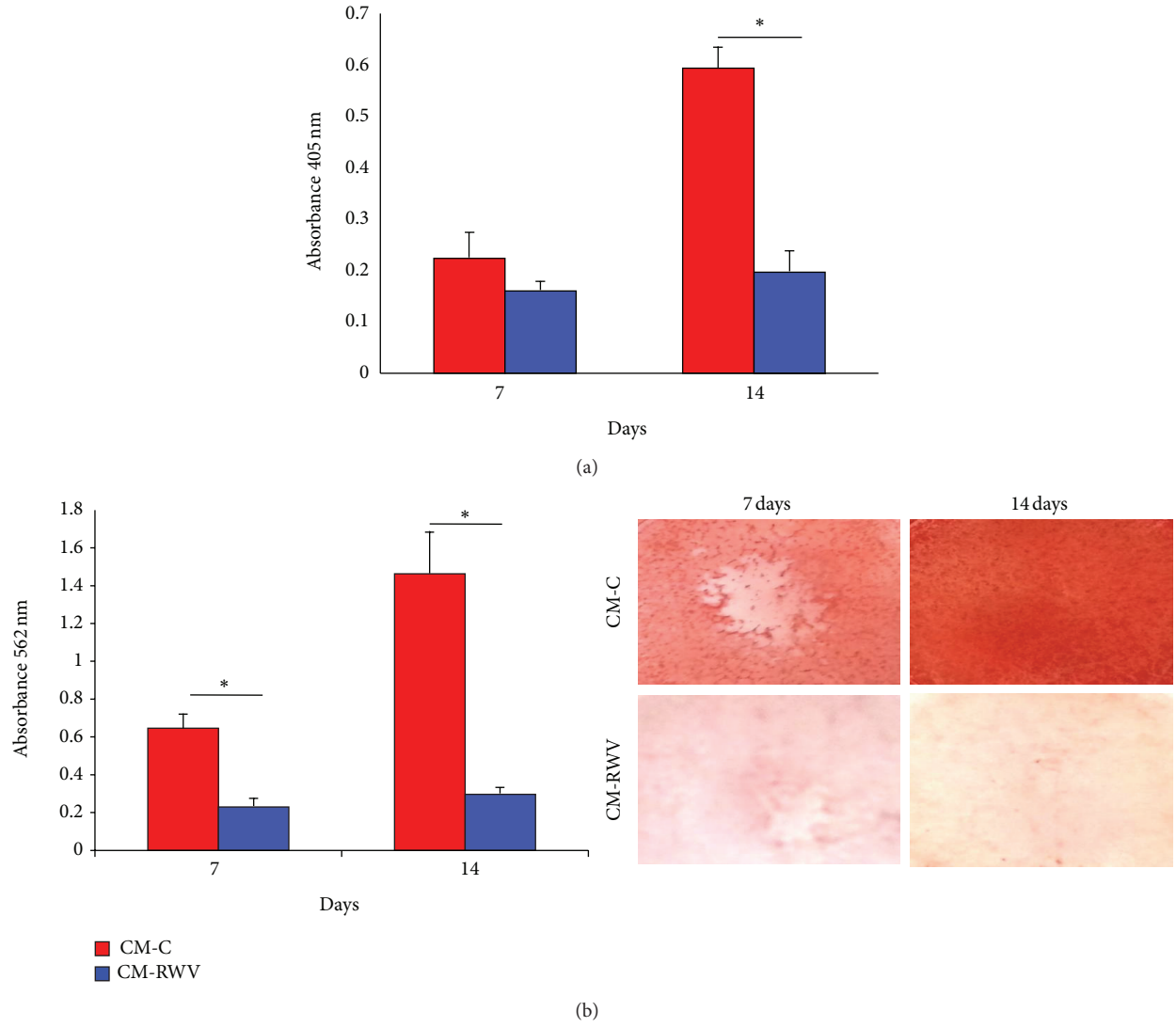

Figure 4: CM from HMEC in simulated microgravity inhibit NHOst activity. NHOst were cultured for 7 and 14 days with medium conditioned by HMEC in simulated microgravity (CM-RWV) or by HMEC controls (CM-C) both added with osteogenic stimuli. (a) ALP enzymatic activity was quantified by spectrophotometric analysis as described. Absorbance was measured at 405 nm. (b) Alizarin Red Staining was performed. Photographs were taken before acid extraction. Absorbance was measured at 562 nm.

Confluent Saos-2 cells were then cultured in CM from HMEC in simulated microgravity or HMEC controls both added with the osteogenic cocktail and were stained with Alizarin Red to evaluate the formation of calcium phosphate in culture [18]. We found that 14-day culture in the conditioned media from HMEC in the RWV inhibited ALP activity (Figure 6(a)). The inhibition of Saos2 cell activity was confirmed by demonstrating lower amounts of deposition of mineral matrix in cell cultured with the CM from HMEC in the RWV (Figure 6(b)).

4. Discussion

Bone loss in space has been reported in humans and in several experimental models [8]. All the *in vivo* results obtained in space point to major alterations of bone cells. Bone cells have been extensively studied *in vitro* both in space and on ground using different devices to simulate microgravity to conclude that microgravity alters the morphology of these cells [24], impairs the differentiation of osteoblasts [25], and increases the activity of osteoclasts [8]. All these results are not surprising since gravitational forces contribute to the maintenance of bone integrity and affect bone remodeling to adjust to mechanical demands.

Bone vasculature is important for skeletal development during the embryonic stage, postnatal growth, and bone remodeling. It supplies oxygen, nutrients, hormones, cytokines, and bone precursor cells. Moreover, the communication between bone endothelium and bone cells is vital to regulate and modulate bone homeostasis. The endothelium contributes to bone health by releasing osteogenic factors [26], and bone cells produce angiogenic factors that are crucial

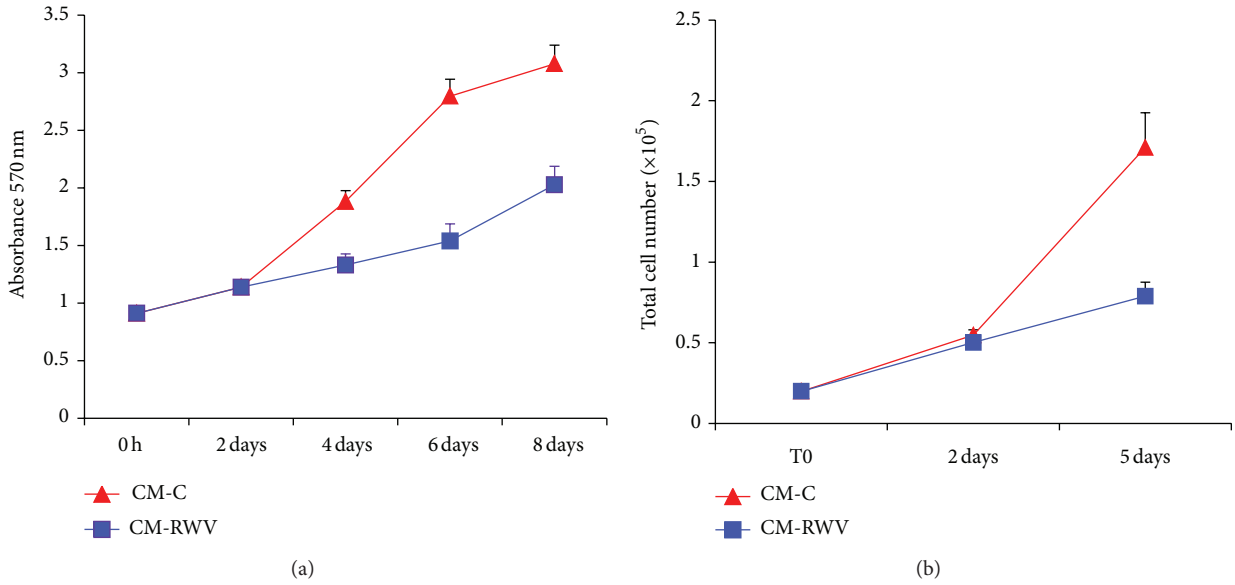

Figure 5: CM from HMEC in simulated microgravity inhibit Saos-2 proliferation. Saos-2 were cultured for different times with CM from HMEC in simulated microgravity (CM-RWV) or by HMEC controls (CM-C). Viable cells were evaluated by MTT assay (a) and the absolute absorbance values are shown. After trypsinization, viable cells were stained with trypan blue and counted (b).

for endothelial viability and survival under physiological conditions and that drive angiogenesis when needed [3].

We have shown that human endothelial cells from the umbilical vein, widely used as a model of macrovascular endothelial cells, are deeply influenced by simulated microgravity [10, 11, 27]. These results were confirmed by our recent study performed on the International Space Station (ISS) [28]. Other experiments have been performed on different types of macrovascular endothelial cells with discordant results, which can be ascribed to poor definition of the endothelial cells used [14, 15], the different culture conditions, the use of different microgravity simulators, and also the inadequate descriptions of how they were operated. Less is known about microvascular endothelial cells, which cover an area 50 times greater than that of all large vessels combined [29]. In an animal model of wound healing and in a rat fibular osteotomy model, microgravity retards neovascularization [30, 31], thus indicating the occurrence of microvascular endothelial dysfunction. Moreover, bed rest, which mimics some aspects of spaceflight, causes impairment of endothelium-dependent functions in the microcirculation [32]. We have previously demonstrated that RWV-simulated microgravity induces an antiangiogenic phenotype in HMEC [11]. In the present study, we confirm and broaden these results by showing that culture in the RWV retards HMEC cell growth without inducing apoptosis. This correlates with the upregulation of p21, an inhibitor of the cyclin/CDK2 complexes necessary for the transition from the G1 to the S phases, through a p53-independent mechanism. Our results are in disagreement with a recent report showing that culture in a clinostat induces apoptosis in pulmonary microvascular endothelial cells [12]. As mentioned above, these contrasting results might be due to differences in the cells used, in the cell culture conditions, and in the microgravity simulator utilized.

The aim of this work was to understand whether simulated microgravity impairs endothelial-osteoblast communication. To this purpose, we evaluated the effects produced on osteoblasts by CM from HMEC cultured in simulated microgravity.

We show that HMEC release factors that retard the growth of osteoblasts and severely impair their osteogenic activity. It is noteworthy that we found increased amounts of secreted TIMP-2 and IL-6, known to affect both endothelial cells and osteoblasts. Interestingly, TIMP-2 inhibits endothelial cell proliferation by a matrix metalloproteases (MMP) independent mechanism [33] and might therefore play a role in HMEC growth retardation in simulated microgravity. TIMP-2 also impairs osteoblast activity. Indeed, TIMP-2 nearly abolishes ALP expression [34] by inhibiting MT1-MMP (membrane type 1-metalloprotease) [34], a protease which is implicated in multiple steps of osteogenic differentiation and is mainly involved in ALP upregulation [35]. Interestingly, TIMP-2 inhibits cell survival of osteoblasts forced to transdifferentiate into osteocytes [36]. This result might offer a molecular explanation, at least in part, to the lysis of osteocytes in spaceflight described by Blaber et al. [37]. In media from HMEC cultured in the RWV, we also found increased amounts of IL-6, a pleiotropic cytokine implicated in acute phase response and inflammation. IL-6 not only promotes endothelial dysfunction [38] but also affects human osteoblast differentiation [39], thus contributing to osteopenia.

We therefore propose that microgravity impacts both directly and indirectly on osteoblasts. Microgravity has been shown to directly inhibit osteoblasts. In addition, by modulating microvascular endothelial cell function, microgravity indirectly exerts inhibitory effects on osteoblasts.

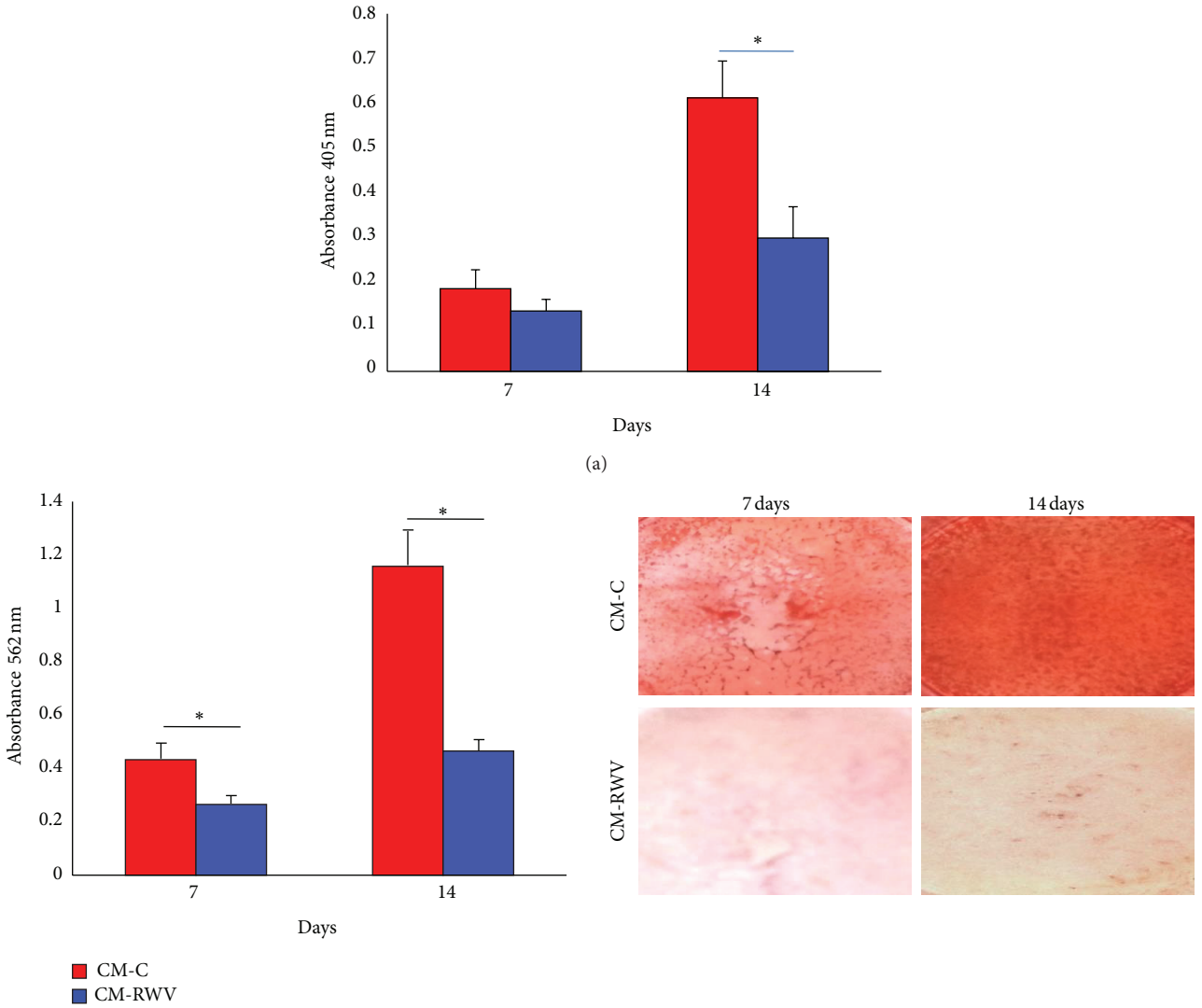

FIGURE 6: CM from HMEC in simulated microgravity inhibit Saos-2 activity. Saos-2 were cultured for 7 and 14 days with CM from HMEC in simulated microgravity (CM-RWV) or by HMEC controls (CM-C) both added with osteogenic stimuli. (a) ALP enzymatic activity and (b) Alizarin Red Staining were performed as above.

The current space programs onboard the ISS and the future human exploration of Mars require long duration missions. However, several biomedical issues still need to be clarified before these missions can take place without causing health problems to the astronauts. Our results suggest that endothelial dysfunction might represent a common denominator for cardiovascular deconditioning and for bone loss and offer a new light to interpret the behaviour of mammalian skeleton in microgravity. Eventually, these results might foster studies to develop countermeasures that target the endothelium to improve both bone homeostasis and vascular function.

Conflict of Interests

The authors declare that there is no conflict of interests regarding the publication of this paper.

Acknowledgment

This work was supported by a grant from the European Space Agency to Jeanette A. M. Maier.

References

[1] T. C. Phan, J. Xu, and M. H. Zheng, "Interaction between osteoblast and osteoclast: impact in bone disease," *Histology and Histopathology*, vol. 19, no. 4, pp. 1325–1344, 2004.

[2] B. Guillotin, C. Bourget, M. Remy-Zolgadri et al., "Human primary endothelial cells stimulate human osteoprogenitor cell differentiation," *Cellular Physiology and Biochemistry*, vol. 14, no. 4–6, pp. 325–332, 2004.

[3] J. Kular, J. Tickner, S. M. Chim, and J. Xu, "An overview of the regulation of bone remodelling at the cellular level," *Clinical Biochemistry*, vol. 45, no. 12, pp. 863–873, 2012.

[4] B. Decker, H. Bartels, and S. Decker, "Relationships between endothelial cells, pericytes, and osteoblasts during bone formation in the sheep femur following implantation of tricalciumphosphate-ceramic," *Anatomical Record*, vol. 242, no. 3, pp. 310–320, 1995.

[5] R. D. Prisby, M. W. Ramsey, B. J. Behnke et al., "Aging reduces skeletal blood flow, endothelium-dependent vasodilation, and no bioavailability in rats," *Journal of Bone and Mineral Research*, vol. 22, no. 8, pp. 1280–1288, 2007.

[6] L. Vico, P. Collet, A. Guignandon et al., "Effects of long-term microgravity exposure on cancellous and cortical weight-bearing bones of cosmonauts," *The Lancet*, vol. 355, no. 9215, pp. 1607–1611, 2000.

[7] A. D. LeBlanc, E. R. Spector, H. J. Evans, and J. D. Sibonga, "Skeletal responses to space flight and the bed rest analog: a review," *Journal of Musculoskeletal and Neuronal Interactions*, vol. 7, no. 1, pp. 33–47, 2007.

[8] M. P. Nagaraja and D. Risin, "The current state of bone loss research: data from spaceflight and microgravity simulators," *Journal of Cellular Biochemistry*, vol. 114, no. 5, pp. 1001–1008, 2013.

[9] S. I. M. Carlsson, M. T. S. Bertilaccio, E. Ballabio, and J. A. M. Maier, "Endothelial stress by gravitational unloading: effects on cell growth and cytoskeletal organization," *Biochimica et Biophysica Acta*, vol. 1642, no. 3, pp. 173–179, 2003.

[10] S. Versari, A. Villa, S. Bradamante, and J. A. M. Maier, "Alterations of the actin cytoskeleton and increased nitric oxide synthesis are common features in human primary endothelial cell response to changes in gravity," *Biochimica et Biophysica Acta—Molecular Cell Research*, vol. 1773, no. 11, pp. 1645–1652, 2007.

[11] M. Mariotti and J. A. M. Maier, "Gravitational unloading induces an anti-angiogenic phenotype in human microvascular endothelial cells," *Journal of Cellular Biochemistry*, vol. 104, no. 1, pp. 129–135, 2008.

[12] C. Y. Kang, L. Zou, M. Yuan et al., "Impact of simulated microgravity on microvascular endothelial cell apoptosis," *European Journal of Applied Physiology*, vol. 111, no. 9, pp. 2131–2138, 2011.

[13] S. M. Grenon, M. Jeanne, J. Aguado-Zuniga, M. S. Conte, and M. Hughes-Fulford, "Effects of gravitational mechanical unloading in endothelial cells: association between caveolins, inflammation and adhesion molecules," *Scientific Reports*, vol. 3, article 1494, 2013.

[14] L. Morbidelli, M. Monici, N. Marziliano et al., "Simulated hypogravity impairs the angiogenic response of endothelium by up-regulating apoptotic signals," *Biochemical and Biophysical Research Communications*, vol. 334, no. 2, pp. 491–499, 2005.

[15] M. Infanger, P. Kossmehl, M. Shakibaei et al., "Induction of three-dimensional assembly and increase in apoptosis of human endothelial cells by simulated microgravity: impact of vascular endothelial growth factor," *Apoptosis*, vol. 11, no. 5, pp. 749–764, 2006.

[16] N. V. Rodionova and V. S. Oganov, "Changes of cell-vascular complex in zones of adaptive remodeling of the bone tissue under microgravity conditions," *Advances in Space Research*, vol. 32, no. 8, pp. 1477–1481, 2003.

[17] P. Dowling and M. Clynes, "Conditioned media from cell lines: a complementary model to clinical specimens for the discovery of disease-specific biomarkers," *Proteomics*, vol. 11, no. 4, pp. 794–804, 2011.

[18] M. Leidi, F. Dellera, M. Mariotti, and J. A. M. Maier, "High magnesium inhibits human osteoblast differentiation in vitro," *Magnesium Research*, vol. 24, no. 1, pp. 1–6, 2011.

[19] B. R. Unsworth and P. I. Lelkes, "Growing tissues in microgravity," *Nature Medicine*, vol. 4, no. 8, pp. 901–907, 1998.

[20] S. Castiglioni, S. Casati, R. Ottria, P. Ciuffreda, and J. A. M. Maier, "N6-isopentenyladenosine and its analogue N6-benzyladenosine induce cell cycle arrest and apoptosis in bladder carcinoma T24 cells," *Anti-Cancer Agents in Medicinal Chemistry*, vol. 13, no. 4, pp. 672–678, 2013.

[21] S. Casati, R. Ottria, E. Baldoli, E. Lopez, J. A. Maier, and P. Ciuffreda, "Effects of cytokinins, cytokinin ribosides and their analogs on the viability of normal and neoplastic human cells," *Anticancer Research*, vol. 31, no. 3, pp. 3401–3406, 2011.

[22] E. M. Czekanska, M. J. Stoddart, R. G. Richards, and J. S. Hayes, "In search of an osteoblast cell model for in vitro research," *European Cells and Materials*, vol. 24, pp. 1–17, 2012.

[23] L. Saldaña, F. Bensiamar, A. Boré, and N. Vilaboa, "In search of representative models of human bone-forming cells for cytocompatibility studies," *Acta Biomaterialia*, vol. 7, no. 12, pp. 4210–4221, 2011.

[24] N. Nabavi, A. Khandani, A. Camirand, and R. E. Harrison, "Effects of microgravity on osteoclast bone resorption and osteoblast cytoskeletal organization and adhesion," *Bone*, vol. 49, no. 5, pp. 965–974, 2011.

[25] G. Carmeliet, G. Nys, and R. Bouillon, "Microgravity reduces the differentiation of human osteoblastic MG-63 cells," *Journal of Bone and Mineral Research*, vol. 12, no. 5, pp. 786–794, 1997.

[26] S. M. Chim, J. Tickner, S. T. Chow et al., "Angiogenic factors in bone local environment," *Cytokine & Growth Factor Reviews*, vol. 24, no. 3, pp. 297–310, 2013.

[27] M. Mariotti and J. A. M. Maier, "Human Micro- and macrovascular endothelial cells exposed to simulated microgravity upregulate hsp70," *Microgravity Science and Technology*, vol. 21, no. 1-2, pp. 141–144, 2009.

[28] S. Versari, G. Longinotti, L. Barenghi, J. A. Maier, and S. Bradamante, "The challenging environment on board the International Space Station affects endothelial cell function by triggering oxidative stress through thioredoxin interacting protein overexpression: the ESA-SPHINX experiment," *FASEB Journal*, vol. 27, pp. 4466–4475, 2013.

[29] S. Danese, E. Dejana, and C. Fiocchi, "Immune regulation by microvascular endothelial cells: directing innate and adaptive immunity, coagulation, and inflammation," *The Journal of Immunology*, vol. 178, no. 10, pp. 6017–6022, 2007.

[30] J. M. Davidson, A. M. Aquino, S. C. Woodward, and W. W. Wilfinger, "Sustained microgravity reduces intrinsic wound healing and growth factor responses in the rat," *The FASEB Journal*, vol. 13, no. 2, pp. 325–329, 1999.

[31] M. E. Kirchen, K. M. O'Connor, H. E. Gruber et al., "Effects of microgravity on bone healing in a rat fibular osteotomy model," *Clinical Orthopaedics and Related Research*, no. 318, pp. 231–242, 1995.

[32] M. Coupé, J. O. Fortrat, I. Larina, G. Gauquelin-Koch, C. Gharib, and M. A. Custaud, "Cardiovascular deconditioning: from autonomic nervous system to microvascular dysfunctions," *Respiratory Physiology & Neurobiology*, vol. 169, supplement 1, pp. S10–S12, 2009.

[33] W. G. Stetler-Stevenson and D. Seo, "TIMP-2: an endogenous inhibitor of angiogenesis," *Trends in Molecular Medicine*, vol. 11, no. 3, pp. 97–103, 2005.

[34] S. Barthelemi, J. Robinet, R. Garnotel et al., "Mechanical forces-induced human osteoblasts differentiation involves MMP-2/MMP-13/MT1-MMP proteolytic cascade," *Journal of Cellular Biochemistry*, vol. 113, no. 3, pp. 760–772, 2012.

[35] P. Manduca, A. Castagnino, D. Lombardini et al., "Role of MT1-MMP in the osteogenic differentiation," *Bone*, vol. 44, no. 2, pp. 251–265, 2009.

[36] M. A. Karsdal, T. A. Andersen, L. Bonewald, and C. Christiansen, "Matrix metalloproteinases (MMPs) safeguard osteoblasts from apoptosis during transdifferentiation into osteocytes: MT1-MMP maintains osteocyte viability," *DNA and Cell Biology*, vol. 23, no. 3, pp. 155–165, 2004.

[37] E. A. Blaber, N. Dvorochkin, C. Lee et al., "Microgravity induces pelvic bone loss through osteoclastic activity, osteocytic osteolysis , and osteoblastic cell cycle inhibi tion by CDKN1a/p21," *PLoS ONE*, vol. 8, no. 4, Article ID e61372, 2013.

[38] S. Wassmann, M. Stumpf, K. Strehlow et al., "Interleukin-6 induces oxidative stress and endothelial dysfunction by overexpression of t he angio tensin II type 1 receptor," *Circulation Research*, vol. 94, no. 4, pp. 534–541, 2004.

[39] B. Peruzzi, A. Cappariello, A. del Fattore, N. Rucci, F. de Benedetti, and A. Teti, "C-Src and IL-6 inhibit osteoblast differentiation and integrate IGFBP5 signalling," *Nature Communications*, vol. 3, article 630, 2012.

Hindawi Publishing Corporation
BioMed Research International
Volume 2014, Article ID 652434, 12 pages
http://dx.doi.org/10.1155/2014/652434

Research Article

Phenotypic Switch Induced by Simulated Microgravity on MDA-MB-231 Breast Cancer Cells

Maria Grazia Masiello,[1,2] Alessandra Cucina,[2] Sara Proietti,[2] Alessandro Palombo,[3] Pierpaolo Coluccia,[2] Fabrizio D'Anselmi,[2] Simona Dinicola,[2] Alessia Pasqualato,[2] Veronica Morini,[2] and Mariano Bizzarri[3]

[1] *Department of Clinical and Molecular Medicine, "Sapienza" University of Rome, Piazza Sassari 3, 00161 Rome, Italy*
[2] *Department of Surgery "Pietro Valdoni", "Sapienza" University of Rome, Via A. Scarpa 14, 00161 Rome, Italy*
[3] *Department of Experimental Medicine, "Sapienza" University of Rome, Systems Biology Group, Viale Regina Elena 324, Via A. Scarpa 14, 00161 Rome, Italy*

Correspondence should be addressed to Mariano Bizzarri; mariano.bizzarri@uniroma1.it

Received 14 May 2014; Accepted 23 July 2014; Published 18 August 2014

Academic Editor: Monica Monici

Microgravity exerts dramatic effects on cell morphology and functions, by disrupting cytoskeleton and adhesion structures, as well as by interfering with biochemical pathways and gene expression. Impairment of cells behavior has both practical and theoretical significance, given that investigations of mechanisms involved in microgravity-mediated effects may shed light on how biophysical constraints cooperate in shaping complex living systems. By exposing breast cancer MDA-MB-231 cells to simulated microgravity (~0.001 g), we observed the emergence of two morphological phenotypes, characterized by distinct membrane fractal values, surface area, and roundness. Moreover, the two phenotypes display different aggregation profiles and adherent behavior on the substrate. These morphological differences are mirrored by the concomitant dramatic functional changes in cell processes (proliferation and apoptosis) and signaling pathways (ERK, AKT, and Survivin). Furthermore, cytoskeleton undergoes a dramatic reorganization, eventually leading to a very different configuration between the two populations. These findings could be considered adaptive and reversible features, given that, by culturing microgravity-exposed cells into a normal gravity field, cells are enabled to recover their original phenotype. Overall these data outline the fundamental role gravity plays in shaping form and function in living systems.

1. Introduction

Space flights induce relevant changes in human physiology, such as bone loss, muscle atrophy, deregulation of immune function, hematological anomalies, and cardiovascular function impairment. Microgravity effects may be ascribed to systemic interferences with body fluids distribution, disappearance of fluid shear, perturbation of the circadian clock, altered endothelial function, and reduced loading on skeletal structures [1]. Yet, a direct effect on cell and signaling pathways inside the cell has been documented, despite the fact that microgravity has been previously thought to be too weak for contrasting the intermolecular forces [2]. Thereby, it is likely that spaceflight could exert its detrimental effects on astronauts via changes in cellular structure and/or functions.

Several studies, performed both in simulated and actual microgravity, have shown that normal as well as neoplastic cells undergo dramatic changes after exposition to a microgravity field. Cell morphology, as well as features of subcellular organelles and cytoskeleton structure, has been reported to be dramatically influenced by gravity [3, 4]. Similarly, relevant modifications in tissue organization have been recorded in microgravity-exposed organs and/or animals [5, 6]. Shape changes are likely to be mediated by concomitant structural rearrangement of cytoskeleton (CSK), which is severely disorganized under microgravity [7, 8]. CSK conveys mechanical signals into the cells, and by that way it influences both biochemical pathways [9, 10] and gene expression [11, 12]. As a consequence, many metabolic, proliferative, and differentiating processes end up to be deeply perturbed [13].

Microgravity effects may be ascribed to both indirect and direct effects [14]. Meanwhile specialized cells and structures in the plant realm have been found to be sensitive to even subtle change in gravity vector [15]; no components in the mammalian cells have been so far identified as having a sufficiently large mass density difference in respect to the surrounding medium: thus, the force exerted by the gravitational field is nowhere higher than the energy of random thermal motion and cannot significantly modify the behaviour of any single subcellular structure. Instead, mammalian cells may be able to sense some environmental changes due to gravity affecting a wide range of biophysical parameters: buoyancy, shear forces, viscosity, diffusion process, and many others. Yet, a lot of gravity-related phenomena at the cellular level, involving shape rearrangement, cytoskeleton disruption, and even modified gene expression, would hardly be explained by only considering changes in "external" environmental biophysical parameters. Indeed, gravity may likely affect some general properties of the systems, acting "directly" as an organizing field parameter. We have previously reported that by "removing" the gravitational constraint, according to the nonequilibrium theory [16], murine osteoblasts underwent a transition after a bifurcation point, thus recovering degrees of freedom enabling the system in accessing new attractor states, that is, new phenotypic configurations [17]. Indeed, microgravity induces the emergence of two distinct phenotypes, characterized by different morphologies. Herein we investigate if a similar pattern could be retrieved in breast cancer cells and how such features are associated with differences in their biochemical pathways. Indeed, conflicting data have been reported by investigations carried out on cancer cells exposed to microgravity: some authors have recorded an overall inhibitory effect on cancer cell proliferation, motility, and survival [18, 19], whereas others have observed the opposite [20–22]. We hypothesize that such results may be likely explained by the emergence of distinct cell phenotypes, characterized by different functional and reproductive features.

2. Material and Methods

2.1. RPM (Random Positioning Machine). Microgravity conditions were simulated by a Desktop RPM, a particular kind of 3D clinostat [23], manufactured by Dutch Space (Leiden, The Netherlands). The degree of microgravity simulation depends on angular speed and on the inclination of the disk. These tools do not actually eliminate the gravity but allow you to apply a stimulus rather than a unidirectional omnidirectional 1 g. Effects generated by the RPM are comparable to those of the real microgravity, provided that the direction changes are faster than the response time of the system to gravity field. The desktop RPM was located in a standard incubator (to maintain temperature, CO_2, and humidity levels) and connected to the control console through standard electric cables.

2.2. Cell Culture. MDA-MB-231 human breast cancer cell line was purchased from European Collection of Cell Cultures (ECACC, Sigma-Aldrich, St. Louis, MO, USA). Cells were seeded into Nunc OptiCell Cell Culture Systems, gas-permeable cell culture disks (Thermo Scientific, Rochester, USA), and cultured in Dulbecco's modified Eagle's medium (DMEM, Euroclone Ltd., Cramlington, UK) supplemented with 10% Fetal Bovine Serum (FBS, HyClone Laboratories, Logan, UT, USA), 200 mM L-glutamine, 100 IU/mL Penicillin, and 100 μg/mL Streptomycin (all from Euroclone Ltd., Cramlington, UK). Then OptiCells containing subconfluent monolayers were fixed onto the RPM, as close as possible to the center of the platform, which was rotated at a speed of 60°/s using the random mode of the machine. On ground control (1 g static cultures) and RPM cultures were kept in the same humidified incubator at 37°C in an atmosphere of 5% CO_2 in air. Experiments were performed for 24 and 72 hours. After 24 and 72 hours of microgravity exposure, cell clumps swimming in culture supernatants were found, in addition to adherent cells, and separately collected. The three cell populations (on ground control cells, RPM adherent cells, and RPM cell clumps) were characterized separately.

2.3. Optical Microscopy. Cell clumps were collected, washed in PBS, and deposited onto a clearly defined area of a glass slide using a Shandon CytoSpin 4 Cytocentrifuge, Thermo Scientific, while maintaining cellular integrity. Cell clumps and adherent and on ground control cells were fixed in 4% paraformaldehyde for 10 minutes at 4°C and photographed with Nikon Coolpix 995 digital camera coupled with Zeiss Axiovert optical microscope. The images were obtained with a 320x magnification, saved as TIFF files, and used for image analysis.

2.4. Image Analysis. Image analysis was performed on 10 images for each group of MDA-MB-231 cells. As the analysis was performed blindly, the image groups were classified as follows: A (on ground cells, 24 h), B (RPM adherent cells, 24 h), C (RPM cell clumps, 24 h), D (on ground cells, 72 h), E (RPM adherent cells, 72 h), and F (RPM cell clumps, 72 h). In each image, single randomly chosen cells (50 for each group) were contoured with a fine black marker by different researchers, simply scanned, and cataloged according to the time of study: 24 and 72 hours. This method was chosen because pathologists are used to correlate the shape the cells acquire with their malignancy by means of morphological, qualitative, and subjective observations. Thus, we decided to perform a semiautomatic analysis, coupling the expertise of researchers with a computerized parameterization method. All the images were processed by Adobe Photoshop CS4. All the pictures (i.e., all the sheets of the groups, for each time point) were resized at 2560 × 1920 pixels according to original scale of image acquisition. For each black contoured cell, edges were refined. Then cells were black filled and threshold was adjusted in order to exclude from the image other cells and background. For each time point a single sheet of all the cells considered was created. To obtain single cell shape parameters (area A, roundness, solidity, and fractal dimension FD), ImageJ v1.47h software was used. Then,

the software analyzed single cells, by the function "shape descriptor." In addition to area A were calculated

$$\text{Roundness} = \frac{4A}{\pi\sqrt{\text{ma}}}$$
$$\text{Solidity} = \frac{A}{\text{CA}}, \quad (1)$$

where A is the area of the cell, ma is the major axis, and CA is the convex area, namely, the area of the convex hull of the region. The convex hull of a region is the smallest region that satisfies two conditions: (a) it is convex and (b) it contains the original region.

As for FD, it was obtained by means of box counting method using FracLac plugin:

$$\text{FD} = \lim_{\varepsilon \to 0} \left[1 - \frac{\log\left[L_\varepsilon(C)\right]}{\log \varepsilon} \right], \quad (2)$$

where C is the considered curve, L is the length of the curve C, and ε is the length of the segment used as unit to calculate L.

Single graphs about roundness, solidity, and FD were obtained for each set of images.

2.5. Fluorescence Microscopy. MDA-MB-231 cells were fixed in 4% paraformaldehyde for 10 minutes at 4°C and incubated over night at 4°C with PBS (CMF, Calcium, and Magnesium Free) 1,5% goat serum plus the following specific antibodies: anti-α-tubulin (T5168, Sigma-Aldrich) and anti-vimentin (sc-6260, Santa Cruz biotechnology). For F-actin visualization rhodamine-phalloidin (Invitrogen Molecular Probes, Eugene) was used. Cells were washed three times with PBS (1% BSA 0.2% Triton X 100) and incubated with rhodamine-phalloidin, the anti-mouse IgG-FITC PN IM1619 secondary antibody (Beckman-Coulter Inc., Fullerton, CA, USA), and HOECHST 33342 (Sigma-Aldrich, St. Louis, MO, USA) to stain the DNA. Finally, cells were washed, mounted in buffered glycerol (0.1 M, pH 9.5), and analyzed using a Zeiss Fluorescent Microscope. The images were scanned under 40x objective.

2.6. Cell Cycle Analysis. Cell clumps were collected and centrifuged and pellets were trypsinized and washed twice with PBS (Phosphate Buffered Saline, Sigma-Aldrich, St. Louis, MO, USA). Adherent and ground control cells were trypsinized and washed twice with PBS. Cells were fixed with 70% ethanol at 4°C for 24 h and stained with DNA PREP Stain (Beckman Coulter, Fullerton, USA) at 4°C overnight. Stained cells were measured by flow cytometry. Cell cycle analysis was performed three times.

2.7. Annexin V/7-AAD Staining. Cell clumps were collected and centrifuged and pellets were trypsinized and washed twice with PBS. Adherent cells and ground control cells were trypsinized and washed twice with PBS. The cells were stained with FITC labeled annexin V/7-AAD (7-aminoactinomycin-D) according to the manufacturer's instructions (annexin V/7-AAD kit; Beckman Coulter, Marseille, France). Briefly, a washed cell pellet (5×10^4 cells/mL) was resuspended in 500 μL binding buffer; 10 μL of annexin V together with 20 μL 7-AAD was added to 470 μL cell suspension. The cells were incubated for 15 min on ice in the dark. The samples were analyzed by flow cytometry. Apoptosis assay was performed three times.

2.8. Flow Cytometry. Flow cytometry was performed using an EPICS Coulter XL (Beckman-Coulter Inc.). The fluorescence of 20,000 events was measured. An excitation wavelength of 488 nm was used in combination with standard filters to discriminate between the FL1 (forward scatter) and FL3 (side scatter) channels. Data were analyzed by ModFit LT Software (Verity Software Inc., USA).

2.9. Western Blot. Cell clumps were washed twice with ice-cold PBS and resuspended in RIPA lysis buffer (Sigma Chemical Co.). Adherent and ground control cells were washed twice with ice-cold PBS and scraped in RIPA lysis buffer (Sigma Chemical Co.). A mix of protease inhibitors (Complete-Mini Protease Inhibitor Cocktail Tablets, Roche, Mannheim, Germany) and phosphatase inhibitors (PhosStop; Roche, Mannheim, Germany) was added just before use. Cellular extracts were then centrifuged at 8,000 ×g for 10 min. The protein content of supernatants was determined using the Bradford assay. For western blot analysis, cellular extracts were separated on SDS-polyacrylamide gels with a concentration of acrylamide specific for the proteins studied. Proteins were blotted onto nitrocellulose membranes (BIO-RAD, Bio-Rad Laboratories, Hercules, CA, USA) and probed with the following antibodies: anti-Cyclin D1 (AB-90009) from Immunological Sciences; anti-survivin (number 2808), anti-phospho-AKT (ser473) (number 9271S), anti-AKT (number 9272S), anti-phospho-ERK1/2 (number 9106), anti-cleaved PARP (number 9541), anti-GAPDH (number 2118), all from Cell Signaling Technology; anti-Bax (sc-493), anti-Bcl-2 (sc-492), anti-ERK1 (sc-94), all from Santa Cruz Biotechnology. Antigens were detected with enhanced chemiluminescence kit (Amersham Biosciences, Little Chalfont Buckinghamshire, England), according to the manufacturer's instructions. All Western blot images were acquired and analyzed through Imaging Fluor S densitometer (Biorad-Hercules).

2.10. Statistical Analysis. Data were expressed as mean ± standard deviation (SD) or mean ± standard error (SE). Data were statistically analyzed with the analysis of variance (ANOVA) followed by the Bonferroni post-test. Differences were considered significant at the level of $P < 0,05$. Statistical analysis was performed by using GraphPad Instat software (GraphPad Software, Inc.; San Diego, CA, USA).

3. Results

3.1. Effect of Microgravity on MDA-MB-231 Morphology. MDA-MB-231 cell line grew as a monolayer when cultured under static 1 g condition (on ground control, Figures 1(a)

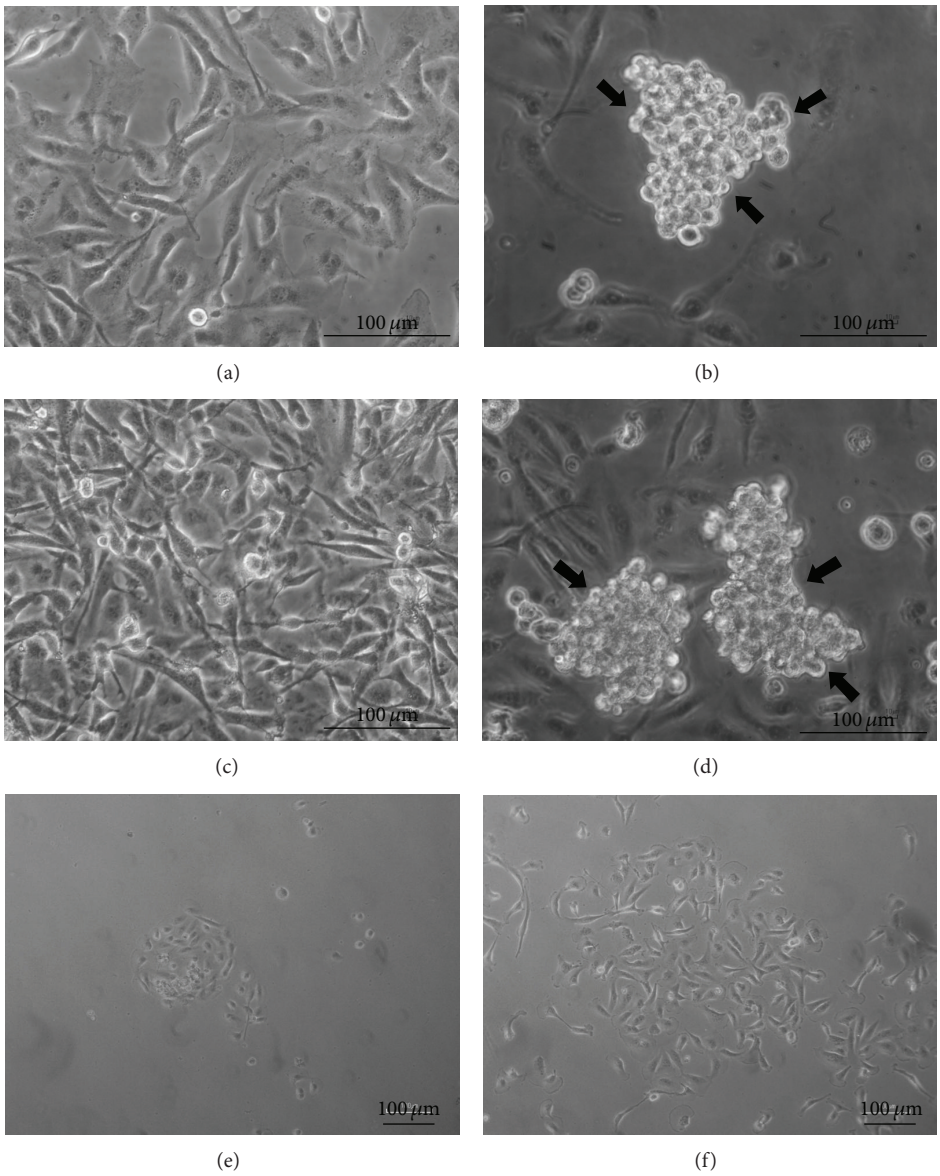

Figure 1: Microphotographs of MDA-MB-231 by optical microscopy. MDA-MB-231 cell line in on ground control condition at 24 (a) and 72 hours (c). MDA-MB-231 cells exposed to microgravity for 24 (b) and 72 hours (d). RPM cell clumps, after reseeding into a normal gravitational field after 6 (e) and 24 hours (f). Magnification ×320 (a), (b), (c), (d), ×100 (e), (f).

and 1(c)). After 24 and 72 hours of simulated microgravity exposure, cells were distributed into two populations: the first, adhering to the substrate, represented by flat, spindle cells; the second, represented by rounded cells, aggregated in cell clumps, floating in the culture medium (Figures 1(b) and 1(d)). This distribution does not represent a transitory state, given that the percentage of cells at both 24 and 72 hours still remains constant. However, beside the fact that such changes are likely to involve several modifications on shape and biological function, the observed nonadherent phenotype is still wholly reversible after 72 hours. Indeed, after reseeding into a normal gravitational field, cell clumps were *de novo* able to adhere to the culture plate already after 6 hours (Figure 1(e)) and to fully recover their native morphological traits and topological distribution after 24 hours (Figure 1(f)).

3.2. Effect of Microgravity on Quantitative Morphological Parameters. Quantitative image analysis was performed by quantifying roundness, solidity, and fractal dimension (FD). Significant differences were recorded among the three cell populations (Table 1). *Roundness*: no statistically significant differences between on ground cells and RPM adherent cells have been observed at both 24 and 72 hours. Instead, RPM cell clumps showed a significant strong increase in roundness compared to control and RPM adherent cells at 24 and 72 hours. *Solidity*: at 24 hours, no statistically significant differences between on ground cells and RPM adherent cells

Table 1

	Roundness	±SE		Solidity	±SE		FD	±SE	
24 hours									
On ground cells	0,4563	0,0301		0,6690	0,0225		1,7482	0,0091	
RPM adherent cells	0,3991	0,0275		0,6499	0,0200		1,7406	0,0063	
RPM cell clumps	0,7894	0,0219	**	0,8966	0,0263	**	1,4625	0,0015	**
72 hours									
On ground cells	0,3227	0,0263		0,4687	0,0136		1,6677	0,0036	
RPM adherent cells	0,4081	0,0311		0,6115	0,0226	*	1,7245	0,0067	
RPM cell clumps	0,7961	0,0208	**	0,8573	0,0469	**	1,4990	0,0015	**

Roundness, solidity, and fractal dimension (FD) mean values ± SE in on ground control cells, RPM adherent cells, and RPM cell clumps. $^{*}P < 0.01$ *versus* on ground control cells; $^{**}P < 0.001$ *versus* on ground control and RPM adherent cells by ANOVA followed by Bonferroni post-test.

were recorded; meanwhile in RPM cell clumps the solidity index was significantly higher with respect to on ground cells and RPM adherent cells. At 72 hours, the solidity index significantly increased in both RPM cell populations, reaching its highest level in RPM cell clumps. *Fractal dimension*: no statistically significant differences between on ground cells and RPM adherent cells were recorded both at 24 and 72 hours. Instead, RPM cell clumps showed a statistically significant decrease in FD compared to control and RPM adherent cells at 24 and 72 hours. These results are coherent with the qualitative morphological assessment and confirmed that microgravity exposure leads to the emergence of two morphologically distinct cell populations.

3.3. Effect of Microgravity on MDA-MB-231 Cytoskeleton Architecture. After 24 hours of microgravity exposure, both MDA-MB-231 RPM adherent cells and RPM cell clumps showed a large rearrangement of F-actin, α-tubulin, and vimentin compared to on ground control cells. In on ground control cells the network of cytosolic F-actin bundles appeared well organized and the microtubules appeared orderly radiating from the perinuclear area throughout the cytoplasm toward the cell periphery (Figure 2(a)). In RPM adherent cells the actin filaments showed a disappearance of the complex cytosolic network which appeared mostly localized on the cell border; microtubules were disorganized, with a more evident thickening in perinuclear position (Figure 2(b)). In floating cell clumps, the actin meshwork appeared completely disrupted, and the filaments were mainly localized behind the cell border. Tubulin meshwork was also completely disrupted and a slight diffuse fluorescence was observed spreading throughout the entire cytoplasm (Figure 2(c)). In the on ground cells vimentin filaments were well organized all over the cytoplasm (Figure 3(a)). In both RPM adherent cells and cell clumps the vimentin network was disrupted, appearing in the form of dense aggregates closely associated with the nucleus (Figures 3(b) and 3(c)). Cytoskeleton rearrangements were almost stable, given that no significant changes have been observed even after 72 hours in microgravity-exposed cells (data not shown).

3.4. Microgravity Modifies MDA-MB-231 Cell Cycle Distribution. MDA-MB-231 cells subjected to microgravity displayed relevant modification in their cell cycle (Figures 4(a) and 4(b)). Nonadherent RPM-treated MDA-MB-231 cells were distributed in a significantly different manner when compared to both control and RPM-adherent cells; indeed, after 24 hours, floating cell clumps in G0/G1 and in S phase were significantly decreased, whereas cells in G2/M phase increase up to 6-fold. On the contrary, adherent RPM-treated cells displayed only a slight increase in the S phase distribution, when compared to controls. After 72 hours of microgravity exposure, MDA-MB-231 RPM cell clumps still showed a relevant decrease in the S phase, thus demonstrating a persistent inhibition of cell growth; cells number in G2/M phase was significantly higher; meanwhile no significant change in G0/G1 was observed (Figure 4(b)). Again, besides minor differences, control and adherent RPM-treated cells displayed an overlapping distribution in the G0/G1 and G2/M phase, whereas the percentage of cells in the S phase was still higher than that recorded in floating RPM cell clumps. These data are exemplarily mirrored by Cyclin D1 data. Cyclin D1 is one of the main factors that regulate the activation of the cell cycle and its increase is required to foster cell growth. As expected, a statistically significant decrease of Cyclin D1 levels in RPM cell clumps was recorded; meanwhile Cyclin D1 levels are higher in adherent proliferating RPM cells, as well as in control samples. These effects were observed at both 24 and 72 hours (Figure 4(c)).

3.5. Microgravity Induces Apoptosis in MDA-MB-231 Cell Clumps. Data obtained by cytofluorimetric assays reported a statistically significant increase in the apoptotic rate after 24 and 72 hours of microgravity exposure in cell clumps with respect to both adherent cells and on ground control cells (Figure 5(a)). Western blot analysis revealed a statistically significant increase of Bax/Bcl-2 ratio at 72 hours in RPM cell clumps compared to RPM adherent cells and on ground control cells (Figure 5(b)). Similarly cleaved-PARP levels, a direct marker of caspase-3 activation [24], were significantly increased at 24 and 72 hours in RPM cell clumps compared to RPM adherent cells and on ground control cells (Figure 5(c)). Overall these data suggest that nonadherent cells were significantly constrained in their viability, given that microgravity inhibits cell growth and, at the same time, enhances the apoptotic process. Adherent cells in microgravity, on the

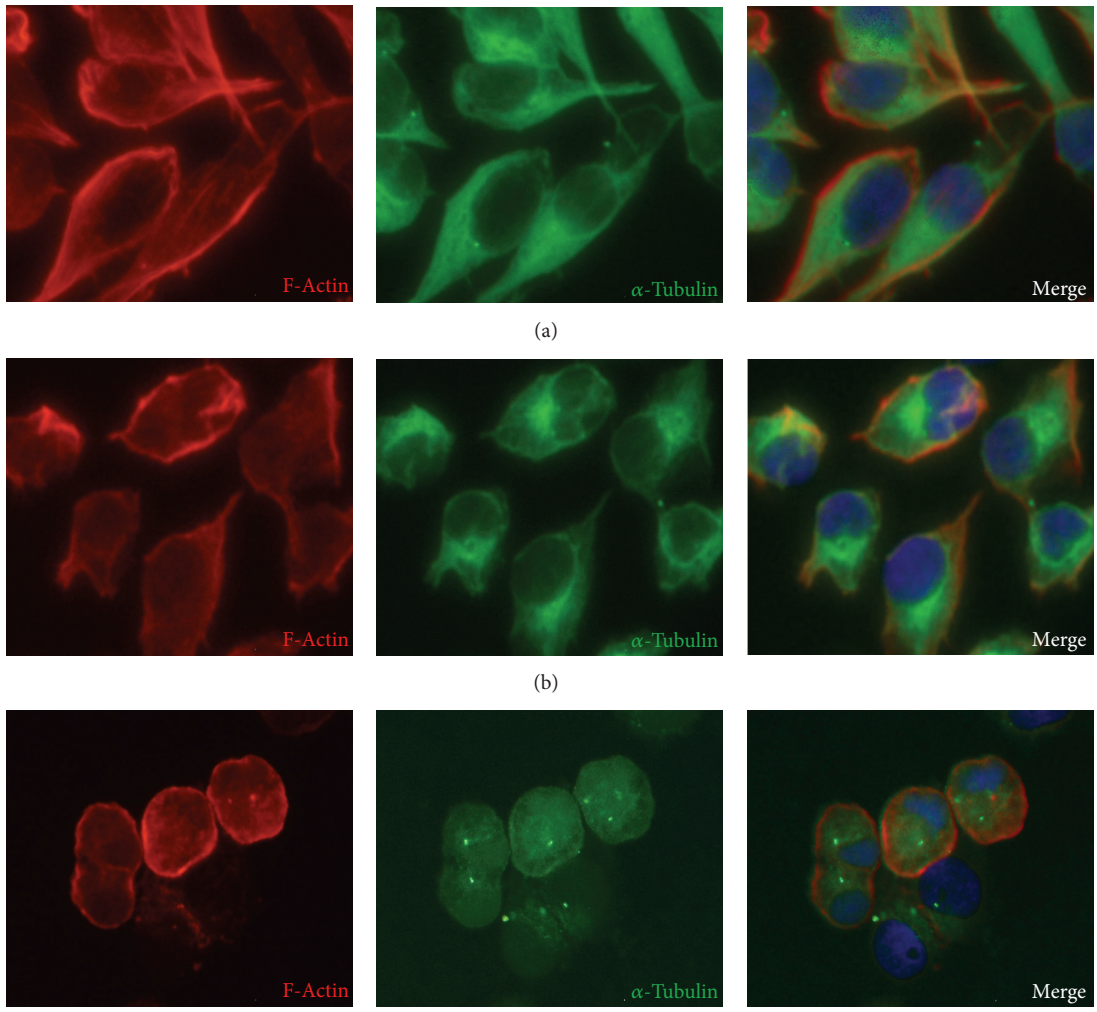

Figure 2: Immunofluorescence images of F-actin and α-tubulin in MDA-MB-231. Rhodamine-phalloidin staining of MDA-MB-231 showing F-actin distribution patterns (red color) and immunostaining of α-tubulin (green color) and HOECHST 33342 to stain nuclei (blue color) after 24 hours in on ground control cells (a), RPM adherent cells (b), and RPM cell clumps (c). Magnification ×400.

contrary, display only minor changes in both apoptosis and proliferation rate.

3.6. Microgravity Modifies MDA-MB-231 Survival Pathways. Microgravity exposure is associated with a statistically significant decrease in the phosphorylation of AKT in adherent cells and cell clumps with respect to on ground control cells after 24 h. Instead, after 72 hours of microgravity exposition, RPM adherent cells showed a statistical increase of p-AKT expression with respect to on ground control cells and RPM cell clumps (Figure 6(a)); such biphasic effect on AKT activation may help explain the biphasic trend observed in apoptosis rate in adherent RPM-exposed cells: apoptosis increases, indeed, at 24 hours when p-AKT values are low; the opposite is observed when p-AKT levels increase at 72 hours. A similar behavior may be described for the two other prosurvival factors, Survivin and phosphorylated-ERK. Microgravity exposure induced a statistically significant decrease in Survivin levels in both adherent and nonadherent RPM-treated cells at 24 hours. However, at 72 hours Survivin levels significantly increased in RPM adherent cells and decreased in nonadherent RPM-treated cells (Figure 6(b)). Likewise, ERK phosphorylation was severely inhibited in RPM cell clumps after 24 and 72 hours, in respect to values observed in both RPM adherent and control cells (Figure 6(c)). Taken as a whole, prosurvival factors increased in adherent RPM-treated cells; meanwhile they decreased in nonadherent RPM-exposed cells, mirroring so far the observed mentioned trend in apoptosis.

4. Discussion

Breast cancer cells exposed to microgravity acquire two distinct phenotypes already after the first 24 hours. Such outstanding result has been previously observed in osteoblasts cultured in microgravity [17] and can be interpreted in the light of the nonequilibrium theory. Briefly, a dissipative, nonlinear system sufficiently far from the equilibrium

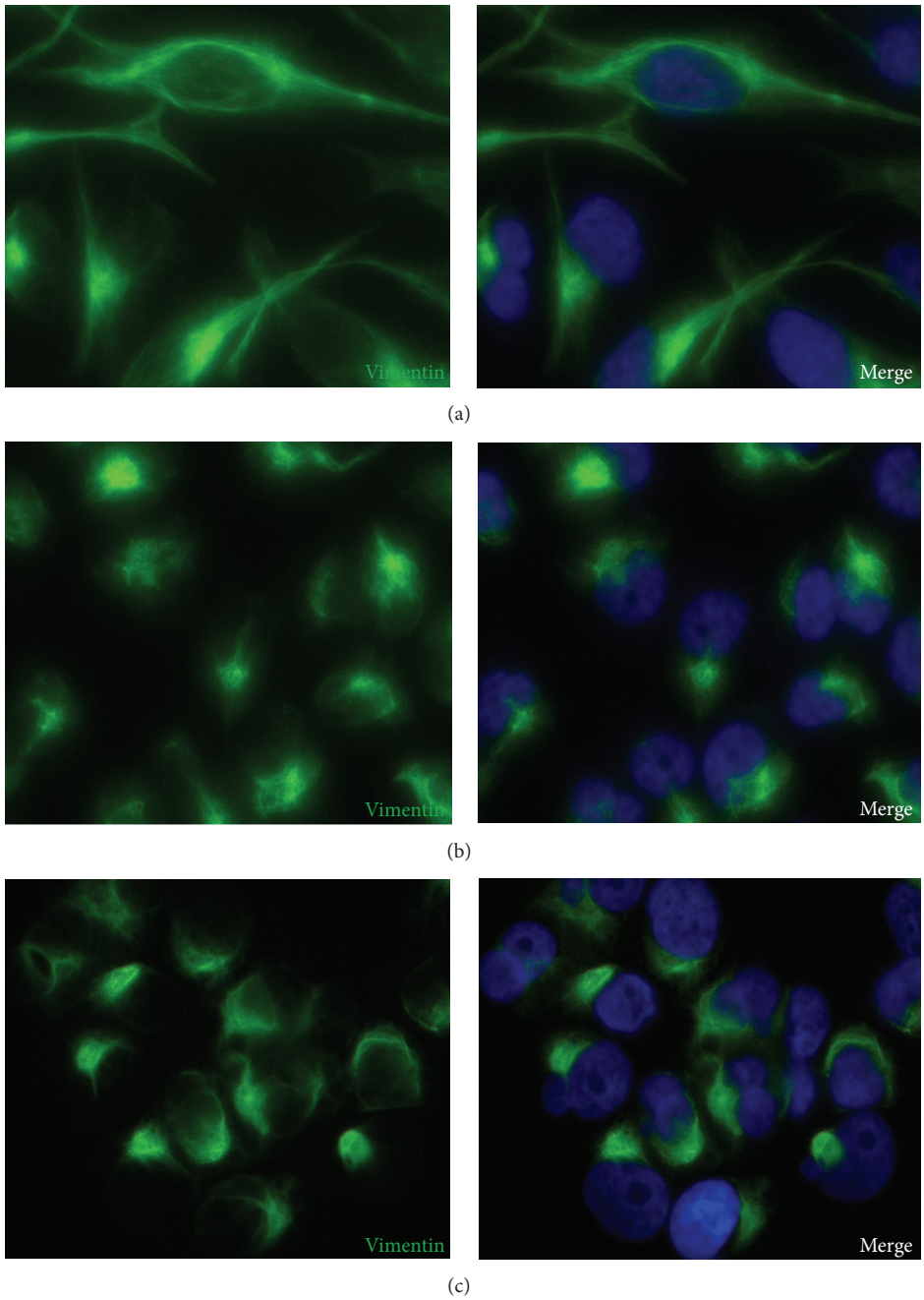

Figure 3: Immunofluorescence images of vimentin in MDA-MB-231. Immunostaining of vimentin (green color) and HOECHST 33342 to stain nuclei (blue color) after 24 hours in on ground control cells (a), RPM adherent cells (b), and RPM cell clumps (c). Magnification ×400.

can form spatial stationary patterns after experiencing a phase transition, leading to new asymmetric configurations [25]. These states are equally accessible, that is to say, that there exists a complete symmetry between the emerging configurations, as it is reflected in the symmetry of the bifurcation diagram. However, the superimposition of an external field, even if a weak one like gravity, may break the system's symmetry, bestowing a preferential directionality according to which the system will preferentially evolve into one of the states and not the others. Indeed, bifurcations far from equilibrium endow a system with a very pronounced sensitivity, allowing it to capture the slightest environmental asymmetry and select a preferred polarity or chirality. In other words, the "weak" force dramatically influences the system in selecting one out of many other configurations [26]. On the contrary, by removing the gravitational constraints the system can freely access different attractor states, recovering henceforth new configuration states ("phenotypes"). Such model has been experimentally confirmed, showing that several cell components characterized by a nonlinear dynamics

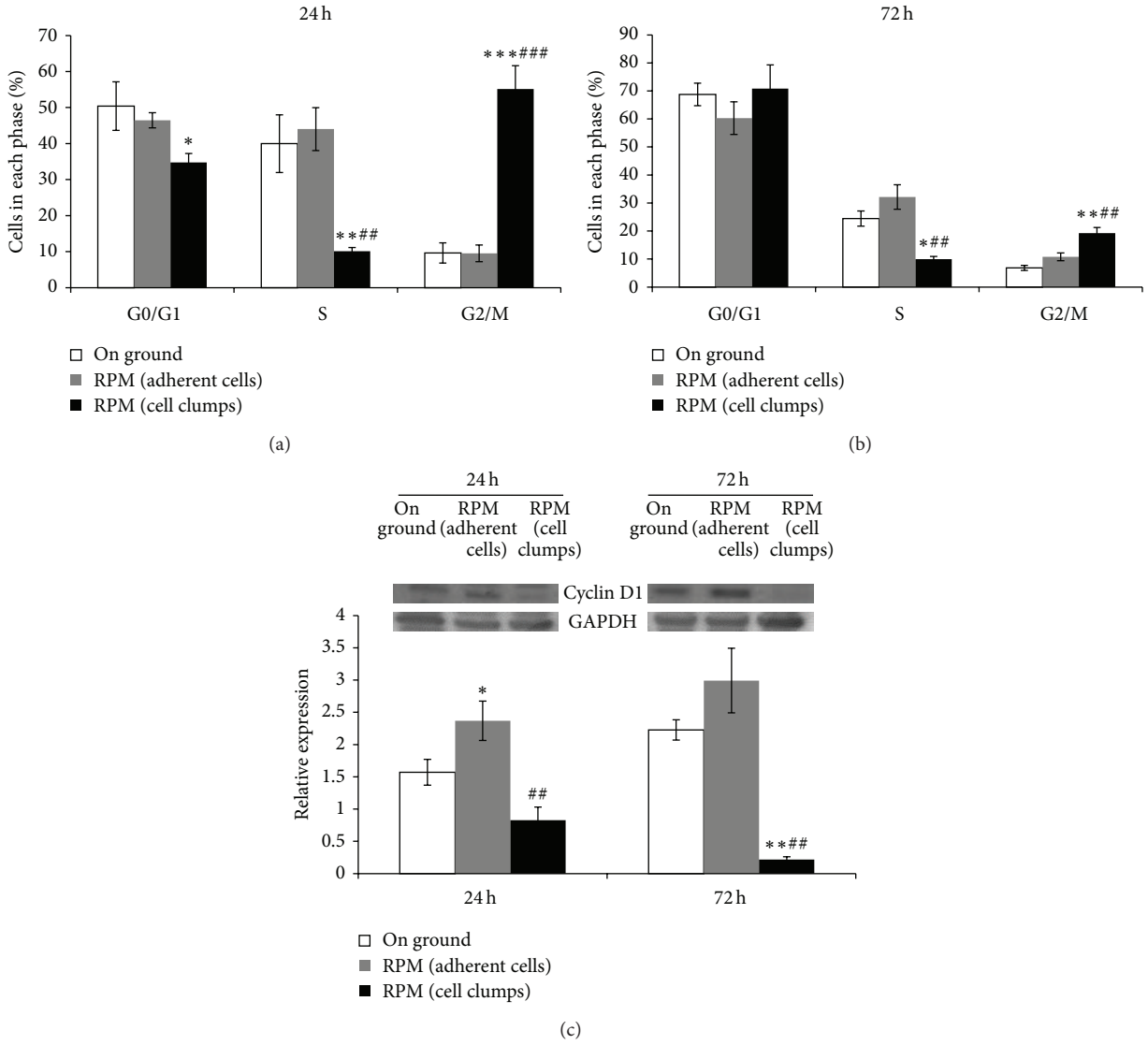

Figure 4: Cell cycle analysis in MDA-MB-231. Cells distribution along the different phases of the cell cycle at 24 (a) and 72 hours (b), in on ground control cells, RPM adherent cells, and RPM cell clumps. (c) Immunoblot bar chart showing the expression of Cyclin D1 in MDA-MB-231 in on ground control cells, RPM adherent cells, and RPM cell clumps at 24 and 72 hours. Columns and bars represent densitometric quantification of optical density (OD) of specific protein signal normalized with the OD values of the GAPDH served as loading control. Each column represents the mean value ± SD of three independent experiments. $^{*}P < 0,05$; $^{**}P < 0,01$; $^{***}P < 0,001$ *versus* on ground control; $^{\#\#}P < 0,01$; $^{\#\#\#}P < 0,001$ *versus* RPM adherent cells by ANOVA followed by Bonferroni post-test.

when exposed to microgravity may experience bifurcation transitions, leading to the appearance of new self-organized states from an initially homogeneous conformation [27, 28]. It is tempting to speculate that such transitions may arise in the cell when self-organization processes (cytoskeleton components assembly and mitosis) take place. In our experiment, the annihilation of gravity enables the system to recover more degree of freedom through subsequent symmetry breakings, with the appearance of new morphological and functional phenotypes.

Indeed, MDA-MB-231 cells exposed to microgravity were almost equally split into two distinct populations, characterized by very different morphologies. The first cluster is represented by cells adherent to the substrate, roughly preserving their native, spindle profile. The second one is represented by rounded, smallest cells, grouped and linked to each other, forming aggregates floating in the supernatant.

Fractal analysis provides a quantitative assessment of those qualitative differences [17, 29]. Adherent cells in microgravity showed fractal values significantly higher than suspended cells; coherently, roundness values were greater in suspended than in adherent cells. Additionally, solidity estimation evidences how different these populations are in terms of "potential" deformability. Solidity is a good descriptor of cell deformability, indeed, as it describes in geometrical terms the stiffness and deformability of an object. Thus, the

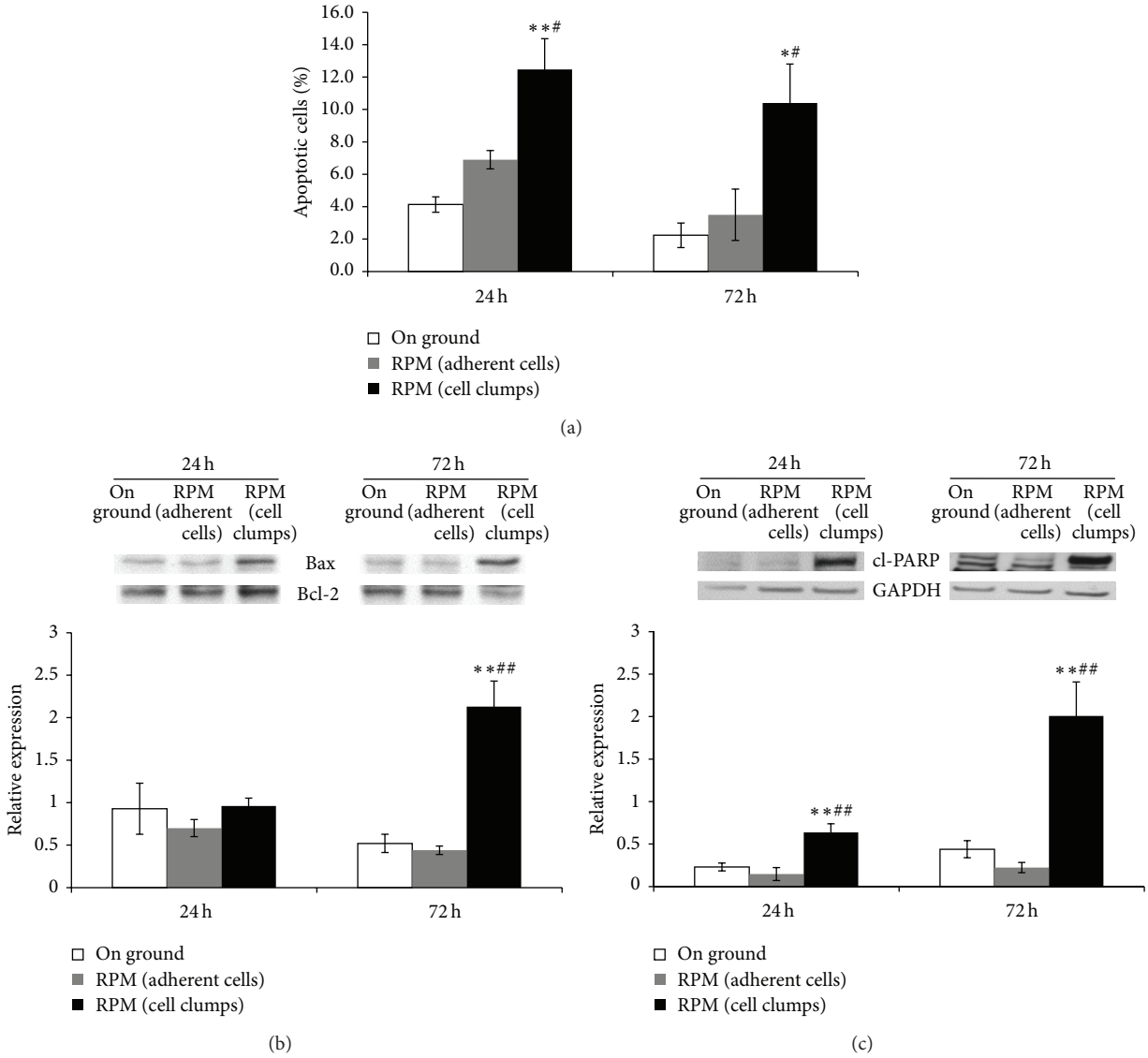

Figure 5: Apoptosis analysis in MDA-MB-231. Apoptotic rate in RPM cultured MDA-MB-231 and on ground cells was determined by a dual parameter flow cytometric assay (a). Histograms show the percentage of apoptotic cells (Annexin V+/7-AAD-); each column represents the mean value ± SD of three independent experiments. Immunoblot bar chart showing the expression of Bax/Bcl-2 ratio (b) and cleaved PARP (c) in on ground control cells, RPM adherent cells, and RPM cell clumps at 24 and 72 hours. Columns and bars represent densitometric quantification of optical density (OD) of specific protein signal normalized with the OD values of the GAPDH served as loading control. Each column represents the mean value ± SD of three independent experiments. $^{*}P < 0,05$; $^{**}P < 0,01$ *versus* on ground control; $^{\#}P < 0,05$; $^{\#\#}P < 0,01$ *versus* RPM adherent cells by ANOVA followed by Bonferroni post-test.

higher the solidity is, the lower the cell deformability is. Nonadherent cells growing in microgravity are grouped in discrete clusters, and they establish tight cell-to-cell contacts. As expected, their solidity value is higher than that recorded in isolated, adherent cells growing in RPM, given that the multiple cell-to-cell adhesion is thought to "stabilize" the cells shape, by mutually reinforcing their stiffness. The combined estimation of these parameters suggests that the two emerging populations significantly exhibit differences in their respective morphological features.

Aggregates of floating cells retain their viability potential and, after reseeding into a normal gravitational field, they are able to fully recover their native morphological traits, already after 24 hours. This is not really an unexpected event, since it has been previously reported that microgravity exposed cells may recover their original profile when replaced in a normal gravity environment [30]. Thereby, gravity-related phenotypic variability may be considered an adaptive, reversible phenomenon.

Changes in cell shape are likely mediated by associated modification in cytoskeleton architecture, which also conveys mechanical stress to the cell biochemical/genetic machinery. Therefore, different cytoskeleton arrangements will end up in activating different gene sequences, leading hence

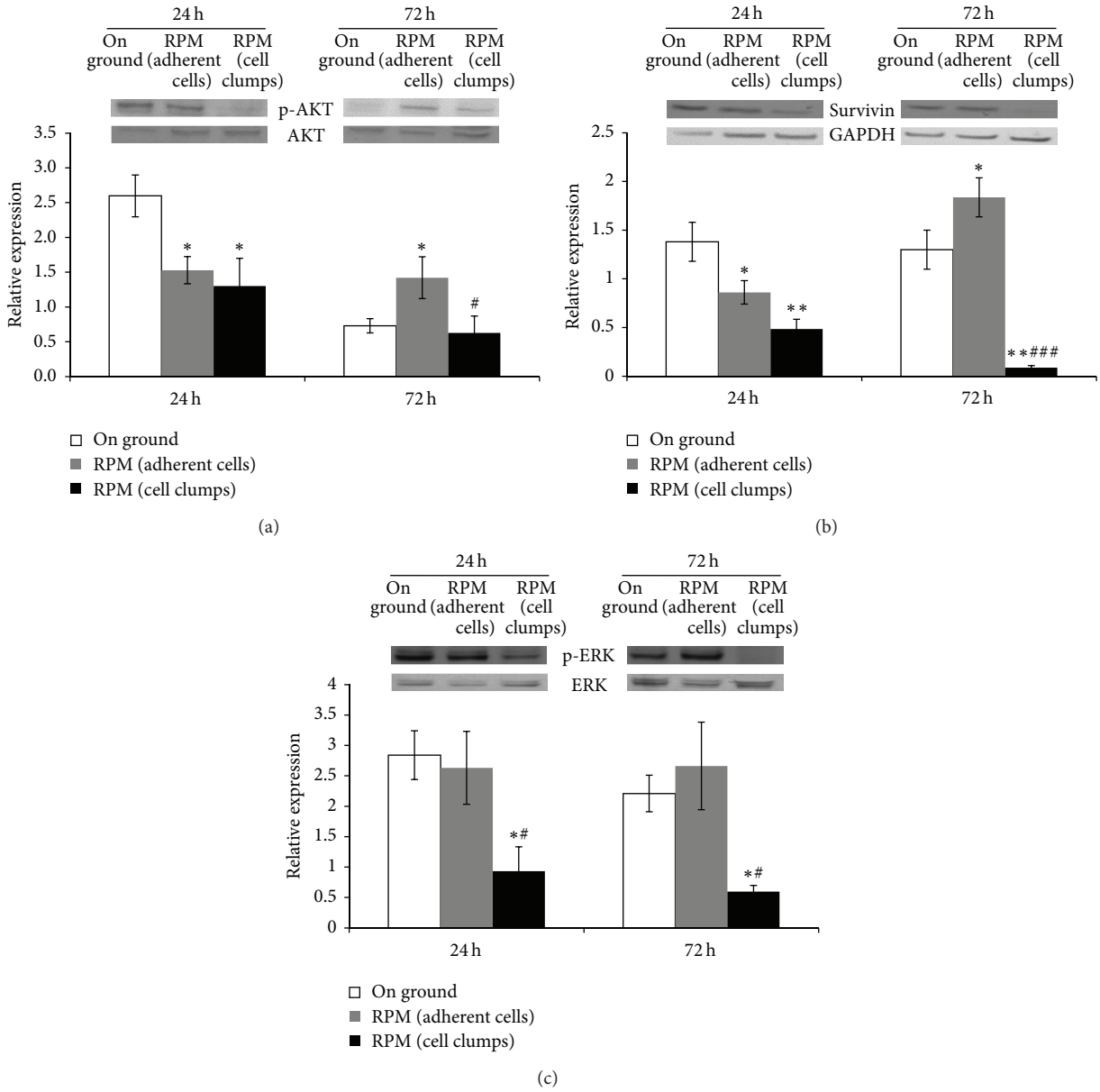

Figure 6: Survival pathways analysis in MDA-MB-231. Immunoblot bar chart showing the expression of p-AKT/AKT ratio (a), Survivin (b), and p-ERK/ERK ratio (c) in on ground control cells, RPM adherent cells, and RPM cell clumps at 24 and 72 hours. Columns and bars represent densitometric quantification of optical density (OD) of specific protein signal normalized with the OD values of the GAPDH served as loading control. Each column represents the mean value ± SD of three independent experiments. $^{*}P < 0,05$; $^{**}P < 0,01$ *versus* on ground control; $^{\#}P < 0,05$; $^{\#\#\#}P < 0,001$ *versus* RPM adherent cells by ANOVA followed by Bonferroni post-test.

to triggering different biochemical pathways. The balance between tensional forces and the cytoskeleton architecture modulates thereupon several complex cell functions like apoptosis, differentiation, proliferation, ECM remodelling, and so forth [31]. Compelling data demonstrated that both simulated and real, space-based microgravity can severely affect cytoskeleton structure and function [8, 32]. The most impressive modifications were observed in nonadherent RPM-exposed cells in which stress fibers disappear and actin architecture is severely compromised, thus jeopardizing the chances of cell anchoring to the substrate. In the same cells, tubulin microfilaments are almost completely disorganized. This finding may help in explaining the cell cycle inhibition observed in floating cell clumps, given that a correct arrangement of the tubulin meshwork is required to ensure a proper functioning of the mitotic process: microtubules perform indeed a special task during mitosis and meiosis by forming the spindle assembly to align and separate the chromosomes [33]. Yet it is worth of noting that cytoskeleton changes greatly differ between the two RPM-cultured populations, outlining therefore that microgravity enacted the emergence of two very different cytoskeleton phenotypes.

That architectural diversity is associated with significant differences in cell cycle and apoptosis. Adherent breast cancer cells growing in RPM are trying to counteract microgravity effects by increasing the number of cells in the S phase and by stabilizing the apoptotic rate. On the contrary, suspended cell aggregates display a very different behavior, characterized by reduced proliferative capability and enhanced apoptosis.

However, most of the cells in the floating clumps resulted to be viable; in fact, these cells readhered and grew up when once they were reseeded in normal gravity environment. Hence, cell population blocked in G2/M underwent apoptosis; meanwhile cell population blocked in G0/G1 recovered the original profile, when they were reseeded.

It is worth noting that such results have been obtained by treating highly malignant growing cancer cells. In this regard, both cell phenotypes cultured in RPM greatly differ from their counterpart growing in 1 g gravity field. Such processes are remarkably mirrored by the concomitant, coherent changes in several biochemical pathways, mechanistically linked to both proliferation and programmed cell death. Cyclin D1, a key regulatory factor for cell cycle G1/S transition, is significantly increased in adherent MDA-MB-231 cells; meanwhile in suspended cell aggregates Cyclin D1 release is almost completely abolished. Likewise, proapoptotic effectors (BAX, PARP) dramatically increase in suspended RPM-cultured cells; meanwhile prosurvival factors (Bcl-2, Survivin) significantly decrease; Survivin, a well-known critical factor triggering a plethora of survival signaling cascades, was indeed dramatically downregulated and resulted to be undetectable after 72 hours of exposition. Opposite findings were observed in adherent breast cancer cells exposed to microgravity: the Bcl-2 inhibitor of caspase activation increases, whereas proapoptotic effectors concomitantly decline.

Regulation of apoptotic processes relies on the modulation of an intricate interplay between several upstream molecular pathways, involving mainly activation of p-ERK and p-AKT expression. As expected, p-AKT and p-ERK were significantly reduced in suspended cell aggregates; meanwhile they increase in adherent, apoptosis-resistant cells. Overall, these results become evident already at early times, that is, after 24 hours of exposition.

5. Conclusions

Our results confirm previous findings, demonstrating that microgravity enacted the emergence of distinct phenotypes, characterized by significant, recognizable differences in shape configuration, biochemical pathways architecture, and behavioral processes [17]. Additionally, it should be remarked that the coexistence of two different cell populations may contribute to explain some contradictory results provided by earlier studies [34, 35]; indeed, increase or reduction in cell proliferation as well as enhanced or reduced apoptosis could well be both found during microgravity experiments, given that such opposite behaviors must be ascribed to very different cell clusters.

Spontaneous emergence of different phenotypes in microgravity after the system has experienced a symmetry breaking is a finding worth of interest and may have relevant consequences for human space flights. Phenotypic switch leading to divergent morphological and biochemical configuration is triggered by nonlinear processes taking place near the transition point. Such transition enables the system to recover new degree of freedom and, as such, it may be viewed as a spontaneous process allowed by the nonequilibrium thermodynamics. That finding highlights the relevance of biophysical constraints in shaping the form biological, dissipative systems acquire [36] and may help understand how cells and tissues behave during development, pathological events, or in extreme environmental fields.

Conflict of Interests

The authors declare that there is no conflict of interests regarding the publication of this paper.

Acknowledgment

This work was partially supported by a grant from ASI (Italian Space Agency), COREA Program.

References

[1] J. C. Buckey, *Space Physiology*, Oxford University Press, 2006.

[2] G. Albrecht-Buehler, "Possible mechanisms of indirect gravity sensing by cells," *ASGSB Bulletin*, vol. 4, no. 2, pp. 25–34, 1991.

[3] M. Hughes-Fulford and M. L. Lewis, "Effects of microgravity on osteoblast growth activation," *Experimental Cell Research*, vol. 224, no. 1, pp. 103–109, 1996.

[4] G. Carmeliet and R. Bouillon, "The effect of microgravity on morphology and gene expression of osteoblasts in vitro," *The FASEB Journal*, vol. 13, no. 8, pp. S129–S134, 1999.

[5] R. Gruener, R. Roberts, and R. Reitstetter, "Reduced receptor aggregation and altered cytoskeleton in cultured myocytes after space-flight," *Biological Sciences in Space*, vol. 8, no. 2, pp. 79–93, 1994.

[6] D. A. Riley, J. L. W. Bain, J. L. Thompson et al., "Thin filament diversity and physiological properties of fast and slow fiber types in astronaut leg muscles," *Journal of Applied Physiology*, vol. 92, no. 2, pp. 817–825, 2002.

[7] M. L. Lewis, L. A. Cubano, B. Zhao et al., "cDNA microarray reveals altered cytoskeletal gene expression in space-flown leukemic T lymphocytes (Jurkat)," *The FASEB journal*, vol. 15, no. 10, pp. 1783–1785, 2001.

[8] D. Vorselen, W. H. Roos, F. C. MacKintosh, G. J. L. Wuite, and J. J. W. A. van Loon, "The role of the cytoskeleton in sensing changes in gravity by nonspecialized cells," *The FASEB Journal*, vol. 28, no. 2, pp. 536–547, 2014.

[9] A. Cogoli, "Signal transduction in T lymphocytes in microgravity," *Gravitational and Space Biology Bulletin*, vol. 10, no. 2, pp. 5–16, 1997.

[10] J. P. Hatton, F. Gaubert, M. L. Lewis et al., "The kinetics of translocation and cellular quantity of protein kinase C in human leukocytes are modified during spaceflight," *The FASEB Journal*, vol. 13, no. 8, pp. S23–S33, 1999.

[11] T. G. Hammond, E. Benes, K. C. O'Reilly et al., "Mechanical culture conditions effect gene expression: gravity-induced changes

on the space shuttle," *Physiological Genomics*, vol. 2000, no. 3, pp. 163–173, 2000.

[12] J. Renn, D. Seibt, R. Goerlich, M. Schartl, and C. Winkler, "Simulated microgravity upregulates gene expression of the skeletal regulator Core binding Factor α1/Runx2 in Medaka fish larvae in vivo," *Advances in Space Research*, vol. 38, no. 6, pp. 1025–1031, 2006.

[13] J. Boonstra, "Growth factor-induced signal transduction in adherent mammalian cells is sensitive to gravity," *The FASEB Journal*, vol. 13, no. 8, pp. S35–S42, 1999.

[14] M. Bizzarri, A. Cucina, A. Palombo, and M. G. Masiello, "Gravity sensing by cells: mechanisms and theoretical grounds," *Rendiconti Lincei. Scienze Fisiche e Naturali*, vol. 25, no. 1, pp. S29–S38, 2014.

[15] M. Braun, "Primary responses of gravity sensing in plants," in *Biology in Space and Life on Earth: Effects of Spaceflight on Biological Systems*, E. Brinckmann, Ed., chapter 2, Wiley, Weinheim, Germany, 2007.

[16] D. K. Kondepudi and P. B. Storm, "Gravity detection through bifurcation," *Advances in Space Research*, vol. 12, no. 1, pp. 7–14, 1992.

[17] F. Testa, A. Palombo, and S. Dinicola, "Fractal analysis of shape changes in murine osteoblasts cultured under simulated microgravity," *Rendiconti Lincei. Scienze Fisiche e Naturali*, vol. 25, no. 1, pp. S39–S47, 2014.

[18] J. Vassy, S. Portet, M. Beil et al., "Weightlessness acts on human breast cancer cell line MCF-7," *Advances in Space Research*, vol. 32, no. 8, pp. 1595–1603, 2003.

[19] A. Qian, W. Zhang, L. Xie et al., "Simulated weightlessness alters biological characteristics of human breast cancer cell line MCF-7," *Acta Astronautica*, vol. 63, no. 7–10, pp. 947–958, 2008.

[20] J. M. Jessup, M. Frantz, E. Sonmez-Alpan et al., "Microgravity culture reduces apoptosis and increases the differentiation of a human colorectal carcinoma cell line," *In Vitro Cellular & Developmental Biology—Animal*, vol. 36, no. 6, pp. 367–373, 2000.

[21] E. N. Grigoryan, H. J. Anton, and V. I. Mitashov, "Real and simulated microgravity can activate signals stimulating cells to enter the S phase during lens regeneration in urodelean amphibians," *Advances in Space Research*, vol. 38, no. 6, pp. 1071–1078, 2006.

[22] K. Nakamura, H. Kuga, T. Morisaki et al., "Simulated microgravity culture system for a 3-D carcinoma tissue model," *BioTechniques*, vol. 33, no. 5, pp. 1068–1076, 2002.

[23] J. J. W. A. van Loon, "Some history and use of the random positioning machine, RPM, in gravity related research," *Advances in Space Research*, vol. 39, no. 7, pp. 1161–1165, 2007.

[24] A. H. Boulares, A. G. Yakovlev, V. Ivanova et al., "Role of poly(ADP-ribose) polymerase (PARP) cleavage in apoptosis. Caspase 3-resistant PARP mutant increases rates of apoptosis in transfected cells," *The Journal of Biological Chemistry*, vol. 274, no. 33, pp. 22932–22940, 1999.

[25] G. Nicolis and I. Prigogine, *Exploring Complexity*, Freeman, New York, NY, USA, 1989.

[26] G. Nicolis and I. Prigogine, "Symmetry breaking and pattern selection in far-from-equilibrium systems," *Proceedings of the National Academy of Sciences of the United States of America*, vol. 78, no. 2, part 1, pp. 659–663, 1981.

[27] J. Tabony, N. Glade, J. Demongeot, and C. Papaseit, "Biological self-organization by way of microtubule reaction-diffusion processes," *Langmuir*, vol. 18, no. 19, pp. 7196–7207, 2002.

[28] S. J. Moorman and A. Z. Shorr, "The primary cilium as a gravitational force transducer and a regulator of transcriptional noise," *Developmental Dynamics*, vol. 237, no. 8, pp. 1955–1959, 2008.

[29] A. R. Qian, D. Li, J. Han et al., "Fractal dimension as a measure of altered actin cytoskeleton in MC3T3-E1 cells under simulated microgravity using 3-D/2-D clinostats," *IEEE Transactions on Biomedical Engineering*, vol. 59, no. 5, pp. 1374–1380, 2012.

[30] R. Coinu, A. Chiaviello, G. Galleri, F. Franconi, E. Crescenzi, and G. Palumbo, "Exposure to modeled microgravity induces metabolic idleness in malignant human MCF-7 and normal murine VSMC cells," *FEBS Letters*, vol. 580, no. 10, pp. 2465–2470, 2006.

[31] M. E. Chicurel, C. S. Chen, and D. E. Ingber, "Cellular control lies in the balance of forces," *Current Opinion in Cell Biology*, vol. 10, no. 2, pp. 232–239, 1998.

[32] M. Infanger, P. Kossmehl, M. Shakibaei et al., "Simulated weightlessness changes the cytoskeleton and extracellular matrix proteins in papillary thyroid carcinoma cells," *Cell and Tissue Research*, vol. 324, no. 2, pp. 267–277, 2006.

[33] J. L. Carminati and T. Stearns, "Microtubules orient the mitotic spindle in yeast through dyne independent interactions with the cell cortex," *The Journal of Cell Biology*, vol. 138, no. 3, pp. 629–641, 1997.

[34] L. Vico, "What do we know about alteration in the osteoblast phenotype with microgravity?" *The Journal of Musculoskeletal Neuronal Interactions*, vol. 6, no. 4, pp. 317–318, 2006.

[35] M. Hughes-Fulford, "Physiological effects of microgravity on osteoblast morphology and cell biology," *Advances in Space Biology and Medicine*, vol. 8, pp. 129–157, 2002.

[36] M. Bizzarri, A. Pasqualato, A. Cucina, and V. Pasta, "Physical forces and non linear dynamics mould fractal cell shape. Quantitative morphological parameters and cell phenotype," *Histology and Histopathology*, vol. 28, no. 2, pp. 155–174, 2013.

Hindawi Publishing Corporation
BioMed Research International
Volume 2014, Article ID 834134, 10 pages
http://dx.doi.org/10.1155/2014/834134

Research Article

Oxidative Stress and NO Signalling in the Root Apex as an Early Response to Changes in Gravity Conditions

Sergio Mugnai,[1,2] Camilla Pandolfi,[1] Elisa Masi,[1] Elisa Azzarello,[1] Emanuela Monetti,[1] Diego Comparini,[1] Boris Voigt,[3] Dieter Volkmann,[3] and Stefano Mancuso[1]

[1] *DISPAA, University of Florence, Viale delle Idee 30, 50019 Sesto Fiorentino, Italy*
[2] *HSO-USB, ESTEC, European Space Agency, Keplerlaan 1, 2200 AG Noordwijk, The Netherlands*
[3] *IZMB, University of Bonn, Kirschallee 1, 53115 Bonn, Germany*

Correspondence should be addressed to Sergio Mugnai; sergio.mugnai@unifi.it

Received 16 May 2014; Accepted 16 July 2014; Published 17 August 2014

Academic Editor: Monica Monici

Oxygen influx showed an asymmetry in the transition zone of the root apex when roots were placed horizontally on ground. The influx increased only in the upper side, while no changes were detected in the division and in the elongation zone. Nitric oxide (NO) was also monitored after gravistimulation, revealing a sudden burst only in the transition zone. In order to confirm these results in real microgravity conditions, experiments have been set up by using parabolic flights and drop tower. The production of reactive oxygen species (ROS) was also monitored. Oxygen, NO, and ROS were continuously monitored during normal and hyper- and microgravity conditions in roots of maize seedlings. A distinct signal in oxygen and NO fluxes was clearly detected only in the apex zone during microgravity, with no significant changes in normal and in hypergravity conditions. The same results were obtained by ROS measurement. The detrimental effect of D'orenone, disrupting the polarised auxin transport, on the onset of the oxygen peaks during the microgravity period was also evaluated. Results indicates an active role of NO and ROS as messengers during the gravitropic response, with probable implications in the auxin redistribution.

1. Introduction

During evolution, plants have developed elaborate sensory and signaling systems to cope with and adjust to rapid environmental changes. Among them, gravity remains a constant stimulus, playing a central role in driving the evolution of plants on Earth [1]. Gravitropism involves a fine and reliable coordination of the activity of different cells and tissues deputed to gravity sensing with a growth response occurring in spatially distinct regions. In roots, for example, the centrally located columella cells in the root cap are the proposed site of gravity sensing, but the growth response (root curvature) occurs in the elongation zone (EZ). The most common and accepted explanation for gravity sensing in plants is the starch-statolith hypothesis (which is the physical sedimentation of starch-filled organelles called amyloplasts (statoliths) in gravity-sensing cells (statocytes) located at the root tip) which triggers biochemical and physiological signals [2]. After the first event (sensing the change in the gravity vector/level) a signal is transduced and then transmitted to the EZ, stimulating the differential cellular growth mentioned above. This response is mainly driven by auxin [3], which accumulates to higher levels along the lower side of the root, thus provoking the inhibition of growth (Cholodny-Went theory). Recently, other investigators highlighted the role of cytoskeleton in the gravitropic response [4, 5]. Its central role in modulating cell polarity, organelle movement, intracellular transport, and cell expansion leads cytoskeleton to be a strong candidate in mediating the gravity signal transduction cascade (tensegrity model, [6]).

In the last years, experimental evidences depicted the structure of the root apex as divided into three different zones: a transition zone (TZ) located between two other regions, the apical division zone (DZ), and the elongation zone (EZ) [7]. The cells belonging to TZ have a specific cytoarchitecture, with centralized postmitotic nuclei surrounded by

perinuclear microtubules radiating toward the cell periphery. In contrast to the mitotically active DZ cells, which are continually assembling and disassembling mitotic spindles, the TZ cells are not deputed to perform these activities but to have more specific sensory activities [3]. Experimental data suggest that the TZ is more a sort of sensory and information processing zone, devoted to a continuous monitoring of the environmental parameters and triggering appropriate responses, rather than being implicated in the division and growth process. The TZ cells are very sensitive to a wide range of stress sources, such as touch [8], water and salt stress [9], aluminium [10], and hypoxia [11, 12]. However, little is known about the role of TZ cells in the graviresponse, especially related to the transduction/transmission phases after gravity sensing by the cells of the root tip.

Among key signalling molecules in plants, nitric oxide (NO) has recently emerged as an essential compound [13]. Among its tasks, NO regulates the actin cytoskeleton [14], endocytosis, vesicle trafficking, and the polarity of growing tip cells [15], root formation [16], and stomatal regulation [17]. In addition, NO is widely implicated in the plant response to environmental stress [18], but its exact role in the response of plants to change in gravity levels is still unclear and not well investigated.

Reactive oxygen species (ROS) such as H_2O_2 are generally considered to be toxic by-products of respiration. However, recent experiments suggest that the production of ROS should have an important and active role as components of intracellular and extracellular signalling [19]. In particular, H_2O_2 is starting to be accepted as a second messenger for signals generated by means of ROS because of its relatively long life and high permeability across membranes [20]. The role of ROS in the gravitropic response is still under debate, as this topic has been rarely investigated [21].

Elucidating the mechanisms behind the signal transmission from the site of gravity sensing to the site of gravibending is therefore the main objective of this paper, with particular interest towards the role of the root apex (and in particular the TZ) in the transduction process and the importance of sensing molecules, such as NO and H_2O_2, in the gravity response process. After preliminary experiments on ground using the method of gravistimulation via a horizontal displacement of the root, the response of maize seedlings to gravity changes has been studied for the first time ever in a real situation of microgravity, thanks to a set of experiments performed during three ESA parabolic flight campaigns and a drop tower campaign.

2. Materials and Methods

2.1. Gravistimulation on Ground. Oxygen flux measurements were performed using the vibrating probe technique [22]. Briefly, healthy *Z. mays* L. root apices (5-6 mm long) were cut, carefully washed with deionized water, and placed individually at the bottom of a measuring chamber containing an electrophysiological solution (10 mM $CaCl_2$, pH 6.5). The flux measurement was performed at 24 ± 0.25°C by positioning a custom-built oxygen-selective microelectrode (tip diameter of 1 μm [23, 24]) near the root surface. To ensure the flux detection on the bottom part of a gravistimulated root (gravistimulation was performed by rotating the seedling and the measurement system by 90 degrees) an electrode with a hooked tip was also built. During the recording, the microelectrode oscillated in a square wave parallel to the electrode axis over a distance of 10 μm (0.1 Hz frequency), moving along the entire root length. The calculation of the difference between the voltage of each electrode position and that of the previous one at the other extreme position as well as the evaluation of a moving average of these differences over any desired time period, producing the potential difference, were computer generated. The O_2 influxes were calculated using Fick's first law of diffusion, assuming a cylindrical diffusion geometry. The flux measurements were performed on at least 10 different root apices per treatment ($n \geq 10$).

To localize the production of NO in the different regions of the root apex with a spatial resolution of a few micrometers, a NO-selective microelectrode of carbon fibers with diameters as small as 5 μm was constructed [12], using the same system described above for the measurement. The dimensions and the response time (<0.5 s) allowed the use of this electrode in a self-referencing mode [23, 25] with a resolution as small as 50 fmol cm^{-2} s^{-1}.

2.2. Parabolic Flight Experiments. All parabolic flight experiments were conducted aboard the Airbus A300 ZERO-G, which is operated by Novespace and is based in Bordeaux, France. Every parabolic flight, which lasts ~3 h including takeoff and landing, encompasses 31 parabolas. Every parabola started from a steady normal horizontal flight and typically included 2 hypergravity (1.8 g) periods of 20 s, separated on average by a 22-s microgravity period (<0.05 g). The first test parabola was followed by 6 series of 5 parabolas, separated by breaks of 4 and 8 min, respectively. The data presented emerged from the 41st and 45th Parabolic Flight Campaigns (PFC) and the "Fly Your Thesis 2012" (student campaign) of the European Space Agency (ESA), representing a total of 8 parabolic flights or 248 parabolas.

During the 41st ESA Parabolic Flight Campaign (PFC), the measurements of oxygen influx/efflux from the seedling roots were conducted. For each parabolic flight of the PFC, a set of three 3-day-old seedlings of *Zea mays* L., with a homogeneous length of 5 ± 0.5 cm, have been installed into an Eppendorf vial (1 seedling = 1 vial) filled with an electrophysiological solution (10 mM $CaCl_2$, pH 6.5). The fourth vial was left empty and used as a control without seedlings. A couple of O_2 needle microsensors (OX50, Unisense, DK) have been horizontally inserted at two different levels for each vial, corresponding to the root apex and to the mature zone of the seedling root. The tip of the electrode was placed close to the root tissues (distance < 1 mm). The vials with the seedlings and the electrodes were placed inside a thermostated chamber (temperature = 24-25°C). Each electrode was connected to a picoammeter (PA2000, Unisense, DK), a four-channel laboratory amplifier that enables the measurement of multiple parameters. The output of the picoammeter was then connected to a datalogger. A dedicated LabView software on

a laptop recorded the oxygen measurement. Concurrently, an accelerometer provided gravity measurement.

During the 45th ESA PFC the respiration rate of detached root apices ($n = 6$, with known weight) from 3-day-old *Zea mays* L. seedlings was measured. The root apices were placed inside an oximeter chamber (Oxytherm, Hansatech Instruments) with controlled temperature (25°C). A small magnetic stirrer provided a continuous stirring of the solution. Measurements have been performed with the apices in distilled water or in a solution containing D'orenone (C_{18} ketone (5*E*,7*E*)-6-methyl-8-(2,6,6-trimethylcyclohex-1-enyl) octa-5,7-dien-2-one, 10 μg/mL). The oximeter chamber was connected to a laptop with a dedicated software for datalogging.

During the "Fly your thesis 2012" PFC campaign the production of H_2O_2 was assessed. The Amplex Red reagent was used after a preliminary evaluation in our lab, due to its high sensitivity and successful use for the measure of H_2O_2 production in plant root, as previously reported by [26]. We used the Amplex Red Hydrogen Peroxide/Peroxidase Assay Kit (Invitrogen, #A22188) in combination with horseradish peroxidase (HRP, Invitrogen), to detect H_2O_2 released from biological samples. In the presence of HRP Amplex red reagent reacts with H_2O_2 in a 1 : 1 stoichiometry to produce the red-fluorescent oxidation product, resorufin. As first step, the tips of maize roots were cut and immediately washed twice for 15 minutes in PBS to eliminate ROS derived from the cut. Tips were divided in samples constituted by 10 mg of fresh tissue. Then 50 μL of working solution (containing dye and HRP) was added to 10 mg of plant tissue (root), and the samples were incubated in a 96-well microplate at room temperature for 30 minutes, in darkness. During the flight, fluorescence was measured using excitation at 530 ± 12.5 nm and fluorescence detection at 590 ± 17.5 nm by using a microplate reader (Tecan Infinite 200 PRO). A datalogger connected to the Tecan and a laptop provided data storage, which were then normalised to plant biomass.

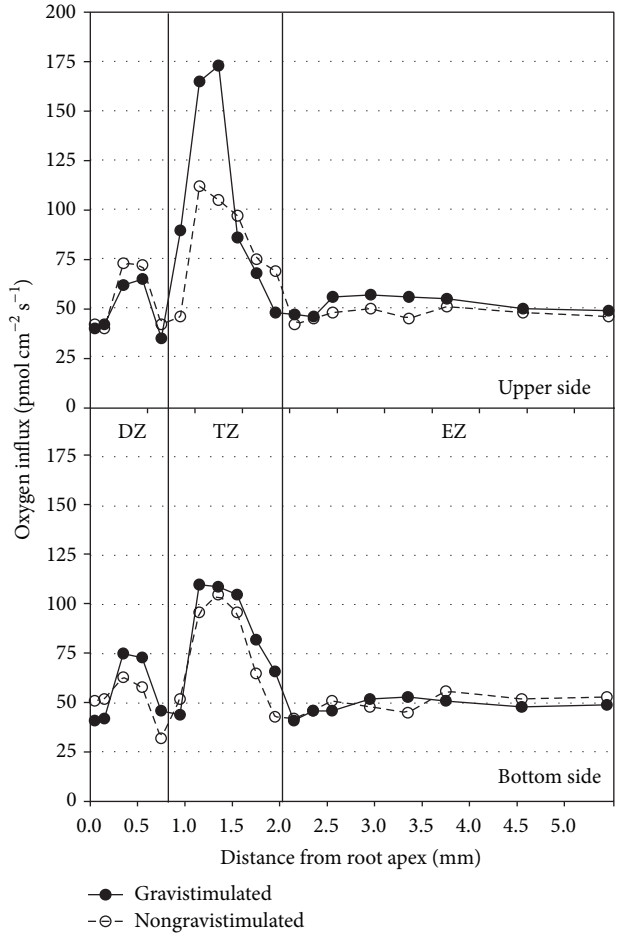

Figure 1: Oxygen influx measured on the two sides of a gravistimulated and a vertical root. Upper graph refers to the upper side of a gravistimulated root, whereas the second graph refers to the bottom side of a gravistimulated root.

2.3. Drop Tower Campaign. The Drop Tower in Bremen (Germany) is one of only a few facilities worldwide providing gravitational forces as small as 10^{-5} g, even if only for a short time of 4.7 seconds. The cylindrical falling capsule of a diameter of 80 cm, a height of 2.8 m, and a mass of 500 kg is dropped from 110 m height of the tower whose inner tube is evacuated within 2 h to an air pressure of less than 10 mPa. On the bottom of the tower the capsule (reaching 170 km h^{-1}) is decelerated within 130 ms by a huge basket of app. 2.5 × 8 m, filled with styropor grains. There the motion energy (6×10^5 Nm) is converted into heat. Gravitational sensors were provided by ZARM. Deceleration of the capsule leads to gravitational values of about 30 g. An oximeter (see Parabolic Flights section) was used and adapted for the measurement of nitric oxide by using selective microelectrodes (amiNO-30, Innovative Instruments Inc., USA) connected to a NO electrochemical detector with automatic temperature compensation (in NO-T-II, Innovative Instruments Inc., USA). The output of the detector was connected to a laptop via

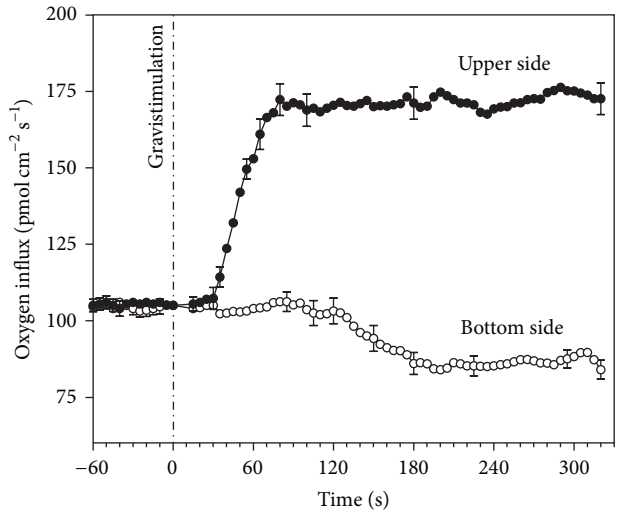

Figure 2: Timeline of the oxygen influx change at TZ level after gravistimulation (time = 0).

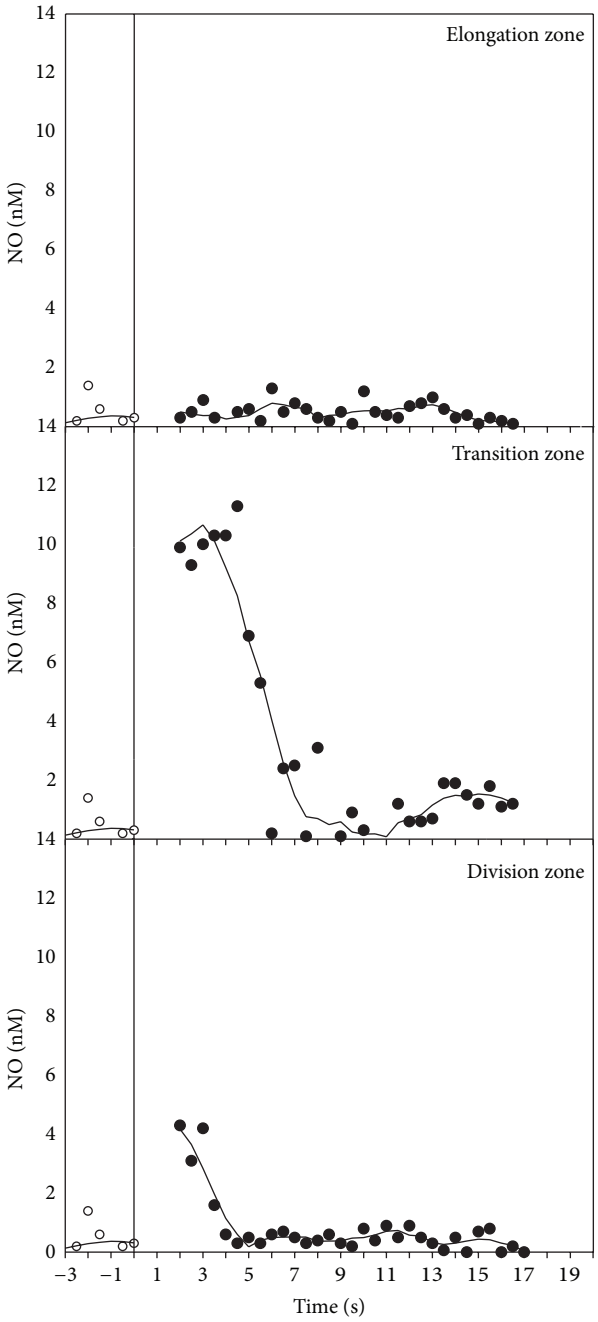

Figure 3: Timeline of the NO production in a maize root apex in the three different constituent zones after gravistimulation (time = 0).

USB port running the inNO-T-II specific software for data acquisition.

3. Results

3.1. Gravistimulation on Ground. In normal (vertical) conditions, strong differences between the constituent zones of the maize root (DZ, TZ, and EZ) were clearly evident. The TZ appeared to be the most active zone in the uptake of oxygen from the surrounding solution (Figure 1). The spatial patterns of the oxygen influxes in the entire root apex showed a marked peak in the TZ (110 pmol cm^{-2} s^{-1}) at 1–1.5 mm from the maize root tip. A minor oxygen influx peak (75 pmol cm^{-2} s^{-1}) was also evident in the DZ. Importantly, the TZ was the only root apex region significantly affected with regards to gravistimulation; in fact, the marked peak of oxygen influx was greatly enhanced in the upper part of the horizontal (gravistimulated) root, whereas the DZ maintained a similar pattern. On the contrary, the bottom side of the horizontal root showed a normal behaviour. The increase of oxygen influx at TZ level appeared as a very quick response following gravistimulation, as it was clearly evident after less than 30 seconds in the upper side of the root (Figure 2), while the bottom part remained unaffected.

Gravistimulation also promoted a very fast NO production from the root apex (Figure 3). A burst of NO was suddenly produced after only 2-3 seconds from gravistimulation, reaching a peak of 10 nM and lasting approximately 8 s before returning to the steady-state values in the TZ. Only a small and negligible efflux of NO was detectable in the DZ, and, importantly, NO bursts were not detected in the EZ region.

Table 1: Average time of burst appearance calculated for different groups of parabolas. Data were analyzed by ANOVA, using Tukey's test ($P < 0.05$).

Group of parabolas	Average time (secs)	Standard deviation	Significance
1–10	2.51	1.08	ns
11–20	2.65	1.22	ns
21–30	2.07	0.99	ns
1–30	2.4	1.1	—

3.2. Parabolic Flight and Drop Tower Campaigns. A typical parabola is shown in Figure 4, with a period of microgravity (<0.05 g, 20–22 secs) inserted between two periods of hypergravity (1.8 g, 20 secs). Oxygen concentrations in the solution measured at two different root levels (root apex and mature zone) are also reported for three different parabolas. Bursts and peaks of oxygen concentration are clearly evident at root apex level during the microgravity periods, with significant detection during the entire flight. Interestingly, no peaks were detected in the mature zone and during hypergravity periods in the root apex. Control without seedlings showed no activity, demonstrating that the results previously shown were not related to a background noise of the microelectrodes during microgravity.

For each parabola, the average detection time (T_1) of the first oxygen peaks from the start of the microgravity period ($g < 1$, T_0; see Figure 5) has been calculated. The average time for all the parabolas is 2.4 secs. In order to evaluate a difference in the appearance of the first peak during the flight, the parabolas have been separated in three different groups (Table 1). Each group was composed of 10 parabolas. The objective was to investigate if a sort of "memory effect" of the stimulus during the repeated parabolas could cause a

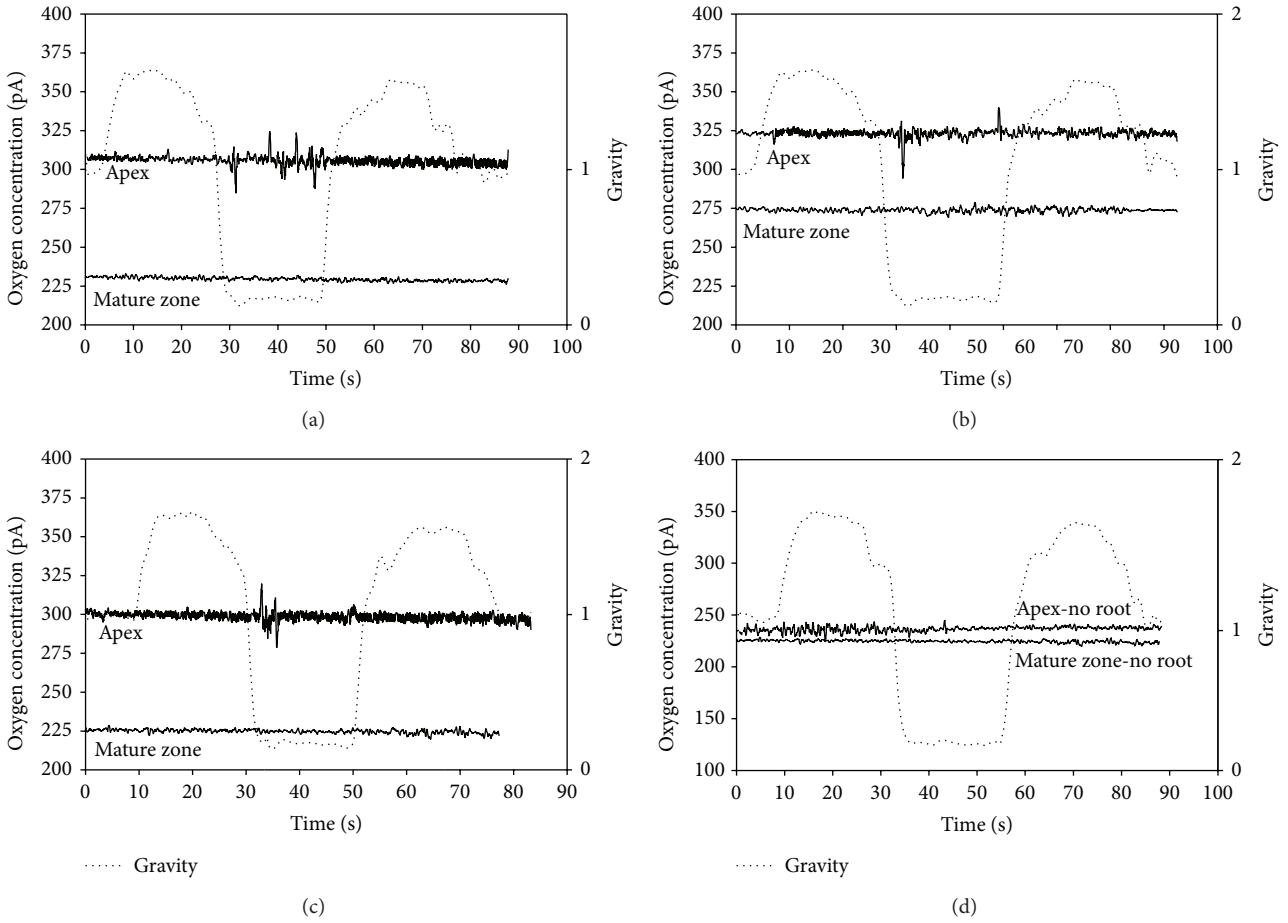

Figure 4: Oxygen concentration in the solution measured at two different levels, close to (distance < 1 mm) the root apex and to the root mature zone during three different parabolas: one parabola at the beginning (a), one in the middle (b), and one at the end of the experiment (c). Control experiment with no roots inside the Eppendorf vial is shown in (d).

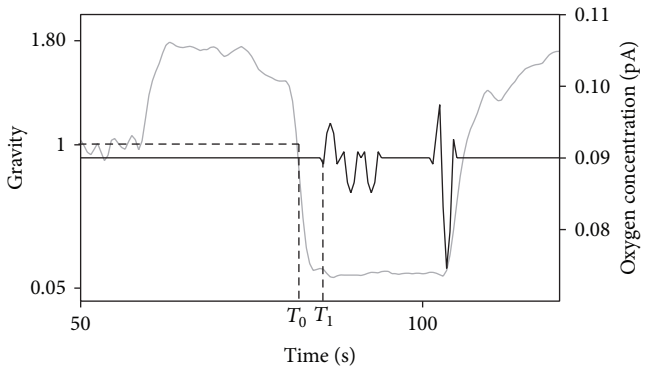

Figure 5: Timeline of burst appearance (T_1) after the onset of microgravity (T_0) during a parabola.

different response during the time of the flight (higher/lower, anticipated/retarded). The results showed a reduction, but not statistically significant, in the onset of the first peak during the last set of parabolas.

Interesting results have been also obtained from the measurement of the respiration rate by oximeters. The respiration rate inside a single parabola has been divided into five segments, each segment being related to a different gravity level: 1 g, 2 g, 0 g, 2 g (after microgravity), and 1 g (after microgravity). Negative values indicate oxygen influx. Respiration by root apices led to an unavoidable reduction of the oxygen content in the solution due to the plant metabolism; thus the parabolas have been divided into different groups by taking into account the real oxygen concentration because the respiration rate is directly related to the amount of oxygen present in the solution. Four groups related to different $[O_2]$ in the solution have been therefore created: >1500 nM, 1000–1500 nM, 500–1000 nM, and <500 nM. The values relative to the control (Figure 6) show no significant differences among the different gravity levels in each parabola for every oxygen concentration group, except for the last group ($[O_2]$ < 500 nM) with an increased respiration rate during the second period of hypergravity. On the contrary, the presence of D'orenone in the solution did not lead to any variation neither in the respiration rate among the different gravity levels nor compared to the control (Figure 7).

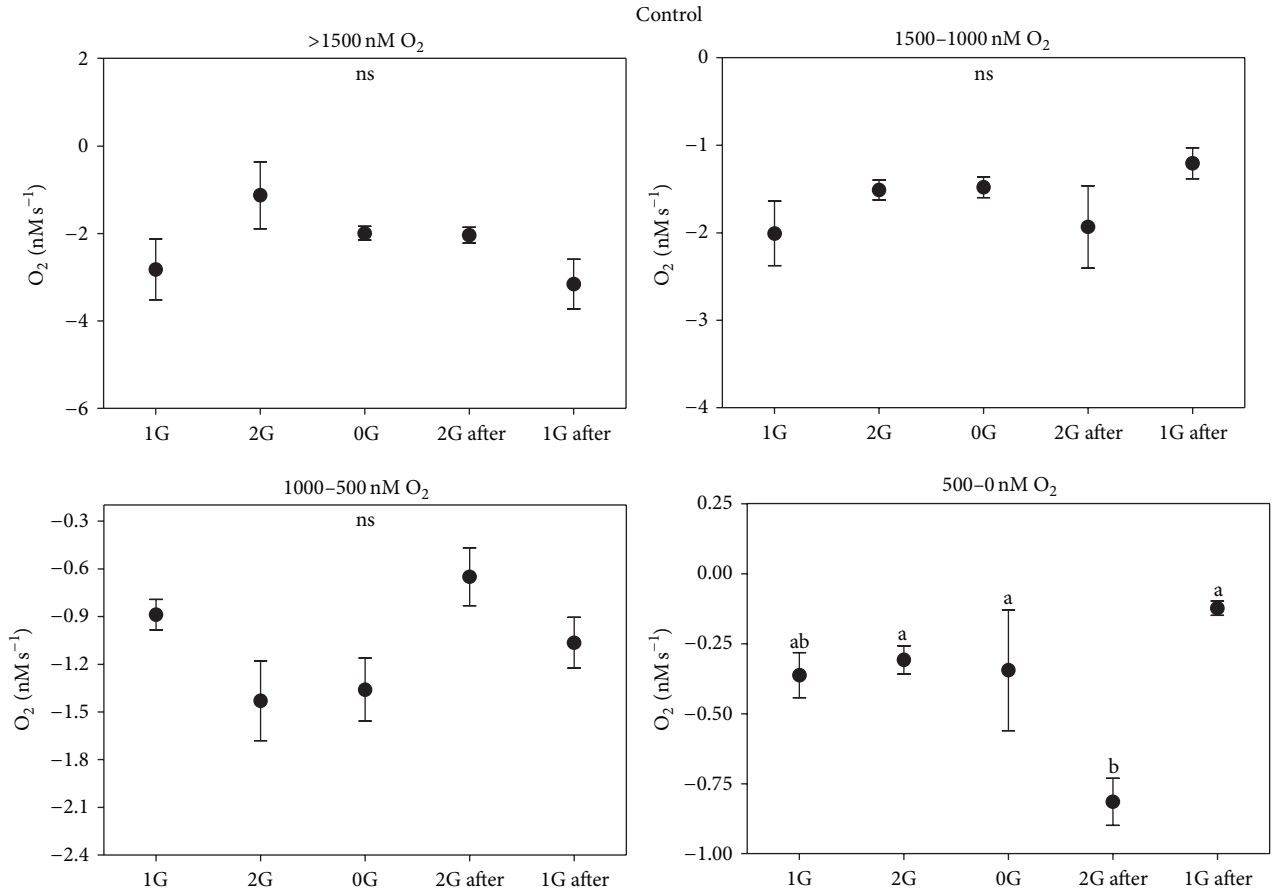

Figure 6: Respiration rate in control roots for the different groups related to the oxygen concentration in the solution.

D'orenone has been utilized in this experiment because it increases PIN2 protein abundance without affecting PIN2 transcripts, with the consequence that the PIN2 expression domain enlarges and shifts basipetally, resulting in more active auxin transport. To deeply analyse the previous results, the behaviour of the respiration rate during a single parabola has been evaluated. It has been noted that when $[O_2]$ was < 700 nM, a sudden burst of oxygen was produced only in the control a few seconds after the onset of microgravity (Figure 8). This large amount of oxygen was quickly absorbed by the roots for respiration, thus explaining the increased respiration rate during the second hypergravity period. This phenomenon was clearly evident during each parabola with $[O_2]$ < 700 nM. The fact that the bursts were evident only when $[O_2]$ < 700 nM was probably due to the electrode sensitivity, which was not able to discriminate very low differences in the respiration rate (around 25 nM) with higher oxygen concentrations in the solution. These oxygen bursts have been characterised by calculating the area inside the curve (Figure 9). The values of area, response time after the onset of microgravity, peak duration, and peak amplitude are reported in Figure 10, with a discrimination based on the parabolas' groups. No significant differences among the groups were noted in the peak area, with an average value of 274.73 nM representing the moles of oxygen produced during the microgravity period and then consumed, in the response time after the onset of microgravity (average value of 0.79 seconds) and the timing of the maximum peak (11.03 seconds). On the contrary, significant differences among groups were registered in the peak duration. The first 20 parabolas had an average peak duration of 20-21 seconds, while the last 10 parabolas had a longer duration (average value around 30 seconds). Finally, peak amplitude showed no significant differences. As expected, when no roots were present in the oximeter, a stable signal was registered (data not shown).

Production of H_2O_2 measured with Amplex Red is shown in Figure 11. Data were grouped according to the class of gravity level. Data recorded during microgravity (0 g) were statistically compared with data recorded during normogravity (1 g) and hypergravity (2 g) conditions. Transition from 1 g to 2 g and 2 g to 1 g had no significant effect on H_2O_2. On the contrary, transition from 2 g to 0 g results stimulated a higher H_2O_2 production from the root samples. Interestingly, we did not observe any difference in H_2O_2 production between 2 g condition in comparison to 1 g. Control experiment without any root tip inside the microplate showed no significant difference between all the gravity levels (data not shown).

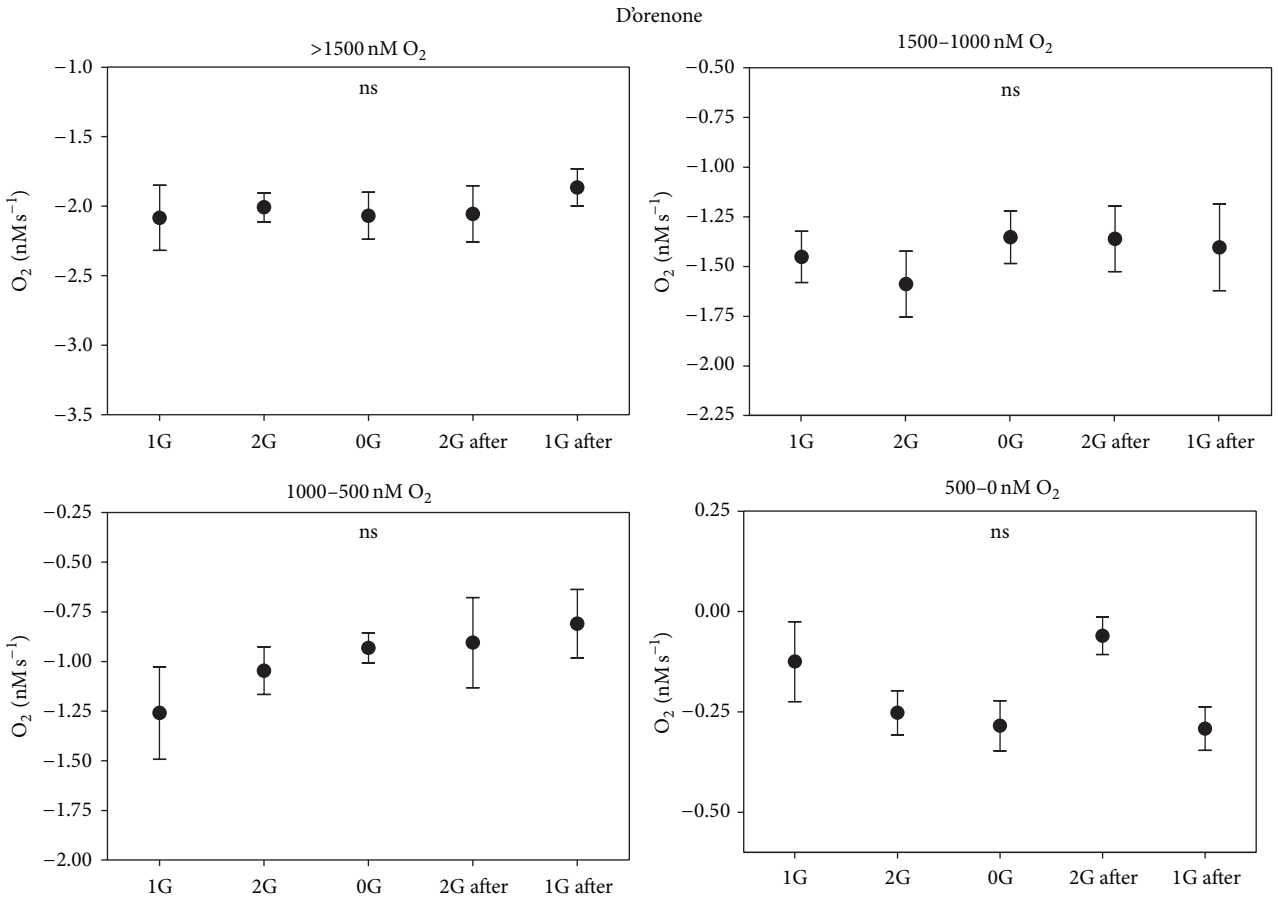

Figure 7: Respiration rate in roots incubated in D'orenone for the different groups related to the oxygen concentration in the solution.

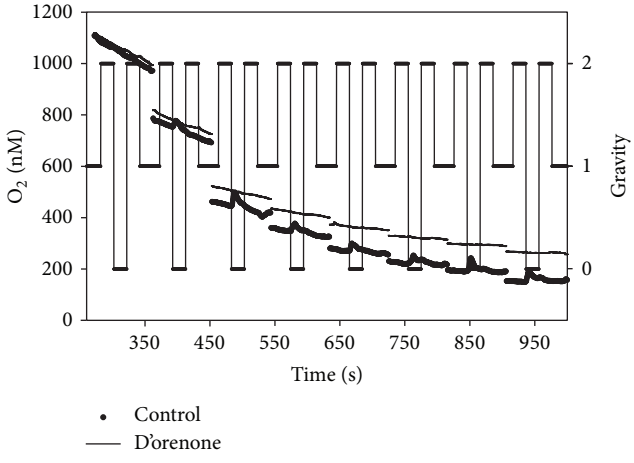

Figure 8: Respiration rate during single parabolas when [O_2] in the solution was <700 nM. Both control roots and roots incubated in D'orenone are reported.

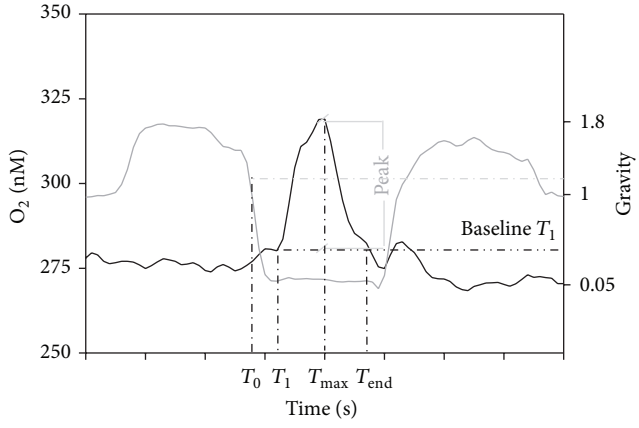

Figure 9: Characterisation of an oxygen burst measured with an oximeter: T_0 is the time of the onset of microgravity; T_1 is the time when the burst of oxygen begins. Its value in the Y-axis is taken as the baseline for the calculation of the area, amplitude, and duration between T_1 and T_{end}.

Finally, the production of NO was detected and evaluated during an ESA Drop Tower campaign (Figure 12). Interestingly, a burst of NO was clearly evident after 2 seconds from the start of the microgravity period, which then started to decline, resembling the behaviour of the gravistimulated roots on ground. Oximeter chambers without roots showed

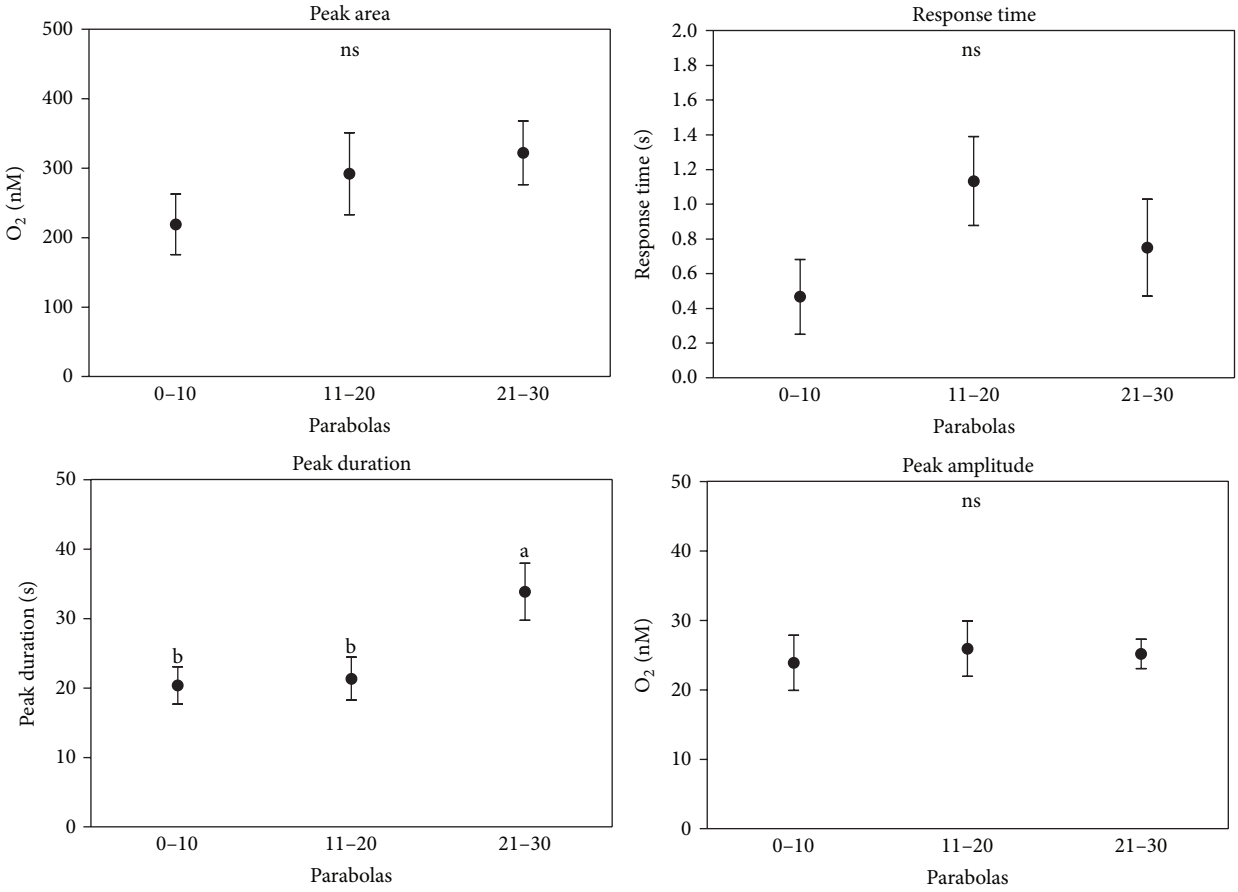

FIGURE 10: Peak area, response time, peak duration, and peak amplitude measured for different groups of parabolas by using the method described in Figure 9.

no bursts or signal detected by the microelectrode (data not shown).

4. Discussion

Although both sensing (Cholodny-Went theory and tensegrity model) and signal transduction (role of auxin in the root bending) in the gravitropic response are well and comprehensively described in the literature, little is known about the grey area of signal transmission, the series of events comprised between sensing and bending. Hu et al. [27] reported that gravistimulation induced the asymmetric accumulation of nitric oxide (NO) on the lower side of the apical region of gravistimulated (horizontal) soybean seedling roots, leading to a subsequent auxin accumulation in the upper part. Our results confirmed this hypothesis, with a massive production of NO in a very short time (2-3 seconds). Moreover, we also integrated these results with the interesting information that the NO is mainly produced at TZ level, thus confirming the role of TZ as a sensing zone of the root, directly and actively implicated in the response to gravity changes.

Gravistimulation also induced a sudden burst of oxygen in the upper part of TZ level 20–30 seconds after gravistimulation. Our results suggest the hypothesis that after the displacement of statolythes under gravistimulation, the chain of events is related to a sudden emission of NO which leads to an improved plant metabolism which needs more oxygen for respiration, especially at TZ level, to produce ATP to be used as a source of energy. Rapid changes in cytosolic Ca^{2+} and pH have been proposed as components of the gravisignaling machinery [28]; therefore it is plausible that the control of Ca^{2+} and H^+ channels would require more ATP (i.e., more oxygen consumption) after gravistimulation and during microgravity. The fact that oxygen burst at TZ level following gravistimulation can be inhibited by BFA [3] and that TZ shows significant higher auxin secretion via the endocytic vesicle recycling [29] might correlate the oxygen bursts observed during gravistimulation/under microgravity and the auxin metabolism, thus provoking a differential growth response.

In plants, the simultaneous generation of O_2 and NO has a synergistic function in defense responses [30], as well as in plants exposed to abiotic stress [31]. NO is also generated at the same time as ROS, such as hydrogen peroxide, for example, during abiotic stress [32]. Root gravitropism appears to be another example of a physiological process in which both NO and ROS play key roles in a simultaneous way [33], as ROS were recently associated with auxin-mediated gravitropic

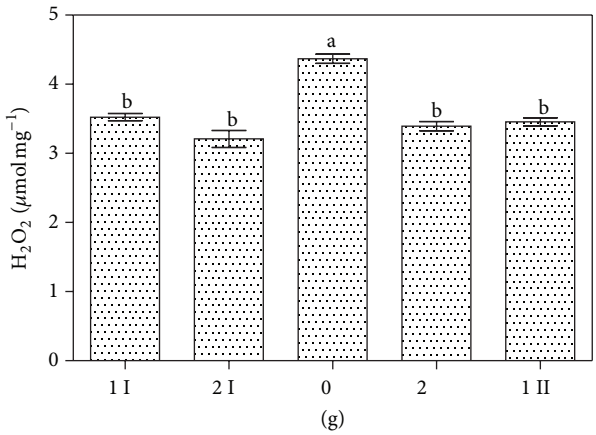

Figure 11: H_2O_2 production measured with Amplex Red during different gravity conditions. The letters I and II refer to the 1 g and 2 g phases prior (I) and after (II) the 0 g condition. Data are presented as average among each parabola of two parabolic flight days (62 parabolas in total are considered). Data were analyzed by ANOVA. Data statistically different are indicated with different letters ($P < 0.05$). Error bars are also indicated.

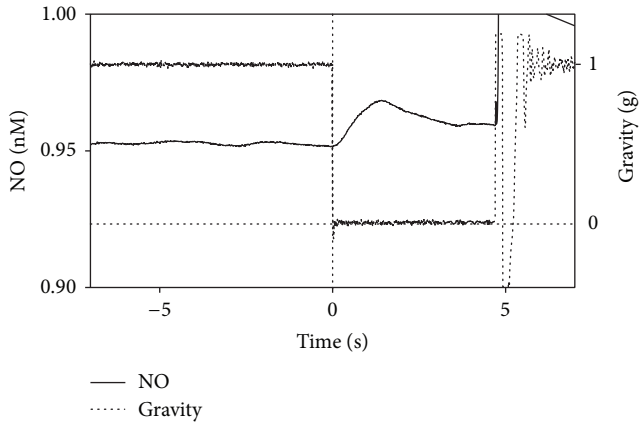

Figure 12: Typical nitric oxide curve measured in the oximeter chamber during a drop in the ESA Drop Tower campaign.

responses in maize [21] and in the graviresponsive pulvinus of maize [34]. In gravistimulated roots, ROS accumulated asymmetrically to the lower cortex within 30 min of reorientation, becoming symmetrical upon longer stimulation [21]. Interestingly, Long et al. [35] have shown that auxin asymmetries are detectable only after 2 h of gravistimulation of the pulvinus, making the ROS changes reported much faster than the generation of gradients in auxin and so, in contrast to the conclusions from the gravitropically responding root, possibly placing them upstream of the action of this hormone. Our results support this hypothesis, with the generation of an oxygen burst after a few seconds after the onset of microgravity, which could be directly linked to the production of ROS as a stress messenger. The fact that the respiration rate in root apices increased during microgravity could also be related to the necessity of activating defensive and scavenging mechanisms for ROS molecules. In fact, the production of ROS during real microgravity has been confirmed during a parabolic flight campaign.

D'orenone rapidly and significantly activates the DR5 promoter [36] and also targets processes that are related to PIN2 degradation [16], causing slower turnover and increased protein levels of this auxin efflux transporter, thus suggesting that this apocarotenoid interacts with auxin signaling at the root apex. Our results indicate that D'orenone has also an inhibitor activity on the respiration rate and on the oxygen production, thus giving indirect clue to a link between the sudden increase of oxygen during microgravity and auxin redistribution via PIN2 activity which is one of the major responses to changes in the gravity vector/levels.

5. Conclusions

For the first time ever, a systemic and comprehensive series of experiments concerning the role of oxygen and stress messengers (NO and ROS) during a real microgravity environment has been conducted. The timeline and the cascade of events detected during these experiments suggest an active role of NO and ROS during the transmission step of the gravity response, with probable implications in the auxin redistribution.

Conflict of Interests

The authors declare that there is no conflict of interests regarding the publication of this paper.

Acknowledgments

The authors would like to thank ESA (European Space Agency), Novespace, and ZARM for their kind support during the parabolic flight campaigns and the drop tower campaigns.

References

[1] D. Volkmann and F. Baluška, "Gravity: one of the driving forces for evolution," *Protoplasma*, vol. 229, no. 2–4, pp. 143–148, 2006.

[2] E. B. Blancaflor, "Regulation of plant gravity sensing and signaling by the actin cytoskeleton," *American Journal of Botany*, vol. 100, no. 1, pp. 143–152, 2013.

[3] F. Baluska and S. Mancuso, "Root apex transition zone as oscillatory zone," *Frontiers in Plant Science*, vol. 4, article 354, 2013.

[4] H. Tatsumi, T. Furuichi, M. Nakano et al., "Mechanosensitive channels are activated by stress in the actin stress fibres, and could be involved in gravity sensing in plants," *Plant Biology*, vol. 16, pp. 18–22, 2014.

[5] F. Baluka and D. Volkmann, "Mechanical aspects of gravity-controlled growth, development and morphogenesis," in *Mechanical Integration of Plant Cells and Plants*, pp. 195–223, Springer, Berlin, Germany, 2011.

[6] Y. Chebli and A. Geitmann, "Gravity research on plants: use of single-cell experimental models," *Frontiers in Plant Science*, vol. 2, no. 56, pp. 1–10, 2011.

[7] F. Baluška, S. Mancuso, D. Volkmann, and P. W. Barlow, "Root apex transition zone: a signalling-response nexus in the root," *Trends in Plant Science*, vol. 15, no. 7, pp. 402–408, 2010.

[8] H. Ishikawa and M. L. Evans, "Induction of curvature in maize roots by calcium or by thigmostimulation: role of the postmitotic isodiametric growth zone," *Plant Physiology*, vol. 100, no. 2, pp. 762–768, 1992.

[9] E. S. Ober and R. E. Sharp, "Electrophysiological responses of maize roots to low water potentials: relationship to growth and ABA accumulation," *Journal of Experimental Botany*, vol. 54, no. 383, pp. 813–824, 2003.

[10] M. Amenós, I. Corrales, C. Poschenrieder, P. Illéš, F. Baluška, and J. Barceló, "Different effects of aluminum on the actin cytoskeleton and brefeldin A-sensitive vesicle recycling in root apex cells of two maize varieties differing in root elongation rate and aluminum tolerance," *Plant and Cell Physiology*, vol. 50, no. 3, Article ID pcp013, pp. 528–540, 2009.

[11] S. Mugnai, A. M. Marras, and S. Mancuso, "Effect of hypoxic acclimation on anoxia tolerance in vitis roots: response of metabolic activity and K^+ Fluxes," *Plant and Cell Physiology*, vol. 52, no. 6, pp. 1107–1116, 2011.

[12] S. Mugnai, E. Azzarello, F. Baluška, and S. Mancuso, "Local root apex hypoxia induces no-mediated hypoxic acclimation of the entire root," *Plant and Cell Physiology*, vol. 53, no. 5, pp. 912–920, 2012.

[13] M. Simontacchi, C. García-Mata, C. G. Bartoli, G. E. Santa-María, and L. Lamattina, "Nitric oxide as a key component in hormone-regulated processes," *Plant Cell Reports*, vol. 32, no. 6, pp. 853–866, 2013.

[14] K. A. Wilkins, J. Bancroft, M. Bosch, J. Ings, N. Smirnoff, and V. E. Franklin-Tong, "Reactive oxygen species and nitric oxide mediate actin reorganization and programmed cell death in the self-incompatibility response of papaver," *Plant Physiology*, vol. 156, no. 1, pp. 404–416, 2011.

[15] M. C. Lombardo and L. Lamattina, "Nitric oxide is essential for vesicle formation and trafficking in Arabidopsis root hair growth," *Journal of Experimental Botany*, vol. 63, no. 13, pp. 4875–4885, 2012.

[16] M. Schlicht, J. Ludwig-Müller, C. Burbach, D. Volkmann, and F. Baluska, "Indole-3-butyric acid induces lateral root formation via peroxisome-derived indole-3-acetic acid and nitric oxide," *New Phytologist*, vol. 200, no. 2, pp. 473–482, 2013.

[17] A. M. Distéfano, D. Scuffi, C. García-Mata, L. Lamattina, and A. M. Laxalt, "Phospholipase Dδ is involved in nitric oxide-induced stomatal closure," *Planta*, vol. 236, no. 6, pp. 1899–1907, 2012.

[18] W. Qiao, C. Li, and L. M. Fan, "Cross-talk between nitric oxide and hydrogen peroxide in plant responses to abiotic stresses," *Environmental and Experimental Botany*, vol. 100, pp. 84–93, 2014.

[19] S. S. Gill and N. Tuteja, "Reactive oxygen species and antioxidant machinery in abiotic stress tolerance in crop plants," *Plant Physiology and Biochemistry*, vol. 48, no. 12, pp. 909–930, 2010.

[20] L. J. Quan, B. Zhang, W. W. Shi, and H. Y. Li, "Hydrogen peroxide in plants: a versatile molecule of the reactive oxygen species network," *Journal of Integrative Plant Biology*, vol. 50, no. 1, pp. 2–18, 2008.

[21] J. H. Joo, Y. S. Bae, and J. S. Lee, "Role of auxin-induced reactive oxygen species in root gravitropism," *Plant Physiology*, vol. 126, no. 3, pp. 1055–1060, 2001.

[22] C. Pandolfi, S. Pollastri, E. Azzarello, E. Masi, S. Mugnai, and S. Mancuso, "The vibrating probe technique in root studies," in *Measuring Roots*, pp. 67–81, Springer, Berlin, Germany, 2011.

[23] S. Mancuso, G. Papeschi, and A. M. Marras, "A polarographic, oxygen-selective, vibrating-microelectrode system for the spatial and temporal characterisation of transmembrane oxygen fluxes in plants," *Planta*, vol. 211, no. 3, pp. 384–389, 2000.

[24] S. Mancuso and A. M. Marras, "Different pathways of the oxygen supply in the sapwood of young *Olea europaea* trees," *Planta*, vol. 216, no. 6, pp. 1028–1033, 2003.

[25] S. Mancuso and M. Boselli, "Characterisation of the oxygen fluxes in the division, elongation and mature zones of Vitis roots: influence of oxygen availability," *Planta*, vol. 214, no. 5, pp. 767–774, 2002.

[26] R. Shin, R. H. Berg, and D. P. Schachtman, "Reactive oxygen species and root hairs in arabidopsis root response to nitrogen, phosphorus and potassium deficiency," *Plant and Cell Physiology*, vol. 46, no. 8, pp. 1350–1357, 2005.

[27] X. Hu, S. J. Neill, Z. Tang, and W. Cai, "Nitric oxide mediates gravitropic bending in soybean roots," *Plant Physiology*, vol. 137, no. 2, pp. 663–670, 2005.

[28] G. B. Monshausen, N. D. Miller, A. S. Murphy, and S. Gilroy, "Dynamics of auxin-dependent Ca^{2+} and pH signaling in root growth revealed by integrating high-resolution imaging with automated computer vision-based analysis," *The Plant Journal*, vol. 65, no. 2, pp. 309–318, 2011.

[29] S. Mancuso, A. M. Marras, V. Magnus, and F. Baluška, "Noninvasive and continuous recordings of auxin fluxes in intact root apex with a carbon nanotube-modified and self-referencing microelectrode," *Analytical Biochemistry*, vol. 341, no. 2, pp. 344–351, 2005.

[30] S. Asai, K. Mase, and H. Yoshioka, "A key enzyme for flavin synthesis is required for nitric oxide and reactive oxygen species production in disease resistance," *Plant Journal*, vol. 62, no. 6, pp. 911–924, 2010.

[31] G. Tanou, A. Molassiotis, and G. Diamantidis, "Hydrogen peroxide- and nitric oxide-induced systemic antioxidant prime-like activity under NaCl-stress and stress-free conditions in citrus plants," *Journal of Plant Physiology*, vol. 166, no. 17, pp. 1904–1913, 2009.

[32] S. J. Neill, R. Desikan, and J. T. Hancock, "Nitric oxide signalling in plants," *New Phytologist*, vol. 159, no. 1, pp. 11–35, 2003.

[33] S. Swanson and S. Gilroy, "ROS in plant development," *Physiologia Plantarum*, vol. 138, no. 4, pp. 384–392, 2010.

[34] A. M. Clore, S. M. Doore, and S. M. N. Tinnirello, "Increased levels of reactive oxygen species and expression of a cytoplasmic aconitase/iron regulatory protein 1 homolog during the early response of maize pulvini to gravistimulation," *Plant, Cell and Environment*, vol. 31, no. 1, pp. 144–158, 2008.

[35] J. C. Long, W. Zhao, A. M. Rashotte, G. K. Muday, and S. C. Huber, "Gravity-stimulated changes in auxin and invertase gene expression in maize pulvinal cells," *Plant Physiology*, vol. 128, no. 2, pp. 591–602, 2002.

[36] M. Schlicht, O. Šamajová, D. Schachtschabel et al., "D'orenone blocks polarized tip growth of root hairs by interfering with the PIN2-mediated auxin transport network in the root apex," *The Plant Journal*, vol. 55, no. 4, pp. 709–717, 2008.

Hindawi Publishing Corporation
BioMed Research International
Volume 2014, Article ID 904396, 14 pages
http://dx.doi.org/10.1155/2014/904396

Research Article

Cytoskeleton Modifications and Autophagy Induction in TCam-2 Seminoma Cells Exposed to Simulated Microgravity

Francesca Ferranti,[1,2] Maria Caruso,[2] Marcella Cammarota,[3] Maria Grazia Masiello,[4,5] Katia Corano Scheri,[2] Cinzia Fabrizi,[2] Lorenzo Fumagalli,[2] Chiara Schiraldi,[3] Alessandra Cucina,[5,6] Angela Catizone,[2] and Giulia Ricci[3]

[1] *Italian Space Agency (ASI), Via del Politecnico snc, 00133 Rome, Italy*
[2] *Department of Anatomy, Histology, Forensic Medicine and Orthopedics, Sapienza University of Rome, Viale Regina Elena 336, 00161 Rome, Italy*
[3] *Department of Experimental Medicine, Second University of Naples, Via Santa Maria di Costantinopoli 16, 80138 Naples, Italy*
[4] *Department of Clinical and Molecular Medicine, Sapienza University of Rome, Viale Regina Elena 291, 00161 Rome, Italy*
[5] *Systems Biology Group, Sapienza University of Rome, Via A. Scarpa 16, 00161 Rome, Italy*
[6] *Department of Surgery "Pietro Valdoni," Sapienza University of Rome, Viale del Policlinico 155, 00161 Rome, Italy*

Correspondence should be addressed to Giulia Ricci; giulia.ricci@unina2.it

Received 12 May 2014; Revised 4 July 2014; Accepted 4 July 2014; Published 17 July 2014

Academic Editor: Mariano Bizzarri

The study of how mechanical forces may influence cell behavior via cytoskeleton remodeling is a relevant challenge of nowadays that may allow us to define the relationship between mechanics and biochemistry and to address the larger problem of biological complexity. An increasing amount of literature data reported that microgravity condition alters cell architecture as a consequence of cytoskeleton structure modifications. Herein, we are reporting the morphological, cytoskeletal, and behavioral modifications due to the exposition of a seminoma cell line (TCam-2) to simulated microgravity. Even if no differences in cell proliferation and apoptosis were observed after 24 hours of exposure to simulated microgravity, scanning electron microscopy (SEM) analysis revealed that the change of gravity vector significantly affects TCam-2 cell surface morphological appearance. Consistent with this observation, we found that microtubule orientation is altered by microgravity. Moreover, the confocal analysis of actin microfilaments revealed an increase in the cell width induced by the low gravitational force. Microtubules and microfilaments have been related to autophagy modulation and, interestingly, we found a significant autophagic induction in TCam-2 cells exposed to simulated microgravity. This observation is of relevant interest because it shows, for the first time, TCam-2 cell autophagy as a biological response induced by a mechanical stimulus instead of a biochemical one.

1. Introduction

An increasing number of experimental observations have demonstrated that tissue homeostasis could be strongly influenced and regulated by physical forces, such as the modulation of gravity vector. In the recent years, many efforts have been made to elucidate the effect of microgravity on cell behavior, and accumulating data show that microgravity alters, permanently or transiently, important biological processes such as mitosis, differentiation, survival, cell morphology, and gene expression profiles [1–7]. However, how cells sense these signals and convert them into a biochemical response remains an important question that needs to be addressed. Recent studies have focused on the cytoskeleton as initial gravity sensor [1, 8]. Cytoskeleton plays important roles in cell physiology being responsible for chromosomal segregation during mitosis, providing a mechanical support to dividing cells, contributing to maintain cell shape and

spatially organizing cell proteins and organelles in cell cytoplasm. Moreover, cytoskeleton is involved in cell motility, membrane trafficking, signal transduction, and cell adhesion. In addition, cytoskeletal proteins can transduce and amplify membrane receptor-captured signals, transmitting the information to the nucleus and finally regulating gene expression [2, 9, 10]. Considering all these observations, it appears easy to understand why cytoskeleton disorganization could compromise a lot of cell functions leading, in some cases, to cell death. It is well known that microgravity exposure could strongly influence cytoskeleton organization [10–17] and it is commonly accepted that cellular tensegrity alteration in microgravity exposed cells could explain, at least in part, the conversion of a mechanical cue into a biological response. In this regard, recent studies have revealed the importance of cytoskeletal integrity, such as F-actin and microtubules, in the physiological specific aspects of autophagy, and some papers described the capability of microgravity to induce autophagy in living cells [18–22]. Autophagy is an important housekeeping physiological process that is involved in cellular remodeling during development, elimination of aberrant organelles, or misfolded proteins and in the recycling of unnecessary cellular components to compensate for the limitation of nutrients during starvation. It is of interesting notice that this biological process is highly conserved from yeast to mammals. Despite several studies suggested a tumor suppressive role for autophagy, other reports support the hypothesis that this process is instead exploited by cancer cells to prime their proliferation and promote their survival [23–27].

Microgravity condition is a stressful change in the physical microenvironment for living cells; however, they seem to be able to adapt to this change of gravitational force since in the major part of studies available in the literature, the behavioral cellular modifications induced by microgravity are transient. This observation has led to the intriguing hypothesis that cells, in response to gravity changes, react triggering adaptive biological processes and autophagy could be one of them.

Testicular cells appear to be sensitive to microgravity: it has been demonstrated, in fact, that testicular function is impaired by microgravity exposure [28–34]. Moreover, some in vitro observations revealed that microgravity influences cell proliferation, apoptosis, and testosterone secretion of testicular organ cultures [35, 36]. In addition, microgravity condition has differentiating effect in cultured spermatocytes and influences germ cell survival [37, 38]. This effect on male germ cell lineage has triggered the hypothesis that also testicular cancer germ cells could be altered by microgravity condition. For this reason, we decided to study the effect of microgravity on TCam-2 cells that are the only accredited seminoma cell line [39–42]. These cells have been recently characterized at molecular and biochemical level [43–51] and thus represent a good tool to investigate male germ cell behavior modification in response to a mechanical force modification. In this paper we report, for the first time, cytoskeletal modifications and the activation of autophagic process induced by acute exposure to microgravity in TCam-2 cell line.

2. Materials and Methods

2.1. Random Positioning Machine. The random positioning machine (RPM; desktop RPM, Dutch Space, Leiden, the Netherlands), we used in the investigation, is a particular kind of 3D clinostat. It consists of two independently rotating frames. One frame is positioned inside the other giving a very complex net change of orientation to a biological sample mounted in the middle. The degree of microgravity simulation depends on angular speed and on the inclination of the disk. These tools do not actually eliminate the gravity but it is a microweight simulator based on the principle of "gravity-vector averaging": it allows you to apply a 1 g stimulus omnidirectionally rather than unidirectionally and the sum of the gravitational force vectors tends to zero. Effects generated by the RPM are comparable to those of the real microgravity, provided that the direction changes are faster than the response time of the system to gravity field. The desktop RPM we used has been positioned within an incubator (for maintaining temperature, CO_2, and humidity levels) and connected to the control console through standard electric cables.

2.2. TCam-2 Cell Cultures. The TCam-2 human cell line was derived in 1993 from a primary testicular tumor sample of pure classical seminoma [42]. TCam-2 cells were cultured in RPMI 1640 (Lonza) supplemented with 10% fetal bovine serum (FBS, Lonza) and penicillin/streptomycin (Invitrogen) at 37°C in a humidified atmosphere with 5% carbon dioxide [41]. The time 0 plating cell density is $3 \times 10^4/\text{cm}^2$. As described in the paragraph above, microgravity condition was simulated using the random positioning machine (RPM). Experiments were performed on cells cultured for 24 and 48 hours at 1 g or in RPM, after additional 24 hours of preplating on glass slides or IBIDI microscopy chambers (IBIDI, 80826). Glass slides were silicone fixed to the culture dishes at least 48 hours before plating. Cell culture dishes, in both 1 g and RPM culture conditions, were completely filled with fresh culture medium in order to avoid air bubbles and to minimize liquid flow, thus making negligible the effects of both buoyancy and shear stress during rotation.

2.3. Proliferation, Apoptosis, and Autophagy Quantification. Cells cultured at 1 g or under microgravity conditions (as described above) were fixed in 4% paraformaldehyde (PFA) in phosphate buffered saline (PBS) 1X for 10 minutes at 4°C and permeabilized with 1% bovine serum albumin (BSA), 0.1%-Triton X-100 in PBS 1X for 1 hour at room temperature (RT). Nonspecific antibody binding was blocked with glycine 1 M pH 8.8 and with 1% BSA, 0.1% Triton X-100, and 5% donkey serum (Jackson ImmunoResearch Laboratories) in PBS 1X. Cells were incubated overnight (ON) in PBS 1X added with 1% BSA/0.1% Triton X-100 at 4°C with the following primary antibodies: anticleaved Caspase-3 (Cell Signaling, rabbit polyclonal #9661, 1 : 200 dilution), anti-p-histone H3 (Santa Cruz Biotechnology, mouse monoclonal sc-374669, 1 : 50 dilution), or anti-LC3 (Sigma-Aldrich, L7543 1 : 120 dilution). After rinsing, samples were incubated with

the opportune secondary antibody (FITC-conjugated donkey anti-rabbit 711-095-152 or donkey anti-mouse 715-095-150 IgG, Jackson ImmunoResearch Laboratories, 1 : 200 dilution) in PBS 1X for 90 min at RT. In negative controls primary antibody was omitted. After secondary antibody incubation, samples were washed and mounted in buffered glycerol (0.1 M, pH 9.5). All experiments were performed at least in triplicate.

For proliferation and apoptosis analyses, samples were photographed with a Zeiss fluorescence microscope (Axioscope) and positive cells were counted. For LC3 immunolocalization a Leica confocal microscope (Laser Scanning TCS SP2) equipped with Ar/ArKr and He/Ne lasers was used. Images were acquired utilizing the Leica confocal software. The laser line was at 488 nm for FITC excitation. The images were scanned under a 20x objective or 40x oil immersion objective. In order to get a quantitative analysis of fluorescence, optical spatial series, each composed of 23/25 optical sections with a step size of 2 μm, were performed in areas in which cells reached confluence both in nonrotated and in RPM cultured samples. The fluorescence intensity was determined by the Leica confocal software, using the following parameters: the maximum amplitude of fluorescence (MAX Amplitude), the sum of intensity (SUM (I)), and the mean amplitude of fluorescence intensity (MEAN (A)), of LC3 positive areas. The MAX Amplitude represents the maximum intensity of fluorescence of each series. The SUM (I) represents the total amount of fluorescence intensity recovered within the entire z-axis of each series. The MEAN (A) represents the arithmetical mean of fluorescence intensity recovered within the entire z-axis of each series. We analyzed 12 equivalent sized regions (regions of interest (ROI)) for each experiment both in 1 g and in RPM culture conditions (36 total ROI for each experimental condition).

2.4. Western Blotting of LC3 Autophagy Marker. Cells cultured at 1 g and in RPM condition for 24 and 48 hours were lysed in RIPA buffer (Sigma-Aldrich). Samples were then clarified by centrifugation at 10000 rpm for 10 min. Equivalent amount of protein (10 μg) from each sample was electrophoretically resolved on 12.5% precast SDS-polyacrylamide gels (ExcelGel, GE Healthcare Biosciences) using horizontal apparatus (Pharmacia Biotech, Uppsala, Sweden). Then, separated proteins were electrotransferred onto nitrocellulose membranes (Schleicher & Schuell) by a semidry system (Novablot, Pharmacia Biotech). Membranes were blocked with 3% nonfat milk in PBS and then were incubated (ON at 4°C) with the LC3B monoclonal antibody (1 : 2000; Sigma). After extensive washing with PBS containing 0.1% tween-20 (TBST), blots were incubated with 1 : 2000 dilution of HRP-conjugated secondary antibody (Amersham Biosciences) for 1 hour at RT. Immunopositive bands were detected with a chemiluminescence's detection system (GE Healthcare Biosciences). To check for equal loading of the gel, membranes were stripped and reprobed with mouse anti-β-actin antibody (1 : 20000, Sigma) and with anti-GAPDH antibody (1 : 1000, Cell Signalling Technology). Densitometric analysis was performed with the Quantity One software (BioRad Laboratories).

2.5. F-Actin and Tubulin Distribution Pattern. For F-actin visualization Rhodamine Phalloidin (Invitrogen Molecular Probes Eugene, 1 : 40 dilution) was used. Cells were fixed in 4% paraformaldehyde (PFA) in PBS for 10 minutes at 4°C and then permeabilized with cold ethanol : Acetone 1 : 1 for 10 minutes at 4°C. After rinsing, cells were incubated with Rhodamine Phalloidin for 25 min in the dark. Cells were then washed in PBS and mounted in buffered glycerol (0.1 M, pH 9.5).

Cell height analysis (z-axis) was performed using the confocal microscope already described (Leica IRE SP2, Laser Scanning TCS SP2) equipped with Ar/ArKr and He/Ne lasers. Images of the optical sections were acquired using the Leica confocal software. The Laser Line was at 543 nm for TRITC excitation. Images were scanned under a 40x oil objective. In order to evaluate cell height three different experiments were performed using cells cultured 1 g and in RPM conditions. For each experiment 4/5 optical spatial series with a step size of 2 μm were recovered and a total of at least 80 optical sections were analyzed for each experimental condition. Cell height of the examined samples was calculated using Leica confocal software.

For microtubules localization immunofluorescence experiments, using anti-α-tubulin (Biomeda, mouse monoclonal V10178, 1 : 75 dilution) as primary antibody, were performed. The protocol used is the same already described in the paragraph above. Donkey anti-mouse (715-095-150 IgG, Jackson ImmunoResearch Laboratories, 1 : 200 dilution), as secondary antibody, was used. Samples were then observed using both fluorescence microscope (Axioscope, Zeiss) and confocal microscope (Leica).

2.6. Scanning Electron Microscopy. Samples were fixed in Glutaraldehyde 2.5% in cacodylate buffer 0.1 M pH 7.3 ON and then postfixed with 1% osmium tetroxide in cacodylate buffer 1 M, dehydrated with increasing ethanol percentage (30–90% in water for 5 min, twice 100% for 15 min), treated in Critical Point Dryer (EMITECH K850), sputter coated with platinum-palladium (Denton Vacuum DESKV), and observed with Supra 40 FESEM (Zeiss).

2.7. Statistical Analysis. All experiments were performed at least in triplicate. All quantitative data are presented as the mean value ± standard error (SEM). Student's t-test and ANOVA test for multigroup comparison were carried out, when appropriate, to evaluate the significance of differences. The significance level was fixed at a P value < 0.05.

3. Results and Discussion

3.1. Microgravity Does Not Affect TCam-2 Cell Proliferation and Apoptosis. Microgravity exposure is known to influence cell proliferation and apoptosis in normal and cancer cells [52]. In order to asses proliferation rate of TCam-2 seminoma cells, maintained at 1 g or in RPM culture conditions for 24 and 48 hours, we performed immunofluorescence analyses of the M-phase marker p-histone H3. We observed that, actually, this acute microgravity exposure does not affect

the number of mitotic cells at all the culture times considered (Figure 1). Literature data have demonstrated that TCam-2 cells do not have a high proliferation rate (58 hours doubling time) when compared with JKT1 (27 hours doubling time), that is, another germ cell tumor cell line [40]. Since the percentage of proliferating cells we expect in the time frame of 24 and 48 hours is not high, we can hypothesize that this altered gravitational stimulus is not long enough to determine a modification of cell proliferation in this particular cell line. Interestingly after 48 hours of culture the number of mitotic cells decreases significantly, in a similar amount, both in 1 g and in RPM cultured samples (Figure 1), indicating that cell proliferation, in this particular cell line, starts to be inhibited by cell-to-cell contact even if these cells are cancer cells. It has to be noticed that we chose to plate cells at high density in order to let them attach each other before the RPM exposure and react, thanks to their tensional forces, to the changes of gravitational field. Due to the high density of plating, at the end of the longer culture time we analyzed, cell culture dishes are crowded of cells so it appears not possible to prolong more the culture without detaching and replate cells. To this regard it is fair to say that we cannot exclude that TCam-2 cell proliferation might be altered by RPM exposure if they would have been cultured at a different density.

To test whether microgravity would be able to modify TCam-2 cell apoptosis, we performed immunofluorescences for the active fragment of the apoptosis marker Caspase-3. We found that the change of gravity vector does not affect the number of apoptotic cells after 24 hours of culture (Figure 2). However, it has to be noticed that, after 48 hours of culture, the number of apoptotic cells increases significantly in the RPM cultured samples, even if the large majority of cells appear to tolerate this mechanical stress (Figure 2) and to survive. The latter observation indicates that a small part of TCam-2 cells appears more sensible to the change of gravity vector, when the mechanical stimulus is prolonged a bit, but this sensibility does not seem related to mechanical cell stability because, due to the high density of plating, all cells are stably attached to each other and to the substrate. In addition, apoptotic cells are observable uniformly dispersed in the culture dish. On the basis of this observation, we hypothesized that TCam-2 cells need to trigger rescue processes that let them survive after a prolonged change of gravity vector. Possibly, rescue processes are not correctly induced or exploited by the whole population of TCam-2 cells and this hypothesis may explain why a small percentage of them appears not able to survive to the change of gravity. The change of physical forces is sensed by the cells through their cytoskeleton components and one of the first features that reveal a cytoskeletal modification is the change in the plasma membrane morphology. We studied first membrane surface and cytoskeletal modifications, due to RPM exposure, to be sure the TCam-2 cells are able to sense and modify their shape in response to this mechanical stress. Then we evaluated, in the same culture conditions, the autophagic process modulation in response to RPM exposure, since autophagy is the most known biological rescue mechanism that let cell to change rapidly and survive to sudden microenvironmental changes.

3.2. Microgravity Strongly Influences TCam-2 Cell Membrane Surface. To study if the alteration of the mechanical forces acting on TCam-2 cells during microgravity simulation may modify cell membrane surface morphology, samples were analyzed by scanning electron microscopy. We observed the presence of two morphologically distinguishable cell populations in the 1 g cultured samples: one has smooth membrane surface and the other one is characterized by the presence of membrane expansions morphologically similar to microvilli (Figure 3). Noteworthy, we found that microgravity strongly affects membrane surface appearance after 24 hours of culture: microvilli appeared collapsed and the differences between the two cell populations are less evident (Figure 3). It is of interesting notice that cell microvilli are considered to be an important site of mechanotransduction both in sensory specialized cells and not-sensory cells [53]. After 48 hours of culture the membrane surface differences appear recovered and microvilli-like structures appear reconstituted in RPM cultured samples (Figure 3). On the basis of these observations, we hypothesized that cell mechanosensor-system was transiently altered by RPM exposure and this strongly suggested the occurrence of cytoskeleton remodeling due to an acute exposure to gravitational vector change.

3.3. Microgravity Induces TCam-2 Cytoskeleton Remodeling. A huge amount of literature data demonstrated that microgravity is able to influence cell cytoskeletal architecture, promoting cell morphofunctional alterations [54]. In the light of these observations and on the basis of our scanning electron microscopy data, we decided to evaluate the possible effects of simulated microgravity on TCam-2 microfilament and microtubule organization. Herein, we report microfilament distribution pattern analyzed by F-actin staining of TCam-2 cells cultured at 1 g or in RPM culture conditions. Even if no apparent significant alterations in the actin cytoskeleton organization were found both in 24 (Figure 4(a)) and 48 hours of culture (not shown), a more detailed analysis by confocal microscopy using Leica confocal software allowed us to evaluate cell height (cell z-axis) (Figures 4(b), 4(c), and 4(d)) in all the considered experimental conditions. We observed that simulated microgravity significantly increases TCam-2 cell height after 24 hours of RPM exposure with respect to 1 g cultured cells ($15.62 \pm 1.10\,\mu$m versus $11.0 \pm 0.66\,\mu$m; $P < 0.001$) indicating that RPM culture condition was able to modify TCam-2 cell shape. Noteworthy, after 48 hours of culture the differences in cell height in 1 g and RPM cultured cells are no more statistically significant (Figure 4(d)), indicating that TCam-2 cells are able to recover rapidly after the exposure to this mechanical stress. The latter observation appears consistent with the reported recovery of surface membrane microvilli-like structures after 48 hours of RPM exposure (Figure 3).

Microtubule distribution pattern was studied by anti-α-tubulin immunofluorescence staining. After 24 hours of culture, we observed that microtubule distribution is altered in TCam-2 cells exposed to RPM culture condition: centriolar polarization is much less visible in these samples and microtubules appear to be distributed in an apparently random

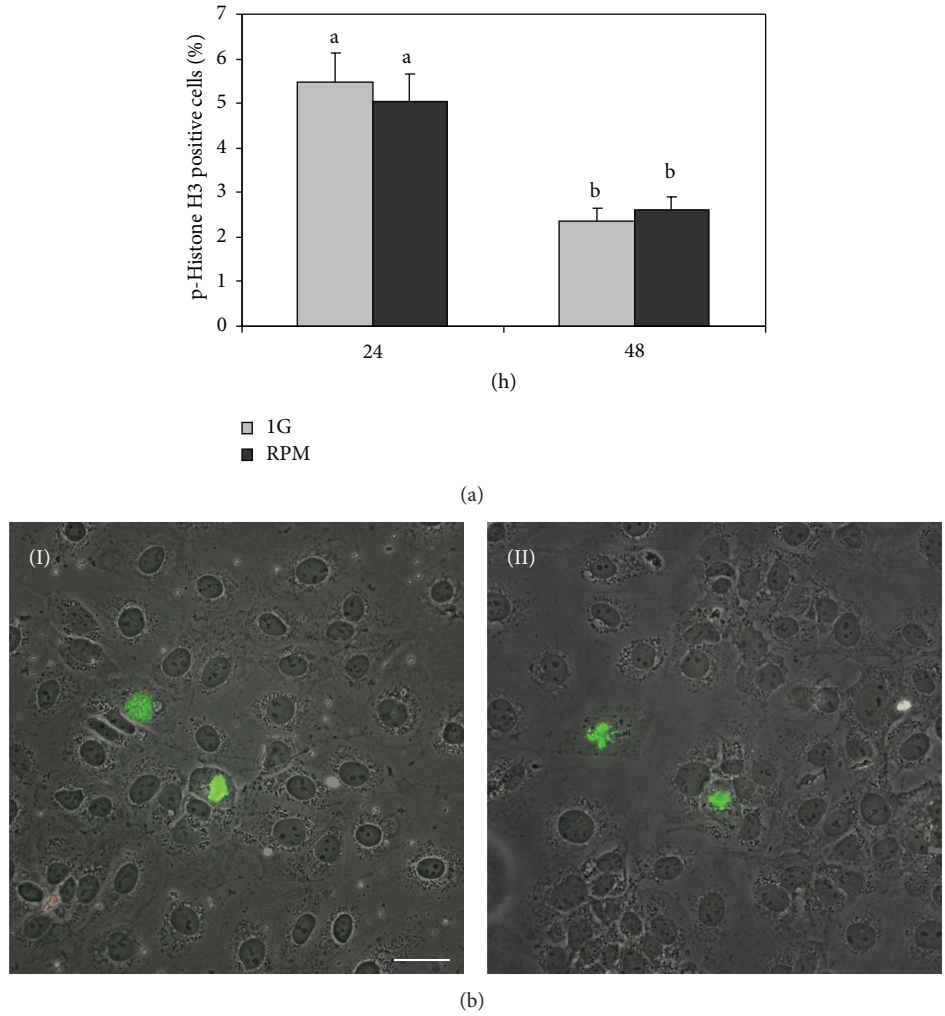

Figure 1: RPM exposure does not influence TCam-2 cell proliferation. (a) Graphical representation of the percentage of proliferating cells (p-histone H3 positive cells) at 24 and 48 hours of culture. No differences were observed between TCam-2 cells cultured at 1 g or in RPM culture conditions. Data are expressed as the mean ± SEM. Same letters indicate no statistical difference. Different letters indicate $P < 0.05$. (b) Representative images of TCam-2 cells cultured for 24 hours at 1 g (I) and in RPM condition (II) after p-histone H3 immunofluorescence. Bar, 50 μm.

manner within the cells (Figure 5). Microtubules are key regulators of membrane trafficking; organelle distribution inside the cells and together with actin microfilaments seems to regulate autophagosome formation [55–57]. In addition it is of interesting notice that LC3, the marker protein of the autophagic process, is a microtubule associated protein (MAP). As well as actin filaments, after 48 hours of culture the microtubule distribution pattern appears recovered in RPM exposed samples since it is not possible to observe significant differences between 1 g and RPM cultured cells. These observations again clearly indicate the capability of TCam-2 cell to sense the change of physical forces in their microenvironment and also to recover rapidly from this physical stress. These data strongly suggest the trigger of rescue mechanisms due to TCam-2 RPM exposure.

It is worth mentioning that the reported microtubule alteration does not appear to significantly alter the proper formation of the mitotic spindle (Figure 5(g) white box). This observation is consistent with the results reported in Figure 1 in which we observed that TCam-2 cell proliferation does not appear to be affected by RPM exposure.

3.4. Microgravity Induces TCam-2 Cell Autophagy. Some papers in the literature reported that, in other cellular systems, microgravity is involved in autophagy induction [18–20] and, as previously stated, cytoskeleton plays important roles in autophagy regulation [22]. In particular, in mammals, microtubules appear to be involved in the fusion of autophagosome with late endosome and to bind and transport autophagosomes, once terminally completed. The role of actin filaments on mammalian autophagy process regulation is still a matter of debate, but it is worth mentioning that microfilaments depolymerization agents are able to block autophagosome formation.

TCam-2 cells cultured at 1 g and in RPM conditions were immunostained to detect the autophagic marker LC3.

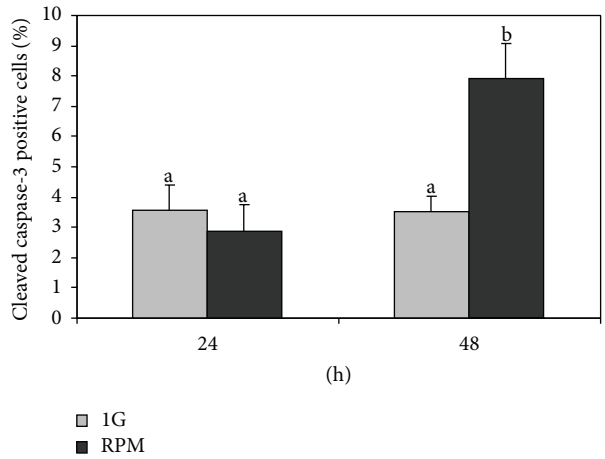

(a)

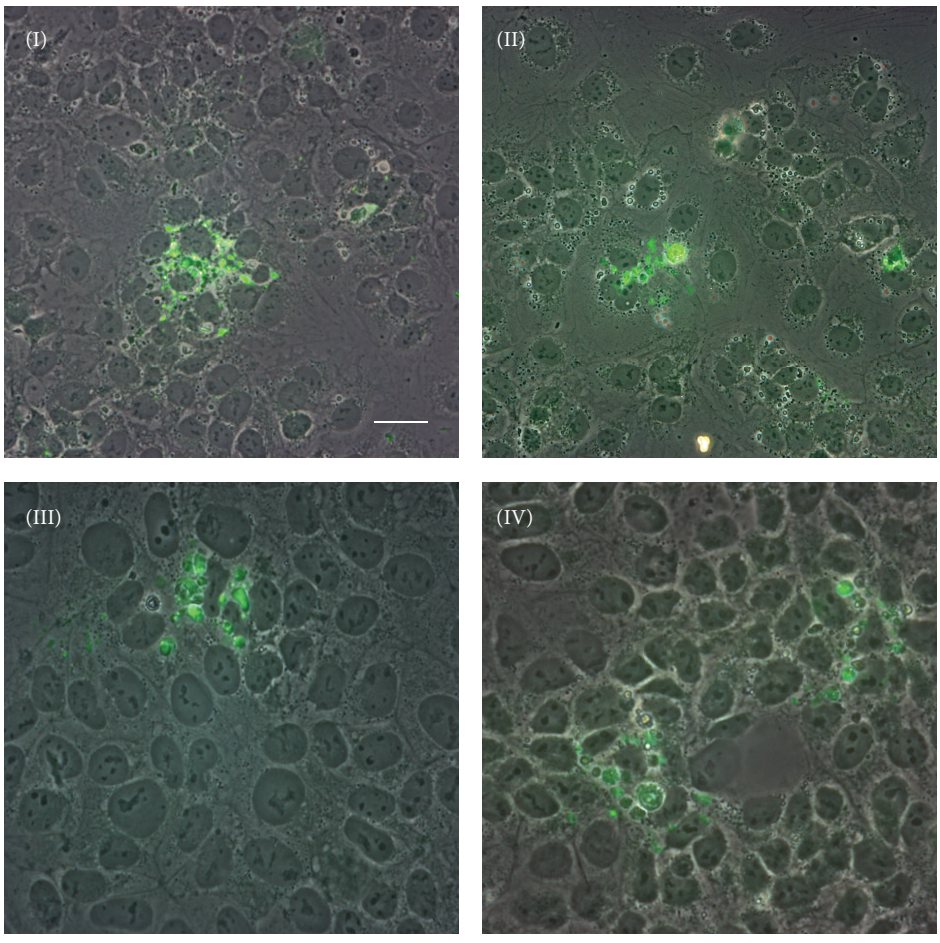

(b)

Figure 2: RPM exposure and TCam-2 cell apoptosis. (a) Graphical representation of the percentage of apoptotic cell number (anticleaved Caspase-3 positive cells). No differences were observed between TCam-2 cells cultured for 24 hours at 1 g or in RPM culture conditions. On the contrary a slight increase in apoptotic cell percentage is observed after 48 hours of culture. Data are expressed as the mean ± SEM. Same letters indicate no statistical difference. Different letters indicate $P < 0.01$. (b) Representative images of 1 g (I, III) and RPM (II, IV) exposed TCam-2 cells in 24 (I, II) and 48 (III, IV) hours of culture after cleaved Caspase-3 immunofluorescence. Bar: 50 μm (I and II); 35 μm (III and IV).

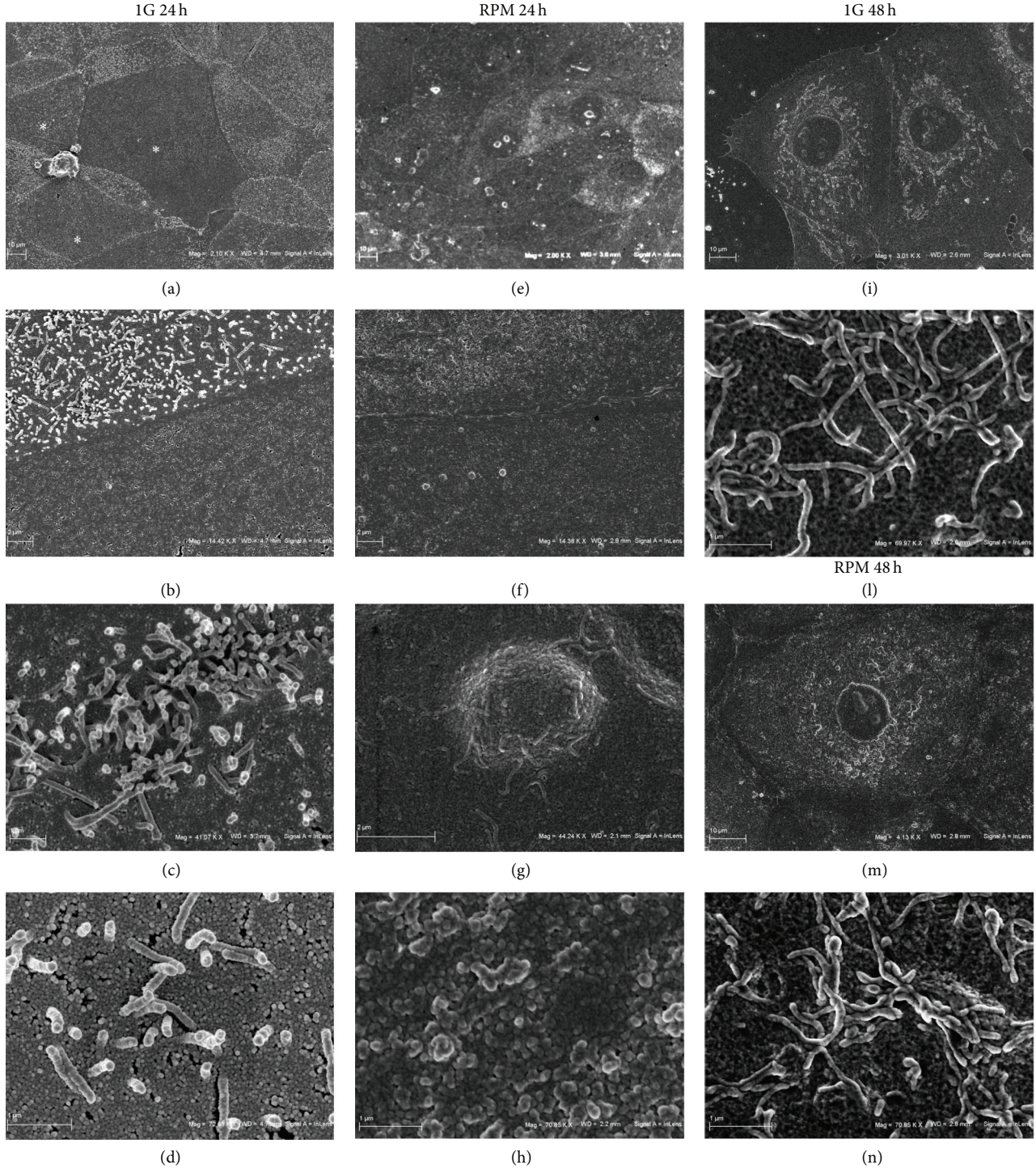

Figure 3: Microgravity effect on TCam-2 cell membrane surface. Scanning electron microscopy pictures with increasing magnification showing cell membrane surface morphology of TCam-2 cells cultured for 24 (a, b, c, and d) and 48 hours (i, l) at 1 g or for 24 (e, f, g, and h) and 48 hours (m, n) in RPM culture conditions. In (a) white asterisks indicate TCam-2 cells with smooth membrane surface while the other TCam-2 cells of the same image are characterized by the presence of microvilli-like structures. In (b) the boundary between one smooth membrane and one microvilli membrane presenting cells is reported. (c) and (d) represent higher magnifications of the microvilli-like structures of TCam-2 cells maintained at 1 g. In (e), (f), (g), and (h) it is well evident that, in RPM cultured cells, membrane surface is more similar in all the cells and it is difficult to clearly identify the two cell populations. In particular in (h) it is possible to observe that microvilli-like structures appeared collapsed in RPM exposed TCam-2 cells. The morphological appearance of cell surface (i, m) and microvilli-like structures (l, n) appeared indistinguishable in 1 g (i, l) and RPM exposed cells (m, n) after 48 hours of culture.

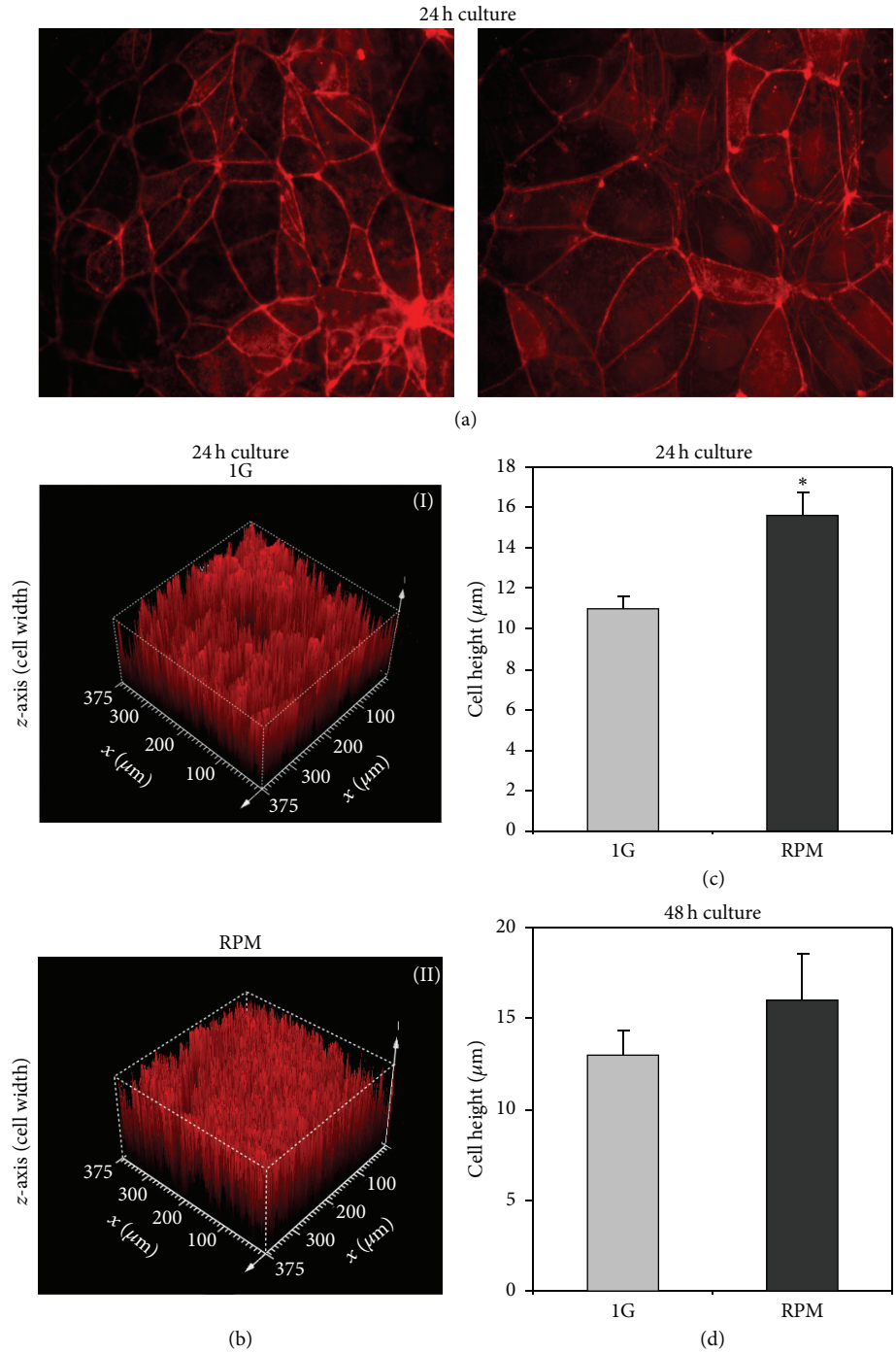

Figure 4: Simulated microgravity influences TCam-2 cell height. (a) Rhodamine-phalloidin staining of TCam-2 cells showing F-actin distribution pattern after 24 hours of culture at 1 g (I) or under RPM (II) conditions. Bar, 20 μm. (b) Representative images of cell height obtained using the Leica confocal software, of samples cultured for 24 hours at 1 g (I) or in RPM (II) conditions. (c) Graphical representation of cell height obtained by confocal microscopy analysis on 1 g and RPM exposed cells after 24 hours of culture (*1 5.62 ± 1, 10 μm versus 11.0 ± 0.66 μm; $P < 0.001$). Data are expressed as the mean ± SEM. (d) Graphical representation of cell height obtained by confocal microscopy analysis on 1 g and RPM exposed cells after 48 hours of culture (13.02 ± 1.32 μm versus 16.02 ± 2.49 μm, resp.). Data are expressed as the mean ± SEM. The values are not statistically significant.

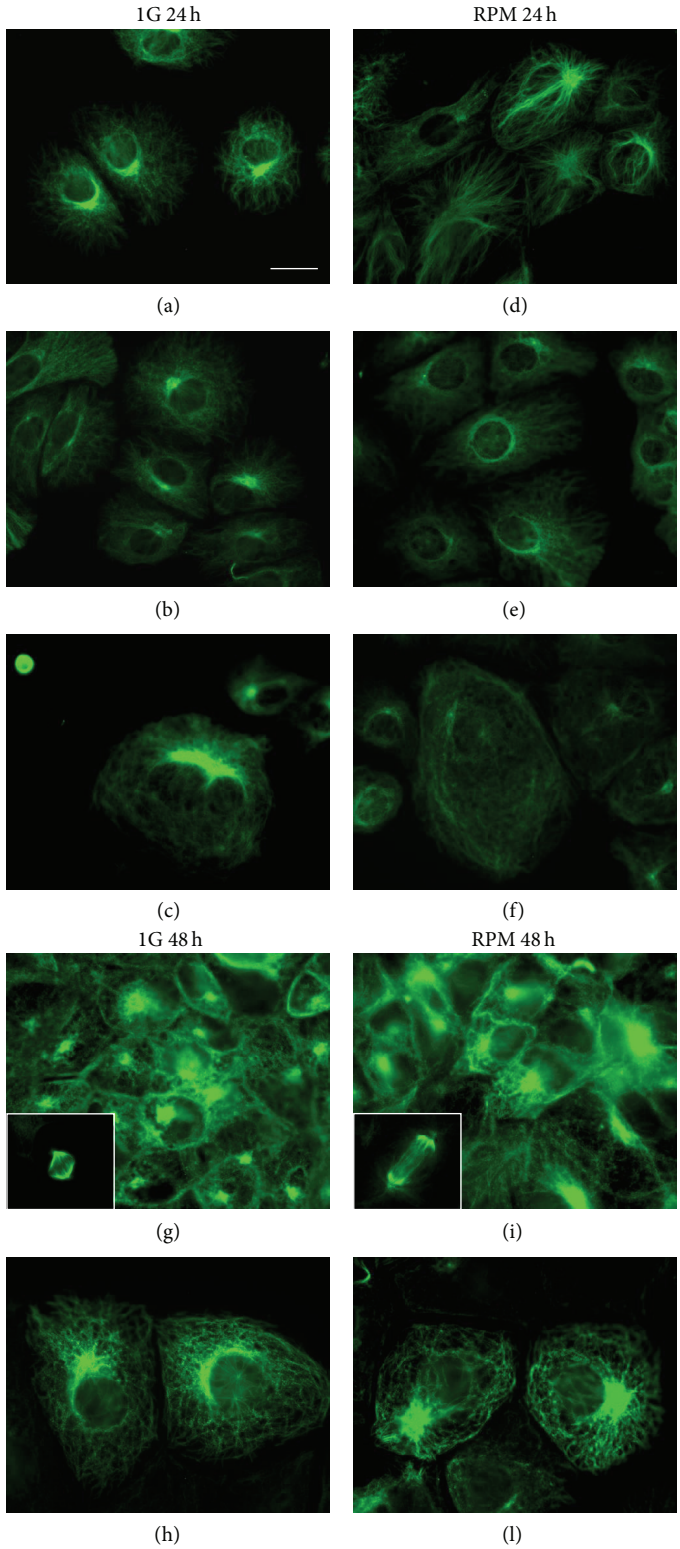

FIGURE 5: Microtubule distribution pattern in TCam-2 cells exposed to simulated microgravity. Immunodetection of α-tubulin in TCam-2 cells cultured for 24 hours (a, b, c, d, e, and f) and 48 hours (g, h, i, and l) at 1 g (a, b, c, g, and h) or under RPM conditions (d, e, f, i, and l). In images (g) and (i), in the white box, representative images of mitotic spindles are also shown. Bar, 20 μm.

As shown in Figures 6(a)(II) and 6(a)(IV), LC3 is detectable both in 1 g and in RPM cultured samples and it is mainly localized in cytoplasmic vesicles. Interestingly, the number of these LC3 positive vesicles appears strongly increased in TCam-2 cells exposed to microgravity conditions (Figure 6(a)(IV)) with respect to 1 g cultured cells (Figure 6(a)(II)) after 24 hours of culture. Moreover, a quantitative analysis, carried out using the Leica confocal software, allows us to quantify the fluorescence intensity increase of LC3 stained cells exposed to simulated microgravity (Figures 6(b) and 6(c)). In particular, Figure 6(b) shows a stack profile of 12 regions of interest (ROI) of a representative experiment both in 1 g (I) and in RPM cultured samples (II). The two groups of peaks reported in this figure represent the Max amplitude of fluorescence detected by the confocal microscope from the beginning to the end of the sample (total z-axis). It is well evident that Max amplitude of fluorescence is increased in simulated RPM exposed samples. We evaluated also the SUM (I) and the MEAN (A) of fluorescence. Consistent with the data reported in Figure 6(b), we observed also an increase of both the SUM (I) and the MEAN (A) in RPM cultured cells after 24 hours of culture (Figure 6(c)). According to the described confocal quantitative analyses, western blots performed with the anti-LC3 antibody showed that, besides the increase of LC3-I protein amount, LC3-II (the LC3 active isoform) protein content is increased in RPM with respect to 1 g cultured samples (Figure 7). Same results were obtained normalizing the LC3 bands versus β-actin (Figure 7) and versus GAPDH signal (not shown). Autophagy induction is a naturally transient process: this phenomenon is called autophagic flux [58], since, when it works, autophagy protein machinery has to be degraded via lysosomes or proteasome together with the portion of the cell that needs to be eliminated. On the contrary, when autophagy is blocked, the autophagy protein machinery is not degraded and is maintained at high level in the cytoplasm. In our samples, after 48 hours of culture autophagy active protein LC3-II, together with LC3-I, appears quantitatively similar in 1 g and RPM cultured cells, demonstrating that autophagy is restored at the same level with respect to 1 g culture condition. Same results were obtained normalizing the LC3 bands versus β-actin (Figure 7) and versus GAPDH signal (not shown). Consistent with this observation, the LC3 cytoplasmic fluorescence is lowered in the RPM exposed cells demonstrating that autophagy was not blocked by this mechanical stress (Figure 6(a)(VI)). It has to be mentioned that LC3-II protein is present at basal level at 24 and 48 hours of culture as well as cytoplasmic LC3 dots, even in cells cultured at 1 g, indicating that autophagy is a housekeeping process that works in TCam-2 cells even in control samples and suggesting that this cancer cell line may exploit autophagy as a survival mechanism.

There is a common agreement indicating that there is a relationship between autophagy and apoptosis: when autophagy is not able to rescue cell from microenvironmental changes, apoptotic process is triggered. On the light of this theory we might interpret the small increase in the apoptotic index at 48 hours of culture in RPM cultured samples (Figure 2) as the autophagy efficiency threshold or the limit of autophagy efficiency in the rescue of cell survival after mechanical stress exposure.

All together these qualitative and quantitative analyses allow us to conclude that microgravity is able to positively modulate the autophagic process in TCam-2 seminoma cell line. Autophagy induced in TCam-2 cells by Estrogen exposure through ERβ activation was recently reported [59]. Herein we reported, for the first time, autophagy induced in TCam-2 cells by a mechanical cue (or, more precisely, by a removal of a mechanical stimulus) instead of a biochemical one. The analysis of the autophagy related pathways induced by RPM exposure and the direct role of microtubules and microfilaments in this process, as well as the other possible biological meanings of RPM induced TCam-2 autophagy, deserves further investigations.

4. Conclusions

Gravitational biology could be considered part of mechanobiology, the science that investigates the impact of forces on living organisms. At cellular level, cytoskeleton elements are likely candidates for force sensing and transduction processes. These biomechanical properties of cell cytoskeleton explain the capability to propagate a mechanical stimulus over long distances in living tissues and represent the basis of the intriguing hypothesis that many, if not all, reported changes in ion fluxes, protein phosphorylation, membrane potential changes, and so forth are indeed provoked by a mechanical modification somewhere within the cell or on its membrane [60, 61]. This paper is in line with this theory and adds experimental data supporting the importance of mechanotransduction and cell behavior. In this paper, in fact, we reported the effects of the exposure to changes of gravity vector on TCam-2 seminoma cells. In this experimental model, simulated microgravity is able to induce TCam-2 cell surface modifications and microvilli-like structure alteration. Moreover, microtubules and microfilaments organization result to be influenced by microgravity: (a) TCam-2 cells show actin cytoskeleton remodeling and cell height increase; (b) centriolar polarization becomes much less visible in these samples and microtubules appear to be distributed in an apparent random manner within the cells. All these modifications appear to be transient, indicating that cells modify their cytoskeletal components in response to gravitational force change, but that are also able to recover their shape when the gravitational change is prolonged. Interestingly, RPM exposure is able to induce TCam-2 cell autophagy. The latter observation allows us to hypothesize that TCam-2 cells are able to rapidly respond to acute exposure to microgravity, inducing adaptive biological processes such as autophagy, that probably allow them to survive in the changing physical microenvironment. Since autophagy is considered a biological survival mechanism the apoptosis induction in a small percentage of TCam-2 cells after 48 hours of culture might be speculated as the limit in the efficiency of this survival process. All together these data provide evidences of TCam-2 sensitivity to changes of gravitational force direction and lay the groundwork to further studies on TCam-2 cell autophagy and its biological meaning.

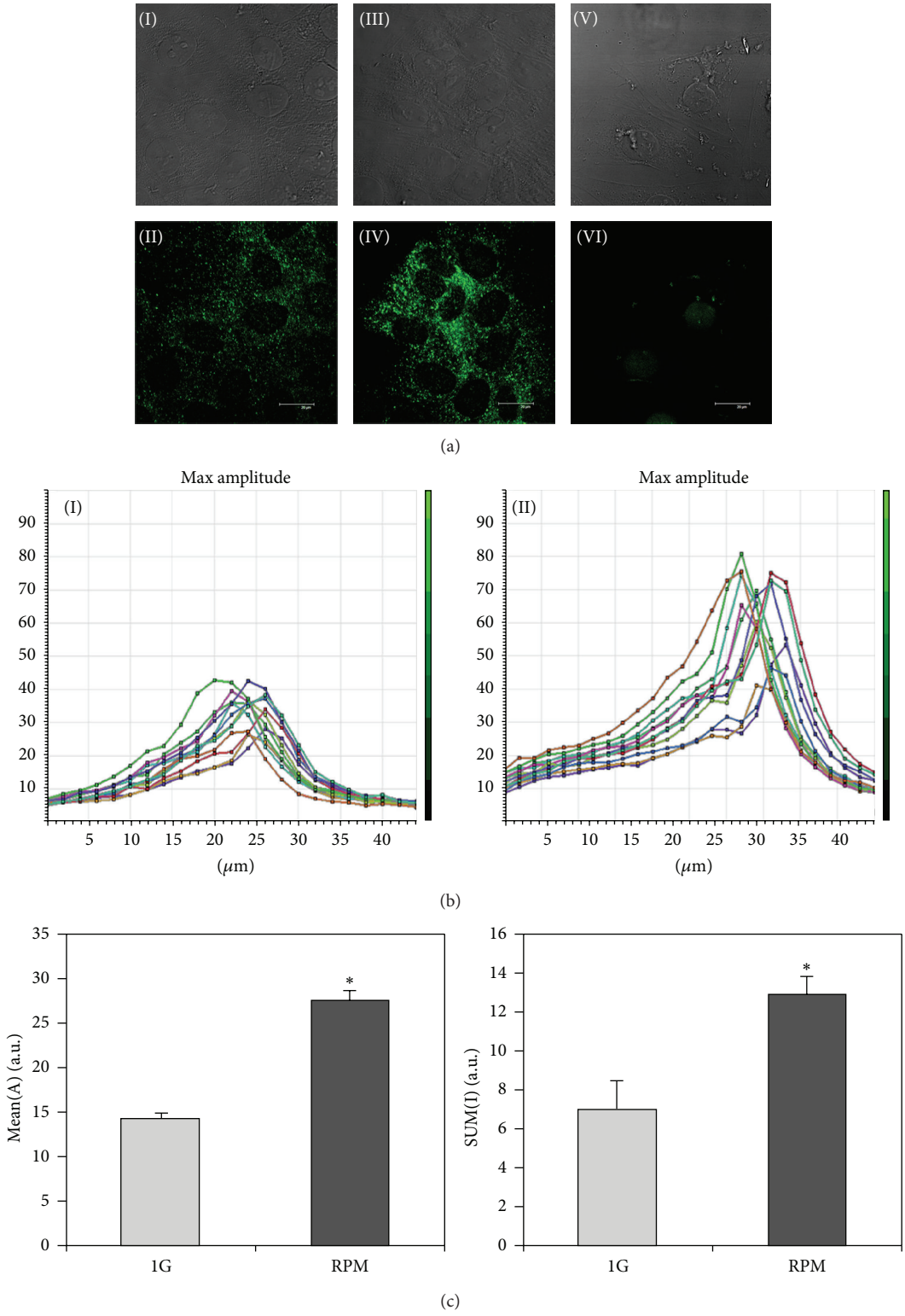

Figure 6: Autophagy induction in TCam-2 cells exposed to microgravity. (a) Immunodetection of LC3 in TCam-2 cells cultured for 24 hours at 1 g (II) or under RPM (IV) conditions. In VI LC3 immunodetection of TCam-2 cells cultured in RPM condition for 48 hours is reported. In I, III, and V the respective bright fields are shown. (b) Stack profile of 24 hours of culture representative experiment showing the maximum amplitude (MAX Amplitude) of fluorescence in 12 regions of interest (ROI), randomly drawn in an area in which the cells reached confluence, in nonrotated (I) and RPM cultured samples (II). It is evident an increase of maximum amplitude of fluorescence in microgravity exposed samples (II) with respect to the 1 g-cultured cells (I). (c) MEAN (A) (^{*2} 7.62 ± 1.04 versus 14.34 ± 0.59; $P < 0.001$) and SUM (I) (^{*1} 2.92 ± 0.85 versus 6.95 ± 1.52; $P < 0.05$) confirm an increase of LC3 positivity in RPM exposed sample with respect to 1 g cells after 24 hours of culture. Data are expressed as the mean ± SEM.

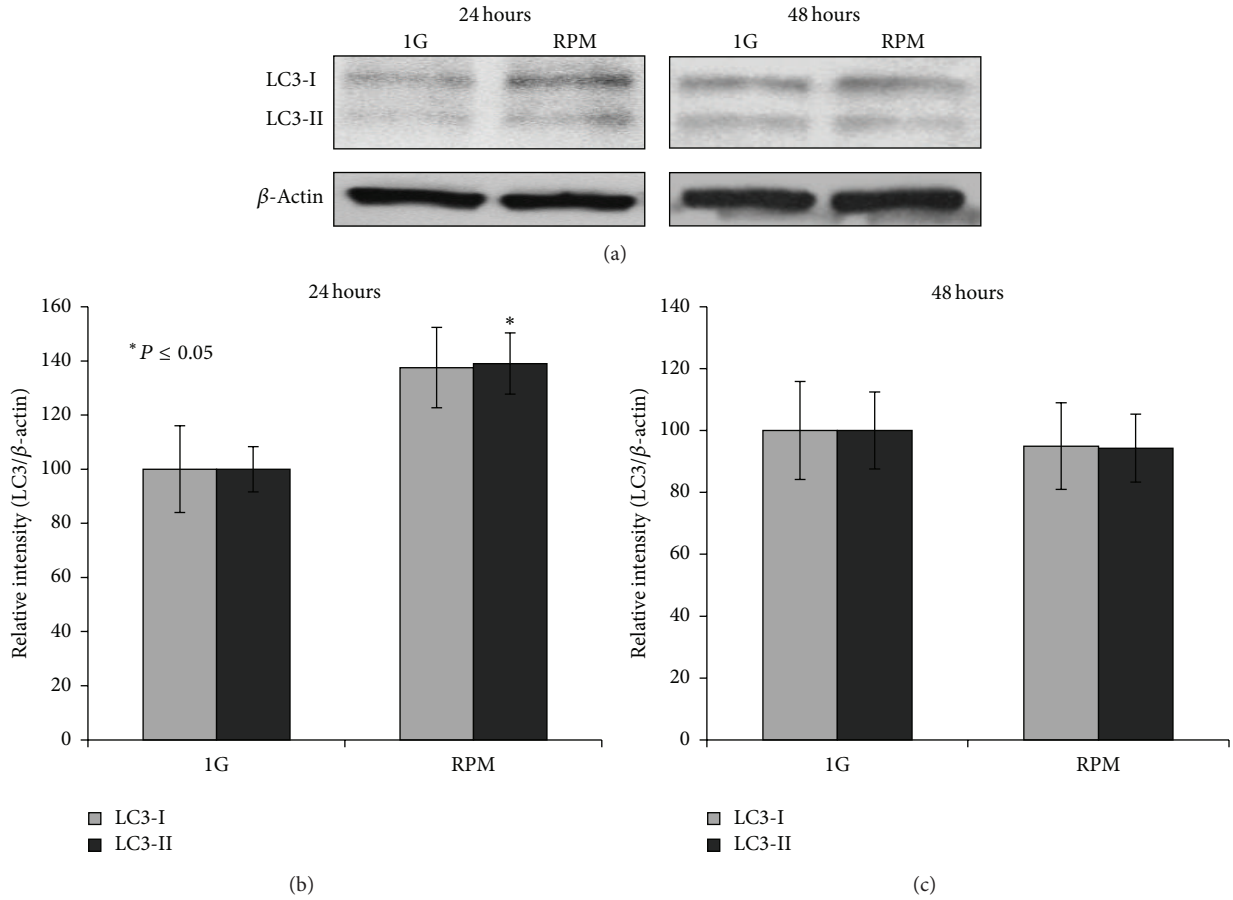

Figure 7: Western blot analysis of LC3 autophagy marker. (a) Representative images of the bands revealed by anti-LC3 western blot analysis on 24 and 48 hours cultured samples. As expected anti-LC3 antibody detected both the LC3 isoforms (LC3-I cytosolic isoform; LC3-II autophagosomal membrane-conjugated isoform). (b) Graphical representation summarizing the densitometric analysis of the LC3-I and LC3-II bands, normalized versus β-actin in 24 hours cultured samples. Data are expressed as the mean ± DS. *versus 1 g $P < 0.05$. (c) Graphical representation summarizing the densitometric analysis of the LC3-I and LC3-II bands, normalized versus β-actin in 48 hours cultured samples. Data are expressed as the mean ± DS. The values are not statistically significant.

Conflict of Interests

The authors declare that there is no conflict of interests regarding the publication of this paper.

Authors' Contribution

Angela Catizone and Giulia Ricci are equal senior authors.

Acknowledgments

The authors wish to thank Professor Mariano Bizzarri for the valuable suggestions and the Italian Space Agency for the support received to carry out this research project.

References

[1] D. Vorselen, W. H. Roos, F. C. MacKintosh, G. J. Wuite, and J. J. van Loon, "The role of the cytoskeleton in sensing changes in gravity by nonspecialized cells," *The FASEB Journal*, vol. 28, no. 2, pp. 536–547, 2014.

[2] G. Aleshcheva, J. Sahana, X. Ma et al., "Changes in morphology, gene expression and protein content in chondrocytes cultured on a random positioning machine," *PLoS ONE*, vol. 8, no. 11, Article ID e79057, 2013.

[3] S. Li, Z. Ma, Z. Niu et al., "NASA-approved rotary bioreactor enhances proliferation and osteogenesis of human periodontal ligament stem cells," *Stem Cells and Development*, vol. 18, no. 9, pp. 1273–1282, 2009.

[4] R. Tamma, G. Colaianni, C. Camerino et al., "Microgravity during spaceflight directly affects in vitro osteoclastogenesis and bone resorption," *The FASEB Journal*, vol. 23, no. 8, pp. 2549–2554, 2009.

[5] S. J. Pardo, M. J. Patel, M. C. Sykes et al., "Simulated microgravity using the Random Positioning Machine inhibits differentiation and alters gene expression profiles of 2T3 preosteoblasts," *American Journal of Physiology-Cell Physiology*, vol. 288, no. 6, pp. C1211–C1221, 2005.

[6] A. Guignandon, M. H. Lafage-Proust, Y. Usson et al., "Cell cycling determines integrin-mediated adhesion in osteoblastic ROS 17/2.8 cells exposed to space-related conditions," *The FASEB Journal*, vol. 15, no. 11, pp. 2036–2038, 2001.

[7] D. Ingber, "How cells (might) sense microgravity," *The FASEB Journal*, vol. 13, pp. S3–S15, 1999.

[8] D. Grimm, P. Wise, M. Lebert, P. Richter, and S. Baatout, "How and why does the proteome respond to microgravity?" *Expert Review of Proteomics*, vol. 8, no. 1, pp. 13–27, 2011.

[9] T. D. Ross, B. G. Coon, S. Yun et al., "Integrins in mechanotransduction," *Current Opinion in Cell Biology*, vol. 25, no. 5, pp. 613–618, 2013.

[10] B. Geiger, A. Bershadsky, R. Pankov, and K. M. Yamada, "Transmembrane extracellular matrix-cytoskeleton crosstalk," *Nature Reviews Molecular Cell Biology*, vol. 2, no. 11, pp. 793–805, 2001.

[11] M. Y. Kapitonova, N. Salim, and S. Othman, "Alteration of cell cytoskeleton and functions of cell recovery of normal human osteoblast cells caused by factors associated with real space flight," *Malaysian Journal of Pathology*, vol. 35, no. 2, pp. 153–163, 2013.

[12] G. Pani, N. Samari, R. Quintens et al., "Morphological and physiological changes in mature in vitro neuronal networks towards exposure to short-, middle- or long-term simulated microgravity," *PLoS ONE*, vol. 8, no. 9, Article ID e73857, 2013.

[13] J. Nakashima, F. Liao, J. A. Sparks, Y. Tang, and E. B. Blancaflor, "The actin cytoskeleton is a suppressor of the endogenous skewing behaviour of Arabidopsis primary roots in microgravity," *Plant Biology*, vol. 16, supplement 1, pp. 142–150, 2013.

[14] C. Nouri, J. A. Tuszynski, M. W. Wiebe, and R. Gordon, "Simulation of the effects of microtubules in the cortical rotation of amphibian embryos in normal and zero gravity," *BioSystems*, vol. 109, no. 3, pp. 444–449, 2012.

[15] J. Li, S. Zhang, J. Chen, T. Du, Y. Wang, and Z. Wang, "Modeled microgravity causes changes in the cytoskeleton and focal adhesions, and decreases in migration in malignant human MCF-7 cells," *Protoplasma*, vol. 238, no. 1–4, pp. 23–33, 2009.

[16] M. A. Meloni, G. Galleri, P. Pippia, and M. Cogoli-Greuter, "Cytoskeleton changes and impaired motility of monocytes at modelled low gravity," *Protoplasma*, vol. 229, no. 2–4, pp. 243–249, 2006.

[17] C. Papaseit, N. Pochon, and J. Tabony, "Microtubule self-organization is gravity-dependent," *Proceedings of the National Academy of Sciences of the United States of America*, vol. 97, no. 15, pp. 8364–8368, 2000.

[18] H. W. Ryu, S. H. Choi, S. Namkoong et al., "Simulated microgravity contributes to autophagy induction by regulating AMP-activated protein kinase," *DNA and Cell Biology*, vol. 33, no. 3, pp. 128–135, 2014.

[19] Y. Sambandam, M. T. Townsend, J. J. Pierce et al., "Microgravity control of autophagy modulates osteoclastogenesis," *Bone*, vol. 61, pp. 125–131, 2014.

[20] Y. C. Wang, D. Y. Lu, F. Shi et al., "Clinorotation enhances autophagy in vascular endothelial cells," *Biochemistry and Cell Biology*, vol. 91, no. 5, pp. 309–314, 2013.

[21] D. Sandonà, J. Desaphy, G. M. Camerino et al., "Adaptation of mouse skeletal muscle to long-term microgravity in the MDS mission," *PLoS ONE*, vol. 7, no. 3, Article ID e33232, 2012.

[22] I. Monastyrska, E. Rieter, D. J. Klionsky, and F. Reggiori, "Multiple roles of the cytoskeleton in autophagy," *Biological Reviews*, vol. 84, no. 3, pp. 431–448, 2009.

[23] J. H. Choi, Y. S. Cho, Y. H. Ko, S. U. Hong, J. H. Park, and M. A. Lee, "Absence of autophagy-related proteins expression is associated with poor prognosis in patients with colorectal adenocarcinoma," *Gastroenterology Research and Practice*, vol. 2014, Article ID 179586, 10 pages, 2014.

[24] N. Orfali, S. L. McKenna, M. R. Cahill, L. J. Gudas, and N. P. Mongan, "Retinoid receptor signaling and autophagy in acute promyelocytic leukemia," *Experimental Cell Research*, vol. 324, no. 1, pp. 1–12, 2014.

[25] C. Cerella, M. H. Teiten, F. Radogna, M. Dicato, and M. Diederich, "From nature to bedside: Pro-survival and cell death mechanisms as therapeutic targets in cancer treatment," *Biotechnology Advances*, 2014.

[26] C. Fabrizi, V. S. De, F. Somma et al., "Lithium improves survival of PC12 pheochromocytoma cells in high-density cultures and after exposure to toxic compounds," *International Journal of Cell Biology*, vol. 2014, Article ID 135908, 7 pages, 2014.

[27] L. Yu, L. Strandberg, and M. J. Lenardo, "The selectivity of autophagy and its role in cell death and survival," *Autophagy*, vol. 4, no. 5, pp. 567–573, 2008.

[28] F. Strollo, G. Riondino, B. Harris et al., "The effect of microgravity on testicular androgen secretion," *Aviation Space and Environmental Medicine*, vol. 69, no. 2, pp. 133–136, 1998.

[29] F. Strollo, M. A. Masini, M. Pastorino et al., "Microgravity-induced alterations in cultured testicular cells.," *Journal of Gravitational Physiology*, vol. 11, no. 2, pp. P187–188, 2004.

[30] Y. Ding, J. Tang, J. Zou et al., "The effect of microgravity on tissue structure and function of rat testis," *Brazilian Journal of Medical and Biological Research*, vol. 44, no. 12, pp. 1243–1250, 2011.

[31] T. Kaneko, S. Sasaki, Y. Umemoto, Y. Kojima, T. Ikeuchi, and K. Kohri, "Simulated conditions of microgravity increases progesterone production in I-10 cells of Leydig tumor cell line," *International Journal of Urology*, vol. 15, no. 3, pp. 245–250, 2008.

[32] M. A. H. Motabagani, "Morphological and morphometric study on the effect of simulated microgravity on rat testis," *Chinese Journal of Physiology*, vol. 50, no. 4, pp. 199–209, 2007.

[33] F. Strollo, G. Strollo, M. More et al., "Changes in human adrenal and gonadal function onboard Spacelab," *Journal of Gravitational Physiology*, vol. 4, no. 2, pp. 103–104, 1997.

[34] U. Engelmann, F. Krassnigg, and W.-. Schill, "Sperm motility under conditions of weightlessness," *Journal of Andrology*, vol. 13, no. 5, pp. 433–436, 1992.

[35] G. Ricci, A. Catizone, R. Esposito, and M. Galdieri, "Microgravity effect on testicular functions," *Journal of gravitational physiology*, vol. 11, no. 2, pp. 61–62, 2004.

[36] G. Ricci, R. Esposito, A. Catizone, and M. Galdieri, "Direct effects of microgravity on testicular function: analysis of hystological, molecular and physiologic parameters," *Journal of Endocrinological Investigation*, vol. 31, no. 3, pp. 229–237, 2008.

[37] S. di Agostino, F. Botti, A. di Carlo, C. Sette, and R. Geremia, "Meiotic progression of isolated mouse spermatocytes under simulated microgravity," *Reproduction*, vol. 128, no. 1, pp. 25–32, 2004.

[38] M. Pellegrini, S. di Siena, G. Claps et al., "Microgravity promotes differentiation and meiotic entry of postnatal mouse male germ cells," *PLoS ONE*, vol. 5, no. 2, Article ID e9064, 2010.

[39] J. de Jong, H. Stoop, A. J. M. Gillis et al., "Further characterization of the first seminoma cell line TCam-2," *Genes Chromosomes and Cancer*, vol. 47, no. 3, pp. 185–196, 2008.

[40] D. Eckert, D. Nettersheim, L. C. Heukamp, S. Kitazawa, K. Biermann, and H. Schorle, "TCam-2 but not JKT-1 cells resemble seminoma in cell culture," *Cell and Tissue Research*, vol. 331, no. 2, pp. 529–538, 2008.

[41] N. C. Goddard, A. McIntyre, B. Summersgill, D. Gilbert, S. Kitazawa, and J. Shipley, "KIT and RAS signalling pathways

in testicular germ cell tumours: new data and a review of the literature," *International Journal of Andrology*, vol. 30, no. 4, pp. 337–348, 2007.

[42] Y. Mizuno, A. Gotoh, S. Kamidono, and S. Kitazawa, "Establishment and characterization of a new human testicular germ cell tumor cell line (TCam-2)," *Nihon Hinyokika Gakkai Zasshi*, vol. 84, no. 7, pp. 1211–1218, 1993.

[43] D. Nettersheim, L. C. Heukamp, F. Fronhoffs et al., "Analysis of TET expression/activity and 5mC oxidation during normal and malignant germ cell development," *PLoS ONE*, vol. 8, no. 12, Article ID e82881, 2013.

[44] F. Ferranti, B. Muciaccia, G. Ricci et al., "Glial cell line-derived neurotrophic factor promotes invasive behaviour in testicular seminoma cells," *International Journal of Andrology*, vol. 35, no. 5, pp. 758–768, 2012.

[45] F. Ferranti, F. D'Anselmi, M. Caruso et al., "Correction: TCam-2 seminoma cells exposed to egg-derived microenvironment modify their shape, adhesive pattern and migratory behaviour: a molecular and morphometric analysis," *PLoS ONE*, vol. 8, no. 10, 2013.

[46] S. M. Russell, M. G. Lechner, A. Mokashi et al., "Establishment and characterization of a new human extragonadal germ cell line, SEM-1, and its comparison with TCam-2 and JKT-1," *Urology*, vol. 81, no. 2, pp. 464–e9, 2013.

[47] R. Franco, F. Boscia, V. Gigantino et al., "GPR30 is overexpressed in post-puberal testicular germ cell tumors," *Cancer Biology & Therapy*, vol. 11, no. 6, pp. 609–613, 2011.

[48] F. Esposito, F. Boscia, V. Gigantino et al., "The high-mobility group A1-estrogen receptor β nuclear interaction is impaired in human testicular seminomas," *Journal of Cellular Physiology*, vol. 227, no. 12, pp. 3749–3755, 2012.

[49] D. Nettersheim, A. J. M. Gillis, L. H. J. Looijenga, and H. Schorle, "TGF-β1, EGF and FGF4 synergistically induce differentiation of the seminoma cell line TCam-2 into a cell type resembling mixed non-seminoma," *International Journal of Andrology*, vol. 34, no. 4, part 2, pp. e189–e203, 2011.

[50] D. Nettersheim, A. Gillis, K. Biermann, L. H. J. Looijenga, and H. Schorle, "The seminoma cell line TCam-2 is sensitive to HDAC inhibitor depsipeptide but tolerates various other chemotherapeutic drugs and loss of NANOG expression," *Genes Chromosomes and Cancer*, vol. 50, no. 12, pp. 1033–1042, 2011.

[51] U. Eppelmann, F. Gottardo, J. Wistuba et al., "Raman microspectroscopic discrimination of TCam-2 cultures reveals the presence of two sub-populations of cells," *Cell and Tissue Research*, vol. 354, no. 2, pp. 623–632, 2013.

[52] J. Pietsch, J. Bauer, M. Egli et al., "The effects of weightlessness on the human organism and mammalian cells," *Current Molecular Medicine*, vol. 11, no. 5, pp. 350–364, 2011.

[53] O. P. Hamill and B. Martinac, "Molecular basis of mechanotransduction in living cells," *Physiological Reviews*, vol. 81, no. 2, pp. 685–740, 2001.

[54] S. J. Crawford-Young, "Effects of microgravity on cell cytoskeleton and embryogenesis," *International Journal of Developmental Biology*, vol. 50, no. 2-3, pp. 183–191, 2006.

[55] A. Aplin, T. Jasionowski, D. L. Tuttle, S. E. Lenk, and W. A. Dunn Jr., "Cytoskeletal elements are required for the formation and maturation of autophagic vacuoles," *Journal of Cellular Physiology*, vol. 152, no. 3, pp. 458–466, 1992.

[56] E. Fass, E. Shvets, I. Degani, K. Hirschberg, and Z. Elazar, "Microtubules support production of starvation-induced autophagosomes but not their targeting and fusion with lysosomes," *Journal of Biological Chemistry*, vol. 281, no. 47, pp. 36303–36316, 2006.

[57] R. Köchl, X. W. Hu, E. Y. W. Chan, and S. A. Tooze, "Microtubules facilitate autophagosome formation and fusion of autophagosomes with endosomes," *Traffic*, vol. 7, no. 2, pp. 129–145, 2006.

[58] N. Mizushima, T. Yoshimori, and B. Levine, "Methods in Mammalian Autophagy Research," *Cell*, vol. 140, no. 3, pp. 313–326, 2010.

[59] C. Guido, S. Panza, M. Santoro et al., "Estrogen receptor β (ERβ) produces autophagy and necroptosis in human seminoma cell line through the binding of the Sp1 on the phosphatase and tensin homolog deleted from chromosome 10 (PTEN) promoter gene," *Cell Cycle*, vol. 11, no. 15, pp. 2911–2921, 2012.

[60] J. J. W. A. van Loon, "Mechanomics and physicomics in gravisensing," *Microgravity Science and Technology*, vol. 21, no. 1-2, pp. 159–167, 2009.

[61] M. Bizzarri, A. Cucina, A. Palombo, and M. G. Masiello, "Gravity sensing by cells: mechanisms and theoretical grounds," *Rendiconti Lincei*, vol. 25, pp. 29–38, 2014.

Hindawi Publishing Corporation
BioMed Research International
Volume 2014, Article ID 964203, 5 pages
http://dx.doi.org/10.1155/2014/964203

Research Article

Gravity Affects the Closure of the Traps in *Dionaea muscipula*

Camilla Pandolfi,[1] Elisa Masi,[1] Boris Voigt,[2] Sergio Mugnai,[1] Dieter Volkmann,[2] and Stefano Mancuso[1]

[1] *DISPAA, University of Florence, Viale delle idee 30, 50019 Sesto Fiorentino, Italy*
[2] *IZMB, University of Bonn, Kirschallee 1, 53115 Bonn, Germany*

Correspondence should be addressed to Camilla Pandolfi; camilla.pandolfi@unifi.it

Received 12 May 2014; Accepted 27 June 2014; Published 15 July 2014

Academic Editor: Monica Monici

Venus flytrap (*Dionaea muscipula* Ellis) is a carnivorous plant known for its ability to capture insects thanks to the fast snapping of its traps. This fast movement has been long studied and it is triggered by the mechanical stimulation of hairs, located in the middle of the leaves. Here we present detailed experiments on the effect of microgravity on trap closure recorded for the first time during a parabolic flight campaign. Our results suggest that gravity has an impact on trap responsiveness and on the kinetics of trap closure. The possible role of the alterations of membrane permeability induced by microgravity on trap movement is discussed. Finally we show how the Venus flytrap could be an easy and effective model plant to perform studies on ion channels and aquaporin activities, as well as on electrical activity *in vivo* on board of parabolic flights and large diameter centrifuges.

1. Introduction

The response of Venus flytrap (*Dionaea muscipula*) to mechanical stimulation has long been known, and it is one of the most rapid movements in the plant kingdom [1, 2].

The plant produces a rosette of leaves, each divided into two parts: a lower part called the lamina and the upper part called the trap. The trap catches prey thanks to a very rapid movement of its bilobed halves that shut when the trigger hairs are stimulated. At room temperature, two touches activate the trap, which snaps shut in a fraction of second [3]. At higher temperature only one stimulus is required for trap closure [4]. The stimulation of the trigger hairs activates mechanosensitive ion channels and generates receptor potentials, inducing the action potentials (APs) that initiate the closure [5]; electrical signals are the immediate cause of the trap movements, irrespective of the way in which the signal is triggered (mechanical stimulation or electrostimulation) [5]. Once the insect is caught, the lobes seal tightly allowing digestion to take place [6, 7]. The APs in *Dionaea muscipula* have been extensively studied (e.g., [5, 8, 9]). Trigger hair-induced generation of action potentials is not exclusively associated with the trap closure. The struggling of the entrapped prey in the closed trap results in the generation of further action potentials which cease to occur just when the prey stops moving. These APs may induce inhibition of the dark reaction of photosynthesis [10] showing that chlorophyll-A fluorescence is under electrochemical control [11]. Although this spectacular example of plant movement has long fascinated scientists, the mechanism by which the trap works remains poorly understood [12]. Some explanations proposed involve an irreversible cell wall loosening, induced by the acidification of the cells [6], or a rapid loss of turgor pressure similarly to what happens in stomata [13]. However, the validity of both mechanisms has been questioned because they cannot explain the speed at which the movement happens. More recently, other two models have been proposed: the elastic deformation that results from a snap-buckling instability [14] and a hydroelastic curvature mechanism based on the fast opening of water channels [9]. Both models may convincingly account for the speed of the movement.

The possibility to study the effect of microgravity on living organisms is a unique opportunity to observe the alteration of phenomena in the absence of the otherwise omnipresent gravity force. Although the understanding of the effect of gravity on animal and plant bodies is crucial, in view of the possible future space travels, the research is moving slowly if

compared with other research fields, due to the accessibility to microgravity conditions and the challenging experimental condition.

In the present study we report the effect of microgravity on trap closure conducted during a parabolic flight campaign. This gave us the opportunity to test *Dionaea muscipula* as possible candidate to study the effect of gravity on the electrical activity of organisms by monitoring the variation in the excitability of the traps and the alteration in the kinetics of their closure. Furthermore, the changes in the kinetics of trap closure gave us important hints on the mechanism at the base of the fast trap snapping.

2. Materials and Methods

Parabolic flight experiments were performed in an A300 airplane (Novespace, France) during the 9th DLR parabolic flight campaign. A typical parabolic flight manoeuvre provides alternating acceleration levels of regular gravity (1 g), microgravity (0 g) for 22 s, and two periods (20 s) of hypergravity (up to 1.8 g for 20 s) before and after each period of microgravity. Twenty *Dionaea muscipula* J. Ellis plants were grown in a growth chamber with 14/10 h light/dark period, in well-drained peat moss in plastic pots irrigated with distilled water. All experiments were performed on healthy adult specimens. The pots were sealed with parafilm to avoid the floating of the substrate during the zero gravity periods, and plants were secured inside a plexiglass growth chamber. Digital HD video recorder Sony HDR-SR11E was used to film the Venus flytraps at 25 fps. Each day experiments were done on 4 different plants. All the traps were mechanically stimulated during 0, 1, and 2 g, using a wooden stick by gently touching the trigger hairs. The wooden stick was immediately removed after stimulation. The collected movies were analysed frame by frame, and the trap closure was quantified by measuring the change of distance between two laminas with ImageJ software [15]. Space and time constraints limited the number of plants that could be carried on board and consequently limited the number of traps available each day. More emphasis was given to the zero gravity condition; therefore 25 traps were tested in microgravity, 20 were tested in 1 g during the flight, and 8 traps were devoted to 2 g. The distance $y(t)$ between the edges of the trap leaf was measured in the closing process. In the open state, the distance between the edges of the trap leaf is $y_{\max}$. As individual plants have different opening distances data were normalized $x = y/y_{\max}$. The speed of trap closure was calculated as $v = dx/dt$ and it has the dimension of s^{-1}.

3. Results

The trap closure was studied at different gravity conditions (Figure 1).

Results showed a low responsiveness of traps in microgravity: 36% of the traps did not close at all and 48% manifested a slower closing motion. The traps stimulated in normal gravity demonstrated a normal closure in 80% of the cases and, finally, the traps stimulated in hypergravity reacted promptly to the stimulation, with 50% of the traps being faster than controls (Table 1).

Table 1: Trap behaviour recorded under different gravity conditions; the number of traps tested n is reported in the table.

	n	No response	Normal closure	Slow closure	Fast closure
0 G	25	36%	16%	48%	0%
1 G	20	10%	80%	10%	0%
2 G	8	0%	50%	0%	50%

In the graph (Figure 2) three representative examples have been reported.

Trap closure is strongly affected by gravity: in microgravity the kinetics of snapping is slower (Figure 2(a)) and the acceleration is low if compared with 1 and 2 g where the speed of closure increases sharply after the trigger (Figure 2(b)).

Because of the constraints involved in performing the experiments on a plane we were unable to measure the reaction time between the trigger and the start of the closure (our time resolution was 40 ms and the traps were stimulated manually). However, visual observation revealed a delayed response in zero gravity, and an anticipated response in hyper-g.

4. Discussion

Volkov et al. described the trap closure as consisting of three different phases [9]: (1) a mechanically silent period with no observable movement immediately after stimulation; (2) the period when the movement starts accelerating; (3) the fast movement of the trap, when the leaves quickly relax to the new equilibrium state. In our results it appears that microgravity acts in *Dionaea* at two different levels: (i) by impairing the signal transduction, as suggested from the high percentage of inactive traps and from the lower responsiveness (phase 1); and (ii) by altering the trap kinetics by significantly reducing the trap closing time (phases 2-3), eventually suggesting that the mechanisms leading to trap closure are gravity-related. The electrical properties of excitable cells are extremely important in higher organisms. Changes of their parameters under microgravity can impair the functionality of the neural systems and have significant consequences for human, especially in view of long space travels. The few reports available on animal cells suggest that action potentials are affected by gravity [16]: in particular, the propagation velocity and their intensity seem to be gravity-dependent; that is, they increase under hypergravity and decrease under microgravity compared to 1 g [17]. Very little is known for higher plants. Masi et al. monitored for the first time the electrical activity of root cells during a parabolic flight and observed alterations of the frequency of APs [18]. Altered parameters have been reported also under hypergravity (Masi et al., unpublished) suggesting that the excitability of both plant and animal cells is heavily affected by altered gravity conditions.

In *Dionaea muscipula* it is well known that the stimulation of trigger hairs generates the two APs required for trap closure [9, 19, 20]. The high number of inactive traps (i.e., no response to the trigger) and the apparent slower response time of

Figure 1: Closing of the trap in micro- (0 g), normal (1 g), and hypergravity (2 g).

the trap closure suggest an alteration in the generation or propagation of the APs in microgravity. In plants, as well as in animals, action potentials are induced by the fast opening and closing of ion channels whose functionality has been little studied and understood in microgravity so far. In fact, ion channels are integral membrane proteins, and they could be affected either directly or indirectly by gravity. Gravity could directly affect the protein integrity, whereas changes in the thermodynamical properties of the membrane could have an indirect effect on the ion channel functionality [21].

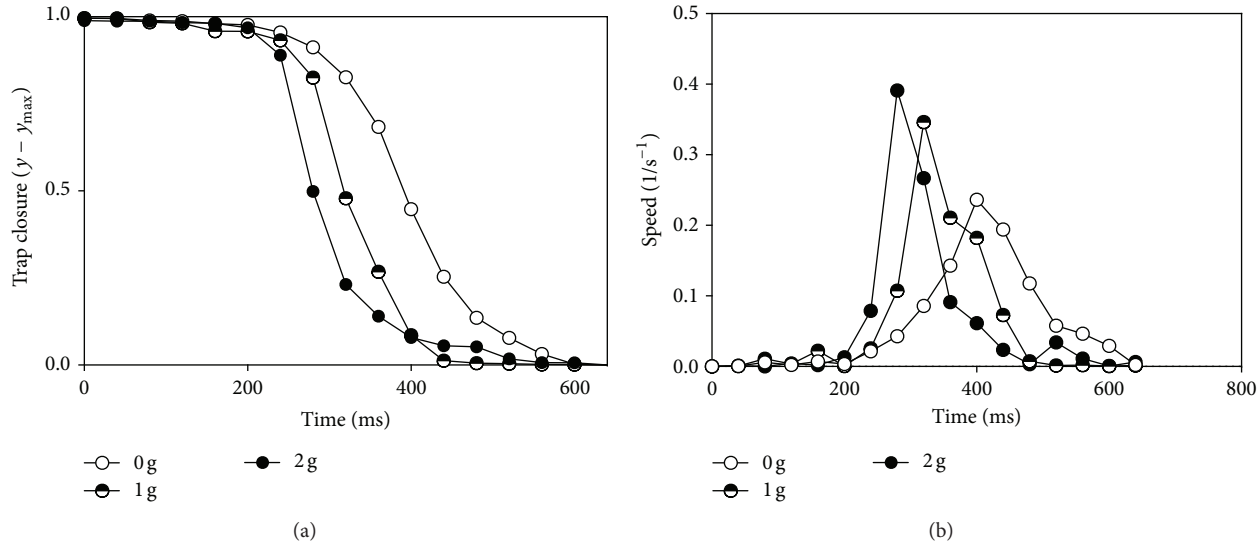

Figure 2: Effect of gravity on trap closure. (a) Kinetics of trap closure under different gravity conditions: y is the distance between the edges of the lobes. (b) Dependency of the speed of trap closure on time after stimulation.

In 2001, Goldermann and Hanke showed for the first time that gravity influences the integral open state probability of ion channels providing a first explanation of the effects of gravity on electrical signalling [22]. Those findings were further confirmed by patch-clamp analysis [21].

Nothing similar has been done for plants. The first silent stage of the trap closing involves transduction of electrical signal and hence it is related to ion channel gating. Interestingly results similar to the ones obtained here under microgravity were observed when applying channel blockers to the traps [9]. The use of BaCl2, ZnCl2, and TEACl significantly delayed trap closure and altered its speed [9].

Of course, the results presented here are just preliminary. Further studies will be necessary to consolidate the results and to investigate in deeper detail the possible effect of gravity on the generation and propagation of action potentials. Particularly interesting would be to stimulate electrically the traps allowing measuring and quantifying the delay in trap closure under altered gravity conditions.

To conclude, our results demonstrate the role of microgravity on the events leading to trap closure. The possible alterations of ion and water channel permeability that could be at the base of the lower responsiveness and slow closure observed in microgravity are a possibility worthy to be investigated. In fact, if properly demonstrated it would strengthen the validity of the hydroelastic curvature model suggested by Volkov et al. [9]. Finally, we want to stress the fact that Venus flytrap could be an easy and effective model plant to perform studies on ion channels and aquaporin activities, as well as on electrical activity *in vivo* on board of parabolic flights and large diameter centrifuges.

Conflict of Interests

The authors declare that there is no conflict of interests regarding the publication of this paper.

References

[1] J. Burdon-Sanderson, "On the electrom otive properties of the leaf of dionaea in the excited and unexcited states," *Philosophical Transactions of the Royal Society of London*, vol. 173, pp. 1–55, 1882.

[2] C. Darwin and F. Darwin, *Insectivorous Plants*, John Murray, London, UK, 1888.

[3] B. B. E. Juniper, R. J. Robins, and D. M. Joel, *The Carnivorous Plants*, Academic Press, London, UK, 1989.

[4] W. H. Brown and L. W. Sharp, "The closing response in dionaea," *Botanical Gazette*, vol. 49, no. 4, pp. 290–302, 1910.

[5] A. G. Volkov, T. Adesina, and E. Jovanov, "Closing of venus flytrap by electrical stimulation of motor cells," *Plant Signaling & Behavior*, vol. 2, no. 3, pp. 139–145, 2007.

[6] S. E. Williams and A. B. Bennett, "Leaf closure in the venus flytrap: an acid growth response," *Science*, vol. 218, no. 4577, pp. 1120–1122, 1982.

[7] J. Scala, K. Iott, D. Schwab, and F. Semersky, "Digestive secretion of *Dionaea muscipula* (venus's flytrap)," *Plant Physiology*, vol. 44, no. 3, pp. 367–371, 1969.

[8] K. Trebacz and A. Sievers, "Action potentials evoked by light in traps of *Dionaea muscipula* ellis," *Plant and Cell Physiology*, vol. 39, no. 4, pp. 369–372, 1998.

[9] A. G. Volkov, T. Adesina, V. S. Markin, and E. Jovanov, "Kinetics and mechanism of dionaea muscipula trap closing," *Plant Physiology*, vol. 146, no. 2, pp. 694–702, 2008.

[10] A. Pavlovič, L. Slováková, C. Pandolfi, and S. Mancuso, "On the mechanism underlying photosynthetic limitation upon trigger hair irritation in the carnivorous plant Venus flytrap (Dionaea muscipula Ellis)," *Journal of Experimental Botany*, vol. 62, no. 6, pp. 1991–2000, 2011.

[11] A. Pavlovič and S. Mancuso, "Electrical signaling and photosynthesis can they co-exist together?" *Plant Signaling and Behavior*, vol. 6, no. 6, pp. 840–842, 2011.

[12] D. Hodick and A. Sievers, "On the mechanism of trap closure of Venus flytrap (Dionaea muscipula Ellis)," *Planta*, vol. 179, no. 1, pp. 32–42, 1989.

[13] B. S. Hill and G. P. Findlay, "The power of movement in plants: the role of osmotic machines," *Quarterly Reviews of Biophysics*, vol. 14, no. 2, pp. 173–222, 1981.

[14] Y. Forterre, J. M. Skotheim, J. Dumals, and L. Mahadevan, "How the Venus flytrap snaps," *Nature*, vol. 433, no. 7024, pp. 421–425, 2005.

[15] C. A. Schneider, W. S. Rasband, and K. W. Eliceiri, "NIH image to imageJ: 25 years of image analysis," *Nature Methods*, vol. 9, no. 7, pp. 671–675, 2012.

[16] M. Wiedemann, F. P. Kohn, H. Roesner, and W. R. Hanke, "Behavior of action potentials under variable gravity conditions," in *Self-Organization and Pattern-Formation in Neuronal Systems under Conditions of Variable Gravity*, pp. 95–109, 2011.

[17] K. Meissner and W. Hanke, "Action potential properties are gravity dependent," *Microgravity Science and Technology*, vol. 17, no. 2, pp. 38–43, 2005.

[18] E. Masi, M. Ciszak, S. Mugnai et al., "Electrical network activity in plant roots under gravity-changing conditions," *Journal of Gravitational Physiology*, pp. 167–168, 2008.

[19] D. Hodick and A. Sievers, "The action potential of Dionaea muscipula Ellis," *Planta*, vol. 174, no. 1, pp. 8–18, 1988.

[20] W. H. Brown, "The mechanism of movement and the duration of the effect of stimulation in the leaves of dionaea," *The American Journal of Botany*, vol. 3, no. 2, pp. 68–90, 1916.

[21] M. Wiedemann, F. P. Kohn, H. Roesner, and W. R. Hanke, "Interaction of gravity with molecules and membranes," in *Self-Organization and Pattern-Formation in Neuronal Systems under Conditions of Variable Gravity*, pp. 57–93, 2011.

[22] M. Goldermann and W. Hanke, "Ion channel are sensitive to gravity changes," *Microgravity Science and Technology*, vol. 13, no. 1, pp. 35–38, 2001.

Hindawi Publishing Corporation
BioMed Research International
Volume 2014, Article ID 928507, 15 pages
http://dx.doi.org/10.1155/2014/928507

Review Article

The Impact of Simulated and Real Microgravity on Bone Cells and Mesenchymal Stem Cells

Claudia Ulbrich,[1] Markus Wehland,[2] Jessica Pietsch,[2] Ganna Aleshcheva,[2] Petra Wise,[3] Jack van Loon,[4,5,6] Nils Magnusson,[7] Manfred Infanger,[2] Jirka Grosse,[8] Christoph Eilles,[8] Alamelu Sundaresan,[9] and Daniela Grimm[10]

[1] *Department of Physiology, Membrane Physiology, University of Hohenheim, 70593 Stuttgart, Germany*
[2] *Clinic for Plastic, Aesthetic and Hand Surgery, Otto-von-Guericke University, 39120 Magdeburg, Germany*
[3] *Hematology/Oncology, Children's Hospital Los Angeles, University of Southern California, Los Angeles, CA 90027, USA*
[4] *Department of Oral and Maxillofacial Surgery/Oral Pathology, VU University Medical Center Amsterdam, 1007 MB Amsterdam, The Netherlands*
[5] *Department of Oral Cell Biology, Academic Centre for Dentistry Amsterdam (ACTA), University of Amsterdam and VU University Amsterdam, 1081 LA Amsterdam, The Netherlands*
[6] *European Space Agency Technology Center, Gravity Lab (ESA-ESTEC-TEC-MMG), 2201 AZ Noordwijk, The Netherlands*
[7] *Medical Research Laboratory, Institute of Clinical Medicine, Aarhus University, 8000 Aarhus C, Denmark*
[8] *Department of Nuclear Medicine, University of Regensburg, 93052 Regensburg, Germany*
[9] *Department of Biology, Texas Southern University, 3100 Cleburne, Houston, TX 77004, USA*
[10] *Institute of Biomedicine, Pharmacology, Aarhus University, Wilhelm Meyers Allé 4, 8000 Aarhus C, Denmark*

Correspondence should be addressed to Daniela Grimm; daniela.grimm@farm.au.dk

Received 4 April 2014; Revised 6 June 2014; Accepted 6 June 2014; Published 10 July 2014

Academic Editor: Mariano Bizzarri

How microgravity affects the biology of human cells and the formation of 3D cell cultures in real and simulated microgravity (r- and s-μg) is currently a hot topic in biomedicine. In r- and s-μg, various cell types were found to form 3D structures. This review will focus on the current knowledge of tissue engineering in space and on Earth using systems such as the random positioning machine (RPM), the 2D-clinostat, or the NASA-developed rotating wall vessel bioreactor (RWV) to create tissue from bone, tumor, and mesenchymal stem cells. To understand the development of 3D structures, *in vitro* experiments using s-μg devices can provide valuable information about modulations in signal-transduction, cell adhesion, or extracellular matrix induced by altered gravity conditions. These systems also facilitate the analysis of the impact of growth factors, hormones, or drugs on these tissue-like constructs. Progress has been made in bone tissue engineering using the RWV, and multicellular tumor spheroids (MCTS), formed in both r- and s-μg, have been reported and were analyzed in depth. Currently, these MCTS are available for drug testing and proteomic investigations. This review provides an overview of the influence of μg on the aforementioned cells and an outlook for future perspectives in tissue engineering.

1. Introduction

It is well known, that microgravity influences different biological systems like bone and muscle as well as the heart and brain, and it enhances cancer risk [1]. During their stay at the MIR, astronauts and cosmonauts did show a distinct loss of bone mineral density in the lumbar spine, the pelvis, and the proximal femur [2], and the extent of bone loss varied up to 20% [3].

As it is not feasible to gather enough material from astronauts to do in-depth investigations, another device has been developed for the International Space Station (ISS), the mice drawer system (MDS), as a facility to study long-time influence of radiation on the biology and behavior of mice.

Tavella et al., for example, report an altered bone turnover in different strains of mice which were kept on the ISS for 91 days. This resulted in bone loss due to increased bone resorption and a decreased bone deposition [4].

While the past biological, physiological, and medical research nearly exclusively focused on investigating the biochemical processes of living cells and organisms, more and more attention was paid to the biomechanical properties and mechanical environment of cells and tissues during the last decades. When culturing cells on Earth, they usually settle on the bottom of the culture flask, forming two-dimensional (2D) monolayers. A three-dimensional (3D) growth, more resembling the tissue environment found in living organisms, is prevented by the presence of the gravitational field. For a scaffold-free 3D tissue growth, it is therefore necessary to circumvent this problem by effectively eliminating the influence of the gravitational pull during cultivation. One of the byproducts of various space flight endeavors is the possibility to perform long-term near-weightlessness or microgravity (μg) experiments [5, 6]. In a μg environment, cells will not settle like on Earth. This provides an increased opportunity for freely floating cells to interact with each other and develop 3D structures [7].

2. Space Flights for Cell-Biological Experiments

Long-term orbital space flight experiments are, however, not trivial. Flight opportunities are very scarce and the costs of hardware development are high. Furthermore, science is not always a priority in space flight activities. Such preconditions are delaying the advancement of research in areas such as cell biology and tissue engineering disciplines, which could profit tremendously from more frequent research options in a real microgravity (r-μg) environment.

Some researchers recently pointed out that osteoblasts undergo a disintegration of their cytoskeleton, which may explain dramatic changes in size and shape of the cells and their surface specializations [47]. Also, other studies have been performed using the ISS or space shuttle flights to learn more about the behavior of bone cells in space [48], but flight opportunities are sparse, and, therefore, other platforms had to be elucidated.

It is due to the aforementioned limitations that, over the years, various devices have been developed in an attempt to reduce the impact of gravity and simulate a near-weightlessness environment (s-μg) on Earth. From a physical point of view, gravity is a force exhibiting both magnitude and direction. Therefore, the influence of gravity can be reduced by either manipulating magnitude or direction. An orbital space flight as on the ISS is physically identical to a free-fall. Here, the gravitation acts in a perpendicular manner on the spacecraft's velocity vector, effectively changing its direction constantly but not affecting its magnitude. Free-fall is also found when using sounding rockets, which provide r-μg during a time span of up to 15 minutes. On Earth, r-μg can also be attained, although only for periods in the range of seconds, in drop towers, and during parabolic flights missions [49, 50]. Although time periods of seconds or minutes limit their use for tissue engineering studies, such periods can be useful to explore various intra- and intercellular processes, responsible for gene expression and protein content changes which can be observed after only a few hours of culturing cells in μg [49–51].

3. Devices Simulating Microgravity on Earth

In this respect, we should mention an instrument that was introduced by the European Space Agency (ESA) in the early nineties, called the free fall machine (FFM) [52]. This instrument was specifically developed for biological experiments and could generate a free fall for a period of about 800 ms with an intermediate "bounce" of ~20 g for around 50 ms. The paradigm of the FFM is that cells might not be sensitive to the relatively short period of 50 ms of hypergravity, while they experience the relatively longer period of free-fall. Long-term experiments (hours, days), which might be useful for tissue engineering studies, could be performed on this platform. However, thus far, only two studies were published using the FFM, one investigating *Chlamydomonas* [53] and another one researching T-lymphocytes [54]. The *Chlamydomonas* study showed similar results to what was found in real space flight while the T-lymphocytes experiments did not. Considering the very limited number of studies performed on this ground-based device, the FFM still might deserve some more exploration.

Levitating magnets are also used to produce s-μg on Earth. Such systems compensate the magnitude of the gravity vector by preventing sedimentation of relatively heavy structures, like cells, by the application of a high gradient magnetic field. This principle was first described for biological systems by Berry and Geim in 1997 [55], who demonstrated that a toad could be levitated and survive while exposed to a 16 Tesla magnetic field. Various experiments in cell biology have made use of such systems [56–58]. The magnetic field acts on individual molecules and atoms within a cell, based on their magnetic susceptibility, preventing them from sedimentation. However, the magnetic field as such confounds possible s-μg effects. The direction of the field might force (bio-)polymers into a certain orientation. Different polymers within a cell or on the cell membrane have different susceptibilities, possibly producing artifacts by forcing polymers into specific arrangements, which may not reflect the actual physiological situation [59–61]. Superconducting high gradient magnets are especially capable of performing long-term experiments and might be useful in the area of tissue engineering [62–64]. In this context, another promising technique should be mentioned. This method is the use of magnetic particles for 3D cell cultures. It is not based on a high-gradient magnetic field, but on ferromagnetic particles attached to cells, which can subsequently be levitated by a conventional magnet facilitating the formation of 3D structures [65, 66].

Another option is to manipulate the direction of the gravity vector with respect to the sample. The reduction of the gravitational impact on biological systems by constantly changing its orientation was shown first in experiments by

the German botanist von Sachs in 1879, growing *Lepidium sativum* and *Linum usit* [67]. He constructed a slowly rotating system and named it a clinostat, in which, for example, a plant can be placed horizontally and rotated around its longitudinal axis. In doing so, the gravity vector stimulus is constantly changing its impact angle on the sample. As a result, a plant grows straight without the characteristic gravitropic curvature seen when the plant is placed horizontally and not rotating. Based on these initial studies, other rotating systems like the fast rotating clinostat have been developed.

The initial clinostats were rotating relatively slowly in a range from one rotation per couple of hours up to a maximum of about 10 rpm. This is adequate for relatively "solid samples" such as plants, but too slow for cell culture systems that involve a large liquid phase. In a biphasic system, that is, a liquid with particles (cells) both of different density, the heavy particles tend to settle. Rotating such a system around a horizontal axis keeps the heavy particles in suspension. This phenomenon depends mainly on the relative density of the liquid and the particles, the viscosity of the liquid, the rotation speed, and the diameter of the rotated container. When a cell is in a static vessel and the vessel is rotated by 90°, the cell will settle in the direction of the gravity vector. One can repeat this for a full 360° and upon an increase in the frequency of rotation, the traveling distance of the cell decreases. If this rotation is performed constantly with increased speed, we finally end up rotating a cell around its own axis. Such a controlled rotation not only applies to the cells, but also its surrounding boundary liquid phase [68].

Another well-known device to simulate μg is the so-called random positioning machine (RPM), a 3D clinostat [69] consisting of two frames, each driven by a dedicated motor. This allows a randomized movement of both frames, independent of each other [69–74]. One of the advantages of the RPM is its size, as cell culture flasks can easily be mounted on it, so it is possible to work with quite large liquid volumes. This ranges from regular T25 flasks [75, 76] to multi-well plates [77], flasks on slides [78], or more dedicated devices [79]. As cells move freely within the liquid, they usually interact with each other and form multicellular spheroids.

The best simulation of μg is achieved in the rotation center of the two axes, which limits the preferred volume size of the samples. Depending on the speed of rotation and the distance from the center, an acceptable residual gravity can be obtained in the order of 10^{-4} g by a maximum angular velocity of $60^{\circ}\,s^{-1}$ at a radial distance of 10 cm [70]. Earlier RPM models had no possibility to add constituents during the experiment, but newer models have been developed to enable fluid management during rotation [73, 74]. RPMs are commercially available by Mitsubishi Heavy Industries (Kobe, Japan) and Dutch Space (Leiden, The Netherlands), while various academic groups developed similar systems on their own [80–84] (Figure 1).

The rotating wall vessel (RWV) prevents cells from settling via a constant rotation. It has been developed by NASA [85] and is now commercially available through Synthecon Inc. (Houston, TX, USA). Basically, RWVs consist of a slow rotating, relatively large liquid filled container (vessel). The rotation speed has to be adapted to the specific weight of the cells, the fluid density, and viscosity. The cells and tissues in the RWV are constantly falling within the fluid. The settling velocity and direction combined with the rotation of the fluid create spiral trajectories within the vessel [86]. This motion of the sample relative to the fluid generates fluid shear forces on a particle surface ranging from 180 to 320 mPa (1.8–3.2 dyne/cm^2) for 50 μm beads [87], ~500 mPa (5 dyne/cm^2) with 3D aggregates of BHK-21 cells [88] to 520–780 mPa (5.2–7.8 dynes/cm^2) for a 200 or 300 μm spherical object [89]. Over the years, various models based on the initial RWV have been developed, differing in vessel geometry, aspect ratio, and gas supply, such as the slow turning lateral vessel (STLV) [90], the high aspect ratio vessel (HARV) [91], or the rotating-wall perfused vessel (RWPV) [92].

Hence, it can be concluded that annulling the gravity forces, which pull the cells constantly towards the Earth, deliver the ultimate trigger to eukaryotic cells to leave a cell monolayer and assemble in 3D aggregates [5].

It is still unknown which cellular and biochemical mechanisms are involved in the altered signal transduction and in the change of the cellular growth behavior.

4. Transition from Two- to Three-Dimensional Cell Growth

A few publications appeared in the literature in recent years, providing some clues for understanding the weightlessness-induced transition from two- (2D) to three-dimensional (3D) cell growth.

Several signaling pathways are affected by annulling gravity forces in the cell interior [93]. However, it is unknown which of these signaling pathways contribute to the formation of three-dimensional aggregates. When endothelial cells form tubes, the nitric oxide signaling pathway appears to be affected [94]. Siamwala et al. reported that iNOS (inducible nitric oxide synthase) acts as a molecular switch, which controls whether the effects of μg on vascular endothelial cells induce angiogenesis via the cyclic guanosine monophosphate (cGMP)-PKG-dependent pathway [94]. iNOS is upregulated in HUVEC by a mechanism dependent on suppression of AP-1, after clinorotation of the cells [95]. In addition, the endothelial nitric oxide synthase is phosphorylated by phosphoinositide 3-kinase under weightlessness, simultaneously with Akt [96]. The organoid formation by PC12 pheochromocytoma cells in a RWV bioreactor is accompanied by prolonged activation of the ERK, p38, and jnk signaling pathways [97].

3D cell culture techniques have attracted much attention, not only among biologists, but also clinicians interested in tissue engineering [98, 99] of artificial vessels [100–104] or cartilage [105–108]. Moreover, osteoarthritis and cartilage trauma occur in patients with a high incidence, but current treatment methods are still limited [109]. Even a minor injury to articular cartilage may lead to progressive damage and degeneration [110].

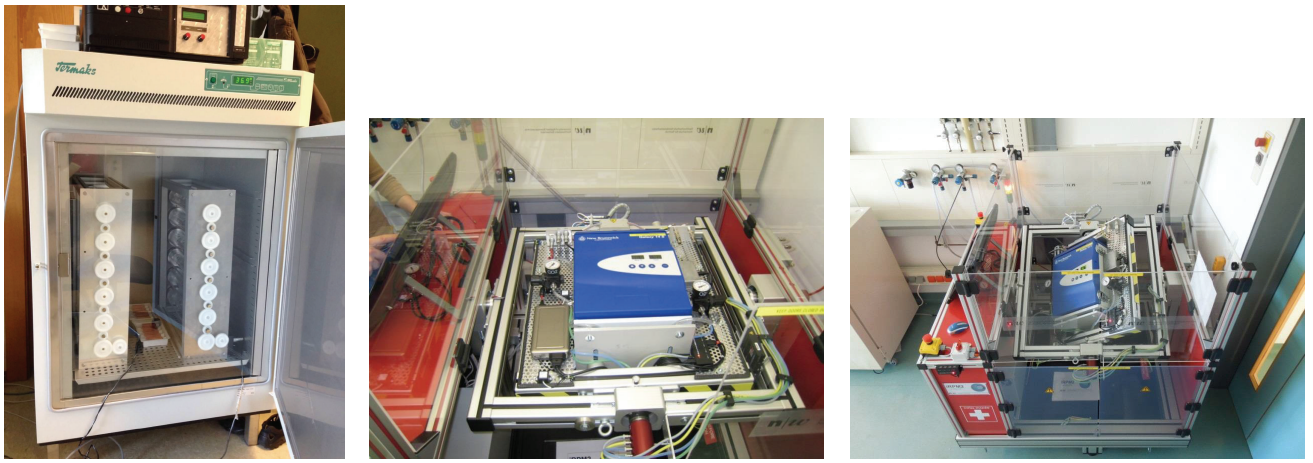

(a) (b) (c)

Figure 1: (a) Two 2D clinostat devices in an incubator constructed by the German Aerospace Center (DLR), Institute of Aerospace Medicine, Biomedical Science Support Center, Gravitational Biology, Cologne, Germany. (b, c): Random Positioning Machine simulating microgravity. It was developed by T. Hoson in Japan and manufactured by Dutch Space (former Fokker Space). The basic principle consists of an inner and an outer frame rotating independently from each other in random direction. The samples in the center of the machine experience low gravity as the gravity vector is averaged to zero over time. The redesign of the classical RPM with a CO_2-Incubator with temperature and CO_2-level control was realized by Professor Jörg Sekler, Fachhochschule Nordwestschweiz (FHNW), Institut für Automation, Switzerland, and tested by PD Dr. Marcel Egli, Hochschule Luzern—Technik & Architektur, CC Aerospace Biomedical Science & Technology, Hergiswil, Switzerland.

5. Tissue Engineering of Bone

Bone loss has been documented for many years in μg (1-2% a month). Increased bone loss and risk of fractures is an identified risk in the bioastronautics critical roadmap for long-term cosmic missions to the moon and mars. *In vitro* drug screening both in 1 g, μg and in artificial gravity is essential to adequately address countermeasures for bone loss. Bone loss in μg is the second most important risk to space missions [5, 6].

Exposure to the μg environment of space causes astronauts to lose calcium from bones [5, 6]. This loss occurs because the absence of Earth's gravity disrupts the process of bone maintenance in its major function of supporting body weight. Exposure to the μg environment of space causes men and women of all ages to lose up to 1% of their bone mass per month due to disuse atrophy, a condition similar to osteoporosis. It is not yet clear whether loss in bone mass will continue as long as a person remains in the μg environment or level off in time.

There are, indeed, four major bone cell types, and each of them seems to be influenced by μg. Bone mesenchymal stem cells (MSC) are able to differentiate into adipocytes, osteoblasts, and osteoclasts. Proliferation and differentiation are very sensitive to μg, as the lack of gravity in space can reduce mechanical stress, leading to a decreased rate of osteogenesis and an increased adipogenesis rate [111]. As the signaling pathways involved in MSC differentiation form a complicated network, it has been found that the reduction in the osteogenesis of MSCs in the presence of μg is mediated by a decrease in the integrin/mitogen-activated protein kinase (MAPK) signaling pathway [112], as well as RhoA and cytoskeletal disruption [113].

Osteoblasts are derived from MSCs, but in μg the differentiation does not function properly, and the resulting bone loss has been attributed to osteoblasts due to their (1) reduced proliferation and activity, (2) reduced differentiation, and (3) decreased responsiveness to bone-related factors in the microenvironment [114]. Observations have also been made regarding the cytoskeleton of osteoblasts; there is growing evidence that the cytoskeleton is closely connected to nuclear morphology and function [115]. The enlarged nuclei observed in flight osteoblasts could be a result of cytoskeletal disruption [116].

Osteocytes regulate bone resorption and formation and are considered the terminal differentiation stage of osteoblasts. The osteocytes in cortical bone and periosteum degenerated after a 12.5-day flight in space on the Cosmos Biosatellite [117]. Osteocyte apoptosis has been observed after a 2-week flight, increasing the number of functionally active osteoclasts [118]. Apoptotic osteocytes are essential for the initiation of bone remodeling, but it is the neighboring nonapoptotic osteocytes that produce proosteoclastogenic signaling [119]. Osteocytes seem to be the key effectors of μg induced bone loss [120].

Osteoclasts are bone-resorbing cells, and their differentiation seems to be enhanced in μg [121]. This could be another explanation of bone-loss in space.

The mystery, for the moment, is what signals permit bone tissue to adapt to a weightless or an Earth (1 g) environment. Researchers do not yet know whether the biomechanical stimuli that are changed by μg directly affect osteoblast and osteoclast function or if other physiological factors such as hormone levels or poor nutrition contribute to bone loss. NASA investigators are studying gravity-sensing systems in individual bone cells by flying cultures of these

cells on the space shuttle and observing how they function. Discoveries made in the course of space biomedical research on bone are already contributing to a better understanding of osteoporosis and the treatment of bone mass loss on Earth as well as in space. The single most important contribution that NASA research has made to the understanding of bone deterioration in osteoporosis is heightened awareness of the importance of gravity, activity, and biomechanics—that is, the mechanical basis of biological activity— in bone remodeling.

Mechanical forces—the action of energy on matter—appear to coordinate bone shaping processes. The standard theory of bone remodeling states the body translates mechanical force into biochemical signals that drive the basic processes of bone formation and resorption. Aging, especially in postmenopausal women, and exposure to μg uncouple bone resorption and formation. When this uncoupling occurs, formation lags behind resorption, and the result is bone loss.

Researchers are not yet certain whether bone resorption speeds up or the bone formation slows down, though recent experimentation in space indicates that μg might somehow affect both processes. Progress in developing methods of preventing or treating disuse atrophy and osteoporosis depends on better understanding of the mechanisms that cause the problem. Determining how the body translates mechanical loading (physical stress or force) into the signals that control bone structure may reveal how aging, inactivity, and space flight uncouple bone formation and resorption. Only in the absence of gravity can we determine the influence of weight and stress on bone dynamics.

By studying what mechanisms translate mechanical stress on bones into biochemical signals that stimulate bone formation and resorption, space life scientists may be able to determine how to maintain bone mass. Researchers do not yet know exactly what type and amount of exercise, hormones, or drugs might prevent bone loss or promote bone formation. However, some combination of sex hormones, growth hormones, and exercise seems to be the key to preventing bone mass loss associated with chronological aging and postmenopausal hormone changes on Earth.

Bone is made up of several different cell populations. Osteoclasts are responsible for the breakdown of mineralized bone, in preparation for bone remodeling. In contrast, the osteoblasts synthesize mineralized bone in the remodeling process. The goal of this project is to develop an "*in vitro*" three-dimensional, cellular model of osteoclasts and osteoblasts (human and rodent) cultured together in μg analog culture conditions to identify the underlying biomarkers related to bone loss in μg and the cellular mechanisms involved in bone resorption. The NASA rotating-wall vessel (RWV) permits the growth of mixed cell cultures for much longer periods than traditional culture methods. This would set the stage for development of countermeasure strategies for bone loss in space as well as in osteoporosis and rheumatoid arthritis which are increased health risks on Earth. Professor Sundaresan and collaborators [122–124] have developed a 3D cell culture bone tissue model using a specialized rotating-wall vessel culture system to address a more physiologically relevant model to the human body. The use of the cells by themselves also eliminates confounding variables such as neuroendocrine stress found *in vivo* (Figure 2(a)).

The human body needs a framework to withstand gravity. This framework is given by the skeletal system. During long-term space missions, bone loss has been reported in astronauts at a rate that is both substantial and progressive with time spent in μg [125–128]. But what is the reason for this massive bone loss? Some studies suggested that this effect might be attributed to increased resorption in load-bearing regions of the skeleton [129–131], and evidence of a decrease in bone formation had also been described. For example, the loss of bone in μg is about 10 times greater than the bone mineral density loss per month of postmenopausal women on Earth, who are not on estrogen therapy [132–135]. The loss of bone mineral density in a six-month mission appeared to be reversible in 1000 days after return to Earth [136, 137], but changes in the bone structure are irreversible and seem to mimic changes in the elderly [137].

Until now there are still knowledge gaps on the mechanism of bone loss, especially on the molecular and cellular mechanisms, also the question of fracture repair arises. Moreover, more information is needed on the influence of radiation, hormones, and fluid shifts.

Investigations in humans and animals are quite difficult due to the lack of long-term flight opportunities, the absence of animal housing facilities in space, and the problem of material collection from returning astronauts. Thus, other possibilities have to be sought in order to investigate bone. So far, most commonly used are bone cell culture experiments, which are a viable opportunity for investigating cells in 3D, acting as tissue like samples while they are cultivated under conditions of weightlessness. However, 3D embryonic bone tissue cultures have been used in the past and show a clear decrease in matrix mineralization, in mineralizing cartilage and by osteoblasts, combined with an increased mineral resorption by osteoclasts [138].

Besides this, tissue engineering is a very up-to-date topic. The ultimate goal is to generate functional 3D constructs, which can be used as replacement organs or structures with normal function or serve for *in vitro* studies [5, 139]. Bone replacement, especially, is quite difficult, as large bone defects usually require reconstructive surgery to restore function [140]. Up to date, the treatment includes autograft or allograft transplantation and the use of synthetic materials [141]. While autograft transplantation is the preferred treatment, it suffers from limited supply and donor site morbidity [142]. As the autogenous origin of cells prevents potential immune rejection, the amount of bone marrow suitable for transplantation is limited. New techniques have been developed, allowing selection of bone marrow osteoprogenitor cells and expanding them in culture, so that a large amount of transplantable cells can be generated after only one biopsy [143–145].

In principle, culturing bone cells is not that easy. A combination of osteoconductive matrices, bone-forming cells, and osteogenic growth factors is needed for the engineering of bone tissue [146]. The first important factor is the cell type. Osteoblasts are in a close to mature stage, showing a low proliferative potential. Mesenchymal stromal cells represent

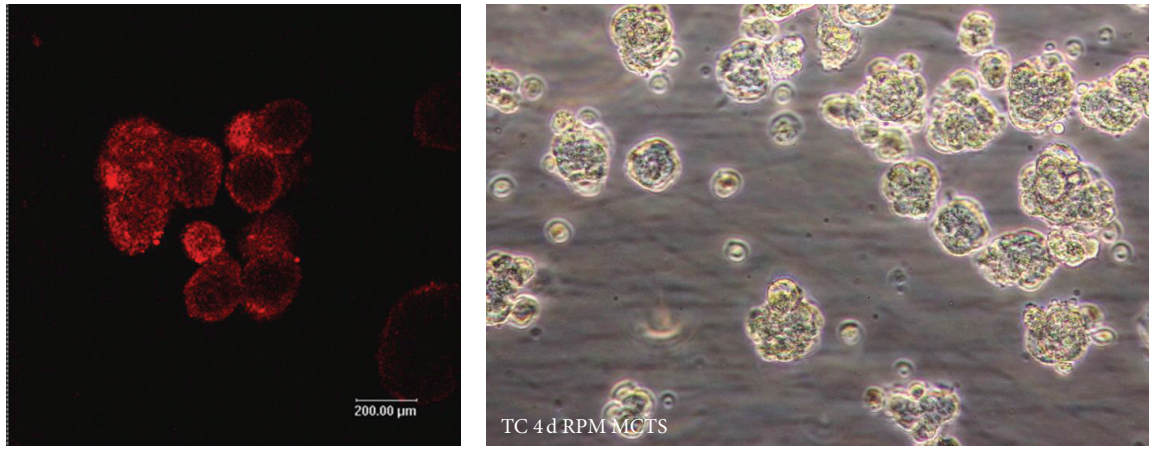

(a) (b)

Figure 2: (a) Production of large numbers of small (200 μm diameter) immature (7-day-old) osteospheres with labeled osteoclast cells (red) viewed by confocal imaging in living constructs-USPTO 80736136 and (b) follicular thyroid cancer cells (TC) cultured on the RPM. Several multicellular tumor spheroids are visible after 4 days.

a proliferating and undifferentiated cell source, but their availability is limited [147, 148]. An option to increase their lifespan *in vitro* is the overexpression of human telomerase reverse transcriptase (hTERT). The second factor is an ideal scaffold, which possesses mechanical properties comparable to bone. It should support cell adhesion and should be biodegradable to facilitate natural bone remodeling [146]. As of now, different studies have shown the advantages and disadvantages of several types of scaffolds like chitin, gelatin, poly(lactic acid), poly(glycolic acid), poly(lactic acid-co-glycolic acid), polycaprolactone, hydroxyapatite, coral, and so forth. Several *in vitro* studies revealed an ideal scaffold pore size for osteoblasts from 200 to 400 μm [149, 150]. It is important to recognize that the scaffold architecture influences the distribution of shear stress, the range of mechanical stimuli, as well as the proliferation and differentiation of osteoprogenitor cells [151, 152].

To simulate an ideal *in vivo* situation for *in vitro* cells, specific cytokines and growth factors are necessary. For bone morphogenesis, the bone morphogenetic proteins (BMP), which belong to the transforming growth factor beta (TGF-β) superfamily, are essential [153]. Currently, only BMP-2 and -7 are commercially available, so alternatives to stimulate osteoprogenitor cells by growth factors are required. It has been reported that autologous platelet-rich plasma is an effective bioactive supplement, as it contains osteogenic and angiogenic growth factors [154].

Several different bioreactor systems are already available for bone tissue engineering. A well-known and simple system is the spinner flask bioreactor. Convective forces are provided by a stirrer and the medium flows around the cells. The emerging shear stress is not applied homogenously, as there appears to form a gradient in the flask [146]. This factor certainly needs to be considered when conducting studies with the spinner flask system.

Other suitable instruments are rotating bioreactor systems, for example, the RWV. It has been used with different kind of bone cells, which are often grown with the help of microcarriers [8, 155] or scaffolds [8–11, 15, 155]. The high aspect ratio vessel (HARV) [91] was used by Lv et al. [12] to engineer tissue on poly(lactic acid glycolic acid)/nano-hydroxyapatite composite microsphere-based scaffolds.

Some researchers used bone marrow mesenchymal stem cells for their investigations. Jin et al. [16] were able to transplant RWV-grown bone constructs in cranial bone defects of Sprague-Dawley rats and found them to be more effective in repairing the defects than the 1 g controls after 24 weeks. Moreover, a 3D environment as in a rotary cell culture system enhanced osteoblast cell aggregation and mineralization [13]. Preosteoblasts cultured in a RWV could be engineered into osseous-like tissue [14].

6. Mesenchymal Stem Cells and Microgravity

Mesenchymal stem cells (MSCs) are cells capable of long-term proliferation and differentiation into various stromal tissue cell types. The state of MSCs rests on the cellular microenvironment and several soluble factors. In addition, gravity can influence MSC features. Disuse, as encountered during long-term bed-rest or space travel, and the accompanying absence of mechanical stimuli lead to an inhibition of osteogenesis and simultaneously to an induction of adipogenesis in MSCs. Hence, it is crucial to provide a proper mechanical stimulation for cellular viability and osteogenesis, particularly under unusual conditions.

In 2004, Merzlikina et al. [27] studied the effects of prolonged clinorotation on cultured human MSC morphology, proliferation rate, and expression of specific cellular markers. After exposure of the cells to clinorotation for time frames from 1 h to 10 days, it was shown that the proliferative rate decreased in the experimental cultures as compared to cells growing under normal conditions. Clinorotated MSCs seemed more flattened and reached confluence at a lower

cell density, which advocates that cultured hMSCs sense the changes in the gravity vector and respond to s-μg by altered functional activity. The group around Myoui [28] examined whether gravity-induced stress is linked to osteoblast differentiation and function. Rat marrow mesenchymal cells (MMCs) were cultured in pores of interconnected porous calcium hydroxyapatite (IP-CHA) for 2 weeks on a 3D clinostat. In MMCs subjected to s-μg, the marker of osteoblastic differentiation alkaline phosphatase activity was decreased by 40%, compared to the control group. Also, the clinostat group exhibited less extensive extracellular matrix formation than the control group. The implantation of the IP-CHA/MMC composites in syngeneic rats showed that bone formation was significantly lower for the clinostat group than for the control group. Yuge et al. [29] also used a 3D clinostat for their experiments on the proliferation behavior of hMSCs. The proliferation rate of the cells of the clinostat group was elevated almost 3-fold in comparison to the control group, and the number of hMSCs double-positive for CD44/CD29 or CD90/CD29 in the clinostat group after 7 days in culture increased 6-fold. The hMSCs cultured in a 3D-clinostat were still able to differentiate into hyaline cartilage after transplantation into cartilage defective mice and displayed the strong proliferative characteristic of stem cells, thus, showing that s-μg may be used to expand stem cell populations *in vitro*. In contrast to these findings, Dai et al. [24] reported in 2007 that μg simulated by a clinostat inhibited population growth of bone marrow mesenchymal stem cells (rBMSCs) and their differentiation towards osteoblasts. The cells grown on the clinostat were arrested in the G(0)/G(1) phase of cell cycle, and growth factors, such as insulin-like growth factor-I, epidermal growth factor, and basic fibroblast growth factor had only a slight stimulatory effect compared to the static control group. Gershovich and Buravkova's [17] work supports this hypothesis. After 20 days of clinostat-exposure, the proliferative activity of hBMCs was reduced, whereas it increased the number of large flat cells in the culture and stimulated migration activity of cells. In 2009, Gershovich and Buravkova [30] demonstrated the effects of s-μg by clinostat and RPM on the interleukin production by hBMSCs and MSC osteogenous derivatives. 20-day exposure on a clinostat increased the interleukin-8 (IL-8) content 1.4 to 3.2 times in the culture medium, while the average increase of IL-production on the RPM amounted to 1.5–6 times (10 days) and 1.6–2.1 times (20 days), respectively. This suggests that results of s-μg vary by the use of different modeling systems. rMSCs grown in a clinostat demonstrate that s-μg can boost the differentiation of MSCs into neurons, as demonstrated by Chen et al. [156] In s-μg, neuronal cells derived from rMSCs were found to express higher microtubule-associated protein-2 (MAP-2), tyrosine hydroxylase (TH) and choline acetyltransferase (CHAT). Furthermore, the excretion of neurotrophins such as nerve growth factor (NGF), brain derived neurotrophic factor (BDNF), or ciliary neurotrophic factor (CNTF) was increased. In comparison to 1 g controls, neuronal cells from the s-μg group generated more mature action potentials and displayed repetitive action potentials. This might benefit the search for new strategies for the treatment of central nervous system diseases.

Zayzafoon et al. [18] demonstrated that s-μg inhibits the osteoblastic differentiation of hMSC and induces the development of an adipocytic phenotype. In the effort of understanding space flight-induced bone loss, the group used the rotary cell culture system (RCCS) to model μg and determine its effects on osteoblastogenesis. Human MSCs were cultured and osteogenic differentiation was induced before the initiation of s-μg. As a result, the important mediator of adipocyte differentiation, peroxisome proliferator-activated receptor gamma (PPARgamma2), and adipsin, leptin, and glucose transporter-4 was highly expressed. These changes were not adjusted after 35 days of readaptation to normal gravity. Moreover, μg decreased ERK- and increased p38-phosphorylation pathways, known to regulate the activity of runt-related transcription factor 2 and PPARgamma2. These results were supported by Saxena et al. [19] in 2007, who demonstrated that s-μg inhibited osteoblastogenesis and increased adipocyte differentiation in hMSCs incubated under osteogenic conditions using the RCCS. They could show that a reduced RhoA activity and cofilin phosphorylation, disruption of F-actin stress fibers, and decreased integrin signaling through focal adhesion kinase were involved in this process. Meyers et al. [20] also investigated the effects of s-μg on integrin expression and function in hMSCs, since a reduced osteoblastic differentiation might be caused by impaired type I collagen (Col I)-integrin interactions or a reduction of integrin signaling. Culturing of hMSCs for 7 days in s-μg, lead to reduced expression of Col I, while Col I-specific alpha2 and beta1 integrin protein expression increased. However, autophosphorylation of adhesion-dependent kinases, focal adhesion kinase (FAK) and proline-rich tyrosine kinase 2 (PYK2) was significantly reduced. These findings indicate that a reduction in osteoblastogenesis in s-μg is, at least in part, caused by a reduced integrin/MAPK signaling. The group around Duan [16] studied the relationships between the composition and mechanical properties of engineered bone constructs. BMSCs were grown for 15 days on ceramic bovine bone scaffolds in different environments, namely, static flasks and the RWV. DNA content and alkaline phosphatase (ALP) were higher for cells grown on the RWV. After transplantation into Sprague-Dawley rats with cranial bone defects, the bone constructs engineered on the RWV repaired the defects better and showed histologically better bone connection.

Sheyn et al. [21] evaluated the effect of s-μg on all genes expressed in hMSCs, with the hypothesis that many important pathways are affected during culture on a rotating wall vessel system. The analysis of gene expression by use of whole genome microarray and clustering showed that 882 genes were downregulated and 505 genes were upregulated after exposure to s-v. A multitude of genes belonging to cell compartment, biological process, and signaling pathway clusters were modulated, as identified by gene ontology clustering. Significant reductions in osteogenic and chondrogenic gene expression and an increase in adipogenic gene expression were shown and could be validated by a parallel adipogenic differentiation assay. In order to investigate the effects of s-μg on chondrogenic differentiation of human adipose-derived MSCs (ADSCs), Yu et al. [22] cultured cells on

a RCCS in pellets with or without the chondrogenic growth factor TGF-β_1. Analysis of real-time PCR and histological results demonstrated that s-μg has a synergistic effect on chondrogenesis with TGF-β_1. The p38 MAPK pathway was activated by TGF-β_1 alone and was additionally stimulated by s-μg. Inhibition of p38 activity with SB203580 suppressed chondrocyte-specific gene expression and matrix production. This indicates that the p38 MAPK signal mediates s-μg-induced chondrogenesis of ADSCs. In MSCs cultured during chondrogenic induction in a rotating culture, combined with polyglycolic acid (PGA), mRNA and proteins of collagen type II and aggrecan were significantly more expressed in the s-μg rotating culture group than the static culture group, as reported by Wu et al. [25]. Zhang et al. [26] described that MSCs spread out in a spindle shape when cultured in normal gravity, while they become unspread and round under s-μg. Also, under s-μg, their cytoskeleton fibers are being reorganized. The function of MSCs was affected by these morphological changes, transmitted through the activity of RhoA. To test the hypothesis that s-μg has the capacity to offer a novel choice in the stimulation of neovascularization, MSCs were cultured under s-μg stimulation followed by VEGF differentiation. The responses revealed that MSCs were differentiated into endothelial-like cells after 72 h incubation and were able to form a capillary network. Their endothelial differentiation potential improved compared with the static control group.

Another approach of modeling μg in hMSCs is the use of a large gradient high magnetic field (LGHMF) produced by a superconducting magnet. Shi et al. [64] analyzed the effects of LGHMF-μg on survival, cytoskeleton and osteogenic potential of hMSCs. Results showed that the LGHMF-μg treatment disrupted the cytoskeleton of hMSCs, a LGHMF-μg treatment for 24 h led to cell death. LGHMF-μg treatments in early stages of osteogenic induction resulted in suppression of osteogenesis of hMSCs. The suppression intensity was reduced gradually as the treatment stage of LGHMF-MG was postponed. A LGHMF-μg treatment during the ending-stage of osteogenic induction had no visual effect on osteogenesis of hMSCs, which indicates that LGHMF-μg affects the initiation of osteogenesis.

Furthermore, a study of Uddin and Qin [23] examined the effects of low intensity pulsed ultrasound (LIPUS) on the osteogenic differentiation of adipose-derived human stem cells (Ad-hMSC) under s-μg conditions. Microgravity was simulated in a 1D clinostat and treated with LIPUS at 30 mW cm^{-2} for 20 min day^{-1}. Hypothetically, the application of LIPUS to s-μg cultures would restore osteogenesis in Ad-hMSCs. The results showed significant increases in *ALP*, *OSX*, *RANKL*, and *RUNX2* and decreases in *OPG* gene expression in LIPUS treated SMG cultures of Ad-MSC compared to nontreated cultures. LIPUS also restored *OSX*, *RUNX2*, and *RANKL* gene expression in osteoblast cells. s-μg significantly reduced ALP positive cells by 70% ($P < 0.01$) and ALP activity by 22% ($P < 0.01$), while LIPUS treatment restored ALP positive cell number and activity to equivalence with normal gravity controls. Extracellular matrix collagen and mineralization was assessed by Sirius red and Alizarin red staining, respectively. s-μg cultures showed little or no collagen or mineralization, but LIPUS treatment restored collagen content to 50% ($P < 0.001$) and mineralization by 45% ($P < 0.001$) relative to s-μg—only cultures.

Table 1: Comparative methods of 3D cell culture systems using simulated μg.

Device		Working principle
Free fall machine	FFM	Free fall for 800 ms, "bounce" of 20 g for 50 ms
Levitating magnets	LM	A high gradient magnetic field prevents sedimentation
2D-clinostat		Rotation along one axis
Random positioning machine	RPM	Two frames with randomized movement
Rotating wall vessel	RWV	Constant rotation prevents cells from settling

7. Multicellular Tumor Spheroids

3D growth of tumor cells creating MCTS *in vitro* has been observed in various tumor cell lines including thyroid and colorectal cancer [31]. MCTS mimic the growth of solid tumors and represent a simple model, approaching some of the characteristics found *in vivo* including physiological characteristics such as multicellular architecture and natural barriers of mass transportation. Therefore, the use of MCTS as an *in vitro* tool for testing anticancer drugs has gained significant interest as MCTS potentially provide a more reliable model for drug testing compared to single layer adherent cell cultures. During the approval process of drugs before clinical testing in trials, the mechanisms of delivery and the effectiveness of the drugs must be determined. The first steps of preclinical drug testing are typically carried out using adherent cell formats growing in two dimensions [157]. However, the outcome of such investigations in two-dimensional cell systems is often very different from what is observed in a whole-body situation. This makes it difficult to draw clear conclusions of the drug properties anticipated *in vivo*. In terms of drug delivery, a spheroid test platform has inherent advantages, providing a natural barrier resembling the natural tumor environment. Spheroids of a particular size exhibit certain gradients of oxygen and nutrition [35–37, 158, 159]. Spheroids larger than 400–500 μm in diameter show characteristics of layered structures with a hypoxic core, consisting of necrotic cells surrounded by quiescent cells and an outer layer of proliferating cells [38, 160, 161]. Hence, 3D tumor cell systems are a valuable tool for studying drug delivery and the response and metabolism of hypoxic tumor cells to cancer therapy. Fang et al. reported that multicellular spheroids of primary human colon cancer cells were resistant to chemotherapy-induced apoptosis and retained the expression of colon cancer marker CD133, mimicking colorectal cancer [162]. Were these cells grown under normal conditions, they did not retain these characteristics. Size control of MCTS is a major challenge in obtaining uniform and reliable high throughput test systems;

Table 2: Overview of various cell types used for tissue engineering and μg-conditions involved.

Cell type	Engineered tissue	Method	References
Osteoblasts	Bone	RWV bioreactor (s-μg)	[8–12]
Osteoprogenitor cells	Bone	RWV bioreactor (s-μg)	[13, 14]
Mesenchymal stem cells	Bone	RWV bioreactor (s-μg)	[12, 15–23]
Mesenchymal stem cells	Divers	RWV bioreactor (s-μg)	[18, 21, 24–26]
Mesenchymal stem cells	Divers	RPM (s-μg)	[27–30]
Several cell types	MCTS	RWV bioreactor (s-μg)	[31–34]
Several cell types	MCTS	Spinner flask (s-μg)	[35–38]
Several cell types	MCTS	RPM (s-μg)	[39–44]
Several cell types	MCTS	Space (r-μg)	[45]
Hepatocytes	liver	RWV bioreactor (s-μg)	[34, 46]

various techniques such as forced aggregation techniques, micro textured surfaces, and porous 3D scaffolds are being employed to solve these issues [163–166]. There are several conventional methods for generating 3D aggregates of cancer cells, including NASA rotary cell culture systems, hanging drops, and culturing of cells using nonadherent surfaces [166–168]. Conditions of s-μg using the RPM (Figure 2(b)) or the HARV have been shown to induce the growth of MCTS without the use of scaffolds in several types of human cancer cells [31–33, 39, 169]. The molecular switches initiating s-μg-induced spheroid formation are still unknown. Several changes in morphology and gene expression profiles have been observed in follicular thyroid cancer cells, grown under s-μg conditions with the main features involving changes in the ECM and early induction of apoptosis [39, 40]. Signaling between exogenous ECM and tumor surface receptors has long been thought to be an essential component in regulating the tumorigenic phenotype in 3D cultures. These phenomena have been demonstrated in studies showing that blocking specific ECM-integrin signaling can cause a shift in the malignant potential of tumor cells, leading to a more benign phenotype [40, 170]. In an attempt to identify gravity sensitive genes responsible for MCTS formation, Grosse et al. [41] identified 487 transcripts, which were differently regulated after 24 h of s-μg in comparison to the ground control. Comparing adherent cells with MCTS under s-μg conditions revealed significant differences in terms of growth patterns and signaling. Interestingly, the rate of apoptosis was increased in adherent cells compared to MCTS, indicating that the early phase induction of apoptosis may be concomitant with the transition of cells shifting from 2D to 3D growth. Several NF-κB-driven genes, involved in the regulation of tumor invasion, were upregulated by s-μg in adherent cells, highlighting that s-μg initiates distinct adaptive mechanisms in the cells.

8. Summary

The development of tools like the RPM or RWV gave new impacts in the field of tissue engineering (Table 1). Growing cells in simulated or real weightlessness, for example, on the RPM, might be a highly promising new technique to generate tissue constructs in a scaffold-free manner. Cultivation of chondrocytes might lead to small cartilage particles, which could be used to replace injured or outworn cartilage. Restoring normal osteogenic differentiation of MSCs from s-μg exposure by daily short-term stimulation could be helpful so that tissue products may become commercially available, like it has already happened for some bone tissues (BioSeed-Oral Bone, co.don osteotransplant and Osteocel).

At the moment, studies analyzing the molecular mechanisms behind spheroid formation of, for example, thyroid cells, chondrocyte, and others have increased the knowledge of the complex regulation of 3D growth in μg [42–45, 171].

To be able to use this new technique more efficiently, further studies are necessary to better understand the exact cellular changes specific to these conditions. Tissue, which was produced under s- or r-μg conditions, might be helpful to better understand cell signaling, intercellular contact, and tissue growth as well as being sufficient for medical transplantation. MCTS can be used as an alternative to animal experiments.

Although the μg environment is not a common field for biologists and medical researchers, recent studies have clearly shown that the loss of gravity impacts the cells and it dramatically changes the genome, proteome, and secretome of these cells [43, 45]. Therefore, it is important to systematically explore the advantages of this new research opportunity. Different space flights have already demonstrated a 3D cell growth (Table 2) and similar results have been detected with the help of devices simulating μg in ground-based laboratories [34, 44, 46, 172–174].

Conflict of Interests

The authors declare that there is no conflict of interests regarding the publication of this paper.

Acknowledgments

This paper was supported by the German Space Agency DLR (Daniela Grimm) (BMWi Grants 50WB0824 and 50WB1124), the European Space Agency (ESA; CORA-GBF-2013-001;

CORA-GBF-2013-004), and Aarhus University, Denmark (Daniela Grimm). The authors would like to thank Mr. Peter Lindborg, Los Angeles, CA, USA, for reviewing the paper for language and grammar errors.

References

[1] R. J. White and M. Averner, "Humans in space," *Nature*, vol. 409, no. 6823, pp. 1115–1118, 2001.

[2] A. I. Grigoriev, V. S. Oganov, A. V. Bakulin et al., "Clinical and physiological evaluation of bone changes among astronauts after long-term space flights," *Aviakosmicheskaia i Ekologicheskaia Meditsina*, vol. 32, no. 1, pp. 21–25, 1998.

[3] L. Vico, P. Collet, A. Guignandon et al., "Effects of long-term microgravity exposure on cancellous and cortical weight-bearing bones of cosmonauts," *The Lancet*, vol. 355, no. 9215, pp. 1607–1611, 2000.

[4] S. Tavella, A. Ruggiu, A. Giuliani et al., "Bone turnover in wild type and pleiotrophin-transgenic mice housed for three months in the International Space Station (ISS)," *PLoS ONE*, vol. 7, no. 3, Article ID e33179, 2012.

[5] J. Pietsch, J. Bauer, M. Egli et al., "The effects of weightlessness on the human organism and mammalian cells," *Current Molecular Medicine*, vol. 11, no. 5, pp. 350–364, 2011.

[6] D. Grimm, P. Wise, M. Lebert, P. Richter, and S. Baatout, "How and why does the proteome respond to microgravity?" *Expert Review of Proteomics*, vol. 8, no. 1, pp. 13–27, 2011.

[7] D. Grimm, M. Wehland, J. Pietsch J et al., "Growing tissues in real and simulated microgravity: new methods for tissue engineering," *Tissue Engineering Part B Reviews*, 2014.

[8] C. Granet, N. Laroche, L. Vico, C. Alexandre, and M. H. Lafage-Proust, "Rotating-wall vessels, promising bioreactors for osteoblastic cell culture: comparison with other 3D conditions," *Medical and Biological Engineering and Computing*, vol. 36, no. 4, pp. 513–519, 1998.

[9] K. Song, Z. Yang, T. Liu et al., "Fabrication and detection of tissue-engineered bones with bio-derived scaffolds in a rotating bioreactor," *Biotechnology and Applied Biochemistry*, vol. 45, no. 2, pp. 65–74, 2006.

[10] K. Song, T. Liu, Z. Cui, X. Li, and X. Ma, "Three-dimensional fabrication of engineered bone with human bio-derived bone scaffolds in a rotating wall vessel bioreactor," *Journal of Biomedical Materials Research A*, vol. 86, no. 2, pp. 323–332, 2008.

[11] K. Kyriakidou, G. Lucarini, A. Zizzi et al., "Dynamic co-seeding of osteoblast and endothelial cells on 3D polycaprolactone scaffolds for enhanced bone tissue engineering," *Journal of Bioactive and Compatible Polymers*, vol. 23, no. 3, pp. 227–243, 2008.

[12] Q. Lv, L. Nair, and C. T. Laurencin, "Fabrication, characterization, and in vitro evaluation of poly(lactic acid glycolic acid)/nano-hydroxyapatite composite microsphere-based scaffolds for bone tissue engineering in rotating bioreactors," *Journal of Biomedical Materials Research A*, vol. 91, no. 3, pp. 679–691, 2009.

[13] S. R. Facer, R. S. Zaharias, M. E. Andracki, J. Lafoon, S. K. Hunter, and G. B. Schneider, "Rotary culture enhances pre-osteoblast aggregation and mineralization," *Journal of Dental Research*, vol. 84, no. 6, pp. 542–547, 2005.

[14] G. B. Schneider, J. K. Boehrs, J. V. Hoopes, and D. A. Seabold, "Use of 3-dimensional environments to engineer osseous-like tissue," *Journal of Developmental Biology and Tissue Engineering*, vol. 3, no. 4, pp. 42–47, 2011.

[15] D. Turhani, E. Watzinger, M. Weißenböck et al., "Analysis of cell-seeded 3-dimensional bone constructs manufactured in vitro with hydroxyapatite granules obtained from red algae," *Journal of Oral and Maxillofacial Surgery*, vol. 63, no. 5, pp. 673–681, 2005.

[16] F. Jin, Y. Zhang, K. Xuan et al., "Establishment of three-dimensional tissue-engineered bone constructs under microgravity-simulated conditions," *Artificial Organs*, vol. 34, no. 2, pp. 118–125, 2010.

[17] J. G. Gershovich and L. B. Buravkova, "Morphofunctional status and osteogenic differentiation potential of human mesenchymal stromal precursor cells during in vitro modeling of microgravity effects," *Bulletin of Experimental Biology and Medicine*, vol. 144, no. 4, pp. 608–613, 2007.

[18] M. Zayzafoon, W. E. Gathings, and J. M. McDonald, "Modeled microgravity inhibits osteogenic differentiation of human mesenchymal stem cells and increases adipogenesis," *Endocrinology*, vol. 145, no. 5, pp. 2421–2432, 2004.

[19] R. Saxena, G. Pan, and J. M. McDonald, "Osteoblast and osteoclast differentiation in modeled microgravity," *Annals of the New York Academy of Sciences*, vol. 1116, pp. 494–498, 2007.

[20] V. E. Meyers, M. Zayzafoon, S. R. Gonda, W. E. Gathings, and J. M. McDonald, "Modeled microgravity disrupts collagen I/integrin signaling during osteoblastic differentiation of human mesenchymal stem cells," *Journal of Cellular Biochemistry*, vol. 93, no. 4, pp. 697–707, 2004.

[21] D. Sheyn, G. Pelled, D. Netanely, E. Domany, and D. Gazit, "The effect of simulated microgravity on human mesenchymal stem cells cultured in an osteogenic differentiation system: a bioinformatics study," *Tissue Engineering A*, vol. 16, no. 11, pp. 3403–3412, 2010.

[22] B. Yu, D. Yu, L. Cao et al., "Simulated microgravity using a rotary cell culture system promotes chondrogenesis of human adipose-derived mesenchymal stem cells via the p38 MAPK pathway," *Biochemical and Biophysical Research Communications*, vol. 414, no. 2, pp. 412–418, 2011.

[23] S. M. Uddin and Y. X. Qin, "Enhancement of osteogenic differentiation and proliferation in human mesenchymal stem cells by a modified low intensity ultrasound stimulation under simulated microgravity," *PLoS ONE*, vol. 8, no. 9, Article ID e73914, 2013.

[24] Z. Q. Dai, R. Wang, S. K. Ling, Y. M. Wan, and Y. H. Li, "Simulated microgravity inhibits the proliferation and osteogenesis of rat bone marrow mesenchymal stem cells," *Cell Proliferation*, vol. 40, no. 5, pp. 671–684, 2007.

[25] X. Wu, S.-H. Li, L.-M. Lou, and Z.-R. Chen, "The effect of the microgravity rotating culture system on the chondrogenic differentiation of bone marrow mesenchymal stem cells," *Molecular Biotechnology*, vol. 54, no. 2, pp. 331–336, 2013.

[26] X. Zhang, Y. Nan, H. Wang et al., "Model microgravity enhances endothelium differentiation of mesenchymal stem cells," *Naturwissenschaften*, vol. 100, no. 2, pp. 125–133, 2013.

[27] N. V. Merzlikina, L. B. Buravkova, and Y. A. Romanov, "The primary effects of clinorotation on cultured human mesenchymal stem cells," *Journal of Gravitational Physiology*, vol. 11, no. 2, pp. 193–194, 2004.

[28] M. Nishikawa, H. Ohgushi, N. Tamai et al., "The effect of simulated microgravity by three-dimensional clinostat on bone tissue engineering," *Cell Transplantation*, vol. 14, no. 10, pp. 829–835, 2005.

[29] L. Yuge, T. Kajiume, H. Tahara et al., "Microgravity potentiates stem cell proliferation while sustaining the capability of differentiation," *Stem Cells and Development*, vol. 15, no. 6, pp. 921–929, 2006.

[30] I. G. Gershovich and L. B. Buravkova, "Interleukine production in culture of mesenchymal stromal cells of humans during simulation of the microgravity effects," *Aviakosmicheskaia I Ekologicheskaia Meditsina*, vol. 43, no. 3, pp. 44–50, 2009.

[31] M. Ingram, G. B. Techy, R. Saroufeem et al., "Three-dimensional growth patterns of various human tumor cell lines in simulated microgravity of a nasa bioreactor," *In Vitro Cellular and Developmental Biology: Animal*, vol. 33, no. 6, pp. 459–466, 1997.

[32] B. Marrero, J. L. Messina, and R. Heller, "Generation of a tumor spheroid in a microgravity environment as a 3D model of melanoma," *In Vitro Cellular and Developmental Biology—Animal*, vol. 45, no. 9, pp. 523–534, 2009.

[33] S. M. Konstantinov, M. M. Mindova, P. T. Gospodinov, and P. I. Genova, "Three-dimensional bioreactor cultures: a useful dynamic model for the study of cellular interactions," *Annals of the New York Academy of Sciences*, vol. 1030, pp. 103–115, 2004.

[34] T. T. Chang and M. Hughes-Fulford, "Monolayer and spheroid culture of human liver hepatocellular carcinoma cell line cells demonstrate distinct global gene expression patterns and functional phenotypes," *Tissue Engineering A*, vol. 15, no. 3, pp. 559–567, 2009.

[35] A. Bredel-Geissler, U. Karbach, S. Walenta, L. Vollrath, and W. Mueller-Klieser, "Proliferation-associated oxygen consumption and morphology of tumor cells in monolayer and spheroid culture," *Journal of Cellular Physiology*, vol. 153, no. 1, pp. 44–52, 1992.

[36] L. A. Kunz-Schughart, C. Groebe, and W. Mueller-Klieser, "Three-dimensional cell culture induces novel proliferative and metabolic alterations associated with oncogenic transformation," *International Journal of Cancer*, vol. 66, no. 4, pp. 578–586, 1996.

[37] M. Wartenberg, F. Dönmez, F. C. Ling, H. Acker, J. Hescheler, and H. Sauer, "Tumor-induced angiogenesis studied in confrontation cultures of multicellular tumor spheroids and embryoid bodies grown from pluripotent embryonic stem cells," *The FASEB Journal*, vol. 15, no. 6, pp. 995–1005, 2001.

[38] R.-Z. Lin and H.-Y. Chang, "Recent advances in three-dimensional multicellular spheroid culture for biomedical research," *Biotechnology Journal*, vol. 3, no. 9-10, pp. 1172–1184, 2008.

[39] D. Grimm, J. Bauer, P. Kossmehl et al., "Simulated microgravity alters differentiation and increases apoptosis in human follicular thyroid carcinoma cells," *The FASEB Journal*, vol. 16, no. 6, pp. 604–606, 2002.

[40] M. Infanger, P. Kossmehl, M. Shakibaei et al., "Simulated weightlessness changes the cytoskeleton and extracellular matrix proteins in papillary thyroid carcinoma cells," *Cell and Tissue Research*, vol. 324, no. 2, pp. 267–277, 2006.

[41] J. Grosse, M. Wehland, J. Pietsch et al., "Gravity-sensitive signaling drives 3-dimensional formation of multicellular thyroid cancer spheroids," *The FASEB Journal*, vol. 26, no. 12, pp. 5124–5140, 2012.

[42] X. Ma, A. Sickmann, J. Pietsch et al., "Proteomic differences between microvascular endothelial cells and the EA.hy926 cell line forming three-dimensional structures," *Proteomics*, vol. 14, no. 6, pp. 689–698, 2014.

[43] X. Ma, J. Pietsch, M. Wehland et al., "Differential gene expression profile and altered cytokine secretion of thyroid cancer cells in space," *FASEB Journal*, vol. 28, no. 2, pp. 813–835, 2014.

[44] J. Pietsch, A. Sickmann, G. Weber et al., "A proteomic approach to analysing spheroid formation of two human thyroid cell lines cultured on a random positioning machine," *Proteomics*, vol. 11, no. 10, pp. 2095–2104, 2011.

[45] J. Pietsch, X. Ma, M. Wehland et al., "Spheroid formation of human thyroid cancer cells in an automated culturing system during the Shenzhou-8 Space mission," *Biomaterials*, vol. 34, no. 31, pp. 7694–7705, 2013.

[46] T. T. Chang and M. Hughes-Fulford, "Molecular mechanisms underlying the enhanced functions of three-dimensional hepatocyte aggregates," *Biomaterials*, vol. 35, no. 7, pp. 2162–2171, 2014.

[47] M. Y. Kapitonova, N. Salim, S. Othman et al., "Alteration of cell cytoskeleton and functions of cell recovery of normal human osteoblast cells caused by factors associated with real space flight," *The Malaysian Journal of Pathology*, vol. 35, no. 2, pp. 153–163, 2013.

[48] E. A. Blaber, N. Dvorochkin, C. Lee et al., "Microgravityinduces pelvic bone loss through osteoclastic activity, osteocytic osteolysis, and osteoblastic cell cycle inhibition by CDKN1α/p21," *PLoS ONE*, vol. 8, no. 4, Article ID 61372, 2013.

[49] C. Ulbrich, J. Pietsch, J. Grosse et al., "Differential gene regulation under altered gravity conditions in follicular thyroid cancer cells: relationship between the extracellular matrix and the cytoskeleton," *Cellular Physiology and Biochemistry*, vol. 28, no. 2, pp. 185–198, 2011.

[50] J. Grosse, M. Wehland, J. Pietsch et al., "Short-term weightlessness produced by parabolic flight maneuvers altered gene expression patterns in human endothelial cells," *The FASEB Journal*, vol. 26, no. 2, pp. 639–655, 2012.

[51] R. Hemmersbach, M. Krause, R. Bräucker, and K. Ivanova, "Graviperception in ciliates: steps in the transduction chain," *Advances in Space Research*, vol. 35, no. 2, pp. 296–299, 2005.

[52] D. A. M. Mesland, "Novel ground-based facilities for research in the effects of weight," *ESA Microgravity News*, vol. 9, 1996.

[53] D. A. M. Meslana, A. H. Anton, H. Willemsen, and H. van den Ende, "The free fall machine—a ground-based facility for microgravity research in life sciences," *Microgravity Science and Technology*, vol. 9, no. 1, pp. 10–14, 1996.

[54] M. Schwarzenberg, P. Pippia, M. A. Meloni, G. Cossu, M. Cogoli-Greuter, and A. Cogoli, "Signal transduction in T lymphocytes—a comparison of the data from space, the free fall machine and the random positioning machine," *Advances in Space Research*, vol. 24, no. 6, pp. 793–800, 1999.

[55] M. V. Berry and A. K. Geim, "Of flying frogs and levitrons," *European Journal of Physics*, vol. 18, no. 4, pp. 307–313, 1997.

[56] J. M. Valles Jr., K. Lin, J. M. Denegre, and K. L. Mowry, "Stable magnetic field gradient levitation of *Xenopus laevis*: toward low-gravity simulation," *Biophysical Journal*, vol. 73, no. 2, pp. 1130–1133, 1997.

[57] M. J. A. Moes, J. C. Gielen, R.-J. Bleichrodt, J. J. W. A. van Loon, P. C. M. Christianen, and J. Boonstra, "Simulation of microgravity by magnetic levitation and random positioning: effect on human A431 Cell morphology," *Microgravity Science and Technology*, vol. 23, no. 2, pp. 249–261, 2011.

[58] R. Herranz, R. Anken, J. Boonstra et al., "Ground-based facilities for simulation of microgravity: organism-specific recommendations for their use, and recommended terminology," *Astrobiology*, vol. 13, no. 1, pp. 1–17, 2013.

[59] T. Higashi, A. Yamagishi, T. Takeuchi et al., "Orientation of erythrocytes in a strong static magnetic field," *Blood*, vol. 82, no. 4, pp. 1328–1334, 1993.

[60] K. A. Mirica, F. Ilievski, A. K. Ellerbee, S. S. Shevkoplyas, and G. M. Whitesides, "Using magnetic levitation for three dimensional self-assembly," *Advanced Materials*, vol. 23, no. 36, pp. 4134–4140, 2011.

[61] J. S. Brooks, J. A. Reavis, R. A. Medwood et al., "New opportunities in science, materials, and biological systems in the low-gravity (magnetic levitation) environment (invited)," *Journal of Applied Physics*, vol. 87, no. 9, pp. 6194–6199, 2000.

[62] B. E. Hammer, L. S. Kidder, P. C. Williams, and W. W. Xu, "Magnetic levitation of MC3T3 osteoblast cells as a ground-based simulation of microgravity," *Microgravity Science and Technology*, vol. 21, no. 4, pp. 311–318, 2009.

[63] C. E. Dijkstra, O. J. Larkin, P. Anthony et al., "Diamagnetic levitation enhances growth of liquid bacterial cultures by increasing oxygen availability," *Journal of the Royal Society Interface*, vol. 8, no. 56, pp. 334–344, 2011.

[64] D. Shi, R. Meng, W. Deng et al., "Effects of microgravity modeled by large gradient high magnetic field on the osteogenic initiation of human mesenchymal stem cells," *Stem Cell Reviews and Reports*, vol. 6, no. 4, pp. 567–578, 2010.

[65] G. R. Souza, J. R. Molina, R. M. Raphael et al., "Three-dimensional tissue culture based on magnetic cell levitation," *Nature Nanotechnology*, vol. 5, no. 4, pp. 291–296, 2010.

[66] F. Castro-Chavez, K. C. Vickers, J. S. Lee, C. Tung, and J. D. Morrisett, "Effect of lyso-phosphatidylcholine and Schnurri-3 on osteogenic transdifferentiation of vascular smooth muscle cells to calcifying vascular cells in 3D culture," *Biochimica et Biophysica Acta*, vol. 1830, no. 6, pp. 3828–3834, 2013.

[67] F. G. J. R. von Sachs, "Über Ausschliessung der geotropischen und heliotropischen Krümmungen während des Wachstums," *Würzburger Arbeiten*, vol. 2, pp. 209–225, 1879.

[68] J. J. W. A. van Loon, "Some history and use of the random positioning machine, RPM, in gravity related research," *Advances in Space Research*, vol. 39, no. 7, pp. 1161–1165, 2007.

[69] S. Murakami and M. Yamada, "Architecture of statocytes and chloroplasts under the microgravity environment," *Biological Sciences in Space*, vol. 2, no. 4, p. 301, 1988.

[70] J. J. W. A. van Loon, "Effects of spaceflight on biological systems," in *Biology in Space and Life on Earth*, E. Brinckmann, Ed., vol. 17, Wiley-VCH, 2007.

[71] T. Hoson, S. Kamisaka, Y. Masuda, and M. Yamashita, "Changes in plant growth processes under microgravity conditions simulated by a three-dimensional clinostat," *The Botanical Magazine Tokyo*, vol. 105, no. 1, pp. 53–70, 1992.

[72] T. Hoson, S. Kamisaka, Y. Masuda, M. Yamashita, and B. Buchen, "Evaluation of the three-dimensional clinostat as a simulator of weightlessness," *Planta*, vol. 203, pp. S187–S197, 1997.

[73] A. G. Borst and J. J. W. A. van Loon, "Technology and developments for the random positioning machine, RPM," *Microgravity Science and Technology*, vol. 21, no. 4, pp. 287–292, 2009.

[74] C. A. D. Leguy, R. Delfos, and M. J. B. M Pourquie, "Fluid motion for microgravity simulations in a random positioning machine," *Gravitational and Space Biology*, vol. 25, no. 1, pp. 36–39, 2011.

[75] S. Wakayama, Y. Kawahara, C. Li, K. Yamagata, L. Yuge, and T. Wakayama, "Detrimental effects of microgravity on mouse preimplantation development in vitro," *PLoS ONE*, vol. 4, no. 8, Article ID e6753, 2009.

[76] M. Z. Luo, R. Meng, S. S. Li et al., "Weightlessness simulated with random positioning machine influences the cytoskeleton and migration of MC3T3-E1 cells," *Journal of the Japan Society of Microgravity Application*, vol. 28, no. 2, pp. S41–S45, 2011.

[77] W. A. Loesberg, X. F. Walboomers, E. M. Bronkhorst, J. J. W. A. Van Loon, and J. A. Jansen, "The effect of combined simulated microgravity and microgrooved surface topography on fibroblasts," *Cell Motility and the Cytoskeleton*, vol. 64, no. 3, pp. 174–185, 2007.

[78] G. Aleshcheva, J. Sahana, X. Ma et al., "Changes in morphology, gene expression and protein content in chondrocytes cultured on a Random Positioning Machine," *PLoS ONE*, vol. 8, no. 11, Article ID e79057, 2013.

[79] L. Prodanov, J. J. W. A. van Loon, J. te Riet, J. A. Jansen, and X. F. Walboomers, "Nanostructured substrate conformation can decrease osteoblast-like cell dysfunction in simulated microgravity conditions," *Journal of Tissue Engineering and Regenerative Medicine*, 2012.

[80] J. Ichigi and M. Asashima, "Dome formation and tubule morphogenesis by Xenopus kidney A6 cell cultures exposed to microgravity simulated with a 3D-clinostat and to hypergravity," *In Vitro Cellular Developmental Biology. Animal*, vol. 37, no. 1, pp. 31–44, 2001.

[81] Y. D. Jiang, W. N. Li, L. F. Wang, Z. Y. Zhang, B. M. Zhang, and H. J. Wu, "Several new types of clinostats," *Space Medicine & Medical Engineering*, vol. 21, no. 4, pp. 368–371, 2008.

[82] J. H. Siamwala, S. H. Reddy, S. Majumder et al., "Simulated microgravity perturbs actin polymerization to promote nitric oxide-associated migration in human immortalized Eahy926 cells," *Protoplasma*, vol. 242, no. 1, pp. 3–12, 2010.

[83] L. Xiang, F. Qi, D. Dai, C. Li, and Y. Jiang, "Simulated microgravity affects growth of *Escherichia coli* and recombinant β-D-glucuronidase production," *Applied Biochemistry and Biotechnology*, vol. 162, no. 3, pp. 654–661, 2010.

[84] R. Hemmersbach, S. M. Strauch, D. Seibt, and M. Schuber, "Comparative studies on gravisensitive protists on ground (2D and 3D clinostats) and in microgravity," *Microgravity Science and Technology*, vol. 18, no. 3-4, pp. 257–259, 2006.

[85] T. J. Goodwin, J. M. Jessup, and D. A. Wolf, "Morphologic differentiation of colon carcinoma cell lines HT-29 and HT-29 KM in Rotating-Wall Vessels," *In Vitro Cellular and Developmental Biology: Animal*, vol. 28, no. 1, pp. 47–60, 1992.

[86] T. G. Hammond and J. M. Hammond, "Optimized suspension culture: the rotating-wall vessel," *The American Journal of Physiology—Renal Physiology*, vol. 281, no. 1, pp. F12–F25, 2001.

[87] T. Liu, X. Li, X. Sun, X. Ma, and Z. Cui, "Analysis on forces and movement of cultivated particles in a rotating wall vessel bioreactor," *Biochemical Engineering Journal*, vol. 18, no. 2, pp. 97–104, 2004.

[88] T. J. Goodwin, T. L. Prewett, D. A. Wolf, and G. F. Spaulding, "Reduced shear stress: a major component in the ability of mammalian tissues to form three-dimensional assemblies in simulated microgravity," *Journal of Cellular Biochemistry*, vol. 51, no. 3, pp. 301–311, 1993.

[89] E. A. Nauman, C. M. Ott, E. Sander et al., "Novel quantitative biosystem for modeling physiological fluid shear stress on cells," *Applied and Environmental Microbiology*, vol. 73, no. 3, pp. 699–705, 2007.

[90] X. Guo, Y. Zhao, H. Chang et al., "Creation of engineered cardiac tissue in vitro from mouse embryonic stem cells," *Circulation*, vol. 113, no. 18, pp. 2229–2237, 2006.

[91] D. L. Tucker, C. M. Ott, S. Huff et al., "Characterization of *Escherichia coli* MG1655 grown in a low-shear modeled micro gravity environment," *BMC Microbiology*, vol. 7, article 15, 2007.

[92] M. N. Cinbiz, R. S. Tıgli, I. G. Beşkardeş, M. Gümüşderelioğlu, and U. Colak, "Computational fluid dynamics modeling of momentum transport in rotating wall perfused bioreactor for cartilage tissue engineering," *Journal of Biotechnology*, vol. 150, no. 3, pp. 389–395, 2010.

[93] A. Puca, G. Russo, and A. Giordano, "Properties of mechanotransduction via simulated microgravity and its effects on intracellular trafficking of VEGFR's," *Oncotarget*, vol. 3, no. 4, pp. 426–434, 2012.

[94] J. H. Siamwala, S. Majumder, K. P. Tamilarasan et al., "Simulated microgravity promotes nitric oxide-supported angiogenesis via the iNOS-cGMP-PKG pathway in macrovascular endothelial cells," *FEBS Letters*, vol. 584, no. 15, pp. 3415–3423, 2010.

[95] Y. C. Wang, S. Zhang, T. Y. Du, B. Wang, and X. Q. Sun, "Clinorotation upregulates inducible nitric oxide synthase by inhibiting AP-1 activation in human umbilical vein endothelial cells," *Journal of Cellular Biochemistry*, vol. 107, no. 2, pp. 357–363, 2009.

[96] F. Shi, Y.-C. Wang, T.-Z. Zhao et al., "Effects of simulated microgravity on human umbilical vein endothelial cell angiogenesis and role of the PI3K-Akt-eNOS signal pathway," *PLoS ONE*, vol. 7, no. 7, Article ID e40365, 2012.

[97] P. I. Lelkes, N. Akhtar, E. Lelkes et al., "Neuroendocrine tissue engineering in rotating wall vessel bioreactors under simulated microgravity conditions," in *Proceedings of the 23rd Annual International Conference of the IEEE Engineering in Medicine and Biology Society*, vol. 3, pp. 2987–2990, October 2001.

[98] A. Abbott, "Cell culture: biology's new dimensions," *Nature*, vol. 424, no. 6951, pp. 870–872, 2003.

[99] B. R. Unsworth and P. I. Lelkes, "Growing tissues in microgravity," *Nature Medicine*, vol. 4, no. 8, pp. 901–907, 1998.

[100] M. Infanger, P. Kossmehl, M. Shakibaei et al., "Induction of three-dimensional assembly and increase in apoptosis of human endothelial cells by simulated microgravity: impact of vascular endothelial growth factor," *Apoptosis*, vol. 11, no. 5, pp. 749–764, 2006.

[101] D. Grimm, M. Infanger, K. Westphal et al., "A delayed type of three-dimensional growth of human endothelial cells under simulated weightlessness," *Tissue Engineering A*, vol. 15, no. 8, pp. 2267–2275, 2009.

[102] D. Grimm, J. Bauer, C. Ulbrich et al., "Different responsiveness of endothelial cells to vascular endothelial growth factor and basic fibroblast growth factor added to culture media under gravity and simulated microgravity," *Tissue Engineering A*, vol. 16, no. 5, pp. 1559–1573, 2010.

[103] M. Infanger, C. Ulbrich, S. Baatout et al., "Modeled gravitational unloading induced downregulation of endothelin-1 in human endothelial cells," *Journal of Cellular Biochemistry*, vol. 101, no. 6, pp. 1439–1455, 2007.

[104] X. Ma, M. Wehland, H. Schulz et al., "Genomic Approach to identify factors that drive the formation of three-dimensional structures by EA.hy926 endothelial cells," *PLoS ONE*, vol. 8, no. 5, Article ID e64402, 2013.

[105] C. Ulbrich, K. Westphal, J. Pietsch et al., "Characterization of human chondrocytes exposed to simulated microgravity," *Cellular Physiology and Biochemistry*, vol. 25, no. 4-5, pp. 551–560, 2010.

[106] L. E. Freed and G. Vunjak-Novakovic, "Cultivation of cell-polymer tissue constructs in simulated microgravity," *Biotechnology and Bioengineering*, vol. 46, no. 4, pp. 306–313, 1995.

[107] L. E. Freed, R. Langer, I. Martin, N. R. Pellis, and G. Vunjak-Novakovic, "Tissue engineering of cartilage in space," *Proceedings of the National Academy of Sciences of the United States of America*, vol. 94, no. 25, pp. 13885–13890, 1997.

[108] V. Stamenković, G. Keller, D. Nesic, A. Cogoli, and S. P. Grogan, "Neocartilage formation in 1 *g*, simulated, and microgravity environments: implications for tissue engineering," *Tissue Engineering A*, vol. 16, no. 5, pp. 1729–1736, 2010.

[109] L. Kock, C. C. van Donkelaar, and K. Ito, "Tissue engineering of functional articular cartilage: the current status," *Cell and Tissue Research*, vol. 347, no. 3, pp. 613–627, 2012.

[110] C. H. Chang, F. H. Lin, T. F. Kuo, and H. C. Liu, "Cartilage tissue engineering," *Biomedical Engineering: Applications, Basis and Communications*, vol. 17, no. 2, pp. 61–71, 2005.

[111] E. Ozcivici, Y. K. Luu, B. Adler et al., "Mechanical signals as anabolic agents in bone," *Nature Reviews Rheumatology*, vol. 6, no. 1, pp. 50–59, 2010.

[112] R. Yang, W. Lin, Y. Chen et al., "Regulation by ultrasound treatment on the integrin expression and differentiation of osteoblasts," *Bone*, vol. 36, no. 2, pp. 276–283, 2005.

[113] H. C. Hsu, Y. C. Fong, C. S. Chang et al., "Ultrasound induces cyclooxygenase-2 expression through integrin, integrin-linked kinase, Akt, NF-κB and p300 pathway in human chondrocytes," *Cellular Signalling*, vol. 19, no. 11, pp. 2317–2328, 2007.

[114] Y. I. Arfat, W. Z. Xiao, S. Iftikhar et al., "Physiological effects of microgravity on bone cells," *Calcified Tissue International*, vol. 94, no. 6, pp. 569–579, 2014.

[115] D. A. Starr, "Communication between the cytoskeleton and the nuclear envelope to position the nucleus," *Molecular BioSystems*, vol. 3, no. 9, pp. 583–589, 2007.

[116] N. Nabavi, A. Khandani, A. Camirand, and R. E. Harrison, "Effects of microgravity on osteoclast bone resorption and osteoblast cytoskeletal organization and adhesion," *Bone*, vol. 49, no. 5, pp. 965–974, 2011.

[117] S. B. Doty, E. R. Morey-Holton, G. N. Durnova, and A. S. Kaplansky, "Cosmos 1887: morphology, histochemistry, and vasculature of the growing rat tibia," *FASEB Journal*, vol. 4, no. 1, pp. 16–23, 1990.

[118] N. V. Rodionova, O. V. Polkovenko, and V. S. Oganov, "Interactions of cells in zones of bone resorption under microgravity and hypokinesia.," *Journal of Gravitational Physiology*, vol. 11, no. 2, pp. P147–151, 2004.

[119] O. D. Kennedy, B. C. Herman, D. M. Laudier, R. J. Majeska, H. B. Sun, and M. B. Schaffler, "Activation of resorption in fatigue-loaded bone involves both apoptosis and active pro-osteoclastogenic signaling by distinct osteocyte populations," *Bone*, vol. 50, no. 5, pp. 1115–1122, 2012.

[120] C. Lin, X. Jiang, Z. Dai et al., "Sclerostin mediates bone response to mechanical unloading through antagonizing Wnt/β-catenin signaling," *Journal of Bone and Mineral Research*, vol. 24, no. 10, pp. 1651–1661, 2009.

[121] R. Tamma, G. Colaianni, C. Camerino et al., "Microgravity during spaceflight directly affects in vitro osteoclastogenesis and bone resorption," *The FASEB Journal*, vol. 23, no. 8, pp. 2549–2554, 2009.

[122] A. Sundaresan, S. F. Clarke, and N. R. Pellis, *Production of Bone Morphogenic Proteins (BMPS) Using a Novel Tissue Culture Platform*, 2011, US Patent 8076136.

[123] A. Sundaresan, S. F. Clarke, and N. R. Pellis, "Constructions osseuses minéralisées en trois dimensions," European Patent Number: EP2013730, 2011.

[124] A. Sundaresan, M. S. F. Clarke, and M. Brinker, Development of a human colloidal bone graft material, US 8506982 B2, 2013.

[125] J. R. Milstead, S. J. Simske, and T. A. Bateman, "Spaceflight and hindlimb suspension disuse models in mice," *Biomedical Sciences Instrumentation*, vol. 40, pp. 105–110, 2004.

[126] H. M. Frost and W. S. Jee, "On the rat model of human osteopenias and osteoporoses," *Bone and Mineral*, vol. 18, no. 3, pp. 227–236, 1992.

[127] J. H. Keyak, A. K. Koyama, A. LeBlanc, Y. Lu, and T. F. Lang, "Reduction in proximal femoral strength due to long-duration spaceflight," *Bone*, vol. 44, no. 3, pp. 449–453, 2009.

[128] S. M. Smith, M. E. Wastney, K. O. O'Brien et al., "Bone markers, calcium metabolism, and calcium kinetics during extended-duration space flight on the Mir Space Station," *Journal of Bone and Mineral Research*, vol. 20, no. 2, pp. 208–218, 2005.

[129] J. M. Vogel, "Bone mineral measurement: Skylab experiment M-078," *Acta Astronautica*, vol. 2, no. 1-2, pp. 129–139, 1975.

[130] S. M. Smith, M. E. Wastney, B. V. Morukov et al., "Calcium metabolism before, during, and after a 3-mo spaceflight: kinetic and biochemical changes," *American Journal of Physiology*, vol. 277, no. 1, part 2, pp. R1–R10, 1999.

[131] J. E. Zerwekh, L. A. Ruml, F. Gottschalk, and C. Y. C. Pak, "The effects of twelve weeks of bed rest on bone histology, biochemical markers of bone turnover, and calcium homeostasis in eleven normal subjects," *Journal of Bone and Mineral Research*, vol. 13, no. 10, pp. 1594–1601, 1998.

[132] T. Lang, A. LeBlanc, H. Evans, Y. Lu, H. Genant, and A. Yu, "Cortical and trabecular bone mineral loss from the spine and hip in long-duration spaceflight," *Journal of Bone and Mineral Research*, vol. 19, no. 6, pp. 1006–1012, 2004.

[133] A. LeBlanc, C. Lin, L. Shackelford et al., "Muscle volume, MRI relaxation times (T2), and body composition after spaceflight," *Journal of Applied Physiology*, vol. 89, no. 6, pp. 2158–2164, 2000.

[134] M. Iki, E. Kajita, Y. Dohi et al., "Age, menopause, bone turnover markers and lumbar bone loss in healthy Japanese women," *Maturitas*, vol. 25, no. 1, pp. 59–67, 1996.

[135] J. Sirola, H. Kröger, R. Honkanen et al., "Factors affecting bone loss around menopause in women without HRT: a prospective study," *Maturitas*, vol. 45, no. 3, pp. 159–167, 2003.

[136] J. D. Sibonga, H. J. Evans, H. G. Sung et al., "Recovery of spaceflight-induced bone loss: bone mineral density after long-duration missions as fitted with an exponential function," *Bone*, vol. 41, no. 6, pp. 973–978, 2007.

[137] T. F. Lang, A. D. Leblanc, H. J. Evans, and Y. Lu, "Adaptation of the proximal femur to skeletal reloading after long-duration spaceflight," *Journal of Bone and Mineral Research*, vol. 21, no. 8, pp. 1224–1230, 2006.

[138] J. J. W. A. Van Loon, D.-J. Bervoets, E. H. Burger et al., "Decreased mineralization and increased calcium release in isolated fetal mouse long bones under near weightlessness," *Journal of Bone and Mineral Research*, vol. 10, no. 4, pp. 550–557, 1995.

[139] R. Langer, "Tissue engineering: a new field and its challenges," *Pharmaceutical Research*, vol. 14, no. 7, pp. 840–841, 1997.

[140] G. M. Crane, S. L. Ishaug, and A. G. Mikos, "Bone tissue engineering," *Nature Medicine*, vol. 1, no. 12, pp. 1322–1324, 1995.

[141] M. J. Yaszemski, R. G. Payne, W. C. Hayes, R. Langer, and A. G. Mikos, "Evolution of bone transplantation: molecular, cellular and tissue strategies to engineer human bone," *Biomaterials*, vol. 17, no. 2, pp. 175–185, 1996.

[142] E. M. Younger and M. W. Chapman, "Morbidity at bone graft donor sites," *Journal of Orthopaedic Trauma*, vol. 3, no. 3, pp. 192–195, 1989.

[143] S. Gronthos and P. J. Simmons, "The biology and application of human bone marrow stromal cell precursors," *Journal of Hematotherapy and Stem Cell Research*, vol. 5, no. 1, pp. 15–23, 1996.

[144] N. Jaiswal, S. E. Haynesworth, A. I. Caplan, and S. P. Bruder, "Osteogenic differentiation of purified, culture-expanded human mesenchymal stem cells in vitro," *Journal of Cellular Biochemistry*, vol. 64, no. 2, pp. 295–312, 1997.

[145] J. E. Aubin, "Osteoprogenitor cell frequency in rat bone marrow stromal populations: role for heterotypic cell-cell interactions in osteoblast differentiation," *Journal of Cellular Biochemistry*, vol. 72, no. 3, pp. 396–410, 1999.

[146] J. Rauh, F. Milan, K. Günther, and M. Stiehler, "Bioreactor systems for bone tissue engineering," *Tissue Engineering B: Reviews*, vol. 17, no. 4, pp. 263–280, 2011.

[147] S. Kern, H. Eichler, J. Stoeve, H. Klüter, and K. Bieback, "Comparative analysis of mesenchymal stem cells from bone marrow, umbilical cord blood, or adipose tissue," *Stem Cells*, vol. 24, no. 5, pp. 1294–1301, 2006.

[148] M. Kassem and B. M. Abdallah, "Human bone-marrow-derived mesenchymal stem cells: biological characteristics and potential role in therapy of degenerative diseases," *Cell and Tissue Research*, vol. 331, no. 1, pp. 157–163, 2008.

[149] J. E. Dennis, S. E. Haynesworth, R. G. Young, and A. I. Caplan, "Osteogenesis in marrow-derived mesenchymal cell porous ceramic composites transplanted subcutaneously: effect of fibronectin and laminin on cell retention and rate of osteogenic expression," *Cell Transplantation*, vol. 1, no. 1, pp. 23–32, 1992.

[150] B. D. Boyan, T. W. Hummert, D. D. Dean, and Z. Schwartz, "Role of material surfaces in regulating bone and cartilage cell response," *Biomaterials*, vol. 17, no. 2, pp. 137–146, 1996.

[151] A. L. Olivares, È. Marsal, J. A. Planell, and D. Lacroix, "Finite element study of scaffold architecture design and culture conditions for tissue engineering," *Biomaterials*, vol. 30, no. 30, pp. 6142–6149, 2009.

[152] S. B. Vangordon, R. S. Voronov, T. B. Blue, R. L. Shambaugh, D. V. Papavassiliou, and V. I. Sikavitsas, "Effects of scaffold architecture on preosteoblastic cultures under continuous fluid shear," *Industrial & Engineering Chemistry Research*, vol. 50, no. 2, pp. 620–629, 2011.

[153] E. Canalis, A. N. Economides, and E. Gazzerro, "Bone morphogenetic proteins, their antagonists, and the skeleton," *Endocrine Reviews*, vol. 24, no. 2, pp. 218–235, 2003.

[154] B. L. Eppley, J. E. Woodell, and J. Higgins, "Platelet quantification and growth factor analysis from platelet-rich plasma: implications for wound healing," *Plastic and Reconstructive Surgery*, vol. 114, no. 6, pp. 1502–1508, 2004.

[155] E. A. Botchwey, S. R. Pollack, E. M. Levine, and C. T. Laurencin, "Bone tissue engineering in a rotating bioreactor using a microcarrier matrix system," *Journal of Biomedical Materials Research*, vol. 55, no. 2, pp. 242–253, 2001.

[156] J. Chen, R. Liu, Y. Yang et al., "The simulated microgravity enhances the differentiation of mesenchymal stem cells into neurons," *Neuroscience Letters*, vol. 505, no. 2, pp. 171–175, 2011.

[157] D. N. Karunaratne, P. S. Silverstein, V. Vasadani et al., "Cell culture models for drug transport studies," in *Drug Delivery:*

Principles and Applications, B. Wang, T. Siahaan, and R. Soltero, Eds., pp. 103–124, John Wiley & Sons, Hoboken, NJ, USA, 2005.

[158] M. Gassmann, J. Fandrey, S. Bichet et al., "Oxygen supply and oxygen-dependent gene expression in differentiating embryonic stem cells," *Proceedings of the National Academy of Sciences of the United States of America*, vol. 93, no. 7, pp. 2867–2872, 1996.

[159] R. M. Sutherland, "Cell and environment interactions in tumor microregions: the multicell spheroid model," *Science*, vol. 240, no. 4849, pp. 177–184, 1988.

[160] L. A. Kunz-Schughart, J. P. Freyer, F. Hofstaedter, and R. Ebner, "The use of 3-D cultures for high-throughput screening: the multicellular spheroid model," *Journal of Biomolecular Screening*, vol. 9, no. 4, pp. 273–285, 2004.

[161] F. Hirschhaeuser, H. Menne, C. Dittfeld, J. West, W. Mueller-Klieser, and L. A. Kunz-Schughart, "Multicellular tumor spheroids: an underestimated tool is catching up again," *Journal of Biotechnology*, vol. 148, no. 1, pp. 3–15, 2010.

[162] D. D. Fang, Y. J. Kim, C. N. Lee et al., "Expansion of $CD133^+$ colon cancer cultures retaining stem cell properties to enable cancer stem cell target discovery," *British Journal of Cancer*, vol. 102, no. 8, pp. 1265–1275, 2010.

[163] S. M. Ong, C. Zhang, Y. Toh et al., "A gel-free 3D microfluidic cell culture system," *Biomaterials*, vol. 29, no. 22, pp. 3237–3244, 2008.

[164] Y.-S. Torisawa, B.-H. Chueh, D. Huh et al., "Efficient formation of uniform-sized embryoid bodies using a compartmentalized microchannel device," *Lab on a Chip*, vol. 7, no. 6, pp. 770–776, 2007.

[165] L. Y. Wu, D. Di Carlo, and L. P. Lee, "Microfluidic self-assembly of tumor spheroids for anticancer drug discovery," *Biomedical Microdevices*, vol. 10, no. 2, pp. 197–202, 2008.

[166] Y. S. Torisawa, A. Takagi, Y. Nashimoto, T. Yasukawa, H. Shiku, and T. Matsue, "A multicellular spheroid array to realize spheroid formation, culture, and viability assay on a chip," *Biomaterials*, vol. 28, no. 3, pp. 559–566, 2007.

[167] J. M. Kelm and M. Fussenegger, "Microscale tissue engineering using gravity-enforced cell assembly," *Trends in Biotechnology*, vol. 22, no. 4, pp. 195–202, 2004.

[168] J. Friedrich, R. Ebner, and L. A. Kunz-Schughart, "Experimental anti-tumor therapy in 3-D: spheroids—old hat or new challenge?" *International Journal of Radiation Biology*, vol. 83, no. 11-12, pp. 849–871, 2007.

[169] J. M. Kelm and M. Fussenegger, "Scaffold-free cell delivery for use in regenerative medicine," *Advanced Drug Delivery Reviews*, vol. 62, no. 7-8, pp. 753–764, 2010.

[170] V. M. Weaver, O. W. Petersen, F. Wang et al., "Reversion of the malignant phenotype of human breast cells in three-dimensional culture and in vivo by integrin blocking antibodies," *The Journal of Cell Biology*, vol. 137, no. 1, pp. 231–245, 1997.

[171] M. Hughes-Fulford, "Function of the cytoskeleton in gravisensing during spaceflight," *Advances in Space Research*, vol. 32, no. 8, pp. 1585–1593, 2003.

[172] Y. Naito, T. Shinoka, D. Duncan et al., "Vascular tissue engineering: towards the next generation vascular grafts," *Advanced Drug Delivery Reviews*, vol. 63, no. 4-5, pp. 312–323, 2011.

[173] C. Kang, L. Zou, M. Yuan et al., "Impact of simulated microgravity on microvascular endothelial cell apoptosis," *European Journal of Applied Physiology*, vol. 111, no. 9, pp. 2131–2138, 2011.

[174] S. M. Grenon, M. Jeanne, J. Aguado-Zuniga, M. S. Conte, and M. Hughes-Fulford, "Effects of gravitational mechanical unloading in endothelial cells: association between caveolins, inflammation and adhesion molecules," *Scientific Reports*, vol. 3, article 1494, 2013.

Hindawi Publishing Corporation
BioMed Research International
Volume 2014, Article ID 615854, 10 pages
http://dx.doi.org/10.1155/2014/615854

Review Article

Multisensory Integration and Internal Models for Sensing Gravity Effects in Primates

Francesco Lacquaniti,[1,2,3] Gianfranco Bosco,[1,2,3] Silvio Gravano,[1,3] Iole Indovina,[1,3] Barbara La Scaleia,[3] Vincenzo Maffei,[3] and Myrka Zago[3]

[1] *Centre of Space Bio-Medicine, University of Rome Tor Vergata, Via Montpellier 1, 00133 Rome, Italy*
[2] *Department of Systems Medicine, University of Rome Tor Vergata, Via Montpellier 1, 00133 Rome, Italy*
[3] *Laboratory of Neuromotor Physiology, IRCCS Santa Lucia Foundation, Via Ardeatina 306, 00179 Rome, Italy*

Correspondence should be addressed to Francesco Lacquaniti; lacquaniti@med.uniroma2.it

Received 2 May 2014; Accepted 26 May 2014; Published 1 July 2014

Academic Editor: Mariano Bizzarri

Gravity is crucial for spatial perception, postural equilibrium, and movement generation. The vestibular apparatus is the main sensory system involved in monitoring gravity. Hair cells in the vestibular maculae respond to gravitoinertial forces, but they cannot distinguish between linear accelerations and changes of head orientation relative to gravity. The brain deals with this sensory ambiguity (which can cause some lethal airplane accidents) by combining several cues with the otolith signals: angular velocity signals provided by the semicircular canals, proprioceptive signals from muscles and tendons, visceral signals related to gravity, and visual signals. In particular, vision provides both static and dynamic signals about body orientation relative to the vertical, but it poorly discriminates arbitrary accelerations of moving objects. However, we are able to visually detect the specific acceleration of gravity since early infancy. This ability depends on the fact that gravity effects are stored in brain regions which integrate visual, vestibular, and neck proprioceptive signals and combine this information with an internal model of gravity effects.

1. Introduction

Intuitively, sensing gravity effects should be a trivial problem for a complex nervous system such as our own. On the one hand, direction and magnitude of gravity are quasi-constant on Earth. Thus, gravitational acceleration varies by <1% by changing latitude or altitude, while the vertical deflection is $<0.05^{\circ}$. On the other hand, our nervous system is computationally high-powered, being endowed with $\approx 10^{11}$ neurons interconnected via $\approx 10^{15}$ synapses. All axons pieced together would cover the distance between the Earth and the Moon (about 400.000 km). One would assume that we are able to monitor gravity directly by means of our sensory systems, but this is not the case. As we shall review in this paper, gravity effects are only extrapolated indirectly by the brain by combining multisensory information with internal models, that is, with neural processes which mimic a physical event.

Sensing and coping with gravity is crucial for space perception, control of upright posture, and generation of movements. Indeed, gravity provides a unique reference axis to which we can anchor body orientation and monitor orientation changes. Gravity effects on limb and body movements are two-sided, insofar as gravity acts both as a perturbing force that must be counteracted to avoid falling down and as a facilitating force which allows walking and running via the ground contact forces.

2. Vestibular Information

The vestibular receptors lie inside the labyrinth of the temporal bone. Somewhat similar sensors evolved first in invertebrates and then in vertebrates about 500 Myrs ago [1]. The vestibular apparatus acts as an inertial navigation system, including in each ear three semicircular canals oriented roughly orthogonal to each other and two otolithic organs, the sacculus and utriculus with sensory epithelia oriented roughly vertically and horizontally, respectively [2].

The vestibular sensors function as accelerometers, the semicircular canals transducing angular accelerations (roll, yaw, and pitch) and the otoliths transducing linear accelerations. Head acceleration bends the cilia of the hair cells in the sensory organs, resulting in a change of the membrane potential and synaptic transmission of the neurons of the vestibular ganglion innervating the receptors. The signals from the vestibular neurons carry information about head velocity and acceleration to the vestibular nuclei in the brain stem. In turn, signals from these nuclei are relayed and processed in several regions of the brain and spinal cord, giving rise to sensations and movements [3].

The widely distributed polarities of response of the otolith receptors in the maculae allow monitoring acceleration vectors in any arbitrary direction (Figure 1(a)). These receptors are extremely sensitive, being able to detect displacements of the cilia as small as 0.3 nm (typical atomic diameter) and correspondingly small accelerations. In fact, the receptors in the maculae respond to the projection of an applied force (or acceleration). Thus, the component of gravitational acceleration projected on the saccular macula is $g \cos\alpha$, where α is the angle of tilt of the head relative to the gravity direction, whereas the component of gravitational acceleration projected on the utricle macula is $g \sin\alpha$. Gravity accelerates the body downwards and is opposed by the ground contact forces. These contact forces are transmitted to all body segments and to the head, where they are monitored by the otolith receptors. These receptors respond to a tilt of the head relative to gravity, but in general they cannot provide a unique measurement of gravity effects. As any accelerometer, also the sacculus and utricle respond to net gravitoinertial accelerations, and they cannot distinguish between the gravitational and the inertial component. For instance, otolith afferents cannot distinguish whether we are accelerating backward (Figure 1(b)) or tilting the head forward (Figure 1(c)). This is because the effect of gravity is locally indistinguishable from the effect of a linear acceleration of the reference system [8]. In fact, the otolith afferents signal the net gravitoinertial acceleration (a) resulting from the vector difference between the gravity vector (g) and the linear acceleration vector (f):

$$a = g - f. \tag{1}$$

All vectors are time-varying, referred to head-fixed coordinates of the vestibular sensors.

This intrinsic ambiguity can give rise to perceptual illusions which become extremely dangerous under some specific conditions. For instance, during takeoff, an airplane pilot may sense an erroneously high value of upward pitch, because the resultant of the vector sum of gravity and backward inertial acceleration is misperceived as the actual orientation relative to the vertical. Under conditions of low visibility and without the aid of instruments, the pilot may then attempt to correct the aircraft attitude by pitching downward, with the risk of impacting the ground. Spatial disorientations originating from sensory ambiguities of this kind are often involved in severe aviation accidents [9].

Under usual conditions, however, we have no difficulty in sensing the orientation of the head relative to the vertical, even with the eyes closed and in the presence of appreciable accelerations, provided the latter have short duration (as those of a car or train). This is because the ambiguity can be solved by the brain using a variety of "tricks." First, the brain filters the otolith signals, so that the low-frequency (longer lasting) signals are automatically interpreted as a change in the tilt angle of the head relative to gravity [10]. Conversely, high-frequency (shorter lasting) signals are interpreted as related to a linear acceleration. Also the perceptual illusion of the aircraft pilot mentioned above is consistent with the frequency segregation hypothesis. A prolonged linear acceleration (such as that at airplane takeoff) is a very rare event; when it occurs, it is interpreted erroneously as a tilt relative to gravity. Notice, however, that, unlike the output of a simple low-pass filter, the phase of perceived tilt has been shown to be relatively constant across a broad frequency range [3, 11].

A second "trick" used to disambiguate gravitoinertial acceleration consists in combining the otolith signals with those of the semicircular canals [11–13], just as the man-made inertial systems which combine accelerometers and gyroscopes. When we turn our heads, the semicircular canals integrate the angular acceleration and signal the corresponding angular velocity for frequencies above about 0.05 Hz [14]. Information about angular head velocity can then be used to keep track of changes in orientation of the gravity vector relative to the head [15, 16]. Formally,

$$\dot{g} = g \times \omega, \tag{2}$$

where $\dot{g}$ denotes the time derivative of the gravity vector, ω denotes the angular velocity, and $\times$ denotes vector cross-product. An internal three-dimensional estimate of the gravity vector in head coordinates can then be obtained by integrating (2), if the initial conditions for g are known:

$$g = \int g \times \omega \, dt. \tag{3}$$

Notice that the angular velocity that needs to be integrated in (3) is represented by the component parallel to the Earth horizon, because this component changes the orientation of the head relative to gravity. Given the estimate of g provided by (3), gravitoinertial accelerations can be disambiguated by solving (1).

A potential problem with the model outlined above is that the semicircular canals do not provide a reliable estimate of angular velocity at steady-state [14]. Errors in the estimate of ω would determine an error in the estimate of tilt relative to gravity provided by (3). A solution consists in correcting the errors by means of the so-called somatogravic feedback (Figure 2), which tends to align the estimate of the gravitational acceleration with the gravitoinertial acceleration [4, 5, 17]. In other words, the time-average of the gravitoinertial acceleration over several seconds yields an estimate of gravity orientation at low frequencies. The somatogravic effect can be incorporated in the model of (2) by including a low-pass

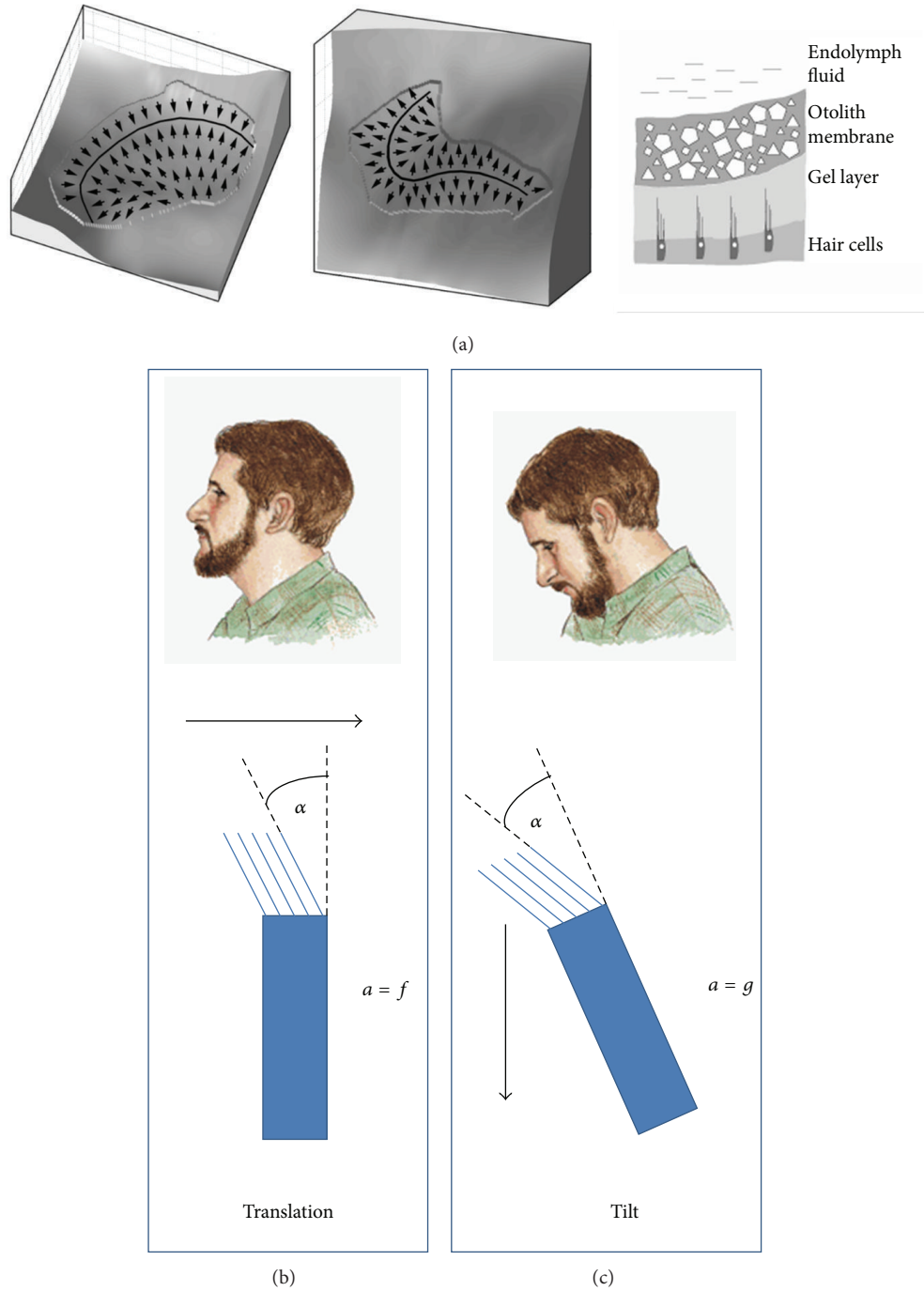

FIGURE 1: (a) Otolith organs. Left: utricle. Center: saccule. Arrows indicate the local on-directions of the hair cells; thick black lines indicate the striola. Right: cross-section through the otolith membrane showing the different layers. Licensed under the Creative Commons Attribution-Share (authors: Thomas Haslwanter and Rudi Jaeger). (b)-(c) Tilt-translation ambiguity of otolith receptors. (b) The upright head is accelerated backward. (c) The head is tilted forward. These two gravitoinertial accelerations cannot be discriminated by the otolith sensory neurons.

filtered term to the tilt estimate, thereby canceling any drift [4]. The resulting equation is

$$\dot{g} = g \times \omega - \frac{g - a}{\tau}. \quad (4)$$

The time constant τ controls the gain and phase of the g estimate when the otolith organs alone are activated, for example, by pure translation. Alternatively, the somatogravic feedback effects can be substituted by a Bayesian prior at zero translational acceleration [4, 17]. This prior is also compatible with the aviation illusion mentioned above. Indeed, while the correction due to the feedback or the prior is beneficial under normal conditions, it can result in the so-called somatogravic illusion [4, 9]. During translation, the tilt

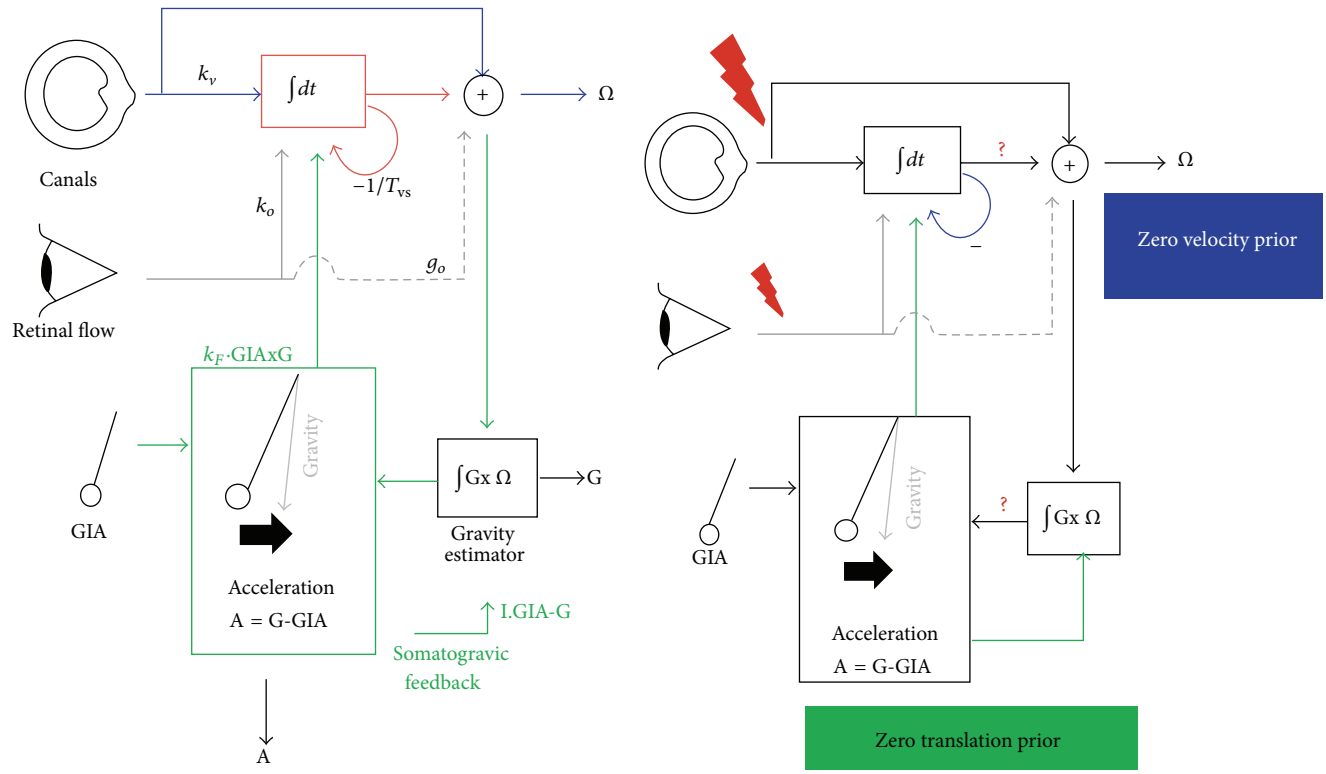

(a) Complete vestibular information processing model

(b) Bayesian model

FIGURE 2: Model of visuovestibular processing proposed by Laurens and Angelaki [4]. (a) Blue lines, vestibular pathways; grey lines, visual pathways; green lines, inertial pathways. (b) Schematic model of Bayesian inference for vestibular processing. Black lines, deterministic model; lightning bolts, sources of noise; question marks, points of error accumulation; blue lines, influence of the zero velocity prior; green lines, influence of the zero translation prior; grey lines, incorporation of visual information (reproduced with permission from [4]).

estimate increases over time as the estimated gravity moves towards the gravitoinertial acceleration. This causes a decrease in the translation estimate and in an aftereffect at the end of the translational acceleration.

Neural correlates of the operations described above have been discovered in the monkey by Angelaki and colleagues, who found that the neural computation of translation (f) occurs in the so-called Vestibular-only neurons of the vestibular nuclei, in the rostral portion of cerebellar fastigium and nodulus [18]. Neurons in these regions combine temporally processed signals from the canals and otoliths as predicted by the internal model hypothesis. Recently, neurons extracting gravity have been discovered in the cerebellum [5]. Laurens et al. identified a group of Purkinje cells in the caudal cerebellar vermis with responses that reflect an estimate of head tilt (Figure 3). These tilt-selective cells are complementary to the translation-selective Purkinje cells mentioned above, such that their population activities sum to the net gravitoinertial acceleration encoded by the otolith organs.

3. Multisensory Integration

As we remarked in the previous section, vestibular sensations result from composite signals, because the otolith signals are centrally combined with those of the semicircular canals already at the level of second-order sensory neurons in the vestibular nuclei of the brainstem. As far as gravity transduction is concerned, the vestibular signals are centrally combined with other sensory information, such as proprioceptive signals from muscle and tendon receptors, visceral signals (from the kidneys, vena cava, etc.), and visual signals. Vision, in particular, provides both static and dynamic (e.g., optic flow) signals about the orientation of the body relative to the vertical. Finally, also the so-called efference copy of motor signals (i.e., a copy of the motor commands sent by higher brain centers) and internal estimates of the body axis orientation [19] contribute to an estimate of body orientation. All these signals are centrally combined yielding accurate multisensory estimates about gravity direction. Indeed, in darkness an erect person makes errors <2° when aligning an initially tilted luminous bar with the expected direction of gravity [20].

Under normal light conditions of daily life, there are several visual cues which point to the direction of gravity [21]. Thus, trees are rooted downwards and grow vertically upwards, and the walls of the houses are also vertical, as are the chandeliers hanging from the ceiling. The visual reference to gravity is so strong that there exist tourist attraction places (so-called mystery spots) where some anomaly of the environment is exploited to provide the illusion that the gravity law is violated. For instance, in some places there is a strong slope of the terrain and trees grow slanted. Similar effects can be obtained with tilted walls in

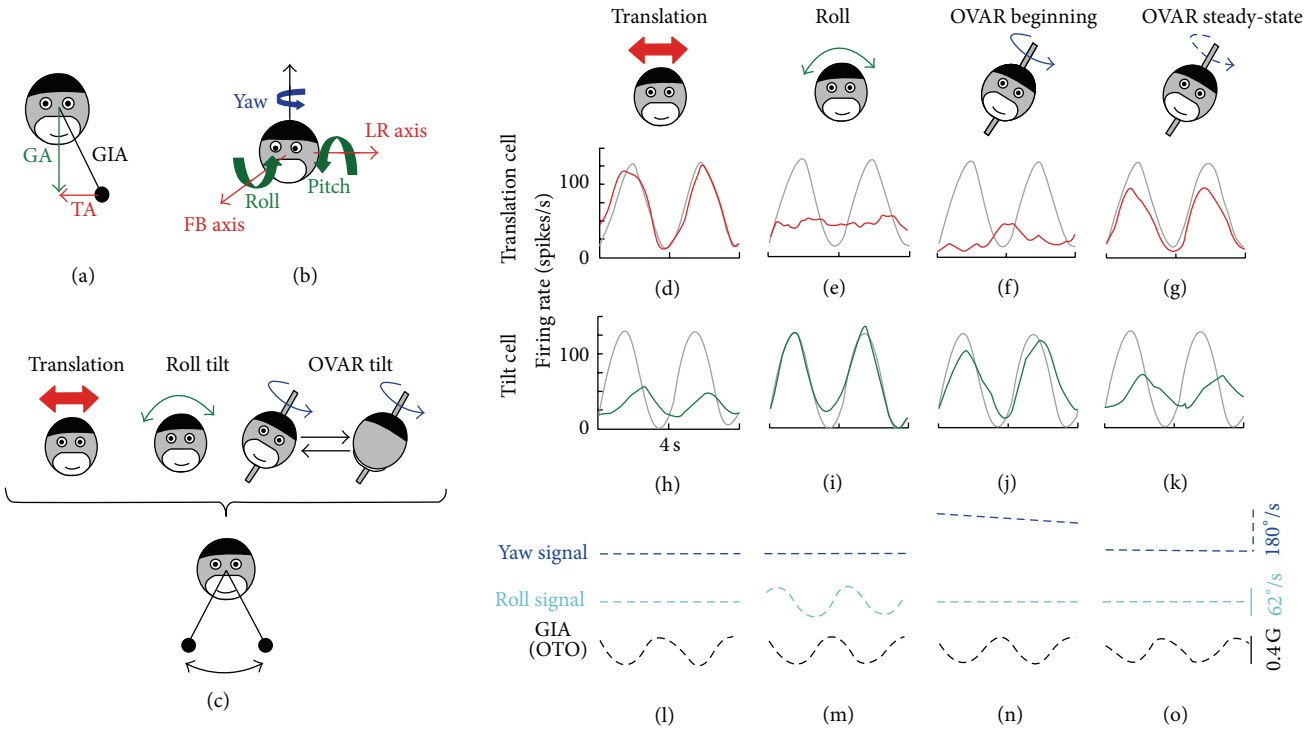

FIGURE 3: (a) Equivalence principle: the otolith organs are sensitive to the gravitoinertial acceleration (GIA), equal to the difference between the gravity vector (GA) and the translational acceleration (TA). (b) Naming conventions of the head's translation and rotation axes. FB, forward-backward; LR, leftward-rightward. (c) Representation of the motion protocols used by Laurens et al. [9]. GIA along the LR axis, represented by a swinging pendulum (bottom), is identical in the 3 protocols (translation, tilt, and off-vertical axis rotation [OVAR]). ((d)–(o)) Responses from a translation-selective cell (red) and a tilt-selective cell (green) during left-right (LR) translation ((d) and (h)), roll tilt ((e) and (i)), and constant velocity OVAR ((f), (g), (j), and (k)). (l), (m), (n), and (o) show the corresponding yaw velocity (detected by horizontal canals, blue), roll velocity (detected by vertical canals, cyan), and GIA along the LR axis (detected by otolith organs [OTO], black). Gray curves: fit to the LR translation response (shown in (d), translation cell) or the roll tilt response (shown in (i), tilt cell) (reproduced with permission from [5]).

houses built for the purpose of creating such illusions. The slope angle distorts the perspective of the observer and may even create the perceptual illusion that a ball can roll upwards by itself. In Italy, such illusions can be felt inside the leaning house designed by Vicino Orsini at Bomarzo (see http://en.wikipedia.org/wiki/File:Bomarzo_parco_mostri_casa_pendente.jpg).

Except when some cue is so strong as to drive space perception by itself (a winner-take all situation), neural estimates of gravity direction normally are computed by the central nervous system as a weighted average of multicue information, including vestibular, visual, neck, and truncal signals, plus a prior distribution about head and body orientation based on experience [20, 22–24]. In Bayesian terms, the posterior estimate is obtained by combining noisy sensory measurements with a prior, each term being weighed inversely to its variance (noise [23]).

4. Visual Perception of Gravitational Acceleration

So far, we considered the problem of monitoring the direction of gravity. A different problem concerns monitoring its magnitude. How do we estimate the gravitational acceleration of an object in a visual scene? This situation occurs quite frequently, as when we experience the vision of objects in free-fall, projectile, or pendulum motion. In addition to object motion, also self-motion may involve visual stimuli (optic flow) accelerated by gravity, as when we fall or jump from a height. When confronted with gravity effects, the visual system faces a unique challenge. In contrast with body graviceptors (such as those of the vestibular system, muscle and tendon proprioceptors, and visceral organs), the visual system does not deal with physical gravity directly, but only with the acceleration of the retinal image. Whereas gravitational acceleration is constant at a given location, the corresponding retinal acceleration varies inversely with the viewing distance (distance between the observer and the scene). Therefore, the visual estimate of gravity effects on a target motion requires accurate estimates of both image acceleration and viewing distance. Both types of estimates are potentially problematic. Indeed, while the visual system is very accurate in velocity estimates, it is rather poor in acceleration estimates. In fact, the visual discrimination of acceleration is about 5 times worse than that of velocity [25]. Also, viewing distance may be difficult to assess. Eye vergence, accommodation, and stereo-disparity contribute

Figure 4: Test with curved tubes in preschoolers (reproduced with permission of Prof. Bruce Hood, University of Bristol).

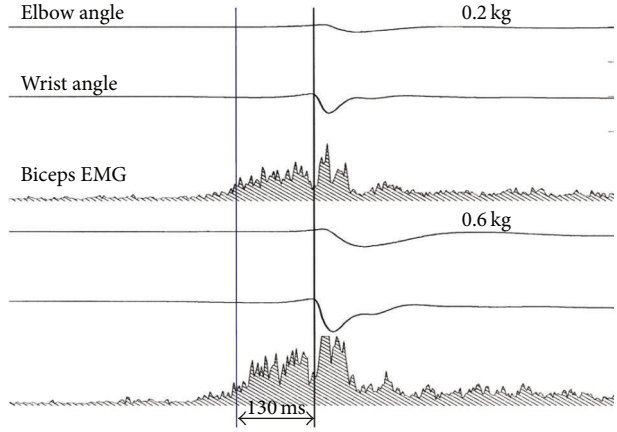

Figure 5: Catching balls of different weight. In different trials, a subject caught a 0.2 kg ball (upper panel) and a 0.6 kg ball (lower panel), dropped from a 1.2 m height. In each panel, traces from top to bottom correspond to elbow flexion angle, wrist flexion angle, and rectified electrical activity (EMG) of biceps muscle. The right-most vertical line denotes the time of impact of the ball on the hand. The left-most vertical line denotes the time of onset of the anticipatory EMG activity (reproduced with permission from [6]).

to estimating viewing distance of target motion in three-dimensional space, but these cues are ineffective when the target is far (because of trigonometry) or when it moves on a two-dimensional video display (as in a videogame). Pictorial information—such as that provided by the presence of objects of known size (people, trees, houses, etc.) in the visual scene—also aids recovering an environmental reference and scale and thus allows the calibration of the retinal image [26].

An internal model of gravity effects represents a critical component of the visual estimates in addition to raw sensory signals. Indeed, gravity represents a special case of visual acceleration to which we are exposed since birth. Therefore, it is very likely that it has been internalized in the brain. In fact, it has been shown that gravity effects on a visual object are detected early in life [27]. Between 5 and 7 months of age, infants expect that an object moving down an inclined plane accelerates and an upwardly moving object decelerates and are surprised to see the effects of an artificial reversed gravity (i.e., objects decelerating while moving downwards and accelerating while moving upwards). Implicit expectation of gravity effects can generate striking judgment errors in preschoolers. Children around 2 years of age believe that a descending object always falls vertically downwards. Thus, when they are asked to find a ball that is dropped along a curved tube, they search directly under the point of fall rather than at the exit of the tube [28]. However, if the ball motion is artificially reversed so that the ball seems to rise upwards, all children solve the task perfectly (Figure 4). Notice that false beliefs about free-fall can still persist in adulthood (so-called naïve physics). For instance, several people without formal scientific background believe that heavier objects fall faster than lighter objects of the same size [6].

Strikingly, however, the motor system has an implicit knowledge of physics which is much better than that available to the cognitive system [6]. Daily life offers several examples of behavior demonstrating the implicit knowledge of physics and the anticipation of the effects of gravitational and centrifugal forces, for instance, when we try to keep equilibrium while riding a bike. Also the automatic motor responses evoked by seeing a falling object are programmed by the brain by taking into account the law of free-fall first formulated by Galileo Galilei. In a laboratory experiment (Figure 5), subjects were asked to catch with the hand a ball that was dropped vertically from 1.2 m height relative to the hand [6]. The ball could weigh 200 g or 600 g in different trials and fell in about 0.5 s. Subjects prestiffened their arm muscles to absorb the impact at about 130 ms, irrespective of the specific mass of the ball. Instead, the amplitude of muscle activation scaled in proportion to the ball mass, because a stronger force is required to counteract a stronger ball momentum [29]. It has also been shown that the time of muscle contraction always leads the impact time by the same amount irrespective of the height of fall (Figure 6) [29]. Therefore, the motor system is accurately tuned to the effects of Earth gravity.

This tuning persists at the beginning of orbital flight, despite the sensory and cognitive evidence of weightlessness, and despite the motor responses being inappropriate to the new conditions [30]. These results are compatible with a Bayesian interpretation of the estimate of gravitational acceleration, if one assumes that the variance in the prior of 1 g acceleration is very small compared with the variance in the sensory likelihood. If so, the 1 g prior would bias strongly the estimate, until it is updated with prolonged exposure to weightlessness [31].

Gravity effects are taken into account not only by the motor system but also perceptually, as when people judge the duration of motion of a falling target [32, 33] or the period of oscillation of a pendulum [34]. Thus, in experiments in which a pendulum oscillates faster or slower than normal, the observers rate the oscillations violating the physical length-period relation as less natural than the oscillations complying with physics [34]. The implicit bias toward gravitational motion when viewing an oscillating pendulum is

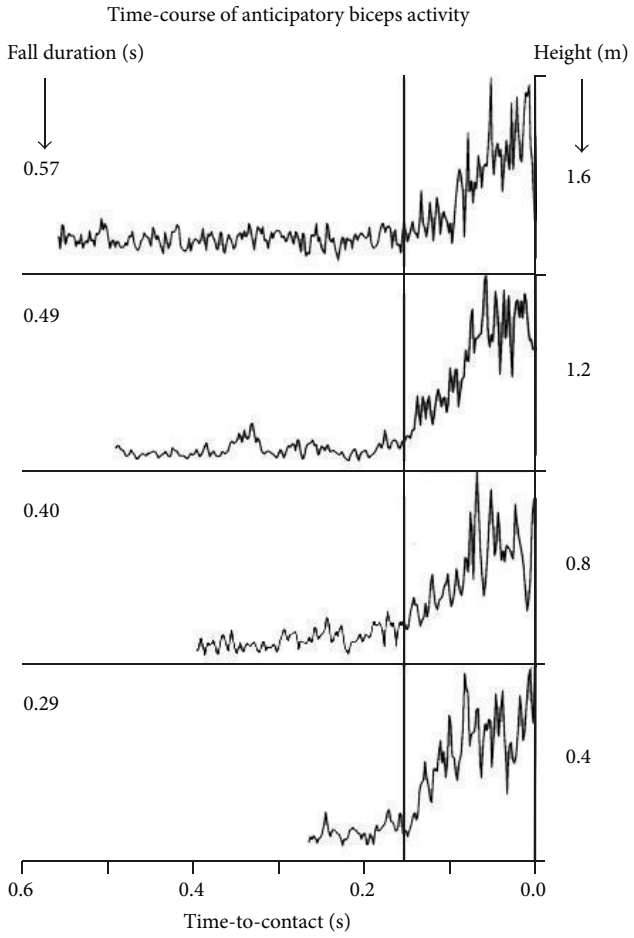

Figure 6: Time course of the EMG anticipatory responses of biceps. Traces correspond to the results obtained for catches of balls dropped from the heights indicated on the right (fall durations are indicated on the left). EMG traces have been scaled in amplitude to their maximum and aligned relative to collision time. Time axis indicates the time remaining prior to collision (reproduced with permission from [6]).

also revealed by the observation that harmonic motion is perceived as uniform [35]. Also, the perceptual judgment of passive egomotion along the vertical direction—simulated by means of immersive visual stimuli—is based on the internal model of gravity [36].

Just as in the case of the estimates of the direction of gravity, also those of visual gravitational acceleration generally depend on a combination of multiple cues, and such combination may obey Bayes' rules. The internal model provides the prior, while various sensory cues provide the likelihood of the estimate with a reliability that depends on the context. In one study, observers were asked to judge the duration of motion of a target accelerating in one of four different directions, downwards, upwards, leftwards, and rightwards, relative to a visual scene [33]. Downward motion complied with the gravity constraint, whereas motion in the other directions violated this constraint. Observers watched either a pictorial or an empty scene, while being upright or tilted by 45° relative to the monitor and Earth's gravity. In another condition, observers were upright and the scene was tilted by 45°. Discrimination precision was significantly better for downward motion than for the other directions. However, the difference in precision was not constant across conditions but was highest when both the observer and the pictorial scene were upright and lowest when the target direction in the empty scene was tilted by 45° relative to an upright observer. Thus, the behaviour observed in the study was consistent with the combination of pictorial cues, orientation of the observer relative to the physical vertical, and orientation of target motion relative to the physical vertical.

The interaction of the visual signals with vestibular signals about subject orientation relative to physical gravity was shown in a study performed during a parabolic flight campaign [37]. During each parabola, a 20 s weightless (0 g) phase was preceded and followed by 20 s of hypergravity (1.5–1.8 g). Strikingly, the timing of interception of a visual target moving along the visual vertical reversed sign during the weightless phases compared with the responses at normal gravity [37]. This reversal depends on the reversal of the otolith responses during the transition from hypergravity to hypogravity, which was sensed as a negative gravity, that is, as a gravitational pull in the upward direction (comparable to when we are suspended upside-down).

5. Neural Substrates of the Internal Model of Gravity Effects on Visual Motion

The hypothesis that the effects of gravity on a target motion are taken into account by combining multisensory information, including visual and vestibular cues, is supported by human neuroimaging studies. In a series of fMRI studies [7, 38–40], visual gravitational acceleration (involving either object motion or simulated egomotion) engaged a network of brain regions located within and around the Sylvian fissure close to the temporoparietal junction (TPJ): posterior insular cortex, retroinsula, parietal operculum, supramarginal gyrus, temporal operculum, and superior and middle temporal gyri. In addition, gravitational motion engaged primary somatosensory and motor cortex, ventral premotor cortex, SMA, cingulate cortex, visual cortex including the lingual gyrus, and several subcortical structures: posterior thalamus, putamen, cerebellum, and vestibular nuclei. A causal link between TPJ activity and the processing of visual gravitational motion has been demonstrated by transiently disrupting the activity of TPJ by means of transcranial magnetic stimulation (TMS) [41].

As reviewed earlier, electrophysiological studies in the monkey showed that a population of Purkinje cells in the caudal cerebellar vermis encodes head tilt, thus reflecting an estimate of gravity direction based on vestibular information [5]. Interestingly, human posterior cerebellar vermis (a homologue region of that studied by Laurens et al. [5] in monkeys) and vestibular nuclei appear to be involved in combining pictorial information with the internal model of gravity to extract gravitational motion from visual scenes (Figure 7) [7].

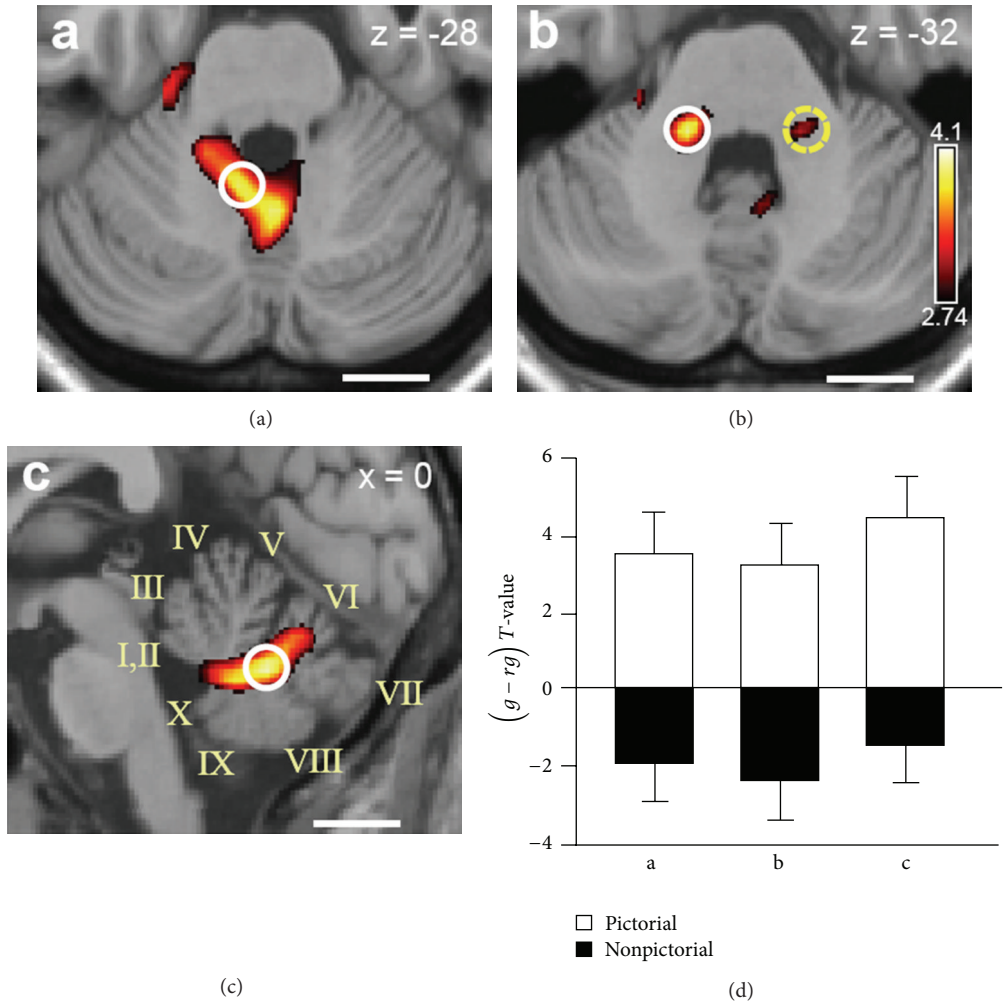

FIGURE 7: Functional magnetic resonance imaging of the cerebellum and brainstem in a task of interception of a ball moving along the vertical. Brain areas showing preferential activation for natural gravity motion specifically for the pictorial visual context. (a), (b), (c) Activations in the midline cerebellum ((a) axial section; (c) medial sagittal section) and vestibular nuclei ((b) axial section). Roman numerals in (c) denote Larsell lobules. White circles are centered on maximal statistical activation peaks. (a) Lobules IX/X. (b) Left vestibular nuclei. (c) Lobules VII/VIII. (d) Bar-graphs of the difference (± between-subjects s.e.m.) t-values for natural gravity (g) and artificial reversed gravity (rg) trials in pictorial (white) and nonpictorial (black) context for the activity peaks circled in (a), (b), and (c) (reproduced with permission from [7]).

In sum, the neuroimaging studies reviewed above indicate that the effects of gravity on visual motion are encoded in a highly distributed cortical-subcortical network. Several regions of this network colocalize with the regions independently activated by vestibular caloric stimuli [38]. These regions then presumably belong to the multimodal vestibular network, which also responds to visual and neck proprioceptive stimuli [42, 43]. Lesions of vestibular cortex can lead to a tilt of the perceived visual vertical and rotational vertigo/unsteadiness [44], while focal electrical stimulation or epileptic discharges can elicit sensations of self-motion or altered gravity [45, 46].

6. Conclusions

We argued that an apparently simple problem such as that of monitoring gravity effects on our body and on the external environment is in fact computationally very demanding, even for a high-powered brain such as that of primates. Measurements derived from individual sensory organs are often ambiguous (due to the intrinsic constraints of physical laws) and noisy (due to biological limitations). However, the combination of multisensory signals (visual, vestibular, proprioceptive, and visceral) and the reliance on internal models of physics yield estimates which are very accurate under normal conditions, but which can fail badly under anomalous conditions (such as the early phases of space flight). Central processing of multisensory information and internal models occurs in a widely distributed network of cortical and subcortical regions. The extensive integration of sensory and motor information in this network makes gravity-related information available to many vital functions of the organism.

Conflict of Interests

The research reviewed in this paper was conducted in the absence of any commercial or financial relationships that could be construed as a potential conflict of interests.

Acknowledgments

The authors' work was supported by the Italian Ministry of University and Research (PRIN grant), and Italian Space Agency (CRUSOE, COREA, SLINK, and ARIANNA grants).

References

[1] K. W. Beisel, Y. Wang-Lundberg, A. Maklad, and B. Fritzsch, "Development and evolution of the vestibular sensory apparatus of the mammalian ear," *Journal of Vestibular Research: Equilibrium and Orientation*, vol. 15, no. 5-6, pp. 225–241, 2005.

[2] M. E. Goldberg, M. F. Walker, and A. J. Hudspeth, "The vestibular system," in *Principles of Neural Science*, E. K. Kandel, J. H. Schwartz, T. M. Jessell, S. A. Siegelbaum, and A. J. Hudspeth, Eds., pp. 917–934, McGraw-Hill, New York, NY, USA, 2013.

[3] D. E. Angelaki and K. E. Cullen, "Vestibular system: the many facets of a multimodal sense," *Annual Review of Neuroscience*, vol. 31, pp. 125–150, 2008.

[4] J. Laurens and D. E. Angelaki, "The functional significance of velocity storage and its dependence on gravity," *Experimental Brain Research*, vol. 210, no. 3-4, pp. 407–422, 2011.

[5] J. Laurens, H. Meng, and D. E. Angelaki, "Neural representation of orientation relative to gravity in the macaque cerebellum," *Neuron*, vol. 80, no. 6, pp. 1508–1518, 2013.

[6] M. Zago and F. Lacquaniti, "Cognitive, perceptual and action-oriented representations of falling objects," *Neuropsychologia*, vol. 43, no. 2, pp. 178–188, 2005.

[7] W. L. Miller, V. Maffei, G. Bosco et al., "Vestibular nuclei and cerebellum put visual gravitational motion in context," *Journal of Neurophysiology*, vol. 99, no. 4, pp. 1969–1982, 2008.

[8] C. Fernandez and J. M. Goldberg, "Physiology of peripheral neurons innervating otolith organs of the squirrel monkey. I. Response to static tilts and to long duration centrifugal force," *Journal of Neurophysiology*, vol. 39, no. 5, pp. 970–984, 1976.

[9] R. Gibb, B. Ercoline, and L. Scharff, "Spatial disorientation: decades of pilot fatalities," *Aviation Space and Environmental Medicine*, vol. 82, no. 7, pp. 717–724, 2011.

[10] R. Mayne, "A systems concept of the vestibular organs," in *Vestibular System: Psychophysics, Applied Aspects and General Interpretations*, H. Kornhuber, Ed., vol. 6, part 2, pp. 493–580, Springer, Berlin, Germany, 1974.

[11] S. Glasauer, "Interaction of semicircular canals and otoliths in the processing structure of the subjective zenith," *Annals of the New York Academy of Sciences*, vol. 656, pp. 847–849, 1992.

[12] D. E. Angelaki, M. Q. McHenry, J. D. Dickman, S. D. Newlands, and B. J. M. Hess, "Computation of inertial motion: neural strategies to resolve ambiguous otolith information," *Journal of Neuroscience*, vol. 19, no. 1, pp. 316–327, 1999.

[13] D. M. Merfeld, L. Zupan, and R. J. Peterka, "Humans use internal models to estimate gravity and linear acceleration," *Nature*, vol. 398, no. 6728, pp. 615–618, 1999.

[14] J. M. Goldberg and C. Fernandez, "Vestibular mechanisms," *Annual Review of Physiology*, vol. 37, pp. 129–162, 1975.

[15] D. M. Merfeld and L. H. Zupan, "Neural processing of gravitoinertial cues in humans. III. Modeling tilt and translation responses," *Journal of Neurophysiology*, vol. 87, no. 2, pp. 819–833, 2002.

[16] A. M. Green and D. E. Angelaki, "An integrative neural network for detecting inertial motion and head orientation," *Journal of Neurophysiology*, vol. 92, no. 2, pp. 905–925, 2004.

[17] J. Laurens and J. Droulez, "Bayesian processing of vestibular information," *Biological Cybernetics*, vol. 96, no. 4, pp. 389–404, 2007.

[18] D. E. Angelaki, A. G. Shaikh, A. M. Green, and J. D. Dickman, "Neurons compute internal models of the physical laws of motion," *Nature*, vol. 430, no. 6999, pp. 560–564, 2004.

[19] H. Mittelstaedt, "A new solution to the problem of the subjective vertical," *Naturwissenschaften*, vol. 70, no. 6, pp. 272–281, 1983.

[20] R. A. A. Vingerhoets, M. de Vrijer, J. A. M. van Gisbergen, and W. P. Medendorp, "Fusion of visual and vestibular tilt cues in the perception of visual vertical," *Journal of Neurophysiology*, vol. 101, no. 3, pp. 1321–1333, 2009.

[21] I. P. Howard, *Human Visual Orientation*, John Wiley & Sons, New York, NY, USA, 1982.

[22] L. H. Zupan, D. M. Merfeld, and C. Darlot, "Using sensory weighting to model the influence of canal, otolith and visual cues on spatial orientation and eye movements," *Biological Cybernetics*, vol. 86, no. 3, pp. 209–230, 2002.

[23] P. R. MacNeilage, M. S. Banks, D. R. Berger, and H. H. Bülthoff, "A Bayesian model of the disambiguation of gravitoinertial force by visual cues," *Experimental Brain Research*, vol. 179, no. 2, pp. 263–290, 2007.

[24] D. E. Angelaki, E. M. Klier, and L. H. Snyder, "A vestibular sensation: probabilistic approaches to spatial perception," *Neuron*, vol. 64, no. 4, pp. 448–461, 2009.

[25] P. Werkhoven, H. P. Snippe, and A. Toet, "Visual processing of optic acceleration," *Vision Research*, vol. 32, no. 12, pp. 2313–2329, 1992.

[26] S. E. Palmer, *Vision Science. Photons to Phenomenology*, MIT Press, Cambridge, UK, 1999.

[27] I. K. Kim and E. S. Spelke, "Infants' sensitivity to effects of gravity on visible object motion," *Journal of Experimental Psychology: Human Perception and Performance*, vol. 18, no. 2, pp. 385–393, 1992.

[28] B. M. Hood, "Gravity does rule for falling events," *Developmental Science*, vol. 1, no. 1, pp. 59–63, 1998.

[29] F. Lacquaniti and C. Maioli, "The role of preparation in tuning anticipatory and reflex responses during catching," *The Journal of Neuroscience*, vol. 9, no. 1, pp. 134–148, 1989.

[30] J. McIntyre, M. Zago, A. Berthoz, and F. Lacquaniti, "Does the brain model Newton's laws?" *Nature Neuroscience*, vol. 4, no. 7, pp. 693–694, 2001.

[31] R. J. White and M. Averner, "Humans in space," *Nature*, vol. 409, no. 6823, pp. 1115–1118, 2001.

[32] M. A. Grealy, C. M. Craig, C. Bourdin, and S. G. Coleman, "Judging time intervals using a model of perceptuo-motor control," *Journal of Cognitive Neuroscience*, vol. 16, no. 7, pp. 1185–1195, 2004.

[33] A. Moscatelli and F. Lacquaniti, "The weight of time: gravitational force enhances discrimination of visual motion duration," *Journal of Vision*, vol. 11, no. 4, pp. 1–17, 2011.

[34] J. B. Pittenger, "Detection of violations of the law of pendulum motion: observers' sensitivity to the relation between period and length," *Ecological Psychology*, vol. 2, no. 1, pp. 55–81, 1990.

[35] B. La Scaleia, M. Zago, A. Moscatelli, F. Lacquaniti, and P. Viviani, "Implied dynamics biases the visual perception of velocity," *PloS ONE*, vol. 9, no. 3, Article ID e93020, 2014.

[36] I. Indovina, V. Maffei, and F. Lacquaniti, "Anticipating the effects of visual gravity during simulated self-motion: estimates of time-to-passage along vertical and horizontal paths," *Experimental Brain Research*, vol. 229, no. 4, pp. 579–586, 2013.

[37] P. Senot, M. Zago, A. le Séac'h et al., "When up is down in 0g: how gravity sensing affects the timing of interceptive actions," *Journal of Neuroscience*, vol. 32, no. 6, pp. 1969–1973, 2012.

[38] I. Indovina, V. Maffei, G. Bosco, M. Zago, E. Macaluso, and F. Lacquaniti, "Representation of visual gravitational motion in the human vestibular cortex," *Science*, vol. 308, no. 5720, pp. 416–419, 2005.

[39] V. Maffei, E. Macaluso, I. Indovina, G. Orban, and F. Lacquaniti, "Processing of targets in smooth or apparent motion along the vertical in the human brain: an fMRI study," *Journal of Neurophysiology*, vol. 103, no. 1, pp. 360–370, 2010.

[40] I. Indovina, V. Maffei, K. Pauwels, E. Macaluso, G. A. Orban, and F. Lacquaniti, "Simulated self-motion in a visual gravity field: sensitivity to vertical and horizontal heading in the human brain," *NeuroImage*, vol. 71, pp. 114–124, 2013.

[41] G. Bosco, M. Carrozzo, and F. Lacquaniti, "Contributions of the human temporoparietal junction and MT/V5+ to the timing of interception revealed by transcranial magnetic stimulation," *The Journal of Neuroscience*, vol. 28, no. 46, pp. 12071–12084, 2008.

[42] S. Bense, T. Stephan, T. A. Yousry, T. Brandt, and M. Dieterich, "Multisensory cortical signal increases and decreases during vestibular galvanic stimulation (fMRI)," *Journal of Neurophysiology*, vol. 85, no. 2, pp. 886–899, 2001.

[43] G. Bottini, H. O. Karnath, G. Vallar et al., "Cerebral representations for egocentric space: functional-anatomical evidence from caloric vestibular stimulation and neck vibration," *Brain*, vol. 124, no. 6, pp. 1182–1196, 2001.

[44] T. Brandt and M. Dieterich, "The vestibular cortex: its locations, functions, and disorders," *Annals of the New York Academy of Sciences*, vol. 871, pp. 293–312, 1999.

[45] O. Blanke, S. Ortigue, T. Landis, and M. Seeck, "Stimulating illusory own-body perceptions," *Nature*, vol. 419, no. 6904, pp. 269–270, 2002.

[46] D. K. Nguyen, D. B. Nguyen, R. Malak et al., "Revisiting the role of the insula in refractory partial epilepsy," *Epilepsia*, vol. 50, no. 3, pp. 510–520, 2009.

Hindawi Publishing Corporation
BioMed Research International
Volume 2014, Article ID 296747, 16 pages
http://dx.doi.org/10.1155/2014/296747

Research Article

Integration Analysis of MicroRNA and mRNA Expression Profiles in Human Peripheral Blood Lymphocytes Cultured in Modeled Microgravity

C. Girardi,[1] C. De Pittà,[1] S. Casara,[1] E. Calura,[1] C. Romualdi,[1] L. Celotti,[1,2] and M. Mognato[1]

[1] *Dipartimento di Biologia, Università degli Studi di Padova, Via U. Bassi 58/B, 35131 Padova, Italy*
[2] *Laboratori Nazionali di Legnaro, INFN, Viale dell'Università 2, Legnaro, 35020 Padova, Italy*

Correspondence should be addressed to L. Celotti; lucia.celotti@unipd.it and M. Mognato; maddalena.mognato@unipd.it

Received 16 April 2014; Revised 22 May 2014; Accepted 22 May 2014; Published 23 June 2014

Academic Editor: Mariano Bizzarri

We analyzed miRNA and mRNA expression profiles in human peripheral blood lymphocytes (PBLs) incubated in microgravity condition, simulated by a ground-based rotating wall vessel (RWV) bioreactor. Our results show that 42 miRNAs were differentially expressed in MMG-incubated PBLs compared with 1 g incubated ones. Among these, miR-9-5p, miR-9-3p, miR-155-5p, miR-150-3p, and miR-378-3p were the most dysregulated. To improve the detection of functional miRNA-mRNA pairs, we performed gene expression profiles on the same samples assayed for miRNA profiling and we integrated miRNA and mRNA expression data. The functional classification of miRNA-correlated genes evidenced significant enrichment in the biological processes of immune/inflammatory response, signal transduction, regulation of response to stress, regulation of programmed cell death, and regulation of cell proliferation. We identified the correlation of miR-9-3p, miR-155-5p, miR-150-3p, and miR-378-3p expression with that of genes involved in immune/inflammatory response (e.g., IFNG and IL17F), apoptosis (e.g., PDCD4 and PTEN), and cell proliferation (e.g., NKX3-1 and GADD45A). Experimental assays of cell viability and apoptosis induction validated the results obtained by bioinformatics analyses demonstrating that in human PBLs the exposure to reduced gravitational force increases the frequency of apoptosis and decreases cell proliferation.

1. Introduction

Exposure to spaceflight environment is known to cause in humans many adverse physiological changes, including skeletal muscle atrophy [1–3], cardiovascular and microvascular disorders [4–6], bone deterioration [7, 8], and impaired immune system function [9, 10]. Immune system dysfunction due to exposure to microgravity has been documented as well in terms of reduced activation/proliferation, altered cytokine production, and altered signal transduction [11, 12]. Alterations in global gene expression patterns have been also observed in space-flown human cells, involving mainly genes of immune system activation [13, 14], cytoskeleton [15], and cell cycle [16, 17]. However, due to the difficulty and limitations of performing experiments in the real microgravity of space, many investigations have been conducted under simulated microgravity conditions, in which cells are cultured in ground-based machines, such as clinostats and rotating wall vessel bioreactors that generate a residual 10^{-3}–10^{-6} g force that approximates microgravity [5, 18–24]. The results indicate that, similar to space microgravity, simulated microgravity affects both cell structure and function, as well as gene expression, in mammalian cells [14, 19, 25], in bacteria [26, 27], or in other living organisms [28–30].

Since molecular changes at the gene level may compromise cell function, it is important to understand the cellular response to reduced gravity at the molecular level. For this purpose, a class of noncoding RNAs, called microRNAs (miRNAs), plays a key role. miRNAs are a large family of small RNAs of 18–24 nucleotides that are involved in post-transcriptional regulation of gene expression by interacting with 3′-untranslated regions (UTR) of target genes. The regulatory process is complex and occurs posttranscriptionally through miRNA interaction with a target site in the mRNA

that has partial or complete complementarity to the miRNA. The binding of miRNAs to complementary sequence of their target mRNAs may repress translation or induce degradation of mRNAs [31]. Recently, the destabilization of target mRNAs, instead of translational repression, has been shown to be the predominant mechanism for reduced protein output [32]. Less often, dsRNA formed by miRNA target complexes can target gene promoters and actually enhance transcription of target genes, sometimes termed RNAa (RNA activation) [33]. A single miRNA may have broad effects on gene expression networks, such as regulating cell lineage specificity, cellular functions, or stress response. Besides a physiological role of miRNAs in a variety of important biological processes including differentiation, apoptosis [34], and fat metabolism [35], the miRNA-mediated gene regulation operates also during viral infection [36], stress response pathway [37], and pathological processes, such as tumorigenesis [38–42].

The present study is addressed to identify alterations in miRNA profiles of human peripheral blood lymphocytes (PBLs) incubated in modeled microgravity (MMG) with respect to those incubated in gravity 1 g. To simulate microgravity, we used a specialized bioreactor developed at the NASA-Johnson Space Center (Houston, TX, USA), the rotating wall vessel, which represents a valid ground model to simulate, as far as possible, a condition of reduced gravity. To identify miRNA-correlated genes whose expression level was significantly altered as a function of MMG, we performed gene expression profiling on the same PBL samples assayed for miRNA profiling and we integrated microRNAome and transcriptome by using MAGIA^2 [43], a web tool for the integrative analysis of miRNA and genes expression data incorporating transcriptional regulation. A group of miRNA-mRNA pairs related to immunity, cell proliferation, and apoptosis was identified in PBLs incubated in MMG. The differences between MMG and 1 g on correlated miRNA-mRNA pairs involved in cell proliferation and apoptosis were investigated by *in vitro* assays of clonogenic ability and apoptosis induction in PBLs incubated in MMG with respect to those incubated in 1 g conditions.

2. Materials and Methods

2.1. Lymphocytes Isolation and Microgravity Simulation. Human peripheral blood lymphocytes (PBLs) were obtained from freshly collected "buffy coats" from blood samples of twelve healthy anonymous donors at the Blood Centre of the City Hospital of Padova (Italy). This study obtained the Ethics Approval from the Transfusion Medicine (TM) Ethics Committee of Blood Centre of the City Hospital of Padova. PBLs were isolated by separation on Biocoll density gradient (BIOCHROM, Berlin, Germany). After isolation, PBLs were preincubated overnight at a concentration of 3×10^6/mL in basal medium RPMI 1640 containing GlutaMAX I (Invitrogen Life Technologies, Carlsbad, CA, USA), 124 U/mL penicillin, 63 μg/mL streptomycin sulfate, and 10% fetal bovine serum (FBS, BIOCHROM, Berlin, Germany). After the overnight incubation, PBLs, consisting of peripheral mononuclear cells depleted of monocytes, were suspended at 1×10^6/mL in basal medium and subjected to modeled microgravity, simulated by the rotating wall vessel (RWV) bioreactor (Synthecon, Cellon), placed inside a humidified incubator, vertically rotating at 23 rpm [44]. In the rotating system, the gravity is balanced by equal and opposite mechanical forces (centrifugal, Coriolis, and shear components), and the gravitational vector is reduced to about 10^{-3} g. In these conditions, single cells are nearly always in suspension, rotating in quasi-stationary manner with the fluid, in a low-shear culture environment [19, 45]. Ground-based (1 g) PBLs were kept at the same cell density in 75 cm^2 flasks (FALCON) in the same medium. After 24, 48, or 72 h of incubation in MMG and 1 g PBLs were activated to enter cell cycle to measure cell proliferation by incubation in culture medium (CM) containing phytohaemagglutinin (PHA, BIOCHROM, Berlin, Germany) and interleukin 2 (IL2, Chiron Siena, Italy) as stimulating factors [46].

2.2. Total RNA Isolation. Total RNA was isolated from 10^7 PBLs at the end of 24 h incubation in MMG and 1 g by using Trizol Reagent (Invitrogen Life Technologies, Carlsbad, CA, USA), according to the manufacturer's protocol. Total RNA was quantified using the ND-1000 spectrophotometer (Nanodrop, Wilmington, DE, USA) and RNA integrity and the content of miRNAs were assessed by capillary electrophoresis using the Agilent Bioanalyzer 2100, as previously described [47]. Only total RNA samples with RNA integrity number (RIN) values ≥6 and with miRNA <20% were used for microarray analysis.

2.3. miRNA and Gene Expression Profiling. MicroRNAs profiling was carried out in PBL samples incubated in MMG versus 1 g. Analyses were performed by using the "Human miRNA Microarray kit (V2)" (Agilent Technologies) that allows the detection of 723 known human (miRBase v.10.1) and 76 human viral miRNAs. Total RNA (200 ng) was labeled with pCp Cy3, according to the Agilent protocol and unincorporated dyes were removed with MicroBioSpin6 columns (BioRad) [48]. Probes hybridization and slides washing were performed as previously reported [47]. Agilent Feature Extraction software version 10.5.1.1 was used for image analysis.

Gene expression profiling was carried out in MMG-incubated PBLs versus 1 g incubated PBLs on total RNA extracted from the same PBL samples assayed for miRNA profiling. We used the "Whole Human Genome Oligo Microarray" (Agilent), consisting of ~41.000 (60-mer) oligonucleotide probes, which span conserved exons across the transcripts of the targeted full-length genes. 800 ng of total RNA was labeled with "Agilent One-Color Microarray-Based Gene Expression protocol" according to the manufacturer's instructions. The method uses T7 RNA polymerase, which simultaneously amplifies target material and incorporates cyanine 3-labeled CTP. The Cy3-labeled cRNAs were purified using Qiagen's RNeasy mini spin columns (Qiagen) and quantified using the ND-1000 spectrophotometer (Nanodrop, Wilmington, DE, USA). Probes hybridization and slides washing were performed as previously reported [47].

Slides were scanned on an Agilent Microarray Scanner System (model G2565CA) and Agilent Feature Extraction software version 10.5.1.1 was used for image analysis. Raw data are available on the Gene Expression Omnibus (GEO) website (http://www.ncbi.nlm.nih.gov/geo/) using SuperSeries accession number GSE57418 that groups microRNA (GSE57400) and mRNA expression profiles (GSE57408).

2.4. Statistical Analysis of miRNA and Gene Expression Data. Interarray normalization of expression levels was performed with cyclic Lowess for miRNA experiments and with quantile for gene expression profiling [49] to correct possible experimental distortions. Normalization function was applied to expression data of all experiments and then values of spot replicates within arrays were averaged. The modalities of spot quality measures and hybridization are reported previously [47]. The identification of differentially expressed genes and miRNAs was performed with one- and two-class Significance Analysis of Microarray (SAM) program [50] with default settings. The expression level of each miRNA and mRNA was calculated as the log2 (MMG/1 g) PBLs of the same donor. Pathway analysis on differentially expressed genes has been performed using Graphite web [51], hypergeometric test on Reactome Pathways, considering significant those categories with FDR < 0.1.

2.5. Identification of miRNA Target Genes and Correlation Analysis of miRNA and mRNA Expression Data. To predict miRNA targets, we performed a computational analysis integrating mRNA and miRNA expression measurements from the same donor using MAGIA^2 web tool [43], freely available at http://gencomp.bio.unipd.it/magia2/. We used http://www.microrna.org/ predictions and Pearson correlation ($r > 0.4$) to estimate the degree of correlation between any putative pairs of miRNA and mRNA [52, 53]. To identify the biological processes most involved in target prediction, we have performed an enrichment analysis on Gene Ontology (GO) using DAVID web tool v6.7 [54] considering significant those categories with FDR < 0.2.

Intraclass analyses have been performed considering MMG and 1 g samples separately. In order to have comparable results, the intraclass analysis has been performed using MAGIA^2 software with the same parameters, predictors, and cutoff described for the previous analysis. Specific interactions for MMG and 1 g networks have been identified and a GO enrichment analysis (FDR < 0.2) was performed separately on the nodes belonging to the specific MMG and 1 g networks using DAVID web tool.

2.6. Quantitative Real-Time PCR (qRT-PCR) Assay. In order to verify the expression data generated by miRNA and mRNA microarrays, we performed qRT-PCR experiments for miRNAs and genes which showed significant expression changes in MMG. The following miRNAs were subjected to the RT-qPCR validation: miR-9-5p, miR-378a, miR-155-5p, and miR-150-3p. Reverse transcription of 10 ng of total RNA with primers corresponding to each miRNA and to U48 small nuclear RNA (RNU48) as endogenous control was performed as directed by the protocol of the two-step TaqMan MicroRNA Assay kit (Applied Biosystems, Foster City, CA, USA) that incorporates a target-specific stem-loop reverse transcription primer to provide specificity for the mature miRNA target. For the PCR reaction, 1 μL of the RT reaction was combined with 0.5 μL of TaqMan MicroRNA Assay 20x and 5 μL of TaqMan Universal PCR Master Mix in a 10 μL final volume. The reactions were incubated in a Mastercycler EP gradient *S* (Eppendorf) in 0.2 mL PCR tubes for 30 min at 16°C and 30 min at 42°C, followed by 5 min at 85°C, and then held at 4°C. The resulting cDNA was quantitatively amplified in 40 cycles on an ABI 7500 Real-Time PCR System, using TaqMan Universal PCR Master Mix and TaqMan MicroRNA Assays.

For mRNA detection, 1 μg of total RNA was retrotranscribed with ImProm-II Reverse Transcription System (Promega). qRT-PCR was performed with the GoTaq qPCR Master Mix (Promega) and gene-specific primers for IFNG, IL17F, TLR4, HLA-DRB1, and BCL6 genes and for GAPDH as reference. qRT-PCR reactions were performed in quadruplicates, in PBL samples from 6 to 8 donors. Real-time PCR was performed using an Applied Biosystems 7500 Fast Real-Time PCR System with cycling conditions of 95°C for 10 min followed by 95°C for 15 sec and 60°C for 60 sec, 45 cycles in total. The relative expression levels of miRNAs and mRNAs between samples were calculated using the comparative delta CT (threshold cycle number) method ($2^{-\Delta\Delta CT}$) implemented in the 7500 Real-Time PCR System software [55]. Primers' pairs used are as follows: GAPDH (glyceraldehyde-3-phosphate dehydrogenase): fw 5′-TCCTCTGACTTCAACAGCGA-3′; rev 5′-GGGTCTTACTCCTTGGAGGC-3′; IFNG (interferon gamma): fw 5′- GGCATTTTGAAGAATTGGAAAG-3′; rev 5′-TTTGGATGCTCTGGTCATCTT-3′; IL17F (interleukin 17): fw 5′-GGCATCATCAATGAAAACCA-3′; rev 5′- TGGGGTCCCAAGTGACAG-3′; TLR4 (Toll-like receptor 4):fw 5′-CCTGCGTGAGACCAGAAAG-3′; rev 5′-TTCAGCTCCATGCATTGATAA-3′; HLA-DRB1 (major histocompatibility complex, class II, DR beta 1): fw 5′-ACAACTACGGGGTTGTGGAG-3′; rev 5′-GCTGCCTGGATAGAAACCAC-3′; BCL6 (B-cell CLL/lymphoma 6): fw 5′-CGAATCCACACAGGAGAGAAA-3′; rev 5′-ACGCGGTATTGCACCTTG-3′.

2.7. Cell Proliferation and Apoptosis Induction. Cell viability was determined by the T-cell cloning assay [44, 46] at the end of 24 h, 48 h, and 72 h incubation in MMG and 1 g. Briefly, four 96-well U-bottomed microtiter plates with two viable lymphocytes/well were seeded in medium CM in the presence of 1×10^4 feeder cells/well (TK6 lymphoblastoid cells lethally irradiated with 40 Gy of γ-rays). Two weeks later, the plates were scored for growing colonies to calculate the cloning efficiency (CE) from the proportion of negative wells assuming a Poisson distribution ($CE = -\ln P_0/N$, where P_0 is the fraction of wells without cells and N is the number of cells seeded into wells) [56].

Apoptotic index was determined in PBLs incubated for 24 and 48 h in MMG and in parallel in 1 g. For detection of apoptotic morphology, PBLs were fixed and stained with

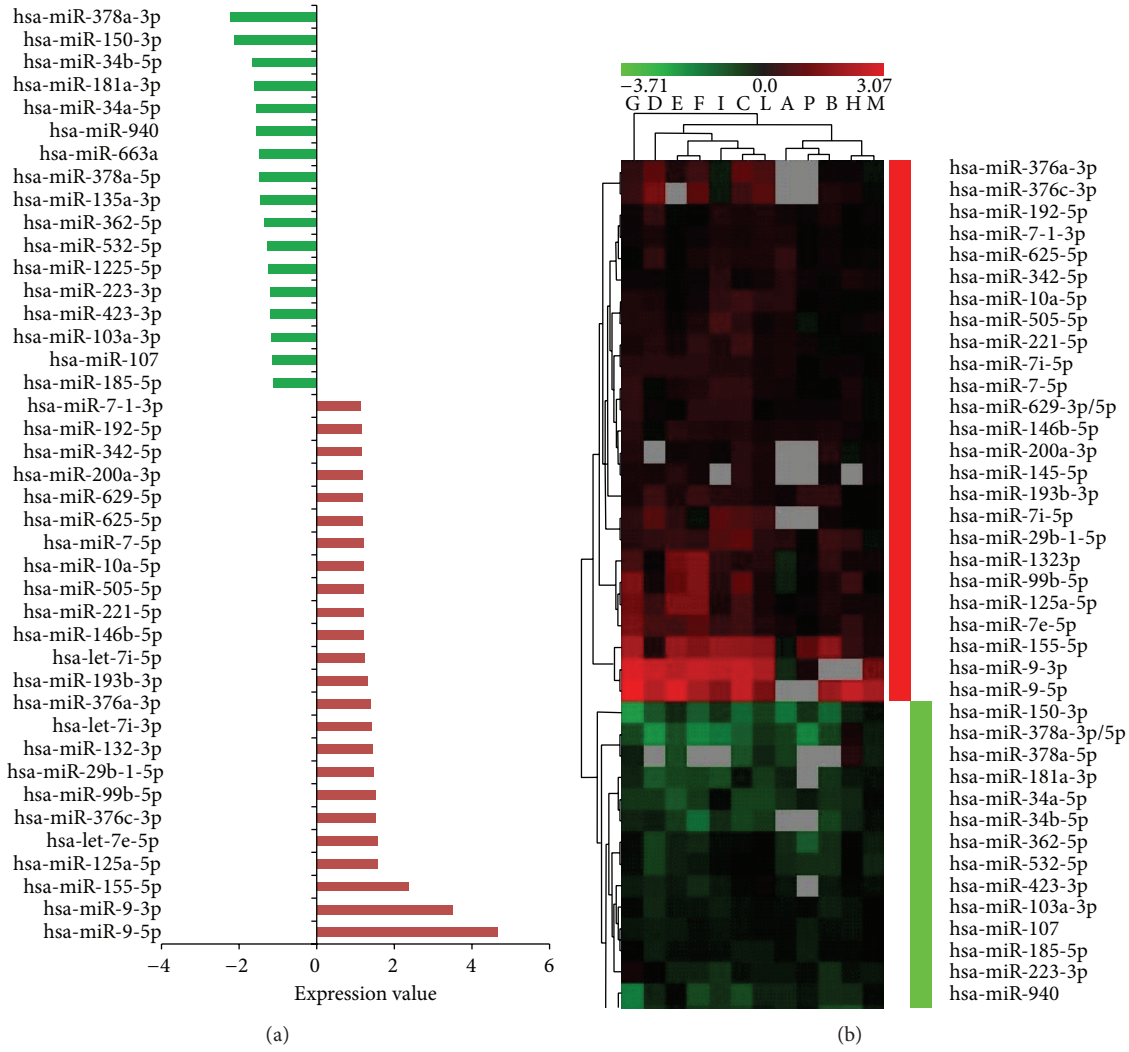

Figure 1: Differentially expressed miRNAs in human PBLs incubated in MMG. (a) The expression level of each miRNA, indicated as fold change, is the mean of the expression values obtained from the transformed log2 ratio (MMG/1 g). (b) Dendrogram of miRNAs differentially expressed in MMG. The range of expression value is from −3.7 (green, downregulation) to 3.07 (red, upregulation). Grey boxes correspond to not available (N/A) fluorescent signal from the microarray platform.

2 μg/mL 4,6-diamino-2-phenylindol (DAPI, Roche), in an antifade solution (Vectashield, Vector Lab) as previously described [57]. At least 2000 cells were scored for each time-point by fluorescence microscopy (1000x magnification). The activation of caspase-3 was measured by the caspase-3 fluorescent assay kit (Clontech BD Biosciences) at the end of incubation in 1 g or MMG, as previously described [58]. The fluorescent emission at 505 nm (excitation at 400 nm) of cleaved 7-amino-4-trifluoromethyl coumarin (AFC) was measured with a PerkinElmer LS-50 B spectrofluorimeter.

3. Results

3.1. Identification of miRNAs Affected by Microgravity. miRNA expression profiling was performed on total RNA extracted from PBLs of twelve healthy donors at the end of 24 h incubation time in MMG and in 1 g conditions. By comparing the expression profile of MMG-incubated versus 1 g incubated PBLs of the same donor, we found 42 differentially expressed miRNAs, 25 upregulated and 17 downregulated, for which raw data and means of miRNA expression values are available at Supplementary Table S1 (see Supplementary Table S1 in the Supplementary Material available online at http://dx.doi.org/10.1155/2014/296747). miR-9-5p, miR-9-3p, and miR-155-5p were the most upregulated (4.6-, 3.5-, and 2.4-fold, resp.), whereas miR-378a and miR-150-3p were the most downregulated (~2-fold) (Figure 1).

3.2. Effect of Microgravity on Gene Expression Profile. Gene expression analysis was performed in PBLs incubated for 24 h in MMG and in 1 g. By comparing the expression profiles of MMG-incubated and 1 g incubated PBLs, we identified 1581 differentially expressed genes in MMG versus 1 g, among

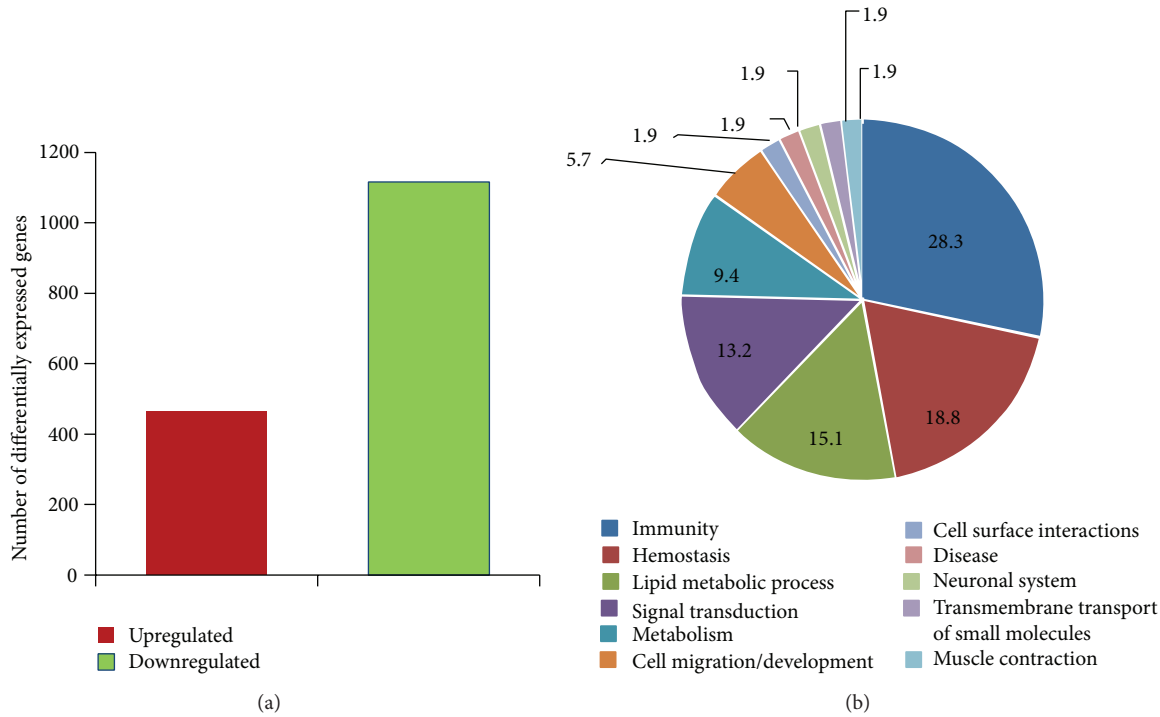

Figure 2: Results of gene expression analysis. Differentially expressed genes (a) and pie chart of biological process (%) containing pathways significantly enriched in PBLs incubated in MMG (b).

which 465 (29%) genes were upregulated whereas 1116 (71%) genes were downregulated (Figure 2(a) and Supplementary Table S2). By selecting a 2-fold cut-off threshold, we identified 312 (19.7%) genes in MMG; 157 genes (10%) showed alterations in expression level with a fold change greater than 4.0, and, among these, 20 genes showed a fold change ≥16.0 (Supplementary Table S3). To identify sets of genes with expression changes in MMG condition, we used Graphite [51], a novel web tool for topological-based pathway analyses based on high-throughput gene expression data analyses. Pathway analysis on differentially expressed genes has been performed by using hypergeometric test on Reactome Pathways as implemented in Graphite web, considering significant those categories with FDR < 0.1. We evidenced biological pathways significantly enriched in MMG: 15 (28.3%) were related to immunity, 10 (18.8%) to hemostasis, 7 (13.2%) to lipid metabolic process and signal transduction, 5 (9.4%) to metabolism, 3 (5.7%) to cell migration/development, and 1 (1.9%) tocell surface interactions, disease, neuronal system, transmembrane transport of small molecules, and muscle contraction (Figure 2(b)). The list of pathways is reported in Supplementary Table S4.

Among the immune pathways significantly enriched in MMG, those of "MHC class II antigen presentation," "Toll Receptor Cascades," and "DAP12 signaling" showed the highest number of differentially expressed genes (30, 20, and 20 genes, resp.). Also the "interferon gamma signaling" pathway was significantly enriched in MMG, with 13 differentially expressed genes. Ten genes codifying for proteins of MHC class II (HLA-DRA, HLA-DRB1, HLA-DRB3, HLA-DRB4, HLA-DRB5, HLA-DQA1, HLA-DQA2, HLA-DPA1, HLA-DPB1, and HLA-DQB1) were common to nine pathways (Figure 3). CD4, codifying for a membrane glycoprotein of T lymphocytes that interacts with the major histocompatibility complex class II antigens, was common to eight immune pathways; RELA, PTEN, and PAK1 were included in three pathways, whereas HLA-DOA and HLA-DMB were included in two pathways.

3.3. Target Prediction and Integration Analysis of miRNA and mRNA Expression Profiles. We examined the regulatory effects of miRNAs on global gene expression under modeled microgravity (MMG) condition in comparison with ground gravity (1 g). To predict the target genes of differentially expressed miRNAs in MMG, we performed a computational analysis using TargetScan tool, which predicts biological targets of miRNAs by searching for the presence of conserved 8 mer and 7 mer sites that match the seed region of each miRNA [59]. However, all available software for target prediction is characterized by a large fraction of false positive; thus, the integration of target predictions with miRNA and gene target expression profiles has been proposed to refine miRNA-mRNA interactions. The correlation analyses on the differentially expressed miRNAs and mRNAs were carried out with MAGIA^2 software [43], by microRNA Pearson prediction analysis, which allowed the identification of miRNA-mRNA interactions (Supplementary Table S5). To discover functional relationships between miRNAs and the transcriptome and uncover the gene pathways that are regulated

Gene symbol	description	Fold change	Interferon gamma signaling	PD-1 signaling	Phosphorylation of CD3′ and TCR zeta chains	Translocation of ZAP-70 to immunological synapse	Generation of second messenger molecules	MHC class II antigen presentation	Downstream TCR signaling	TCR signaling	Costimulation by the CD28 family	DAP12 signaling	Toll receptor cascade
HLA-DPA1	Major histocompatibility complex, class II, DP alpha 1	−1.78	■	■	■	■	■	■	■	■	■		
HLA-DPB1	Major histocompatibility complex, class II, DP beta 1	−1.83	■	■	■	■	■	■	■	■	■		
HLA-DQA1	Major histocompatibility complex, class II, DQ alpha 1	−1.51	■	■	■	■	■	■	■	■	■		
HLA-DQA2	Major histocompatibility complex, class II, DQ alpha 2	−1.64	■	■	■	■	■	■	■	■	■		
HLA-DQB1	Major histocompatibility complex, class II, DQ beta 1	−1.4	■	■	■	■	■	■	■	■	■		
HLA-DRA	Major histocompatibility complex, class II, DR alpha	−1.55	■	■	■	■	■	■	■	■	■		
HLA-DRB1	Major histocompatibility complex, class II, DR beta 1	−1.61	■	■	■	■	■	■	■	■	■		
HLA-DRB3	Major histocompatibility complex, class II, DR beta 3	−1.85	■	■	■	■	■	■	■	■	■		
HLA-DRB4	Major histocompatibility complex, class II, DR beta 4	−1.74	■	■	■	■	■	■	■	■	■		
HLA-DRB5	Major histocompatibility complex, class II, DR beta 5	−1.59	■	■	■	■	■	■	■	■	■		
HLA-DOA	Major histocompatibility complex, class II, DO alpha	−0.95						■	■				
HLA-DMB	Major histocompatibility complex, class II, DM beta	−1.47						■	■				
CD4	CD4 molecule	−0.78		■	■	■	■	■	■	■	■		
RELA	v-rel reticuloendotheliosis viral oncogene homolog A	0.51							■	■			■
PTEN	Phosphatase and tensin homolog	−0.26							■	■		■	
PAK1	p21 protein (Cdc42/Rac)-activated kinase 1	−1.32					■			■	■		

Figure 3: Differentially expressed genes common to immune-related pathways identified by Reactome database in PBLs incubated in MMG. The expression value of each gene, indicated as fold change, is the mean of expression levels calculated as the log2 ratio (MMG/1 g) on PBL samples (see Supplementary Table S2).

by miRNAs in MMG, we performed Gene Ontology (GO) analysis using DAVID [54].

In our analysis, we used high classification stringency and considered only GO terms that have $P < 0.1$ after permutation corrections (Benjamini) (Table 1). Several GO terms belonged to immune system function (i.e., "innate immune response," "inflammatory response," "regulation of cytokine production," "positive regulation of immune system process," and "response to bacterium"), in accordance with the results of pathway analysis on transcriptome (see Supplementary Table S4). GO terms of "cell development," "regulation of cell differentiation," "regulation of cell communication," "cell motility," and "cell migration" were significantly enriched in MMG, together with the category "organ development." In addition, the biological categories of "regulation of signal transduction," "regulation of response to stress," "regulation of cell death," and "regulation of cell proliferation" were enriched in PBLs incubated in MMG.

To determine whether different miRNAs within a GO category interact with the same target genes, we performed network analysis using MAGIA^2 [43], a software platform for the visualization of complex miRNA-mRNA interactions. We focused on miRNAs that correlated both positively and negatively with the GO categories of immune/inflammatory response, regulation of programmed cell death, and regulation of cell proliferation. As shown in Figure 4, most transcripts are associated with more than one miRNA, as in the case of TLR4 transcript, correlated with eight different miRNAs (miR-10a-5p, miR-7-5p, miR-135a-3p, miR-103a-3p, miR-7-1-3p, miR-107, miR-629-5p, and miR-362-5p).

By using Cytoscape [60], we visualized the functional interactions between miRNAs whose expression levels changed the most in PBLs incubated in MMG, such as miR-9-5p, miR-9-3p, miR-155-5p, miR-150-3p, and miR-378a-3p, and correlated target genes involved in GO categories of immune/inflammatory response, regulation of programmed cell death, and regulation of cell proliferation (Figure 5).

Our results show that miR-155-5p correlates with IFNG, IL17F, BCL6, and RELA involved in immune/inflammatory response, with PTEN, BNIP3L, APAF1, and PDCD4 involved in regulation of programmed cell death, and with NKX3-1 involved in regulation of cell proliferation; miR-150-3p correlates with immune-related genes (IFNG, IL1A, and HLA-DRB1) and with proapoptotic gene PDCD4; miR-9-3p correlates with genes regulating cell proliferation (NKX3-1, GADD45A, and TP53BP1), apoptosis (APAF1, BNIP3L), and immunity (CCL7, CXCL5, and BCL6). Among genes enriched within the three functional categories, miR-9-5p

Table 1: Selected GO terms of biological processes significantly affected by microgravity. The complete list of GO terms can be found in Supplementary Table S6.

GO:ID	Term	Count	P value	Fold enrichment	FDR
GO:0045087	Innate immune response	25	$2{,}42 \times 10^{-5}$	2,566978193	0,040412626
GO:0009966	Regulation of signal transduction	88	$1{,}67 \times 10^{-4}$	1,471577879	0,27973741
GO:0048468	Cell development	62	$1{,}71 \times 10^{-4}$	1,610338849	0,285253218
GO:0045595	Regulation of cell differentiation	54	$2{,}68 \times 10^{-4}$	1,648	0,448057857
GO:0006954	Inflammatory response	41	$3{,}23 \times 10^{-4}$	1,787513228	0,539044451
GO:0080134	Regulation of response to stress	37	$5{,}43 \times 10^{-4}$	1,806696296	0,90478009
GO:0010646	Regulation of cell communication	95	$8{,}22 \times 10^{-4}$	1,380599647	1,366092587
GO:0048513	Organ development	139	$8{,}22 \times 10^{-4}$	1,290910116	1,366713032
GO:0042060	Wound healing	26	$8{,}38 \times 10^{-4}$	2,025910165	1,393334889
GO:0007165	Signal transduction	198	0,001398603	1,211224944	2,313943814
GO:0001817	Regulation of cytokine production	27	0,001406003	1,926233766	2,326052387
GO:0048514	Blood vessel morphogenesis	26	0,001709187	1,93009009	2,820918727
GO:0001817	Regulation of cytokine production	15	0,001406003	1,926233766	2,326052387
GO:0007399	Nervous system development	88	0,002097026	1,359812471	3,450524099
GO:0022603	Regulation of anatomical structure morphogenesis	28	0,002408369	1,831111111	3,953172097
GO:0048870	Cell motility	33	0,002838826	1,710188679	4,64407324
GO:0048522	Positive regulation of cellular process	159	0,003551259	1,221594406	5,777298149
GO:0002684	Positive regulation of immune system process	31	0,003855111	1,711490787	6,256755641
GO:0050865	Regulation of cell activation	26	0,003880839	1,819447983	6,297247375
GO:0051174	Regulation of phosphorus metabolic process	51	0,003964604	1,486259947	6,428964883
GO:0001944	Vasculature development	28	0,003981783	1,767969349	6,455956993
GO:0043066	Negative regulation of apoptosis	41	0,004040803	1,56952381	6,548633436
GO:0010941	Regulation of cell death	83	0,004115909	1,341019608	6,666445839
GO:0009617	Response to bacterium	22	0,004991824	1,9032021	8,030143455
GO:0043067	Regulation of programmed cell death	82	0,00552374	1,328770895	8,849108723
GO:0008285	Negative regulation of cell proliferation	40	0,00576007	1,54741784	9,210770389
GO:0010557	Positive regulation of macromolecule biosynthetic process	62	0,006543793	1,39014966	10,4004889
GO:0016477	Cell migration	30	0,006706505	1,664646465	10,64564555
GO:0042127	Regulation of cell proliferation	71	0,009848433	1,331149033	15,2576907
GO:0048523	Negative regulation of cellular process	139	0,012514364	1,19870225	18,9945349

correlates with BCL6. miR-378a-3p is correlated with HLA-DRB1, GPNMB, and NKX3-1; the same transcripts, together with IL17F, are correlated also with miR-378a-5p.

The microarray data from miRNA and gene expression profiling were validated by real-time qPCR experiments for four miRNAs (miR-9-5p, miR-155-5p, miR-378a, and miR-150-3p) and five mRNAs (IFNG, IL17F, BCL6, HLA-DRB1, and TLR4) whose expression level was significantly altered by MMG incubation (Figure 6). miR-9-5p and miR-155-5p, together with IFNG, IL17F, and BCL6 transcripts, were upregulated in MMG, whereas miR-378a and miR-150-3p together with HLA-DRB1 and TLR4 transcripts were downregulated in MMG.

3.4. Intraclass Integrated Analysis. Recently, Censi and colleagues [61] observed a significant increase in the number and strength of genes correlation under stress conditions, such as disease and environmental or physiological changes. To evaluate whether the stress induced by MMG increases the amount of correlation of the system with respect to 1 g control condition, we integrated mRNAs and miRNAs data separately for MMG and 1 g using MAGIA^2. By comparing the two regulatory networks, we observed a similar number of interactions between MMG (190 interactions) and 1 g (218 interactions) (Figure S1), indicating that there was no significant connectivity enrichment under modeled microgravity. By contrast, Gene Ontology analysis performed on MMG- and 1 g-specific interactions reported 50 GO categories significantly enriched in only MMG condition ($P < 0.2$ after Benjamini corrections, Supplementary Table S7); 10 out of these were previously described in Table 1. In particular, the GO categories "regulation of cellular process" and "cell differentiation" were significantly affected by MMG. With intraclass analysis, the GO categories of immunity and cell death were not enriched in MMG probably because, in our study, the number of PBL samples available for such analysis was relatively small. On the whole, the intraclass analysis shows that modeled microgravity does not increase the general connectivity of miRNA-gene interaction network but rather increases the transcriptome plasticity with respect

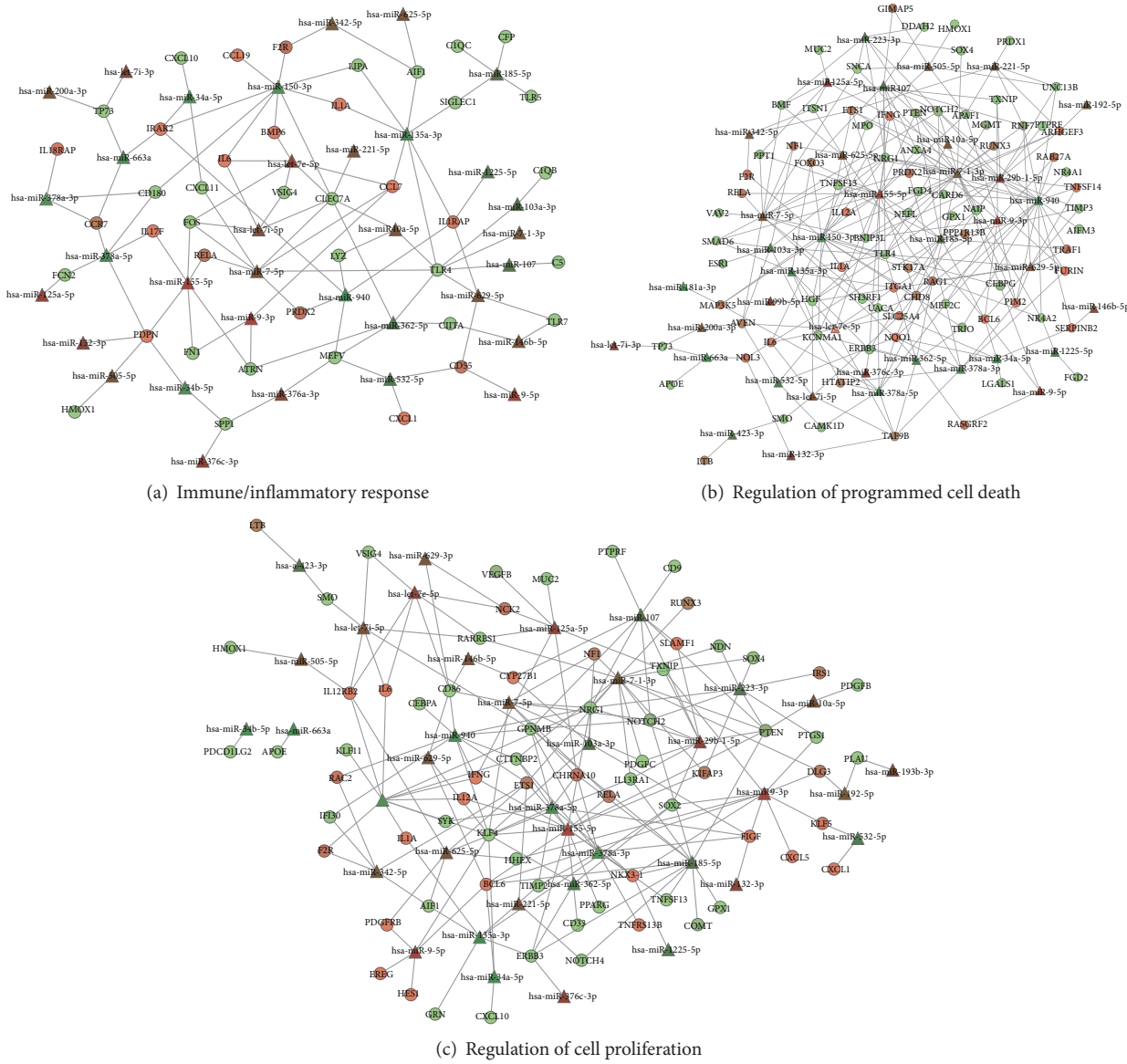

(a) Immune/inflammatory response

(b) Regulation of programmed cell death

(c) Regulation of cell proliferation

FIGURE 4: Network analysis on correlated miRNA-mRNA pairs in PBLs incubated in MMG. Network analyses were performed by MAGIA[2] software using miRNAs correlating both positively and negatively with transcripts involved in immune/inflammatory response (a), in regulation of programmed cell death (b), and in regulation of cell proliferation (c). Circles represent transcripts and triangles represent miRNAs.

to 1 g gravity condition, as evidenced by the enriched GO categories.

3.5. In Vitro Validation of GO Analysis: Effects of MMG on Cell Proliferation and Apoptosis. Experimental assays were performed to validate the results obtained by bioinformatics analyses on the GO categories "regulation of cell proliferation" and "regulation of programmed cell death" associated with variations in miRNA expression under MMG. To measure cell proliferation, quiescent (G_0) PBLs from the same donor were incubated for different times (24 h, 48 h, and 72 h) in 1 g and in MMG. At the end of incubation times, the colony forming ability has been determined by the T-cell cloning assay [44], in which cells were incubated in medium containing mitogen factors (i.e., PHA and IL2) to trigger their cell cycle entry. Our results showed that cloning efficiency (CE) decreased with time in both gravity conditions; however, MMG incubation affected the ability of PBLs to form colonies ($P < 0.05$ at 24 h, Figure 7(a)). To investigate whether MMG incubation increased the frequency of apoptotic cells, PBLs were scored for the presence of apoptotic bodies. Apoptotic index was very similar at 24 and 48 h and significantly higher in PBLs incubated in MMG than in 1 g (Figure 7(b), $P < 0.05$). In the same PBL samples, caspase-3 activation, assayed by the cleavage of the peptide substrate DEVD-AFC,

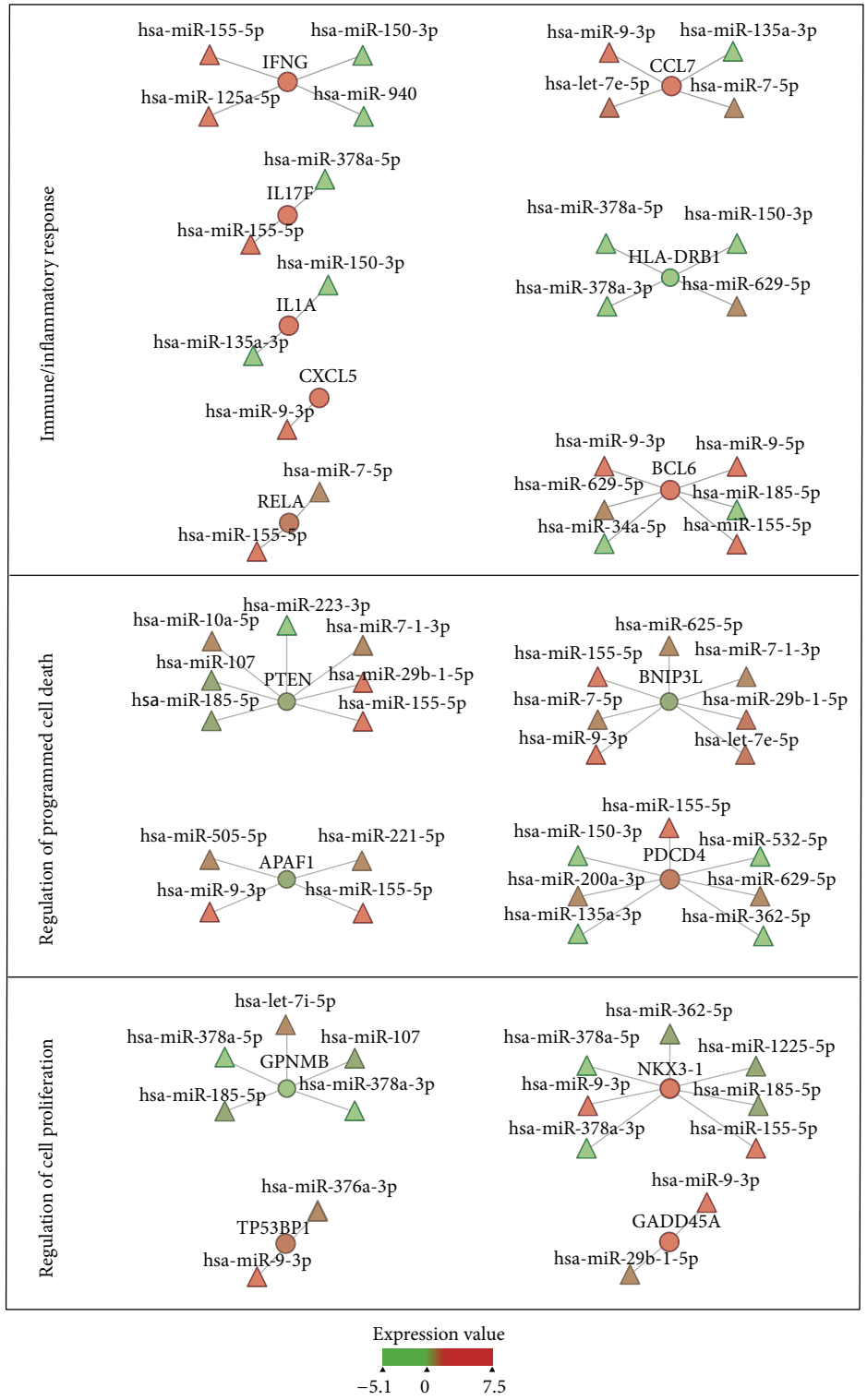

Figure 5: Cytoscape visualization of miRNA-mRNA correlations in PBLs incubated 24 h in MMG. Relationships between miRNAs and correlated target genes involved in "immune/inflammatory response" (IFNG, CCL7, IL17F, HLA-DRB1, IL1A, CXCL5, RELA, and BCL6), "regulation of programmed cell death" (PTEN, BNIP3L, APAF1, and PDCD4), and "regulation of cell proliferation" (GPNMB, NKX3-1, TP53BP1, and GADD45A). Circles represent transcripts and triangles represent miRNAs; the expression levels of each feature are represented as color scale.

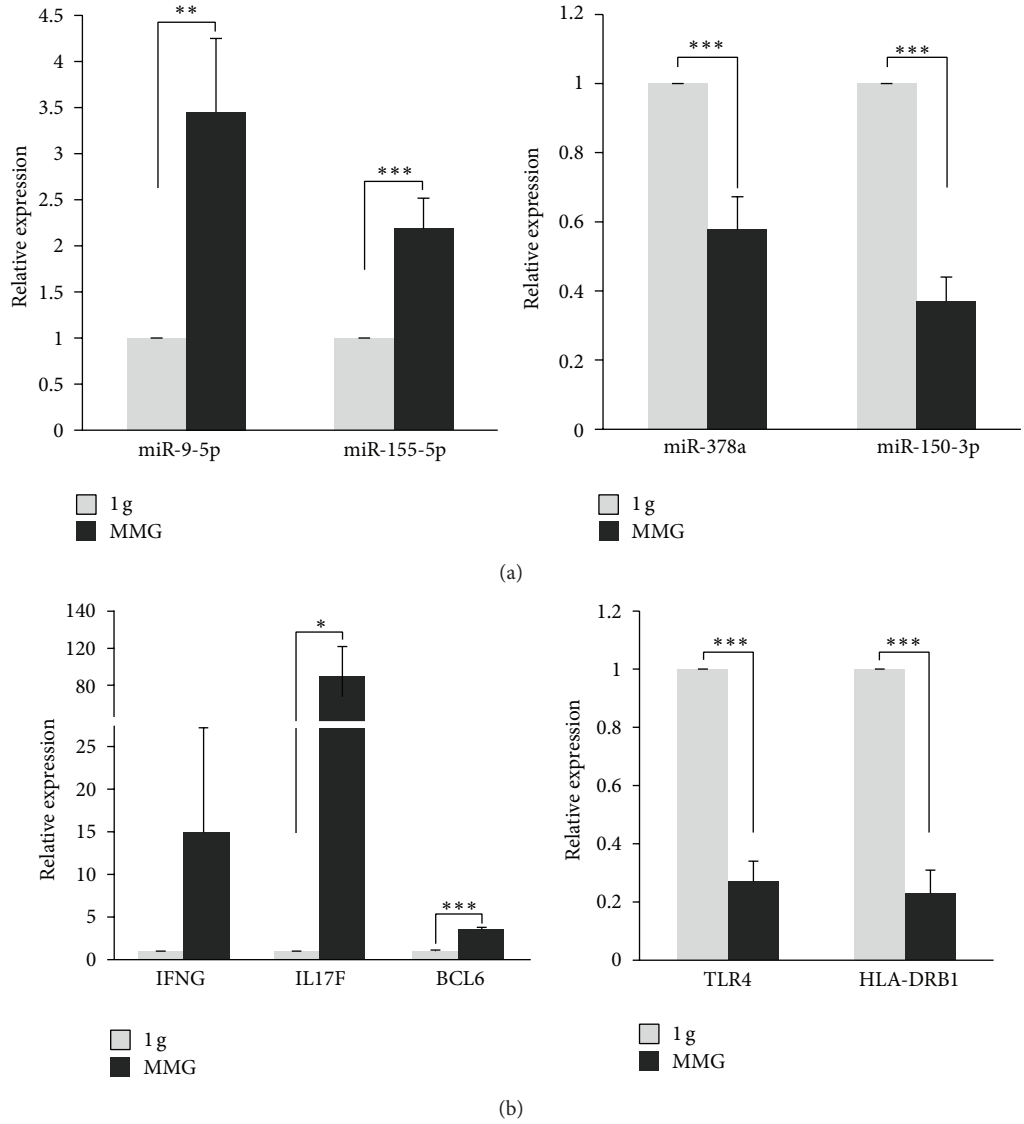

Figure 6: Microarray data validation by quantitative real-time PCR (qRT-PCR). Validation of microarray data by qRT-PCR in MMG-incubated versus 1 g incubated PBLs. The results are consistent with the cumulative microarray data of miRNAs (a) and mRNAs (b). Values (fold change, dark grey bars) are means ± S.E. of expression levels calculated as the log2 (MMG/1 g) on PBL samples from 4 to 6 different donors. The value "1" of control 1 g PBLs (light grey bars) is arbitrarily given when no change is observed ($^{***}P < 0.001$, $^{**}P < 0.01$, and $^{*}P < 0.05$, t-test).

increased significantly in PBLs incubated 48 h in MMG with respect to those in 1 g (Figure 7(c), $P < 0.05$).

4. Discussion

In the present study, we evaluated the effects of modeled microgravity (MMG) on human PBLs by analyzing miRNA and gene expression profiles in comparison with PBLs cultured in Earth gravity condition (1 g). Our results reported 42 differentially expressed miRNAs in PBLs cultured for 24 h in MMG with respect to 1 g, of which 14 (miR-34a-5p, miR-34b-5p, miR-663a, miR-135a-3p, miR-1225-5p, miR-940, miR-221-5p, miR-29b-1-5p, miR-10a-5p, let-7i-3p, miR-200a-3p, miR-7-5p, miR-7-1-3p, and miR-505-5p) were found altered also by γ-irradiation, as assessed in our previous study [47]. The most dysregulated miRNAs identified in the present work are the upregulated miR-9-5p, miR-9-3p, and miR-155-5p, and**a** the downregulated ones are miR-150-3p and miR-378a-3p. Such miRNAs have been found altered in human tumors; in particular, miR-9 is an oncogenic miRNA overexpressed in mixed lineage leukemia- (MLL-) rearranged acute myeloid leukemia [62], in muscle-invasive bladder cancer [63], and in osteosarcoma cell lines [64]. miR-155 is commonly upregulated in hematological malignancies [65, 66] and has been linked to the development of breast, lung, and stomach tumors [67–70]. miR-150 is significantly downregulated in most cases of acute myeloid leukemia [71] and colorectal cancer [72]; in addition, miR-150 has an important role in

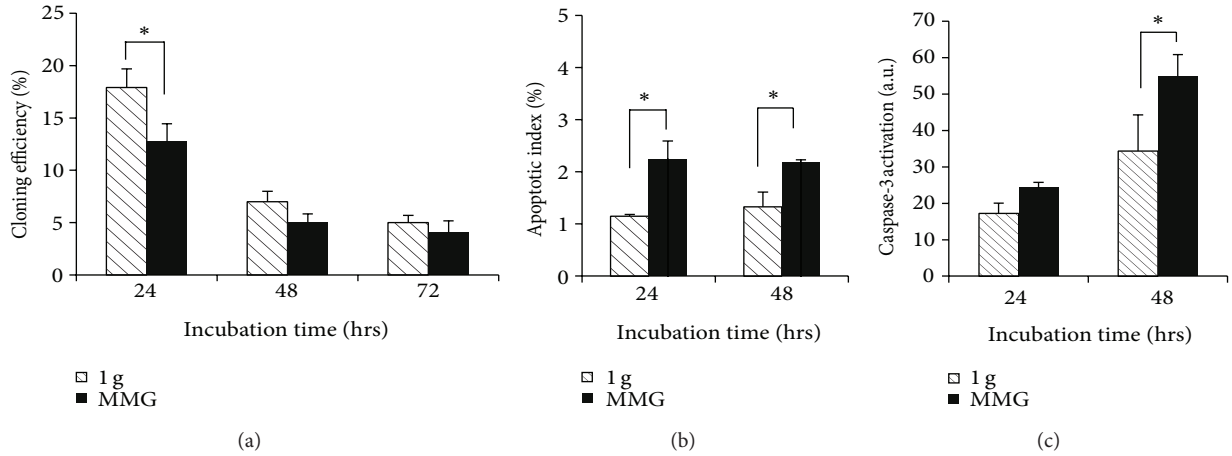

Figure 7: Cell proliferation and apoptosis induction in human PBLs incubated in MMG and in 1 g. (a) T-cell cloning assay performed at the end of 24 h, 48 h, and 72 h of incubation in the two gravity conditions. Data are means ± S.E. from thirteen independent experiments. (b) Apoptotic index at the end of incubation for 24 h and 48 h in MMG and 1 g determined by nuclear chromatin condensation with DAPI staining. (c) Caspase-3 activation at the end of 24 h and 48 h incubation in MMG and 1 g assessed by fluorimetric assay (a.u. arbitrary units). Data in (b) and (c) are means ± S.E. from 3-4 independent experiments ($^*P < 0.05$, t-test).

normal hematopoiesis and its aberrant downregulation is a sensitive marker indicative of lymphocyte depletion and bone marrow damage [73]. miR-378 (actually annotated as miR-378a) is significantly downregulated in colorectal cancer [74], in cutaneous squamous cell carcinoma [75], and in renal cell carcinoma [76]. The effects of microgravity on miRNA expression profile are currently reported in only one study carried out in human lymphoblastoid TK6 cells incubated under simulated microgravity for 72 h [77]. Among the dysregulated miRNAs, only two were common to our data, miR-150 and miR-34a, although the direction and intensity of fold change were different, demonstrating the cell type specific signature of miRNA profile.

miRNAs modulate gene expression by interacting with the 3′UTR of target genes, and since a single miRNA could have hundreds to thousands of predicted target genes [25], it is difficult to determine the true target regulated by the miRNA which affects a biological function. Moreover, binding of multiple miRNAs to one target could further increase the complexity of target prediction. The identification of miRNA target genes is usually performed by bioinformatic prediction algorithms based on (i) sequence similarity search, possibly considering target site evolutionary conservation, and (ii) thermodynamic stability. However, it is known that the results of target prediction algorithms are characterized by very low specificity [78]. For this purpose, the integration of target predictions with miRNA and gene expression profiles has been recently proposed to improve the detection of functional miRNA target relationships [79, 80]. Therefore, to identify the most likely target genes of miRNAs differentially expressed in MMG, we defined gene expression signature on the same samples of PBLs assayed for miRNA profiling; then, we integrated expression profiles from both miRNAs and mRNAs with *in silico* target predictions to reduce the number of false positives and increase the number of biologically relevant targets [81–83]. Our results of gene expression profiling reported the downregulation of multiple genes in MMG (71%), in accordance with previous findings in activated human T lymphocytes incubated for 24 h in simulated microgravity [21]. Moreover, we found that about 20% of genes responded to MMG by more than 2-fold change in expression level and twenty genes showed a ≥16-fold change in expression. Most of these top dysregulated genes were immune-related, such as those codifying for inflammatory cytokines (CCL1, CCL7, CXCL5, CXCL11, and IL1A) and for proteins with a role in immunoregulatory functions (IFNG, TNIP3, TREM1, APOC1, FCN1, FCN2, and CPVL) (Supplementary Table S3). Biological pathways enriched in PBLs exposed to MMG were mainly involved in immunity (Figure 2(b)), including adaptive immune system response (i.e., PD-1 signaling, phosphorylation of CD3 and TCR zeta chains, translocation of ZAP-70 to immunological synapse MHC class II antigen presentation, TCR signaling, and costimulation by the CD28 family), innate immune system response (i.e., Toll Receptor Cascades), and cytokine signaling in immune system (i.e., interferon gamma signaling) (Supplementary Table S4). All these pathways included ten downregulated genes codifying for MHC molecules class II (HLA-DPA1, HLA-DPB1, HLA-DQA1, HLA-DQA2, HLA-DQB1, HLA-DRA, HLA-DRB1, HLA-DRB3, HLA-DRB4, and HLA-DRB5), which are expressed in antigen presenting cells (APC) and play a central role in the immune system by presenting peptides derived from extracellular proteins [84]. Therefore, the downregulation of these genes suggests that the display of antigens at the cell surface of APC may be disturbed by gravity reduction, affecting the efficiency of immune response as observed in astronauts during spaceflight and immediately afterwards [85–87]. Moreover, our data are in accordance with the inhibition of immediate early genes in T-cell activation observed in space microgravity [14]

and with alterations of gene expression in human activated T-cells incubated in modeled microgravity, including the downregulation of HLA-DRA gene [21].

By integrating the transcriptome and microRNAome, we detected significant miRNA-mRNA relationships under MMG. Since miRNAs act prevalently through target degradation, expression profiles of miRNAs and target genes are generally expected to be inversely correlated. Nevertheless, since miRNA activity is part of complex regulatory networks and gene expression profiles are the result of different levels of regulation, also positive correlation (i.e., upregulated miRNA/upregulated mRNA or downregulated miRNA/downregulated mRNA) is expected. Indeed, in an *in vivo* mouse model, the activated expression of miRNAs has been shown to correlate with activated expression of mRNAs rather than with mRNA downregulation [88]. Gene Ontology (GO) analysis conducted on the significantly correlated miRNA-mRNA pairs evidenced the biological categories significantly overrepresented in MMG (Table 1). Many GO terms of immune response were enriched, such as "innate immune response," "inflammatory response," "regulation of cytokine production," "positive regulation of immune system process," and "response to bacterium." Notably, the most dysregulated miRNAs detected in the present study, miR-378a-3p, miR-150-3p, miR-155-5p, miR-9-3p, and miR-9-5p, are significantly correlated with immune-related genes. In particular, miR-378a-3p is positively correlated with transcripts of MHC molecules class II such as HLA-DRB1 (Figure 5) and HLA-DOA, HLA-DRB5, and HLA-DQA2 (not shown). miR-150-3p is negatively correlated with HLA-DRB1, IFNG, and IL1Atranscripts, whereas miR-155-5p is positively correlated with IFNG and IL17F and negatively correlated with RELA and BCL6 (Figure 5). IL1A, IL17F, and IFN-γ are proinflammatory cytokines acting during the immune response; IFN-γ is a soluble cytokine having broader roles in activation of immune responses, in part through upregulating transcription of genes involved in antigen processing/presentation, in cell cycle regulation and apoptosis, and its correlation with miR-155 has been recently validated [89]. BCL6, which encodes a nuclear transcriptional repressor, has a role not only in regulation of lymphocyte function, but also in cell survival and differentiation. Similarly, the pleiotropic transcription factor RELA has a role in immune biological process and it is also involved in cell growth and apoptosis. Besides miR-155-5p, BCL6 is correlated with four miRNAs including miR-9 (3p and 5p); in addition, miR-9-3p is positively correlated with CCL7 and CXCL5 (Figure 5). Recent evidences show that miR-9 is highly involved in immunity and inflammatory diseases [90–92] by enhancing IFN-γ production in activated human CD4(+) T-cells [91]. Moreover, Gao et al. [90] have shown that miR-9 disturbs the display of antigens at the cell surface by suppressing the expression of MHC class I gene transcription.

Together with the categories of immune response, GO analysis reported that also the categories of regulation of cell proliferation and regulation of programmed cell death were significantly enriched in MMG, as previously reported in γ-irradiated PBLs [47]. Interestingly, such categories were not enriched from pathway analysis conducted on transcriptome and the reason could be that integrated analysis of miRNAs and mRNAs expression profiles evidences the posttranscriptional effect mediated by miRNAs on gene expression. Among genes involved in cell proliferation, the transcription factor NKX3-1 (2.4-fold upregulated), which mediates non-cell autonomous regulation of gene expression and inhibits cell proliferation, is correlated with miR-9-3p, miR-155-5p, miR-378a-3p, and miR-378-5p (Figure 5). TP53BP1 (1.4-fold upregulated), encoding for a chromatin-associated factor involved in cell cycle checkpoint and growth, is correlated with miR-9-3p. GADD45A (1.5-fold upregulated), regulating cell cycle arrest, DNA repair, cell survival, senescence, and apoptosis, is also correlated with miR-9-3p. GPNMB (32-fold downregulated), expressed in a wide array of normal tissues, such as bone, hematopoietic system, and skin, where it influences cell proliferation, adhesion, differentiation, and synthesis of extracellular matrix proteins [93], is targeted by five miRNAs including miR-378a-3p. Among miRNA-correlated genes involved in apoptosis, we identified PDCD4 (proapoptotic, 1.4-fold upregulated) and found out that it is correlated with seven miRNAs, including miR-155-5p and miR-150-3p; BNIP3L (proapoptotic, 1.5-fold downregulated) also correlated with seven miRNAs, including miR-155-5p and miR-9-3p; APAF1 (proapoptotic, 1.3-fold downregulated) correlated with four miRNAs including miR-155-5p and miR-9-3p; and PTEN (proapoptotic) correlated with seven miRNAs including miR-155-5p. Notably, many transcripts (i.e., BCL6, PTEN, BNIP3L, PDCD4, NKX3-1, and GPNMB) are targeted by multiple miRNAs, indicating a pleiotropic effect in gene regulation by coexpressed endogenous miRNAs in MMG. Moreover, our results suggest that under MMG condition a small group of miRNAs regulates transcriptome by modulating the same transcripts within one pathway.

To validate the results of Gene Ontology analysis, we evaluated whether the GO categories "regulation of cell proliferation" and "regulation of programmed cell death" were affected by MMG incubation by performing biological assays of T-cell cloning and apoptosis induction. Our results show that cloning ability of PBLs was lower after 24 h incubation in MMG than in 1 g, in accordance with the suppression of proliferative response of human lymphocytes to mitogenic stimulation in microgravity [94, 95]. The ability to originate clones in PBLs incubated for 48h and 72 h decreased in both gravity conditions probably because the longer G_0-phase condition experienced by PBLs affected their responsiveness to enter into cell cycle. The antiproliferative effect of microgravity has been recently reported also in human thyroid cancer cells [96] and in human lung adenocarcinoma cells [97]. Our results of apoptosis induction demonstrated that both the formation of apoptotic bodies activation and caspase-3 activation increased significantly in PBLs incubated in MMG than in 1 g. The activation of apoptotic process seems related to the overexpression of PDCD4 and RELA rather than to the underexpression of BNIP3L and APAF1, indicating the existence of complex regulatory networks between miRNAs and mRNAs that occur at different levels of regulation. IFN-γ, besides having an important role in activating innate and adaptive immune responses, plays important roles in

inhibiting cell proliferation and inducing apoptosis. Its overexpression in MMG, mediated by miR-9-3p and miR-155-5p, could thus mediate the antiproliferative effect and the apoptosis induction. In addition, the correlation between miR-9-3p and TP53BP1 could explain the clonogenicity decrease and apoptosis increase in PBLs incubated in MMG. Indeed, overexpression of TP53BP1 has been demonstrated to decrease the clonogenicity and induce apoptosis in ovarian cancer cells [98].

5. Conclusions

Our results show that MMG leads to changes in expression level of a considerable fraction of microRNAome and transcriptome in human PBLs. miRNAs differentially expressed in MMG are correlated with immune/inflammatory-related genes, as IFNG, accordingly with the important role of miRNAs in immune function regulation. Since inflammation works as a tumor-promoting agent, the abnormal expression of such miRNAs under microgravity condition could influence the carcinogenic process by affecting cancer cell immune escape. Moreover, miRNAs mostly dysregulated in MMG, such as miR-9, miR-155, and miR-150, are oncogenic, suggesting that their abnormal expression can influence the carcinogenic process. The results of miRNA-mRNA integration analysis demonstrate that MMG increases the transcriptome plasticity compared with 1 g condition and that categories of regulation of cell proliferation and programmed cell death are affected by MMG, as confirmed by *in vitro* experimental validation. Taken together,our results of high-throughput expression analysis and miRNA-mRNA integration analysis give new insight into the complex genetic mechanisms of cell response to stress environment under reduced gravity.

Conflict of Interests

The authors declare that there is no conflict of interests regarding the publication of this paper.

Authors' Contribution

M. Mognato and C. De Pittà conceived and designed the experiments. C. Girardi, S. Casara, and M. Mognato performed the experiments. C. De Pittà, C. Romualdi, E. Calura, L. Celotti, and M. Mognato analyzed the data. M. Mognato and L. Celotti wrote the paper. Cristina Girardi and Cristiano De Pittà contributed equally to this work.

Acknowledgments

The authors gratefully acknowledge M. De Bernard for critical discussion and R. Mazzaro for graphical support. This work was done with the support of the Italian Space Agency (ASI, XMAB, from Molecules to Man, 1/014/06/0) to L. Celotti and of the University of Padova (CPDA061783) to M. Mognato. The authors also apologize to the authors whose work could not be cited due to space limitations.

References

[1] R. H. Fitts, D. R. Riley, and J. J. Widrick, "Functional and structural adaptations of skeletal muscle to microgravity," *Journal of Experimental Biology*, vol. 204, no. 18, pp. 3201–3208, 2001.

[2] M. Narici, B. Kayser, P. Barattini, and P. Cerretelli, "Effects of 17-day spaceflight on electrically evoked torque and cross-sectional area of the human triceps surae," *European Journal of Applied Physiology*, vol. 90, no. 3-4, pp. 275–282, 2003.

[3] S. Trappe, D. Costill, P. Gallagher et al., "Exercise in space: human skeletal muscle after 6 months aboard the International Space Station," *Journal of Applied Physiology*, vol. 106, no. 4, pp. 1159–1168, 2009.

[4] S. I. M. Carlsson, M. T. S. Bertilaccio, E. Ballabio, and J. A. M. Maier, "Endothelial stress by gravitational unloading: effects on cell growth and cytoskeletal organization," *Biochimica et Biophysica Acta*, vol. 1642, no. 3, pp. 173–179, 2003.

[5] M. Infanger, P. Kossmehl, M. Shakibaei et al., "Induction of three-dimensional assembly and increase in apoptosis of human endothelial cells by simulated microgravity: impact of vascular endothelial growth factor," *Apoptosis*, vol. 11, no. 5, pp. 749–764, 2006.

[6] R. M. Baevsky, V. M. Baranov, I. I. Funtova et al., "Autonomic cardiovascular and respiratory control during prolonged spaceflights aboard the International Space Station," *Journal of Applied Physiology*, vol. 103, no. 1, pp. 156–161, 2007.

[7] J. D. Sibonga, H. J. Evans, H. G. Sung et al., "Recovery of spaceflight-induced bone loss: bone mineral density after long-duration missions as fitted with an exponential function," *Bone*, vol. 41, no. 6, pp. 973–978, 2007.

[8] J. H. Keyak, A. K. Koyama, A. LeBlanc, Y. Lu, and T. F. Lang, "Reduction in proximal femoral strength due to long-duration spaceflight," *Bone*, vol. 44, no. 3, pp. 449–453, 2009.

[9] O. Ullrich, K. Huber, and K. Lang, "Signal transduction in cells of the immune system in microgravity," *Cell Communication and Signaling*, vol. 6, article 9, 2008.

[10] B. E. Crucian, R. P. Stowe, D. L. Pierson, and C. F. Sams, "Immune system dysregulation following short- vs long-duration spaceflight," *Aviation Space and Environmental Medicine*, vol. 79, no. 9, pp. 835–843, 2008.

[11] G. Sonnenfeld, J. S. Butel, and W. T. Shearer, "Effects of the space flight environment on the immune system," *Reviews on Environmental Health*, vol. 18, no. 1, pp. 1–17, 2003.

[12] G. Sonnenfeld, "Editorial: space flight modifies T cell activation—role of microgravity," *Journal of Leukocyte Biology*, vol. 92, no. 6, pp. 1125–1126, 2012.

[13] A. Semov, N. Semova, C. Lacelle et al., "Alterations in TNF- and IL-related gene expression in space-flown WI38 human fibroblasts," *The FASEB Journal*, vol. 16, no. 8, pp. 899–901, 2002.

[14] T. T. Chang, I. Walther, C.-F. Li et al., "The Rel/NF-κB pathway and transcription of immediate early genes in T cell activation are inhibited by microgravity," *Journal of Leukocyte Biology*, vol. 92, no. 6, pp. 1133–1145, 2012.

[15] M. L. Lewis, L. A. Cubano, B. Zhao et al., "cDNA microarray reveals altered cytoskeletal gene expression in space-flown leukemic T lymphocytes (Jurkat)," *The FASEB Journal*, vol. 15, no. 10, pp. 1783–1785, 2001.

[16] S. J. Pardo, M. J. Patel, M. C. Sykes et al., "Simulated microgravity using the Random Positioning Machine inhibits differentiation and alters gene expression profiles of 2T3 preosteoblasts," *American Journal of Physiology*, vol. 288, no. 6, pp. C1211–C1221, 2005.

[17] M. Monticone, Y. Liu, N. Pujic, and R. Cancedda, "Activation of nervous system development genes in bone marrow derived mesenchymal stem cells following spaceflight exposure," *Journal of Cellular Biochemistry*, vol. 111, no. 2, pp. 442–452, 2010.

[18] D. Grimm, J. Bauer, P. Kossmehl et al., "Simulated microgravity alters differentiation and increases apoptosis in human follicular thyroid carcinoma cells," *The FASEB Journal*, vol. 16, no. 6, pp. 604–606, 2002.

[19] M. Maccarrone, N. Battista, M. Meloni et al., "Creating conditions similar to those that occur during exposure of cells to microgravity induces apoptosis in human lymphocytes by 5-lipoxygenase-mediated mitochondrial uncoupling and cytochrome c release," *Journal of Leukocyte Biology*, vol. 73, no. 4, pp. 472–481, 2003.

[20] S. J. Crawford-Young, "Effects of microgravity on cell cytoskeleton and embryogenesis," *International Journal of Developmental Biology*, vol. 50, no. 2-3, pp. 183–191, 2006.

[21] N. E. Ward, N. R. Pellis, S. A. Risin, and D. Risin, "Gene expression alterations in activated human T-cells induced by modeled microgravity," *Journal of Cellular Biochemistry*, vol. 99, no. 4, pp. 1187–1202, 2006.

[22] J. Q. Clement, S. M. Lacy, and B. L. Wilson, "Gene expression profiling of human epidermal keratinocytes in simulated microgravity and recovery cultures," *Genomics, Proteomics and Bioinformatics*, vol. 6, no. 1, pp. 8–28, 2008.

[23] R. Kumari, K. P. Singh, and J. W. DuMond Jr., "Simulated microgravity decreases DNA repair capacity and induces DNA damage in human lymphocytes," *Journal of Cellular Biochemistry*, vol. 107, no. 4, pp. 723–731, 2009.

[24] C.-Y. Kang, L. Zou, M. Yuan et al., "Impact of simulated microgravity on microvascular endothelial cell apoptosis," *European Journal of Applied Physiology*, vol. 111, no. 9, pp. 2131–2138, 2011.

[25] J. Krützfeldt, M. N. Poy, and M. Stoffel, "Strategies to determine the biological function of microRNAs," *Nature Genetics*, vol. 38, no. 1, pp. S14–S19, 2006.

[26] C. A. Nickerson, C. M. Ott, J. W. Wilson et al., "Low-shear modeled microgravity: a global environmental regulatory signal affecting bacterial gene expression, physiology, and pathogenesis," *Journal of Microbiological Methods*, vol. 54, no. 1, pp. 1–11, 2003.

[27] K. Arunasri, M. Adil, K. Venu Charan, C. Suvro, S. Himabindu Reddy, and S. Shivaji, "Effect of simulated microgravity on *E. coli* K12 MG1655 growth and gene expression," *PLoS ONE*, vol. 8, no. 3, Article ID e57860, 2013.

[28] O. Marcu, M. P. Lera, M. E. Sanchez et al., "Innate immune responses of Drosophila melanogaster are altered by spaceflight," *PLoS ONE*, vol. 6, no. 1, Article ID e15361, 2011.

[29] Y. Honda, A. Higashibata, Y. Matsunaga et al., "Genes down-regulated in spaceflight are involved in the control of longevity in *Caenorhabditis elegans*," *Scientific Reports*, vol. 2, article 487, 2012.

[30] A. I. Manzano, J. J. W. A. van Loon, P. C. M. Christianen, J. M. Gonzalez-Rubio, F. J. Medina, and R. Herranz, "Gravitational and magnetic field variations synergize to cause subtle variations in the global transcriptional state of Arabidopsis in vitro callus cultures," *BMC Genomics*, vol. 13, no. 1, article 105, 2012.

[31] D. P. Bartel, "MicroRNAs: target recognition and regulatory functions," *Cell*, vol. 136, no. 2, pp. 215–233, 2009.

[32] H. Guo, N. T. Ingolia, J. S. Weissman, and D. P. Bartel, "Mammalian microRNAs predominantly act to decrease target mRNA levels," *Nature*, vol. 466, no. 7308, pp. 835–840, 2010.

[33] V. Huang, Y. Qin, J. Wang et al., "RNAa is conserved in mammalian cells," *PLoS ONE*, vol. 5, no. 1, Article ID e8848, 2010.

[34] L. B. Frankel, N. R. Christoffersen, A. Jacobsen, M. Lindow, A. Krogh, and A. H. Lund, "Programmed cell death 4 (PDCD4) is an important functional target of the microRNA miR-21 in breast cancer cells," *The Journal of Biological Chemistry*, vol. 283, no. 2, pp. 1026–1033, 2008.

[35] M. N. Poy, M. Spranger, and M. Stoffel, "microRNAs and the regulation of glucose and lipid metabolism," *Diabetes, Obesity and Metabolism*, vol. 9, no. 2, pp. 67–73, 2007.

[36] N. Stern-Ginossar, N. Elefant, A. Zimmermann et al., "Host immune system gene targeting by a viral miRNA," *Science*, vol. 317, no. 5836, pp. 376–381, 2007.

[37] C. J. Marsit, K. Eddy, and K. T. Kelsey, "MicroRNA responses to cellular stress," *Cancer Research*, vol. 66, no. 22, pp. 10843–10848, 2006.

[38] P. M. Voorhoeve, C. le Sage, M. Schrier et al., "A genetic screen implicates miRNA-372 and miRNA-373 as oncogenes in testicular germ cell tumors," *Cell*, vol. 124, no. 6, pp. 1169–1181, 2006.

[39] E. A. C. Wiemer, "The role of microRNAs in cancer: no small matter," *European Journal of Cancer*, vol. 43, no. 10, pp. 1529–1544, 2007.

[40] W. C. S. Cho, "OncomiRs: the discovery and progress of microRNAs in cancers," *Molecular Cancer*, vol. 6, article 60, 2007.

[41] S. Mi, J. Lu, M. Sun et al., "MicroRNA expression signatures accurately discriminate acute lymphoblastic leukemia from acute myeloid leukemia," *Proceedings of the National Academy of Sciences of the United States of America*, vol. 104, no. 50, pp. 19971–19976, 2007.

[42] S. M. Hammond, "MicroRNAs as tumor suppressors," *Nature Genetics*, vol. 39, no. 5, pp. 582–583, 2007.

[43] A. Bisognin, G. Sales, A. Coppe, S. Bortoluzzi, and C. Romualdi, "MAGIA2: from miRNA and genes expression data integrative analysis to microRNA-transcription factor mixed regulatory circuits (2012 update)," *Nucleic Acids Research*, vol. 40, no. 1, pp. W13–W21, 2012.

[44] M. Mognato and L. Celotti, "Modeled microgravity affects cell survival and HPRT mutant frequency, but not the expression of DNA repair genes in human lymphocytes irradiated with ionising radiation," *Mutation Research*, vol. 578, no. 1-2, pp. 417–429, 2005.

[45] B. R. Unsworth and P. I. Lelkes, "Growing tissues in microgravity," *Nature Medicine*, vol. 4, no. 8, pp. 901–907, 1998.

[46] S.-M. Hou, F. J. Van Dam, F. De Zwart et al., "Validation of the human T-lymphocyte cloning assay—ring test report from the EU concerted action on HPRT mutation (EUCAHM)," *Mutation Research*, vol. 431, no. 2, pp. 211–221, 1999.

[47] C. Girardi, C. de Pittà, S. Casara et al., "Analysis of miRNA and mRNA expression profiles highlights alterations in ionizing radiation response of human lymphocytes under modeled microgravity," *PLoS ONE*, vol. 7, no. 2, Article ID e31293, 2012.

[48] H. Wang, R. A. Ach, and B. O. Curry, "Direct and sensitive miRNA profiling from low-input total RNA," *RNA*, vol. 13, no. 1, pp. 151–159, 2007.

[49] B. M. Bolstad, R. A. Irizarry, M. Åstrand, and T. P. Speed, "A comparison of normalization methods for high density oligonucleotide array data based on variance and bias," *Bioinformatics*, vol. 19, no. 2, pp. 185–193, 2003.

[50] V. G. Tusher, R. Tibshirani, and G. Chu, "Diagnosis of multiple cancer types by shrunken centroids of gene expression," *Proceedings of the National Academy of Sciences of the United States of America*, vol. 98, pp. 5116–5121, 2001.

[51] G. Sales, E. Calura, P. Martini, and C. Romualdi, "Graphite web: web tool for gene set analysis exploiting pathway topology," *Nucleic Acids Research*, vol. 41, pp. 89–97, 2013.

[52] F. Xin, M. Li, C. Balch et al., "Computational analysis of microRNA profiles and their target genes suggests significant involvement in breast cancer antiestrogen resistance," *Bioinformatics*, vol. 25, no. 4, pp. 430–434, 2009.

[53] H. Wang and W.-H. Li, "Increasing MicroRNA target prediction confidence by the relative R2 method," *Journal of Theoretical Biology*, vol. 259, no. 4, pp. 793–798, 2009.

[54] D. W. Huang, B. T. Sherman, and R. A. Lempicki, "Systematic and integrative analysis of large gene lists using DAVID bioinformatics resources," *Nature Protocols*, vol. 4, no. 1, pp. 44–57, 2009.

[55] K. J. Livak and T. D. Schmittgen, "Analysis of relative gene expression data using real-time quantitative PCR and the $2^{-\Delta\Delta C}$T method," *Methods*, vol. 25, no. 4, pp. 402–408, 2001.

[56] R. J. Albertini, K. L. Castle, and W. R. Borcherding, "T-cell cloning to detect the mutant 6-thioguanine-resistant lymphocytes present in human peripheral blood," *Proceedings of the National Academy of Sciences of the United States of America*, vol. 79, no. 21 I, pp. 6617–6621, 1982.

[57] M. Mognato, C. Girardi, S. Fabris, and L. Celotti, "DNA repair in modeled microgravity: double strand break rejoining activity in human lymphocytes irradiated with γ-rays," *Mutation Research*, vol. 663, no. 1-2, pp. 32–39, 2009.

[58] S. Canova, F. Fiorasi, M. Mognato et al., ""Modeled microgravity" affects cell response to ionizing radiation and increases genomic damage," *Radiation Research*, vol. 163, no. 2, pp. 191–199, 2005.

[59] B. P. Lewis, C. B. Burge, and D. P. Bartel, "Conserved seed pairing, often flanked by adenosines, indicates that thousands of human genes are microRNA targets," *Cell*, vol. 120, no. 1, pp. 15–20, 2005.

[60] M. S. Cline, M. Smoot, E. Cerami et al., "Integration of biological networks and gene expression data using Cytoscape," *Nature Protocols*, vol. 2, no. 10, pp. 2366–2382, 2007.

[61] F. Censi, A. Giuliani, P. Bartolini, and G. Calcagnini, "A multiscale graph theoretical approach to gene regulation networks: a case study in atrial fibrillation," *IEEE Transactions on Biomedical Engineering*, vol. 58, no. 10, pp. 2943–2946, 2011.

[62] P. Chen, C. Price, Z. Li et al., "miR-9 is an essential oncogenic microRNA specifically overexpressed in mixed lineage leukemia-rearranged leukemia," *Proceedings of the National Academy of Sciences of the United States of America*, vol. 110, no. 28, pp. 11511–11516, 2013.

[63] G. Pignot, G. Cizeron-Clairac, S. Vacher et al., "MicroRNA expression profile in a large series of bladder tumors: identification of a 3-miRNA signature associated with aggressiveness of muscle-invasive bladder cancer," *International Journal of Cancer*, vol. 132, no. 11, pp. 2479–2491, 2013.

[64] H. M. Namløs, L. A. Meza-Zepeda, T. Barøy et al., "Modulation of the osteosarcoma expression phenotype by microRNAs," *PLoS ONE*, vol. 7, no. 10, Article ID e48086, 2012.

[65] P. S. Eis, W. Tam, L. Sun et al., "Accumulation of miR-155 and BIC RNA in human B cell lymphomas," *Proceedings of the National Academy of Sciences of the United States of America*, vol. 102, no. 10, pp. 3627–3632, 2005.

[66] Y. Pan, M. Meng, G. Zhang, H. Han, and Q. Zhou, "Oncogenic microRNAs in the genesis of leukemia and lymphoma," *Current Pharmaceutical Design*, 2014.

[67] M. V. Iorio, M. Ferracin, C.-G. Liu et al., "MicroRNA gene expression deregulation in human breast cancer," *Cancer Research*, vol. 65, no. 16, pp. 7065–7070, 2005.

[68] Z. Lu, Y. Ye, D. Jiao, J. Qiao, S. Cui, and Z. Liu, "MiR-155 and miR-31 are differentially expressed in breast cancer patients and are correlated with the estrogen receptor and progesterone receptor status," *Oncology Letters*, vol. 4, no. 5, pp. 1027–1032, 2012.

[69] F. Gao, J. Chang, H. Wang, and G. Zhang, "Potential diagnostic value of miR-155 in serum from lung adenocarcinoma patients," *Oncology Reports*, vol. 31, no. 1, pp. 351–357, 2014.

[70] G. Higgs and F. Slack, "The multiple roles of microRNA-155 in oncogenesis," *Journal of Clinical Bioinformatics*, vol. 3, no. 1, p. 17, 2013.

[71] H. Fayyad-Kazan, N. Bitar, M. Najar et al., "Circulating miR-150 and miR-342 in plasma are novel potential biomarkers for acute myeloid leukemia," *Journal of Translational Medicine*, vol. 11, no. 1, article 31, 2013.

[72] M. Yanlei, P. Zhang, F. Wang et al., "miR-150 as a potential biomarker associated with prognosis and therapeutic outcome in colorectal cancer," *Gut*, vol. 61, no. 10, pp. 1447–1453, 2012.

[73] N. K. Jacob, J. V. Cooley, T. N. Yee et al., "Identification of Sensitive Serum microRNA Biomarkers for Radiation Biodosimetry," *PLoS ONE*, vol. 8, no. 2, Article ID e57603, 2013.

[74] G. J. Zhang, H. Zhou, H. X. Xiao, Y. Li, and T. Zhou, "MiR-378 is an independent prognostic factor and inhibits cell growth and invasion in colorectal cancer," *BMC Cancer*, vol. 14, no. 1, p. 109, 2014.

[75] M. Sand, M. Skrygan, D. Georgas et al., "Microarray analysis of microRNA expression in cutaneous squamous cell carcinoma," *Journal of Dermatological Science*, vol. 68, no. 3, pp. 119–126, 2012.

[76] S. Hauser, L. M. Wulfken, S. Holdenrieder et al., "Analysis of serum microRNAs (miR-26a-2∗, miR-191, miR-337-3p and miR-378) as potential biomarkers in renal cell carcinoma," *Cancer Epidemiology*, vol. 36, no. 4, pp. 391–394, 2012.

[77] L. S. Mangala, Y. Zhang, Z. He et al., "Effects of simulated microgravity on expression profile of microRNA in human lymphoblastoid cells," *The Journal of Biological Chemistry*, vol. 286, no. 37, pp. 32483–32490, 2011.

[78] P. Alexiou, M. Maragkakis, G. L. Papadopoulos, M. Reczko, and A. G. Hatzigeorgiou, "Lost in translation: an assessment and perspective for computational microrna target identification," *Bioinformatics*, vol. 25, no. 23, pp. 3049–3055, 2009.

[79] J. Nunez-Iglesias, C.-C. Liu, T. E. Morgan, C. E. Finch, and X. J. Zhou, "Joint genome-wide profiling of miRNA and mRNA expression in Alzheimer's disease cortex reveals altered miRNA regulation," *PLoS ONE*, vol. 5, no. 2, Article ID e8898, 2010.

[80] L. Ma, Y. Huang, W. Zhu et al., "An integrated analysis of miRNA and mRNA expressions in non-small cell lung cancers," *PLoS ONE*, vol. 6, no. 10, Article ID e26502, 2011.

[81] J. C. Engelmann and R. Spang, "A least angle regression model for the prediction of canonical and non-canonical miRNA-mRNA interactions," *PLoS ONE*, vol. 7, no. 7, Article ID e40634, 2012.

[82] N. Bossel Ben-Moshe, R. Avraham, M. Kedmi et al., "Context-specific microRNA analysis: identification of functional microRNAs and their mRNA targets," *Nucleic Acids Research*, vol. 40, no. 21, pp. 10614–10627, 2012.

[83] S. Artmann, K. Jung, A. Bleckmann, and T. Beißbarth, "Detection of simultaneous group effects in microRNA expression and related target gene sets," *PLoS ONE*, vol. 7, no. 6, Article ID e38365, 2012.

[84] R. N. Germain, "MHC-dependent antigen processing and peptide presentation: providing ligands for T lymphocyte activation," *Cell*, vol. 76, no. 2, pp. 287–299, 1994.

[85] I. V. Konstantinova, E. N. Antropova, V. I. Legenkov, and V. D. Zazhirey, "Study of the reactivity of blood lymphoid cells in crew members of Soyuz 6, 7 and 8 before and after space flight," *Kosmicheskaia Biologiia i Meditsina* , vol. 7, no. 6, pp. 35–40, 1973 (Russian).

[86] A. Cogoli and A. Tschopp, "Lymphocyte reactivity during spaceflight," *Immunology Today*, vol. 6, no. 1, pp. 1–4, 1985.

[87] N. Guéguinou, C. Huin-Schohn, M. Bascove et al., "Could spaceflight-associated immune system weakening preclude the expansion of human presence beyond Earth's orbit?" *Journal of Leukocyte Biology*, vol. 86, no. 5, pp. 1027–1038, 2009.

[88] Y. O. Nunez, J. M. Truitt, G. Gorini et al., "Positively correlated miRNA-mRNA regulatory networks in mouse frontal cortex during early stages of alcohol dependence," *BMC Genomics*, vol. 14, p. 725, 2013.

[89] R. P. Sullivan, L. A. Fogel, J. W. Leong et al., "MicroRNA-155 tunes both the threshold and extent of NK cell activation via targeting of multiple signaling pathways," *The Journal of Immunology*, vol. 191, no. 12, pp. 5904–5913, 2013.

[90] F. Gao, Z.-L. Zhao, W.-T. Zhao et al., "MiR-9 modulates the expression of interferon-regulated genes and MHC class I molecules in human nasopharyngeal carcinoma cells," *Biochemical and Biophysical Research Communications*, vol. 431, no. 3, pp. 610–616, 2013.

[91] F. Bazzoni, M. Rossato, M. Fabbri et al., "Induction and regulatory function of miR-9 in human monocytes and neutrophils exposed to proinflammatory signals," *Proceedings of the National Academy of Sciences of the United States of America*, vol. 106, no. 13, pp. 5282–5287, 2009.

[92] S. Thiele, J. Wittmann, H.-M. Jäck, and A. Pahl, "miR-9 enhances IL-2 production in activated human $CD4^+$ T cells by repressing Blimp-1," *European Journal of Immunology*, vol. 42, no. 8, pp. 2100–2108, 2012.

[93] M. Singh, F. Del carpio-Cano, J. Y. Belcher et al., "Functional roles of osteoactivin in normal and disease processes," *Critical Reviews in Eukaryotic Gene Expression*, vol. 20, no. 4, pp. 341–357, 2010.

[94] M. Cogoli-Greuter, M. A. Meloni, L. Sciola et al., "Movements and interactions of leukocytes in microgravity," *Journal of Biotechnology*, vol. 47, no. 2-3, pp. 279–287, 1996.

[95] I. Walther, P. Pippia, M. A. Meloni, F. Turrini, F. Mannu, and A. Cogoli, "Simulated microgravity inhibits the genetic expression of interleukin-2 and its receptor in mitogen-activated T lymphocytes," *FEBS Letters*, vol. 436, no. 1, pp. 115–118, 1998.

[96] X. Ma, J. Pietsch, M. Wehland et al., "Differential gene expression profile and altered cytokine secretion of thyroid cancer cells in space," *The FASEB Journal*, vol. 28, no. 2, pp. 813–835, 2014.

[97] D. Chang, H. Xu, Y. Guo et al., "Simulated microgravity alters the metastatic potential of a human lung adenocarcinoma cell line," *In Vitro Cellular and Developmental Biology—Animal*, vol. 49, no. 3, pp. 170–177, 2013.

[98] S. Hong, X. Li, Y. Zhao, Q. Yang, and B. Kong, "53BP1 suppresses tumor growth and promotes susceptibility to apoptosis of ovarian cancer cells through modulation of the Akt pathway," *Oncology Reports*, vol. 27, no. 4, pp. 1251–1257, 2012.